Methodological Development of Visual Electrodiagnostic of Records with poor SNR: With application in Calibration, Quality Assurance, Collaboration and Training

Thesis submitted following the requirements of the University of Liverpool for the degree of doctor in philosophy

by

RASAM ALIAZIZI

FEBRUARY 2020

Acknowledgements

The following work was produced with the help of number people to whom I am forever grateful. I wish to express my sincere gratitude to Dr. Richard Hagan and Prof Tim Greenshaw for guiding me through my Ph.D. thesis and providing a detailed review of my work.

At the University of Liverpool, I also would like to thank Mr Ashkan Eliasy for his support. Without it, I would not have continued with this work, and without his help, it would not have been possible for me to have a Ph.D. thesis that is adequately structured, organised, worded, and specific. I also wanted to thank Dr Antonio Eleuteri, who has always been there from the beginning of this work through to the end. Antonio has supported me on the technical work, mathematical and programming work as well as almost all other aspects of the work that I am presenting here. I have had the opportunity of numerous meetings with Antonio not only to prepare, structure, and organise my work but also to adequately prepare for my defence. Although he has not been an official supervisor of mine, I have had access to his time, whenever I needed it.

Also, at the University of Liverpool, I wish to thank Mr. Peter Watt, whose support with the electronics and testing side of the work allowed me to efficiently follow through with the technical aspects of the work presented here. Throughout the years working and studying at the University of Liverpool and Royal Liverpool and Broadgreen University Hospital, I have learned and gained a considerable amount of electronics expertise, working alongside Peter.

I especially wanted to thank my dear girlfriend, Sepideh Rad (aka, Sep Sep). The support she gave me in the last couple of years was magnificent. Her help allowed me to finish this work while having a full-time job. Without her support and understanding, it would not have been possible for me to spend any time on my Ph.D. write up.

Furthermore, I wanted to thank my mother & sister for keeping me in their prayers and wishing me all the success. Without their support and my Uncle's, I would not be where I am today.

Declaration

I hereby declare that the following thesis has been composed by me, the research work of which it is record has been carried out by myself and has not been presented in any previous application for a higher degree.

_____

Rasam Aliazizi

Abstract

This thesis describes the design, construction and testing of an instrument that provides realistic test signals from an internet-based reference data library for the calibration and characterisation of electrodiagnostic instruments. The platform, with its attendant software and data libraries (termed ISIM), improves the reliability of these measurements and enables alignment of recording regimes across clinical laboratories. The platform introduces a novel method to share de-identified clinical and research datasets, including the centre's specific normal data (centre's measurement reference point). This could improve the patient's data transferability across different centres over time and facilitates the integration of new theories, techniques and tools (e.g. signal processing toolboxes used to extract signals from records with a weak signal to noise ratios (SNR)) into the critical clinical community and to equipment manufacturers. The latter has the potential to improve the quality assurance and informs the ethos of the standardisation, which is so valued by the International Society for Clinical Electrophysiology of Vision (ISCEV) so that clinical best practice can advance.

A realistic visual electrophysiological data (clinically-based and synthetic) reference library using deterministic and stochastic models is available. The library provides explicitly characterised recordings over a range of SNR's with autoregressive continuous noise and mains supply interference as well as spontaneous electromyography (EMG), eye movement and blinks artefacts. These digital records are freely accessible over the Internet from the Liverpool MatSOAP server using an MS Excel-based toolset acting as a thin internet client. The records are used to objectively assess and validate visual electrophysiological signal processing algorithms as well as characterising the clinical instruments using a physical device termed iSim.

Visual electrophysiological data (Photopic full-field ERG, flicker ERG, ON-OFF ERG) are collected from twelve healthy volunteers with experience in visual electrophysiological data collection and processing. These clinically-based records are conditioned and used as the initial reference data for inclusion within the ISIM back-end library. The context of the data is also provided, allowing maintained traceability. Liverpool thread electrodes and a bespoke Liverpool bio amplifier integrated with Roland ganzfeld stimulator are used for collecting visual biosignal data and continuous record of noise and spontaneous artefacts. The normal data from Liverpool electrodiagnostic laboratory as well as mathematically synthesised data (traceable to specific publications) is also made available to download. The functionality of ISIM is tested with Roland RETIscan system, including characterising Roland's artefact rejection algorithm post scrutinising its underpinning maximally-length sequence used for multifocal ERG (mfERG) measurements.

List of Figures

to reduce the distortion by reversing some of the amplifier's output and feeding it back into the input led into designing a general-purpose differential amplifiers using vacuum tubes during the early 1940s and forms the basis of operational amplifiers) and lacked the required high-level of Common Mode (CM) rejection as well as low input impedance of 200 KΩ. (b) the designed oscillograph by B.H.C Matthews to work with the differential amplifier in (a).

Figure 2.8. (a) The analogue correlator system developed at MIT together with magnetic tape to record the data. (b) ARC (1958) built at Lincoln Laboratory (Lincoln Lab was formed in 1951, funded by US Department of Defense and administrated by MIT) and a digital successor to the Correlator system in (a). (c) Block diagram for the analogue correlator system. Where from the mathematical definition for the auto- or cross-correlation, one can readily see the time-delay, multiplication and integration operations. The signals to be correlated and the correlation result is recorded onto a magnetic tape where the latter would also be plotted using the plotter module. Due to the limitation in storage capacity of the magnetic tapes, a frequency modulation technique was employed in which a carrier wave is frequency modulated by the recorded neurological potential signal and is recorded. The technique is a post record processing of the neuroelectric potentials. (d) Left: Block diagram of ARC allowing for "on-line" processing of neuroelectric potentials. Right: illustration of improvement in signal power compared to the noise power as the number of averages is increased.

Figure 2.9. (a) Relative or normalised spectral luminous efficiency curved under both photopic and scotopic conditions where maximum sensitivity under scotopic and photopic condition are 507 nm and 555 nm, respectively. (b) The spectral characteristic of freshly enucleated human eyes (transmittance curve of the cornea, aqueous humour, lens and vitreous humour for the wavelength range from 0.22 to 2.8 nm). Results are measured made on 9 eyes from people in the range of 4 weeks to 75 years of age. In this study, the author found that the maximum total transmittance (direct and scatter) of the eye is about 84%, and this is in the range of 650-850 nm.

Figure 2.10. (a) Apparatus used by Stiles and Crawford to measure the luminance efficiency curves. Where S is the light source, O_1, O_2, O_3 and O_4 are diffusing glasses providing a uniform illumination at the A_1 and A2 apertures. Prism 1 and 2 (P_1 and P_2) will turn the light and Lenses 1 and 2 will ensure parallel beams of uniform light (Maxwellian system setup). Through turning and adjustment of P1 and P2 it was then possible to create the traversing beam of light required to perform the measurement. (b) The luminance efficiency decreases as the point of entry move away from the centre of a dilated pupil. At the periphery, the luminance efficiency falls by approximately 70%. The luminance efficiency curve is approximately symmetrical for both measured eyes (in this figure left eye measurements are indicated by X, and right eye measurement by Θ) and the peak value does not always match the centre point. Image from. The measurements in the figure are from the author B. H. Crawford (1932) when entering rays are traversed horizontally away from the centre of the pupil in both temporal and nasal directions. (c) Same subject, same experimental conditions and methods (flicker method) when traversing the vertical plane. It is observed that the shape of the curves is the same, but the peak value is now differently paced in the vertical traverses. (d) Graphical representation of SCE for dilated eyes (8 mm). An attempt to create a normal set for human SCE peak and spread value by.

Figure 2.11. (a) A demonstration of Hippus at constant illumination from data collected by H. Bouma and L. C. J. Baghuis. Initially, the authors were under the impression that the spontaneous disturbances of pupil diameter were due to the unsteady state of the light stimulus. This was rejected post further investigation by the authors. (b) Effect of luminance on natural (mean diameter of 5.78 mm) and dilated (mean diameter of 8.41 mm) pupils.

Figure 2.12. (a) A typical setup (Maxwellian system) before Ganzfeld introduction for retinal illumination during experimental and diagnostic examinations. Such installation includes a series of neutral, coloured and calibrated filters (indicated by F), optical lens system to bring the beam of light to focus at point P. If the subject is correctly in position, the beam will be concentrated on the pupil. The use of artificial pupils may be included to ensure the focus of the beam to the pupillary region. The visual angle subtended by the stimulus is then calculated and reported accordingly. The light stimulus is also traced on the final record so that the calculation of waveform subcomponent latencies could be determined. (b) Illustration of changes to ERG morphology (amplitude and time course) with varying intensity (bright and dim stimulation) and distribution of light on the retina, when gross electrode, placed at the cornea, is used to record the ERG responses. (c) & (d) constructed Ganzfeld stimulator by Gouras to allow for whole field or homogenous stimulation of the entire visual field. He further explained that if any stimulus other than a ganzfeld is used, the retina is not evenly illuminated, resulting in the overall recorded ERG waveform to be an integral of localised responses with varying shape and amplitude, making the comparability of records between clinics more difficult. Early changes in amplitudes and latencies of different components of ERG can be used to detect abnormalities, for example, to detect early retinitis peigmentosa before it is evident under conventional ophthalmic imaging.

Figure 2.13. (a) Gunkel Ganzfeld design specification. A indicates flash tube. B & C slots for inserting calibrated filters for stimulus and background light respectively. D, indicates background illumination source. E, background intensity control (through a feedback mechanism adjusted to monitor dome illumination at all times) and I, diffusing filter. (b) Ganzfeld dome constructed by Robin and Berson with a patient sitting in front of the full field dome. (c) and (d) illustration of the overall computerised and variable intensity Ganzfeld stimulator for ERG measurements by Smith and Diprose (1985).

Figure 2.14. (a) Density plot of rod and cone photoreceptors on a horizontal cross-section of the human retina. It is demonstrated that there exist no rods at the centre of the retina and they peak at 5 mm out from the centre. Also, no rods or cones at the optic disk area. (b) Ophthalmic image of the human retina where the optic disk and foveal area are marked. This image gives a visual appreciation of the size of the fovea with respect to the rest of the retina**.** (c) fmERG response generated sue to long stimulus duration where the ON and OFF responses, as well as the PHNR and OPs, are visible. Low signal levels of such responses would mean low SNR and hence require long test durations for any meaningful results.

Figure 2.15. Illustration of the block diagram for the system set up by Fricker and Sanders (1974). The patient was dilated, and cotton wick electrode was used as an active electrode. Grass PS22 stimulator was used to deliver the flashes at a distance from the subject's eye. The flashes were triggered using the flash trigger pulses generated from the rising edge of the waveform output of the PRBS generator. The "*basic*" frequency of 100 Hz was adjusted although this was variable and not fixed. The cross-correlation was carried for 65.5 seconds equating to 1640 averages per the probability distribution of inter-flash intervals of (b). (c) Image taken from Eric Sutter's patent in 1989, demonstrating an array of controllable elements (he used 256 elements in his initial work although more resolution could be obtained if needed) activated and governed by m-sequences. These sequences are then used through the use of cross-correlation technique to extract the regional responses accordingly.

Figure 2.16. Illustration of coding the localised retinal responses and decoding of the record using m-sequences. This figure also illustrates how ISIM could be used to calibrate and a better understanding of the recording data acquisition system.

Figure 2.17. Eye position during one-minute fixation for an elite shooter and a normal control subject under the standard condition and when distracters are present to the parafoveal region.

Figure 2.18. (a) The stimulus array of 509 elements superimposed on fundus image of a normal test subject, where the diameter of the elements is increased from 0.8^{o} (approaching fixation limit) at the centre of the field to 2.8^{o} at the peripheral area. Such variation in stimulating area is to ensure a constant SNR across all stimulating patches. (b) First-order kernel response density function together with the response array of the same test subject to a binary stimulating trigger. A white flash corresponds to an intensity of 8 $cd.sm^{-2}$. The rate of screen update was adjusted to 75 Hz that is every 13.33 ms, and the total recording lasted about one hour. The subject was under photopic condition, dilated and anaesthetised before fitting Burian-Allen contact lens electrodes. The signal was amplified by a factor of 5000 and band-passed filtered at 10-300 Hz and sampled at 1.2 kHz.

Figure 2.19. (a) The strategy selected by Hood et al for comparison of full-field and mfERG summed responses. (b) Left: Results of the comparison for various mfERG stimulation rate (slowest = 7F) while the luminance and contrast were kept at the same level. Right: summed responses of the mfERG for the frame rate of 7F at various background illumination.

Figure 2.20. (a) The calculated number of occurrences of specific pulse trains and the associated effective frequency of these occurrences. The first row in (a) is the first slice of SOK, the second is the SOSS (Second Order Second Slice), the third is the third slice of the second-order kernel and so on. (b) Illustrates the extracted slices of the second-order kernel through performing the selective cross-correlation. The calibration axis demonstrates the base-period of 13 ms, corresponding to a frame rate of 77 Hz. Such high frame rate allows an increased level of nonlinearity in the recorded waveform and as such the impact of previous flashes on the flash of interest becomes more and more pronounced. From (a) one can see that the SNR is reducing for higher-order nonlinearities as the number of occurrences of the specific pulse trains reduces.

Figure 2.21. (a) And (b) An image of the LED-based MFS along a calibrating ruler. The ruler is used to create the calibration axis when imported into a developed MATLAB software application. (c) The application allowed for the calculation of hexagonal area, ring area and ultimately the scaling factor.

Figure 2.22. A proposed system for calibration of visual electrodiagnostic instruments by Ding and Liu et al.

Figure 2.23. (a) transparent, perforated Multi-Electrode Arrays (pMEAs) implemented with 60 Titanium nitride electrodes with 200 um electrode distance and 30 um electrode diameters, ensuring high SNR and maintained the supply of oxygen and nutrition to the ganglion cells in the detached retina. (b) A detached retina is placed on the electrodes where all electrodes are visible, and retina is checked to ensure it is not torn, does not have any holes it is flat and homogeneous.

Figure 2.24. (a) Sundmark (1958-1959) attempt to characterise the impact of b-wave potential at various corneal positions using Cotton wick electrode on human subjects. (b) First attempt (since Sundmark's during the late 1950s) to simultaneously measure the topographical distribution of ERG using multi-electrode ERG (meERG) from rat cornea using 25 electrode arrays (2014). The soft contact lens electrode is constructed to ensure that it fits well on the cornea.

Figure 2.25. Set up of the monkey's eye for full-field ERG and mfERG recordings using GRACE electrode (bottom left) and Jet corneal contact lens electrode (bottom right). The scale white bars in the figures are 5 mm in length.

Figure 2.26. (a) Contact lens sensor developed by Google and Novartis (called "*smart lens technology*"). This product has an embedded glucose biosensor embedded into a hydrogel matrix that senses the glucose level in the tear and transfers the data wirelessly using the embedded controller and antenna to a nearby computer or phone. Several patents granted to Google, Johnson and Johnson Vision Care Inc and others on continuous monitoring of the tear glucose from 2009 to 2014. Such a contact lens system cannot currently be used in electroretinography applications. However, with the trend of increasing miniaturisation of devices and systems, it is becoming increasingly possible to make even smaller, multifunctional, higher speed devices that can potentially provide many of the critical features requirements of a laboratory ERG instrumentation. (b) Left: The first handheld system (RETeval LKC Technologies) developed and commercially made available for VEP, ERG and flicker examinations using skin electrodes without the requirement for pupil dilation and administration of anaesthesia. Right: placement of the device sensor strip, the setup requires no skin preparation. The effect of position of this electrode array is investigated by Hobby and Kozareva et al (2018).

Figure 2.27. Illustration of the LED contact lens electrode as a new and cheap alternative to Ganzfeld dome in veterinary ophthalmology. The setup is used to obtain ERG recording from 15 sedated, healthy beagle dogs. The setup allowed to obtain ERG responses at 12 different intensities including ISCEV SF (Standard Flash, 3.0 cd/m^2/sec) under both photopic and scotopic conditions. Flicker responses, according to ISCEV standards were also performed.

Figure 2.28. Contact lens electrode with four LEDs. These LEDs are the light source for both background and stimulus light. The LEDs are independently controlled using a custom-built power supply unit, and intensities were adjusted per the ISCEV standards. A gold ring electrode mounted on a contact lens is used to record the generated ERG response. The developers of the schema, tested the electrodes on 12 normal subjects and two patients with progressive cone dystrophy to further investigate the ERG parameters.

Figure 2.29. FFT of response recorded using active and passive electrodes, demonstrating a significant reduction in line interference.

Figure 3.1. Illustration of an orthogonal multi-component control system (retina). ISIM is made up of hardware and software components, allows user-defined output through simple multipliers identified as Amplification Matrices ($AM_{i,j}$).

Figure 3.2. Demonstration of methods used to generate and prepare simulated response waveform for the orthogonal multi-component system model.

Figure 3.3. Illustration of edge-effect and its impact on the original or intended data.

Figure 3.4. Digitisation of a standard ERG signal (a) and data transfer to Excel® for further processing (b).

Figure 3.5. (a) Linear feedback shift register resulting in the generation of the sequence shown in (b). Correlation test results with significant peaks are shown in (c).

Figure 3.6. (a) cross-correlation results of a generated m-sequence. (b) using technique demonstrated in (c), an adaptive length is added to the m-sequence and cross-correlation is performed again.

Figure 3.7. Relative location of FOK, SOK, SOSS and TOK obtained from Roland system by Hagan during his PhD work in 2004.

Figure 3.8. Verification of m-sequence & calculation of higher-order kernel slice sequences.

Figure 3.9. (a) Illustrates the recorded raw data from iSim built-in photodiode circuitry for the sequence 0 (centre sequence) of Roland Consult system when a run of 511 m-sequence was initiated with a base-period of 83 ms (5 filler frames, where the stimulation rate is 60 Hz or 16.6 ms time-interval in-between frames). (b) Illustration of peak identification of recorded raw data from photodiode in MATLAB®. A simple difference equation could then be implemented to identify the time interval between flashes. (c) Illustrates the calculated flash sequence or stimulation sequence that also contains the initial adaption or settlement period of length 0.5 seconds. (d) Shows the calculated and plotted data for (using MATLAB® Scatter function) run property of the true m-sequence after performing extraction algorithm on the calculated flash sequence. This shows that there is a certain number of each number of steps between

flashes, i.e. one eight-step gap, two seven-step gaps, four six-step gaps and so on. This is a property specific to m-sequences.

Figure 3.10. Based on memory-length, m-transform matrix is calculated. This together with generated or scanned sequence array, sampling frequency and measured base-period, allows for determination of application multi-dimensional m-transform. Based on discussion in chapter 3, this transformation is used for kernels extraction from recorded retinal response (probed using the generated or scanned m-sequence array) or the inverse, that is estimation of retinal response from kernel-slice tables. Kernel-slice tables are represented mathematically by First and Higher-Order-Kernel slices, i.e. FOK and HOK, which are functions of both time and spatial locations (i.e. encoded/decoded spatiotemporal information). In field of visual electro-diagnostic, kernel slices are illustrated as density map (i.e. extracted localized response function amplitude per square of subtended retinal angle, e.g. nV/deg^2).

Figure 3.11. The "Estimate Response" block in figure 3.10, is represented in this figure, simulating the j^{th} location response. It is easy to realize that, a filter implementation of integer multiple of such blocks in a parallel configuration, would result in full simulation. The output of these filters would be summed together providing a single retinal response estimation under a specific test configuration of N spatial locations probed using a pre-configured m-sequence as the visual excitation signal. Alternative is a sequential approach, which could be implemented having access to j^{th} location governing m-sequence, the shift table for FOK_j and physical synchronization signal defining the starting point.

Figure 3.12. In a clinical system, as frames are presented approx. 50% of hexagons are off, and the other 50% are on. This triggers the iSim (when a flash at a specific location is present) system to start recording the response of the j^{th} retinal location. This response is accompanied by a phase termed implicit time, which is a fixed parameter of the response due to its time-invariance characteristic.

Figure 3.13. Illustrating estimation of location 1 response with stimulation cycle at index 121 of an m-sequence of length 512. The estimation of current response depends on flash content of a memory register that extends by three base-period as highlighted in yellow and demonstrated by blue borders in the GUI. Since this corresponds to three flashes (fff) from table 3.1, it would mean that FOK and TOK kernel slices will contribute to the next response.

Figure 3.14. Arbitrary kernel slices for FOK, SOK, SOSS and TOK obtained from figure 2 in Eric Sutter paper.

Figure 3.15. the boundary region through sequence is demonstrated by the red box for the initial two elements of the sequence for a second order system. As the first term is always a zero a zero vector of length base-period is generated (the content of memory register is [don't care, don't care, 0]. As one moves through the sequence memory register becomes [don't care, 0, 0/1] that is implementation of a SOK response based on table 4.1 and whether second element of the sequence is a 0 or 1. This will satisfy the initial boundary condition in signal estimation.

Figure 3.16. GUI written in C++ that is used to extract kernel slices of a second order system up to TOK slice.

Figure 3.17. Kernel slice extraction algorithm. Synchronous recovery of the kernel slices and cross-correlation vector from estimated or actual signal input vector.

Figure 3.18. Illustration of defocusing in signal generation using ISIM toolbox for a second order system of up to TOK as its most significant higher-order kernel slice. Blue waveform represents the actual kernels and Orange waveform represents extracted kernels post contamination through defocusing. The kernels are for demonstration purposes only. The response vector is created through execution of GUI demonstrated in figure 3.13 by setting the base-period to 25 ms and the governing m-sequence of length 4095. The sequence is mixed with a shifted version simulating the governing m-sequence of the secondary location. Kernel slices are then extracted using GUI in figure 3.16.

Figure 3.19. Example of artefactual signal that does not exceed artefact rejection threshold.

Figure 3.20. This figure illustrates the effect of a blink which completely masks the signal of interest.

(a) Shows a blink occurrence prior to application of the flash, its impact is lasting through the complete period of next retinal response.
(b) Shows occurrence of an eye movement, pulling negative on trough of the signal cycle and is roughly of small amplitude, this could cause significant error in calculation if averaged and as it is evident, it is very difficult to be spotted for an untrained eye.
(c) Shows occurrence of a blink, right after the occurrence of the flash, this is the most common location for an unwanted eye movement or blink. Again, this is contaminating the signal of interest.

(d) Shows a large magnitude blink signal, these are easy to spot for the background clinical software system and the corresponding period would be rejected in prior to averaging process.

Figure 3.21. (a) Full record of EMG artefact signal data at sampling frequency of 10204 Hz using thread electrode. Subject is instructed to perform various facial muscle activity while sat comfortably on chair. Subject were instructed to perform no eye movement or blinks while staring at a dot on the screen ahead when background lights were dimmed and comfortable. (b) & (c) zoomed section of the data record in (a). (d) demonstrates application of Tukey Window to avoid any edge-effects in processing (MATLAB® responsible function: *tuk = tukeywin(length(EMG(:,2)), 0.3)*). (e) a comparison of post windowing vs actual data record. (f) post filtering application with a lowpass corner frequency of 150Hz. The amplitude of the record is maintained while unwanted high-frequency noise data is removed.

Figure 3. 22. National Grid UK, reports that, system frequency is a continuously changing variable that is determined and controlled by the second-by-second (real time) balance between demand and total generation or supply. If demand is greater than generation then the frequency falls and vice versa. It is also reported that national grid must control the frequency to be plus or minus 1% of the nominal frequency of 50.00 Hz. A sudden drop in frequency would indicate that the grid is under stress as there is a surge in demand. This figure demonstrates historical data with 1 second resolution over the month of June 2018. As it can be seen from this published data, the variations in frequency is such that, on average the supply mains frequency is 50.00171 Hz with maximum recorded data of 50.226 Hz and a minimum recorded data of 49.677 Hz.

Figure 3.23. Illustrate the setup used to measure, digitize and record mains signal directly through wall socket.

Figure 3.24. Trigger mode operation and record segmentation.

Figure 3.25. Graphical illustration of stimulator trigger signal preparation for various operational mode. The trigger signal will ensure perfect synchronization between data collected and trigger timing of the stimulator.

Figure 3.26. (a) The apparent isolation path and the use of optoisolators to transmit the signal across the isolation barrier. The component used to isolate the DC power supply, $\pm$12V, is also present. The ground plate in this design is isolated from earth (main's earth) and driven to 0 V using buffer amplifiers. This signal is also fed to the common (reference) electrode that is placed on the patient's forehead during ERG measurement (colour-coded as a green electrode). The ADC amplifiers and respective gain blocks (resistive blocks) are illustrated at the right where these are isolated from the danger of EMI through shielding. In between the isolation barrier and shielded ADC instrumentation amplifiers (32 bit) there exists power regulations circuitry and multiplexing stages. In the left-hand side of this figure, the control unit and power management circuitry are populated. The board is a two-layer board with components and signal tracks on one side of the board, as shown and an almost undisturbed ground plan on the other side of the board. Good electronics practice is visible throughout the layout. For example, most of the tracks on the analogue and digital side are not at the right angle, which further reduces the electronic noise introduced due to reflection. (b) The amplifier's common is different from earth, and it could be connected to the earth. In which case, there is no patient isolation, hence more significant noise interference. The amplifier common is the reference plane. There is no direct path to the earth from the amplifiers common. This is purely for patient safety and results in breaking the ground loops interference, making it a complicated task to make this common reference, electrically quiet. Ripples on this line are common to both inputs of the differential amplifier. In the figure above, there is no direct path from patient to earth. This is performed via isolating the amplifier common and using an isolation amplifier. This results in patient floating. The amplifier common is floating, that means it can be sitting on any voltage and the output of the instrumentation amplifier is measured with respect to this common terminal. It is therefore required to have this terminal, electrically, very quiet. (b) is for illustration purposes only and does not represent the actual placement of the electrodes during ERG measurement. The isolation also allows for accurate transfer of signals across the barrier without cross-coupling or interaction between adjacent signals.

Figure 3.27. Frequency analysis of a PERG waveform.

Figure 3.28. (a) illustration of the clinical/study setup and the required connections. As well system being powered through an isolation transformer block allowing the measurement units and the subject connected to it to float for safety and noise reduction purposes. (b) illustration of designed and developed bio-amplifier showing input and output terminals including amplifier's two recording channels, optical trigger in/out, USB terminal, other exposed input and out digital pins (DIO lines) as well as MCC onboard LED. The gain switch between a gain of unity and 5000 is also demonstrated. (c) illustrates the initial signal channel bio-amplifier prior to advancing to development of a two-channel bio-amplifier with higher specification.

Figure 3.29. illustration of bio-amplifier electronic schematic demonstrating the pin configuration of all integrated units. These pin configurations are carefully recorded during implementation of governing software and are hard coded respectively.

Figure 3.30. (a) Illustration of the MATLAB® GUI to communicate with bio-amplifier and stimulator. (a) shows the interface and a popup dialogue box that allows user to select the stimulator type. (b) Illustration of bio-amplifier main GUI during study subject test run using Ganzfeld Roland system while performing flash stimulation of -25 dB below ISCEV specified standard flash intensity of 3 $cd.s.m^{-2}$. There are two plot areas, the one on the left is a plot of collected data filtered at 500 Hz low-pass corner frequency with no other signal processing and the one on the right which demonstrates the signal average in real-time. The pause button on the top right corner is only visible when the system is running and provides a mechanism to pause signal averaging and storing while still reading and plotting the biological waveform. The artefact auto-rejection mechanism is active when collecting data, the operator will have access to raw data including all recorded artefacts. (b) Also demonstrates recording from both eyes through activating both bio-amplifier channels.

Figure 3.31. (a) illustration of MATLAB® GUI to configure Roland Ganzfeld stimulator. (b) MATLAB® GUI to generate m-sequences, prepare the sequence (e.g. adaptation length, correction term, and intensity level assignment, peripheral adaptation intensity setting as well as configuring the Kelvin Vision LED Multifocal Stimulatot (MFS).

Figure 3.32. MatSOAP© three-tier architecture design to carry out the communications between the application logic and back-end storage. Connections between the user interface and the application logic usually use a remote procedure call (RPC). The latest version of this is called Simple Object Access Protocol (SOAP) and is typically transferred using hypertext transport protocol (http).

Figure 3.33. MatSOAP© gateway representation.

Figure 3.34. Implementation of MatSOAP© and ISIM back-end server.

Figure 3.35. (a) MS Excel® GUI design and developed for generation of user defined visual electro diagnostic records. (b) Once processing at the back-end server is finalized and returns, the spreadsheet will unpack the returned data and present the result to the end-user.

Figure 3.36. application of design control to waterfall design process (figure used with permission from Medical Devices Bureau, Health Canada.

Figure 3.37. Illustration of various developmental phases (with multiple iterations within each phase) laid out on top of three major interconnected work streams. These work streams are developed in a modular design format that expose standard interfaces allowing for integration of modules. For example, the GUI communicates through SPI interface with embedded firmware using commands and acknowledgments (CMD/ACK module).

Figure 3.38. iSim Version 1, risks and opportunities:
At this evolutionary stage, the following key components of ISIM was evaluated, studied, and implemented:

- Verification of top-level user needs – simple usability study through multiple formative validation studies of the process to better inform the overall product requirements which would ultimately translate into a sound hardware and software design
- Ensure portability, lightweight and small size
- Characterisation of MBED prototyping board and maturing the embedded software program
- Implementation of the trigger unit
- Implementation of host computer communication interface using simple MATLAB® GUI
- Characterisation of signal requirements and better understand the challenges of SNR in conjunction with the allowable dynamic range of selected DAC
- Implementation of mathematical engine responsible for signal generation and implementation of associated Excel® GUI to utilise the engine through consumption of the MatSOAP© server

Figure 3.39. iSim Version 2, evaluation of a potential working prototype:
At this evolutionary stage, the following key components of ISIM was evaluated, studied, and implemented:

- Identified Dynamic Range (DR) requirements
    - DAC selection and its associated low-level embedded programming class
    - Design power requirements and associated stable voltage booster circuitry

    - Implementation of output summing amplifier and implementation of hardware and software calibration capability
- Onboard hardware memory storage (SD implementation and its associated low-level embedded software implementation)
    - Low-level file management system and development of an internal buffer system for efficient and accurate data handling taking advantage of a low-level multi-threaded programming technique
- Hardware filter implementation
- Optical trigger-in circuitry

Figure 3.40. iSim Version 3, a working prototype.
At this evolutionary stage, the following key components of ISIM was evaluated, studied, and implemented:

- System noise analysis and reduction (through multiple iterations of PCB design, manufacture, assembly and testing)
- High-level GUI fine-tuning (implementation of a simple and thin User mode to the GUI)
- Further trigger development (Optical, TTL voltage and software-based trigger implementation)
- System verification and validation (V&V)
- Enclosure selection and final assembly including labelling and generation of Instruction For Use (IFU)

Figure 3.41. Schematic design circuit for iSim version 3. The schematic was next evaluated in EAGLE to generate a 2-layer PCB board. This PCB board was then constructed through outsourcing and populated in the department of Medical Physics and Clinical Engineering. Throughout phase three the high-level and low-level software implementation were also optimized and fine-tuned for best user experience.

Figure 3.42. Dynamic range requirements based on the selected signal amplitude.

Figure 3.43. Illustrating that for a signal amplitude of peak-to-peak value in the range of 29.5-600 µV, DAC dynamic range of 5 Volts and a minimum SNR of -20 dB. The DAC with 12-bit resolution can faithfully represent the final waveform.

Figure 3.44. Illustrating that for a signal amplitude of peak-to-peak value in the range of 2-400 µV, DAC dynamic range of 5 Volts and a minimum SNR of -40 dB. The DAC with 19-bit resolution can faithfully represent the final waveform.

Figure 3.45. (a) Illustration of DAC evaluation board with MBED microcontroller during iSim stage two development. (b) demo DAC output when a standard PERG signal at arbitrary amplitude is programmed. (c) zooming to a section of the output waveform illustrates stepped functionality of the DAC, this clearly demonstrates requirements for a reconstruction filter at the output stage of iSim to smooth the signal and avoid contamination due to these unwanted high-frequency components (stepped edges of the square function).

Figure 3.46. DAC update rate vs configured serial peripheral clock frequency.

Figure 3.47. Demonstration of Bit rate manipulation using MATLAB® simulation of a simple sinewave. Even zooming to small areas on the left plot in this figure won't make seeing the individual steps any easier. The left plot demonstrates the signal resampled by a factor of 14200. The number of samples in the right plot is 100. The high sample rate mode is used in iSim calibration mode, when one channel is enough to output a clean signal to calibrate the device. That is the software is at its bare minimum operational mode and will not need to spend much time to service other routines.

Figure 3.48. Measured iSim output update rate against the number of active channels.

Figure 3.49. Illustration of iSim device board zoning where the placements of the top-level components are defined and mapped.

Figure 3.50. illustration of ground star connections.

Figure 3.51. Illustration of top and bottom plane and signal routing. Particularly it is evident that the ground plane is kept free of routing where possible ensuring no breaks or discontinuity.

Figure 3.52. Illustration of iSim PCB assembly iteration and enclosure testing.

Figure 3.53. Example of the software system, items and units.

Figure 3.54. Captures the high-level functional inputs and outputs of the firmware software Item.

Figure 3.55. High-level functional inputs and outputs of iSim firmware software Item.

Figure 3.56. iSim embedded firmware architecture. All SOUPs are borrowed pieces of software in the implemented modular design architecture that are fully tested and where needed modified to fit the required design criteria.

Figure 3.57. Illustration of iSim main thread program flow.

Figure 3.58. Expected iSim noise file structure.

Figure 3.59. Illustration of implemented low and high-level circular buffer in low and high-level software iSim software design. Figure also shows the data flow from the SD storage unit to the client's GUI.

Figure 3.60. Illustrating the timing of the read and write operations and assigned SPI clock frequency to ensure no read and write violation and sustained iSim output sample rate. RI is the Read Index variable holding the position of the next read from the buffer while WI is the Write Index variable that holds the position of the next write to the circular buffer. From the figure and performed calibration, the write and read operations does not occur at the same speed.

Figure 3.61. illustration of iSim GUI notifying user of missing packets (red box at the footer).

Figure 3.62. Execution time during the implementation of fread function. Impact of this is shown in figure 3.63.

Figure 3.63. Irregular effect and negative impact on signal morphology due to iSim timing error.

Figure 3.64. The ISR, is kept very simple to avoid timing issues and set its priority to high to avoid it being interrupted by other ISRs.

Figure 3.65. Initial MATLAB® GUI to communicate with iSim.

Figure 3.66. iSim GUI. (a) User mode loaded but iSim device is not connected. (b) Same as (a) but iSim device is now connected, micro SD card is connected and iSim channels are powered, communication is established, and device is ready for operation. (c) Same as (b), both signal and noise files are successfully loaded. (d) Device is running. (e) iSim is switched to engineering mode. (f) Engineering mode showing DAC settings applied. (g) iSim is switched to terminal mode of operation. (h) iSim is switched to terminal+ mode of operations with generic waveforms such as sine, square and triangular waveforms available to calibrate iSim itself. (i) and (j) Illustrating, how iSim downloads and installed (accordingly prompting user) the required driver software for a successful operation.

Figure 3.67. iSim GUI. (a) and (b) Illustrating iSim downloading the required driver software and instantiating the installation of these software for a successful operation. (c) iSim integrated DAC GUI. This interface is used to setup iSim channels including, power setting and dynamic range of the individual channels. (d) Illustrating the integrated, on-board oscilloscope that provides the end-user with visualization of data samples that iSim is outputting when in running mode.

Figure 3.68. Placement of electrodes and subject preparation prior to data collection.

Figure 4.1. Results of Medical Safety testing of the bio-amplifier before using test subjects for data collection for inclusion within the ISIM library. The test was carried out following the medical safety testing procedure under Medical Physics and Clinical Engineering (MPCE) department of the University of Liverpool.

Figure 4.2. (a) bio-amplifier measured Gain Band Width (GBW). Where the grey horizontal line demonstrates the 10% attenuation point, and the orange line represents the 29.3% attenuation point. (b) bio-amplifier measured Common Mode Rejection Ratio (CMRR).

Figure 4.3. Amplifier recorded noise level when inputs are shorted together, and output is measured. Amplifier bandwidth is 0-1000Hz. The sampling frequency is adjusted to 40 kHz. The test is performed in a clinical room at Royal Liverpool and Broadgreen University Hospital. Y-axis is in units of mV with scaling factor of 10^{-3}, I.e. y-values are in µV. The peak-to-peak measured noise level is smaller than 3.5 µV. Roland RETIscan amplifier is reported noise level less than 4 µV (RMS) which is equivalent to approximately 5 µV peak-to-peak.

Figure 4.4. Verification of some of the assumptions made about noise and ERG response prior to performing data collection on normal (healthy) subject with no known eye-condition. (a) Record of global or full-field ERG response from a normal subject using Liverpool bio-amplifier and DTL electrodes, under photopic condition using ISCEV standard flash intensity. (b) Record of noise data from the same subject when no stimulus is present. The highlighted section in this

record is used for spectral subtraction. (c) Record of ERG response data post spectral subtraction using data record in (a) and (b). (d) A single cycle of the waveform in (a). (e) A single cycle of the data post spectral subtraction procedure. (f) Frequency-time analysis of the record in (c) illustrating stationarity of the data. All voltage records (in a, b, c, d and e) are in mV and time records are in samples (sampling frequency is 8000 Hz, and the bandwidth of the amplifier is set to 500 Hz).

Figure 4.5. (a) Record of full-field photopic ERG from a normal subject at standard flash intensity at a stimulus rate of 2 Hz. A total 240 cycles is recorded. The vertical red lines demonstrate the onset of a flash stimulus minus 100 ms of added pre-flash period (synchronisation point). (b) The record is chopped up into individual cycles, and the resulting array is plotted accordingly. A three-dimension plot in MATLAB® would further help to differentiate the noisy epochs before the averaging process.

Figure 4.6. The record of figure 4.5 is averaged (post removal of epochs with sharp spikes – potential EMG presence) and filtered (0-100 Hz) and the result is plotted. A pre-flash period of 50 ms is included for accurate windowing of the signal record in later processing. (a) Cursor adjustment to measure the a-wave and b-wave amplitude and implicit time. (b) Cursor adjustment to measure the i-wave amplitude and implicit time.

Figure 4.7. The average results in figure 4.6 are transferred to Excel® automatically using the "send to Excel®" button on the analysis GUI. Note that a 50 ms pre-flash period is added to ensure accurate windowing of the record in later processing.

Figure 4.8. Illustration of manual artefact rejection from the raw data record (removal of potential eye-twitches) and automatic transfer of the rejected epochs to Excel® for record storage and further analysis.

Figure 4.9. (a) Results of averaging the selected epochs, post manual artefact rejection of the waveform in figure 4.8. Seven epochs were removed prior to averaging and filtering. (b) Averaged result of the epochs without any artefact rejection of the waveform in figure 4.8. The impact is noticeable (black circled area) with and without any artefact rejection, on the c-wave.

Figure 4.10. (a) An example of an artefact that triggers the auto rejection algorithm of the amplifier – blinks. (b) Averaged result post manual rejection of the raw data record.

Figure 4.11. Illustrating the effect of EMG, drift, eye-movement and blinks on masking the data (ERG responses) during experimental data collection. (a) The raw data record is discarded due to extensive noise contamination. (b) The data record is retained for further processing; however, the contaminated level of noise is considered too much, and the experiment had to be repeated to ensure a cleaner run.

Figure 4.12. Averaged data post manual artefact rejection, averaging and filtering, for the record of figure 5.11.b.

Figure 4.13. Averaged photopic ERG response (photopic with standard flash) from a normal subject with no known eye condition. The data in this figure is filtered from 0-350 Hz, leaving Oscillatory Potentials (OPs) visible on the rising edge of complex b-wave. The average response is band-passed filtered, [100-150] Hz to isolate oscillatory potential through the elimination of the slow, large-amplitude a- and b-waves as illustrated at the left side of the figure.

Figure 4.14. ERG response collected from right eye of normal subjects with no eye condition per experimental design in chapter 4 using Roland full-field flashes at flash rate of 2 Hz. Liverpool bio-amplifier was used with sampling frequency set at 40 kHz, and artefact rejection ratio turned off. Individual responses are collected post manual artefact rejection, decimation by factor of 40 (to simulate sampling frequency of 1 kHz), averaging of the respective epochs and filtering, [0 – 350] Hz. (a) Xenon flash intensity. (b) +5 dB flash intensity. (c) 0 dB (STANDARD) flash intensity. (d) -5 dB flash intensity. (e) -10 dB flash intensity. (f) -15 dB flash intensity.

Figure 4.15. ERG response collected from the right eye of normal subjects with no eye condition per experimental design in chapter 4 using Roland full-field flashes at flash rate of 2 Hz. Liverpool bio-amplifier was used with sampling frequency set at 40 kHz, and artefact rejection ratio turned off. Individual responses are collected post manual artefact rejection, decimation by factor of 40 (to simulate sampling frequency of 1 kHz), averaging of the respective epochs and filtering, [0 – 350] Hz. (a) -20 dB flash intensity. (b) -25 dB flash intensity. (c) -30 dB flash intensity. (d) -35 dB flash intensity and (e) -40 dB flash intensity.

Figure 4.16. Grand average ERG response for all intensity levels (for example, the 0 dB waveform is average of all waveforms in figure 5.14.(c)). All plots are resampled to 1 kHz and filtered to remove DC and high-frequency components, i.e. [0.02 Hz – 350 Hz]. Using Tukey window, ensured no frequency leakage due to presence of any discontinuity. The length of signals are bounded to 500 ms with a 100 ms pre-flash phase. The 0 dB flash intensity (white trace) is equivalent to 3 $cd.s.m^{-2}$, -10 dB (light blue trace) is equivalent to 0.3 $cd.s.m^{-2}$ etc.

Figure 4.17. (a) a-wave amplitude. (b) b-wave amplitude. (c) a-wave implicit time. (d) b-wave implicit time. In all plots, blue trace represents the measured group average values, orange trace represents the maximum measured value at each intensity level and grey trace represents the minimum measured value at each intensity level.

Figure 4.18. (a) Demonstration of normal subject flicker response, using ISCEV standard LED flashes flickering at a rate of 29.4118 Hz. Flash duration is measured to be 1 ms (green trace in (a)) and 100 cycles are averaged (individual epochs or cycles are illustrated in (b)) resulting in the waveform in (c) that is incorporated into ISIM library. (d) concatenating, five copies of (c) resulting in the synthesis of flicker response waveform.

Figure 4.19. Experimentally collected ON-OFF full-field ERG response using standard flash intensity (ISCEV) with a duty cycle of 50%. Five normal subjects with no known eye conditions were tested using Liverpool DTL electrodes and bio-amplifier recording at a sampling rate of 8 kHz. The average cycle (of all subjects) is shown in white and is incorporated into ISIM library for re-use. (a) Subject one, collected raw data (blue trace), and synchronisation signal (green trace). ((b) Illustration of the ON & OFF period of flashes with a duty cycle of 50%. (c) Subjects averaged cycle data together with the grand average in the white trace, marked with the flash onset (yellow vertical line) and flash offset (black vertical line), clearly demonstrating two distinguished ERG ON and OFF responses. This result is a close match with that of ISCEV published results showing re-producibility and repeatability of the experiment to the published standards (lower-right side of (c)).

Figure 5.20. Dark-adapted 10.0 ERG response digitised and simulated at a sampling rate of 1 kHz with an added pre-flash period of 50 ms. The response is low-pass filtered at 150 Hz and has a length of 205 ms.

Figure 4.21. Dark-adapted 30.0 ERG response digitised and simulated at a sampling rate of 1 kHz with an added pre-flash period of 50 ms. The response is low pass filtered at 150 Hz and has a length of 212 ms.

Figure 4.22. (a) GUI used to simulate a mfERG waveforms based on a number of hexagonal locations to simulate: base-period (overlap), imported m-sequence array, noise file and kernel table. (b) simulated waveform for one hexagonal location with a base-period of 25 ms, and an m-sequence of length 4095. Noise is zero and kernel table consists of FOK, SOK, SOSS and TOK slices obtained from Sutter paper.

Figure 4.23. The GUI used to extract the nonlinear simulated or actual retinal kernel responses. In this validation, the top waveform is the estimated waveform illustrated in figure 5.22.b. The central plot demonstrates the calculated cross-correlation in real-time against the received m-sequence. The m-sequence could be collected from the actual mrERG monitor screen using iSim or could be provided and imported as a text or CSV file, in this example the sequence has been imported and is the same as the coding sequence of figure 5.22. The cross-correlation is then calculated based on the provided base-period (25 ms) and a memory length of two previous base-periods. The decoded results are next plotted based on the requested signal duration (100 ms in this example, however if longer duration is requested, user will obtain 0 everywhere after the 100^{th} sample point if the coding/decoding sequence contains the correction term; otherwise a DC offset will be evident). The interface will only require the mother m-sequence or the sequence responsible for the FOK response, as it will calculate the SOK, SOSS and TOK sequences and will have these saved as CSV files as illustrated at the bottom, right-hand side of this figure.

Figure 4.24. The averaged ERG signal at a flash intensity of -20 dB below standard flash intensity is used to simulate two runs of 120 cycles (flash frequency simulation of 2 Hz), totalling one minute of recording. The estimated noise is ARMA generated (ARMA filter coefficients are those from subject 4), and the SNR is calculated to be -19.875 dB. The sampling frequency of the bio-amplifier was set at 40 kHz. The blue waveform is signal trace (superimposed red waveform for comparison purposes) plus ARMA generated noise, and even when one zooms in, it is extremely difficult to recognise presence of any signal components. No blinks, eye movements, mains noise or other harmonics, EMG or drift signal is assumed during this simulation.

Figure 4.25. Time-domain representation of averaged noisy cycle (black trace), clean signal (green trace, for reference only) and the MSC re-constructed signal cycle (red trace) where only the significant (p-values at or below 0.05), frequency components below 350 Hz are considered to re-construct the signal.

Figure 4.26. Frequency spectrum analysis of the averaged noisy data (brown trace), clean signal (yellow trace) and MSC re-constructed signal (blue trace), where only the significant (p-values at or below 0.05), frequency components below 350 Hz are used to reconstruct the signal.

Figure 4.27. Frequency spectrum analysis (same as figure 5.26 with frequency limits set to 0-2kHz) of the averaged noisy data (brown trace), clean signal (yellow trace) and MSC re-constructed signal (blue trace), where only the significant (p-values at or below 0.05), frequency components below 350 Hz are considered to re-construct the signal based on the observed noisy waveform.

Figure 4.28. Frequency-time analysis. (a) Spectrogram of the averaged noisy signal. Presence of high-frequency noise components are clear compared to the clean signal and reconstructed signal spectrogram of (b) and (c) respectively. (b) Spectrogram of the original clean signal. It is evident that most of the energy of the signal is contained at low () below 45 Hz) frequency band. (c) Spectrogram of the reconstructed signal through identification of significant frequency components present in the noisy waveform using MSC algorithm and low-pass filtering. The bandwidth of the signal is smaller than 350 Hz, and as it can be seen there are distinct high-energy lines in the estimated, re-constructed signal.

Figure 4.29. Roland RETISCAN artefact rejection ratio verification & m-sequence capture using iSim.

(a) Placement of photodiode (as part of initial development) on the Roland RETIscan CRT screen.
(b) Collected raw photodiode data as recorded on the Roland RETIscan system.
(c) Generated test signal (at – 20 dB SNR) at the sampling frequency of 1000 Hz with known locations of the injected artefacts) using ISIM with blinks and eye-movement to verify the Roland RETIscan artefact rejection algorithm.
(d) Roland RETIscan setup at RLUBH.

Roland RETIscan "biofile". The raw data collected from Roland RETIscan system over the entire 511 steps of the governing m-sequence, with the blinks and eye-movements (artefacts), removed.

Figure 4.30. (a) a segment of data produced using ISIM contaminated with small and large amplitude artefacts. The Red trace is the input waveform into the Roland RETIscan preamplifier head-box. The blue trace is the processed biofile obtained from Roland. The first few small-amplitude artefacts are not recognised as artefacts by the automatic rejection algorithm of the Roland RETIscan system. The ample amplitude artefact at the end of the trace is registered as an artefact by the system. (b) The blue trace provides clues as to how the system has recovered from the artefact. That is the system has been off-line for approximately 0.5 seconds (greyed-out box), and the system has stitched the traces together to form a continuous signal with no artefacts. The way the two traces are stitched together can introduce artificial jump in the baseline of the signal and hence introduce unwanted artificial noise (this is illustrated using the green ovals where the traces are stitched together).

Figure 4.31. The highlighted red steps show periods where an artefact is occurring, blue steps (b) show where the stimulus was repeated but another artefact was encountered so the attempt was discarded. The green steps in the sequence show a second and successful attempt to recover from the artefact and continue through the remainder of the sequence steps. From this quick verification using iSim, it is evident that (without going into any further investigation) the number of steps to be skipped back is dependent upon several factors. These are the step that the sequence is currently running; the length of the preceding steps in the sequence; and the length of the artefact. Using iSim, the procedure (the clinical system under investigation) carries out to perform artefact rejection could be outlined (not further studied here). iSim can help to accurately and objectively determine this procedure with no impact (or change) to the clinical setup and minimal impact on the clinic hours.

Figure 4.32. The highlighted red steps show periods where an artefact is occurring. The green highlight show where Roland RETIscan attempted a sequence skip back followed immediately by another artefact. The blue regions show a successful attempt to recover from artefact/s. (a) Illustrates the Roland artefact rejection algorithm in dealing with artefacts separated by greater than 0.5 seconds. The backout region in the plot of artefactual m-sequence shows where Roland RETIscan is stationary while the artefact returns toward the baseline. (b) Illustrates the behaviour of Roland RETIscan artefact rejection algorithm when dealing with artefacts separated by less than 0.5 seconds. The greyed-out region shows the recording segment of the signal ignored when Roland tries to recover from the three-consecutive artefacts. Careful examination of this figure shows how Roland stitches the signal segments to create the artefact-free trace (blue trace).

Figure 4.33. Illustrating stitching mechanics of the Roland RETIscan system to recover from the artefact. This has introduced a pronounced DC offset into the artefact-free trace (blue trace).

Figure 4.34. (a) Obtained UK National Grid generated mains supply frequency data over two consecutive days with a resolution of 1 minute. (b) The plot of a sample of the data from the population (a), in MATLAB®. The red horizontal line marks the 50 Hz, black horizontal lines mark the boundaries of [49.95, 50.05] Hz and the green horizontal lines mark the boundaries of [49.9, 50.1] Hz. (c) The histogram plot of the population data. The red fit is one for a normal distribution, where comparing this with that of the histogram of the data, one can see that the distribution is not normal.

Figure 4.35. The recorded data is resampled first (1000 Hz) where the change in signal power (recorded mains data) due to resampling process was calculated to be three orders of magnitude lower than the total mains data power and hence insignificant. Next zero-crossings were measured per the MATLAB® script illustrated in this figure. The positive differential zero-crossing points are marked using the red square in (b). The frequency variation from cycle-to-cycle was then measured, and histogram of the result is plotted in (a).

Figure 4.36. (a) Power spectral density (PSD) for collected mains supply data. (b) Respective spectrogram plot.

Figure 4.37. Power Spectral Density (PSD) for collected mains supply data, and the associated MATLAB® script for plotting it.

Figure 4.38. THD (top plot) and SNR calculation for collected mains supply data from the clinic wall socket, using MATLAB® PSD calculation.

Figure 4.39. SIND calculation for collected mains supply data from the clinic wall socket, using MATLAB® PSD determination.

Figure 4.40. Mains supply interference estimation/modelling using a single 50 Hz and 1st and 2nd harmonics.

Figure 4.41. Histogram of the frequency data selected at random to be used for simulation of mains interference while varying the fundamental (and associated harmonics) frequency.

Figure 4.42. (a) time-domain plot of simulated mains interference (red) against a single 50 Hz component simulation (blue). The length of generated data is 1 second. Red trace contains the following fundamental frequency components and its associated harmonics:
[49.9236,50.0315,50.0181,49.9939,49.9772,50.0286,49.9134,50.0007,50.0885,49.9977,50.0421,50.0499,49.9822,50.0172,50.0033,49.9551,49.9986,50.0300,49.9840,50.0261,49.9752,49.9751,50.016,50.0338,49.9780]
(b) illustrates the frequency domain representation of the simulated data.

Figure 4.43. Normal probability plot of the frequency data supplied by the UK national grid (blue trace) against the normal probability plot of a theoretical normally distributed data (red trace).

Figure 4.44. The frequency spectrum of the variations in mains frequency of the recorded data (a) against the ARMA simulated mains data frequency variations (b).

Figure 4.45. Illustrating of drift simulation.

Figure 4.46. Illustrating plots of some of the generated coloured noise in both time-domain (plots in the left-hand column) and frequency-domain (plots in the right-hand column). Time-domain plots are arbitrary amplitudes against the requested number of samples. The frequency-domain plots are those obtained through application of the Pwelch function in MATLAB® (Log-Log plots). (a) white noise. (b) Brownian noise. (c) pink noise. (d) blue noise.

Figure 4.47. (a) Frequency spectrum of the noise data triggering the filter to generate the recorded data segment. This resembles the spectrum for white noise. (b) Original noise record collected at a Nyquist frequency of 500 Hz, using Liverpool bio-amplifier & thread electrode on subject's right eye with no flash stimulus present and no background light. A section of this record (red brushed area) is selected with no blinks, EMG or eye-movements, to be used for ARMA filter coefficient estimation (filter order is 200 for this subject). (c) Black trace: Selected region of the voltage record in (a), Red trace: simulated data using the subject's ARMA filter. (d) Frequency-power spectrum of the selected region. (e) Frequency-power spectrum of the simulated data (red waveform in ((c)).

Figure 4.48. Illustration of nonuniform sampling period using ISIM waveform generation toolset. (a) Red trace is the clean waveform for reference and blue trace is the same waveform as in (a) with introduced nonuniform sampling intervals. (b) The black circles show points in in the waveform where the error is introduced.

Figure 4.49. A record of simulated ERG response (photopic) contaminated with noise and simulated missing samples or packets of information as illustrated by the region enclosed by vertical red lines.

Figure 4.50. Examples of generated waveforms using Liverpool ERG simulator GUI. (a) 5 cycles of PERG signal with ARMA generated noise at +2 dB without eye-movement, blinks, EMG, mains interference or drift. (b) 20 cycles of photopic ERG (standard flash) with a +2 dB ARMA generated noise, 3 Blinks and 2 eye-movements.

Figure 4.51. Examples of generated waveforms using Liverpool ERG simulator GUI. (a) 20 cycles of PERG signal without noise, eye-movement, blinks, EMG, mains interference or drift. (b) 20 cycles of PERG signal without noise, 2 blinks and 1 eye-movement.

Figure 4.52. The back-end ISIM engine, will create text, CSV, mat and image (JPEG) files once it is finished with waveform synthesis. All these files are then available to download through the Liverpool ERG simulator GUI. Once the CSV/Text file is received, the interface will parse the data accordingly and will present the data in two separate

worksheets as demonstrated by (a) through to (d). These worksheets are generated automatically by the background macro written in VBA.

Figure 4.53. iSim device simulating PERG signal (driving the inputs of an oscilloscope) and filtering the output accordingly with a lowpass corner frequency of 45, 150, 200, 300 and 500 Hz to measure the channels specific SNR and the SNR at the output of the summing amplifier.

Figure 4.54. Illustration of glitch response due to DAC register update and comparison with DAC data sheet as part of Critical To Function (CTF) component inspection and verification.

Figure 4.55. iSIm device is tested and verified at RLUBH eye clinic centre using ROLAND visual electro-diagnostic system with a record of photopic ERG signal (at standard flash). The record in this picture was obtained after three cycles having no noise or other types of artefacts added to the input trace.

Figure 5.1. The proposed calibrator able to provide objective measures on the phase delay and phase linearity of the amplifier and signal processing system, implemented by the clinical setup. Torok states that most visual electrodiagnostic laboratories are potentially unable to do the basic, ISCEV recommended calibration procedure of their setup as they may lack suitable test equipment. Torok claims that the presented device solves this problem and allows accurate calibration of the recording equipment without experience in electronics.

Figure 5.2. Proposed standalone iSim (currently work in progress) device without requirements to connect to a nearby host computer for operations. (a) Left: Push-Button based application of iSim with few selected waveforms. Right: Illustrating input and output connections. (b) Illustrating the implemented battery operation device – This is currently under verification testing by Mr Peter Watt ant MPCE. (c) A modified DS2715 (Maxim Dallas Semiconductor) charger controller switch mode application circuitry for five NiMH battery cells in series.

Figure A.1. (a-d) Illustrating an elegant method of calculation of the system's higher-order nonlinear interactions in a double-pulse experiment. It also demonstrates the difference between a linear and nonlinear system characteristic. X-axes demonstrate time after first and second pulses and y-axes demonstrate, amplitudes in units of measurement. Figure (d) is magnified by a factor of 2 along the amplitude axis (y-axis).

Figure A.2. Illustration of binary stimulus allowing to derive non-zero kernel responses. This illustration provides an assessment of the impact of the previous two flashes on current flash (at $t_0 = 0$). Therefore, two delay operations are considered resulting in adaptation of a second-order nonlinear model. Each section of this figure is termed in line with the same language adapted by Sutter (that is FOK, SOK, SOSS and TOK). To derive the kernel responses for a second-order system, a window of three base-period is selected. However, the system remains a second-order nonlinear system as only changes at input, extending to 2 pervious b.p. (i.e. a memory-length of 2b.p.) are considered to deviate the response of the system at $t = t_0$ from that of an LTI system (higher-order delays considered to have negligible impact and hence are ignored). The adaptive model uses a window of length three b.p. to estimate the future response of the system and hence it is a third-order system with respect to this response-estimation and a second order with respect to assessment of LTI-response-deviation.

Figure A.3. System characterisation, operations and transformation through the use of powerful m-transform, which is in the same equivalent class of Walsh transform.

Figure A.4. Methods of defining G-Functional.

Figure B.1. Liverpool bio amplifier control software flowchart. The control software is fully synchronised with Roland Ganzfeld stimulator and Glasgow MFS LED-based stimulator.

Figure B.2. Liverpool bio amplifier MBED embedded software code implementation flowchart. This software provides the required synchronisation with the high-level MATLAB control software and the stimulators (Roland Ganzfeld and Glasgow MFS).

Figure B.3. Memory array represented in each (a) – (h) illustrates how signal memory buffer is managed at each call to timer object callback function. Each array represents the buffer state in between frames separated by b.p + 1 ms. This example assumes a b.p of 25 ms is selected. The asterisk denotes the time at which the timer object is triggered, and its call back is due execution. Arrows represent the index ($Index_{(l,\,j)}$) to the memory block (M_i) where the next signal sample is taken from and sent to the output. Each block is of length 100 ms and assuming a fixed sampling output rate of 1 kHz, it would contain 100 floating-point number. Since timer object is called four times before iSim scans through one memory block, four such blocks are required to be initialised so that 100 ms second of signal could be generated and sent to the Digital to Analogue Conversion (DAC) unit. The amplitude values (A) stored in each memory block is

determined during timer object callback function based on values of memory register and signal array binary string representation. The output of Sample-Vector-Calculation module is then represented by:
$output\ sample = \sum_{i=1}^{4} A(index_{(i,j)}), where\ j = 1, 2, 3, \ldots, 100$
If measured or selected b.p = 10 ms, then one would require initialising ten such arrays to accurately calculate signal output samples. If b.p = 100 ms, then the system is assumed to be linear and only FOK will be used to represent the output signal.
White regions demonstrate unread samples, black regions demonstrate scanned areas and grey regions demonstrates areas that are in the process of being scanned at a rate of 1 kHz in-between frames.

Figure B.4. The client application (MS Excel) – MatSOAP – MATLAB communication algorithm.

Figure C.1 (a) The proposed timing for a study to investigate and assess the reproducibility, reliability, variability (inter- and intra-subject and session) and SNR of different protocols for mfERG (per the proposed study design), using a multi-variate, multiple regression statistical model and analysis approved by Dr Antonio Eleuteri (b).
It is clear from the timeline that, a study (single-centre) of this size (see Appendix D) would take roughly 12 months to perform the analysis and write up. The timing for peer review and publications are not included.

Chapter 1: Introduction

1.1 Introduction

The mammalian retina is an extension of the brain's neural circuitry and one of the best-studied areas of the central nervous system[1]. To fully understand its role in sensation and interpretation of a visual scene, one requires to identify and assess the cellular components including their intrinsic properties, such as their shape, location and synaptic connections as well as the functional characterisation of various cell types[2]. Comprehensive high-resolution functional and structural maps of mammalian neural wiring such as the retina is central in advancing our understanding of the neural circuitry of these structures through large-scale anatomical reconstruction such as connectomics[3][4]. Advances in imaging, data acquisition and analysis capability of large-scale structural meta-data allowed scientist to validate and further reveal the topological complexities in retinal structure compared to the previously known retinal anatomy[5]. Other advanced ocular imaging techniques, such as ultra-high resolution Optical Coherence Tomography (OCT) has provided three-dimensional high-definition retinal images that correlate with functional loss, enabling assessment of retinal disorder[6][7]. In contrast to many advanced imaging techniques, visual electrophysiology is objective and functional whereas other currently available imaging techniques are subjective and structural. Despite the recent rise of advanced imaging techniques, the functional examination of the retina remains a validated technique in support of a definitive diagnosis of ocular disease[8]. Most "suspected" retinal disorders and cases of unexplained vision loss are often referred for visual electrodiagnostic testing[9].

The International Society for Clinical Electrophysiology of Vision (ISCEV) founded in 1958 with one clear and longstanding target; "*to establish worldwide standard clinical protocols for electrophysiological examinations*". This ambitious target helped to focus our efforts to create the necessary knowledge and validate the findings in both laboratory and clinic. The standard aims at "*extending the knowledge of clinical electrophysiology of vision and promote co-operation and communication among workers in the field of clinical and basic electrophysiology of vision*". This chapter presents an overview of human retinal structure, the basics of visual electrophysiology and its origin, as well as a range of factors impacting the reliability and repeatability of the human electroretinography (ERG) response. The chapter describes what has been achieved to standardise the recorded ERG response and describes the remaining gaps in our knowledge, covering calibration of visual electrodiagnostic instruments, methods to verify and validate new signal processing toolboxes and current training techniques in the field of visual electrodiagnostic. It explains that while much remains unknown in retinal behaviour when exposed to a complex visual scene, we are now in an excellent position to use available knowledge to progress predictive and realistic modelling. Such modelling is used in actual practice, promoting knowledge re-use, sharing and improved collaboration in line with the aim of ISCEV standards. The discussion throughout the thesis and this chapter focus on the human retina and views this structure from an engineering perspective as an adaptive control filter (system).

1.2 The retinal structure

The optical requirements to achieve an image at the retina and its neural processing are the two requirements of vision. Light enters the eye through the pupil surrounded by a pigmented circular muscle, the iris, that gives the individual his or her eye colour. The light-transmitting part of the eye is compromised of the transparent external surface that covers both the pupil and iris, the cornea, the anterior chamber lens and the vitreous chamber (see figure 1.3).

The visual light-transmitting pathway allows the formation of sharp images on the retinal photoreceptor layer, where the visual information is converted to nerve impulses and transferred to the higher brain for further processing, figure 1.1[10] demonstrates the various major cell types of the human retina. The deepest layer of the retinal neurons processes the light first. These neurons are the photoreceptors (rod and cone cells) where the light energy is converted into electrical

impulses[11], which are transmitted to bipolar cells in the second layer, and then up to the ganglion neurons in the third layer.
Rod photoreceptors and rod-connected nerve cells through the retina are responsible for the pathways concerned with night vision and the increased sensitivity of our visual system under what is termed scotopic conditions (little ambient light)[12]. Such increased sensitivity is through huge convergence and divergence of cell contacts in the rod pathway. In contrast, the cone photoreceptors are bright light sensors with sensitivity to different wavelengths of light. As such, they are sensitive in photopic conditions (bright light) and come in several types according to the structure of the visual pigments in their outer segment regions[12]. The cone pathway is inherently different from the rod pathway, providing contrast-detection through installed ON and OFF pathways. (Cones hyperpolarise to light but have two bipolar channels, one carried by a depolarising bipolar and the other by a hyperpolarising bipolar, splitting the original cone signal into a lightness or ON-centre and a darkness or OFF centre[13])
Bipolar cells are where the photoreceptor signal is first divided into ON and OFF pathways, which encode increments and decrements, respectively, in light intensity. Increments depolarise ON bipolar cells and hyperpolarise OFF bipolar cells (and vice versa) by well-understood synaptic mechanisms[14]. The axons of the ganglion cells form the optic nerve and exit the eye at the optic disk (or the blind spot in the visual field) carrying the generated nerve impulses to the brain.
The direct or vertical pathway from the photoreceptor to bipolar, ganglion cells and finally to the brain is not the only pathway in the parallel processing circuitry of the retina (these parallel input signals must be elaborated upon and integrated within the cortex to provide a unified and coherent perception)[15]. The horizontal and amacrine cells also receive information from photoreceptors and transmit to several surrounding bipolar cells and from bipolar cells to a number of surrounding ganglion cells (these cells form the lateral pathway within the retina)[16].
The ganglion cells are substantially fewer in numbers than the photoreceptors, suggesting a convergence and mixing of signals in neural pathways of the retina[17]. The degree of convergence is not consistent across the retina, it is higher at the periphery and lower at the fovea. In the foveal region, the ratio becomes 1:1 from the photoreceptor to bipolar (either ON or OFF bipolar cell) to the ganglion cell. Mammalian retinal circuits constructed from approximately 100 specific cell types. These include 3-4 types of photoreceptors (1 rod and 2-3 cones), 50-70 types of interneurons (horizontal, bipolar and amacrine cells) and 20-30 types of ganglion cells. Cells of each type tile the retina with varying degrees of overlap and cells sizes, where neurons with smaller dendritic fields are found in areas devoted to high acuity vision[2]. This parallel, lateral and feedback circuitry, generates, encodes[17] and integrates the visual information in the form of nerve pulses that are sent to the higher brain for further processing[1].

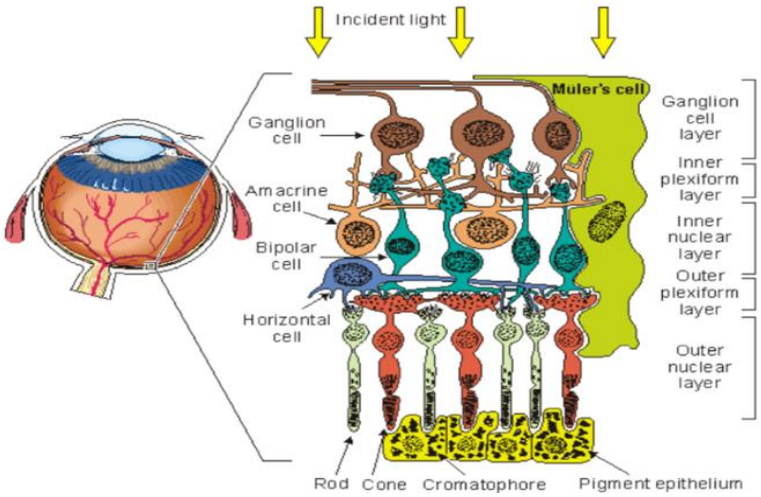

Figure 1.1. Illustrating the human retinal layer and major cell types[10].

1.3 Origins of the Electroretinogram (ERG)

The Electroretinogram (ERG) is the electrical response generated by the retina in response to a flash of light[13]. The retinal response to such an excitation is not a simple electrical waveform, but rather a complex electrical integration of potentials generated[18] as the result of ionic current flows in various light-transmitting pathways produced by several cells and neurons interacting as the visual pathway tries to best describe the visual scene it is exposed to, see figure 1.2[10]. The ERG is an electrical surrogate biomarker for physiology. Its primary purpose is to reflect the health of the retina. As ERG is a complex waveform with many wavelets being produced by different generators, tailoring different stimuli to isolate generators and their origin has been the topic of many past, recent and ongoing discussion[19]. Such analysis is of clinical relevance if the healthy ERG is understood before the ERG of a human patient can attain its maximum value in the diagnosis of the retinal disorder[19].

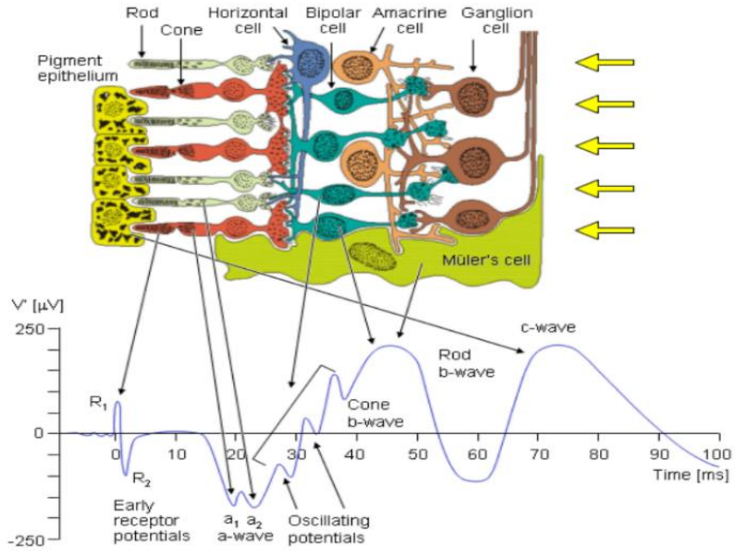

Figure 1.2. The ideal response signal is not itself a simple voltage equation that outputs a known waveform under all experimental conditions, but it is rather a complex electrical summation of potentials originating from different retinal layers that heavily relies on the test conditions such as retinal adaptation status, flash intensity and frequency, etc[10].

The ERG responses are recorded using an active electrode, that can be placed on the surface of the cornea, in the vitreous humour or at different levels inside the retina along the visual transmission pathway. The latter can provide clues to where the responses are likely generated, utilising a weak micro-illumination of the retinal region, where the micro intraretinal electrode is used, ensuring (as much as possible) locally generated electric fields[20][21][22]. Reference and ground electrodes are also required and are placed at sites remote from the visual pathways. This electrode system will pick up the generated potential which is the result of ionic current flow triggered by absorption and bleaching of photopigments in radially (parallel) arranged photoreceptors in the Outer Plexiform Layer (OPL) of the retina. These currents are parallel and will sum together, giving rise to a strong radially oriented extracellular current. In contrast, laterally generated currents tend to cancel each other since the retinal lateral arrangement is entirely symmetrical, provided that the excitation light triggering the ERG response is a perfectly diffuse/homogenous and uniform across the retina. For an ionic current flow to exist, there must be a current source and current sink, making the current pathway a closed one. Each component of the eye on this pathway will have an associated effective impedance, and as current flows through this resistive structure, a potential drop occurs that can be measured using the active electrode as it advances along this pathway[13]. Clinical ERG is a non-invasive manner of measuring the elicited response using various types of active electrodes that can be placed on the skin near the eye or on the surface of the cornea as is illustrated in figure 1.3[13].

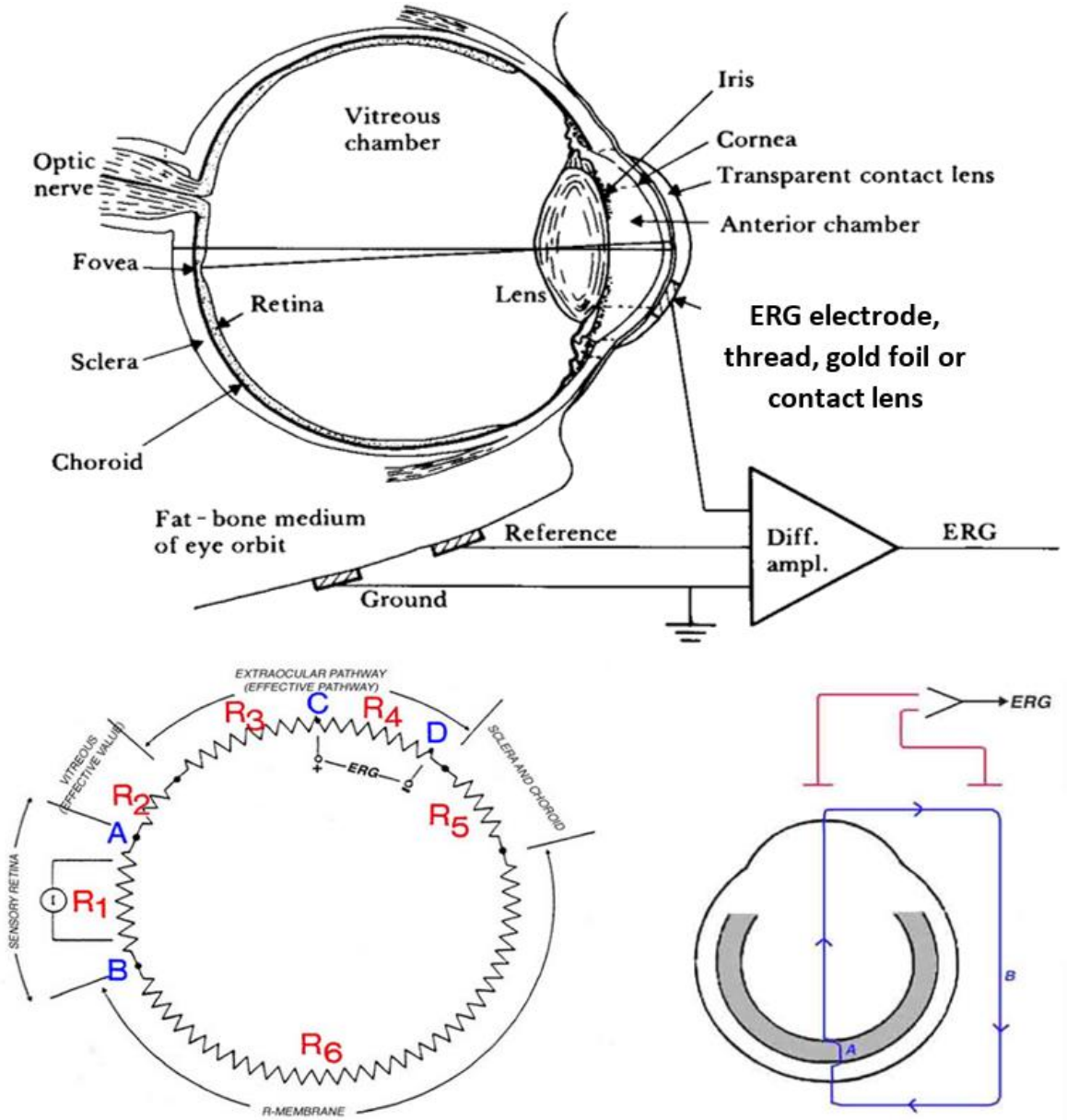

Figure 1.3. Light induced ERG response will induce ionic currents that travel away from the source and to the current sink. The pathway contains different regions that are simulated using a resistive network. Using non-invasive ERG electrodes one can pick up the response at the surface of cornea. Such signal requires further application and processing to improve its SNR prior to post processing[13].

1.3.1 Approaches to determine the origins of ERG

There are three basic approaches to better understand the cellular origins of different principal components of the ERG response:

1- Physiological analysis; the generators of the specific ERG components are in distinct retinal layers. As these layers passed by the intraretinal microelectrodes, the polarity of the particular ERG component will reverse[23][24].
2- Neuron morphology and electrophysiology analysis; the form, structure of cells including their dendritic field, cell body, axial projections as well as the number and type of cells they project to, their locations within the retinal layer and their electrical responsiveness are used to provide clues as to their roles and functions underpinning the various ERG components in single-cell analysis.
3- Pharmacological analysis; specific agonists and antagonists of the cellular mechanism are applied, and their effect on the ERG analysed [25][26][27][28][29], i.e. as opposed to single-

cell analysis, where one investigates the interaction between cells. The effects of lesions, pathology and targeted mutation analysis and the subsequent absence of ERG components can also be considered under this category. For example, in cases of glaucoma, one can determine the contribution of ganglion cells to the elicited ERG response through a comparison with normal ERG recordings, as it is known that the function of ganglion cells is severely degraded under glaucoma.

There exists a strong hypothesis linking various ERG components to associated physiological origins when the evidence from these different approaches converges.

Granit and Riddell[30] demonstrated that the ERG waveform is a summation of 3 processes or potentials called PI, PII and PIII, see figure 1.4[30].

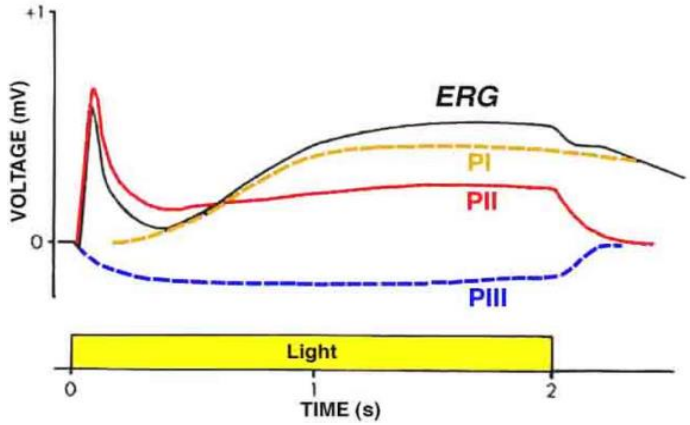

Figure 1.4. Demonstration of three phases contributing to cat's ERG response[30]. The influence of stimulus duration on the c-wave component of the ERG is investigated and it is understood that time-to-peak and amplitude of this wave are dependent on delivered stimulus energy (stimulus intensity and duration)[31][32].

Each of these wavelets is generated by/originates from a group of cells. They give rise to the principal components of the ERG waveform known as the a-wave, b-wave, c-wave and d-wave. The c-wave is a slow positive ERG component with a latency of 1.5-4 seconds. The c-wave and other late and slower potentials have high intra-subject and inter-subject variability[33]. Recording these slower potentials clinically is challenging as it requires a recording setup that is stable enough over several seconds, without blinks and eye-movements. To record c-wave, a long duration, high luminance stimulus using a direct coupling system, is used[34].

1.3.2 Full-field, focal and multifocal ERG

The full-field ERG records the summed transient electrical responses from the entire retina, derived from cells within different retinal layer elicited by exciting the retina with a uniform flash delivered in a full field dome[35]. Clinically the most critical components of this response are a- and b-waves[36][18] with faster (in the range of 100-150 Hz) components known as oscillatory potentials that could occur on the rising edge of the b-wave under both scotopic and photopic conditions[37]. The full-field ERG is essential in the diagnosis of numerous disorders such as cone dystrophy, retinoschisis, congenital stationary night blindness, etc.

Several debilitating maculopathies can go undetected with full-field testing, including Age-related Macular Degeneration (AMD)[38][39]. The percentage of cones contained within the macular region is about 10%. Given that the variations of recorded ERG amplitudes within normal subjects could be as high as 150%, a 10% drop in response due to macular degeneration could undoubtedly leave the response within the normal range. The focal ERG is a useful technique to determine the health of a subsection of the retina and is specifically used to obtain the response elicited from the macular or foveal region. The retinal response isolation in focal ERG measurement requires good fixation, and subject's cooperation (which could be difficult with those subjects with reduced central vision) with

almost no objective feedback on how well the subject has performed (whether normal or not). To ensure the focal ERG waveform provides an accurate estimate of the latencies measured, the amount of light scatter must be reduced[40][41].

Eric Sutter introduced the mfERG (multifocal ERG) as a method of simultaneously collecting several local ERG responses using a maximal length, binary, pseudo-random, periodic sequence (m-sequence) governing the excitation of the retina[42][43][44][35]. The mathematical properties of the m-sequence[45], makes it possible to extract the localised responses and form a topographical map of the retinal function. Due to the nature of the stimulation, the mfERG is a photopic response where, due to increased cone density in the foveal region, poor fixation could result in response spikes away from the fovea[46][47][35].

Sutter patented (US patent number: 4,846,567. Date of patent: 11th of July 1989) the application of m-sequence in visual electrodiagnostic setting and developed the electrodiagnostic system, VERIS. Various methods of delivering the stimulus to the retina are proposed and are currently in clinical use. These include LCD, LED and CRT screens where the governing mother m-sequence, the sequence length[48][49] and its decimation may be different. For example, Roland created the RETIscan system, which uses a correction term to ensure the number of binary 1's and 0's in the sequence is equal. Different centres also run the sequence at various speeds through adding or removing "filler frames" in between the actual stimulation frames to slow down the stimulation or speed it up, respectively, allowing investigation of the retinal temporal properties[50]. The continuity of a session may not be guaranteed; where one session is defined as the time, it takes to cycle through one period of the m-sequence. The longer the session, the better the SNR and the more random the sequence becomes. However, longer sessions are more uncomfortable and may need to be broken into multiple runs.

In contrast, the shorter the session is (keeping the same spatial resolution or subtended retinal angle) the poorer the SNR and hence multiple sessions may be required to perform more averaging. Artefacts such as eye-movement, eye-twitches, EMG, blinks as well as fixation and defocus[51][52] error can seriously damage the outcome, impacting the clinical diagnosis. In a mfERG setting, each stimulus patch is, typically, hexagonally shaped and scaled to ensure approximately equal responses from each hexagon, with the most central hexagon having the smallest area[53] (see figure 1.4).

The final localised waveform is normalised to the unit area giving the fixating point the largest signal density in the topographical map. The typical unit is, therefore, nano-volt per degree squared-$\frac{nV}{deg^2}$ [54][55]. The colour-coded, three-dimensional (3D) response density is an attractive way for visualisation of the topographical response map. This map is accompanied with the trace array to avoid mistakes in response interpretation by the automated paradigm producing the 3D map[56] (grouped-responses which are the average of responses from several elements within the trace array are the focus of clinical reports), see figure 1.5.

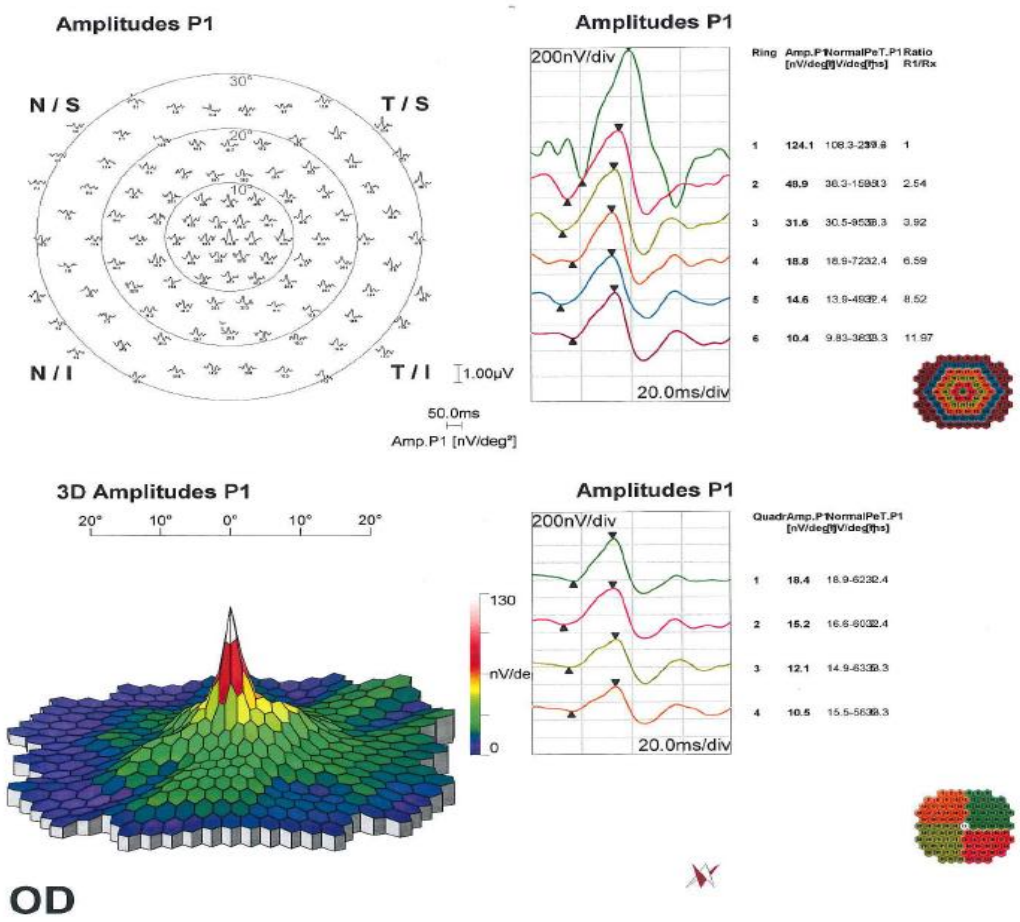

Figure 1.5. Illustration of multifocal data represented in amplitude density format alongside the trace array as well as grouping the recorded localised data into rings and quadrants for a normal subject (the author) logged from his right eye (OD) through the clinical set up at St Paul's eye clinic at RLUBH using a standard thread electrode.

1.4 Factors impacting the retinal ERG response and ISCEV standards

Factors impacting variability in ERG responses can be bundled together, as illustrated in figure 1.6. These factors grouped into four main categories, as described by Keating and Parks [57]. The suggested categories, colour coded in figure 1.6, are the method of stimulus delivery variables (blue); data acquisition variables (orange); patient variables (green); and measurement variables (brown). Anomalies in ERG (and other visually evoked potential) responses could be due to retinal dysfunction and/or contribution from uncontrolled factors, where the latter could lead to misleading interpretation of the ERG recordings due to introduced variability and impact the repeatability and reproducibility of the recordings[58][57][59][60][61]. These factors range from clinical settings and protocols followed by a specific centre or study, clinician skill-set and training, subject co-operation and previous experience with such testing as well as the subject's health and habits (e.g. smoking, diet and alcohol consumption)[62]. Clinical environment and equipment used such as stimulator type [63], type of electrode[64][65][66][67][68][69][70][71][72][73][74] and its placement[60], flash intensity[75], frequency[50], spectrum and contrast presented, type of stimulation[76][57], retinal subtended angle and adaptation state[77], will also affect the ERG response[56]. Visually evoked potentials are typically compared with the centre's normative database, to obtain any meaningful diagnosis. Ideally, the database should consider age group[78][79][80][81][82][83][84], ethnic diversity[65] & gender[85][86][87], eye colour[88], pupil size[89][90] and other factors that can impact such recordings[56][61]. The normative database should be of an appropriate size per variable, so a meaningful conclusion can be drawn when comparisons are made. There are many attempts to form normative databases that can be used as a comparative index of expected normal

values in a clinical setting for both humans and animals[91]. Research Conducted by S. Simao and Co-Researchers as part of the EUROCONDOR (European Consortium for the Early Treatment of Diabetic Retinopathy) project was an attempt to create a large (the largest at the time of writting) normative database (111 eyes) using multifocal electroretinography in the context of a multicentre clinical trial[92]. The author of this thesis received specialized training and was certified as one of the site investigators to collect normal data within St Paul's eye unit Royal Liverpool and Broadgreen University Hospital (RLBUH) electrodiagnostic unit.

The ISCEV founded with the following purpose:

1- Extending the knowledge of clinical electrophysiology of vision and guide education and training.
2- Promotion of communication and co-operation of clinical scientists and researchers active in the electrophysiology of vision.
3- Developing, maintaining and publishing guidelines and recommendations for various diagnostic and non-diagnostic tests.
4- Developing, maintaining and publishing guidelines for calibration of stimulus and recording parameters, although this guideline was last updated in 2003.
5- Providing technical guidance to scientists who are new to the field.
6- Standardising ERG responses.
7- Providing minimum specifications expected for equipment used in triggering, recording, monitoring and processing of ERG responses.
8- Encouraging the establishment of a single worldwide point of reference for electrophysiological examinations.

Using centre-specific normal database[56] reduces the transferability of tracing and results between laboratories making any attempt to interpret ERG recordings between centres or overtime a challenge as recording standards, techniques and instruments are continually changing[65]. This is also a significant hindrance to changing or updating the visual electrodiagnostic system. To date, a normative database cannot be supplied by an external partner, implying that on-site testing must be performed to establish site-specific normative values.

The exact details of data acquisition, data reduction and information extraction procedures are dependent on the specific implementations of individual instrument manufacturers. The lack of universally available reference datasets against which the clinical user can characterise their instrument and cross-reference their results with colleagues in other laboratories limits quality assurance, clinical governance and impedes co-operative work across institutions. It has hindered the utility of ERG testing in drug development and clinical trials and reduced the significance of results obtained in the context of multicentre clinical trial and longitudinal investigations[93][65].

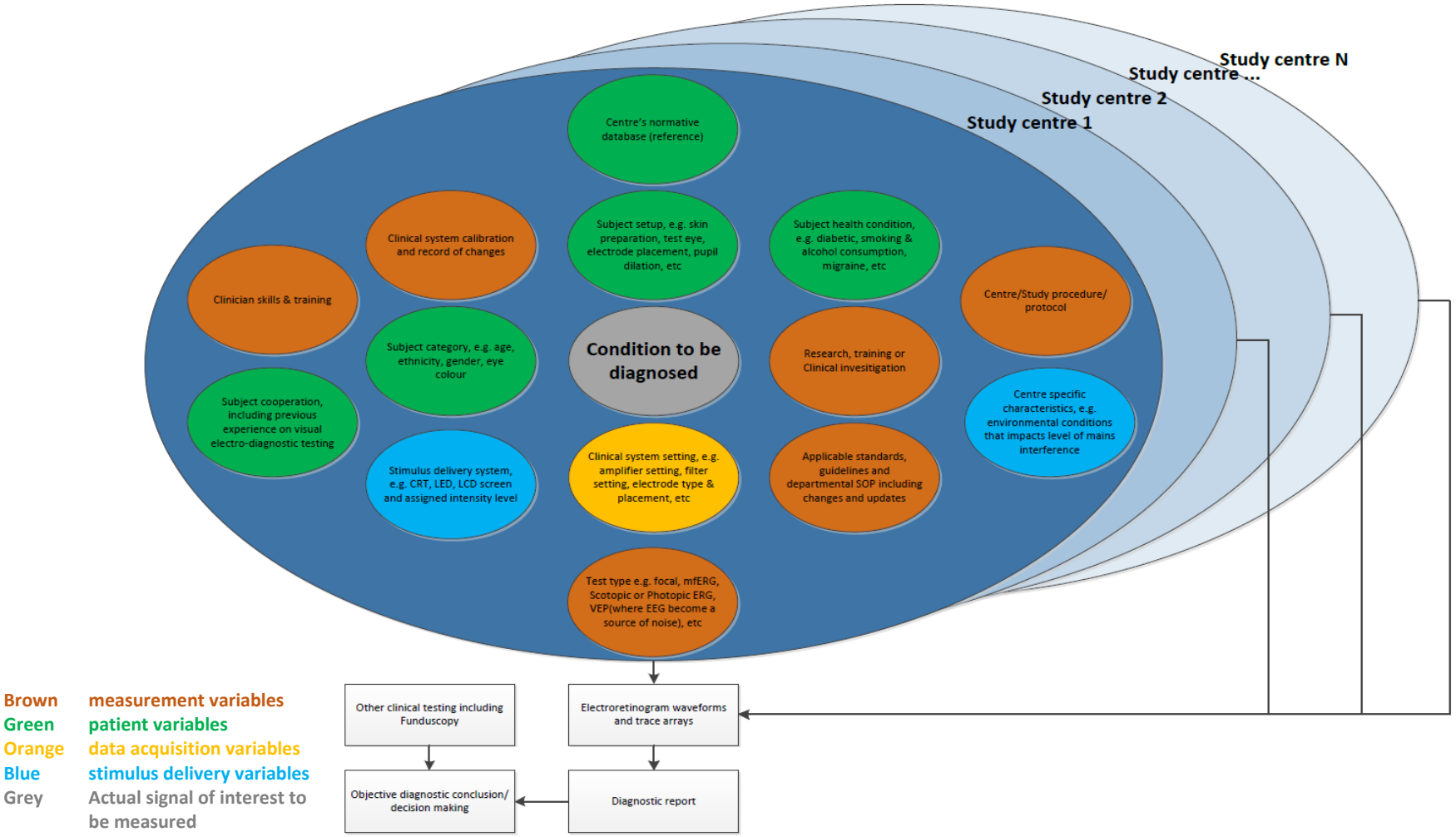

Figure 1.6. Illustration of factors (variables) impacting the recorded ERG waveform from subjects (normal or patient) under study (experimental/research or clinical investigation). The ERG waveform analysis (identifying various significant waveform characteristics such as amplitude and implicit time of b-wave), requires a normal database as the reference ground to compare the clinically or experimentally recorded values against. ISCEV standards and guidelines try to constrain aspects impacting the ERG records under clinical setting to provide a more harmonized approach. In an investigational study, the respective protocols will most certainly be different again impacting the obtained records. Other factors such as subject cooperation and familiarity with the investigation as well as operator skills and level of training plays significant role in obtaining accurate measurements. It is also advised to perform routine calibration and such procedure must be clearly defined under centres quality management system (QMS). The calibration of the medical device system is required through regulations and ensure system credibility in recording and use for clinical decision making.

1.4.1 ERG response modelling: A realistic approach

The mathematical construction of deterministic artificial records based on templates agreed by experts is, in principle, trivial. Such simple noise-free data are of limited relevance, as the highly challenging effects of electrical interference arising from the EMG, blinks, eye-movements and undefined external electrical sources are ignored. To be realistic and useful as reference sources, these factors must be modelled and included as stochastic processes. A clear distinction between signals and noise must be made. The signal is the variable that contains information on the biological object (e.g. the retina) under study, and noise is all other components in a measurement which determines the lowest perceivable amplitude in a biopotential recording[94].

Most stochastic models of clinical electroretinograms employ naive noise sources based on simple Gaussian White Noise (GWN). These are of limited use as they are unrealistic and statistically predictable. The lack of realistic noise models continues to hinder progress in developing our understanding and objective characterisation of electrodiagnostic responses, discouraging the development of algorithm innovation.

Real-life noise, as observed during visual electrodiagnostic measurements, have several orthogonal components. These components would distort the frequency, phase, and amplitude of the signal of interest, directly or indirectly. As ERG is used to provide an objective assessment of retinal function in clinical and laboratory settings and signals are in the nano-volt to milli-volt amplitude range, such interference could significantly reduce the Signal-to-Noise Ratio (SNR) and potentially compromise the diagnosis (or at least increase the length of the investigation, which would raise the fatigue factor, introducing new uncertainties).

To successfully implement an orthogonal multi-component noise model, one must either theoretically and realistically predict the actual noise of each noise component, which is practically impossible, or lump these components (or at least a group of these components) into series and/or parallel filter block representations. This makes the analysis of noise sources easier and allows for the fabrication of new methods to suppress them. Such methodology ultimately provides the separation of active noise sources from the biological signal source; hence the latter could be considered as an ideal source of ERG signal.

Dealing with signals of small SNR, infected with spontaneous, large-amplitude artefacts, can be extremely challenging[95], not only from a technical perspective but also from the clinician's and patient's perspective. This ultimately adds to the costs of treatment, monitoring, and diagnosis. Poor SNR means more variability in ERG recordings and greater test duration before the clinician can confidently report, to the consultant ophthalmologist for accurate clinical decision-making. New innovative signal processing packages such as adaptive filtering and new artefact rejection algorithms, could help to clean the raw data record and improve the SNR during run-time or post data collection. These innovations directly impact the clinician's decision on diagnosis as well as their decision on the length of recording before a conclusion made. Medical device regulations must be respected to protect patient safety as a clinician's decision making could be influenced by such innovations. If such solutions are to be available globally or regionally, then the respective manufacturer must comply with relevant national and international standards, such as IEC 62304, ISO 14971 and ISO 13485 as well as GDPR and 21 CFR 820 (US FDA regulation code for medical devices)[96]. These standards require full implementation of design and change-control processes. Extensive testing as part of verification and validation of the Software as a Medical Device (SaMD)[97][98][99] and software integral to a medical device based on risk assessment and Residual Risk Report (RRR), must be in place to demonstrate compliance with regulations and reliability and consistency of the solution. As part of the verification and validation phase, the developer must show the effectiveness of the solution in a clinical setting through approved ethical applications and performed clinical trials. Usability of the software through documented and planned formative and

summative usability studies must also be in place to show the applicability of the solution for the intended users.

As part of the quality assurance, one would significantly benefit from a platform that could produce realistic, non-naïve ERG waveforms that could be used to truly challenge new ideas ensuring their robustness and feasibility at all stages of the design process. This ultimately reduces time-to-market, allowing the realisation of benefits through improved care.

Advances in technology allow for ever-growing research in the field of visual electrophysiology. The ability to validate any research results is limited as the research, and its source data from normals or patients largely remain within the boundaries of the acquiring institute. Data protection obligations may also add challenges to sharing any data that may be considered personal under GDPR. The various formats of data may also hinder sharing and integration across organisations. The protocols for study design and the study conditions vary widely, and most of the data collected are stored locally. For the data to be useful, one needs to be able to interpret it correctly without any risks to personal data breaches, i.e. the data is useless without its contexts such as test protocol, instruments used, test conditions, subject age group, gender, pupil size, electrode type and placement. This makes the data to be shared a meta-data which further adds to the complexity of sharing it. The only way to compare experimental methods and assess the validity of newly developed protocols and algorithms is to have access to the same data under similar conditions. Major funding agencies are interested in multi-centre studies which require significant investment in data sharing and data protection infrastructure, such as the recent €7.8 million EUROCONDOR project, funded by European Commission to investigate the early treatment of diabetic retinopathy. A collaborative data sharing venue, such as a centralised ERG database, could significantly improve studies of novel algorithms, increasing study power allowing an objective, data-driven approach[100]. Such an approach will better inform the panel of experts responsible for publishing standards and guidelines, ultimately improving healthcare services delivered to the patients. Sustainability of such a data-sharing platform, after its initial funding phase, requires resource and close collaboration across the organisations. Such joint efforts will also result in the collection of normal databases of individual centres, ultimately improving the transferability of patient tracing and includes between laboratories[101].

The foundations of visual electrodiagnostic include the disciplines of psychophysics, neurophysiology, electronics, mathematics, computer science, statistic and medicine. The know-how necessary for this multi-disciplinary field, coupled with the requirements for closer collaboration between clinicians and electrodiagnostic departments as well as the needs for a tailored set of examination protocols that are better suited to the specific patient problem, make visual electrodiagnostic a highly specialised field. Significant investment must be in place to train scientists in the field of ophthalmological electrodiagnostic[102][103][104]. Such training is a combination of self-development through available literature, attending educational courses, reviewing case studies and attending/contributing to clinical sessions so that they can truly understand the clinical value of the tests involved and the way these testing affect the diagnosis and management of patients.

Training involves both, extending one's knowledge on inherited and acquired visual disorders, as well as understanding technical challenges present to the clinician when preparing for and performing the tests[102][8]. For a beginner in this field, the first few patient visits can be overwhelming, mainly if patient cooperation and tolerance are low, making it difficult to concentrate on the technical aspects of the test. Although managing a patient during the clinical investigation is a soft skill that needs to be gained over time and with experience, the trainee scientist could benefit if a realistic simulation is in place allowing him or her to practice the necessary technical requirements before attending a real-life diagnostic session.

1.4.2 Clinical system calibration

It is through standardisation of stimulation, recording procedures and instruments that one can elicit normal values with minimal variability[95]. Without consistent normal values, abnormal responses will become difficult to detect, and monitoring of neurofunctional characteristics of the retina becomes difficult if not impossible. Standardisation requires calibration and standardised calibration procedures to minimise uncertainty in measurements. It is critical to the goal of having comparable data worldwide[105].

Typically, the calibration of recording equipment is performed based on each manufacturer's recommendations[105]. Some devices may provide automatic built-in calibration mechanisms. For the normalcy of responses to be determined, the input impedance characteristics, the gain of the system, the artefact rejection algorithm and levels, the frequency bandwidth of the system, the filtering implementation and associated delay must be known and maintained so conclusions can be drawn on the "fitness for purpose" of the calibration procedure[95][105].

Currently, a calibrated signal generator is used to drive the inputs of the clinical system using a simple square or sine wave to check the frequency and amplification settings of the system when it drives all available channels of the front-end bio-amplifier. Although this may seem a simple way of calibrating the system, many clinicians (without an engineering background) find it challenging to interpret the results and adjust the system's setting accordingly. Also, often the clinician may decide to connect a "normal" subject to the system and compare the system recording with that of the reference (centre's normal database). This could potentially raise ethical questions, even if the testing is not particularly risky. Other unwanted outcomes could include unnecessary anxiety developed as part of a false-positive result on a subject thought to be "normal" or providing false re-assurances (from both subject and laboratory perspective) if false-negative results are obtained. The regulatory environment could be vague in such scenarios where formal ethical approval may not be needed. For example, in low-risk self-examination as part of research or routine maintenance of clinical instrumentation or other reasons that may not completely align with professional purpose of medicine, which is stated by Emanuel[106] to mean "*devoted service to people who are ill, protection of the health of those who are well and defence of healthcare values that might otherwise be undervalued or forgotten*"). However, future confusions can result if something goes wrong or if the researcher decides to transfer the data from one centre to another or publishes it. Consuming the valuable clinic time that would otherwise be available for patients would also need to be considered, for example, when one is to test the performance of the system in a scotopic examination setting.

1.5 Scope

The scope of this thesis is to provide an engineering solution to some of the above problems as a platform, termed ISIM (eye Simulate). This platform is to provide means to perform accurate calibration of clinical instruments in visual electrodiagnostic centres, verification and validation of new or existing signal processing algorithm and improved training with minimal impact on regular clinic hours. The design shall be scalable so it can accommodate the normal database of various centres and making these available to all connected devices and user interfaces (sharing centre specific, de-identified clinical and research data with other centres).

This platform will include both software and hardware modules connected through cloud programming to a designated server component. The server is called MatSOAP© that provides access to a MATLAB® back-end engine responsible for generating user-defined ERG waveforms. The waveform synthesis shall maintain traceability, repeatability and reproducibility and occurs at the back-end server.

The hardware module in ISIM platform, termed iSim, is to provide a physical mean of driving the inputs of the visual electrodiagnostic instruments using downloaded, explicitly defined user

waveforms. iSim should do this by accurate simulation of the electrode connections from a test subject or patient to the bio amplifier during visual electrophysiology measurement. To that end, iSim shall provide a three-wire connection carrying the synthesised waveform, ground and reference signals. iSim interfaces with the clinical instrument in a way that it avoids changes to the setup. iSim contains a photosensor that is sensitive enough (enabling user adjusting the sensitivity to accommodate for various types of commercially available stimulators) to register changes in the luminance as a trigger and synchronisation signal. This signal is used to output an explicitly defined, realistic visual electrophysiological waveform to drive the inputs of the clinical instrument (e.g. for calibration of the data acquisition system) as well as to characterise the system such as its governing maximally length sequence (m-sequence) used to drive the retinal stimulation in mfERG measurement.

1.6 Aim and Objectives

This study aims to implement a novel platform (ISIM) to deliver exactly specified, highly realistic ERG-like signals, with applications in, calibration, collaboration, training, innovation and improved transferability of patient data across the boundaries of globally distributed visual electro-diagnostic centres.

To achieve this, the study will:

1. Develop a solid understanding of the clinical practice, and the mathematical and engineering background of some of the existing visual electrodiagnostic instruments.
2. Develop methods, tools and devices to perform an objective functional assessment of the human eye (retina) in a clinical environment.
3. Develop methods, hardware and software (ISIM) to generate highly realistic ERG-like signals, deliver these to visual electrodiagnostic instruments and other signal processing packages and process the results.
4. Generate an ERG reference library using deterministic and stochastic models which provide explicitly characterised recordings over a range of SNR's with autoregressive continuous noise, spontaneous noise and periodic noise artefacts.
5. Develop the methodology and infrastructure to expand the software library, ensure scalability, maintainability, reproducibility, repeatability and encourage closer cross-centre collaboration.
6. Demonstrate and verify the effectiveness of the platform to scrutinise the governing m-sequence of a chosen clinical system and provide objective results to further investigate this system (such as objective investigation of the manufacturer's implemented blink-rejection-algorithm).
7. Demonstrate and verify the effectiveness of the platform at validating novel signal processing algorithm.

1.7 Thesis structure

This thesis is arranged as follows:

- Chapter 1 provides a brief background on the eye and ERG. It identifies gaps in ERG methods that need to be addressed to improve patient care.
- Chapter 2 describes how visual electrodiagnostic has progressed to the present day, concentrating on factors impacting on ERG records and discusses the relevant international standards providing a clinical background of continuum visual electrodiagnostic.
- Chapter 3 describes the development of tools to perform an objective functional assessment of the retina, and the development of a new toolset package, providing realistic ERG-like signals.
- Chapter 4 presents an experimental study on 11 normal subjects and the data collected for inclusion within the final solution package.

- Chapter 5 describes the analysis of results obtained with reference to current practice, the limitation of this study and a brief discussion on future development.

Chapter 2: Literature search

2.1 Introduction

This chapter presents studies of retinal function and progress made on visual electrophysiology instrumentation and techniques. Despite significant recent advances, current standards and guidelines remain imperfect in setting a single global reference point across visual electrodiagnostic laboratories. Further progress and collaboration are much needed to ensure this longstanding ISCEV (International Society of Electrophysiology of Vision) objective is met. It is also imperative to recognise that practice in the field of visual electrodiagnostic requires specialist training that is not usually the focus of conventional ophthalmic courses. Such specialism is required due to the variety of scientific and engineering disciplines involved in this field.

The rationale behind visual electrodiagnosis testing is to provide the clinician with objective evidence on the function of the visual pathway at various levels, allowing isolation of dysfunction of the visual system[12]. This functional assessment tells the clinician about the function of the retina, complementing other available visual assessment[107]. Different forms of visual electrophysiological testing are available, allowing investigation of different parts of the visual pathway. As such, various standards, guidelines, protocols and procedures have been produced, based on scientific evidence, arming the clinician with the tools to localise the origin of the disease. These are, electroretinography (ERG), electro-oculography (EOG), and Visually Evoked Potential (VEP) testing. The focus of this chapter is on ERG and a special sub-category of electroretinography, termed multifocal electroretinography (mfERG). The chapter will next discuss the variability in such recordings, where a clear need for a set of harmonized standards across the visual electrophysiology community becomes evident. Such standards emphasize the importance of a normal database that is centre specific, allowing monitoring of the visual pathway pathology against the normal reference point. The chapter closes by discussing the importance of accurate and regular calibration of electrodiagnostic instrumentation to try and maintain reproducibility and repeatability of the test results. There is a clear need for a platform that enables workers in the field of visual electrodiagnostics to share data, accurately calibrate their instruments and ensure high standards in in signal detection and processing. Training in the use of this toolset is also essential.

2.2 History of ERG, mfERG and emergence of ISCEV standards/guidelines

2.2.1 A brief history of electrophysiology

Electrophysiology can be traced back to Luigi Galvani (1787-1791), who first announced what he called "*intrinsic animal electricity*" in the Commentaries of the Institute and Academy of Sciences of Bologna, based on his famous experiments on frogs[108]. From these experiments, he concluded that animal tissues existed in a state of disequilibrium and that there exists an electrical gradient intrinsic to animal tissue. This fascinating conclusion predates the physiological knowledge of cell membranes, the existence of iconic pumps and the way these pumps work to maintain a concentration gradient of ions across the cell membrane, generating a delta potential. Galvani's discovery not only laid the foundation for electrophysiology but also gave rise to the "*most passionate scientific debates in the 18th century when Alessandro Volta postulated that Galvani had confused intrinsic animal electricity with small currents produced by metals*", figure 2.1[109]. This debate may have resulted in the invention of the electric batteries by Volta (1800)[110].

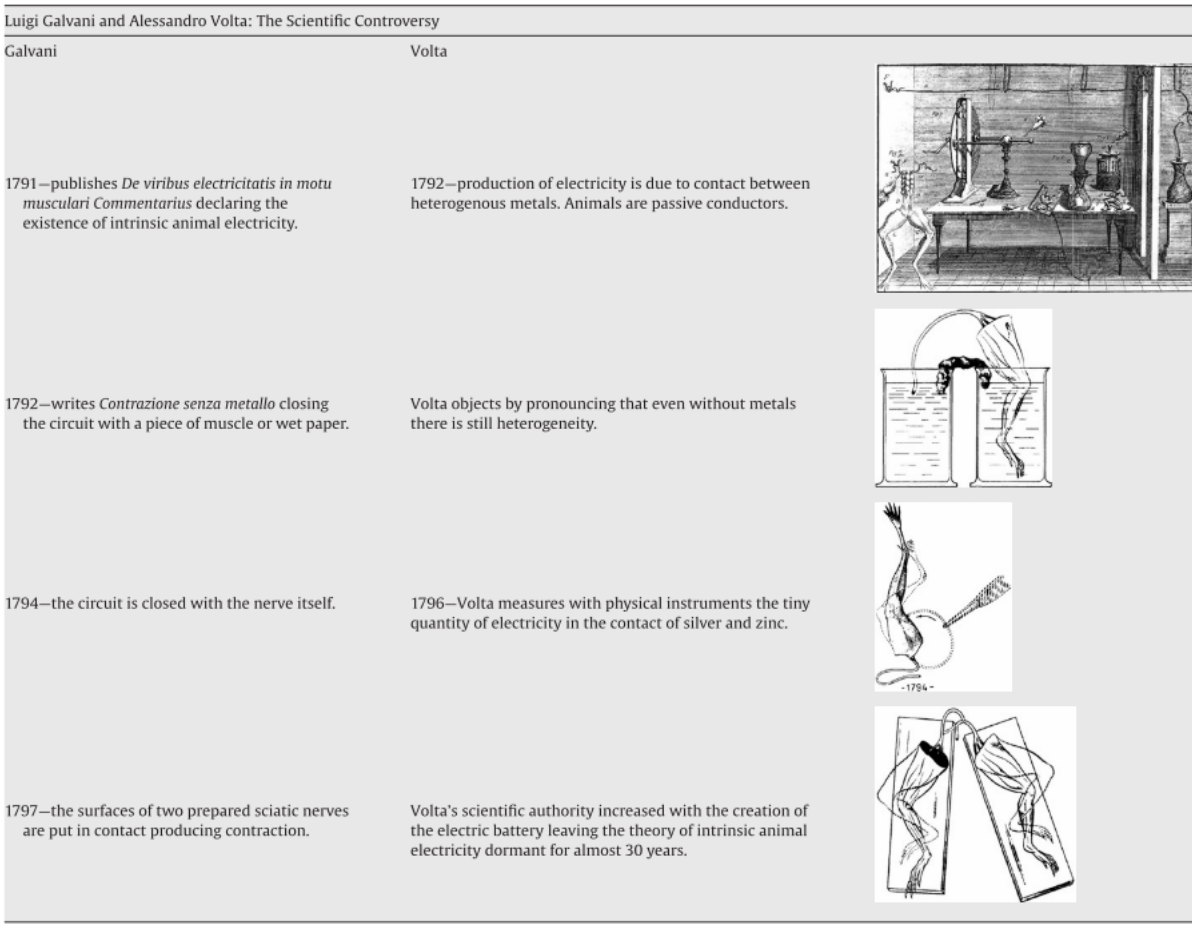

Figure 2.1. Illustration of the Galvani and Volta controversies[109]**.**

Hans Christian Oersted (1820) discovered electromagnetism and demonstrated that electric current in a loop causes deflection of a magnetic needle and that the direction of deflection depends on the direction of current in the loop. DuBois-Reymond introduced the term "*action potential*" for the alternating current he observed due to muscle contraction. He worked on the concept of electromagnetism discovered by Oersted and developed the first galvanometer (1843) sensitive enough (with a magnetic coil of more than 4000 turns) to record the results of his experiments. He also developed the first non-polarizable electrodes used to couple stimulation and recording equipment to the tissue. Due to these developments, he was able to record action currents (termed "*muscular current*") in frog muscle in 1843[111], putting an end to the debate between Volta and Galvani.

2.2.2 Discovery of ERG and early instrumentations

DuBois-Reymond first identified a standing potential of the order of millivolts that existed between the anterior and posterior pole of a resting eye (1848). This source of resting potential behaves as if it was a single dipole, oriented from the retina to the cornea[112]. At the time of this discovery, the available instrumentation did not make it possible to detect if light stimuli would change this voltage gradient, due to the small (less than a second) time constant of the generated potentials [113]. Homgren (1865) first took an electroretinogram (ERG) in the eyes of a frog caused by the transient changes at both the onset and cessation of light stimulation. Independently, Dewar and McKendrick (1873) demonstrated that light stimulus to a previously covered and dark-adapted eye would produce a response. They registered this response, using a Thompson galvanometer (DC instrument), as a positive electrical change in the cornea to the back of the eye[19][13][114][115]. They called this response "*variations*"[116] in the observed potentials and compared their finding on

various fish species. They found the responses differed and noted the presence of nonlinearity as they varied the intensity of the stimuli. Kuhne and Steiner (1880) investigated the reaction of the isolated frog and fish retina to onset and cessation of light stimuli and found a complex response originating from the receptor layer of the retina[117].

There followed work by Gotch using a capillary electrometer (1903)[118] and then Einthoven and Jolly (1908) on isolated frog's eye. Einthoven and Jolly used a series of lenses to concentrate light on the frog's retina and recorded the signal using a string galvanometer[119] (invented in 1901 by Einthoven and first used to obtain quantifiable human ECG recordings[120], figure 2.2[121]). This instrument has significantly increased sensitivity (approximately 2 mV) and reduced the settling time (less than 1 ms) compared to its predecessors. This invention dominated instrumentation in electrophysiology for 20 years, until electronic amplification became available during world war one. These studies were the first to assign letters to ERG components. The first negative deflection, the second positive deflection and the third slow positive deflection were termed a, b and c-wave, respectively (figures 2.4.a and 2.4.b)[122].

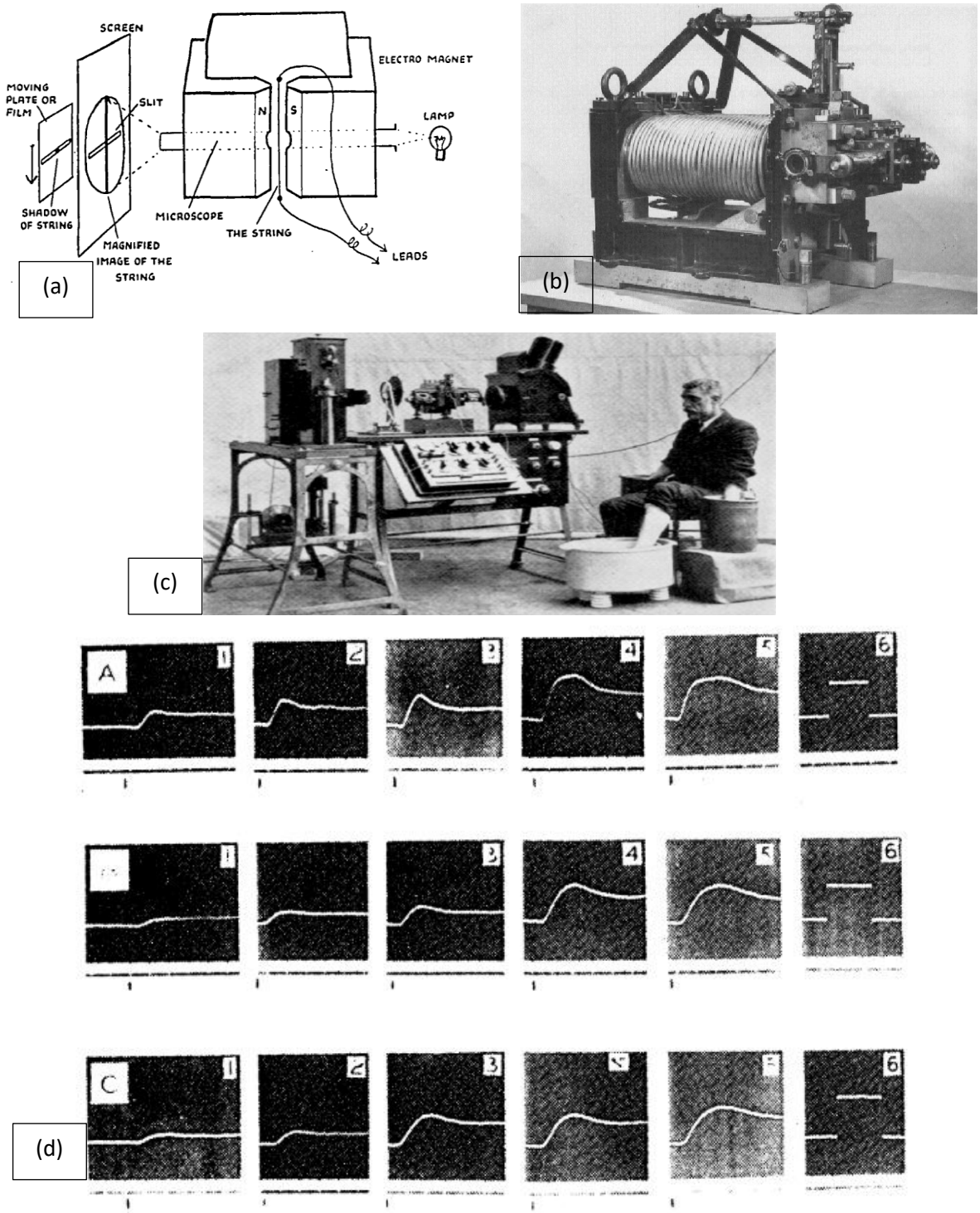

Figure 2.2. (a) Devised Einthoven string galvanometer that was sufficiently fast and sensitive for a recording of electrophysiological action potentials like those from the retina, without any amplification[123]. (b) Einthoven string galvanometer[119]. (c) The first table model of Einthoven electrocardiograph manufactured by Cambridge Scientific Instrument Company of London in 1911 where the string galvanometer is placed at the centre of the table, the lamp is on the right side of the table and the film or display is on the left[121]. (d) Records of frog ERG using string galvanometer. A-C: decreasing the flash intensity and left to right: increased dark-adaptation[123]. The calibration files were not available in the original file.

More than 30 years after the invention of the string galvanometer by Einthoven, Gasser and Erlanger (1922) refined and applied the Cathode-Ray Oscillograph (CRO) in combination with the string galvanometer to not just record but also trace the neurological action potentials travelling through

the nerve fibres [124], figure 2.3. This tracing mechanism significantly enhanced the research in neurophysiological centres as it enabled information to be gained on the time-relation of the action potentials that are triggered through stimulation[125].

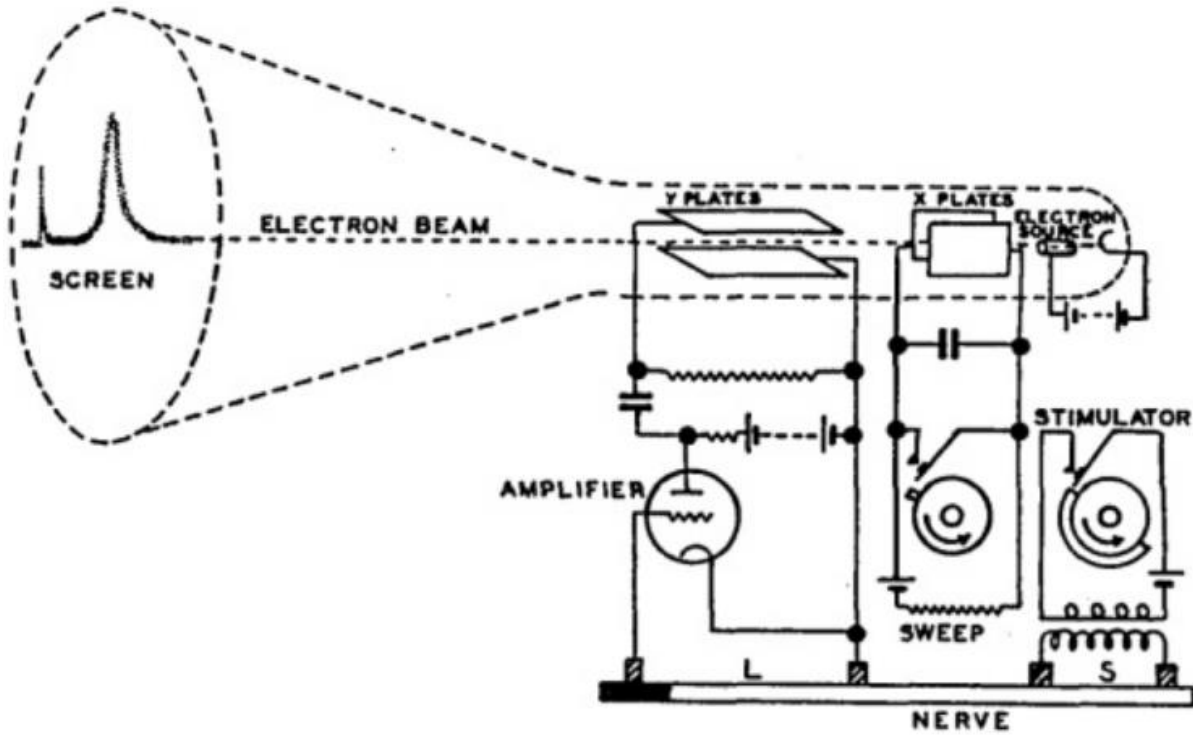

Figure 2.3. Gasser and Erlanger CRO consisting of a nerve stimulator, amplifier and display system to trace the generated action potentials as electrodes are moved through the network of nerve cells[124].

Professor Kahn and Lowenstein (1924) presented the first recorded ERG wavelets from humans using Einthoven's string galvanometer (figure 2.4.c). Their goal was to introduce ERG investigations into standard ophthalmic diagnostics. However, they were unable to provide a method suitable for clinical conditions.

2.2.3 Discovery of ERG components: Granit ERG component analysis

The complex ERG waveform was further explored by Granit[30] (1933), who performed a component analysis of the anaesthetised cat ERG waveform (which he referred to as the "*composite waveform*"). He hypothesised that an infinite number of wavelets could be added or subtracted (a model that he termed "*mechanism of sensory integration*") to produce the recorded response. These waveforms would have to have varying characteristics with regards to sign, strength and timing. Accordingly, he set out to further investigate the processes resulting in the generation of these ERG components. He proposed biological means of splitting the composite waveform into its underlying components. Granit termed these components the first, second and third processes or PI, PII and PIII, respectively. The numbering of the processes was due to the sequence in which Granit successfully removed the component from the composite waveform. The c-wave was the first to be removed by using ether as the differentiating agent and was hence termed PI, while the faster components of the ERG waveform were unaffected. Further narcotization started to reduce the b-wave amplitude and delay it's time to peak for all light intensities. As Granit deepened the anaesthesia, he observed that the b-wave was abolished and hence he termed this PII. The narcotization was induced through inhalation and if it was removed a complete recovery was possible. It was evident to Granit that the a-wave was the most resilient of the components, and once this is removed through progressive narcotization, the retina may cease to respond. Granit termed this component the third process or PIII (figure 2.4.d) and further analysed the a-wave

through occlusion of arterial blood flow. Granit's comprehensive study used a powerful (and drift-free), vacuum tube and direct-coupled amplification circuitry (an advanced technology at the time). He received the 1967 Nobel prize for his discoveries.

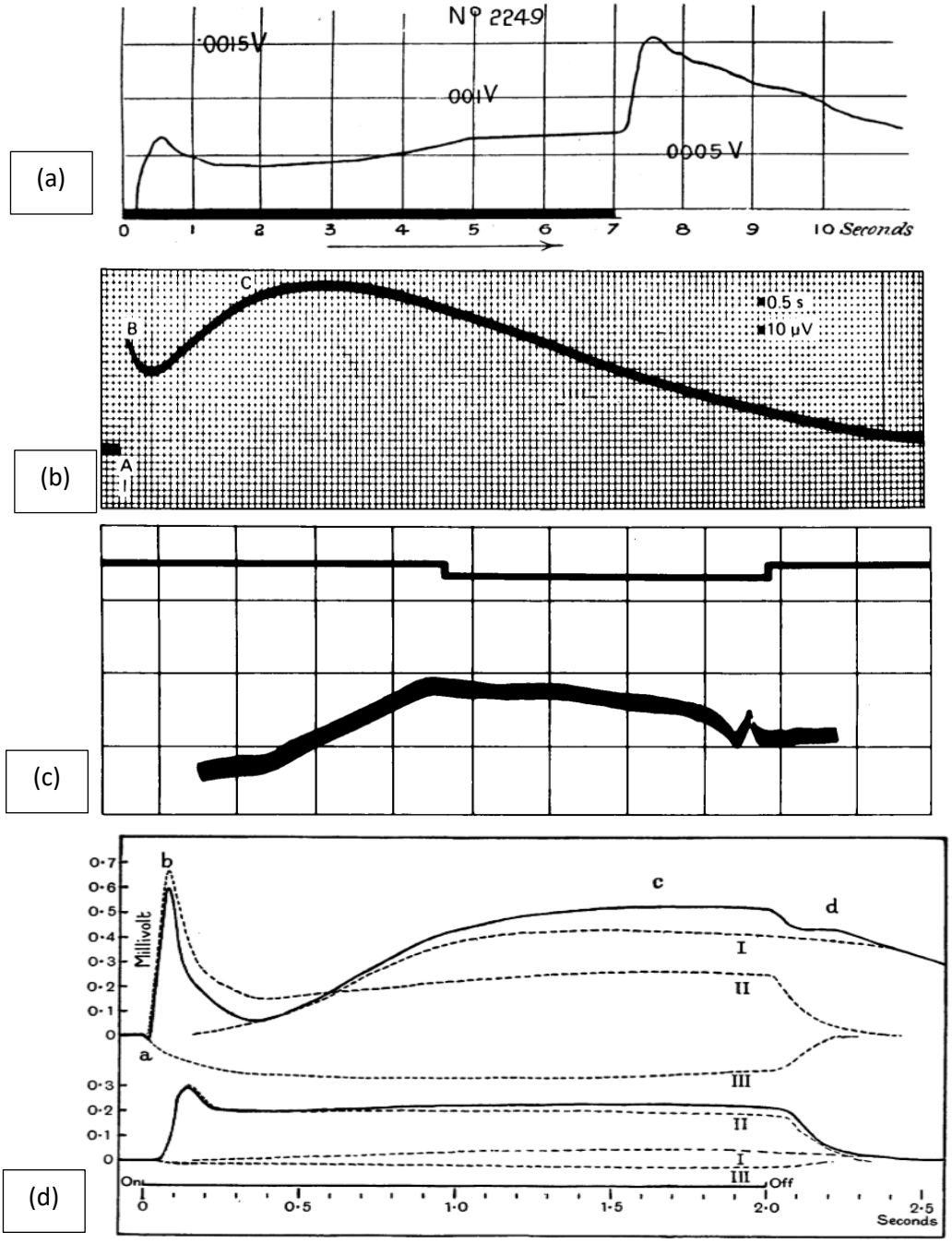

Figure 2.4. (a) The recorded ERG by Gotch (1903) from the eyeball of the frog, illustrating the ON, OFF effect of light stimuli as well as the peak ON response delay of 500 ms as reported by Gotch[118]. (b) Recorded ERG waveform by Einthoven and Jolly (1908), with designated a-, b- and c-wave components of the complex waveform[122]. (c) First human ERG record (Kahn and Lowenstein) where the curve is to be read from right to left (each square in (c) has 500 µV across the y-axis or amplitude axis and 1.2 seconds across the time-axis[117]. (d) Granit (1933) ERG recording of a cat retina to a 2 seconds light stimulus (at two different intensities) where PI, PII and PIII are isolated through the respective state of anaesthesia [30].

2.2.4 Introduction of ERG as a routine clinical and diagnostic tool

The use of electroretinography in human subjects as a research and clinical diagnostic tool must be credited to Riggs[126] (1946) who introduced the contact lens electrode. Before that, contact with the cornea was made through cotton wicks electrodes, which are a great deal more uncomfortable[127]. The need for greater comfort and better signal to noise ratio drove the development of other forms of electrodes, such as the gold foil electrode by Arden (1979) [128], figure 2.5.a. Dawson, Trick and Litzkow (1979) invented a low-mass, conductive thread, corneal electrode and termed this the DTL electrode, which is most commonly used in today's clinical investigation. The objective of this was increased comfort and reduced risks of corneal abrasion (through electrode placement and blinking). They further performed a comparative study between the DTL and Burian-Allen electrode and quantitatively assessed the signal quality and inter-patient variability[129], figure 2.5.b.

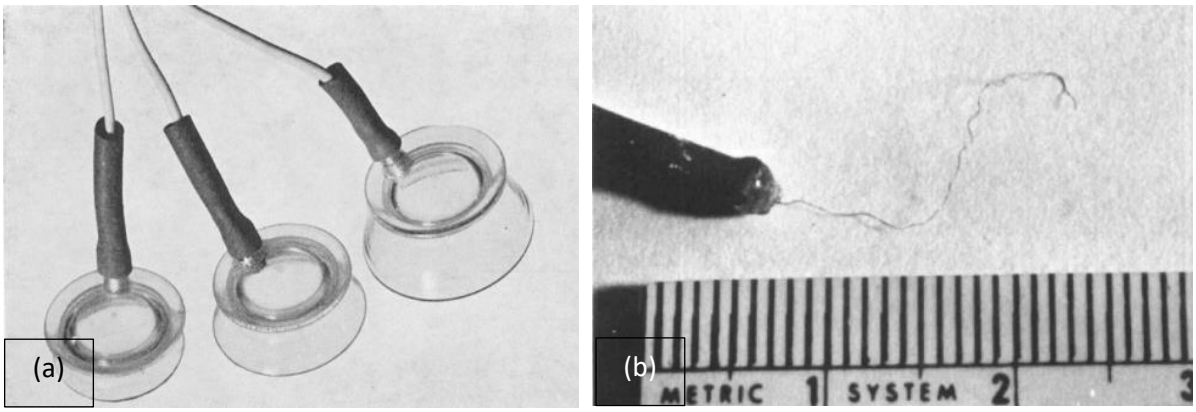

Figure 2.5. (a) Three different sizes of contact glass electrode used as an active electrode by Karpe[130]. (b) DTL electrode, connecting wire tip, and conductive thread developed by Dawson, Trick and Litzkow (1979)[129].

Professor Gosta Karpe (1945) developed techniques that made it possible to improve ERG recording as a routine clinical practice and for the first time reported the absence of ERG in RP (Retinitis Pigmentosa)[131]. Karpe recognised that his new method required specialised training and what he termed "*much patience*" on the part of the investigator if it was to be of widespread clinical value. He designed his method and apparatus with the simplicity in mind, hoping to make it more generally available in "*all important centres for the treatment of eye diseases*". His studies were published in 1947[132] and 1962[130]. These publications discussed the standardisation of the electroretinogram examination[133] and were backed up by years of experience (1946-1961) at the Eye Clinic of Karolinska Sjukuset in Stockholm. The factors discussed are summarised below (figure 2.6):

- Requirements for a screened room.
- Electrode system (both active and reference electrodes) preparation and placement.
- Attention to extraneous electrical disturbances and ways of shielding from such interference.
- Stimulus delivery system and methods of controlling retinal illumination through adjustment of the distance between the subject's eye and the stimulus bulb.
- Calibration of stimulus delivery system before use and further requirements for regular calibration of the light bulb.
- Importance of and methods for recording the stimulus trigger point (synchronisation signal allowing the quantification of the implicit times of the various wavelets of the ERG composite response) by means of a photocell placed near eye and away from the subject's sight.
- Importance of fixation point and method to achieve this to avoid disturbances caused by eye movement.

- Methods to avoid retinal abrasion and contamination of the recordings through the subject's blinking.
- Methods to record the retinal ON and OFF responses and importance of variation in intensity for such recordings; developing recommendations and examination protocols.
- Requirements for a normal database for comparison with the recordings obtained from patients with the suspected retinal disease[134].
- Effect of stabilisation time required for the stimulus delivery to reach the desired intensity and its relation to the normal subject's a- and b-wave amplitude and implicit times.
- Recording amplifier setup and trace display mechanism and its calibration to ensure that it will follow the rapidly changing potential (effect of aliasing).
- Comparative studies using different stimulus delivery systems and amplifier setups to ensure reproducibility and repeatability of results.
- Use of a calibration device that is integrated into the setup to ensure the amount of amplification is regulated throughout the examination.
- Verification and validation of the whole setup prior to clinical use and the reporting of this.
- Patient setup, including requirements for light- and dark-adaption[135], skin preparation prior to electrode placement, use of anaesthesia, its type and concentration.
- Demonstration of normal and a range of pathological types of ERG [136][137][133][138].

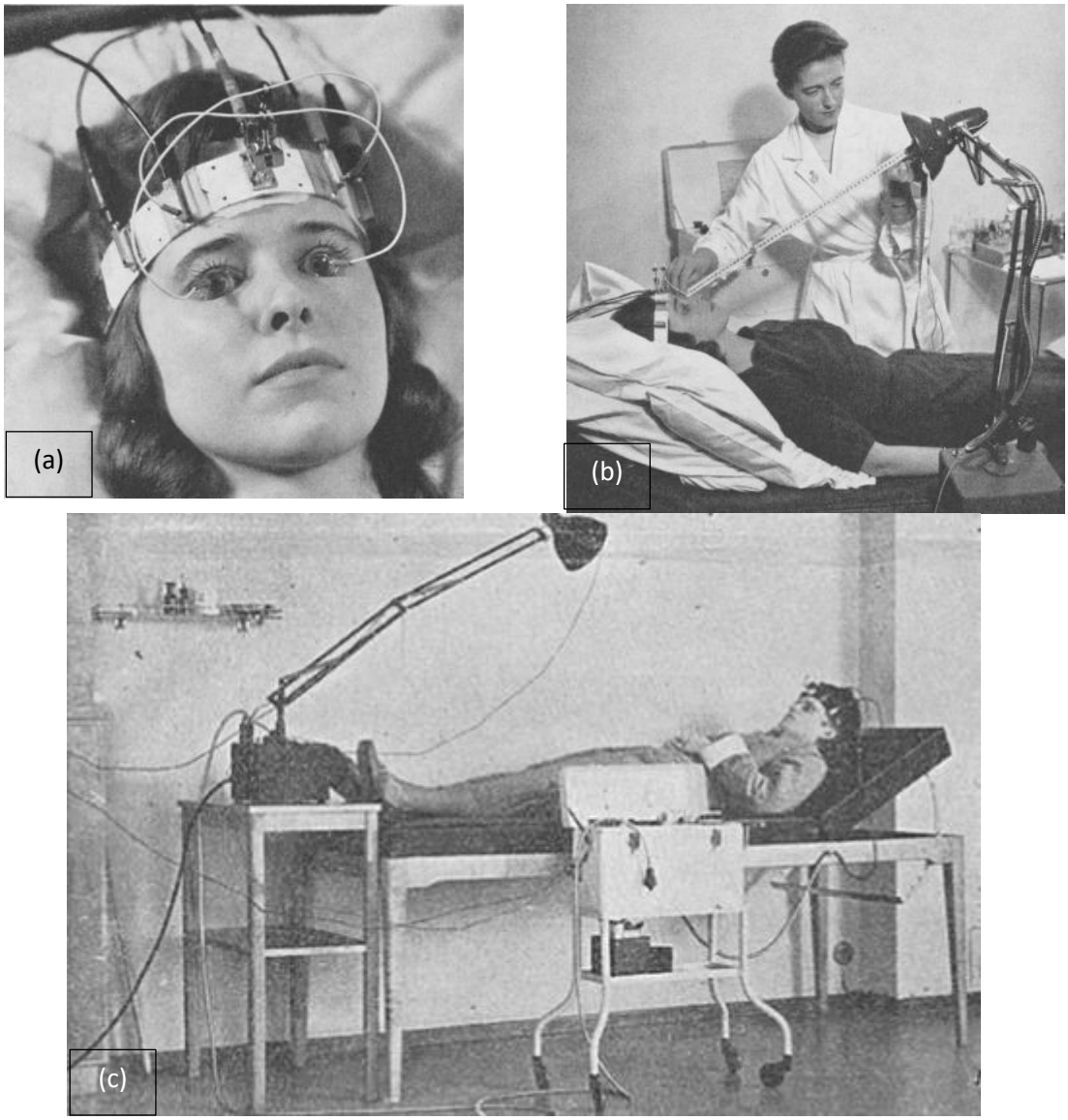

Figure 2.6. (a) The arrangement of the electrode system. (b) Methods to regulate the intensity of light stimuli. (c) dark-adapted subject ready for examination.[130][132]

The same apparatus (where possible) and the method was soon being used by other workers to perform visual electroretinography in a clinical setting[139]. For example, Dhanda (1956) adopted the same technique to first collect normal ERG recordings in multiple age groups within an Indian population and then used the same method (except for the amplifier) to perform clinical ERG studies on patients with blindness due to vitamin-A deficiency. He confirmed the practicality of the method developed by Karpe[140].

Investigations up to this point in time were mainly focused on the slow components of the ERG, the c-wave (1-5 seconds for a response to develop), the fast oscillation trough and the light peak(5-6 minutes for a response to develop)[32]. Compared to other components of the ERG, these are typically very difficult to record clinically due to drift, blink and eye movement artefacts[141][142] as well as high inter- and intra-subject variability[143][144][143]. The c-wave is composed of a negative subcomponent originating from the neural retina and a positive subcomponent (which tends to be larger than the negative subcomponent), originating from the Retinal Pigment Epithelium (RPE). This arises from the interaction of the RPE with the photoreceptors of the retina through ion and water transport and electrical responses as described by Steinberg[145]. The normal variations in these

two subcomponents tend to cancel each other out, giving the apparent absence of the c-wave. Therefore, the c-wave is not a pure index of the RPE functionality, which takes away the precision that one would enjoy in using the electroretinogram to evaluate the retina. These factors make these components less appealing in the routine clinical setting. Electro-oculogram (EOG) is the only widely used test that is concerned with the RPE, measuring the light response of the standing potential that exists between the cornea and Bruch's membrane, Miles (1940)[146]. Arden and Kelsey (1961, 1962) further characterised the EOG signals by proposing a single quantitative index, known as light peak-to-dark trough ratio, or the Arden index. This facilitated comparison of data between centres and different investigators, allowing for EOG to become a widely used clinical test within the visual electrodiagnostic setting and a complement to the ERG testing[147][144].

2.2.5 Signal processing techniques: the emergence of averaging computers

Before the early 1950s [148], procedures for obtaining a good picture of the electro-neuroanatomy of the nervous system were limited, as it was not possible to record response potentials of less than 10 micro-volts (μV) [113][149]. It was generally necessary to use intense stimuli to detect the presence or absence of the response. The following two factors are recognised as the cause of this limitation:

- The remote location of electrode placement from the source of response, i.e. distant from the retina and cortex in visually triggered electrical responses. Animal studies allowed for closer-to-source analysis and provided some clue as to the origins of these responses in correlation with those collected from the human skull or cornea[150].
- Background noise and other uncontrolled sources such as EEG, ECG and EMG or other non-evoked responses.

It was not until the late 1920s/early 1930s that instruments were designed that could be used in the recording of an electric response accompanying a single impulse in one neuron or from living tissue (the apparatus was termed A biological amplifier or bio-amplifier for short). B.H.C Matthews (1934) designed the first AC coupled (capacitively coupled) vacuum tube, two-stage differential amplifier used in electrophysiology. In collaboration with Adrian, a three-channel (allowing the independent and parallel recording of multiple sites) amplifier was designed to record EEG signals. This amplifier, together with the moving-iron oscillograph designed by Matthews, allowed for detailed analysis of EEG signals, establishing many of the basic principles of the EEG, figure 2.7 (the instruments and their working principles were patented)[151][113][152][153]. The bio-amplifier was further refined during the 1930s, and in the 1940s, significant development of differential amplifiers took place.

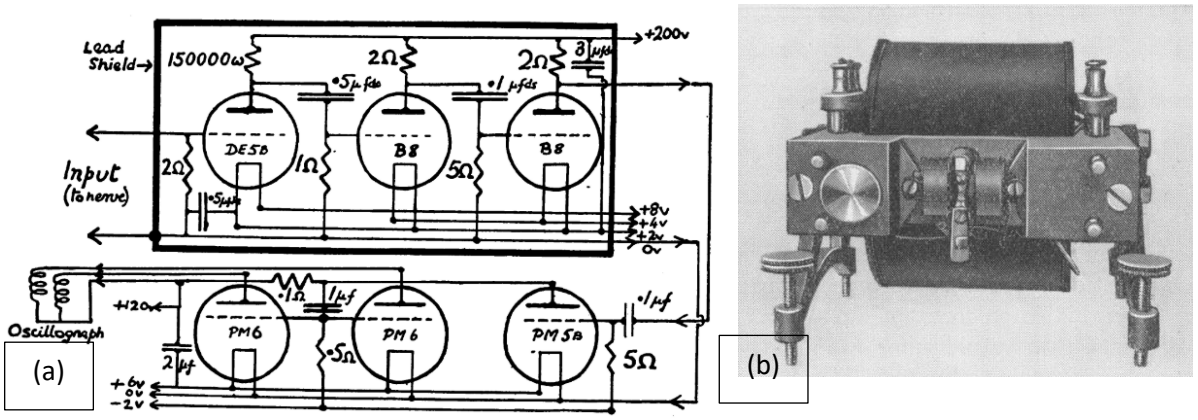

Figure 2.7. (a) Schematic diagram of the differential amplifier demonstrating a two-stage amplifier with connection to the oscillograph, designed and developed by B.H.C Matthews. The design did not apply the concept of feedback and stability (later developed in the Bell's lab by Harold S. Black during the early 1930s. The invention of negative-feedback to reduce the distortion by reversing some of the amplifier's output and feeding it back into the input led into designing a general-purpose differential amplifiers using vacuum tubes during the early 1940s and forms the basis of operational amplifiers[154]) and lacked the required high-level of Common Mode (CM) rejection as well as low input impedance of 200 KΩ. (b) the designed oscillograph by B.H.C Matthews to work with the differential amplifier in (a).[151]

Electrophysiology entered an era of significant growth thanks to the technological advances in amplifiers, oscilloscopes and digitisation techniques, allowing workers in the field to quantify responses and findings as the recording instrument's sensitivity and resolution increased. These advances also allowed the use of more complex stimulus patterns and raised questions as to the fundamental limitations of electrophysiological techniques [155][156][157].

In 1954, an analogue correlator system for analysis of brain potentials was developed at MIT, figure 2.8[148]. The autocorrelator could detect small potential responses which are periodically evoked. Two downsides to the correlator system were[155]:

- It loses the time information of the stimuli-locked evoked neurological responses.
- "*On-line*" processing of the neuroelectric potentials, could not be provided.

The digital successor of the correlator system was the Averaging Response Computer (ARC) system (1958). This allowed the reduction of the noise level, as long as there was access to the synchronisation trace, allowing for enhancement of responses which are time-locked to the stimuli and reduction of those signals that are not, figure 2.8[155][156].

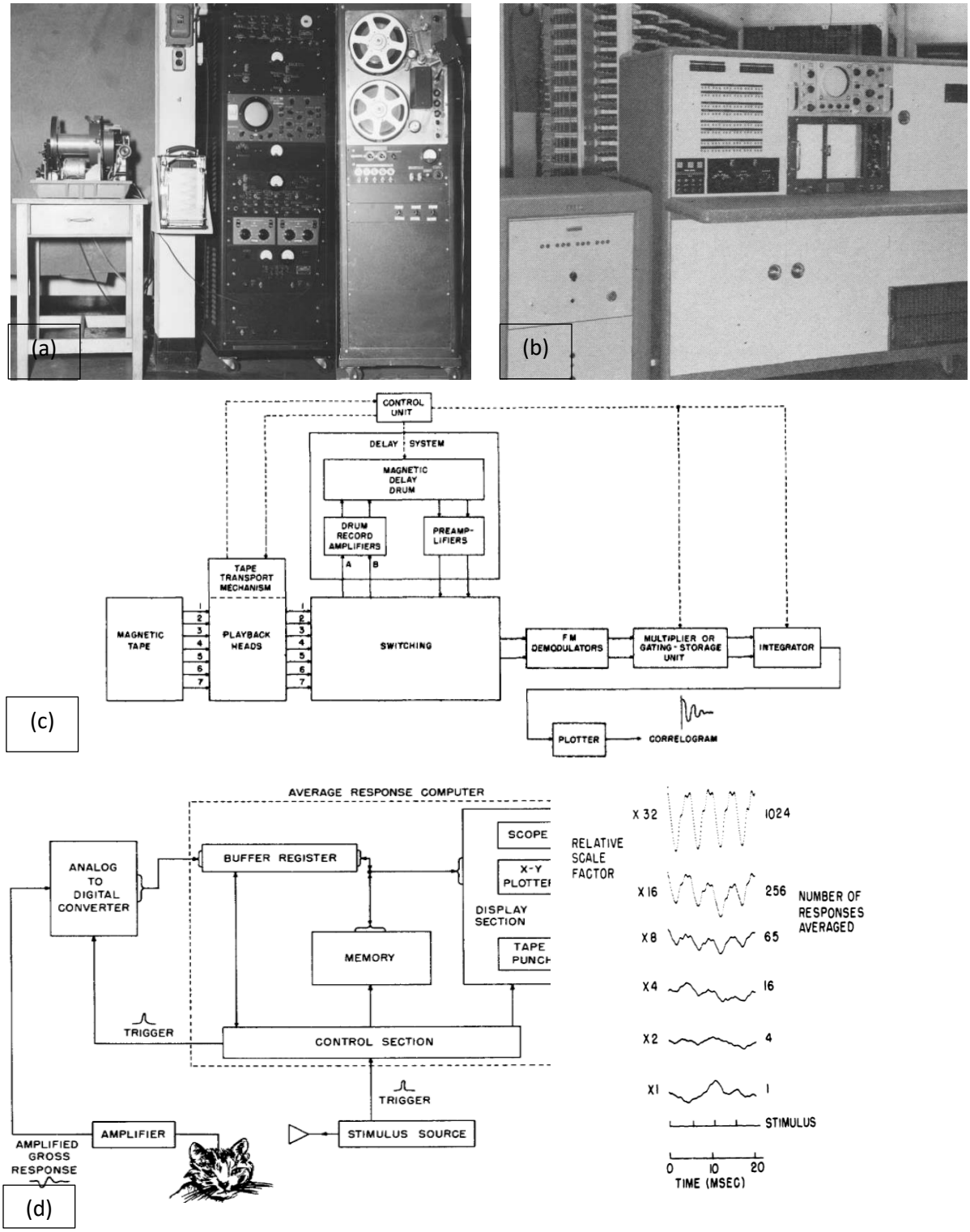

Figure 2.8. (a) The analogue correlator system developed at MIT together with magnetic tape to record the data[148]. (b) ARC (1958) built at Lincoln Laboratory (Lincoln Lab was formed in 1951, funded by US Department of Defense and administrated by MIT[158]) and a digital successor to the Correlator system in (a). (c) Block diagram for the analogue correlator system. From the mathematical definition for the auto- or cross-correlation, one can readily see the time-delay, multiplication and integration operations. The signals to be correlated and the correlation result is recorded onto a magnetic tape where the latter would also be plotted using the plotter module. Due to the limitation in storage capacity of the magnetic tapes, a frequency modulation technique was employed in which a carrier wave is frequency modulated by the recorded neurological potential signal and is recorded. The technique is a post record processing of the neuroelectric potentials[155]. (d) Left: Block diagram of ARC allowing for "on-line" processing of neuroelectric potentials[155]. Right: illustration of improvement in signal power compared to the noise power as the number of averages is increased[156].

Signals obtained in visual electrodiagnostic measurements due to repeated stimulation may change with time. The inherent variability associated with physiological systems as well as drifts in the experimental apparatus can change the response. The impact of this variability may be reduced by defining experimental systems that result in a more repeatable class of evoked responses[123]. Such design adds averaging as a tool to the statistical description of periodic neurophysiological responses.

2.2.6 Photometry: ocular light transmission pathway

Familiarity with photometry is another essential part of visual electrophysiological testing, providing the electrophysiologist with tools to ensure consistency in the quantification of retinal illumination. Although the history of photometry can be traced back to early 1700 (when Pierre Bougure (1729)[159] first published his discovery of practical means of measuring light as well as many fundamental theories), it was not until the early twentieth century that international committees were formed write standards for radiometry, photometry and colourimetry[160], driven by the needs of civil and military aviation[161]. A radiometric system is not the right measurement unit when considering applications in visual electrophysiology due to the selective spectral sensitivity of the human eye. This spectral bandwidth is not uniform across the visible region. It is impacted by various factors such as age (reducing the quality of the image on the retina due to a combination of pupillary miosis, increased light absorption, increased light scatter as well as neural cell degeneration and neurotransmitter changes)[162][163][164], retinal adaptation (scotopic, mesopic and photopic conditions), light source and eye pathology. It is also proposed (Peter Kaiser, 1987) that since spectral sensitivity differs from one individual to another, a more standardised unit of measurement (Troland) is required when discussing retinal illumination [165]. Figure 2.9.a demonstrates the weighted functions (also known as luminance efficiency functions) for photopic and scotopic conditions (normalised values obtained from International Commission on Illumination or CIE[166] and adapted by International Bureau of Weights and Measures or BIPM[167]).

L. T. Troland (1916)[168] noted the importance of measurement of the visual response in absolute units to standardize the conditions and results of experiments so that they can be described as "*exact and scientific*" rather than "*results that can be employed in the support of almost any hypothesis, at the experimenter's pleasure*". In his paper, published in 1917[169], he pointed to the significance of pupillary size upon visual stimulus intensity and proposed a new standard unit of measure that he termed "*photon*" (later during 1920, the unit of retinal illumination was called Troland or Td). One Troland is defined as the measured illumination when viewing a surface with a luminance of 1 cd/m^2 through a pupil with an area of 1 mm^2.

The Troland unit does not take into account the transmittivity of the ocular media [170][171][172][173] and the size of the eye, and as such, it cannot serve as a comparable and "*exact*" unit of measure when it comes to eyes that are "markedly" different with regards to these parameters[174], see figure 2.9.b.

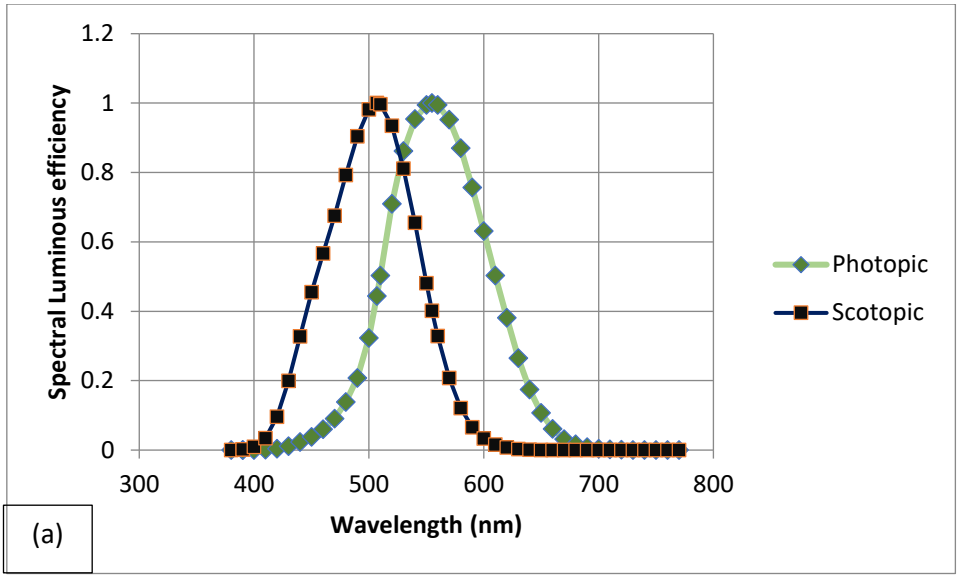

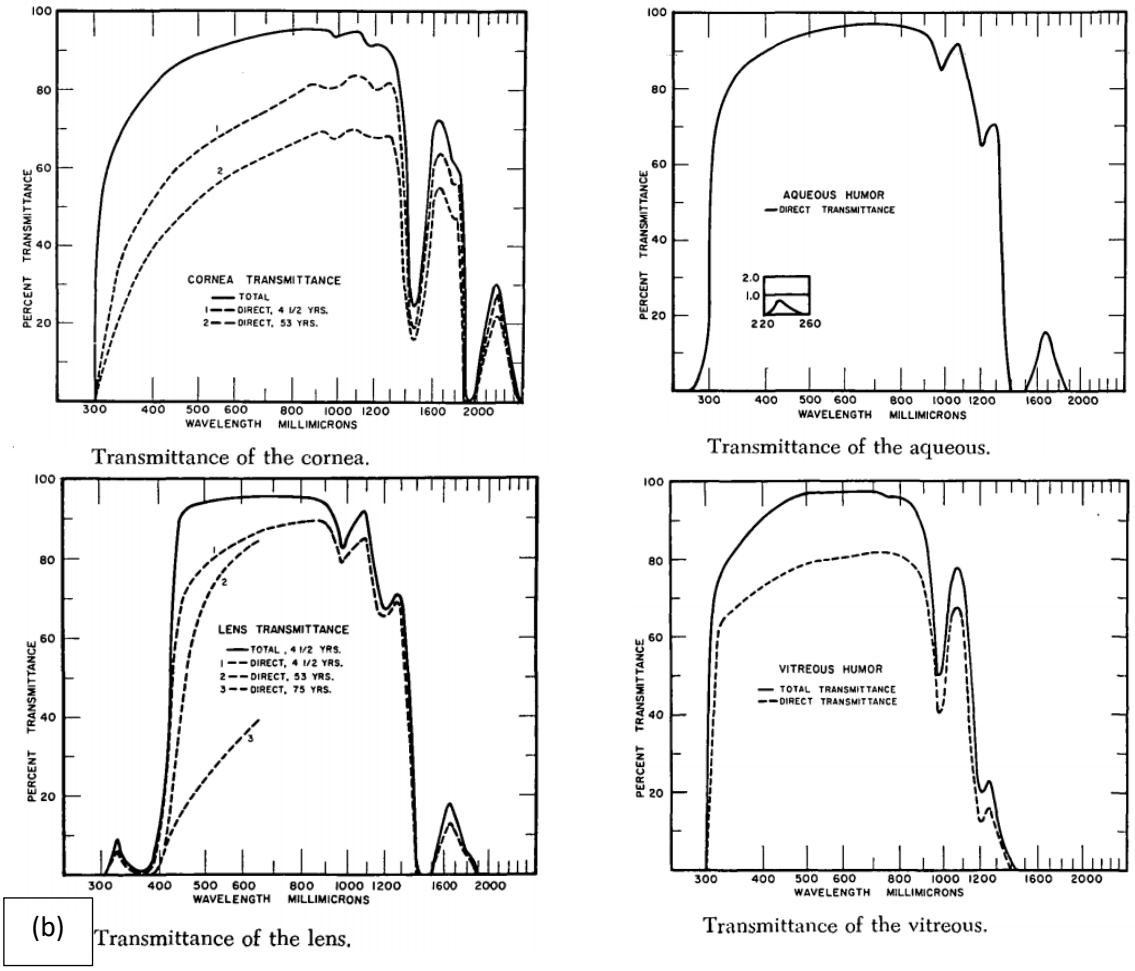

Figure 2.9. (a) Relative or normalised spectral luminous efficiency curved under both photopic and scotopic conditions where maximum sensitivity under scotopic and photopic condition are 507 nm and 555 nm, respectively[166]. (b) The spectral characteristic of freshly enucleated human eyes (transmittance curve of the cornea, aqueous humour, lens and vitreous humour for the wavelength range from 0.22 to 2.8 nm). Results are measured made on 9 eyes from people in the range of 4 weeks to 75 years of age. In this study, the author found that the maximum total transmittance (direct and scatter) of the eye is about 84%, and this is in the range of 650-850 nm[175].

The absolute unit of measurement is the number of quanta or photons that are absorbed per receptor within the stimulated retinal area. The concept of measuring the overall quantum efficiency dates back to 1942 when Rose[176] performed a series of experiments to compare the performance of a human observer with that of an ideal observer. The calculation requires the measured illumination at the eye's object space, the ocular path transmittance factor, the proportion of stimulus scatterer[177], the location of the stimulation on the retina and the number of different photoreceptors in that region, the retinal adaptation state, the viewing system used (e.g. Maxwellian or free viewing system) and stimulus type (e.g. duration, frequency, colour)[178]. This is assuming that the photons absorbed by the photoreceptors will result in signals to the higher visual centres, ultimately leading to optimal processing of the received information by the higher brain[179]. Even if such measurement was feasible and could practically be performed during a routine visual electrodiagnostic examination, it would yield a very subject-specific and variable estimate of the observer's quantum efficiency[180].

Age-related changes in visual function have also been extensively studied and found to impact Visual Acuity (VA), visual field, colour vision, dark adaptation, spatial and temporal Contrast Sensitivity Function (CSF), degree of light scatter, pupillary dynamics, etc. Degradation of these functions and factors in older adults result in poorer visual function[181][182][183][184][185][186]. Several techniques have been developed to, subjectively and objectively evaluate the optical and neural quality of the human eye, providing information on the nature and extent of the optical and neural imperfections. These techniques include wavefront sensing and double-pass instruments[187] to provide information on the optical quality of the eye and multifocal ERG techniques to measure localised neural activities of the retina.

In 1932, the Stiles-Crawford effect was first described[188][189]. It was shown that the effects of a stimulus are dependent on the angle of incidence of the light beam falling on cone photoreceptors (i.e. waveguide properties of human photoreceptors[190][191]). This effect has been demonstrated many times[192] and shown to apply to both vertical and horizontal displacement in the pupil. Is reported as the Stiles-Crawford Effect (SCE) factor for foveal peak location and spread, figure 2.10.d. The effect shows that, under the photopic condition and with dilated pupils, Troland values will overestimate the effective retinal illumination. Therefore, one needs to consider correcting for this effect during electrophysiological measurement[160][193]. The effect can also be used to objectively assess the alignment of cones in humans with different types of macular diseases [190][194]. Although in a study by P. Gonzalez[195] it was concluded that the Stiles and Crawford effect is negligible during mfERG (multifocal ERG) examination, it remains unclear if one needs to include a Stiles-Crawford correction (e.g. increased luminance of background and/or stimulus intensity) during objective examinations[160][196][197]. Bach and Poloschek (2009) suggested the mfERG stimulus luminance should be increased by a factor of 5.4 to compensate for the Stiles-Crawford effect[198].

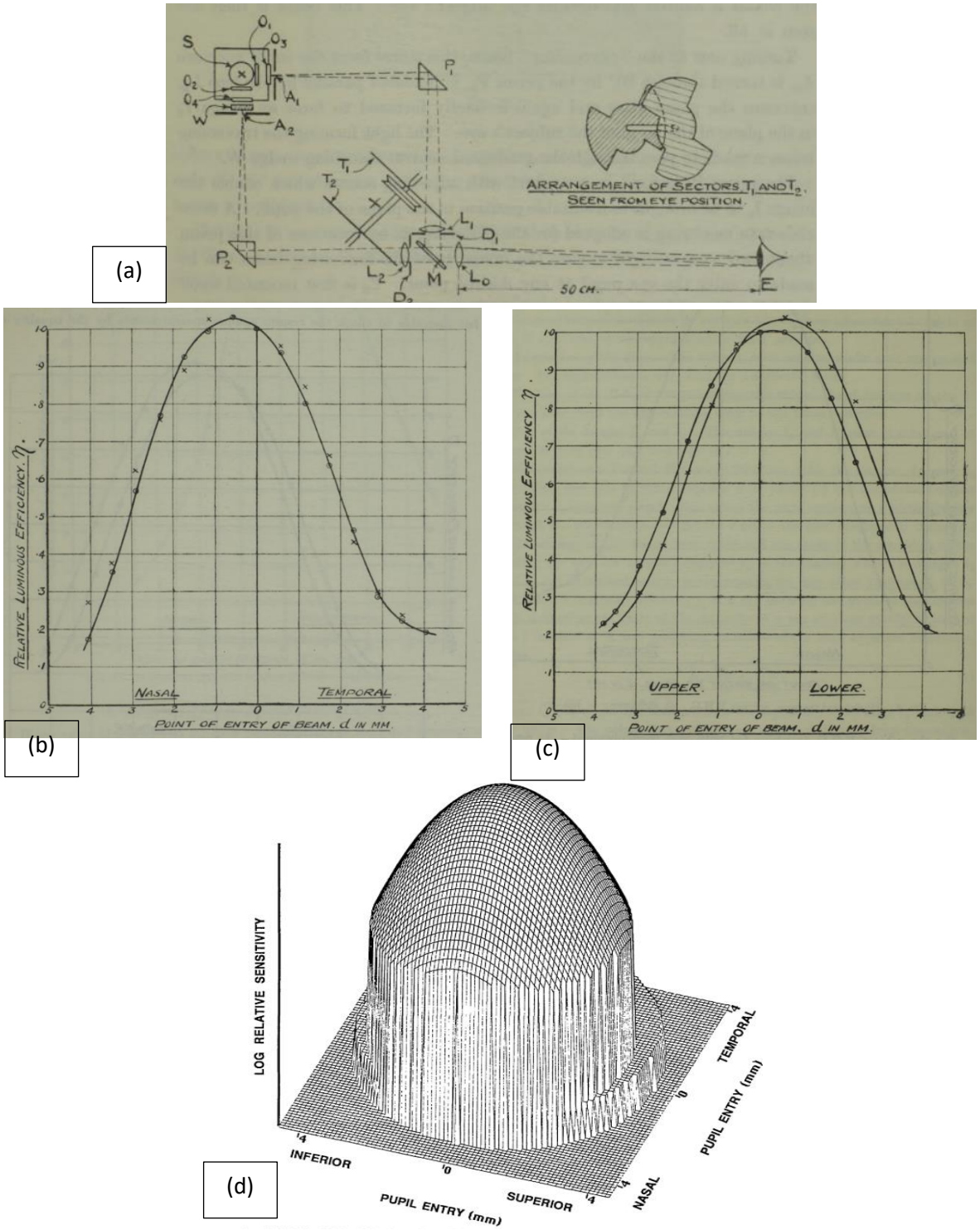

Figure 2.10. (a) Apparatus used by Stiles and Crawford to measure the luminance efficiency curves. Where S is the light source, O_1, O_2, O_3 and O_4 are diffusing glasses providing a uniform illumination at the A_1 and A2 apertures. Prism 1 and 2 (P_1 and P_2) will turn the light and Lenses 1 and 2 will ensure parallel beams of uniform light (Maxwellian system setup). Through turning and adjustment of P1 and P2 it was then possible to create the traversing beam of light required to perform the measurement. (b) The luminance efficiency decreases as the point of entry move away from the centre of a dilated pupil. At the periphery, the luminance efficiency falls by approximately 70%. The luminance efficiency curve is approximately symmetrical for both measured eyes (in this figure left eye measurements are indicated by X, and right eye measurement by Θ) and the peak value does not always match the centre point. Image from [188]. The measurements in the figure are from the author B. H. Crawford (1932) when entering rays are traversed horizontally away from the centre of the pupil in both temporal and nasal directions. (c) Same subject, same experimental conditions and methods (flicker method) when traversing the vertical plane. It is observed that the shape of the curves is the same, but the peak value is now differently paced in the vertical traverses. (d) Graphical representation of SCE for dilated eyes (8 mm). An attempt to create a normal set for human SCE peak and spread value by [191].

Under static conditions of illumination, the pupil of the human eye is not at rest but rather fluctuates periodically in size. This effect is known as pupil unrest or Hippus. Such movement is low in frequency and is shown to be influenced by the state of mind of the test subject[199][200], the type of mental activity[201], fixation and the background illumination level. The dilation and constriction, although of low frequency (measured to be in the range of 0.05 – 0.3 Hz) is large in amplitude (1-2 mm) [202][203], see figure 2.11.a [204]. The presence of Hippus was recognised as early as 1765[205] in both normal subjects and those with pathological conditions. Its origin and clinical significance are still under investigation. Many studies correlate the presence of this phenomenon to epilepsy and diseases of the Autonomic Nervous System (ANS) as the sympathetic and parasympathetic nervous systems control the function of pupil[202][206]. In a study carried out by Emma J. German and colleagues, the impact of luminance on the size of the natural (un-dilated) pupil was determined to be significant and if the pupils are dilated then changes in luminance had no impact on the pupilometer mechanics of the eye. Results are illustrated in figure 2.11.b[207]. Age was also determined to be a major factor in impacting the shape and size of the natural pupil in normal subjects[184] as well as the dynamics of the pupillary response, including the spontaneous Hippus response that decreases with age[208].

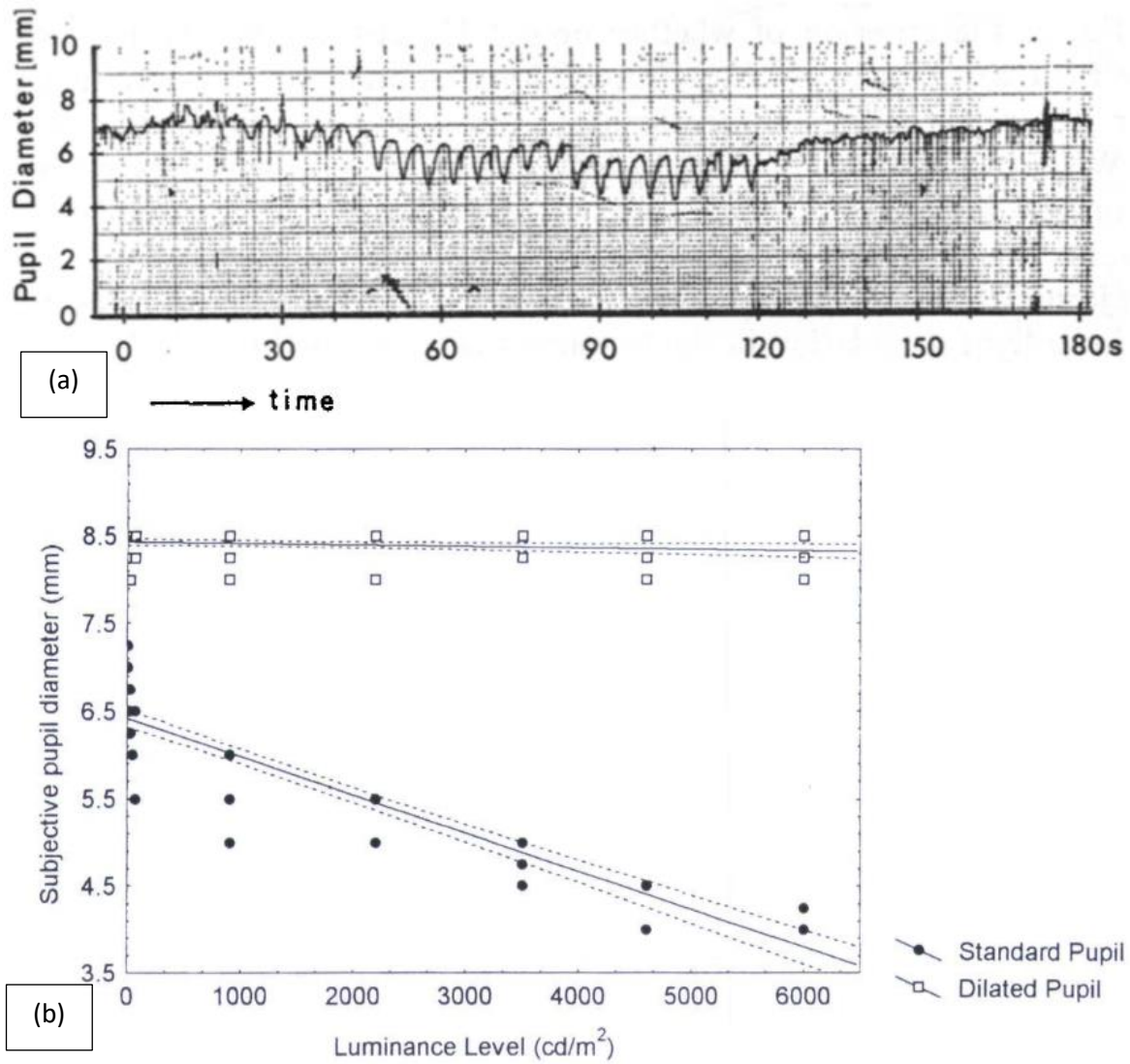

Figure 2.11. (a) A demonstration of Hippus at constant illumination from data collected by H. Bouma and L. C. J. Baghuis [204]. Initially, the authors were under the impression that the spontaneous disturbances of pupil diameter were due to the unsteady state of the light stimulus. This was rejected post further investigation by the authors. (b) Effect of luminance on natural (mean diameter of 5.78 mm) and dilated (mean diameter of 8.41 mm) pupils.

2.2.7 Introducing full-field (Ganzfeld) stimulation

Towards the end of the 1960s and during the 1970s, the contribution of the spatial distribution of the light stimulus reaching the retina to the standardisation of the ERG was well known. Ganzfeld stimulation overcomes the problems of poor visual fixation and stray light. The effect of uneven retinal illumination in recorded ERG is best described by Gouras (1970), as illustrated in figure 2.12.b [209].

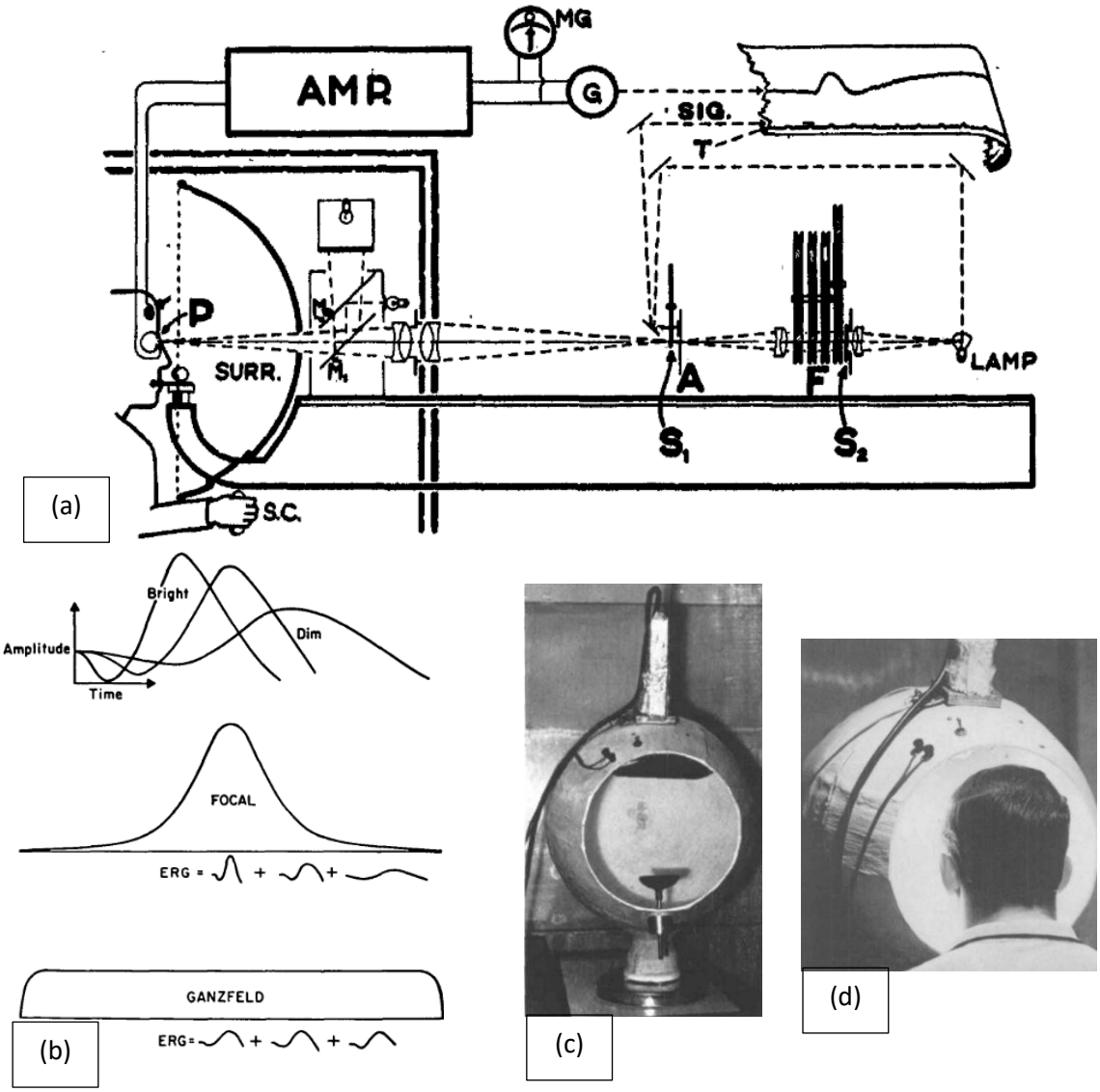

Figure 2.12. (a) A typical setup (Maxwellian system) before Ganzfeld introduction for retinal illumination during experimental and diagnostic examinations. Such installation includes a series of neutral, coloured and calibrated filters (indicated by F), optical lens system to bring the beam of light to focus at point P. If the subject is correctly in position, the light beam is concentrated on the pupil. The use of artificial pupils may be included. The visual angle subtended by the stimulus is then calculated and reported accordingly. The light stimulus is also traced on the final record so that the calculation of waveform subcomponent latencies could be determined[139][210][211][212]. (b) Illustration of changes to ERG morphology (amplitude and time course) with varying intensity (bright and dim stimulation) and distribution of light on the retina, when gross electrode, placed at the cornea, is used to record the ERG responses. (c) & (d) constructed Ganzfeld stimulator by Gouras[209] to allow for whole field or homogenous stimulation of the entire visual field. He further explained that if any stimulus other than a ganzfeld is used, the retina is not evenly illuminated, resulting in the overall recorded ERG waveform to be an integral of localised responses with varying shape and amplitude, making the comparability of records between clinics more difficult[209]. Early changes in amplitudes and latencies of different components of ERG can be used to detect abnormalities, for example, to detect early retinitis peigmentosa before it is evident under conventional ophthalmic imaging.

The first Ganzfeld dome was constructed by Gunkel (1968)[213]. Robin and Berson (1974)[149] introduced modifications to this design. In 1967, Gunkel[214] produced a comprehensive publication on the design features and requirements for Ganzfeld stimulators. Smith and Diprose (1985) designed and constructed the required circuitry to control Ganzfeld stimulation as well as the stimulus/background intensity using a computer, allowing for a broader range of intensity stimulation [215]. Their Ganzfeld device was based on the guidelines provided by Gunkel (1974). See figure 2.13.

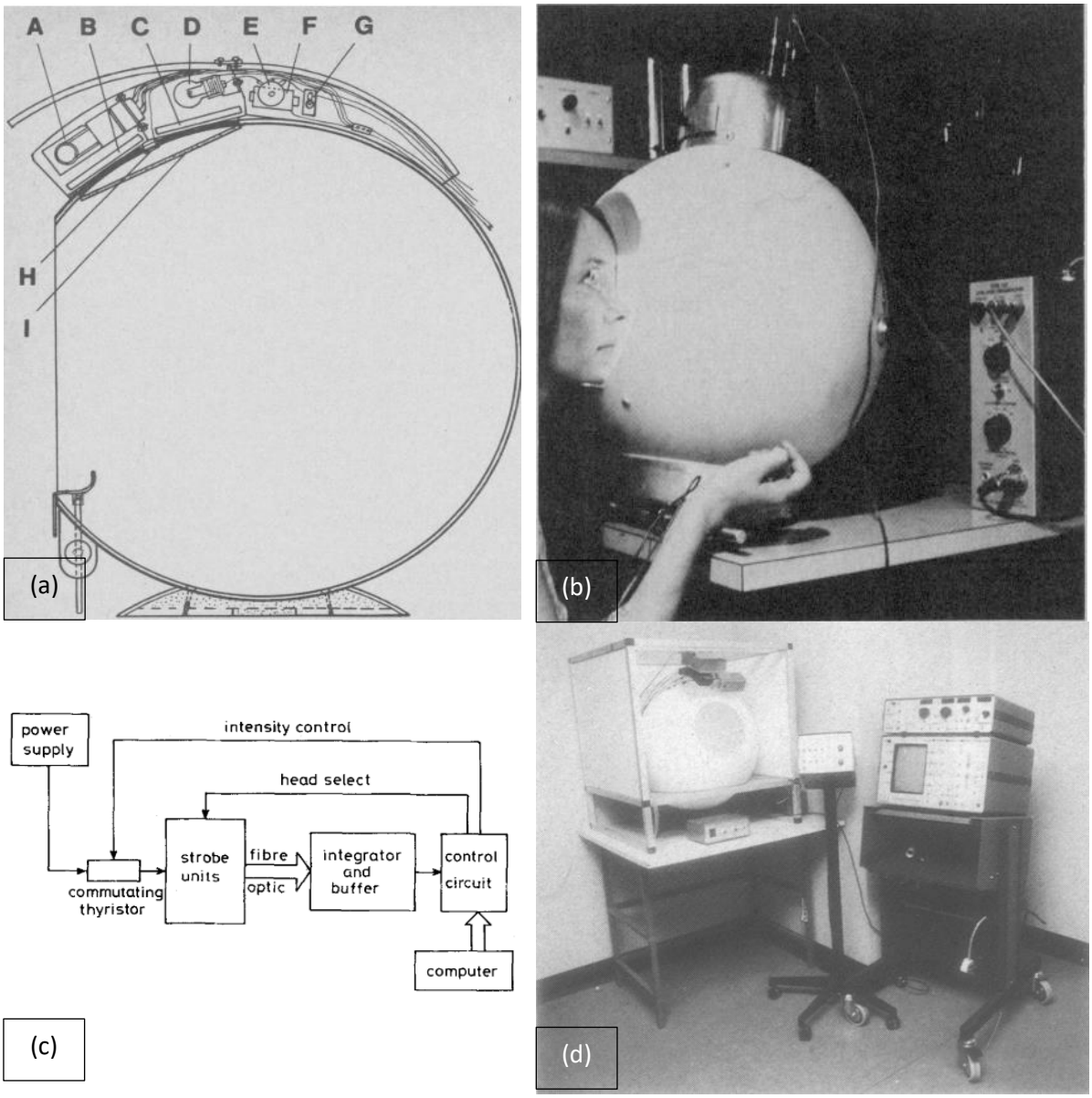

Figure 2.13. (a) Gunkel Ganzfeld design specification. A indicates flash tube. B & C slots for inserting calibrated filters for stimulus and background light respectively. D, indicates background illumination source. E, background intensity control (through a feedback mechanism adjusted to monitor dome illumination at all times) and I, diffusing filter.[214] (b) Ganzfeld dome constructed by Robin and Berson with a patient sitting in front of the full field dome[149]. (c) and (d) illustration of the overall computerised and variable intensity Ganzfeld stimulator for ERG measurements by Smith and Diprose (1985)[215].

2.2.8 High-frequency ERG components: Oscillatory Potentials (OPs)

The current understanding of the processes resulting in ERG signals has not dramatically evolved from that provided by Granit in 1933. The three independent processes he described are still accepted and strongly influences developments in electroretinography[216][217]. Clinically, it is the

early, faster components of the ERG that are of most interest. These are the a- and b-waves of the ERG response to a bright flash of light.

Cobb (1954) was first to report the presence of "*rapid* oscillation" or a "*staircase effect*" on the ascending limb of the b-wave. This was later confirmed by others[218], found in other species and designated as Oscillatory Potentials or OPs by Yonemura, Masuda and HATA (1963)[219]. Yonemura et al also pointed to the clinical significance of these wavelets, elicited using xenon discharge lamps. For example, they found that "*OPs were absent or diminished in almost all cases of slight diabetic retinopathy although in such cases the a- and b-wave were not necessarily reduced*"[220]. OPs occur under both scotopic and photopic conditions using high-intensity flashes[19]. These high-frequency components of the ERG are seen on the rising slope of the both ON and OFF responses (b- and d-wave respectively) and could be recovered through bandpass filtering the signal between 100 and 160 Hz.

2.2.9 Focal ERG and emergence of multifocal ERG technique (mfERG)

2.2.9.1 Focal ERG

The function of the discrete retinal locations cannot be described using the traditional ERG methodology. This limitation is of significance when considering pathologies associated with the macular region (such as age-related macular degeneration, diabetic retinopathy and Stargardt macular dystrophy) or the extent of the spread of pathologies in the retinal areas. The responses elicited from the macular region using focal ERG techniques is also called the focal macular ERG responses or fmERG [41], see figure 2.14.c. Focal and multifocal ERG measurements are those that are recorded from the small regions of the retina. The focal ERG is mainly concerned with generated responses from the macular or foveal region, where the concentration of cone photoreceptors is highest. It can also be used to describe the extent of damage through varying the diameter of the stimulation area[221][222]. The macular region contains about 10%[223][224] of all the cones (see figure 2.14[225]), allowing the recorded full-field ERG fall within the normal range even in the presence of central vision loss (i.e. a false-positive result). Isolating the macular region unmasks the localised response, allowing for measurement and monitoring of deviations from the normal response. This response isolation is not without its technical challenges such as[226]:

- Small signal to noise ratio (SNR).
- Fixation issue (dependent on the subject's willingness and cooperation with the examination in his or her ability to fixate on the target throughout the test duration).
- Long test period (to improve SNR).
- Impact of scattered light.
- Retinal area and location of stimulation, as well as stimulus colour and intensity.
- Potential adaptation impact of the retinal region to previous stimulation steps.

These challenges will be more pronounced if the spatial resolution is increased in the hope of obtaining a more precise functional characterisation of the retinal area under investigation. Before the emergence of averaging computers, any attempt to isolate the ERG response from the macular region was doomed[227]. High-intensity flashes were used to increase the magnitude of elicited responses, but Boynton (1951) and others found that such records may not originate from the stimulated area but also other regions of the retina due to the strong light scattering. They conclusively established this when they observed that a stimulus bound to the blind spot (a highly reflective region in the retina) gave an electroretinogram that could not be differentiated from the same geometrical stimulus falling on the fovea[228]. Armington (1961) was the first to propose that the surroundings (including the stimulus area) should be kept at a constant level of illumination and the required stimulus superimposed over this steady background to reduce the effects of scattering. This attempt was not successful[229], and later Brindley and Westheimer (1965) showed that (using corneal electrode and averaging over hundreds to thousands of sweeps) a much larger and brighter

surround (than those proposed by Armington) can be very effective in discarding the effects of light scatter. They conclusively showed that the human ERG is spatially additive[228], matching their initial findings in the frog's eye (1956, 1957). Arden (1966) showed that the experimental technique of Brindley and Westheimer could be used clinically, to obtain "*true ERGs*"[230] and he successfully performed the first set of clinical trials (using a modified Karpe's contact lens electrode and the same averaging technique) on patients with macular degeneration.

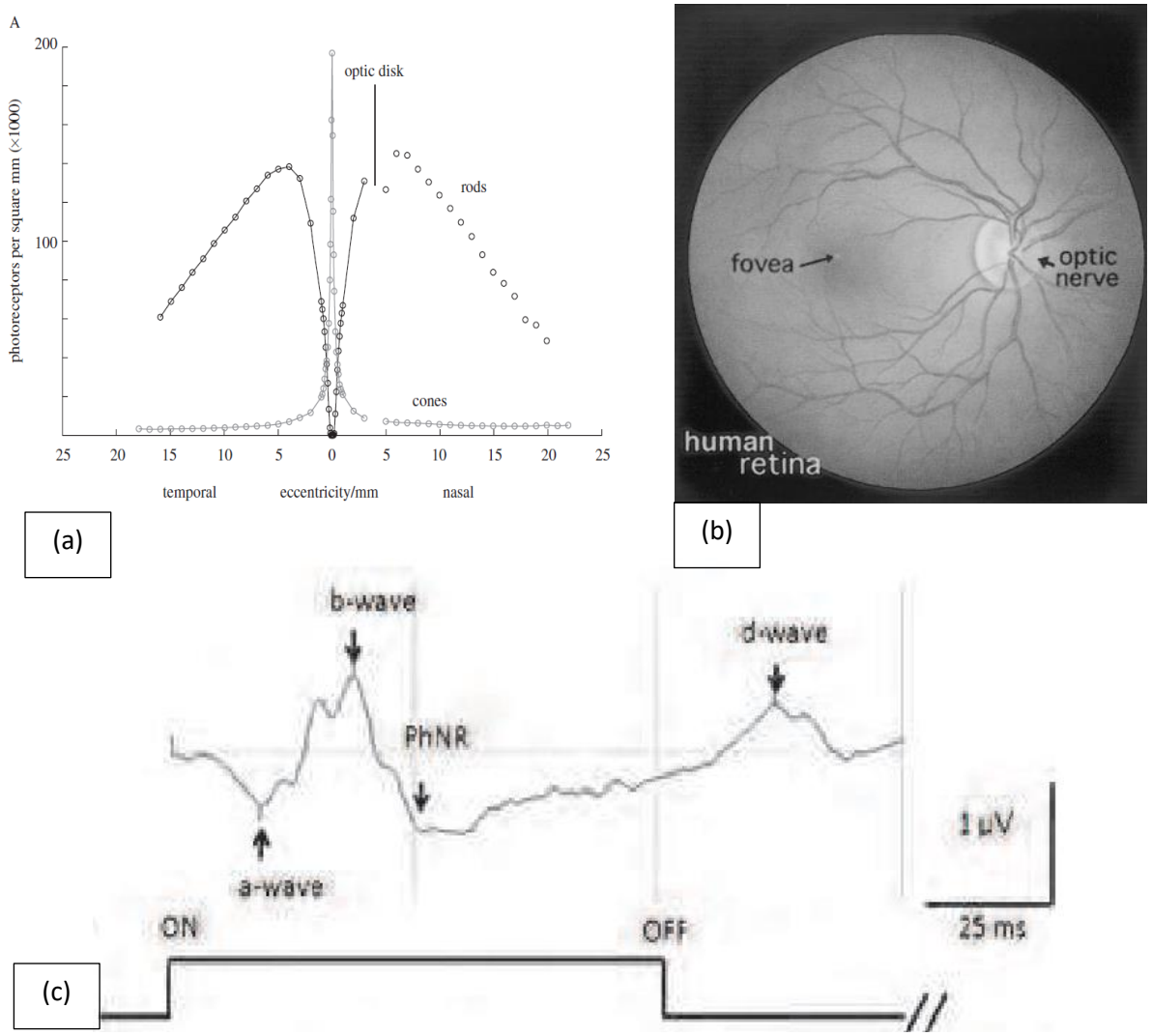

Figure 2.14. (a) Density plot of rod and cone photoreceptors on a horizontal cross-section of the human retina. It is shown that there exist no rods at the centre of the retina and they peak at 5 mm out from the centre. Also, no rods or cones at the optic disk area.[231] (b) Ophthalmic image of the human retina where the optic disk and foveal area are marked. This image gives a visual appreciation of the size of the fovea to the rest of the retina. [225]**.** (c) fmERG response generated sue to long stimulus duration where the ON and OFF responses, as well as the PHNR and OPs, are visible. Low signal levels of such responses would mean low SNR and hence require long test durations for any meaningful results[41].

Obtaining focal ERGs from several locations on the retina is possible but extremely time consuming if performed sequentially. This, together with signal variability in between consecutive sessions, makes any comparisons difficult. Clinical focal ERG is, therefore, an unattractive strategy for most workers in the field[54]. Also, the effect of background noise on the signal of interest is to modify it in a way that depends on the statistical properties of both signal and noise (such as their probability density function). One must identify a signal buried in noise that is not detectable using conventional signal processing methods. For repetitive signals, the length of time that observations must be made is

significant. On the other hand, as SNR increases, the probability of signal detection increases, resulting in a reduced error in implicit time and amplitude measurements.

Various specific ERG techniques have been and are being developed to enhance the response function of various retinal networks, such as rod and cone pathways. These include adjusting background illumination, stimulus intensity, stimulus spectrum and rate of application of the stimulus. For example, rods are most sensitive at low background illumination and function at low frequencies (up to approximately 17-18 Hz). Whereas cones best function under the photopic conditions and high flicker frequencies of up to 80-90 Hz (although research experiments at flicker frequencies as high as 200 Hz[232], to unmask nonlinear interactions between different stimulus frequencies, has been performed. These high frequencies are not delivered as a routine clinical tool). Although these techniques enhance the signal of interest in the recording, however, they will not result in a reduction in the inherent ERG noise. As such, if robust measurements of amplitudes and implicit times are to be made one must seek some noise reduction strategy.

2.2.9.2 Multifocal ERG

Solomon W. Golomb (1954) started working with shift register sequences when the most advanced electronics computers still used vacuum tubes. He was particularly interested in formulating the properties of the maximal length, binary, linearly recurring sequences (termed m-sequences for short by Neal Zierler) (1959)[233]. Neal noted the remarkable properties of m-sequences, such as their, pseudo-randomness, periodicity and autocorrelation properties and viewed the subject from a purely mathematical standpoint. Later, these properties made m-sequences extremely useful in applications in communication systems, making use of the direct sequence spread spectrum, and form the basis of Code Division Multiple Access (CDMA) technology, allowing multiple signals to occupy a single transmission channel without interference and hence optimising the use of available bandwidth. Golomb formulated the properties of m-sequences and discussed shift registers with nonlinear feedback in his publication in 1967[234].

The use of Pseudo-Random Binary Sequences (PRBS) in the field of electroretinography was pioneered by Fricker and Sanders (1974)[235]. Their primary interest was to improve the signal to noise ratio compared to the conventional photopic ERG by using cross-correlation methods, allowing shorter test durations and/or improving the statistical significance of the estimate of ERG amplitudes and implicit times. Figure 2.15.a and (b)[235] show their experimental setup and the probability distribution of inter-flash intervals in milliseconds, respectively.

From an engineering perspective, the setup of Fricker and Sanders allowed characterisation of the retina as a Single Input, Single Output control system (SISO). That is, the response from a single area of the retina (calculated through pupil diameter and distance of the flash tube from the subject eye) is collected using a single stimulation source. Eric Sutter patented[236] (July 1989) the use of m-sequences in conjunction with ERG as a Multi-Input, Single-Output control system (MISO)[54] and created the electrodiagnostic system VERIS, see figure 2.15.c.

mfERG is an objective, non-invasive assessment which allows for simultaneous collection of responses from several locations of the retina using m-sequences to steer the stimuli[237]. The responses are confined to a single recording channel. Sutter developed a fast algorithm termed the Fast Walsh Transform (FWT) and published the result in 1991[42]. His algorithm allows for the reduction of data analysis to a single cross-correlation between the retinal response and the governing m-sequence to recover all localised data. This significantly reduced the required computational processing time, which was limited due to the technology available at the time. The mathematical extraction is only valid if the temporal modulation of different areas is carefully selected, and only then it allows for independent or orthogonal stimulation locations.

(a)

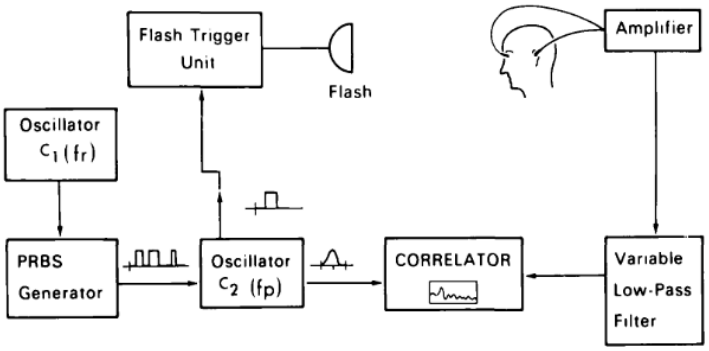

(b)

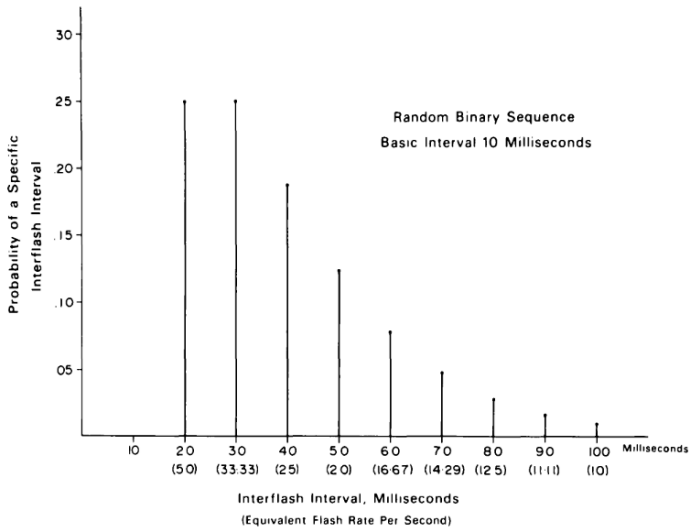

(c)

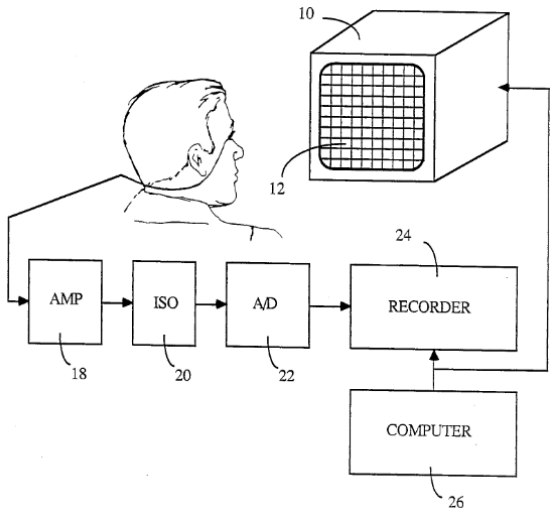

Figure 2.15. Illustration of the block diagram for the system set up by Fricker and Sanders (1974)[235]. The patient was dilated, and a cotton wick electrode was used as an active electrode. Grass PS22 stimulator was used to deliver the flashes at a distance from the subject's eye. The flashes were triggered using the flash trigger pulses generated from the rising edge of the waveform output of the PRBS generator. The "*basic*" frequency of 100 Hz was adjusted although this was variable and not fixed. The cross-correlation was carried for 65.5 seconds equating to 1640 averages per the probability distribution of inter-flash intervals of (b). (c) Image taken from Eric Sutter's patent in 1989, demonstrating an array of controllable elements (he used 256 elements in his initial work although more resolution could be obtained if needed) activated and governed by m-sequences. These sequences are then used through the use of cross-correlation technique to extract the regional responses accordingly[236].

2.2.9.3 mfERG from an engineering perspective

From an engineering perspective, the human visual function is inhomogeneous. Reid and Victor et al[238] described the visual receptive field as a functional transform of a visual stimulus (that varies in both space and time), to a time-varying neural output (referred to as system output or response). mfERG characterises this visual system. Denoting the time-varying response as $y(t)$, and visual stimulus by S which is a function of the spatial plane represented by (x, y) and temporal axis, t, the transformation can be written as: $S(x, y, t) \rightarrow y(t)$. The neural response, which contains encoded spatiotemporal information, recorded and digitised post-filtering and amplification, forming a discrete-time series represented by $y(n)$. The Retina, like most other biological systems is nonlinear, and as described by Korenberg and Hunter[239], one can propose an appropriate nonlinear model to describe the system's response to a restricted class of inputs. Wiener's orthogonal functional series[240] is one such model. It allows for system identification by estimating the kernels in the functional series and is shown to be capable of characterising the overall dynamics of the retinal sensory system. Provided that the time-invariance property of the retina is maintained, one can use the generated kernels to implement a filter allowing for accurate system modelling and implementation (see figure 2.16)[241].

Sutter's original mfERG protocol had an array of 241 elements, subtending a minimum retinal visual angle of 7^{o}, governed through an m-sequence of length 65,535 at a fast frame rate of 67 Hz (without the use of any filler frames). The examination was broken into 32 sessions (of approximately 30 seconds each) to avoid patient fatigue. The clinical stimulus resolution most used, consists of 103 hexagonal elements. Widefield stimulation was first performed in Glasgow and reported by Keating and Parks et al (2000)[57], where Digital Polysilicon devices were used to generate a 61 hexagonal element display spanning a stimulation field of 120^{o}. In Liverpool eye clinic, a CRT monitor is used to display 19 hexagonal elements running at a base-period of 83 ms using short binary sequences of length 511. Hagan, Brown et al (2006) demonstrated that all mathematical requirements for a reliable mfERG can still be met using short m-sequences, although the effective SNR will suffer compared to use of longer sequences[49].

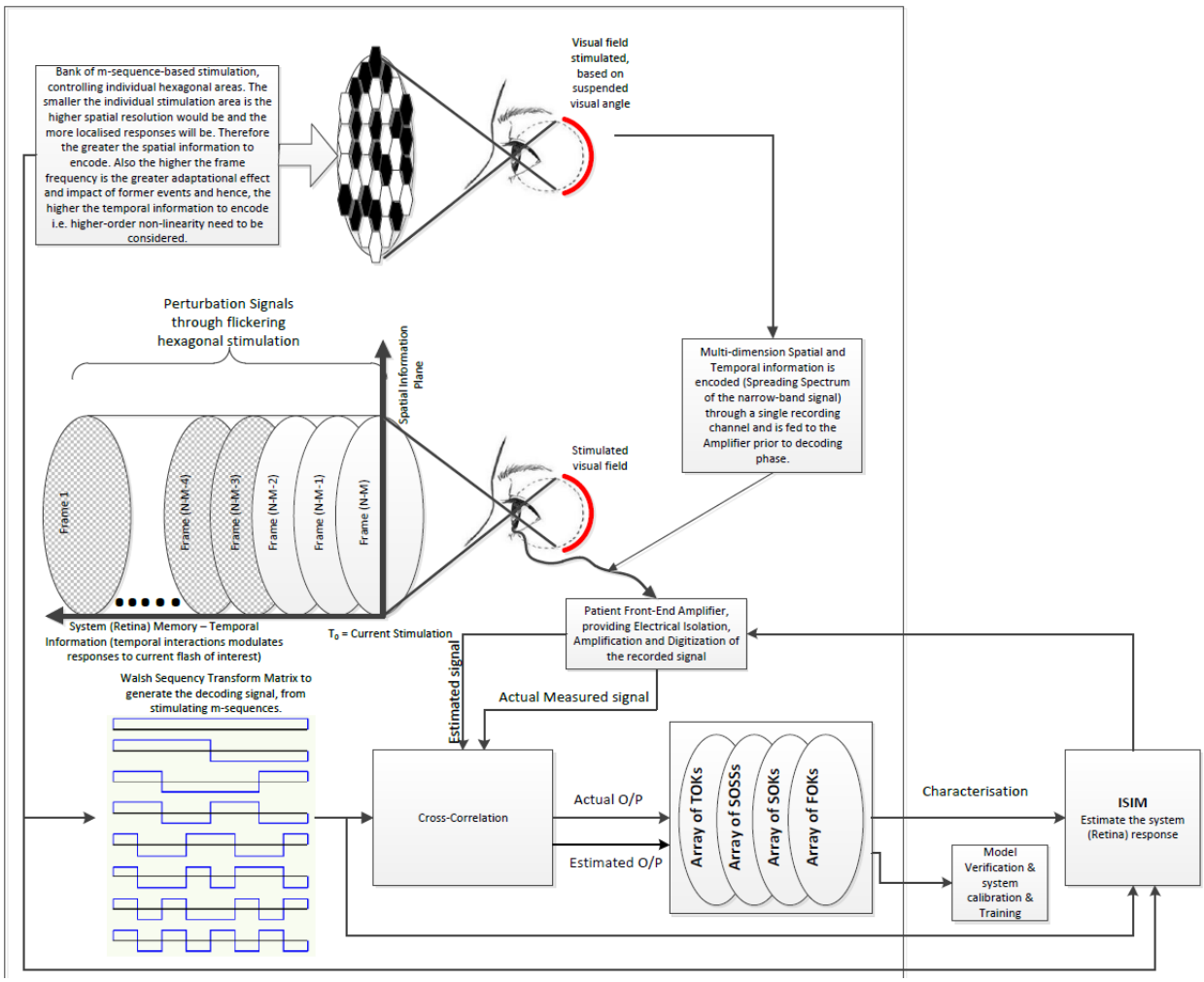

Figure 2.16. Illustration of coding the localised retinal responses and decoding of the record using m-sequences. This figure also illustrates how ISIM could be used to calibrate and improve our understanding of the recording data acquisition system.

2.2.9.4 Major sources of variability in mfERG

The two most common causes of interference and errors in interpreting the mfERG results are unsteady fixation[242][46] and signal contamination due to blinks and eye movement. Stable fixation varies considerably in normal sighted people and even more in patients suffering from macular pathologies (such as AMD) and Stargardt disease[243]. These patients tend to use their peripheral regions for fixation; therefore mfERG records must be treated with care in such cases [244]. Other recent experiments on fixation stability in patients with AMD found that steadier fixation is expected under binocular conditions[245]. It is reported that the duration of 30 seconds to one minute for subjects fixating on a target image could put the fixation system (gaze control mechanism[246]) under stress[247]. In a study by Russo and Pitzalis et al (2003)[248], a group of high calibre elite shooters were compared with a control group of normal subjects to objectively assess any significant difference between these two groups with regards to fixation stability and saccadic latency. The study protocol included a fixation on a stable target alone (standard condition) or fixation on the same target but when distracters were flashed in the parafoveal region. The result of this study for one professional shooter and one control subject is shown in figure 2.17. The effect of the shape of the fixation target was also investigated and one such study found that a cross-hair target is most effective in experiments requiring stable fixation for 17 seconds[47]. Other studies tried to quantify the fixation deviation due to slow drifts and resetting microsaccades and found this to be in the range of 0.1-0.2° of visual angle[249]. This puts a limit to the highest possible resolution of mfERG element sizes and therefore, the visual angle subtended. Keating et al[250] investigated

the effect of the complex multifocal flicker stimulus on fixation quality and tried to quantify this effect. They found 2.4° to be the upper-resolution threshold for stimuli where the fixation quality is adequate for the purpose of mfERG examination, and any higher resolution would be more susceptible to fixation fluctuations during the recording process. Chu and Chan et al[46] concluded that the effect of unsteady fixation is negligible as long as fixation is maintained within the central hexagon. They found that the FOK responses are significantly impacted if the amplitude of unsteady fixation increases beyond 4° where the central hexagonal area subtended an angle of 2.4° and hexagon in ring 3 (the middle ring) subtended an angle of 4°.

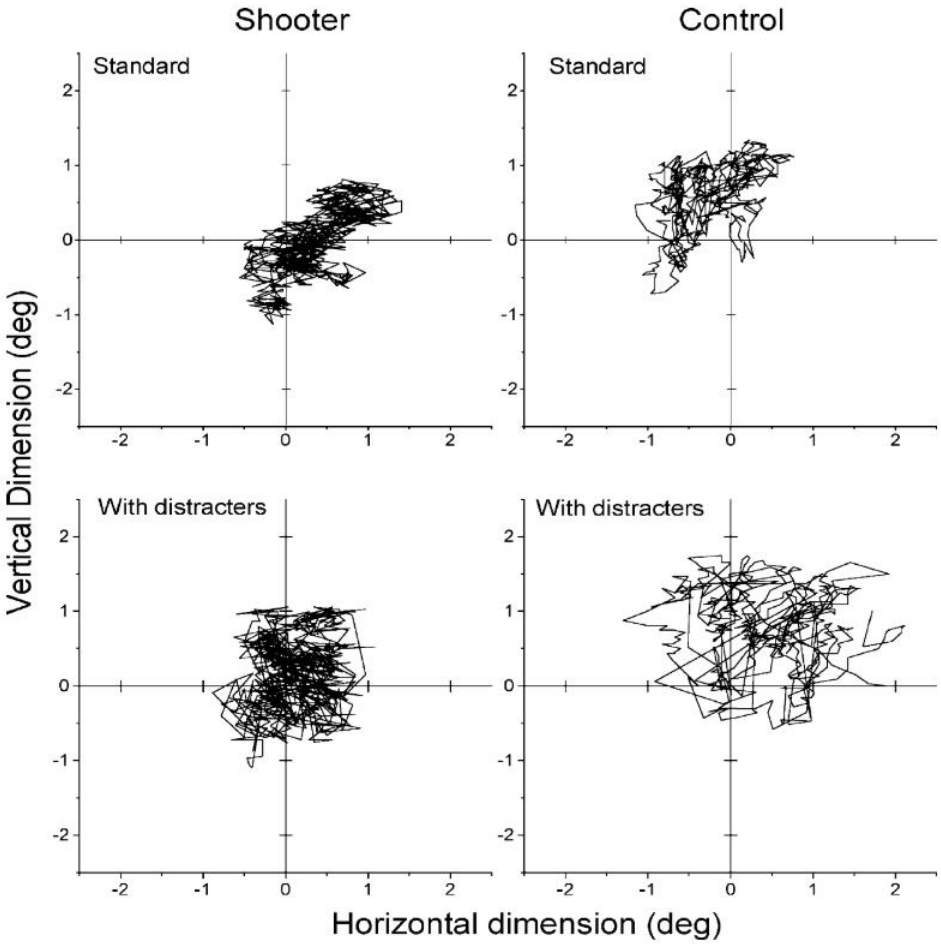

Figure 2.17. Eye position during one-minute fixation for an elite shooter and a normal control subject under the standard condition and when distracters are present to the parafoveal region[248].

Eric Sutter and Charlotte Poloschek published the result of stimulation of an array of 509 elements in 2002 in an attempt to determine the extent to which mfERG is capable of showing fine anatomical and physiological details which could be attributed to response variability across the human retina (see figure 2.18)[55]. This was the first time such high spatial resolution was attempted, pushing the recording time to one hour. They proposed that some of the peaks and valleys in the response array may be due to relative angioscotomata and others are may be due to local differences in the physiological and anatomical properties of the retina. To date, no concrete study conclusively demonstrates any meaningful clinical outcome can be achieved by using such high resolutions and recording times.

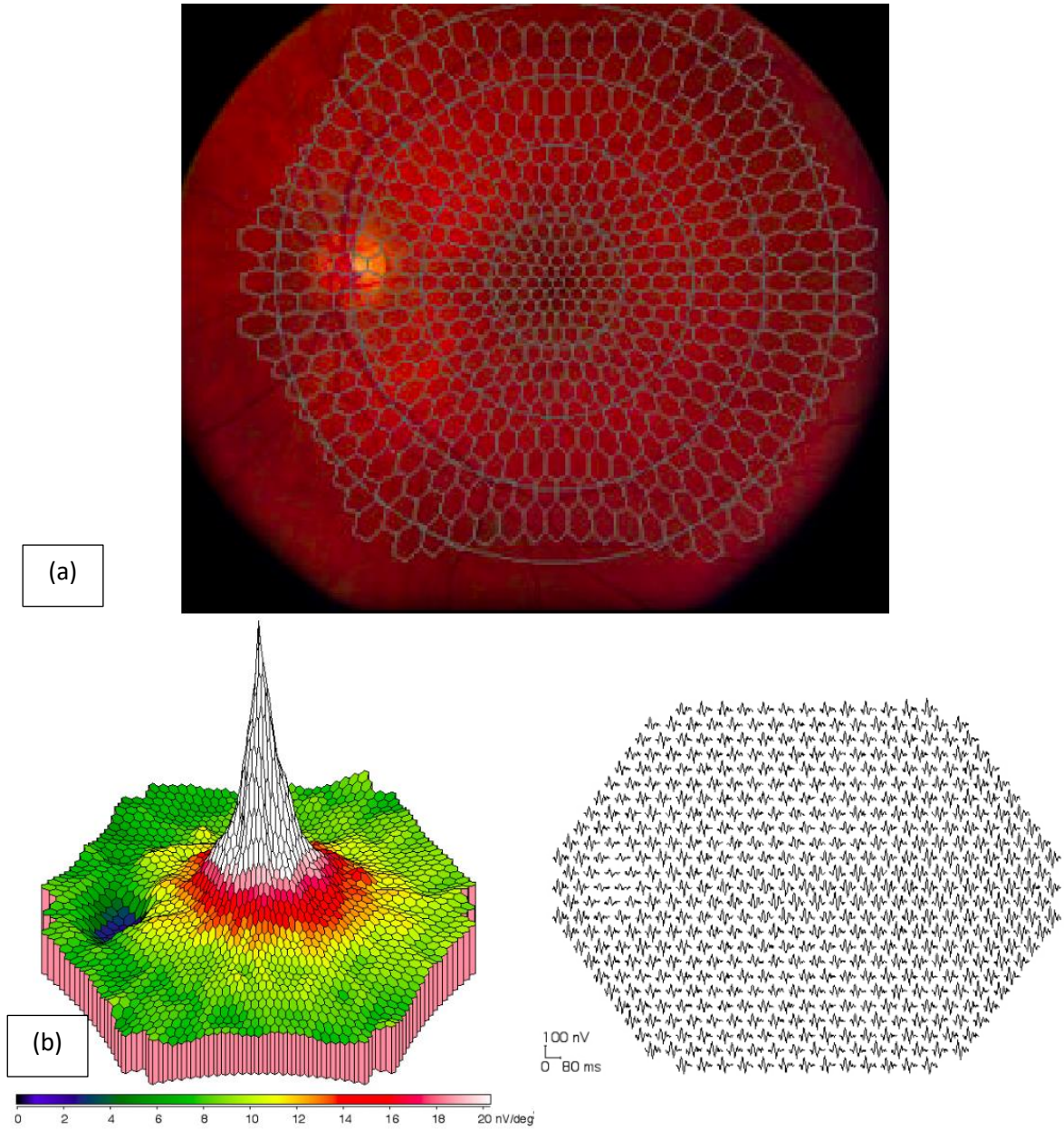

Figure 2.18. (a) The stimulus array of 509 elements superimposed on fundus image of a normal test subject, where the diameter of the elements is increased from 0.8° (approaching fixation limit) at the centre of the field to 2.8° at the peripheral area. Such variation in stimulating area is to ensure a constant SNR across all stimulating patches. (b) First-order kernel response density function together with the response array of the same test subject to a binary stimulating trigger. A white flash corresponds to an intensity of 8 cd.sm^{-2}. The rate of screen update was adjusted to 75 Hz that is every 13.33 ms, and the total recording lasted about one hour. The subject was under photopic condition, dilated and anaesthetised before fitting Burian-Allen contact lens electrodes. The signal was amplified by a factor of 5000 and band-passed filtered at 10-300 Hz and sampled at 1.2 kHz.

2.2.9.5 Relations between mfERG and full-field ERG

The mfERG responses are not the actual potential responses from the retina but rather are mathematical extractions from the recorded waveform. Kondo and Miyake et al (1995)[251] and Hood and Seiple et al (1996)[252] compared the components of the mfERG with those of the conventional full-field ERG. Their work was a significant step for mfERG, as their reports demonstrated that the underlying waveforms were similar to full-field ERG when the stimulation rate, contrast and luminance were adequately adjusted. Kondo confirmed that the mfERG can be used at the clinical level for electroretinography field mapping (what Sutter termed "*ERG*

topography" in his original paper). At the time of his report, the origin of various components of the ERG was not well understood. Therefore, a direct comparison with that of full-field ERG waveform, could not conclude if the components of the "*first negative deflection*" (also termed N1) and "*second positive deflection*" (termed P1) were of the same neural origin as that of the well understood a- and b-waves of the ERG (full field or focal). Hood et al, further investigated the mfERG at various rates (through the addition of filler frames) altering the background luminance. Their main objective was to determine the operating conditions of the mfERG test protocol to try and reconcile the mfERG response to the response from the conventional photopic ERG obtained in compliance with ISCEV standards (see figure 2.19[252]). He then concluded that "*there is a surprisingly good correspondence between the components of mfERG and full-field ERG with the slowest frame rate of 7F, the multifocal component being the same as those compromising the full-field ERG*". He also concluded that N1 corresponds to a-wave, and P1 corresponds to b-wave of the full-field ERG.

Wu and Sutter (1995)[253] further investigated the mfERG, with the goal of better recovery of the Oscillatory Potentials (termed mOPs) through slowing down the stimulation rate by introducing blank filler frames between the stimulation frames. Bearse and Sutter et al (2000)[254] further investigated the oscillatory potentials in both the first and second-order kernels of the mfERG response using a slow mfERG stimulation paradigm. They found these recovered components in both kernel arrays to be similar to those of the conventional OPs (obtained using Ganzfeld and focal ERG stimulation).

Since the introduction of m-sequences into the field of visual electrophysiology, various other protocols have been implemented to isolate specific pathways. Kondo and Yozo (2000)[255] developed the technique of using long-duration mfERG stimuli to identify localised cone, ON and OFF responses and provided the clinical significance of this testing. They showed that the OFF response increased with eccentricity when within a visual field of 60^{o} and plotted a topographical density map of both ON and OFF responses.

Tan and Kondo (2001)[256] used an optimised mfERG technique to assess the pupillary light response fo various locations on the retina through the optic tract. They found the mfERG method to be useful due to its high SNR, ability to operate under photopic condition (minimising the effect of light scatter), short test duration (reducing the impact of fatigue) and allowing the investigation of the temporal factors.

The mfERG recording is most frequently performed at high rates, causing the overlap of responses as there is not enough time for a complete response recovery from preceding stimulation steps. The increased nonlinearity makes it challenging to interpret the data obtained. Mathematically, it is possible to reconstruct the original waveform provided all nonlinear kernels are available, i.e.it is possible to restore the original waveform using the respective kernels and their slices. Keating and Parks (2002)[257], performed mfERG experiments at 77 Hz (a base-period of 13 ms) intending to provide greater insight into the second-order kernel (SOK) of the human retina. They developed their own (now commercially available under the brand name of Kelvin Vision) LED-based stimulator. This development provided the opportunity to perform a true simultaneous stimulation across the visual field that does not suffer from any scan delay compared to the CRT monitors. A comprehensive study by Matsumoto and Shinoda et al (2014) examined CRT, OLED and LCD screen stimulators and found the elicited mfERGs using CRTs and OLEDs are comparable. The evoked responses using LCDs are significantly different in both P1 amplitude and implicit time to, those obtained using OLED or CRT monitors.[258]. Keating developed the required software to perform what he called "*selective cross-correlation*" to recover waveforms of different slices of the SOK (see figure 2.20). Hagan and Brown et al (2011)[50] investigated the effect of stimulation rate on the higher-order kernels (HOKs) using a single (central) hexagonal element (subtending a visual angle of 8^{o}) stimulated using an m-sequence of length 511. A 60 Hz, CRT monitor, was used with an

appropriate number of filler frames (FF) to control the rate of stimulation. They found that at 4FF or slower stimulation rate, the higher-order kernels could not be detected above the noise level.

Both data from Keating and Hagan suggest that the impact of higher-order kernels on the first-order kernel are not statistically significant when a base-period of approximately 65 ms or higher is used. This is an interesting finding across these two independent studies. Hagan currently runs his clinic using a base-period of 83 ms, allowing the retina to "fully" recover before the next stimulation step.

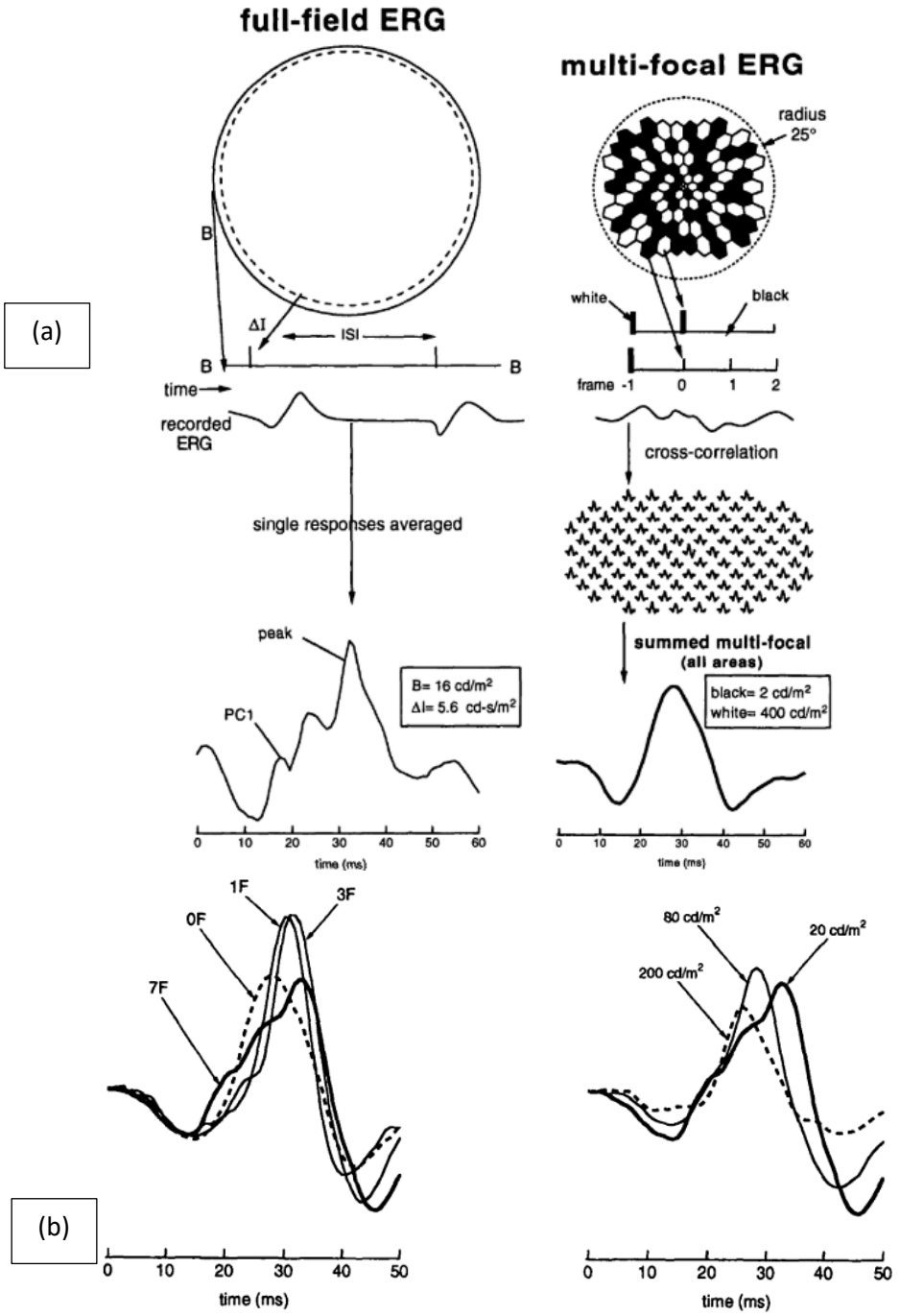

Figure 2.19. (a) The strategy selected by Hood et al for comparison of full-field and mfERG summed responses. (b) Left: Results of the comparison for various mfERG stimulation rate (slowest = 7F) while the luminance and contrast were kept at the same level. Right: summed responses of the mfERG for the frame rate of 7F at various background illumination.[252]

Sequence	Effective frequency	Number of occurrences
1-1	77	8192
1-0-1	38.5	4096
1-0-0-1	25.5	2048
1-0-0-0-1	19	1024
1-0-0-0-0-1	15.5	512
1-0-0-0-0-0-1	13	256
1-0-0-0-0-0-0-1	11	128

(a)

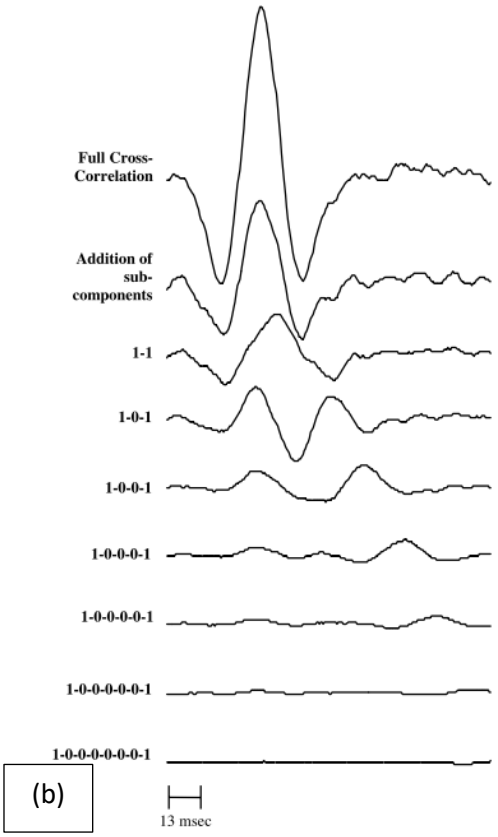

(b)

Figure 2.20. (a) The calculated number of occurrences of specific pulse trains and the associated effective frequency of these occurrences. The first row in (a) is the first slice of SOK, the second is the SOSS (Second Order Second Slice), the third is the third slice of the second-order kernel and so on. (b) Illustrates the extracted slices of the second-order kernel through performing the selective cross-correlation. The calibration axis demonstrates the base-period of 13 ms, corresponding to a frame rate of 77 Hz. Such high frame rate allows an increased level of nonlinearity in the recorded waveform and as such the impact of previous flashes on the flash of interest becomes more and more pronounced. From (a) one can see that the SNR is reducing for higher-order nonlinearities as the number of occurrences of the specific pulse trains reduces.[257]

2.2.10 Need for calibration, quality assurance, standardisation

The discussion to this point demonstrated many sources of potential variation in human ERG and mfERG recordings, such as luminance, contrast, adaptation state, pupil size, and refractive errors. Controlling and standardising these factors across different laboratories would result in better reproducibility with time and between different instruments.

Since the introduction of mfERG as a clinical technique, various multifocal ERG systems have been developed and are currently in use in different centres. The first such system was the VERIS, created by Sutter in 1989. Roland created RETIscan within Europe using m-sequences with an added correction term allowing the exploitation of the mfERG technique without infringing on Sutter's patent.

The signals recorded vary between systems due to the differences in features such as filtering, amplification, sampling, averaging, artefact rejection, stimuli, etc. Bock et al (1999)[63] compared the VERIS and RETIscan systems and found that with the manufacturer's standard parameters, the two systems gave different topographical response array, specifically with regards to the P1 amplitudes. He further showed a significant reduction in differences between the response arrays when the required parameters are adjusted. They confirmed that the m-seqeunce-timing, sampling rate are the main parameters that need to be adjusted to obtain similar results. They also confirmed that it is not possible to truly compare these systems together based on many other factors that impact the variability of recordings.

The reproducibility of the mfERG within the same and different sessions on normal subjects are studied in [75][259][76] using a variety of systems and protocols. It is shown that the inter- and intra-session and subject variability can potentially mask the effects of some of the differences between various recording systems. Therefore, limiting the ability to compare instrument variations. The few system comparison studies carried out by the date of this publication, are of limited use due to variations in external sources (such as electromagnetic coupling) and, study design. This can impede the comparability and effectiveness of combining data in longitudinal and multicentre

studies that use more than one recording instruments or different versions of the same instrument. Transferability of patient data across the boundaries of clinical centres is also limited.[260]

Various signal processing methods and techniques in both the time and frequency domains [261][262][263] such as Fourier Analysis, Principal Component Analysis[264] and, Wavelet Analysis[265][266] are proposed to extract the signal of interest from the background noise. This aids the clinician in distinguishing pathological traces from healthy ones[267]. Utilising effective signal processing techniques will not only improve the speed of ERG recognition, especially when automated but also help to objectify the identification of pathologies and reduce the rate of false positives and negatives in the clinical setting[268].

Improving the SNR post-examination using area averaging in mfERG is a common and useful technique that results in improved repeatability, for example, ring and quadrant averages (see figure 1.5) are shown to be more repeatable than local response measurements [269][59]. It is worth noting that scaling of the hexagonal stimulation area with eccentricity (distance from the foveal region) is performed to ensure similar SNRs from all stimulated areas. Similar SNRs facilitate clinical judgment based on a mfERG trace array. This scaling is also called the "*stretch factor (SF)*" and was studied by Poloschek and Bach (2009)[53] as a method of compensating for the cone density changes with eccentricity, see figure 2.14.a. The variation in cone density is minimal at approximately 8^{o} of visual angle. In the paper, of Poloschek and Vach, it is suggested the SF should be adjusted for each clinical setting depending on the spatial resolution and subtended angle of stimulation, using ring averages to compensate for local variability of mfERG responses. They also found that variability in recording with the same SF across subjects is relatively high, due to inter-subject variation in cone density.

Adjusting the scaling factor is not available on all commercially available multifocal stimulator systems. The Kelvin Vision Multifocal Stimulator (MFS) is a LED-based stimulation device with a fixed number of hexagons (61) and a fixed number of rings (5), pre-scaled with eccentricity in terms of element area[257]. In collaboration with NHS Greater Glasgow and Clyde, the author had access to this stimulator in 2012 and performed calculations of its ring ratios and scaling factor (see figure 2.21).

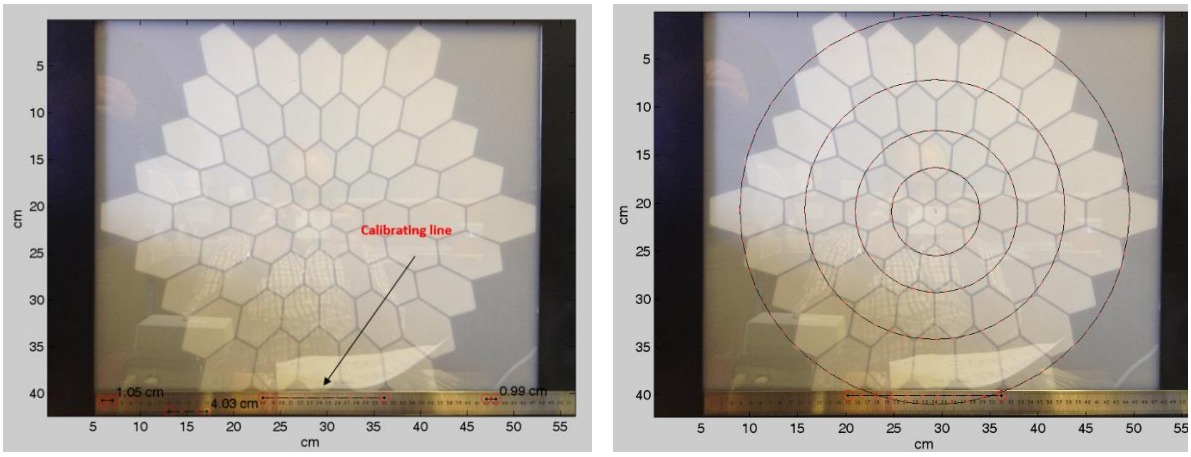

Average Hexagonal Area within each ring (cm^2)				
Ring1	Ring 2	Ring 3	Ring 4	Ring 5
4.4	6.9	12.3	18.2	26.4
Ring Radius measurement (cm)				
Ring1	Ring2	Ring3	Ring4	Ring5
1.23	4.77	8.46	13.55	20.32
Ring area calculation (cm^2)				
Ring1	Ring2	Ring3	Ring4	Ring5
5	67	153	352	720

Figure 2.21. An image of the LED-based MFS along a calibrating ruler. The ruler is used to create the calibration axis when imported into a developed MATLAB software application. The application allowed for the calculation of hexagonal area, ring area and ultimately the scaling factor as illustrated in the table in this figure.

Other filtering methods such as an adaptive neural network (ANN) filters with nonlinear transfer functions have also been studied as methods of enhancing SNR[270]. ANN has been introduced as a learning tool to support clinical decision-making processes since 1959, where Ledley and Lusted[271] mathematically formulated the clinicians understanding of "*the reasoning process*" of medical diagnosis. It was not until the early 1990s that ANN became a routine tool in clinical practice, thanks to further advances in computer science and technology. This is evident from the increased number of patents in the United States granted in biomedical science with a significant contribution in computational intelligence (amounting to 50% of the total number of granted biomedical patents between 1990 to 2000)[272]. The successful implementation of ANN requires that the nonlinear characteristics of the filter match the nonlinear behaviour of the signal[273].

2.2.11 Need for training

The required level of expertise and training in this field should not be underestimated and has been recognised as a key factor since the beginning of electroretinography. Experience in the field of neurophysiology and extensive practice in identifying tiny signal components is useful when it comes to accurate diagnosis, as suggested by Wright and Nilsson (2008)[268]. They modified data obtained from control (normal) groups to simulate the presence of disease (but did not change the waveform morphology). Next, they used three automated scoring templates and human experts, to score the performance (sensitivity and specificity) of all methods in identifying signal in the modified mfERG trace map. They found that prior knowledge of the expected effect of a disease process could increase the sensitivity. This suggests that a fully automated process may not always accurately inform the investigator and could not be used as a generalisation for all types of pathologies. Advances in the logical analysis of medical diagnosis and mathematically mapping the diagnosis process are only an aid to the clinician and cannot take over the investigator's duties. Indeed, such

advances can imply more burden on the investigator to extend their knowledge and gain experience with novel techniques and methodologies.

2.2.12 Birth of ISCEV

The international organisation for electroretinography was founded in 1958 with the mandate to regulate the ERG. Its objective was to "*establish norms for instrumentation, recording, procedure, and measurement in clinical electroretinography*"[274]. The first symposium of the ISCERG (International Society for Clinical Electroretinography), later called ISCEV (International Society for Clinical Electrophysiology), was held in Stockholm in 1961 and focused on ERG standardisation. Van der Tweel (1962)[275] published a report on this meeting and compiled a set of proposals and recommendations for the international community. Tweel started his report with the statement that "*ERG work belongs to the technique of signal analysis*"[275]. From an engineering perspective, the retina is a complex nonlinear system. Different retinal responses are elicited depending on the characteristics of the input light stimulus. An exhaustive study is difficult as it contains a large number of different control systems. Therefore, the retina cannot easily be characterised as a single mathematical model.

Tweel initiated the first structured and fundamental discussion of light stimulus in clinical ERG. He published a much more detailed and specific report in 1981[276] on instrumentation, recording parameters and procedures for clinical electrophysiology of vision, in agreement with both the ISCEV and International Council of Ophthalmology. The EEG instrumentation standards published through the International Federation of Societies for EEG and Clinical Neurophysiology (1977)[277] is the precursor to Tweel's 1981 report for the committee on instrumentation and procedures in visual electrophysiology. Tweel suggested that his latest report should be viewed as a guideline and minimal requirements for electrophysiology of vision (ERG, VEP and EOG) instrumentation as well as an agreement on methods and terminology in clinical ERG, VEP and EOG. The first ISCEV guideline for ERG was published in 1989[274], followed by updates in 1994[278], 1999[279], 2004[280], 2008, and in 2015[105]. The ISCEV now provides standards and guidelines on ERG, mfERG, EOG, PERG, VEP, Calibration and Recording as well as extended protocols for the Photopic Negative Response (PhNR), dark-adapted and red flash ERG and photopic ON-OFF responses. The calibration and recording standards were last updated in 2003[281], though draft guidelines are now in circulation for 2019. The author of this thesis asked why the calibration standard has not been updated since 2003 and what are the upcoming changes to this standard, through email communication with professor Michael Bach (ISCEV director International Communication). The response to this query was that "*the changes to calibration standard would not be major and will be more specific. Calibration guidelines do not need regular update since the physical laws in the field of visual electrodiagnostic do not change. In contrast to other guidelines, the (patho)physiological understanding progresses and changes more rapidly as technology improves and new techniques become available*".

The importance of accurate calibration of visual electrodiagnostic instruments cannot be overestimated. It is a mandatory requirement of many national and international standards and regulatory bodies (such as the US FDA and ISO13485) and has been discussed in [282][281]. The ISCEV calibration standard does not go into much details on the calibration of the acquisition system. It requires a simple calibrated benchtop signal generator that can produce a low amplitude (1 µV to 1 mV) periodic signal with wide enough frequency bandwidth to allow it to be adjusted beyond the low and high pass corner frequencies of the diagnostic system. It is noted that ISCEV requirements are the bare minimum which one needs to follow and are intended as guidance for beginners in the field. Most centres and manufacturers state that their implementation meets and exceeds ISCEV standards. The calibration standard also states a minimum of one year as the calibration interval.

Ding and Liu et al (2017)[283] proposed and implemented a system (see figure 2.22) to simulate "*human electrophysiological activities*" as a high precision calibration device. This paper was

published well after the author of this thesis presented ISIM at national (BriSCEV, 2014[284]) and international (ISCEV, 2014[285] and 2015[286][287] and later in 2018[288]) gatherings. The author of this thesis won the 2014 Marmor award for clinical innovation in visual electrophysiology serving ISCEV and clinical electrophysiology by encouraging new work that improved electrophysiology test practicality and clinical applicability[284]. The initial award granted in 2014 is made as ISIM was concluded as a promising project that can potentially add significant clinical value. The author of this thesis also claimed the follow-up award in 2016[289] demonstrating that the preliminary work had successfully translated into clinical value.

Ding et al[283] also claimed that their system could be used for calibration of other electrophysiological activities such as ECG, EEG, EMG etc. It should be mentioned that no specifics are given on how the presented system could adjust and handle parameters such as dynamic range when used to simulate human electrophysiological activities. It is also stated that the signal generator (see figure 2.22) is capable of producing waveforms in the amplitude range of 1 µV to 1 mV, with a latency of 10 ms to 100 ms over a frequency range of 1 Hz to approximately 1000 Hz for both trigger and continuous modes of operation. The memory capacity of the system, together with methods of accessing it for device parameter settings and waveform manipulation, are not discussed.

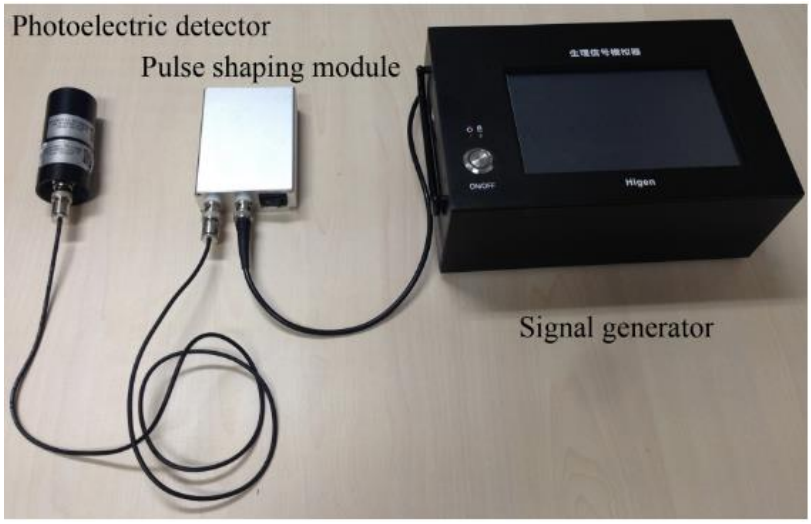

Figure 2.22. A proposed system for calibration of visual electrodiagnostic instruments by Ding and Liu et al [283].

The primary aim of ISCEV is now shifted to extend the knowledge of clinical and research electrophysiology of vision through the promotion of collaboration and better communication between co-workers in this field. The standards also seek true comparability of retinal responses over time and place as well as providing a beginner in the field with a starting point in terms of best practice. The standards also recommend that each clinic must establish a normal database per age group per response type to enable determination of any pathological variations from the centre's reference point.

2.3 The state-of-the-art in visual electrophysiology

All neural recordings and stimulation involve design trade-offs amongst several factors, including, spatial resolution, temporal resolution, degree of invasiveness and optimisation for electrical potential recording and stimulation. An optimal system is one that provides the best performance in all mentioned areas. The state-of-the-art in today's electrophysiology is specifically accelerated through advances in miniaturisation technology (this is due to advances in electronics, microfabrication techniques, nanotechnology, materials and sensing technologies).

Multi Electrodes Arrays (MEA) allow for parallel electrical response recording of retinal layers to presented visual stimuli. The local changes in the retina are essential in studying the degenerative processes which are masked by the mass response in full-field ERG recording. The focal and mfERG techniques could be used in animal studies to define local changes in disease processes, but the challenge of maintained focus could result in misleading data. The MEA electrodes can contain thousands of microelectrodes allowing for single neural characterisation of the detached retinal layer[290], see figure 2.23. The usefulness of the MEA for recording ex vivo micro ERGs was studied by Fuji and Sunagawa et al (2016)[291] in isolated mouse retinas. They used biological antagonists and blockers to further investigate the neural origins of a- and b-wave of the micro ERGs.

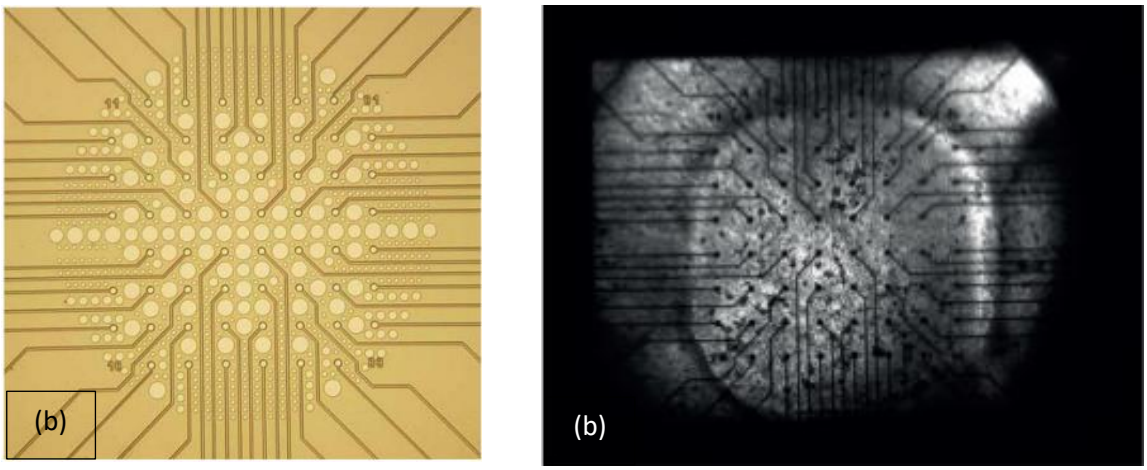

Figure 2.23. (a) transparent, perforated Multi-Electrode Arrays (pMEAs) implemented with 60 Titanium nitride electrodes with 200 um electrode distance and 30 um electrode diameters, ensuring high SNR and maintained supply of oxygen and nutrition to the ganglion cells in the detached retina. (b) A detached retina is placed on the electrodes where all electrodes are visible, and retina is checked to ensure it is not torn, does not have any holes; it is flat and homogeneous. [290]

Advances in miniaturised electrodes have allowed the introduction of multi-electrode arrays on soft contact lenses to perform non-invasive and simultaneous spatial characterisation in the ERG across the cornea in response to flash stimuli [292], see figure 2.24. These spatial differences have been discussed previously in section 1.3. Differences in spatial ERG are due to variations in the impedance between current sources and sinks, which are developed when flashes of light are presented to the eye. The current source, current sink and impedance result in generated electric dipole fields that extend radially away from the retina to the cornea. The conventional ERG electrode would register the sum of all these electrical dipoles in a single potential recording. This is the case whether the stimulus is presented globally or locally using the mfERG technique. The sum of these potentials extends to the extraocular tissues where they can still be recorded using skin electrodes at reduced SNR.

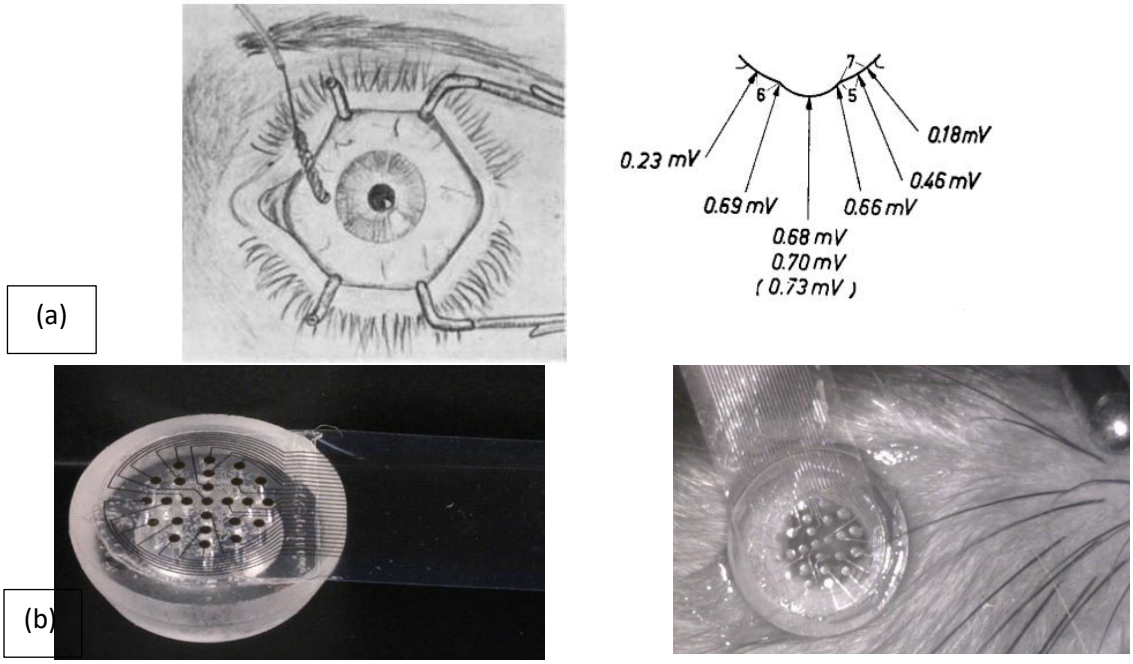

Figure 2.24. (a) Sundmark (1958-1959) attempt to characterise the impact of b-wave potential at various corneal positions using Cotton wick electrode on human subjects.[293] (b) First attempt (since Sundmark's during the late 1950s) to simultaneously measure the topographical distribution of ERG using multi-electrode ERG (meERG) from rat cornea using 25 electrode arrays (2014). The soft contact lens electrode is constructed to ensure that it fits well on the cornea.[292]

In a recent paper by Rongang, Zheng et al (2018) the development and fabrication of a new ocular contact lens electrode with combined optical transparency and softness are discussed, see figure 2.25. The electrode is termed GRACEs (Soft Graphene Contact Lens Electrodes) and was tested in monkeys. It was shown that the SNR was significantly improved compared to the conventional ERG corneal contact lens electrode.

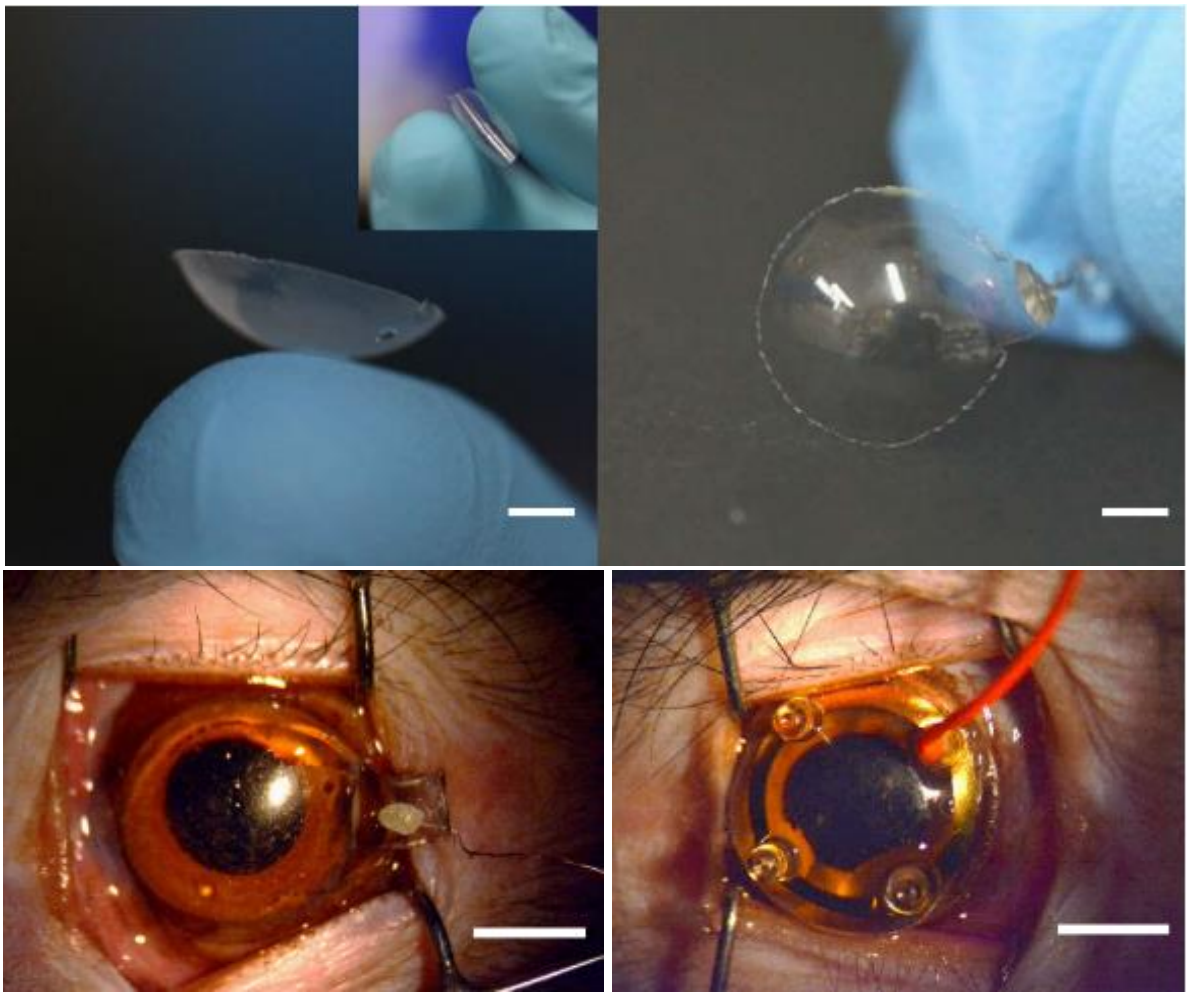

Figure 2.25. Set up of the monkey's eye for full-field ERG and mfERG recordings using GRACE electrode (bottom left) and Jet corneal contact lens electrode (bottom right). The scale white bars in the figures are 5 mm in length.[294]

Advances made in minimally invasive platforms, together with incremental improvement in analytical power enable point of care (POC) diagnostics[295]. Patients may no longer be confined to conventional medical laboratories (e.g. hospitals) for diagnostic testing. This means less costly care could be provided at primary care centres; in the community or the patient's home. Developing contact lens sensors with application in monitoring and diagnostics of ocular disease is one such successful attempt by Google and Novartis, see figure 2.26.a [296]. Wearable devices that allow users to monitor their health at home can provide a continuous record of valuable diagnostic parameters[297].

Another category of devices that can provide POC diagnostics are those laboratory instruments which have been reduced in both size and complexity, so they are now small handheld devices. One such example is the RETeval (LKC Technologies) system (2013)[298] which is the first FDA cleared, ISCEV compliant, completely portable, handheld, full-field flash ERG and VEP testing device (figure 2.26.b). The system is only compatible with its customised skin electrodes (providing integration of active, reference and ground electrodes into a single electrode array strip[299], patent technology, No. 10,010,261, initially filed on Nov. 9, 2016) and has an integrated, age-adjusted normal data set. The reference data were collected through a large randomised study, termed RETeval All Comers Trial or REACT for short. It was performed on normal and abnormal subjects and sponsored by KCL Technologies, Inc. The study was completed in April 2018. The reference data was then integrated into its latest software release 2.8.0. The study included 244 normal subjects in the age range of 4 to

85 years, dilated and un-dilated. RETeval does not require artificial pupil dilation and has a patented algorithm to compensate for pupil size through maintaining a constant retinal illumination (Photopic Td.s) by adjusting the stimulus luminance (Photopic cd.s.m^{-2}) in real-time [300].

Figure 2.26. (a) Contact lens sensor developed by Google and Novartis (called "*smart lens technology*"). This product has an embedded glucose biosensor embedded into a hydrogel matrix that senses the glucose level in the tear and transfers the data wirelessly using the embedded controller and antenna to a nearby computer or phone [296]. Several patents granted to Google, Johnson and Johnson Vision Care Inc and others on continuous monitoring of the tear glucose from 2009 to 2014 [301]. Such a contact lens system cannot currently be used in electroretinography applications. However, with the trend of increasing miniaturisation of devices and systems, it is becoming increasingly possible to make even smaller, multifunctional, higher speed devices that can potentially provide many of the critical features requirements of a laboratory ERG instrumentation. (b) Left: The first handheld system (RETeval LKC Technologies) developed and commercially made available for VEP, ERG and flicker examinations using skin electrodes without the requirement for pupil dilation and administration of anaesthesia. Right: placement of the device sensor strip, the setup requires no skin preparation. The effect of position of this electrode array is investigated by Hobby and Kozareva et al (2018)[299].

Wearable contact lens electrodes with in-built, multi-colour, stimulus and background LED light sources have also been developed and successfully tested on various species. LEDs have many satisfying features that are extremely useful when it comes to electroretinography. These features include rapid ON and OFF responses, high efficiency in energy conversion to light, steady illumination and a much narrower spectral bandwidth than the more conventional light sources. Another advantage of LEDs is their low electromagnetic interference (EMI) emission in comparison with CRT monitors. Teikari and Najjar et al (2012)[302] recently proposed an inexpensive, modular design, USB driven, visual stimulator based on LEDs for vision research. In their prototype, they used

off-the-shelf and open-source components as much as possible, allowing the use of the system by users without advanced electronics expertise. They further measured the EMI emitted from their system and found this to be acceptable for EEG recordings. Integration of LEDs with contact lens electrodes provides a compact and portable configuration, allowing quick setup for ERG recordings [303][304]. The installation, shown in figure 2.27, and 2.28, has the advantage of recording ERGs at the patient's bedside and in remote locations away from hospitals. However, these devices can only provide full-field responses, including flicker. Eye movement and fixation are still a challenge in these systems, with reduced feedback to the investigator on how well the subject is fixing.

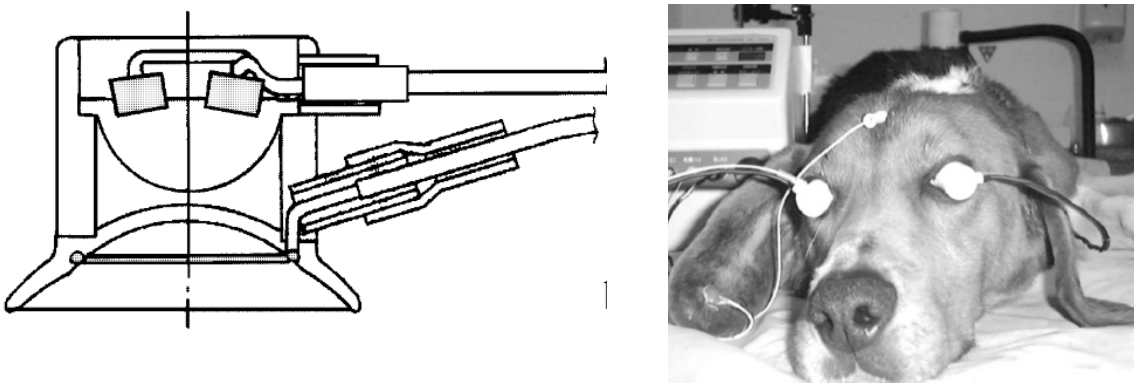

Figure 2.27. Illustration of the LED contact lens electrode as a new and cheap alternative to Ganzfeld dome in veterinary ophthalmology. The setup is used to obtain ERG recording from 15 sedated, healthy beagle dogs. The setup allowed to obtain ERG responses at 12 different intensities including ISCEV SF (Standard Flash, 3.0 cd/m^2/sec) under both photopic and scotopic conditions. Flicker responses, according to ISCEV standards were also performed. [303]

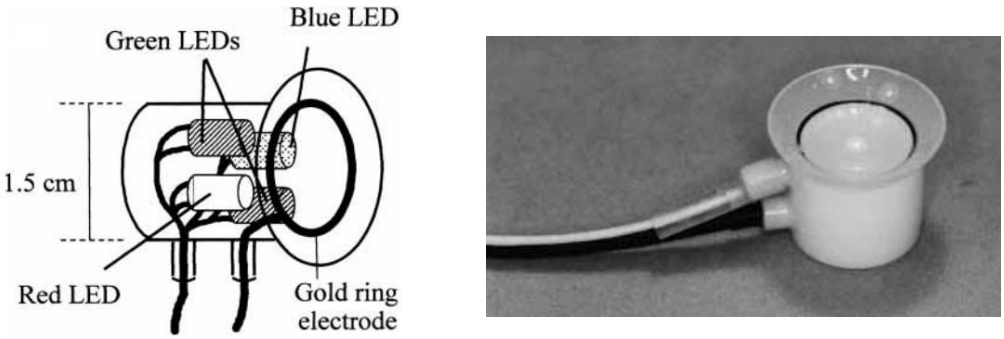

Figure 2.28. Contact lens electrode with four LEDs. These LEDs are the light source for both background and stimulus light. The LEDs are independently controlled using a custom-built power supply unit, and intensities were adjusted per the ISCEV standards. A gold ring electrode mounted on a contact lens is used to record the generated ERG response. The developers of the schema, tested the electrodes on 12 normal subjects and two patients with progressive cone dystrophy to further investigate the ERG parameters. [304]

The development of active electrodes (AEs) and the comparison of their performance with conventional passive electrodes are also investigated by Wong, Yip et al (2018) [305]. They constructed active electrodes using a standard ERG-jet electrode with its cables cut short and soldered directly to the input of an operational amplifier. The amplifier selected is an analogue-to-analogue amplifier. They showed that the SNR is significantly improved by using active electrodes (AEs) and hence, lower stimulation intensities could be used to trigger a response. The disadvantage of AEs in comparison to conventional (e.g. Ag/AgCl, which is the most extensively used electrode in bioelectric recording applications[94]) electrodes is that they are more complex and expensive. However, the traditional electrodes have limitations that prevent their use in wearable applications and POC testing [306]. The AE's robustness to environmental interference [307] (especially that of the line interference at around 50/60 Hz, see figure 2.29[305]) results in reduced inter and intra-session variability and improved reproducibility of the recorded responses. AEs will therefore also

facilitate the recording of ERGs outside the clinical setting (e.g. without the luxury of a Faraday cage) where more significant interference could be expected.

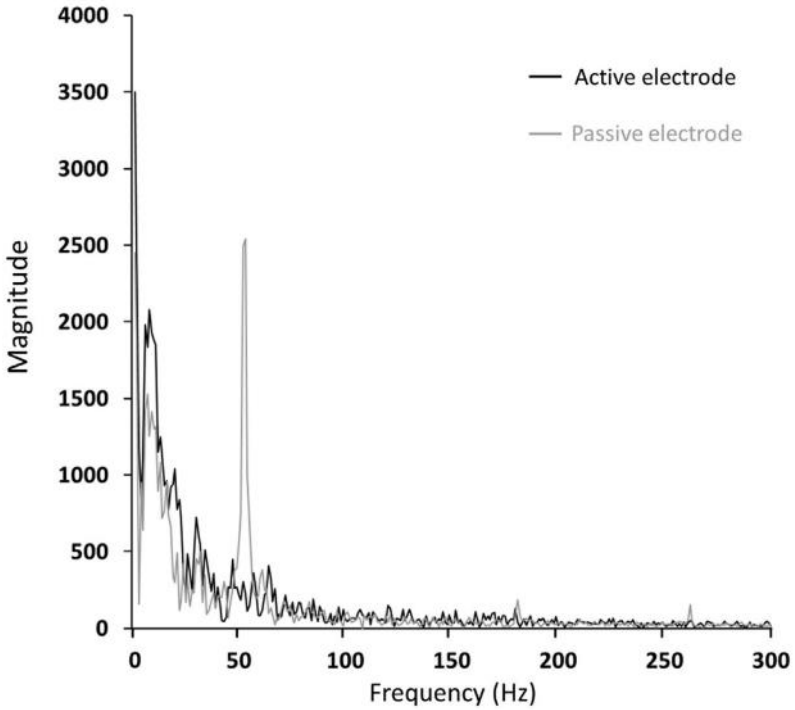

Figure 2.29. FFT of response recorded using active and passive electrodes, demonstrating a significant reduction in line interference.[305]

2.4 Chapter summary

A history of visual electrophysiology is provided. Many experiments on a variety of species and using a range of instrumentation with increasing sophistication have been performed. All such studies aim to identify the components of the complex ERG waveform and relate these to their physiological origin as well as and recognising their clinical significance in both animals and human subjects.

The progress in recording techniques, instruments and technology is discussed. The most notable technological advances which are shaping this field are in recording, acquisition, signal processing and novel mathematical algorithms with application in engineering. Advances in electrode development (mainly the contact lens by Riggs and gold foil by Arden), provide the means to perform clinical and diagnostic ERG. The increased sophistication of amplifiers, storage devices and oscilloscopes, allows the acquisition of tiny electrophysiological traces and provides the means to perform on-line analysis and signal tracking. Improvements in signal processing packages allow cross-correlation and averaging to be performed, thereby significantly improving SNR and ultimately enabling focal ERG examinations. Developments in mathematical algorithms, such as application of m-sequences, provide the means to simultaneously assess many local responses through a single recording channel. Finally, advances in photometry and stimulation techniques allow better characterisation of the retina.

The emergence of Point-of-Care (POC) testing is discussed, facilitated by technological advances in miniaturisation and integration. Development of POC is likely to continue, as it is mainly driven by changes in healthcare strategy, aiming at delivering a more effective diagnosis, continuous monitoring and preventative screening at a lower cost and closer to the patient's home. This trend provides more patient-centred testing, as opposed to the current centralised testing commonly practised in the field of visual electrodiagnostic.

Many sources of variability in visual electrophysiological recording are also discussed. Advances in technology are not enough to ensure comparability, reproducibility and transferability of ERG across recording sessions, subjects, and clinical centres. The need for normalisation improved training techniques, and collaboration between workers in the field and those in manufacturing/developing new instrumentation is discussed. In particular, it is essential to standardise visual electrophysiological recordings. This is the objective of the International Society of Electrophysiology of Vision.

CHAPTER 3: Methodology (Design & implementation of a system to provide synthetic characterised visual electrodiagnostic records)

3.1 Introduction

From an engineering perspective, the retina is a non-autonomous, BIBO stable (Bounded Input, Bounded Output), time-invariant (stationary, or no changes to the frequency content of the visual electrophysiological signal as a function of time. Stationarity property enables averagers and lock-in amplifiers to extract the signal of interest from the noisy record. Where the noise is assumed to be non-stationary) control system with finite memory[308]. Depending on the experimental setup, it can be considered as a static or dynamic, linear or nonlinear, Multi-Input-Single-Output (MISO) or Single-Input-Single-Output (SISO) control system.

The importance of the trigger input (stimulus input signal) to the retina is described when Gaussian White Noise (GWN)[48], a derivative of Brownian motion, is used to characterise the retina[309]. GWN is shown by Sakai et al[309] and in a more recent study by Zele et al[310], to be a capable input (rich input with sufficient temporal variability to identify the dynamics of the system[311]) to study physiological characteristics of the retina allowing for independent variations in mean luminance and stimulus strength. Wiener (1958)[312] combined GWN with the idea of functional representation introduced by Volterra (1930)[313] to define a complex, continuous, finite memory system, e.g. the retina. His work provided a solid mathematical background before advancing to maximal length sequence (m-sequence for short) and its unique properties. These properties offer a more effective and practical way of modelling of the retina as a MISO system[48]. The orthogonal Walsh-Hadamard Transform (WHT) is discussed in [314], which, together with maximally length sequence (a mathematical sequence abbreviated with m-sequence) result in the formation of the f a powerful transformation called m-transform. m-transform is introduced by Sutter[42] as a mathematical procedure to quickly and efficiently characterise the retina and estimate its output through careful selection of the input signal.

In the field of multifocal ERG (mfERG), nonparametric modelling[311] constitutes the most general, tested, and reliable methodology for modelling of nonlinear parameters of the retina. Nonparametric models require one to carefully design the experiment to model the system and employ a mathematical tool, called functional (a term introduced by Hadamard in his book in 1910[315][316], which means a function of function). The objective of nonparametric modelling is to obtain an explicit mathematical representation of the functional. No prior assumption is made during model development, and hence the retina is considered as a biological black-box[317][318].

The importance of time-invariance becomes evident, as the mapping or transformation defined through functionals is fixed through time, assuming the retina remains in the same operational state during the entire length of the experiment. This property would allow for the development of multi-dimensional convolution formulism to model the retinal response when its inputs are a set of delayed and identical flash stimuli.

When the retina behaves linearly, under a very restricted and controlled stimulus input, then it can be modelled (in its entirety) by its unit-impulse response. This first level approximation may reveal the complexity of the retina, which may force the investigator to consider a more complex model representation (for example, as the stimuli rate has increased, the retina may no longer behave linearly). When the retina acts as a time-invariant nonlinear control system, provided the following two conditions are satisfied, the first-order convolution[319] operation could be extended to formulate the higher-order nonlinearities. This is performed through evaluation of higher-order multi-dimensional convolution integral operations[240]:

1- Response or output is linear with respect to its functionals.
2- Functionals are orthogonal (uncorrelated).

The retinal response could be considered as time-invariant when one views it as purely, first-order, second-order, third-order, and so on. In a double input experiment, the retina may behave linearly (or may show strong linear component)[320]. As the temporal distance between the two stimuli is reduced, the retinal response may not be the same as the superposition of single-input-responses. Therefore the retinal responses can no longer be considered time-invariant (i.e. an indication of the fact that the output signal is originated from a nonlinear dynamical system)[311]. However, if one considers the retinal response as the sum of first- and second-order convolution terms, then its response to a double-input experiment could be regarded as time-invariant to the first- and second-order convolution integrals. It is therefore clear that the retinal memory is linked to the time-invariance property, a relationship that is formulated using multi-dimensional convolution operations, i.e. Volterra modelling.

Orthogonality is a powerful tool that is used to sequentially generate the parameters of the control system (the retina) and check its estimated output simultaneously. If the investigator is satisfied with the estimated response of the filter (post-filter performance measurement), then the parameter identification procedure could stop. Such an approach is implemented through the construction of an adaptive filter to model the retina.

Wiener theory is a well-known approach used to construct the input-output relationship of a nonlinear system. Eric Sutter patented[236] (US patent number: 4846567, date of patent: July/11/1989) the idea of using m-sequences to obtain localised ERG signals. He used m-sequences to identify and locate visual disorders by simultaneously stimulating many retinal locations through a pattern of programmable optical elements governed by the array of m-sequence.

The Lee-Schetzen[321] method with GWN as input has been extended to system (e.g. the retina) characterisation with non-white Gaussian input or even certain classes of non-Gaussian inputs[322]. The mfERG is a technique that uses m-sequences for encoding visual information and permits a clean mathematical signal extraction of focal response contributions using a single recording channel with short test duration.

The precise algorithm that is implemented amongst different commercially available systems (such as VERIS Scientific system, the AccuMap ObjectiVision, the RETIscan Roland system, MetroVision, and SHIL Multifocal Imager) to extract the localised ERG signals may vary. However, the main principle is that the sequences must be generated so they remain independent in both the time and space domain. Cross-correlation would then allow extraction of the overlapping, spatiotemporal signals as well as the cross-kernel responses (effect of the stimulus of one region on another) and/or induced components.

In this chapter, the design and engineering implementation of a platform known as ISIM (eye Simulator) is described. This system, models the retinal behaviour within a visual electrodiagnostic setting, allowing an objective assessment of the clinical instruments. The engineering complexity of the design is hidden from the end-user through a simple Graphical User Interface (GUI) that controls the simulator. The ISIM consists of physical hardware and software modules that enable implementation of an orthogonal, multi-component filter, allowing estimation of non-naïve, realistic retinal ERG-like responses. It can be used to simulate both linear and nonlinear waveforms as well as providing methods to create and analyse stimulus input, as presented on CRT, LCD or LED screens by a visual electrodiagnostic clinical instrument.

ISIM's modular design, gives the end-user flexibility in testing and calibrating all components of visual electrodiagnostic instruments. The generated output waveform is comprised of an ideal signal and an additive background noise component. The final waveform is created through the addition of a user-specified combination of ISIM signal and noise sub-components, as demonstrated by figure 3.1.

The orthogonal model implemented in ISIM back-end algorithm to synthesis the user-defined waveform is illustrated as an array of multipliers termed Amplification Matrices ($AM_{i,j}$) in figure 3.1. In the amplification matrix, i, is the index to the system component being modified and j, is the index to the sub-component of the i^{th} component of the system (entries of the matrix are real numbers). The user supplies the modification parameters through a designated Graphical User Interface. For example, if the user requests an ideal linear signal source without any DC component, then the only non-zero term would be $AM_{2,j}$. The response type depicting a test regime is then identified by the j^{th} term in $AM_{2,j}$ matrix. For example, a rod or cone response, PERG, standard ERG etc. As the system is time-invariant the same cycle of the response is generated at the onset of the system (iSim) trigger.

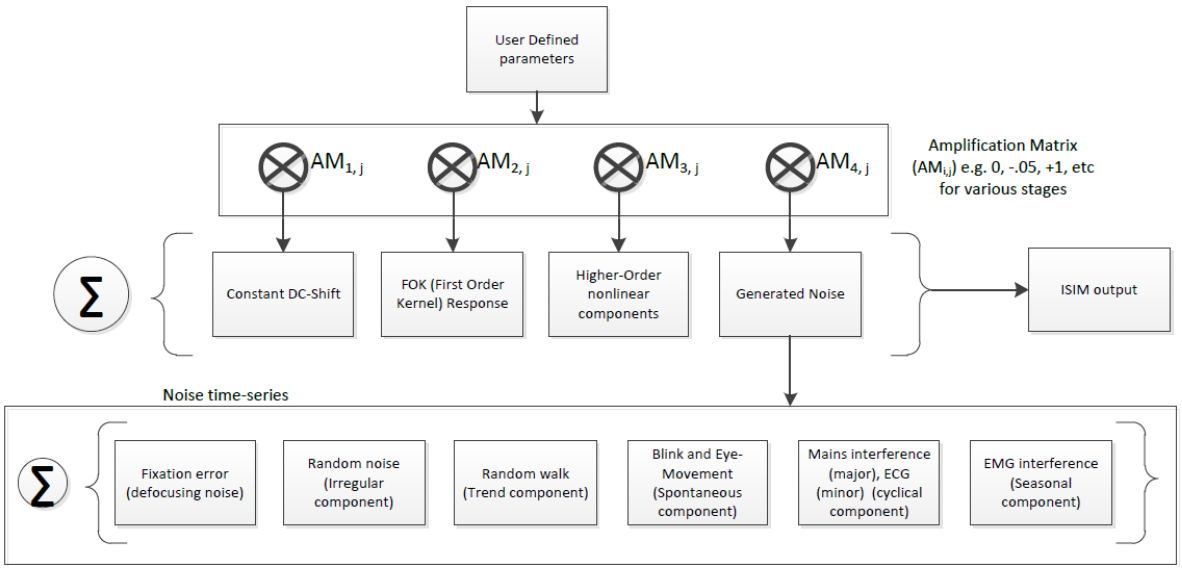

Figure 3.1. Illustration of an orthogonal multi-component control system (retina). ISIM is made up of hardware and software components, allows user-defined output through simple multipliers identified as Amplification Matrices ($AM_{i,j}$).

The physical hardware and the embedded software are termed iSim, while the entire platform including, iSim, the high-level GUI, the back-end MATLAB® engine, and the remote server and other included software components, is termed ISIM. iSim is the device that interfaces with the clinical instrument (the front-end amplifier system) through a three or two-wire electrode array emulating the active, reference and/or ground electrode connections. iSim has a photosensor with user-adjustable sensitivity that allows the device to register changes in the luminance of the clinical stimulator. Registration of flash stimuli triggers the iSim's internal circuitry to output a user-defined waveform. The flash registration also provides the device with the required synchronisation signal so it can accurately characterise the clinical instrument, e.g. characterisation of the system's artefact rejection mechanism or scrutinising the system's underlying m-sequence.

3.2 Building a theoretical and experimental library

The development of an expandable, extensive, and realistic library of theoretical and experimental ERG responses are described here. The library can be shared and used by visual electrodiagnostic centres for accurate calibration, signal processing, and training. The library includes multiple components, as described in figure 3.1, which are made available over the internet through a custom-built, simple-to-use, and robust server application termed MatSOAP©. MatSOAP© server consumes MATLAB® resources over an internet connection. MatSOAP© was developed by Lake et al[323][324][325] and applied in various fields to assist clinicians. Each component in the ISIM library is either mathematically generated without any knowledge of real-life data (e.g. representing harmonics and mains interference through a simple 50 Hz sinewave component) or is based on experimental data. Once the user has specified the requirements for a test waveform, the MATLAB®

back-end algorithm will process the request and synthesise the waveform as described by the orthogonal implementation of figure 3.1. The iSim device provides a mechanism to present a physical signal to a visual electrodiagnostic system, allowing an objective assessment of the system.

An overview of the implemented methodology to digitise and prepare the signal is shown in figure 3.2. This method is used to generate both linear and nonlinear components of the signal.

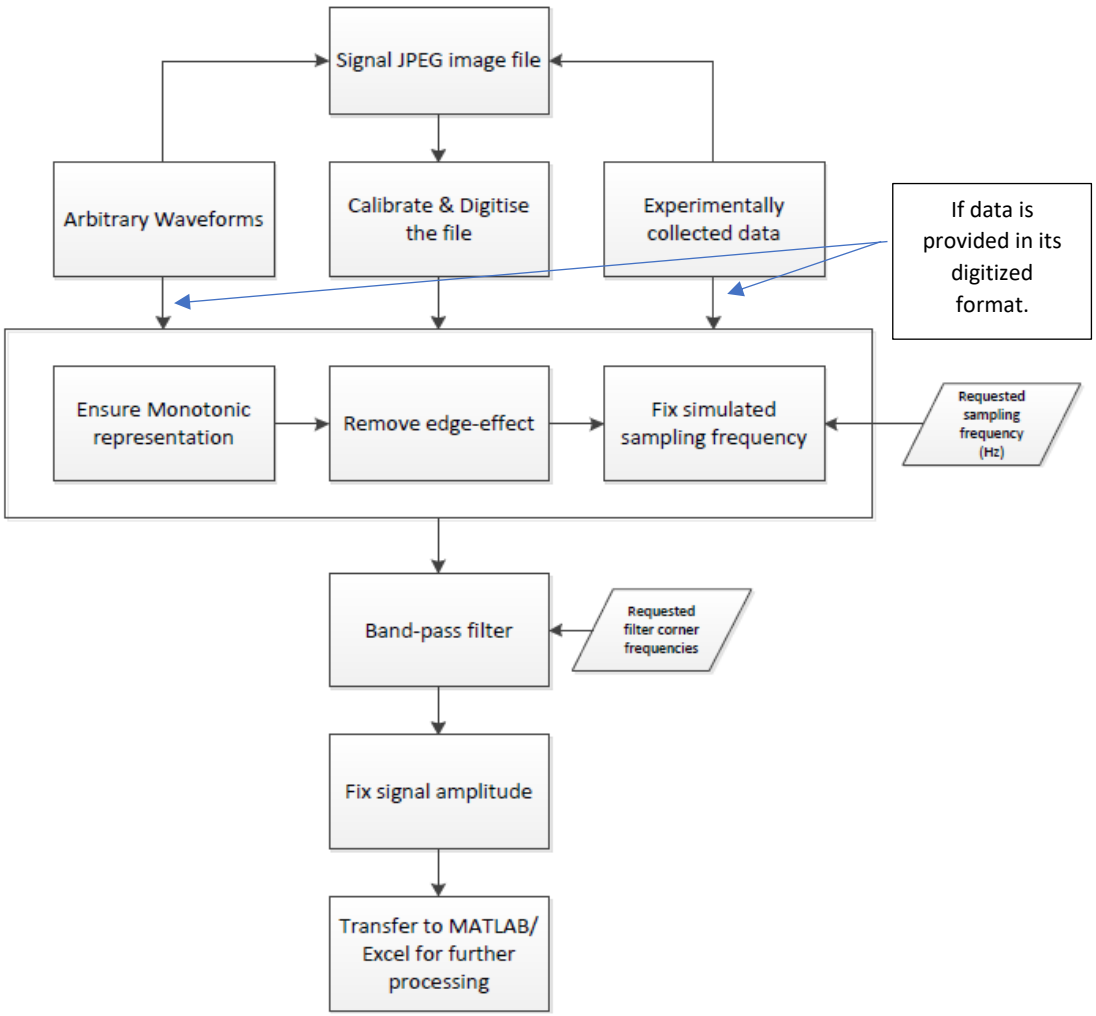

Figure 3.2. Demonstration of methods used to generate and prepare simulated response waveform for the orthogonal multi-component system model.

Nonlinear implementation of signal components is based on the concept of Wiener series, kernel expansion, estimation, and extraction, as described by Sutter in [42]. Simulation and method verification for a multifocal response estimation using Sutter's m-transform method for a nonlinear retina, as well as retinal linear system response estimation, is described later in this chapter.

The origin of signal and spontaneous noise components can come from any validated source, e.g. books, studies, and other experimental data collections and publications.

A MATLAB® library is developed that allows for digitisation, calibration, and processing of recorded waveforms. These waveforms can be in the form of an image file in any format. The only essential requirement is to have the calibration axis available alongside the image. The digitisation may result in irregular samples with respect to time, that potentially suffer from non-monotonicity. The final waveform response is synthesised in a predetermined order. The first step is to create the required length of signal followed by the addition of spontaneous noise components such as eye movement,

blinks and/or EMG. Then any requested mains and associated harmonic interference are added. Finally, the stochastic system noise is generated and added. Frequency leakage is avoided by using a windowing technique (e.g. a Tukey window) and appropriate padding of the signal at its either ends to eliminate any edge-effects. These components are further filtered through the implementation of a bandpass filter and then adjusted in amplitude based on the user-requested SNR. Figure 3.3 demonstrates the edge-effect simulated in MATLAB® for a waveform of a single frequency component (a sinewave with a frequency of 7 Hz sampled at 100 Hz) when one observes 2.1 seconds of the data.

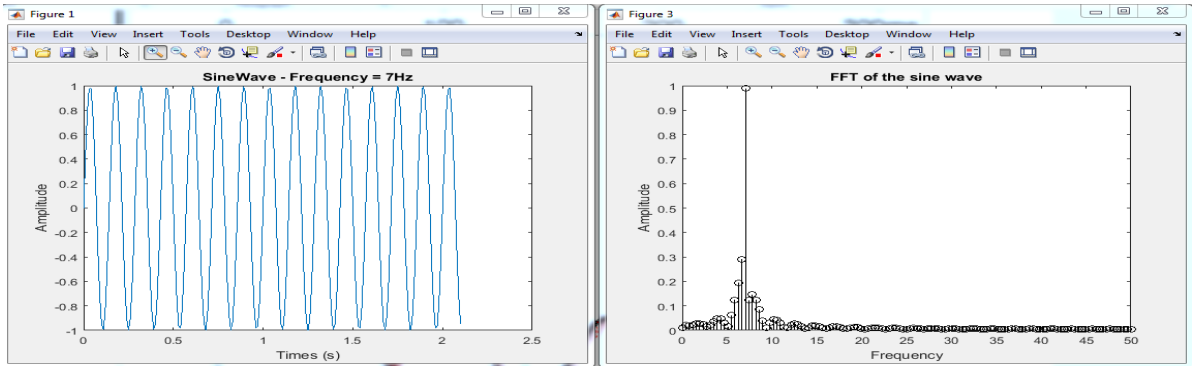

Figure 3.3. Illustration of edge-effect and its impact on the original or intended data.

3.2.1 Linear signal synthesis and simulation

For linear signal estimation, one cycle of the waveform is first digitised and calibrated. Figure 3.4 demonstrates an example where the digitisation of a JPEG image of the multifocal first-order kernel (FOK) response along its time and amplitude data axis is performed.

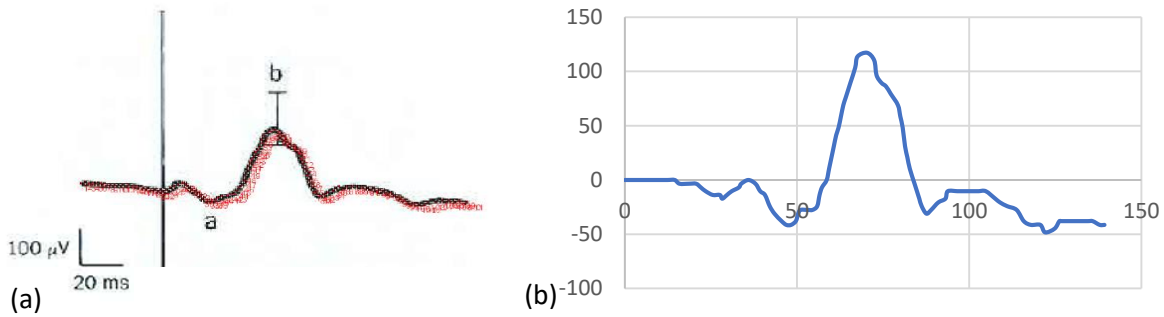

Figure 3.4. Digitisation of a standard ERG signal (a) and data transfer to Excel® for further processing (b).

The digitised data vector representing the waveform is made strictly monotonic and resampled at 1kHz using MATLAB®. The resampled data may demonstrate signs of discontinuity at its endpoints, causing edge-effects and smearing the signal's frequency spectrum. The undesirable edge-effects are avoided by using a Tukey window and then appropriately padding the signal using 0's at both ends. The signal cycle is then filtered to smooth the high-frequency jitters. This waveform is now ready to be uploaded into iSim onboard memory, and the device will output the same cycle every time it is triggered.

3.2.2 Nonlinear signal synthesis, simulation and verification

The synthesis of nonlinear signals is more complicated than that of linear signals. However, thanks to Wiener and the linear expansion of the signal kernel, it is possible to use the same method to prepare the individual kernel slices as if they were linear responses. However, the complexity of multifocal nonlinear estimation means that more considerable effort is required to implement the

estimator filter (the kernel table) and expand the back-end library. The following criteria must be considered when preparing the kernel table for inclusion in the ISIM's library:

- Experimental or clinical settings, ranging from equipment type to specific centre or study procedures, frame rate, m-sequence length, number of runs, pupil dilation, sampling frequency, filter settings, methods of noise rejection, presence or absence of adaptation period, retinal pre-stimulation adaptation, subtended retinal angle (distance to stimulation screen).
- Population demographics, e.g. age, background.
- Type of stimulator, e.g. LED, CRT or LCD.
- Electrode types used.
- Operator experience.

3.2.3 Scrutinising the system's m-sequence

ISIM provides the mechanism to capture and verify m-sequences, calibrate, and test the diagnostic system objectively. In designing ISIM, it was crucial to keep intrusion to ongoing clinics to minimum while probing the system. As most manufacturers provide little information regarding their design and tend to protect commercially sensitive data, one may not have the luxury of knowing the tab positions and the length of the m-sequence underpinning the stimulus. The simulation of a sequence that is not of maximal length is seen in figure 3.5. Autocorrelation is used to allow the investigator to measure the periodicity of the sequence. Figure 3.5 illustrates that the sequence is not maximal in length, as its period is less than 2^n-1, where n is the number of bits in the feedback shift register. The impact of the added adaptation sequence to a generated m-sequence is also shown in figure 3.6, where it is demonstrated how autocorrelation is used to determine the lag in the sequence where the adaptation phase ends/starts.

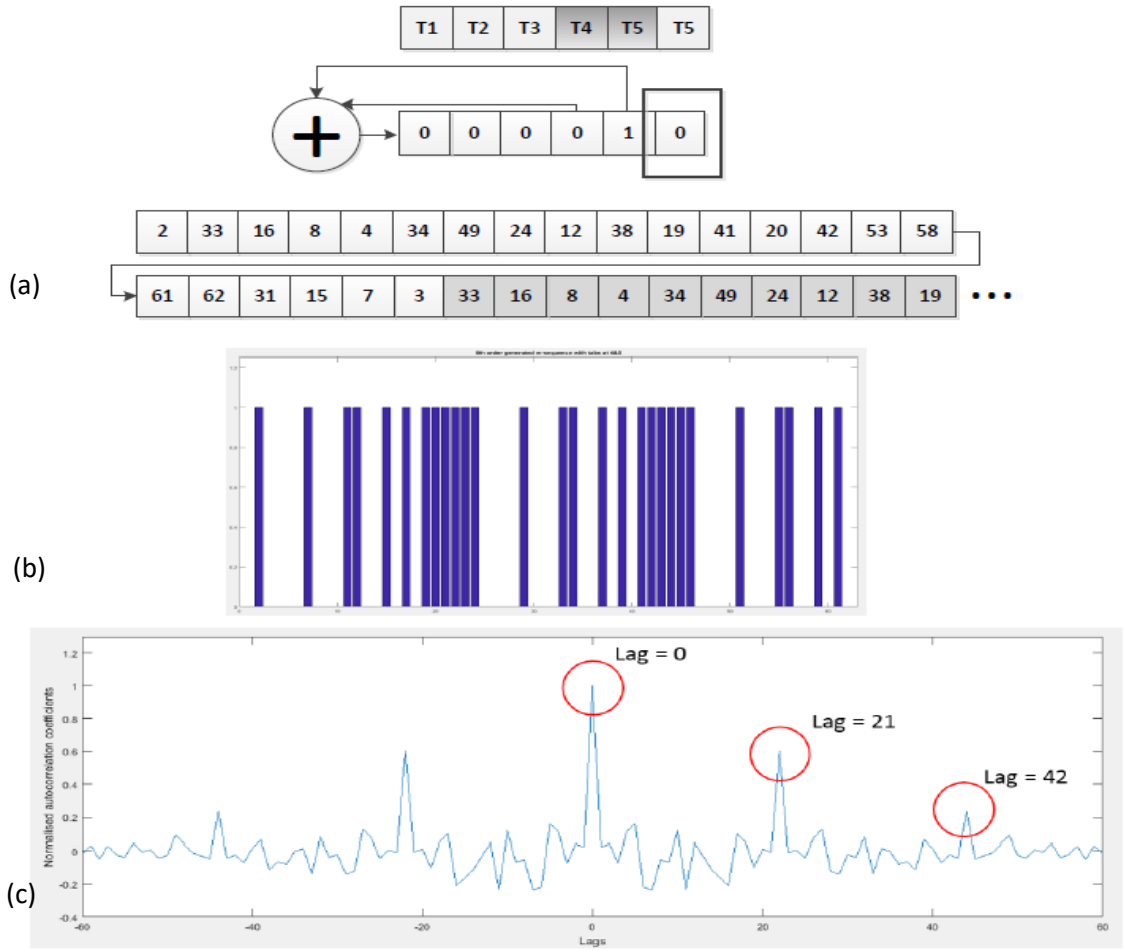

Figure 3.5. (a) Linear feedback shift register resulting in the generation of the sequence shown in (b). Correlation test results with significant peaks are shown in (c).

When iSim registers the flash sequence from a single hexagon (governed by an m-sequence or an m-sequence plus added adaptation sequence), it can only try to extract the m-sequence. This means iSim cannot make any assumptions about the state of the first frame concerned with the selected hexagon. This was also Hagan's finding[49] when he scrutinised the Roland RETIscan's short m-sequence to verify that it is capable of keeping responses of both first- and higher-order kernel slices separate for each stimulating area. For example, if the photodiode probe is placed over the j^{th} hexagonal location when the clinical system is running, if the site is governed by a daughter sequence that starts with zero (absence of a flash), iSim will not register this. Hence, the internal timing of the device will not be triggered (that is, it lags or is out of synchronisation by at least one b.p). The worst-case scenario is when the j^{th} location starts with the longest trail of zeros. For example, for a sequence of length 511, the longest trail of zero is 8 (the j^{th} hexagon is the last to flash). Meaning if the investigator is solely relying on iSim reading from a single location, then there is a danger of an out-of-synchronization error, which, cannot be recovered.

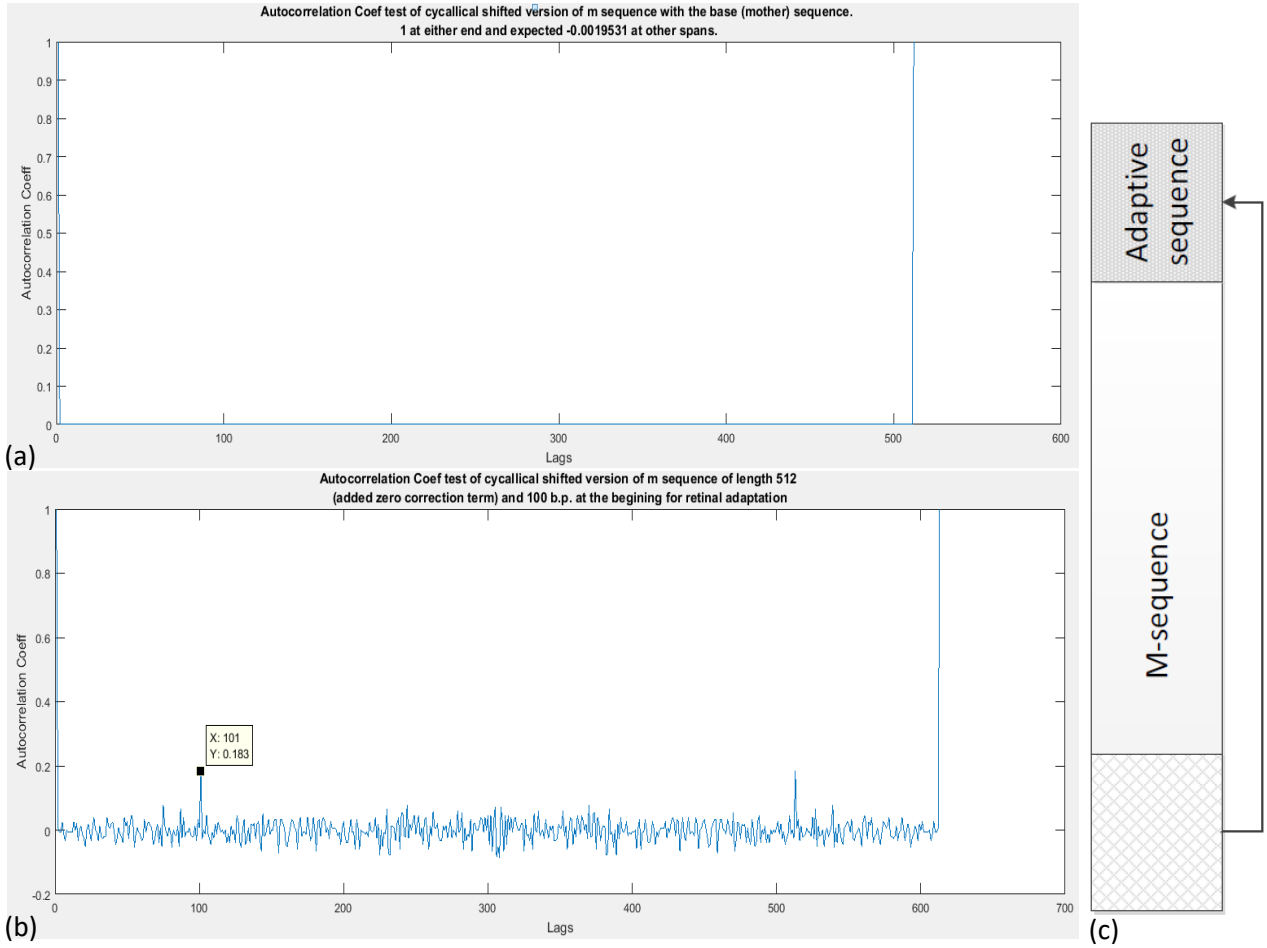

Figure 3.6. (a) cross-correlation results of a generated m-sequence. (b) using technique demonstrated in (c), an adaptive length is added to the m-sequence and cross-correlation is performed again.

However, if the purpose is:

- To extract the sequence and ensure it is, in fact, an m-sequence, or
- To ensure the sequence can contain the required temporal and spatial information without any overlap or crosstalk, then

the error will have no impact as ISIM will add zeros at the end of the sequence until its length is rounded up to the nearest power of 2. That is ISIM assumes the missing b.ps is a trail of zeros at the end of the sequence.

The overlap calculation is based on externally implied shifts and does not represent the way the clinical systems implement governing sequences for other locations. Therefore, although the sequence may have the capability of encoding spatiotemporal information, the actual clinical system's implementation of shifts may be different. For example, Hagan[49] found that the Roland system ensures the FOK sequences are maximally separated. That is, for an m-sequence length of 511, this is 26 steps or b.ps. Roland's selected shift is the length of the sequence divided by the number of stimulation areas which is justified by ensuring all FOKs are well separated from one another, minimising any signal bleed from/to FOK_j, where j is the spatial index. Hagan[49] further analysed and calculated the relations between FOK, SOK, SOSS and TOK in a tabular format, illustrated in figure 3.7 for the Roland system.

Seg	FOK	SOK	SOSS	TOK
19	1	383	254	224
18	27	409	280	250
17	53	435	306	276
16	79	461	332	302
15	105	487	358	328
14	131	2	384	354
13	157	28	410	380
12	183	54	436	406
11	209	80	462	432
10	235	106	488	458
9	261	132	3	484
8	287	158	29	510
7	313	184	55	25
6	339	210	81	51
5	365	236	107	77
4	391	262	133	103
3	417	288	159	129
2	443	314	185	155
1	469	340	211	181

Figure 3.7. Relative location of FOK, SOK, SOSS and TOK obtained from Roland system by Hagan[49] during his PhD work in 2004.

The higher-order kernel slice sequences (HOK_j) are based on calculations from the governing FOK_j sequences as described by the model constructed by Sutter[44][42]. In this calculation, the HOK_j sequence is first identified from the corresponding FOK_j sequence, and then the amount of shift is determined.

The out-of-synchronization risk materializes into an error when one creates an estimation of the system response from the kernel slices using the extracted sequence and further tries to extract these kernel slices using the clinical system under investigation.

The mitigation for this risk is to:

- Provide iSim with a synchronisation signal, indicating the onset of the first frame.
- Repeat the same reading from other hexagonal locations (that is a sweep across index j). This would allow the user to determine the system's implemented shift across all stimulation areas and hence correct the sequence for all index j. Hagan[49] has performed and reported this for the Roland system when he further scrutinised the captured sequence. The good news is that, the clinical systems are not expected to alter their m-sequence from one run to another (assumption here is a fixed number of stimulation areas). Therefore, capturing the sequence for a specific number of stimulation areas can be done once and reused.
- If the system does not implement adaptive sequence, then a synchronisation signal is required to provide iSim with a time reference. Otherwise, it is not advised to use the scanned sequence for the retinal response estimation unless investigator knows that the first scanned location is the location with a governing sequence that starts with a flash (a one).

The length of the adaptation sequence depends on how the clinical system is configured. For example, if it is fixed based on units of time, then the faster the m-sequence is executed, the shorter the b.ps would be. Therefore, the longer the number of steps in the adaptation period (assuming a fixed-length m-sequence governs the stimulation area).

If the synchronisation trigger pulse is available, and the measured b.p is defined, ISIM can estimate the multifocal ERG response. From the measured b.p, and the assumptions that:

- FOK kernel response will return to zero under 100 ms, and
- Memory length of the retina will not increase above 2nd order nonlinearity,

ISIM will estimate the memory and then access the required hyper-plane kernel table from the micro SD storage area. If the required table is not available, it will adjust to the lower-order system and so on. If the measured b.p is smaller than 83 ms, ISIM will not be satisfied with FOK table only and will not run the simulation. This will provide a fail-safe mechanism, ensuring the clinical instrument is not calibrated wrongly.

From this table, ISIM will construct the response vector, and assuming the retina is time-invariant, it will use the m-transform matrix to set up the ISIM memory accordingly. This is shown in figure 3.8, where it is split into the following major blocks:

- Scan the stimulator, e.g. Roland CRT, and register the flash sequences governing each hexagon and calculate the base-period. See figures 3.9.a and 3.9.b.
- Create binary (0 or 1) sequences and extract “potential” m-sequences as well as adaptation sequence, see figure 3.9.c.
- Identify shifts across all spatial locations. See figure 3.9.d.
- If the clinical system implements adaptation period, it will then correct for the assumption of the number of trailing zeros and due to cyclical periodicity and shift property of m-sequences, it will calculate the amount of leading and trailing zeros for each segment. Otherwise, the algorithm requires a synchronisation signal providing iSim internal circuitry with a time-reference.
- The verification of the m-sequence is performed throughout the algorithm against known properties of m-sequences, as shown in figure 3.8.
- Determines the FOK sequences for all spatial locations and then calculates the Higher-Order-Kernel (HOK) sequences for all areas.

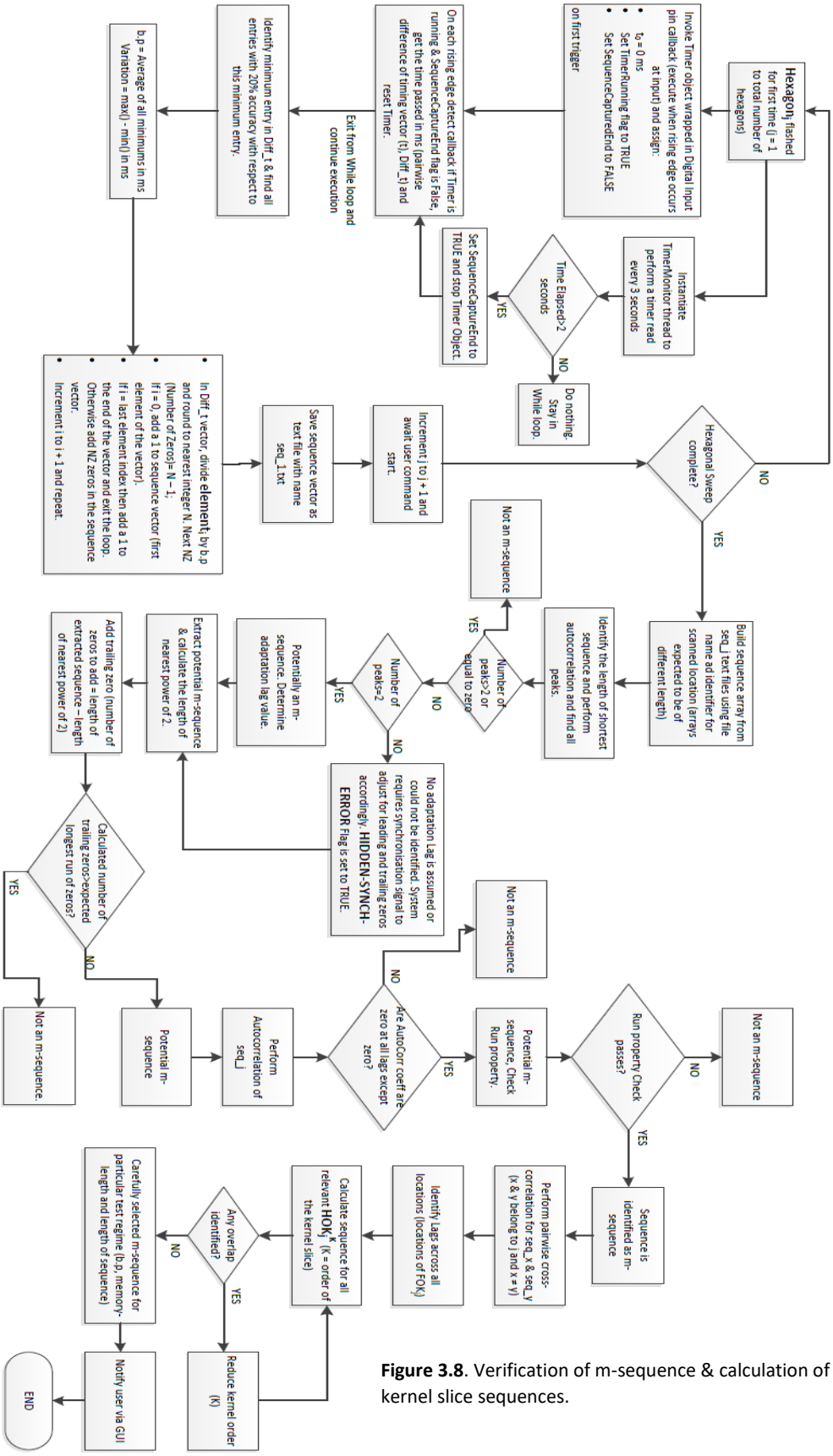

Figure 3.8. Verification of m-sequence & calculation of higher-order kernel slice sequences.

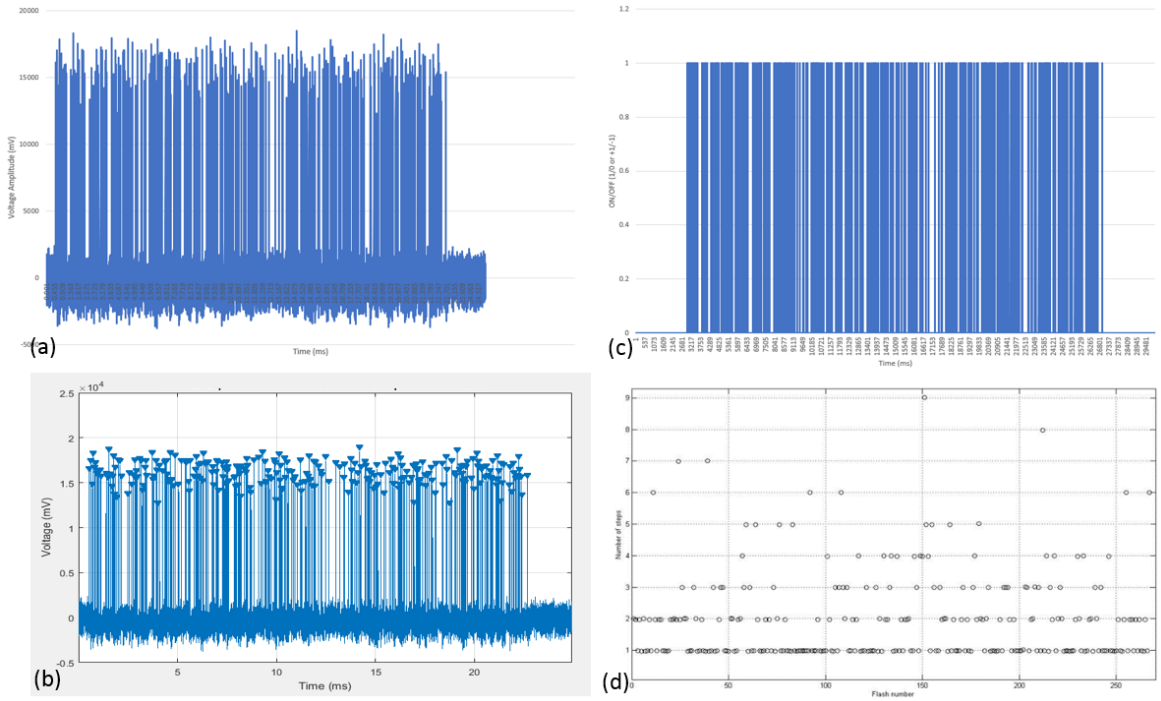

Figure 3.9. (a) Illustrates the recorded raw data from iSim built-in photodiode circuitry for the sequence 0 (centre sequence) of Roland Consult system when a run of 511 m-sequence was initiated with a base-period of 83 ms (5 filler frames, where the stimulation rate is 60 Hz or 16.6 ms time-interval in-between frames). (b) Illustration of peak identification of recorded raw data from photodiode in MATLAB®. A simple difference equation could then be implemented to identify the time interval between flashes. (c) Illustrates the calculated flash sequence or stimulation sequence that also contains the initial adaption or settlement period of 0.5 seconds in length. (d) Shows the calculated and plotted data for (using MATLAB® Scatter function) run property of the true m-sequence after performing extraction algorithm on the calculated flash sequence. This shows that there is a certain number of each number of steps between flashes, i.e. one eight-step gap, two seven-step gaps, four six-step gaps and so on. This is a property specific to m-sequences.

3.2.4 The retinal response synthesis using kernel slices

ISIM can estimate the retinal response to a pre-configured test regime using extracted kernel slices derived from experimentally obtained kernel tables. The test setup and settings, equipment used, and compliance to standards as well as investigator techniques and test population characteristics such as age group will influence the extracted kernel slices and must be accurately reported to ensure traceability. Once these kernels are extracted, it is possible to estimate or synthesis the original spatiotemporal waveform, sometimes referred to as raw bio-signal data. The synthesis could also be performed if one had access to individual responses for single, double, and triple flashes (assuming a second-order nonlinear system). However, these individual responses are not readily available, and most clinical settings extract and present the kernel slices in a density map data array format. See figure 3.10. In this figure, the choice of sampling period will not impact the methodology described. By default, iSim will assume a sampling frequency of 1000 Hz, therefore avoiding aliasing due to the bandwidth of the signal of interest being in the range of 0-350 Hz.

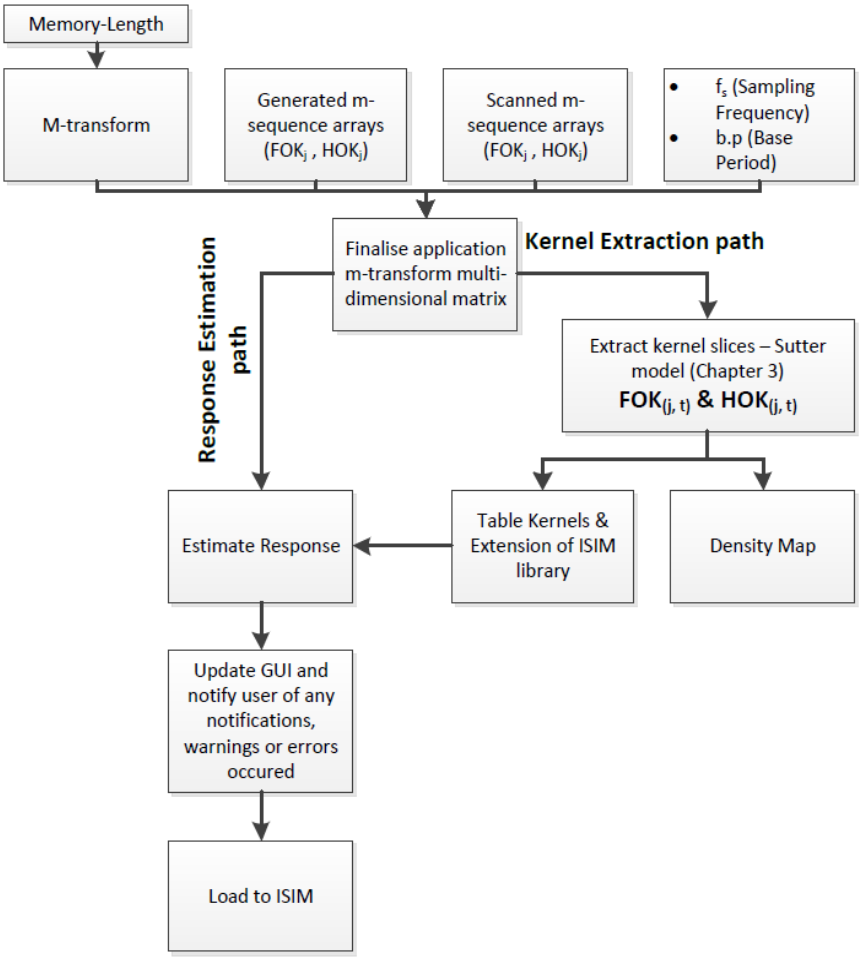

Figure 3.10. Based on memory-length, m-transform matrix is calculated. This together with generated or scanned sequence array, sampling frequency and measured base-period, allows for determination of application multi-dimensional m-transform. This transformation is used for kernels extraction from recorded retinal response (probed using the generated or scanned m-sequence array) or the inverse, that is estimation of retinal response from kernel-slice tables. Kernel-slice tables are represented mathematically by First and Higher-Order-Kernel slices, i.e. FOK and HOK, which are functions of both time and spatial locations (i.e. encoded/decoded spatiotemporal information). In field of visual electro-diagnostic, kernel slices are illustrated as density map (i.e. extracted localized response function amplitude per square of subtended retinal angle, e.g. nV/deg^2).

iSim is capable of storing (using onboard memory) a signal vector of length 500 float-type where, for nonlinear estimation, the first 100 are reserved for FOK, the second 100 for SOK, the third 100 for SOSS and the fourth 100 is reserved for TOK. This vector represents the retinal memory of a maximum of 2nd order plus 2nd order kernel third slice (SOTS). The kernel tables, noise files (simulated noise, blinks & eye movement, EMG and mains/harmonic interference), and other relevant information are stored in the onboard SD card. These will be loaded to the system runtime memory buffer as required, during iSim initialisation and run-time. See figure 3.11.

The computing power is improved significantly since 1991 when Sutter[42] published his paper on m-transforms as an efficient method of deriving kernels (moving away from convolution in the time domain to addition and subtraction in the frequency domain using FWT). However, iSim is an embedded system that is aimed to be friendly and low-profile, where the calculation complexity is abstracted from the user via the consumption of simple GUI and a managed cloud programming service operation. The onboard memory of iSim is limited, even though a hardware storage unit (SD card) is implemented. Slow access time to hardware through implemented filing system is still a limitation, making onboard RAM and registers a preferred method to store critical-to-functions (CTF) parameters and signal arrays. The use of SD allows for permanent storage of data, accessible through Serial Peripheral Interface (SPI) communication.

The signal array consists of five blocks of length 100 ms each, which is equivalent to one hundred samples at the sampling frequency of 1 kHz. This array, together with the m-transform array, is loaded into iSim RAM during initialisation. The loading of the kernel slices into the memory during initialisation period is analogous to the retinal adaptation period when the adaptative input

sequence presents the retina before commencing with the actual test. This adaptation period during an actual objective assessment of the retina is needed as visual neurons must faithfully encode the incoming stimulation signals. iSim, as operated per algorithm in figure 4.8, will not know any difference between adaptive sequence or the actual test sequence.

iSim allows only for estimation of signal from a single spatial location, see figure 3.11. As iSim does not need prior knowledge of the actual governing sequence for the j^{th} location, this location could be anywhere within the subtended visual field. The noise buffer is loaded into memory in chunks of binary samples. Each block represents a noise sample vector or packet containing individual samples of different categories of noise. For example, ARMA (Auto Regressive Moving Average) generated samples, white or other types of coloured-noise, blink, eye movements, EMG noise samples as well as mains or other harmonic type interference samples. The only limitation on the length of the noise signal (N in figure 3.11) is the iSim internal clock counter register, which allows for noise presentation of maximum length of 30 minutes at iSim's default output rate of 1kHz.

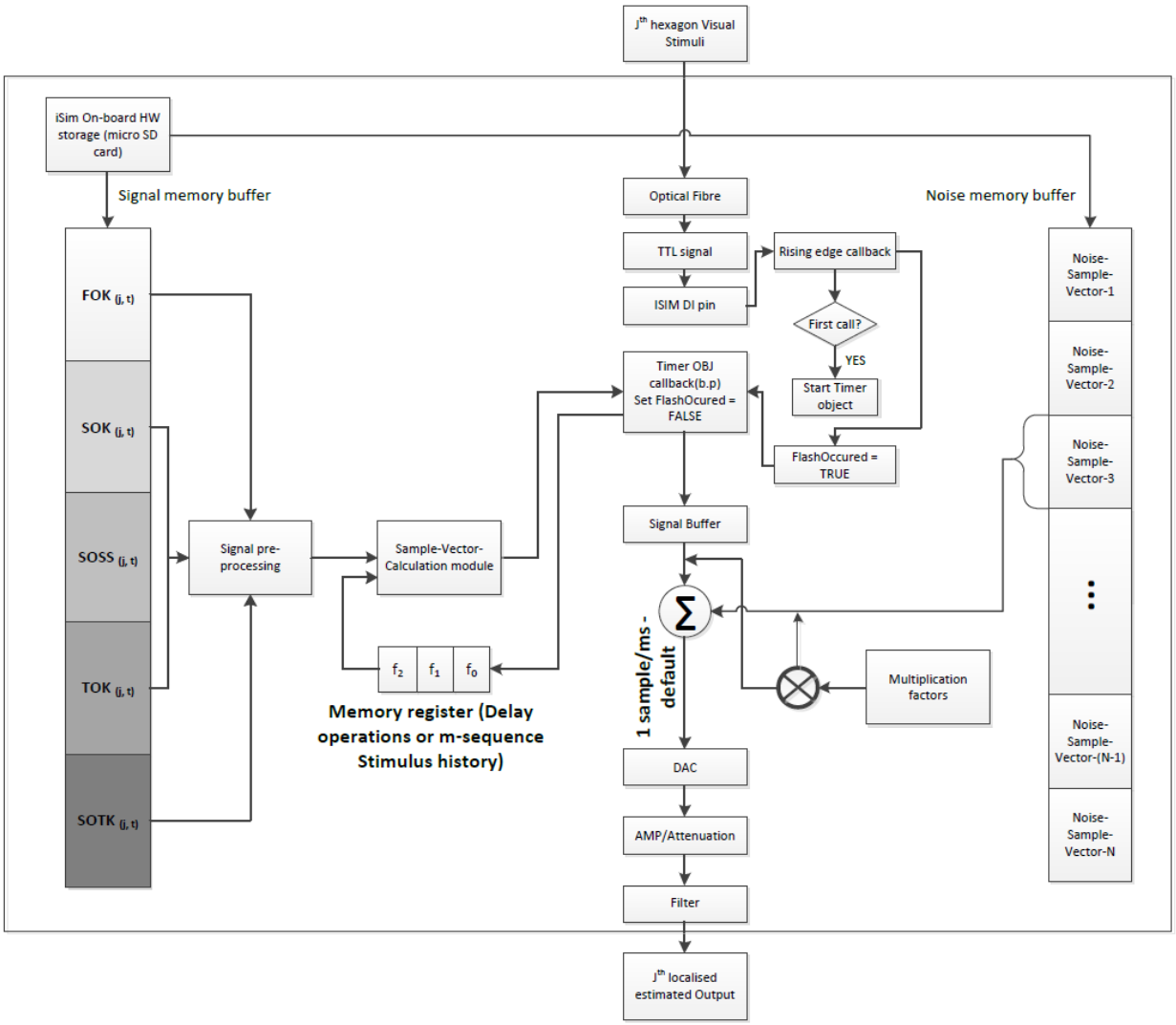

Figure 3.11. The "Estimate Response" block in Figure 4.10, is represented in this figure, simulating the j^{th} location response. It is easy to realize that, a filter implementation of integer multiple of such blocks in a parallel configuration, would result in full simulation. The output of these filters would be summed together providing a single retinal response estimation under a specific test configuration of N spatial locations probed using a pre-configured m-sequence as the visual excitation signal. Alternative is a sequential approach, which could be implemented having access to j^{th} location governing m-sequence, the shift table for FOK_j and physical synchronization signal defining the starting point.

As the retina is assumed to be a time-invariant system, the same kernel slices are used to construct the signal output at the onset of each base-period (b.p). As such, the kernel slices will need to be loaded into the memory during the initialisation phase. The trigger for iSim to output the estimated response comes from a visual stimulus. Importance of this arises from the requirement of perfect timing between presented visual stimuli and output signal when it comes to decoding the response back into its building components, i.e. kernel slices. The implementation of figure 3.11 also requires the clinical setting to present frames at an exact pre-determined b.p.

The visual stimuli are transmitted to the logic circuitry of iSim through the optical fibre. They are converted to a standard Transistor-Transistor Logic (TTL) voltage signal connected to a Digital Input (DI) pin of the microcontroller. Object-Oriented Programming (OOP) in C++ allows for event-driven programming through the multi-threaded application (threading the programming logic clock signal to run multiple applications in parallel on a multi-core or single-core operating system. In the latter,

the illusion of parallel processing is created through a fast context switching mechanism based on the assigned priority levels to individual modules or functions).

There are two categories of triggers for this implementation, as shown in figure 3.12.

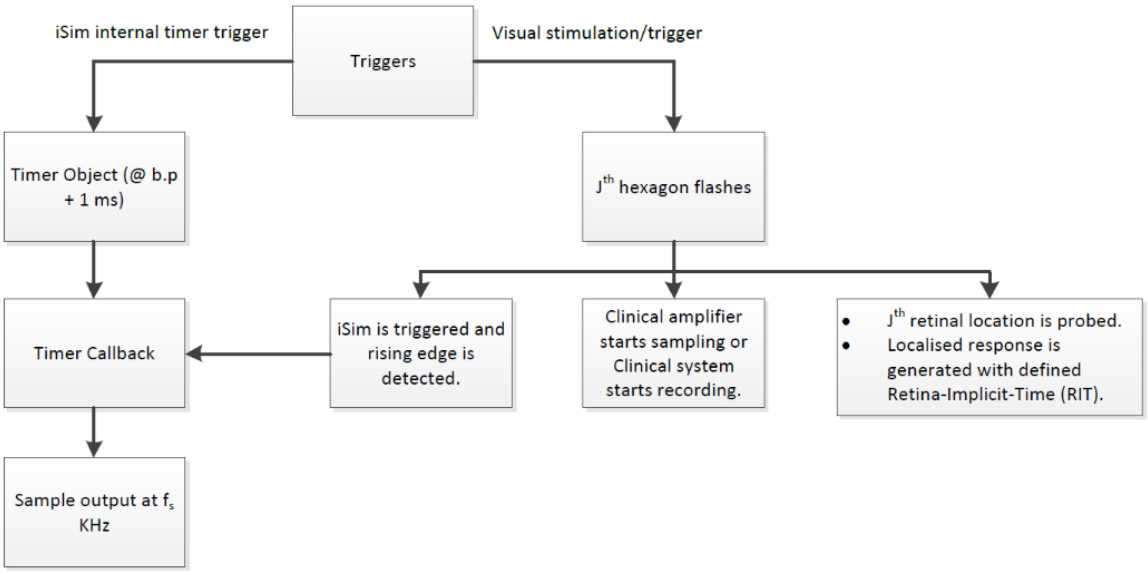

Figure 3.12. In a clinical system, as frames are presented approx. 50% of hexagons are off, and the other 50% are on. This triggers the iSim (when a flash at a specific location is present) system to start recording the response of the j^{th} retinal location. This response is accompanied by a phase termed implicit time, which is a fixed parameter of the response due to its time-invariance characteristic.

The two triggers have associated callback functions as described below:

- One that triggers every time that (b.p + 1) ms is elapsed and is internal to iSim.
- One that triggers when a rising edge is detected on the DI pin and is due to external visual events at the j^{th} spatial location.

The rising-edge-callback function is simple in a sense that it will set the `FlashOccured` iSim internal flag (logical variable signifying the occurrence of a visual stimulus) to TRUE every time it is invoked. If it is the first call, it will instantiate the timer object and will begin counting. The timer object callback is the next high priority function to execute, and it performs the following tasks every time it is called:

- Sets global `FlashOccured` flag to FALSE.
- Updates the memory register (set $\{f_0, f_1, f_2\}$ in figure 3.11), where the set represents a system that its response at time $t_0 = 0$ (i.e. now) depends on its current input and the input to the system at previous two lags (that is two delay operations or a second-order nonlinear system). f_i (i = 0, 1 or 2) is a binary set where zero represents the absence of flash, and a binary one represents, presence of a flash. The initial state of the memory register is all zero and is set during the initialisation period.
- Calls the Sample-Vector-Calculation module (see figure 3.11) to construct the response and update the Signal Buffer array, see figure 3.11.

iSim assumes simulation of the retina with memory extending to the two previous flashes (where nonlinear behaviour is expected) and a vanished memory at a b.p of 100 ms or larger (where a linear operation is expected). Sutter[44][42] provided a simple model to code and decode the nonlinearity through addition and subtraction operations (Appendix A). If the base-period is smaller than 100 ms,

the response of the retina will continue and overlaps with future responses, and hence, the engineering implementation becomes even more complicated as the nonlinearity order is increased. Sutter's model has significantly improved the calculation's power and time as well as memory requirements to estimate the response of a complex nonlinear system, ultimately allowing for the implementation of the algorithm in figure 3.11.

Each output signal sample is then added to a calculated/estimated noise sample, and the result is sent to the digital-to-analogue converter (DAC), amplification/attenuation modules and finally filtered, see figure 3.11.

Each memory block, represented in figure 3.11 is filled in line with the synthesis of the original signal waveform as described below:

- The four kernels ($FOK_{(j,t)}$, $SOK_{(j,t)}$, $SOSS_{(j,t)}$ and $TOK_{(j,t)}$) are assigned a binary string of length 3, where a one indicates if a specific point in time is relevant for the corresponding kernel. These binary strings are (001, 011, 101 and 111). Refer to table A.1 in Appendix A.
- The memory register is described by the pre-stimulus history (the first two digits) and the current stimulus, i.e. the third digit. Table A.1 (Appendix A) is used to extract the kernels slices from the response epochs through the averaging process known as cross-correlation. We are assuming a noise-free signal estimation through the constructed multi-component orthogonal system (allowing separation of signal and noise and a simple addition/subtraction operation to estimate the original waveform). Therefore, iSim will output a zero segment into the corresponding memory block provided that the AND operation described by Sutter in [42] between kernel slice binary representation and stimulus history (memory register) result in even number of 1s. That is, replace all +1, in table A.1 (Appendix A) by 0 and all -1s in the table by +1, where +1 indicates the kernel slice is included in estimation and a zero indicates the kernel slice is not included. This is equivalent to cancelling out the effect of noise and induced HOK ERG components when decoding the raw retinal response data to obtain the kernel slices.
- Based on Sutter's model[44], if the three digits in the kernel slice binary string include an odd number of 1s, the corresponding kernel slice is added, and if they contain an even number of 1s, the corresponding kernel slice will be subtracted.
- The higher-order kernel slices (e.g. second-order third slice) is ignored as the system is assumed to be a second-order system.

Above is summarised in table 3.1, which is used for estimation of the retinal response from all kernel orders and slices up to and including second-order when the system is probed through any m-sequence, whether the adaptation period is included or not.

Table 3.1: Kernel slice multiplication factors for a second-order nonlinear operation.

Extracted kernel slices		$FOK_{(j,t)}$	$SOK_{(j,t)}$	$SOSS_{(j,t)}$	$TOK_{(j,t)}$
Kernel slice binary rep		(001)	(011)	(101)	(111)
Flash train (Memory register)					
$***$	(000)	0	0	0	0
$** f$	(001)	+1	-1	-1	+1
$* f *$	(010)	0	-1	0	+1
$* ff$	(011)	+1	0	-1	0
$f **$	(100)	0	0	-1	+1
$f * f$	(101)	+1	-1	0	0
$ff *$	(110)	0	-1	-1	0
fff	(111)	+1	0	0	+1

Throughout the implementation, the boundary conditions are kept in check via ensuring the following terms and assumptions are satisfied:

- Arrays and registers are set and initialised, e.g. memory register, and the signal buffer is set to all zero and signal array is loaded and checked during the initialisation period, as well as b.p and signal frequency is determined where $\frac{100}{b.p} \in Integer\ set$, and $10 \leq b.p \leq 100\ ms$.
- ISIM can handle minor errors in b.p between frames. It does this by reducing the RIT (retinal implicit time) by 1 ms and triggering the timer object by adding 1 ms, to the measured or provided base-period, ensuring that, it captures the presence of a potential flash in its memory register before performing response calculations.
- In the Sample-Vector-Calculation module, iSim will avoid read/write conflicts and a subsequent system crash by extending the last sample of each memory block by one sample.
- iSim output signal as soon as it enters into run-time and will continue outputting signal when frame presentation stops (i.e. timer object will not stop and will resume normal operations) until iSim is reset. The output is noise (or zero DC if no noise contamination was requested). This will ensure that that iSim will not miss the longest trail of zero in an m-sequence of any length.
- Fixes the output rate to 1 kHz to avoid out of memory error. If a higher output rate is selected, then more signal samples are needed to maintain the signal morphology.

3.2.5 Implementation of response synthesis simulation using arbitrary kernel slices

Response synthesis simulation using arbitrary kernel slices is implemented in C++ using Microsoft Visual Studio Integrated Development Environment (IDE). The implementation code is reported in Appendix B. This is a standalone GUI provided as an installation package where its user front-end interface is shown in figure 3.13. The interface requires three files to operate:

- Sequence Array file (Excel® or CSV format)
- Noise file (text or CSV format)
- Signal Kernel Slice file (text or CSV format)

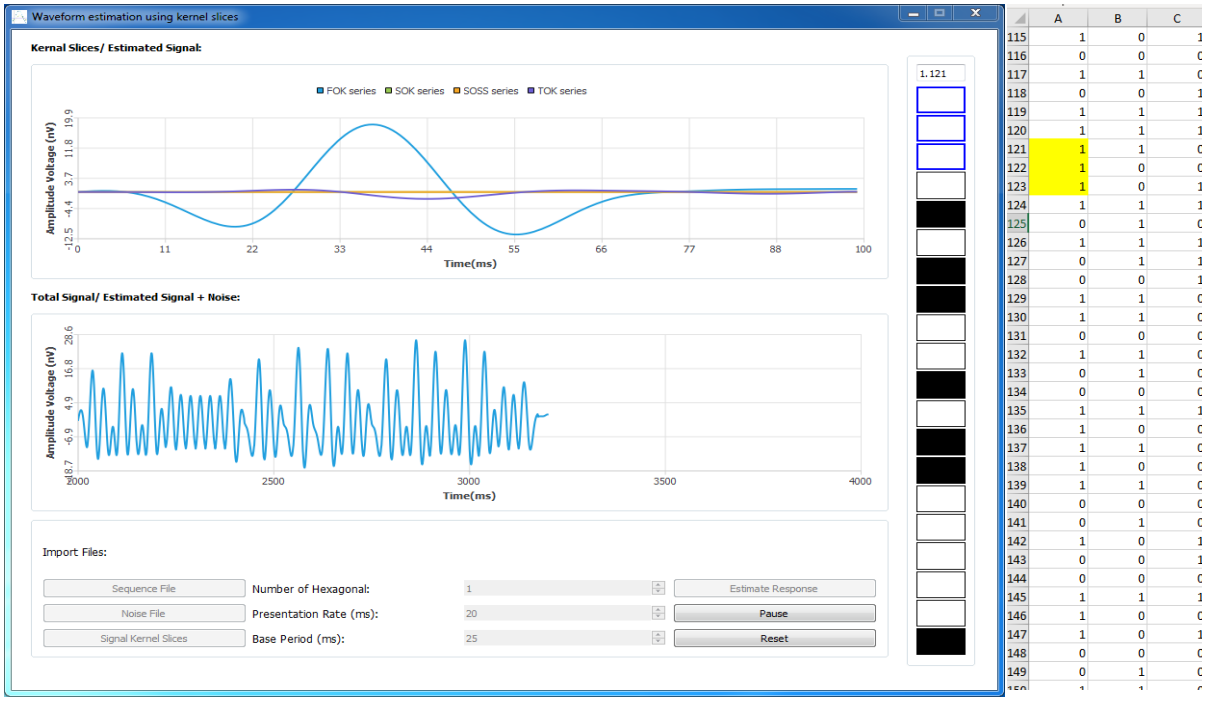

Figure 3.13. Illustrating estimation of location 1 response with stimulation cycle at index 121 of an m-sequence of length 512. The estimation of current response depends on flash content of a memory register that extends by three base-period as highlighted in yellow and demonstrated by blue borders in the GUI. Since this corresponds to three flashes (fff) from table 3.1, it would mean that FOK and TOK kernel slices will contribute to the next response.

The sequence file is an N x M array where M is the number of columns representing the stimulation patches or locations, and N is the number of rows representing the length of the sequence. The sequence is expected to be an m-sequence with or without correction term or adaptation sequence added. If the sequence is not generated through the ISIM package back-end engine, then it is expected to be a binary sequence where binary 1 represents a flash stimulus, and binary 0 represents the absence of a flash stimulus. If the sequence is generated through the implementation of a shift register, then this must be followed by m-transformation. In this transformation, the binary 0 is replaced by element +1, and binary 1 is replaced by element -1, allowing preservation of the mathematical properties of the m-sequence, where the multiplication operation replaces modulo-2 summation and finally replacing all -1's in the transformed array by binary 0.

The noise file can be of any length, greater than or equal to the estimated signal length and may be replaced by an all-zero text file, if the user does not want to include any contaminating noise waveform. Further flexibility is provided for the end-user to omit noise components through simple button clicks on the GUI which communicates through SPI protocol with iSim.

The kernel slice table is required in the form of FOK, SOK, SOSS, and TOK as the implementation assumes a second-order system output estimation. An all-zero text file can replace any of these files if they are not expected to have an impact on the final waveform.

This implementation also requires the number of stimulation locations or hexagons to be provided and will sum the localised response estimate to form the final response vector. The presentation rate defines the GUI update rate, while the selected base-period defines the clinical mfERG frame rate that was set to extract the kernel table.

Using data from figure 2 in the Eric Sutter paper in [44], the FOK, SOK, SOSS and TOK kernel slices are digitised, calibrated, and processed to simulate arbitrary kernel waveforms sampled at 1 kHz and filtered through a low pass corner frequency of 40 Hz, resulting in figure 3.14.

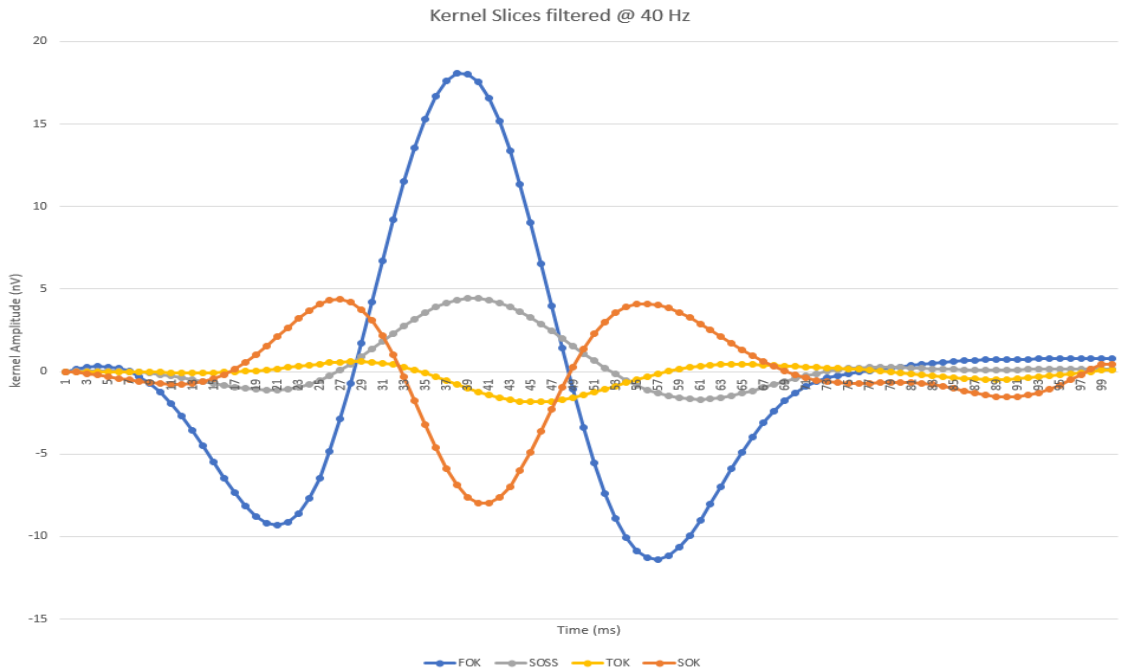

Figure 3.14. Arbitrary kernel slices for FOK, SOK, SOSS and TOK obtained from figure 2 in Eric Sutter paper[44].

The implementation then uses table 3.1 with a memory register length extending to three base-periods to simulate the summed response, sequentially scanning through all columns in the sequence array, see figure 3.13.

The sequence generated by the ISIM package will have a row of zeros added at the beginning of the sequence array as the correction term, which then simplifies the estimation of the signal as described by figure 3.15. Figure 3.15 also demonstrates how iSim deals with the initial boundary condition.

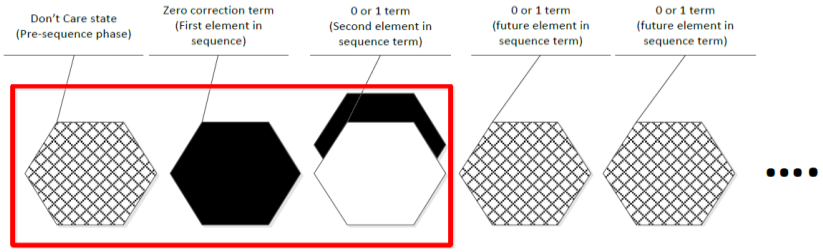

Figure 3.15. the boundary region through sequence is demonstrated by the red box for the initial two elements of the sequence for a second order system. As the first term is always a zero a zero vector of length base-period is generated (the content of memory register is [don't care, don't care, 0]. As one moves through the sequence memory register becomes [don't care, 0, 0/1] that is implementation of a SOK response based on table 4.1 and whether second element of the sequence is a 0 or 1. This will satisfy the initial boundary condition in signal estimation.

Finally, the implementation could easily be extended to that of a linear system response estimation for a theoretically or experimentally selected first-order response if a longer base-period than signal duration is selected (base-period of greater than 100 ms).

3.2.6 Verification of response synthesis algorithm

The synthesised or actual response waveform is decoded using the extraction GUI of figure 3.16, implemented in C++. The interface is independent of the implementation in figure 3.13 and requires the response waveform (response vector), encoding m-sequence (FOK_J), and implemented base-period (`Base_Period` variable) as the required variables. It also provides the user with an option to select the length of extracted kernel slices (`Signal_Duration` variable). The last optional variable helps the user to extract any induced components if they exist in the original response vector. The output of the implementation is the cross-correlation vector allowing visual inspection of kernel slice locations (spatial and temporal) as well as the kernel slices which are locked to the input trigger sequence. The cross-correlation plot is updated in real-time through the implementation of a timer object that is triggered at a user-specified presentation rate in milliseconds, while the kernel plots require a full scan of the input J^{th} location FOK governing m-sequence. Each time the timer object is elapsed, the input sequence is shifted by a default value of 1, and the response epoch matrix is calculated. The response epoch in each column is multiplied by the either 1 or -1 (m-sequence value corresponding to the specific point in time, where the -1 represents the absence of stimuli and +1 the presence) and are summed across the matrix row resulting in a segment of the cross-correlation vector. The implementation has been tested manually using Microsoft Excel® for m-sequences of length 7, 15, 31, 511 and 4095 and further verified and validated using MATLAB®.

The response synthesis and extraction GUIs allow the user to perform computer-based simulations using different kernel tables, base-periods, signal durations and m-sequences before uploading any data into iSim memory to test and validate the mfERG clinical setup.

The implementation algorithm is shown in figure 3.17 and the C++ code in Appendix B.

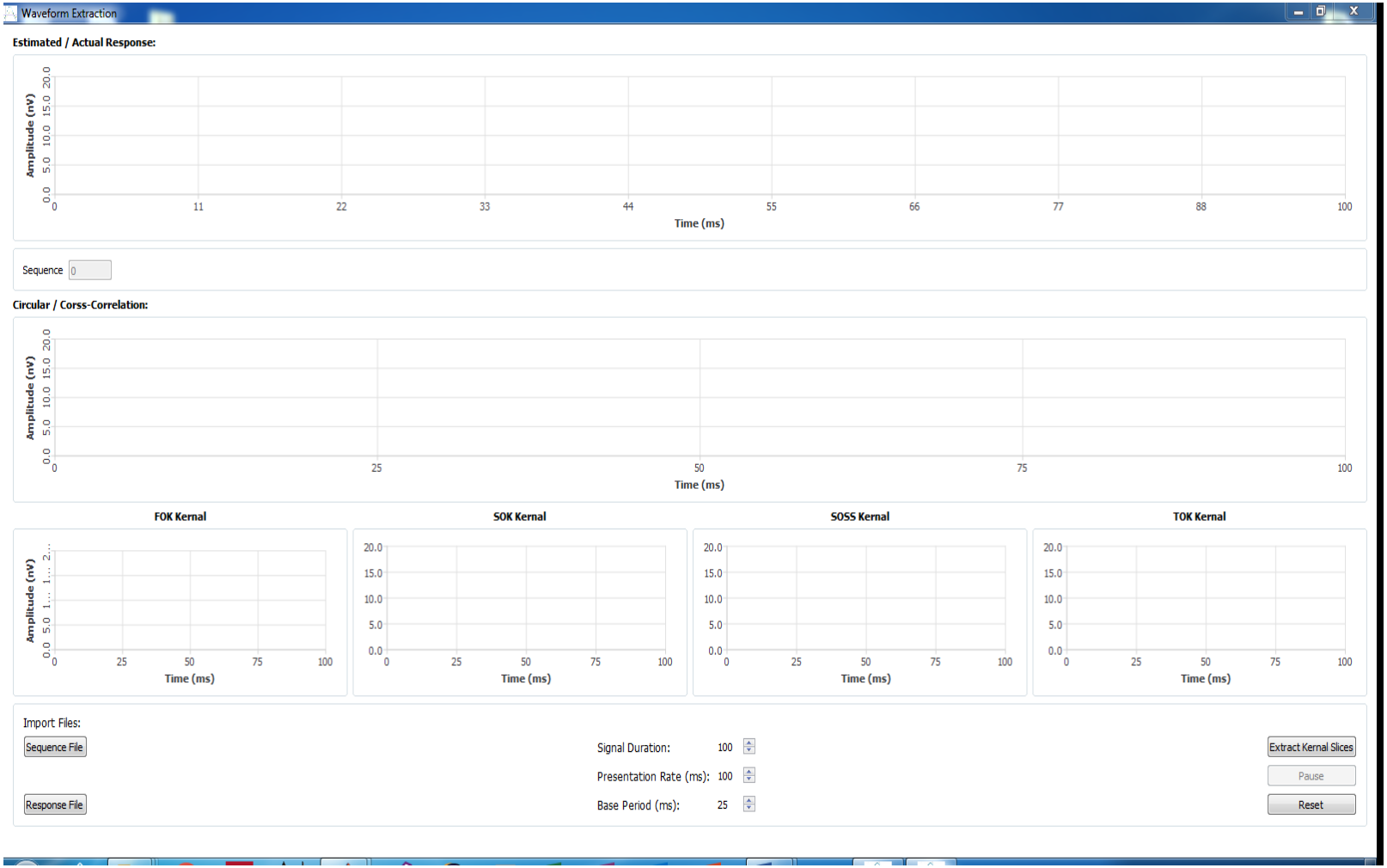

Figure 3.16. GUI written in C++ that is used to extract kernel slices of a second order system up to TOK slice.

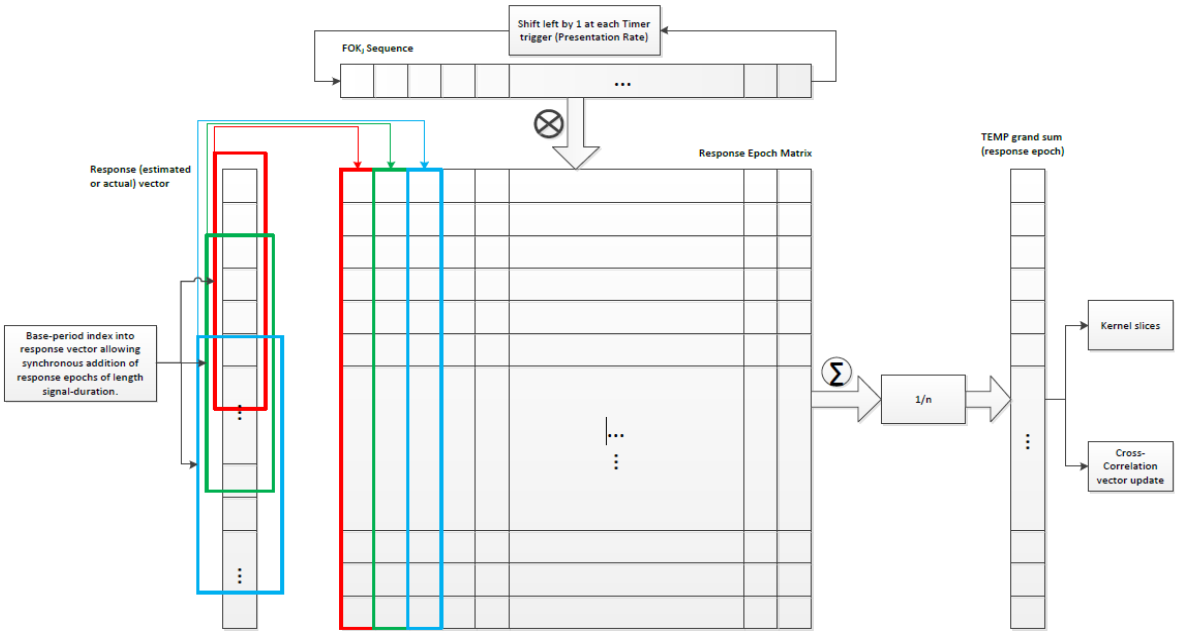

Figure 3.17. Kernel slice extraction algorithm. Synchronous recovery of the kernel slices and cross-correlation vector from estimated or actual signal input vector.

3.2.7 Implementation of fixation error

Eccentric fixation error artefacts are simulated using ISIM providing the end-user with a mechanism to realise how much defocusing could destroy the extracted kernel slices to the degree that they are no longer usable. The effect of defocusing for two spatial locations, governed through two m-sequences of length 4095, is demonstrated in figure 3.18 using arbitrarily kernel slices of figure 3.14. No noise is added, enabling isolation of the impact of defocusing. The illustrated effect is created by putting the governing sequences of the two-spatial location next to each other and swap segments of the sequence. This assumed that when the focus is on one location, the stimulation pattern of the other location contaminates the response of the first location and vice versa. Using this technique, one can quickly determine that the longer the length of the sequence is, the smaller the impact of defocusing if they are not occurring too often as there are a higher number of epochs to average. Also, one quickly realises that the higher-order kernels are much more susceptible to the impact of defocusing. The degree of the impact is determined by considering the following factors when creating the simulation sequence and responses:

- The frequency of occurrence.
- The out of focus duration.
- The length of the sequence or test duration.
- The base-period selected or the number of significant higher-order kernels.
- The number of stimulation location.
- The length of response.

All these factors are considered when generating the estimated response using ISIM package. The fixation error is not available on ISIM when a global flash response is selected, i.e. when localised responses are not considered.

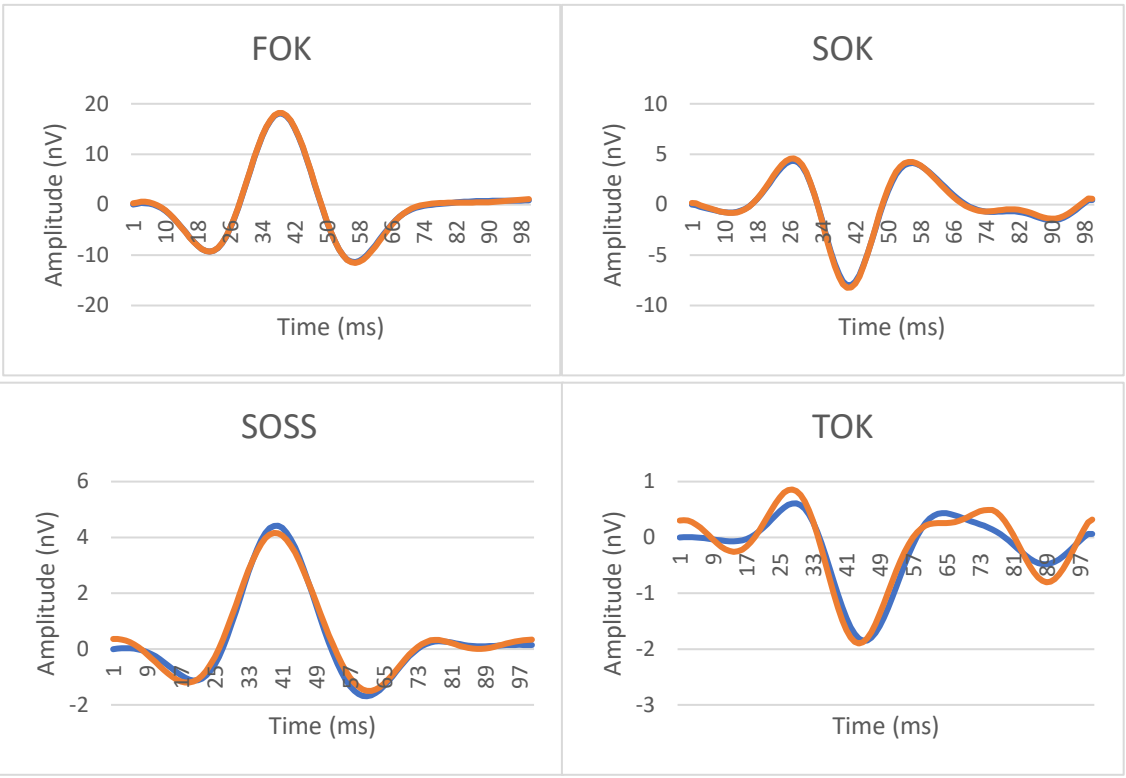

Figure 3.18. Illustration of defocusing in signal generation using ISIM toolbox for a second order system of up to TOK as its most significant higher-order kernel slice. Blue waveform represents the actual kernels and Orange waveform represents extracted kernels post contamination through defocusing. The kernels are for demonstration purposes only. The response vector is created through execution of GUI demonstrated in figure 3.13 by setting the base-period to 25 ms and the governing m-sequence of length 4095. The sequence is mixed with a shifted version simulating the governing m-sequence of the secondary location. Kernel slices are then extracted using GUI in figure 3.16.

3.2.8 Implementation of blinks & eye movement artefacts

iSim could be used not only to scrutinise the governing m-sequence of the clinical instrument when no artefacts are introduced but also when artefacts are injected to learn and verify the system operations. Changes to normal mode of operation on a clinical system may vary due to the presence of artefacts when the system recognises one. Such recognition tends to be amplitude-based. For example, the artefact rejection level used in the Roland RETIscan at RLUH is 5% of the amplifier level, which is 200 µV. This gives an artefact threshold level of 10 µV. Therefore, not all artefacts, like those illustrated in figure 3.20,

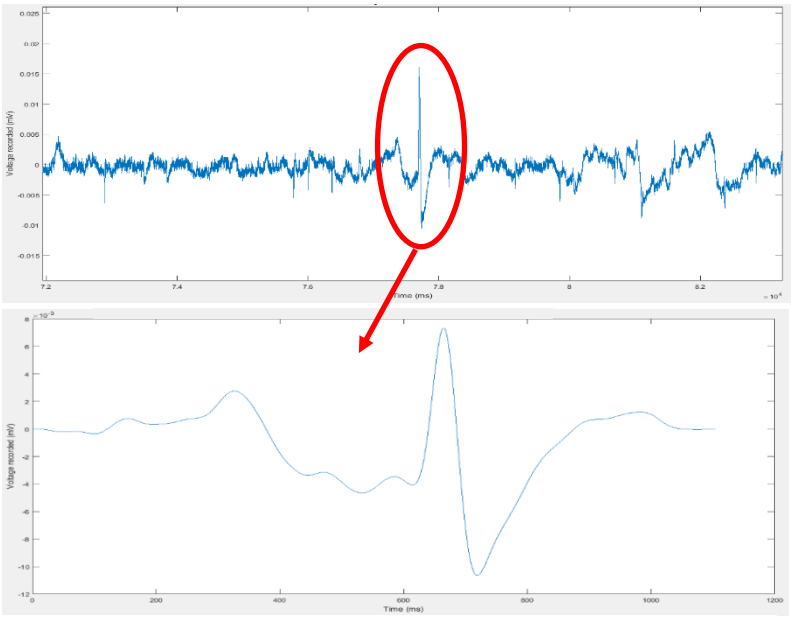

Figure 3.19. Example of artefactual signal that does not exceed artefact rejection threshold.

will cause the system to enter its artefact rejection subroutine, such artefact is demonstrated in figure 3.19 where small eye movements could produce small amplitudes artefacts. iSim can objectively assess the system behaviour in presence of the artefacts as it knows the precise moment when it introduces artefacts as a form of biological signal. iSim can also synchronise this with the reading from stimulator through its optical fibre. This system capability provides the investigator with an objective method to assess the clinical instrument behaviour when artefacts are registered.

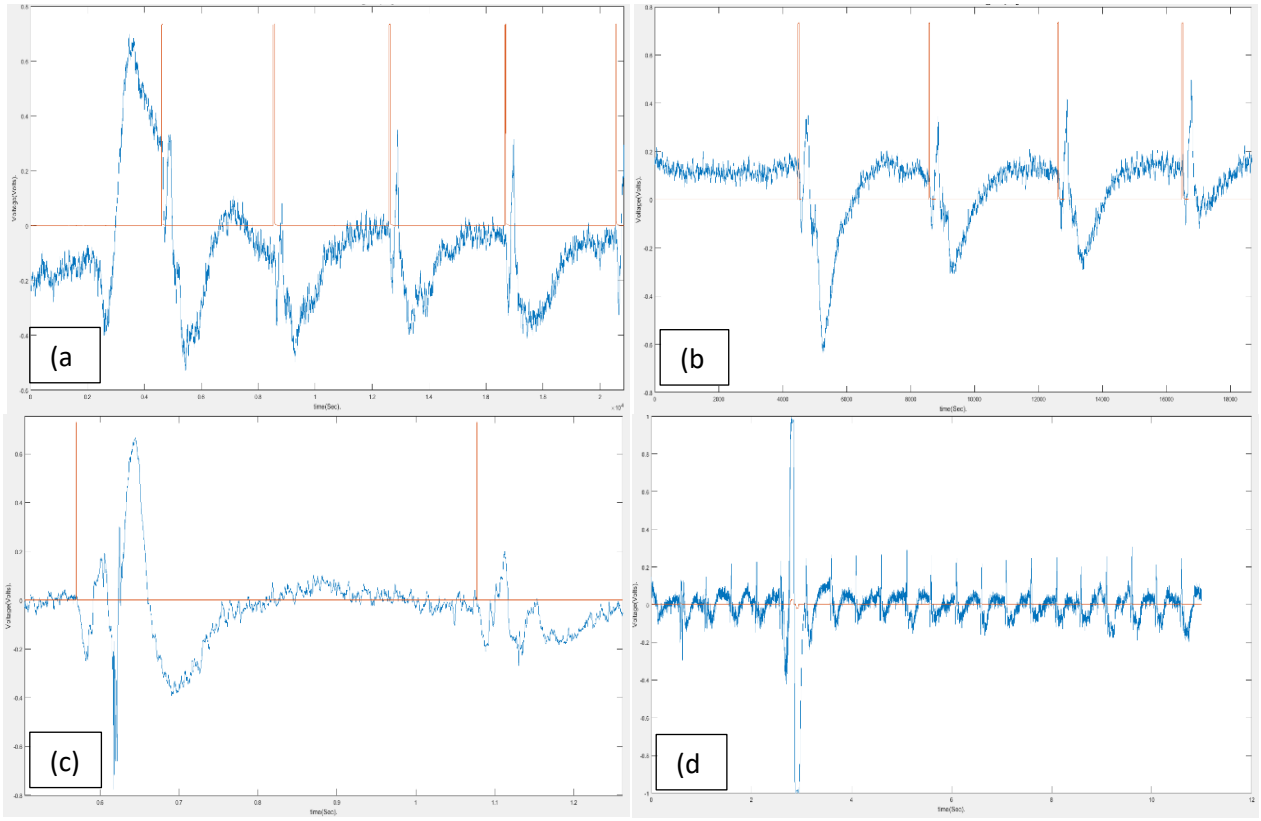

Figure 3.20. This figure illustrates the effect of a blink which completely masks the signal of interest and result in a potential front-end amplifier saturation

(a) Shows a blink occurrence prior to application of the flash, its impact is lasting through the complete period of next retinal response.
(b) Shows occurrence of an eye movement, pulling negative on trough of the signal cycle and is roughly of small amplitude, this could cause significant error in calculation if averaged and as it is evident, it is very difficult to be spotted for an untrained eye.
(c) Shows occurrence of a blink, right after the occurrence of the flash, this is the most common location for an unwanted eye movement or blink. Again, this is contaminating the signal of interest.
(d) Shows a large magnitude blink signal, these are easy to spot for the background clinical software system and the corresponding period would be rejected in prior to averaging process.

The classification, impact and implementation of the artefact rejection algorithm is discussed else where[326][327][328][329][330][331][332] and is beyond the scope of this thesis, although the required infrastructure is in place, to support investigation of artefact rejection mechanisms that are deployed in the clinical setting.

iSim will output the simulated response (for a single location) based on the real-time calculation of its internal memory register variable and the provided kernel slice table. If the clinical system enters the artefact rejection algorithm, iSim will continue to output the waveform based on the registered

stimuli flashes as the clinical system progresses through and tries to recover from the registered artefacts.

3.2.9 Implementation of EMG artefact

The artefacts produced by facial muscle activity such as teeth grinding, jaw clenching, and frowning or smiling are variable in magnitude. This type of noise presents the most problems for the clinical system's artefact rejection algorithm as the 'recovery' from the artefact is a slow process. This causes the clinical system to stay in its artefact rejection mode for longer periods compared to the short-burst blink and eye movements. Most of these artefacts, like those in figure 3.20, have a typical waveform that is a sharp rising spike followed by a deflection of the opposite polarity with an exponential return to the baseline. In some cases, the artefact is not of high enough amplitude to trigger the artefact rejection algorithm. Therefore, these small-amplitude artefacts will go undetected, contaminating the final grand averages.

These commonly recurring artefacts will vary more significantly from subject to subject. It seemed to happen frequently when subjects are first introduced to the stimulus and were concentrating hard on the stimulator screen. This is where the adaptation period could be most beneficial, as not only the retina is settling down and adapting to the incoming flashes but also there is time for subjects to settle into the test.

ISIM does not create EMG types of artefacts using computer-generated simulation. Instead, it uses pre-recording data to contaminate all (or a random section) of the signal with EMG noise data. To avoid any edge effects, the EMG record is smoothed at its ends, i.e. starts from the baseline and returns to it. See figure 3.21.

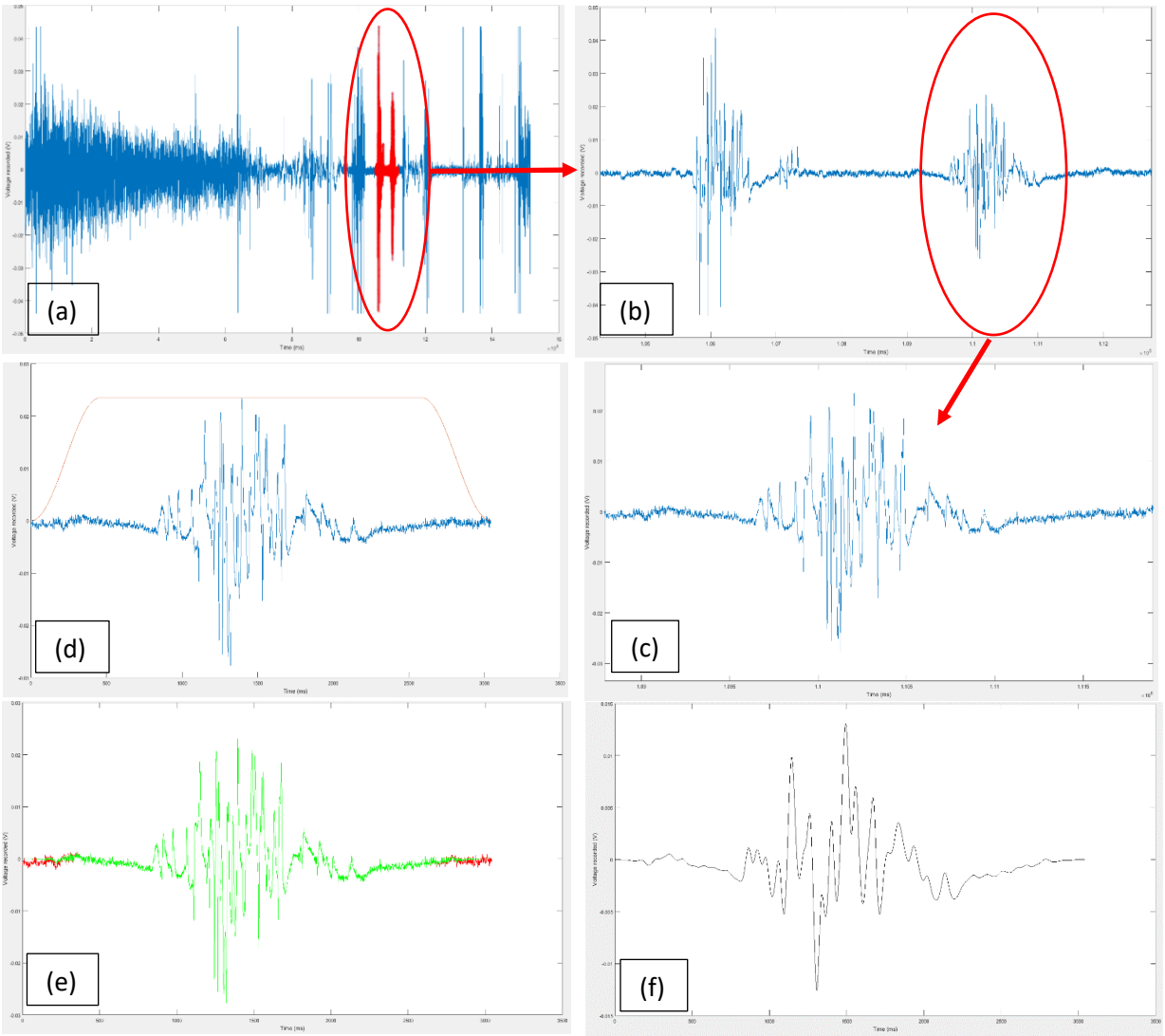

Figure 3.21. (a) Full record of EMG artefact signal data at sampling frequency of 10204 Hz using thread electrode. Subject is instructed to perform various facial muscle activity while sat comfortably on chair. Subject were instructed to perform no eye movement or blinks while staring at a dot on the screen ahead when background lights were dimmed and comfortable. (b) & (c) zoomed section of the data record in (a). (d) demonstrates application of Tukey Window to avoid any edge-effects in processing (MATLAB® responsible function: *tuk = tukeywin(length(EMG(:,2)), 0.3)*). (e) a comparison of post windowing vs actual data record. (f) post filtering application with a lowpass corner frequency of 150Hz. The amplitude of the record is maintained while unwanted high-frequency noise data is removed.

3.2.10 Implementation of harmonic noise interference

Three models are generated and described in this section that could be used for implementing mains interference:

- Pure 50 Hz sine wave with associated harmonics (amplitude, phase and frequency are kept constant with varying SNR).
- A 50 Hz nominal waveform and associated harmonics where the frequency can vary within a range of 1% based on collected data from the UK National Grid.
- A dynamic model based on ARMA that allows considering variations due to the presence of time-dependencies in recorded frequency data.

These methods are used to represent mains interference and challenge the signal processing packages designed to remove such interference from the recorded data. For this challenge to be of any value, one needs to know the characteristics of mains interface. There are many studies, and reports published that propose different methods for removing mains interference from various biological records, such as ECG, EMG, ERG, etc.[333][334][335] When simulating mains interference, it is usual to assume that the interference is at a set frequency of 50 Hz [336] within the UK and develop a simple back-end program module to generate a sine wave at 50 Hz for the requested duration of the signal. Here, a more detailed approach was followed. National Grid UK was contacted and a record of mains frequency over two consecutive days was requested for further analysis.

Methods of reducing such interference were carefully considered, and experiments were made to record various noise and signal components of ISIM. For example:

- Powering the measurement system through isolating transformers and floating the patient and measurement equipment through isolation from power lines.
- Most clinical measurement rooms are faraday cages; this will reduce the patient's decoupling capacitance to power and earth lines.
- Maintained maximum distance of the measurement system and test subjects from the mains supply.
- Twisting long electrical wirings to cancel out harmonically generated interference.
- The interference is also reduced by using proper cabling (shielding and guarding – guarding refers to actively driving the cable shield) to minimise inductive and capacitive coupling.
- Careful skin preparation to ensure low skin-electrode impedance also reduces interference. (It is difficult to obtain high-quality bio-electric signals because they typically have very low amplitudes and wide bandwidths, hence they can easily be corrupted by electrical noise etc. Lowering the skin-electrode impedance increases the strength of the signal as less signal energy is lost across the impedance. This also reduces the effect of common-mode signals. An increase in signal strength will result in improved SNR at the source).
- Power line interference is assumed to be common to the pair of electrodes and will ideally be completely removed by a differential amplifier with a high common-mode rejection ratio (CMRR).

A simple MATLAB® program was created that allows generation and simulation of mains interference consisting of a single 50 Hz sine wave with the addition of higher-order harmonics as required, refer to Appendix B. In this approach, the mains frequency was assumed to be constant at 50 Hz, which results in constant-frequency harmonics. Appendix B provides an improved MATLAB® function that allows variations in the frequency of the mains interference (amplitude and phase remain constant) and its accompanying harmonics. The latter approach is based on a static analysis of observed changes in mains frequency based on observed data from the UK National Grid (figure 3.22). Such data is also available in its historic format on the UK National Grid main webpage.

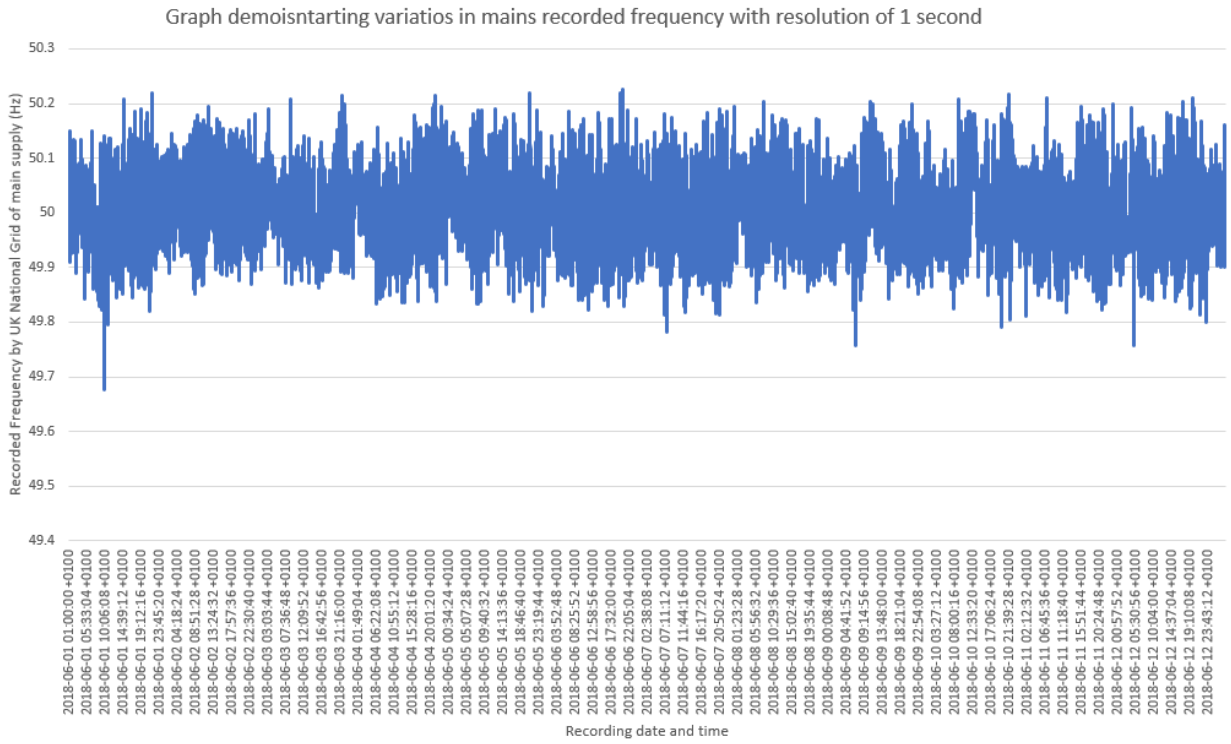

Figure 3. 22. National Grid UK, reports that, system frequency is a continuously changing variable that is determined and controlled by the second-by-second (real time) balance between demand and total generation or supply. If demand is greater than generation then the frequency falls and vice versa. It is also reported that national grid must control the frequency to be plus or minus 1% of the nominal frequency of 50.00 Hz. A sudden drop in frequency would indicate that the grid is under stress as there is a surge in demand. This figure demonstrates historical data with 1 second resolution over the month of June 2018. As it can be seen from this published data, the variations in frequency is such that, on average the supply mains frequency is 50.00171 Hz with maximum recorded data of 50.226 Hz and a minimum recorded data of 49.677 Hz.

The analysis of national grid data (chapter 4) suggests that there are time-dependencies in the frequencies reported by the UK National Grid. To further evaluate this hypothesis, an experiment was set up to record the mains signal directly from the wall socket in the visual electro-diagnostic unit of St Paul's Eye Unit, when clinic room was not in use. The setup is shown in figure 3.23 and the recording software is presented in Appendix B.

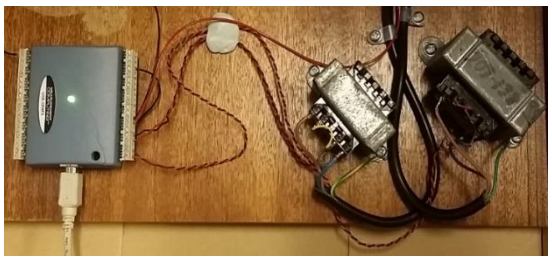

Figure 3.23. Illustrate the setup used to measure, digitize and record mains signal directly through

3.2.10.1 Measurement accuracy and a brief discussion:

The accuracy of frequency measurement using digitised data depends on the sampling frequency of the device and the resampling factor used. This effect was investigated in MATLAB® and found to be insignificant.

From the Power Spectral Density (PSD) analysis, the record shows peaks at odd harmonics and not even harmonics. This suggests that the harmonics may not be part of the mains signal recorded but due to some other nonlinear effects that are present. Such nonlinear effect can be due to attachment of a nonlinear load to the mains network at a nearby place.

A more dynamic model is also made available to represent the effect of mains interference based on the ARMAsel (AR, MA selection) algorithm. This is presented in Appendix A. It is worth noting that enough data were collected from the mains socket and resampled to allow for direct use in noise generation as an alternative to the three models described here.

3.2.11 The ARMA model selection algorithm

3.2.11.1 Introduction

Noise estimation using a Gaussian White Noise (GWN) generator is not realistic and will not provide any knowledge of the system characteristics and its inherent structure. A simple linear $ARMA$ model can provide an adequate model of the system noise. The stationarity assumption of the retina as a control system further justifies the selection of $ARMA$ as the model and $ARMAsel$ as the algorithm, implemented in MATLAB® and embedded within the ISIM package (refer to Appendix A and B for mathematical background and implementation detail and code). The $ARMA$ implementation is used to estimate biological noise data further corrupted by noise from the measurement system. These time series estimations assume that such noise sources can be treated as orthogonal components and produce the noise data through a stationary or at least weakly stationary stochastic process, i.e. non-deterministic with statistical properties (mean, variance, covariance, etc.) that are independent of time. A sample of a user-defined length is generated. Estimation using $ARMA$ assumed that harmonics, DC drift and other spontaneous noise data such as blinks and eye-movements as well as EMG interference are not present in the recorded data used to estimate the model coefficients. Experiments used to collect data for model coefficient estimation were designed, allowing confidence in developing the model. The components are estimated or generated separately and added to generate the final noise data time-series. This allows one to use a sufficiently large segment of the recorded data to estimate the model parameters and ensures the order of the model is kept reasonably low. A model which depends only on the previous outputs of the system is called an autoregressive model (AR), while a model which depends only on the inputs to the system is called a moving average model (MA), and of course a model based on both inputs and outputs is an autoregressive-moving-average model ($ARMA$).

3.3 Bio-Amplifier Hardware Design, Development and Implementation

A prototype bio-amplifier is designed and developed, to allow quick and accurate preliminary data collection for construction of the ISIM signal and noise library. The amplifier was integrated with the Roland Ganzfeld (Ganzfeld Q450HF, SN 9905H-414, Roland Consult) and Glasgow MFS systems[257] as stimulators. The prototype design takes into account relevant quality, clinical, environmental and economic factors. The finished amplifier, illustrated in figure 3.28.b is the working and tested prototype that is comprised of:

- A front-end amplifier block (referred to as Black Box in figure 3.28.a and figure 3.29).
- A gain block (user hardware selectable to 5000 or unity gain).
- A power block.
- A filter block (a simple low pass filter with a low-pass corner frequency of 500 Hz).
- A data acquisition block (USAB-ADC-1608FS data acquisition, measurement computing™ (MCC) hardware that communicates with primary GUI using a supported library in MATLAB® Data Acquisition Toolbox).
- A synchronisation block (MBED or PIC microcontroller unit) and
- A data buffer block (embedded within MCC DAQ hardware and software implementation).

The unit interfaces with flash stimulation unit (Roland Ganzfeld or Glasgow MF LED-based stimulator[257]), through a GUI written and developed in MATLAB®.

The unit operates in either of two modes:

- Triggered acquisition
- Continuous acquisition

These modes are accessible to the user through software. If the trigger data acquisition mode is selected, then the MCC unit will look for a trigger signal from a synchronisation unit to start sampling over a specified window of time. Outside this window, the system will not collect any samples. This technique is used in most clinical instruments like the Roland system, which imposes limitations on signal processing and effectively rules out high-quality Fourier-based filters and other statistical artefact rejection techniques, due to the introduced discontinuities at either ends of the individual data cycles. An example of this record treatment is shown in figure 3.24 using yellow boxes to represent the recorded windows in a triggered operational mode of a continuous record trace. The continuous trace is generated through mixing a standard PERG signal with 3-dB of noise for presentation purposes.

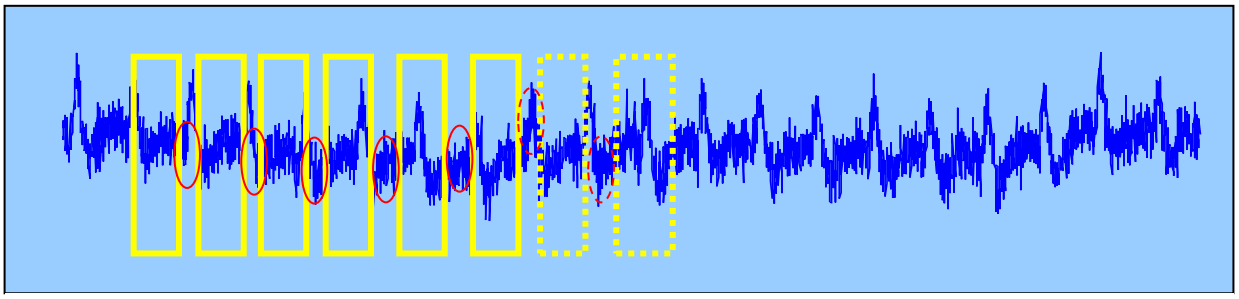

Figure 3.24. Trigger mode operation and record segmentation.

In a continuous mode, the MCC unit will start collecting data as soon as it is started and will dictate the synchronisation pulses to the MBED synchronisation unit. Therefore, there exists a reversible master-slave relationship between the data acquisition unit and the synchronisation unit, which is determined via the selected operational mode.

The amplifier can handle a sampling rate of up to 100 kHz and a minimum rate of 10 Hz (with a 16-bits resolution per sample) that is again user-selectable through the GUI (figure 3.30). Filtering is performed in both hardware and software. In hardware, a low-pass filter with a corner frequency of 500 Hz. In the software, a user-adjustable band-pass filter is implemented as well as performing running averages based on the selected sampling frequency and the user-provided decimation factor.

The amplifier has eight simultaneous single-ended recording channels, which can also be configured through software as four differential recording channels.

The on-chip buffer provided by the MCC unit is exceptionally useful. It allows the GUI to be updated in real-time and gives the control software enough time to collect data, perform some initial signal processing, provide a display, and store the data on the hard drive before any overwrite error occurs. It, therefore, allows for a real-time display of data and notifications so that the investigator can monitor the state of the subject and collect data accordingly. Further, it allows for a pause mode, which temporarily halts data collection and storage but continues to read and display samples. This is important if the test duration is long, and the subject requires some rest or

electrodes and/or other environmental factors that need to be re-adjusted before recommencing the measurement.

The MCC and MBED units communicate through Digital Input and Output (DIO) pins to ensure synchronisation between the two units to the collected samples. The MCC unit provides absolute and relative time information tagged with each collected sample. This useful feature is not present on the MCC DIO lines. These digital lines are used to provide the governing flash stimulus TTL pulses. The user will specify the sampling frequency as well as the trigger frequency (flash presentation rate) and duration of flash ON and OFF periods. The MBED then ensures the trigger frequency is set, and flash ON and OFF durations are kept as requested when it generates the trigger TTL pulse train. This pulse train is used to trigger the stimulator (Ganzfeld or MFS). These stimulators will typically perform a flash when their internal logic circuitry detects a rising edge on the TTL trigger-in and may keep the flash ON for the duration that the TTL line is kept high (this technique is typically used to separate the retinal ON and OFF pathways), see figure 3.25.

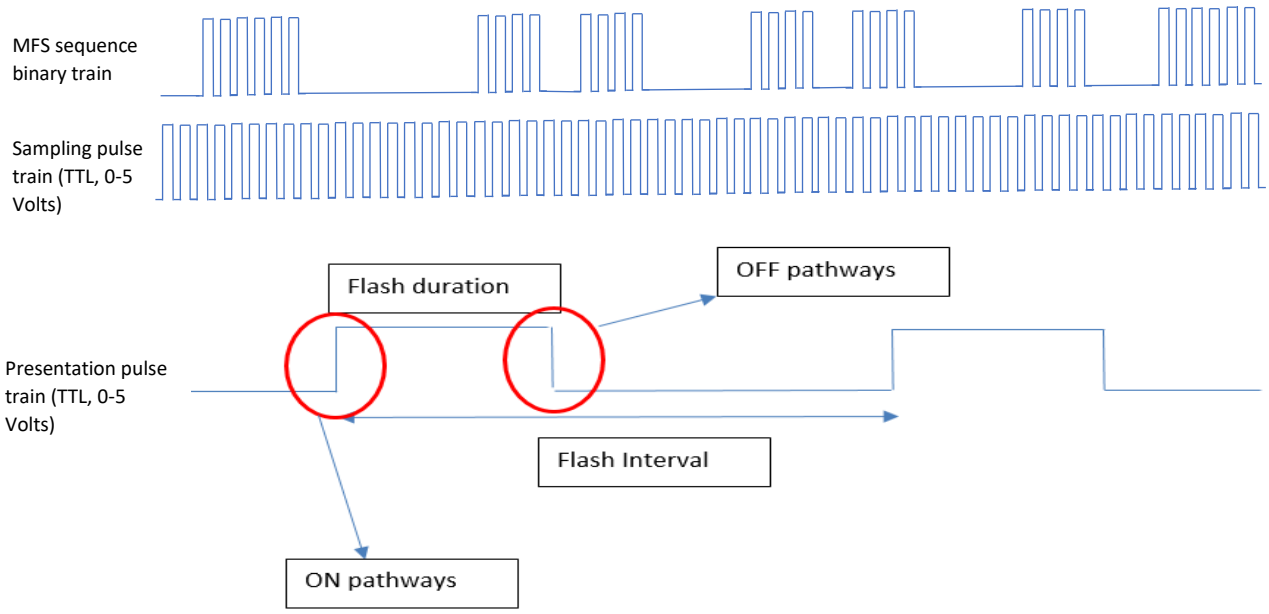

Figure 3.25. Graphical illustration of stimulator trigger signal preparation for various operational mode. The trigger signal will ensure perfect synchronization between data collected and trigger timing of the stimulator.

During the bio-amplifier initialisation, the following information is transferred to the MBED unit:

- Flash duration.
- Trigger frequency.

The Handshaking mechanism is implemented in both the MATLAB® and MBED embedded code. Once the MCC communicates the user requested sampling frequency, presentation rate and flash duration, MBED calculates the actual trigger frequency and flash duration and communicates these to the MCC unit. The MCC checks this and updates the user, at which point the top-level MATLAB® GUI is updated with the actual settings. The implemented two-way communication channel will ensure that the two units are in sync with one another. The synchronisation is imperative, as there is a certain window of time that is used for initialisation when the user presses the start button on the GUI before the system starts sampling (housekeeping activities). Activities during this time-window

include capturing all user-defined inputs such as sampling rate, recording channel/s, presentation rates, flash durations, etc. as well as setting up the analogue object and clearing the internal MCC buffer and initialising of the MATLAB® buffer. These activities take time and require that the internal program gets a timestamp for the first sample captured to determine the exact timing of the stimulation presentation.

As soon as the MCC unit starts acquisition (the analogue object is invoked), it outputs the sampling clock signal through a designated Digital Output (DO) pin. This is fed into the MBED synchronisation unit. The MBED synchronisation unit is programmed to monitor and count the number of rising edges on this line. The MBED then outputs the required TTL pulse train through the trigger-out pin of the bio-amplifier system in synchronisation with the received sampling frequency pulse train from the MCC unit. The trigger-out pulse train is also fed back to the MCC unit and consequently to MATLAB® to perform the following activities:

- Update the GUI with the time at which the flash stimulus occurred.
- Update the GUI with the duration of the trigger-out ON and OFF pulses.
- Verify the above two bullet points with respect to the requested settings.

Having this signal train, the MATLAB® interface can chop up the recorded data in-between flashes for averaging purposes and can perform the required running averages to smooth the displayed data in real-time.

In the case of multifocal stimulation of the LED-based Kelvin Vision system, two mechanisms are used to prepare the sequence file (binary 1 or 0) as well as the pulse train (trigger/synchronisation signal). The MATLAB® GUI in figure 3.31.b is used to create the sequence file, prepare or condition this sequence file and upload the file into the MFS on-board SD storage memory. The file preparation process involves the following steps:

Mechanism 1:

- Generate the sequence, this includes the m-sequence and the adaptation period if requested. The generated sequence is binary 0 (-1) or 1 (+1) after performing the m-transformation.
- Calculate the base-period, the inverse of presentation rate requested by the user.
- Based on the calculated base-period and sampling frequency, calculate the number of filler frames that are required to synchronise the sequence with the sampling frequency pulse train.
- A binary zero in the sequence refers to the minimum intensity, and a binary one represents the maximum flash intensity. The GUI requires a calibration file to adjust the required local intensity of the stimulator (individual LED-based hexagons) and maintain a linear response of the luminance of the stimulator across all requested hexagonal areas.
- The GUI assigns the pulse duration in frames where a binary one is requested by the user and assumes a pulse duration of 1 ms, if this field is left empty or cannot be assigned due to calculations errors.

Mechanism 2:

- The same GUI is used as in mechanism 1 to prepare the file before uploading it to MFS memory. The method for generating the sequence and assigning intensity levels are as

above. The only difference is the length of the prepared sequence file which can be much smaller. This is advantageous, as frees up storage area in the MFS onboard SD card. This is possible through avoiding filler frames in the sequence and adjusting the trigger-out pulse train of the MBED synchronisation unit.

The Ganzfeld stimulation can be both LED and Xenon based and can be programmed through the implemented MATLAB® GUI (figure 3.31.a), while the MFS stimulation is LED-based.

The bio-amplifier communicates with the top-level user GUI through a USB port and the implemented Serial Peripheral Interface protocol (SPI). The SPI port is automatically configured and requires no further input from the user. The unit is powered through the USB port. The implemented power supply block will ensure a maximum default dynamic range of +/- 12 V that can be further configured using the MATLAB® GUI.

The whole system is set up in a designated room that is isolated from mains supply using transformer blocks, therefore floating the test subject or patient and the measurement system during the examination. The setup would allow for “genuine” continuous measurement of biological waveforms (whether noise, blink, eye movement, EMG or signal such as standard ERG and mfERG) and its reliability means it will not miss any data packets. The measured Common Mode Rejection Ratio (CMRR) is at a minimum of 110-dB, and a maximum of 120-dB and its adjustable and high sampling rate means enough data can be collected to model the biological system in later analysis accurately.

When the bio amplifier system is used to collect noise data, its artefact rejection algorithm can be disabled, allowing the capture of records of data such as blinks without the system automatically rejecting the data segments. The bio-amplifier also provides communication with selected interfaces such as the Glasgow MFS system. Right Leg Driven circuitry (RLD) is also provided by the front-end analogue-to-analogue isolation amplifier block, which has a gain of unity and a reported CMRR of 180-dB. The design of the bio amplifier system has therefore reduced this CMRR by 60-dB without implementing the RLD functionality. This is still comparable with most of the commercially available bio-amplifiers such as the Roland system which has a CMRR of 120-dB when common-mode signals are applied to both of its differential inputs. The CMRR could further be increased by twisting the wires carrying biological signals to the amplifier and through good design and experimental practice such as shielding the system as shown by in figure 3.28.b (the front-end yellow boxes), floating the measurement system and avoiding any EMI during measurements from instruments such as mobile phones.

Analogue-to-digital conversion close to the signal source reduces the chance of corruption of the signal with noise. It is also easier to transport a digitised signal across the patient physical isolation barrier. For example, using optical electronics chips that convert the electrical digitised signal to pulses of light and convert the light pulses back to electrical binary 1 and 0 once the barrier is crossed. This is the technique implemented in the Kelvin Vision bio-amplifier system of figure 3.26.a.

The Kelvin Vision amplifier uses high resolution (32 bit) instrumentation, sigma-delta ADC amplifiers (four recording channels, two front-end ADC amplifier ICs) as its front-end digital biopotential amplifier rather than the more traditional, high-quality analogue front-end components. Due to its high resolution, there is no need for front-end amplification of biopotential signals with low amplitude[337]. This method of amplification, if coupled with online or offline signal processing packages (that would traditionally be performed by the front-end analogue circuitry and hardware-implemented filters), provides a powerful setup for the recording and processing of biosignals.

Advances in signal processing Integrated Development Environments (IDEs) and platforms such as SPSS and MATLAB® have provided a suitable environment for signal processing. Also, advances in embedded, inexpensive and powerful microprocessors, microcontrollers, and specialised or generic digital processing boards allow one to perform fast onboard signal processing of data. The Kelvin Vision amplifier was reliant on fast streaming interfaces such as USB as it did not implement any significant built-in data buffering system. The amplifier application interface operates on a Windows Operating System (OS). It is known that Windows is not efficient when it comes to real-time processing and as such the author had significant difficulties storing, displaying and processing the received data using this application interface with MATLAB, or any other signal processing IDEs. Such attempts would result in discontinuities in recorded data, termed "*missing packets*" by the developers of the Kelvin Vision amplifier. Such discontinuities constitute a significant problem when it comes to processing the information accurately, as there are no tools available to interpolate the data accurately.

The Kelvin Vision Multi-Focal Stimulator (MFS) was also investigated as part of this work, to ensure the suitability of the system for data collection. Of particular interest were the following areas:

- Element-size analysis, including ring area calculation using custom-built MATLAB® functions, see figure 2.21.
- Detailed calibration of the unit, including a procedure and tools such as an Excel® spreadsheet allowing for semi-automatic calibration. This tool considers, background & retinal periphery illumination, pupil diameter, the retinal angle subtended, light bleed from neighbouring hexagonal locations and other factors to provide the best estimate of the retinal illumination (see Appendix B for further details).
- A MATLAB® GUI to configure the MFS, including loading the stimulation sequence onto the internal device storage. This interface is then fully integrated with bio-amplifier main GUI, see figure 3.30 and Appendix B. This interface provides a user-friendly tool for building the stimulation sequence and requires (optional but recommended) the calibration and element-size files to accurately assign the intensity levels of individual hexagonal locations.

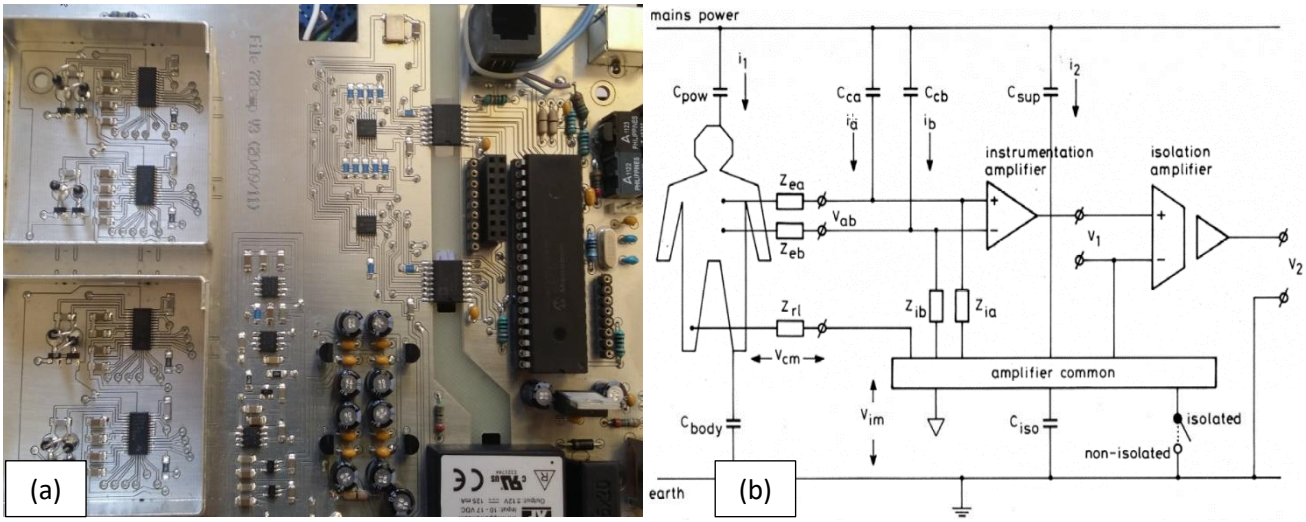

Figure 3.26. (a) The apparent isolation path and the use of optoisolators to transmit the signal across the isolation barrier. The component used to isolate the DC power supply, $\pm$12V, is also present. The ground plate in this design is isolated from earth (main's earth) and driven to 0 V using buffer amplifiers. This signal is also fed to the common (reference) electrode that is placed on the patient's forehead during ERG measurement (colour-coded as a green electrode). The ADC amplifiers and respective gain blocks (resistive blocks) are illustrated at the right where these are isolated from the danger of EMI through shielding. In between the isolation barrier and shielded ADC instrumentation amplifiers (32 bit) there exists power regulations circuitry and multiplexing stages. In the left-hand side of this figure, the control unit and power management circuitry are populated. The board is a two-layer board with components and signal tracks on one side of the board, as shown and an almost undisturbed ground plan on the other side of the board. Good electronics practice is visible throughout the layout. For example, most of the tracks on the analogue and digital side are not at the right angle, which further reduces the electronic noise introduced due to reflection. (b) The amplifier's common is different from earth, and it could be connected to the earth. In which case, there is no patient isolation, hence more significant noise interference. The amplifier common is the reference plane. There is no direct path to the earth from the amplifiers common. This is purely for patient safety and results in breaking the ground loops interference, making it a complicated task to make this common reference, electrically quiet. Ripples on this line are common to both inputs of the differential amplifier. In the figure above, there is no direct path from patient to earth. This is performed via isolating the amplifier common and using an isolation amplifier. This results in patient floating. The amplifier common is floating, that means it can be sitting on any voltage and the output of the instrumentation amplifier is measured with respect to this common terminal. It is therefore required to have this terminal, electrically, very quiet. Figure (b) is for illustration purposes only and does not represent the actual placement of the electrodes during ERG measurement. The isolation also allows for accurate transfer of signals across the barrier without cross-coupling or interaction between adjacent signals.

The MSC (Magnitude Squared Coherence) algorithm (mathematically represented by equation 3.2[338]), was implemented in MATLAB® for use in signal extraction or at least identification of significant frequency components of signal of interest in very noisy waveforms with small recorded SNR. This method has been used frequently in signal processing areas to measure the coherence between real- or complex-valued signals[339]. Most recently, this method has been used in pattern recognition and interpretation of low SNR Pattern Electroretinograms (PERGs) by Fisher et al[323].

$$MSC(f) = \frac{\left[\sum_{i=1}^{M} X_i(f)\right]^2}{M\sum_{i=1}^{M}[X_i(f)]^2} \tag{3.2}$$

$$where\ X_i(f) is\ the\ i^{th}\ of\ each\ epoch\ in\ the\ series\ length\ M\ \left(\begin{matrix}DFT:\\ Discrete\ Fourier\ Transform\end{matrix}\right)$$

The significant frequency components of a standard PERG response, as represented by ISCEV, and its respective frequency series representation are shown in figure 3.27.a.

It is noted that an added noise component also has frequency components in this band. However, the MSC algorithm looks for coherence (in the frequency domain) which is analogous to correlation

in the time domain. Figure 3.27.b demonstrates the synthesised signal using all ten frequency components of a standard PERG, the first seven frequency components and finally (in red) the primary three frequency components only. 40% of PERG power is in its first three harmonics (f_1, f_2 and f_3). The MSC algorithm will identify the significant frequency components, where the larger the number of cycles provided (the greater measurement duration) or, the better the SNR, the more accurate the estimation becomes for a higher number of frequency components.

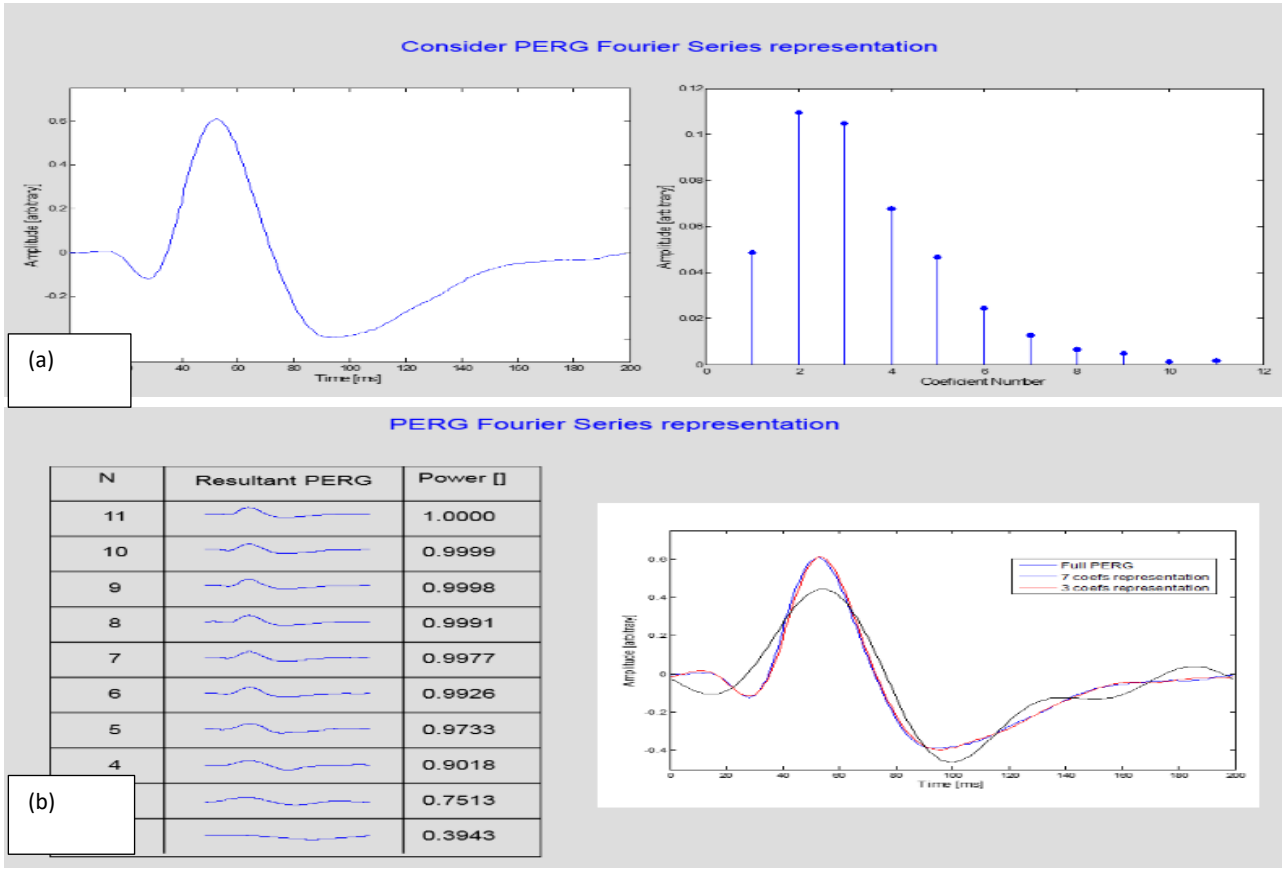

Figure 3.27. Frequency analysis of a PERG waveform.

The MSC implementation requires the following three inputs:

1. The collected matrix data (chopped response waveform at the indices where flash stimulation has occurred).
2. Sampling frequency.
3. An optional window function. If this is not provided, a rectangular window is taken by default.

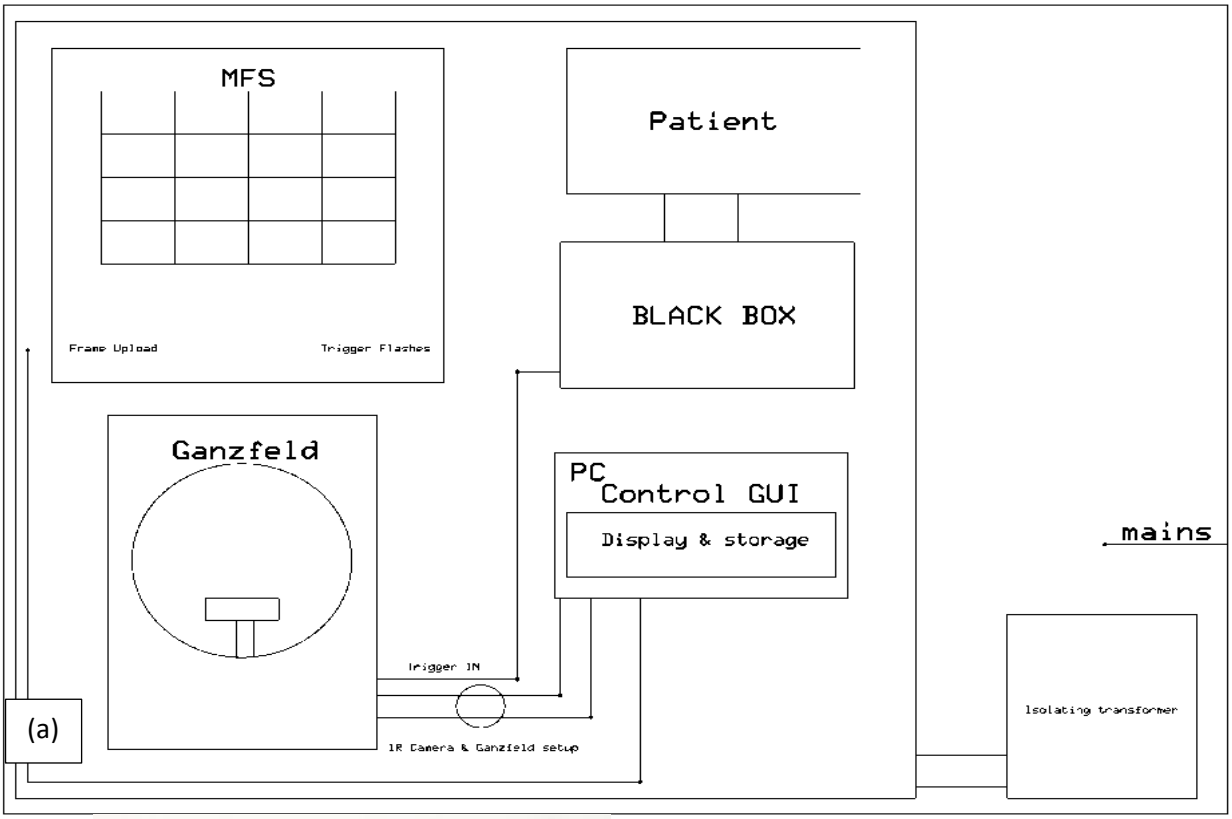

(b)

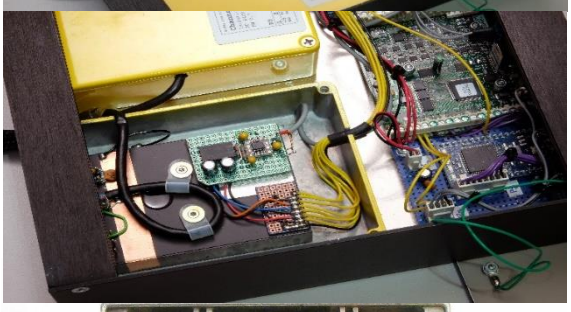

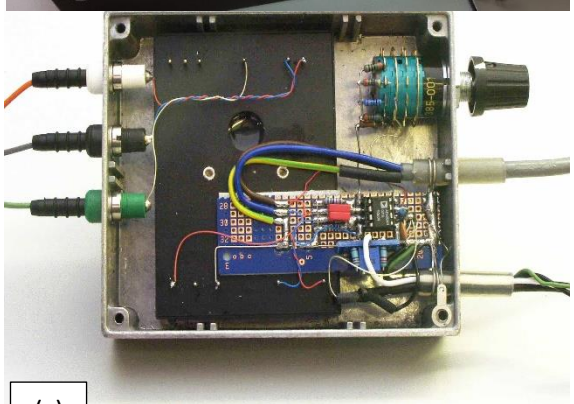

(c)

Figure 3.28. (a) Illustration of the clinical/study setup and the required connections. As well system being powered through an isolation transformer block allowing the measurement units and the subject connected to it to float for safety and noise reduction purposes. (b) Illustration of designed and developed bio-amplifier showing input and output terminals including amplifier's two recording channels, optical trigger in/out, USB terminal, other exposed input and out digital pins (DIO lines) as well as MCC onboard LED. The gain switch between a gain of unity and 5000 is also demonstrated. (c) Illustrates the initial signal channel bio-amplifier prior to advancing to development of a two-channel bio-amplifier with higher specification.

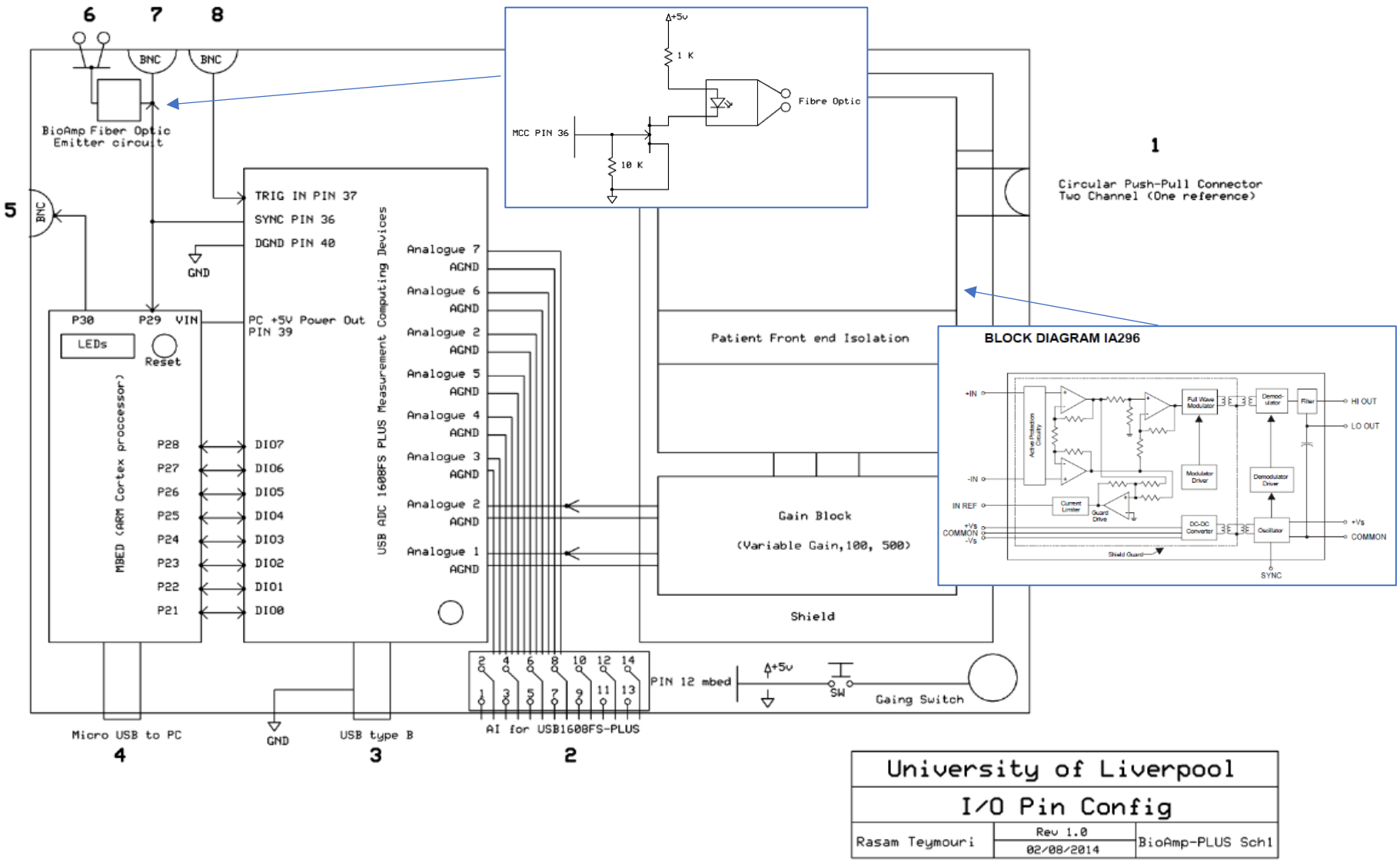

Figure 3.29. illustration of bio-amplifier electronic schematic demonstrating the pin configuration of all integrated units. These pin configurations are carefully recorded during implementation of governing software and are hard coded respectively.

Figure 3.30. (a) Illustration of the MATLAB® GUI to communicate with bio-amplifier and stimulator. (a) shows the interface and a popup dialogue box that allows user to select the stimulator type. (b) Illustration of bio-amplifier main GUI during study subject test run using Ganzfeld Roland system while performing flash stimulation of -25 dB below ISCEV specified standard flash intensity of 3 cd.s.m^{-2}. There are two plot areas, the one on the left is a plot of collected data filtered at 500 Hz low-pass corner frequency with no other signal processing and the one on the right which demonstrates the signal average in real-time. The pause button on the top right corner is only visible when the system is running and provides a mechanism to pause signal averaging and storing while still reading and plotting the biological waveform. The artefact auto-rejection mechanism is active when collecting data, the operator will have access to raw data including all recorded artefacts. Figure (b) also demonstrates recording from both eyes through activating both bio-amplifier channels.

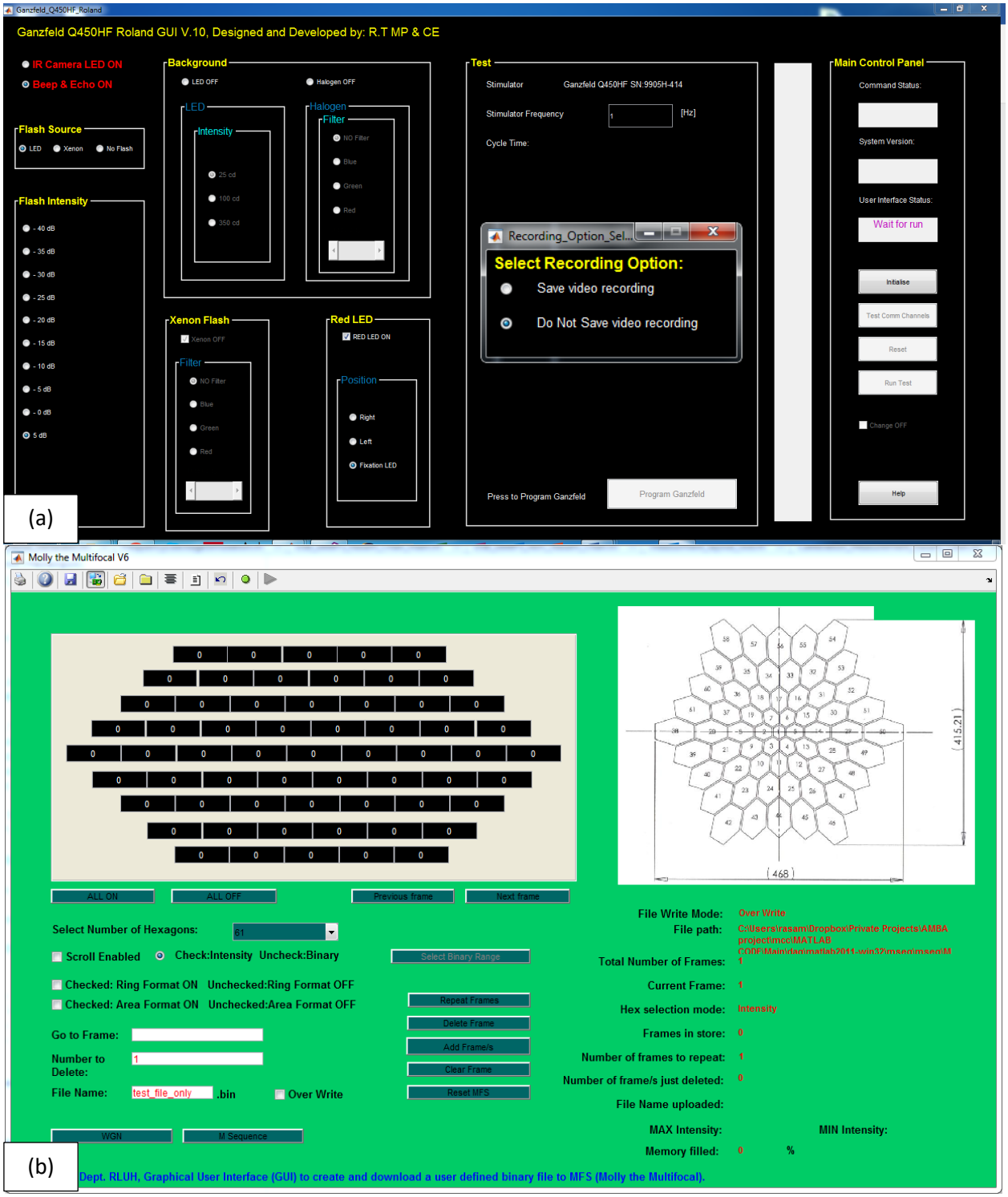

Figure 3.31. (a) Illustration of MATLAB® GUI to configure Roland Ganzfeld stimulator. (b) MATLAB® GUI to generate m-sequences, prepare the sequence (e.g. adaptation length, correction term, and intensity level assignment, peripheral adaptation intensity setting as well as configuring the Kelvin Vision LED Multifocal Stimulatot (MFS).

3.4 Cloud Software and remote access – a tool for collaboration

An in-house server that allows remote access to the back-end mathematical engine was developed by Lake et al[324], providing a mechanism to keep the user front-end simple and focused on the presentation while performing heavy-duty mathematical calculations in a resourceful back-end server. A three-tier architecture design for the IT system splits the user interface (presentation layer) away from the application logic (application layer) which, in turn, is split apart from the data storage (data layer). The presentation layer, which may be a web page, does not carry out any processing, it only interacts with the operator. Any processing is packaged up and sent to the application layer. Similarly, the data storage layer only reads, writes and possibly lists data from the storage. The application layer, therefore, must carry all the know-how, see figure 3.32.

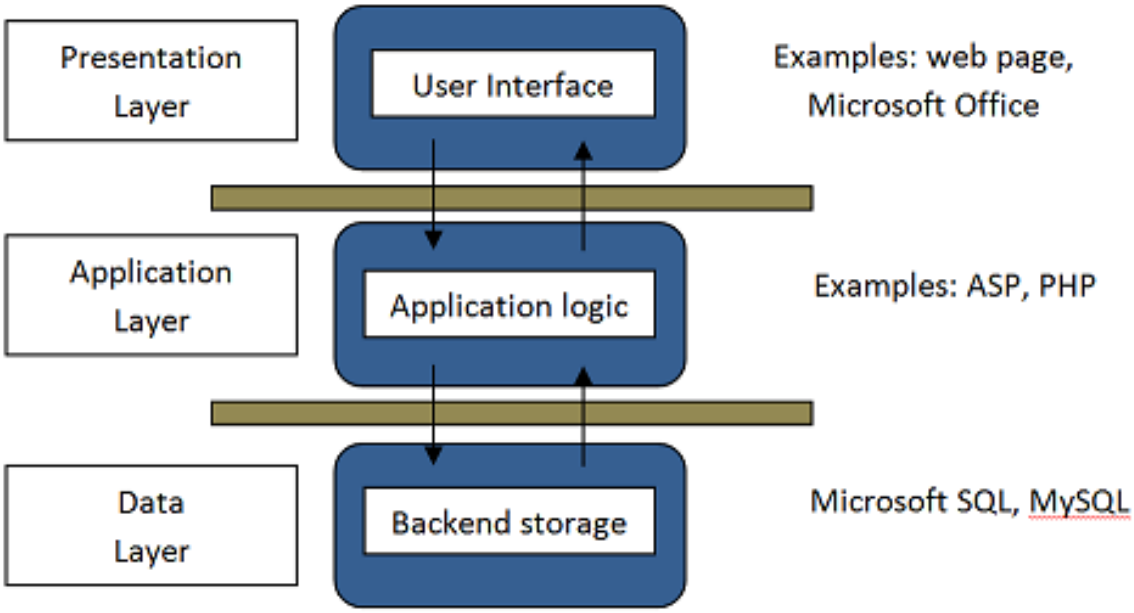

Figure 3.32. MatSOAP© three-tier architecture design to carry out the communications between the application logic and back-end storage. Connections between the user interface and the application logic usually use a remote procedure call (RPC). The latest version of this is called Simple Object Access Protocol (SOAP) and is typically transferred using hypertext transport protocol (http).

3.4.1 Design of MatSOAP©

The MatSOAP© design framework is based on the three-tier architecture of figure 3.32, where MATLAB® command line is the designated application logic engine. The choice of MATLAB® is due to its extensive features in data processing and its rich "almost" human readable programming language. MATLAB® can also be used to automate other storage or presentation layer software via communication through the COM (Component Object Model) interface. SOAP is the selected protocol to communicate with various presentation layers. To pass remote procedure calls (which reference an m-files) from the user interface client to MATLAB®, an in-house gateway called MatSOAP© was designed and developed.

Aliazizi et al[340] further exploited MATLAB® capabilities to handle large and complex data analysis that is hidden from the user and provides the user with a familiar, light and easy to use environment such as Microsoft Excel®. The bridge between the two settings is made possible by the MatSOAP© server (see figure 3.33[325]).

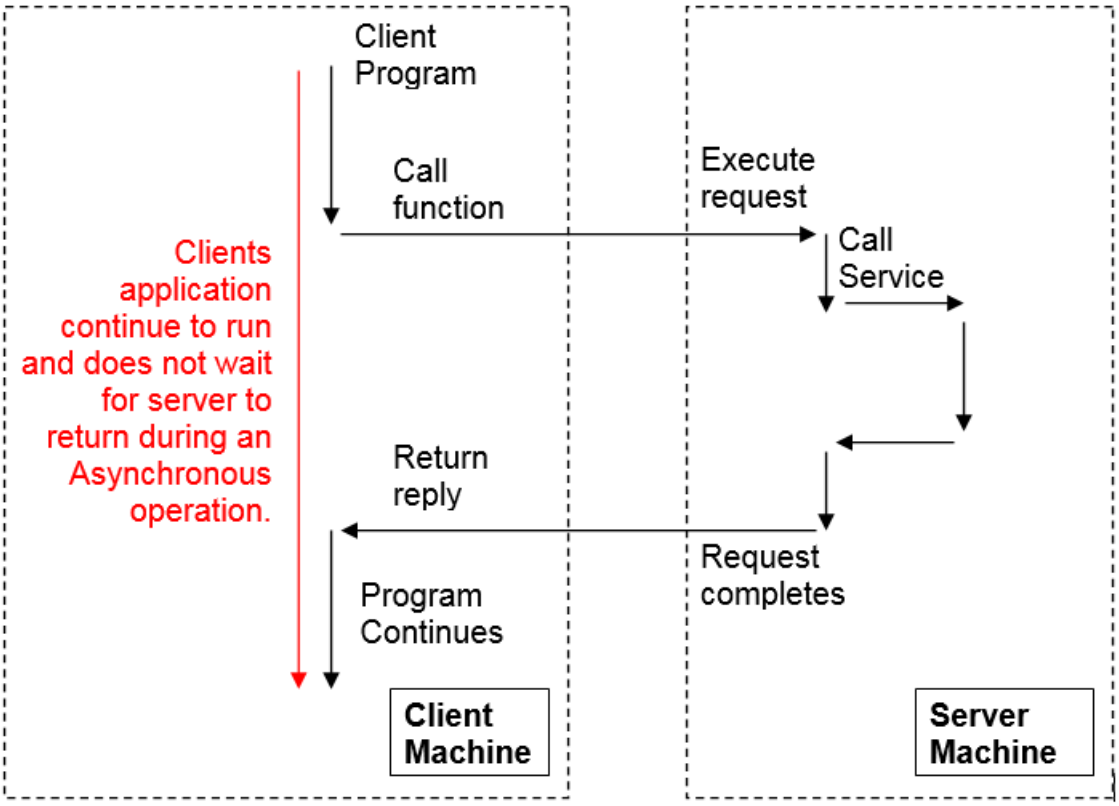

Figure 3.33. MatSOAP© gateway representation.[325]

In the ISIM design, a large quantity of data is extracted directly from the user interface (e.g. Excel®). The information is then validated against a master template and put into a structure that is passed to MATLAB® for further processing. At the back-end server, an additional check on the input data is performed. The entry point is a single m-file that manages the processing through a calling helper m-files to perform checking, analysis, synthesis, storage and packing of the result and any output files, ready to be sent back to client's interface.

For lengthy analysis (greater than 60 seconds), MATLAB® is invoked at the background on the server-side and the control is returned back to client-side, allowing the user to execute other functions while analysis is performed. This means that if the call to the MatSOAP© server would take longer than 60 seconds then, another instance of MATLAB® is invoked/automated at the back-end server to perform the task. This frees up the automation thread of MatSOAP© to take other incoming or stacked calls. It is then possible to check or ping the server periodically (again a background activity on the client-side) to see if the results are available for collection.

MATLAB® can then produce the results in any file format, depending on the user's needs, such as images, text files, etc. Here again, we used MATLAB® to provide a master-slave relationship with Excel®, Excel® being the slave. In this fashion, results are exported in a very presentable manner into an Excel® workbook which is saved and returned to the user. Excel® objects can also be invoked through VBA (Visual Basic for Application), meaning that if data presentation will not take long and is not too processing heavy, the client's Excel® spreadsheet can be coded to perform some of the data processing, see figure 3.34.

Since all complex and extensive analysis is performed at the server back-end, and MatSOAP© allows the presentation end (client-end) to be stripped off the server-end, very presentable and light mobile front ends for complex tasks are possible.

3.4.2 MatSOAP© Gateway

SOAP or Simple Object Access Protocol is a protocol specification used in the implementation of MatSOAP© for exchanging information in a computer network. MatSOAP© relies on XML for its message format and HTTP protocol specification for message transfer. MatSOAP© receives calls or requests through the HTTP server (an in-built web-server) and if the file extension excludes the XML SOAP construct, the file is passed to the HTML directory of the server, i.e. MatSOAP© processing is bypassed, and a conventional return is made to the calling client page. If an XML SOAP call is received, then the information packet is unpacked (i.e. the MATLAB® function name to be invoked is identified, together with the required input string) and passed to the MATLAB® instance for processing. This service supports both synchronous and asynchronous operations or calling modes. While MATLAB® is processing the call, the automation thread is busy and locked to the session. MatSOAP© by default instantiates four MATLAB® sessions and can, therefore, execute four MATLAB® functions simultaneously. Other calls will be stacked within a First-In-First-Out (FIFO) buffer. This method lends itself to signal and image processing, as well as providing teaching and other material and as such fits with the objective of this work. It is not necessary for the developer, host administrator or the client/user to have any specialised knowledge relating to web-interfacing, HTML/XML coding or server management. The MatSOAP© method is constructed as a ready-to-go software tool. A SOAP message is a simple XML package with defined tag names that can be built within any programming application and is human-readable, making it perfect for applications where the client's side needs to be kept simple due to limitations on resources.

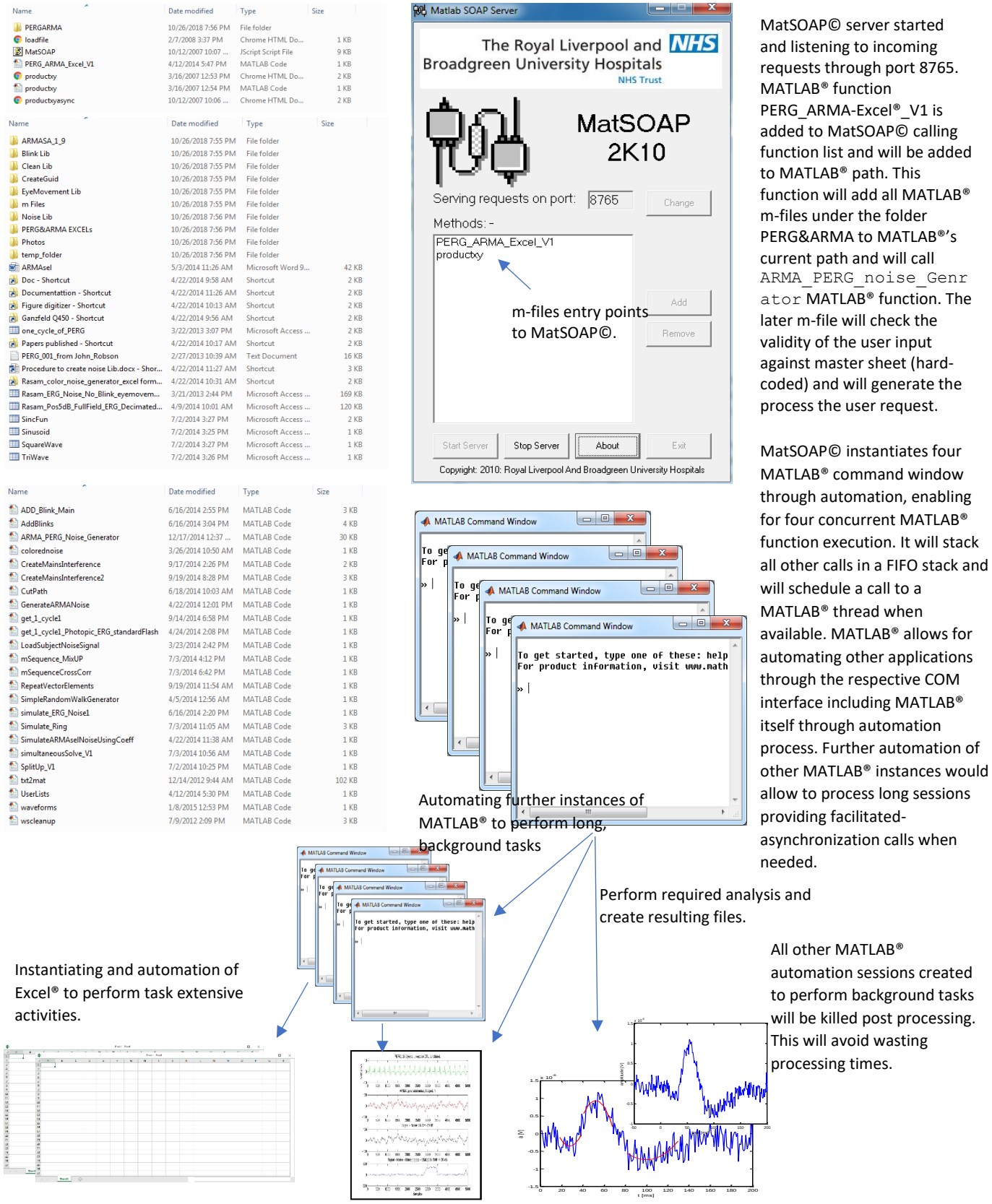

MatSOAP© server started and listening to incoming requests through port 8765. MATLAB® function PERG_ARMA-Excel®_V1 is added to MatSOAP© calling function list and will be added to MATLAB® path. This function will add all MATLAB® m-files under the folder PERG&ARMA to MATLAB®'s current path and will call `ARMA_PERG_noise_Genrator` MATLAB® function. The later m-file will check the validity of the user input against master sheet (hard-coded) and will generate the process the user request.

MatSOAP© instantiates four MATLAB® command window through automation, enabling for four concurrent MATLAB® function execution. It will stack all other calls in a FIFO stack and will schedule a call to a MATLAB® thread when available. MATLAB® allows for automating other applications through the respective COM interface including MATLAB® itself through automation process. Further automation of other MATLAB® instances would allow to process long sessions providing facilitated-asynchronization calls when needed.

All other MATLAB® automation sessions created to perform background tasks will be killed post processing. This will avoid wasting processing times.

Figure 3.34. Implementation of MatSOAP© and ISIM back-end server.

3.4.3 Soap call implementation and parsing within Visual Basic for Application (VBA)

The application (standalone or instantiated from the ISIM main GUI) collects and sorts the following parameters in preparation for a SOAP call to the MatSOAP© server (figure 3.35):

- All user input data from within the sheet (i.e. various combo-boxes). This is packaged into a comma-separated string to be parsed by the invoked MATLAB® file at the server-side.
- Sorts out the target URL address (where MatSOAP© server is located. This is either local or remote to the host machine), the target Folder address (where the back-end MATLAB® engine is stored) and finally, sets the MATLAB® pointer (first MATLAB® program to be executed by the MatSOAP© server when the soap call is received).

A module called `getMatSOAPResults` has been implemented, which requires the above inputs to perform a user-defined, synchronous, or asynchronous call to the server (MatSOAP©). If an asynchronous call is specified (default), then the client Excel® spreadsheet is in the client's control and not frozen until MatSOAP© returns the results. Such functionality is essential to the design to provide a friendly user interface to the end-clients when working with this spreadsheet. This ensures the user of this platform is free to perform multiple calls to the server while the earlier requests are being processed. Once the call from `getMatSOAPResults` returns, the execute button is enabled again. This allows the user to make another request to the server if required. When results are returned the Execute button sub-function automatically updates the User Interface. If other calls are in the queue, then a message box appears that provides the opportunity to the client to save the results before proceeding.

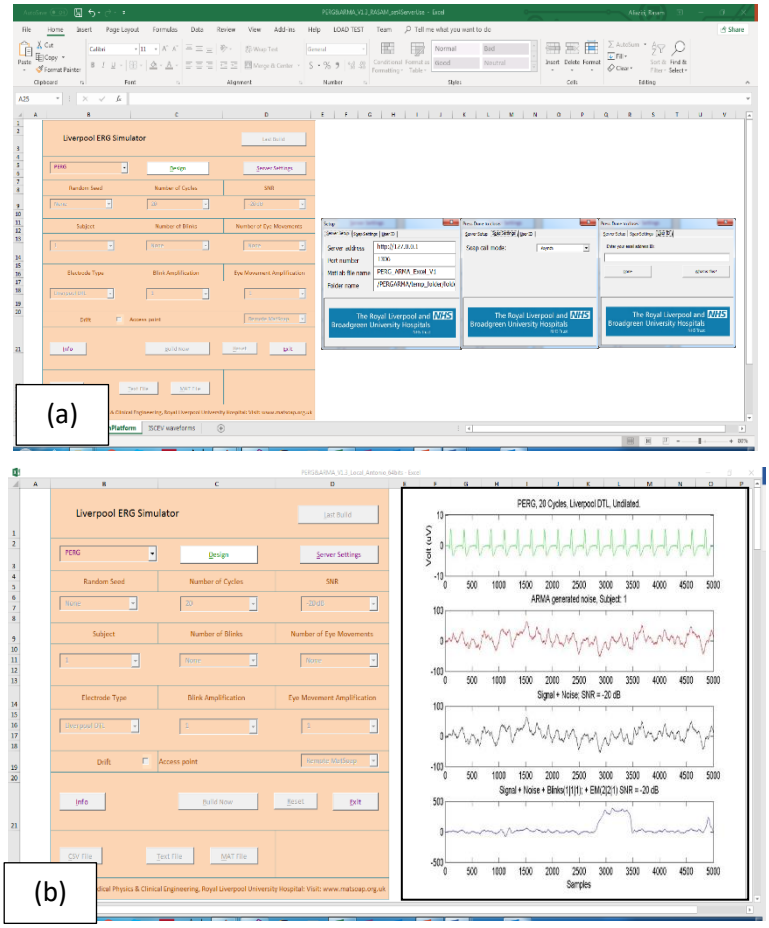

Figure 3.35. (a) MS Excel® GUI design and developed for generation of user defined visual electro diagnostic records. (b) Once processing at the back-end server is finalized and returns, the spreadsheet will unpack the returned data and present the result to the end-user.

3.5 iSim intended use, performance and expected benefits

iSim is designed to generate an exactly described, realistic waveform that can characterise the clinical measurement instrument. The iSim device produces the same signal consistently and hence removes the intra-subject variability, present when testing with human or animal subjects. iSim will produce the same signal, reliably regardless of the clinical system used or the clinic's geographical location.

3.5.1 iSim high-level design specification

ISIM is designed to provide a reliable, flexible platform through a user-friendly framework, allowing for re-using codes and components of the ISIM system within and across centres. This is achieved through implementation of abstraction, instantiation and integration. The goal is to improve collaboration across the boundaries of centres by providing a high-quality toolset to the electro-diagnostic community.

The design framework brings together elements of current best practice, guided through various standards such as ISCEV and IEEE.

3.5.2 iSim high-level Customer and Product Requirements (CRs, PRs)

The waterfall approach is used during the design and development of ISIM to ensure quality control is maintained allowing the design to meet the intended use and performance of the device and deliver the expected outcomes and benefits, see figure 3.36.

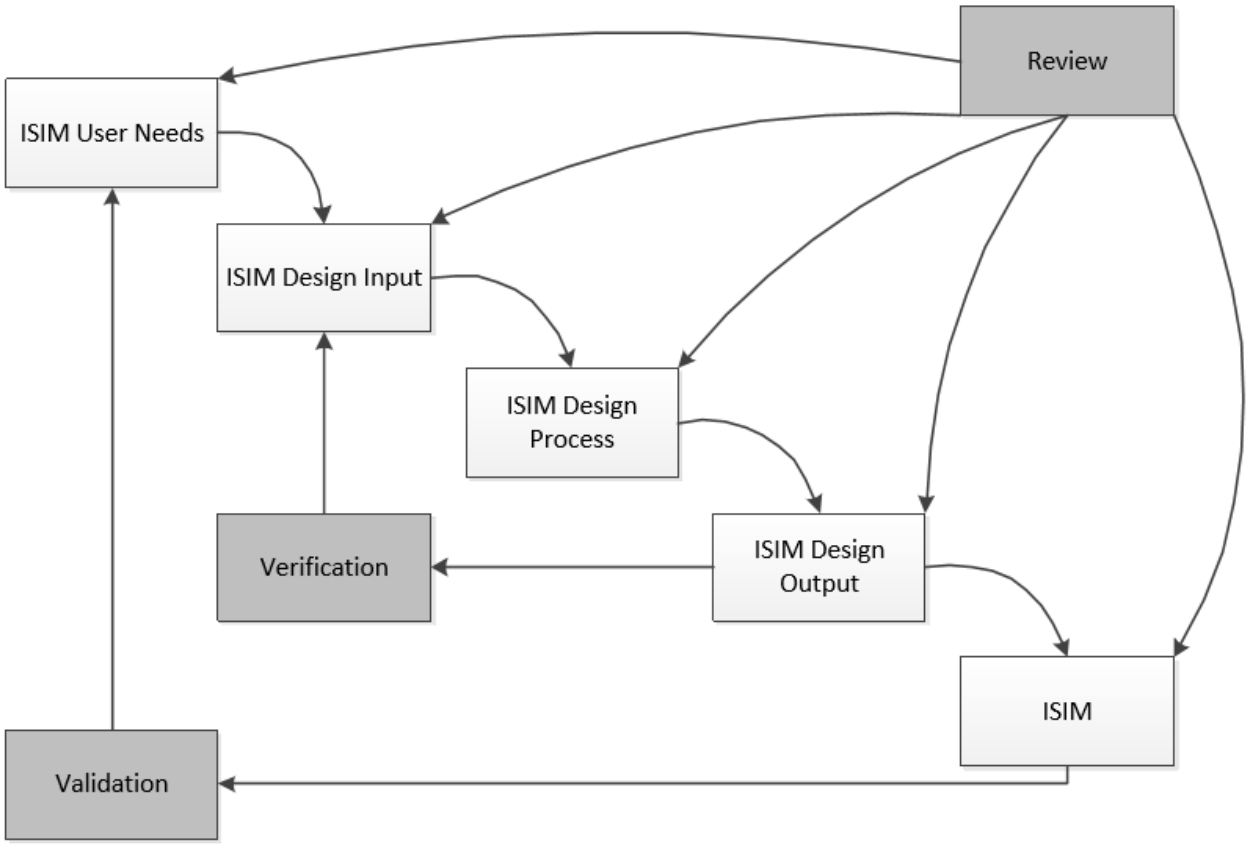

Figure 3.36. application of design control to waterfall design process (figure used with permission from Medical Devices Bureau, Health Canada.

3.5.3 iSim User Needs

User needs are captured using the Voice of Customer (VoC) approach, where a customer is defined by those expected to use and benefit from ISIM, i.e. clinicians, researchers, academics, students, consultants and calibrating engineers or assistants. The focus group is clinicians, and their voices were captured through different forums such as verbal and written communication as well as conference presentations and feedback on the intended use and purpose of ISIM. Further to this focus group, trainee clinical consultants in the department of Physics and Clinical Engineering

(MPCE) of the University of Liverpool (UoL) were consulted to obtain their insight on user needs. The list of captured user needs is summarised below:

- ***U1***: Easy to use.
- ***U2***: Small, portable and lightweight.
- ***U3***: Provide realistic visual electrodiagnostic signals, under relevant clinical setting.
- ***U4***: One button press and output the desired signal.
- ***U5***: Plug and play (PnP).
- ***U6***: No limit on the length of file output.
- ***U7***: Large storage.
- ***U8***: Bluetooth operations.
- ***U9***: Connected to the Internet, download signals online.
- ***U10***: Operate where no internet or network is available.
- ***U11***: Operate within a clinical setting.
- ***U12***: Device to help HCP for calibrating visual electrodiagnostic units and equipment using realistic signals and capable of use for training clinical consultants within visual diagnostic centres.
- ***U13***: Obey all relevant medical device regulations and standards.
- ***U14***: Safe to operate.
- ***U15***: Demo mode.
- ***U16***: Turbo mode of operation. I.e. quick setup, quick test to allow HCP to calibrate equipment within a few minutes before the next patient arrives.
- ***U17***: Device to be connected to cloud for collaboration across centres within the UK.

3.5.3.1 Criteria arising from User Needs

The following criteria arise from the user needs and other constraints:

Quality:

- Ensure the intended use and performance of the device are met and maintained.
- Ensure reliability is met and maintained.

Time for development and thesis write up:

- Ensure conceptualisation, design and development, prototyping, verification & validation testing, reports and thesis write up will be managed on the agreed timeline.

Cost:

- Ensure costs are kept low. The cost indication given was no more than £100.00 cost of goods sold (COGS) on the final representative product/prototype, and to keep within the agreed timeline to ensure reasonable development costs. The writer of the thesis had no control over the budget for this PhD work, except that of COGS.

Based on the above criteria, the system requirements were reduced as indicated below:

- **U1**: Easy to use.
- **U2**: Small, portable and lightweight.
- **U3**: Provide realistic visual electrodiagnostic signals, under relevant clinical setting.
- ~~***U4**: One button press and output the desired signal.*~~

Reason for exclusion: This user need is captured under easy to use (U1) and will be expanded accordingly to a CR and multiple PRs.

- **U~~4~~*4***: Plug and play.
- ~~***U6**: No limit on the length of file output.*~~
  Reason: This is translated to long-duration rather than no limit on file size and is captured under U3.
- **U~~7~~*5***: Large storage.
- ~~***U8**: Bluetooth operations.*~~
  Reason for exclusion: this user need is not required to ensure the reliability of the device/system. It can also add to design and development costs and increase the COGs. It is also argued that such functionality would increase the EMC noise and hence reduce the reliability of the system.
- **U~~9~~*6***: Connected to the Internet, download signals online.
- **U~~10~~*7***: Operate where no internet or network is available.
- **U~~11~~*8***: Operate within a clinical setting.
- **U~~12~~*9***: Device to help HCP for calibrating visual electrodiagnostic units and equipment using realistic signals and capable of use for training clinical consultants within visual diagnostic centres.
- ~~***U13**: Obey to all relevant medical device regulations and standards.*~~
  Reason for exclusion: After a discussion with senior quality and Regulatory responsible person in the department, it is understood that the system is not classed as a Medical Device, but it is rather classed as an accessory to a Medical Device.
- **U~~14~~*10***: Safe to operate.
- ~~***U15**: Demo mode.*~~
  Reason for exclusion: this user need is not required to ensure reliability or for the device/system to meet its intended use and purpose.
- ~~***U16**: Turbo mode of operation. I.e. quick setup, quick test to allow HCP to calibrate equipment within a few minutes before the next patient arrives.*~~
  Reason for exclusion: This User Need is captured under U1.
- ~~***U17**: Device to be connected to cloud for collaboration across centres within the UK.*~~
  Reason for exclusion: This User Need is translated to:
  ***U11**: System to allow collaboration across centres within the UK.*

3.5.4 Design Input (DI)

Collection of accepted Customer Requirements (CR) and the relevant Product Requirements (PR) will form the Design Input Criteria (DI).

3.5.4.1 Customer Requirements (CRs)

Customer requirements (CRs) are developed from the user needs in such way that they allow for formal and objective validation. The customer requirements are summarised below:

- ***CR1***: ISIM GUI to be operable within Windows operating system, irrespective of its version.
- ***CR2***: Access all device capabilities from within the ISIM GUI.
- ***CR3***: iSim to connect to host computer via USB.
- ***CR4***: ISIM GUI to automatically detect when the iSim device is connected to USB port of the end-user computer.
- ***CR5***: Device to allow for three modes of operations, normal, user, engineering.
- ***CR6***: ISIM to initiate in USER mode when connected or reset.

- ***CR7***: Signal morphology to remain unchanged throughout the operation of the device, irrespective of the operational mode.
- ***CR8***: Device to allow easy calibration.
- ***CR9***: ISIM to provide an Instruction For Use (IFU).
- ***CR10***: ISIM to allow for both flash and TTL trigger points.
- ***CR11***: Maximum signal duration (iSim output) to mimic worst case scenario in a clinical setting.
- ***CR12***: iSim to store large number of files.
- ***CR13***: Easily powered.
- ***CR14***: Small and portable.
- ***CR15***: Lightweight.
- ***CR16***: Plug and play.
- ***CR17***: Scalable.
- ***CR18***: ISIM to output clean ERG signal with +3-dB SNR by one button click when first connected. i.e. device is ready to output a pre-determined signal as fast as possible and as soon as it is connected to the host computer.
- ***CR19***: ISIM ready for user to operate within thirty seconds of when it is first connected, when it is reset or when it is unplugged and then plugged back in again.
- ***CR20***: ISIM to be provided with plugs to connect to any bio-potential amplifiers.
- ***CR21***: Friendly Graphical User Interface (GUI).
- ***CR22***: Provide demo mode.
- ***CR23***: Provide manual trigger mode.
- ***CR24***: No hardware buttons should be required for operation, irrespective of mode of operation.
- ***CR25***: Provide a visual confirmation to user that software is running when operating in any operational mode.
- ***CR26***: Allow end-users to build custom noise and signal files.
- ***CR27***: Allow installation on computers within clinical settings. I.e. not requiring any special Windows system access such as administrator rights.
- ***CR28***: Allow remote collaboration.
- ***CR29***: Provide both TTL trigger in and output. Provide option for optical trigger in and output.
- ***CR30***: User-friendly “calibration device”.
- ***CR31***: Record generation length, from a minimum of a “few” seconds to a maximum of a “few” minutes.
- ***CR32***: “Fast” device setup.
- ***CR33***: Robust, consistent and realistic signal generation.

3.5.4.2 Product Requirements (PRs)

PRs are defined and agreed upon the agreed and approved list of CRs. Each CR can be broken down into one or more PR/s. Each PR is written in such a way that it can be objectively verified (forming the design verification stage).

In designing a calibration device, it is vital to know what is being calibrated. This determines the scope of aspects of the project and shapes the technical aspects of the design. The Product Requirements are:

- Bandwidth of 0.1-500 Hz.

- Dynamic range:
    - Smallest signal of interest is PERG i.e. 2 μV_{PP} and the ability to output all available noise components including EMG, blinks and harmonic interference without degradation of signal.
    - Smallest signal of interest is mfERG i.e. minimum of 20 nV/deg2 when considering ARMA generated noise component as the only noise component allowed.
    - Largest signal of interest is blinks/eye movement artefacts, 0.2 V PP.

  This means a dynamic range of 90 dB (this measured criterion is one of the design output parameters and is brought up here so that one can see how DIs and DOs are linked).
- Sample output rate of greater or equal than 1 kHz (default).
- Output impedance of less than 5 kΩ and more than 2.5 kΩ.
- It is also essential for a calibration device to be traceable to a national or international recognised standard. The internationally recognised standard is that of the ISCEV.
  ISCEV does not define the level of accuracy required for such a calibration device. Thus the author has set the system accuracy level by its ability to produce signals with SNR of at least 60-dB for the smallest generated signal.
- The iSim design aims to provide a user-friendly calibration device that not only allows for frequent periodic calibration of the clinical instrument but also allows for a quick calibration test whenever required by the user. This means a PnP requirement must be considered:
    - USB for both communication and to supply electrical power to the device with no other external or internal power source.
    - Complete device control via a friendly GUI.
    - Easy device setup such as the installation of software packages.
    - Fast device initialisation allowing for a quick (less than 30 seconds from the time the device is connected) calibrations.
    - Consistent and robust signal morphology.

Various factors are considered in the process of implementing the electronic circuit for the iSim device. These are captured through the process of refining and fine-tuning; user needs through to Customer Requirements (CRs), which would ultimately define and inform the Product Requirements (PRs). Detailed design and development steps are then identified and implemented through the design and development process, ensuring PRs are verified, and CRs are validated, a process known as Verification and Validation (V&V), which is captured in the Design and Development Plan (DDP).

ISIM design is broken down into the following three main categories:

- Hardware (PCB design and implementation) – iSim.
- Software (embedded, high-level, cloud programming).
- Accessories and ancillary developments (design and development of a bio-amplifier, study and calibration of various clinical measurement systems).

3.5.5 iSim device evolutionary implementation

The approach that perhaps best expressed as a black-box strategy is taken throughout the design. One regards the challenge of implementing the circuit as being equivalent to designing a black-box with inputs and outputs clearly defined through the list of approved PRs.

The key feature of this technique utilised in the iSim developmental phases is that the details of the black box are subject to the usual processes of an evolutionary design phase and are modified where

needed and abstracted from the end-user. In this technique, the fitness of a module (software or hardware) is measured purely as the degree to which the black-box outputs behave in the desired way. Any changes from the expected behaviour are thoroughly investigated and documented to avoid any future design uncertainties.

An evolutionary technique, with the main objectives set at the design stage, is best suited to the ISIM project. In the author's approach, several iterations (build, test and debug) were made and investigated before the design of each part was finalised (e.g. power supply unit, MBED unit, DAC unit, anti-aliasing filters and the final summing and attenuation stages). The evolutionary design allowed for the exploration of a rich set of possibilities, such as allowing for further future developments and improvements. Throughout this approach the Critical To Function (CTF) parameters were identified and, based on these parameters, the accepted behaviour is recognised and captured under Acceptance Criteria within Design Output (DO). Three developmental phases are shown in figure 3.37.

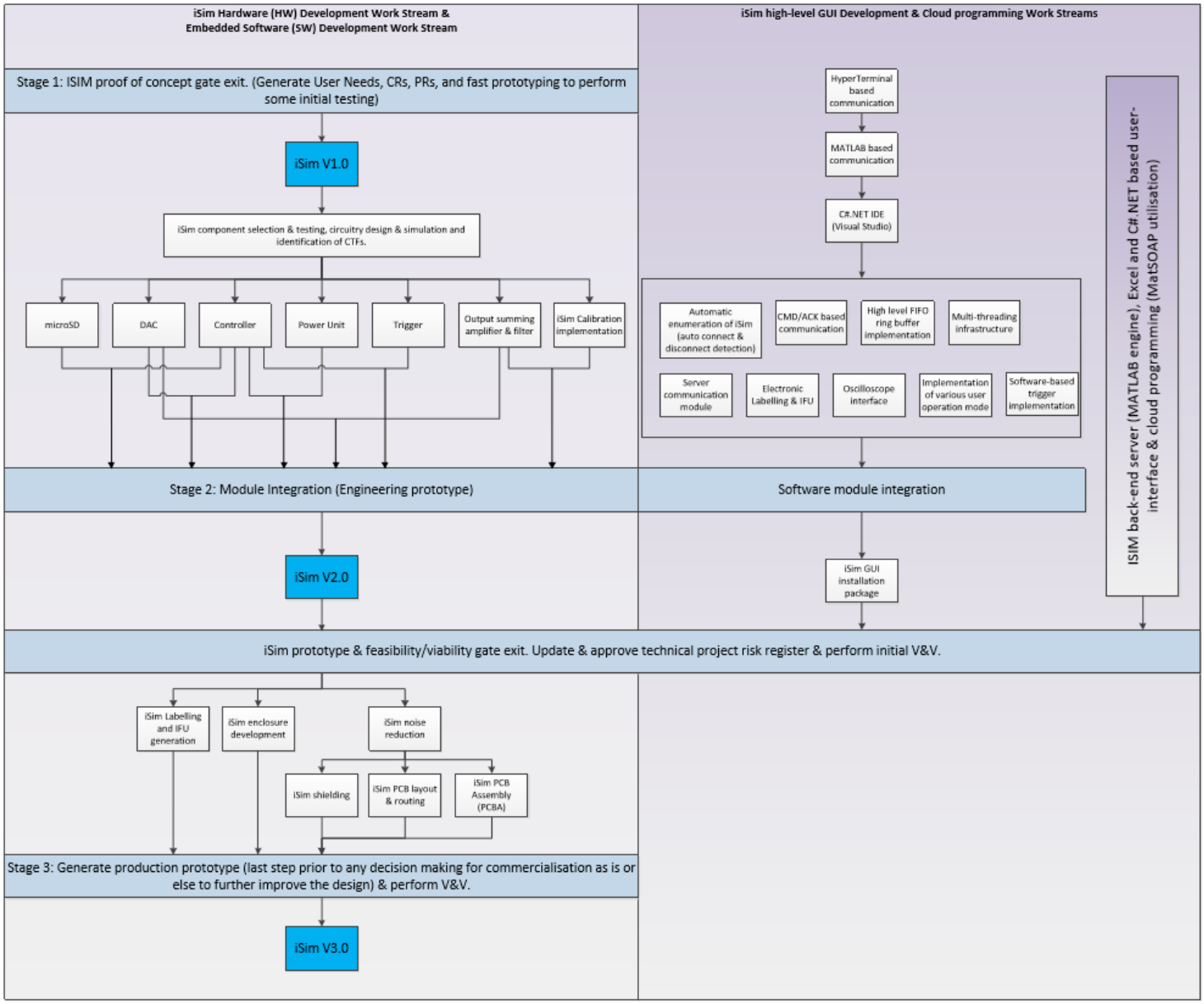

Figure 3.37. Illustration of various developmental phases (with multiple iterations within each phase) laid out on top of three major interconnected work streams. These work streams are developed in a modular design format that expose standard interfaces allowing for integration of modules. For example, the GUI communicates through SPI interface with embedded firmware using commands and

3.5.5.1 iSim development: phase one

The separate but interconnected workstreams (four streams in total) and design stages are shown in figure 3.37. This figure also shows how various modules are integrated. The outcome of the initial prototype phase (proof of concept) is shown in figure 3.38. In the fast prototype phase, the iSim components, such as microSD card, DAC, operational amplifiers, filters, DC-to-DC converters are tested and compared against their stated performance. During stage one development, the MBED microcontroller was thoroughly investigated as a CTF component. MBED is an ARM-processor-based integrated development environment. The LPC1768 is the microcontroller, exploiting some of the capabilities of the powerful M3 Cortex ARM processor (LPC1768 has 100 pins 40 of which are exposed by the MBED board). The downside of using MBED is that not all the features are exposed

to the developer. This, however, is not a limiting factor and reduces the complexity of the design significantly.

The cleverness of the MBED hardware design is the way which this device manages the USB link and acts as a USB terminal to the host computer. In its most common configuration, it receives program code files through the USB and transfers those programs to a 16 Mbit memory (the flash memory), which acts as the USB disk.

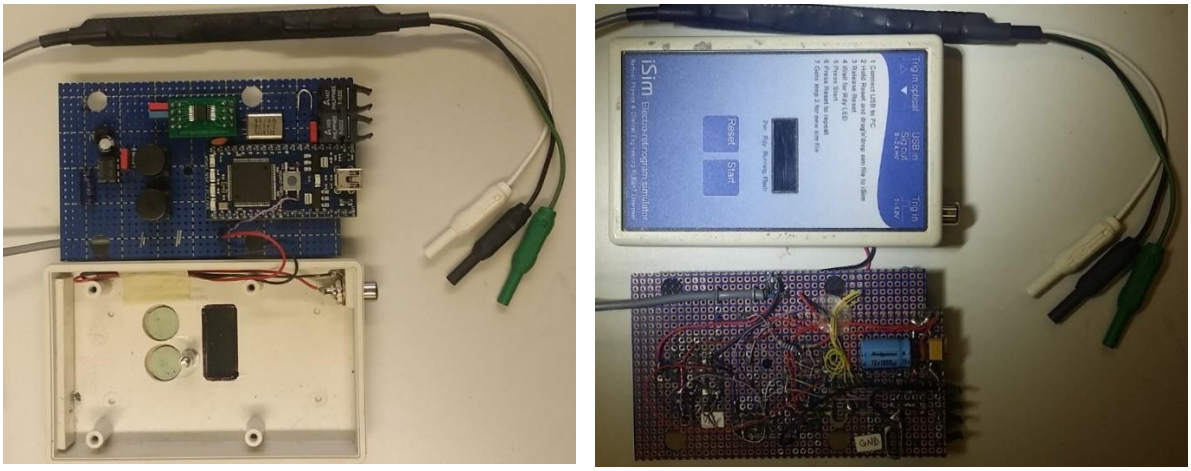

Figure 3.38. iSim Version 1, risks and opportunities:
At this evolutionary stage, the following key components of ISIM was evaluated, studied, and implemented:

- Verification of top-level user needs – simple usability study through multiple formative validation studies of the process to better inform the overall product requirements which would ultimately translate into a sound hardware and software design
- Ensure portability, lightweight and small size
- Characterisation of MBED prototyping board and maturing the embedded software program
- Implementation of the trigger unit
- Implementation of host computer communication interface using simple MATLAB® GUI
- Characterisation of signal requirements and better understand the challenges of SNR in conjunction with the allowable dynamic range of selected DAC
- Implementation of mathematical engine responsible for signal generation and implementation of associated Excel® GUI to utilise the engine through consumption of the MatSOAP© server

When a program, ARM binary, is downloaded to the MBED (MBED comes with an online platform to develop the code, debug it, and finally compile and download it), it is placed in the USB disk. This means that the developer needs no driver to program and re-program the MBED, which makes it easy to swap programs via a simple file transfer that can be automated for further convenience. Implementation of iSim version 1.0 allowed a successful first attempt to better understand the building blocks of the ISIM package, including identification and verification of requirements on other interfaces within the system, ultimately informing the design and development stages before committing to a significant investment. As such, further hardware and software integration, as well as the implementation of all user “nice-to-haves”, is halted at this stage, ensuring the bare minimum is achieved to test the ISIM platform. To that end, a modular design approach is chosen to ensure the feasibility of various design modules as we progress through future development stages. Each component of ISIM is therefore treated as a standalone module.

3.5.5.2 iSim development: phase two

Stage two (see figure 3.39) in the evolutionary design phase is concerned with ensuring a wide dynamic range (DR), allowing coverage of the signal range from nV to volts, as well as dealing with memory constraints and any potential overhead in loading the output signal into the onboard RAM. The wide DR required the implementation of power management circuitry. The MBED provides an

unregulated 0-5 V voltage to power up the digital circuitry. The implemented power management circuitry gives iSim a regulated (through two implemented Low Drop Out (LDO) regulators and ripple filters) $\pm$ 12 V range (through drawing current as required from the host computer providing the required power) that stabilises within the first 220 ms post connection to the host machine. This voltage range will power up the DAC, and output summing amplifier as illustrated in figure 3.41.

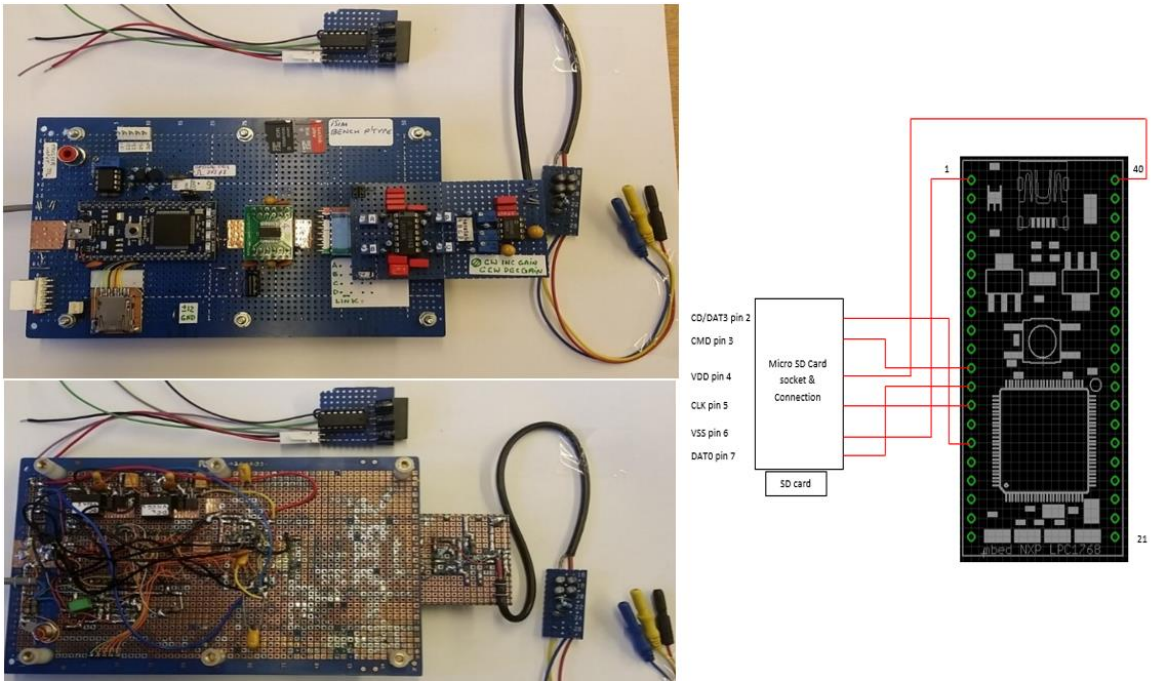

Figure 3.39. iSim Version 2, evaluation of a potential working prototype:
At this evolutionary stage, the following key components of ISIM was evaluated, studied, and implemented:

- Identified Dynamic Range (DR) requirements
    - DAC selection and its associated low-level embedded programming class
    - Design power requirements and associated stable voltage booster circuitry
    - Implementation of output summing amplifier and implementation of hardware and software calibration capability
- Onboard hardware memory storage (SD implementation and its associated low-level embedded software implementation)
    - Low-level file management system and development of an internal buffer system for efficient and accurate data handling taking advantage of a low-level multi-threaded programming technique
- Hardware filter implementation
- Optical trigger-in circuitry

3.5.5.3 iSim development: phase three

Stage three is mainly concerned with the reduction of system noise as well as implementing the calibration mechanism for iSim itself. This involved finalising the schematic for the design, routing and generating a 2-layer PCB board and populating the board. Significant noise analysis was performed, resulting in three iterations of routing and PCBA design. The implemented PCB was next enclosed within a dedicated enclosure as illustrated in figure 3.40.

In designing the pictured PCBA in figure 3.40, the following standards and guidelines (some industry-specific) and other resources describing the best practice for PCB design were considered:

- PCB design guidelines for reduced EMI (Texas instrument)
- Printed Circuit Board (PCB) Design Checklist (Quick-Tec)
- Engineer's Guide to High-Quality PCB Design (electronic design)

- A Practical Guide to High-Speed Printed Circuit Board Layout (Analogue Devices)
- Various other Analog Devices application notes
- Quick-Tec PCB Standard Specification (our PCB manufacturing supplier)
- PCB layout Consideration for mixed-signal PCB design layout (Analog Devices)

Figure 3.40. iSim Version 3, a working prototype.

At this evolutionary stage, the following key components of ISIM was evaluated, studied, and implemented:

- System noise analysis and reduction (through multiple iterations of PCB design, manufacture, assembly and testing)
- High-level GUI fine-tuning (implementation of a simple and thin User mode to the GUI)
- Further trigger development (Optical, TTL voltage and software-based trigger implementation)
- System verification and validation (V&V)
- Enclosure selection and final assembly including labelling and generation of Instruction For Use (IFU)

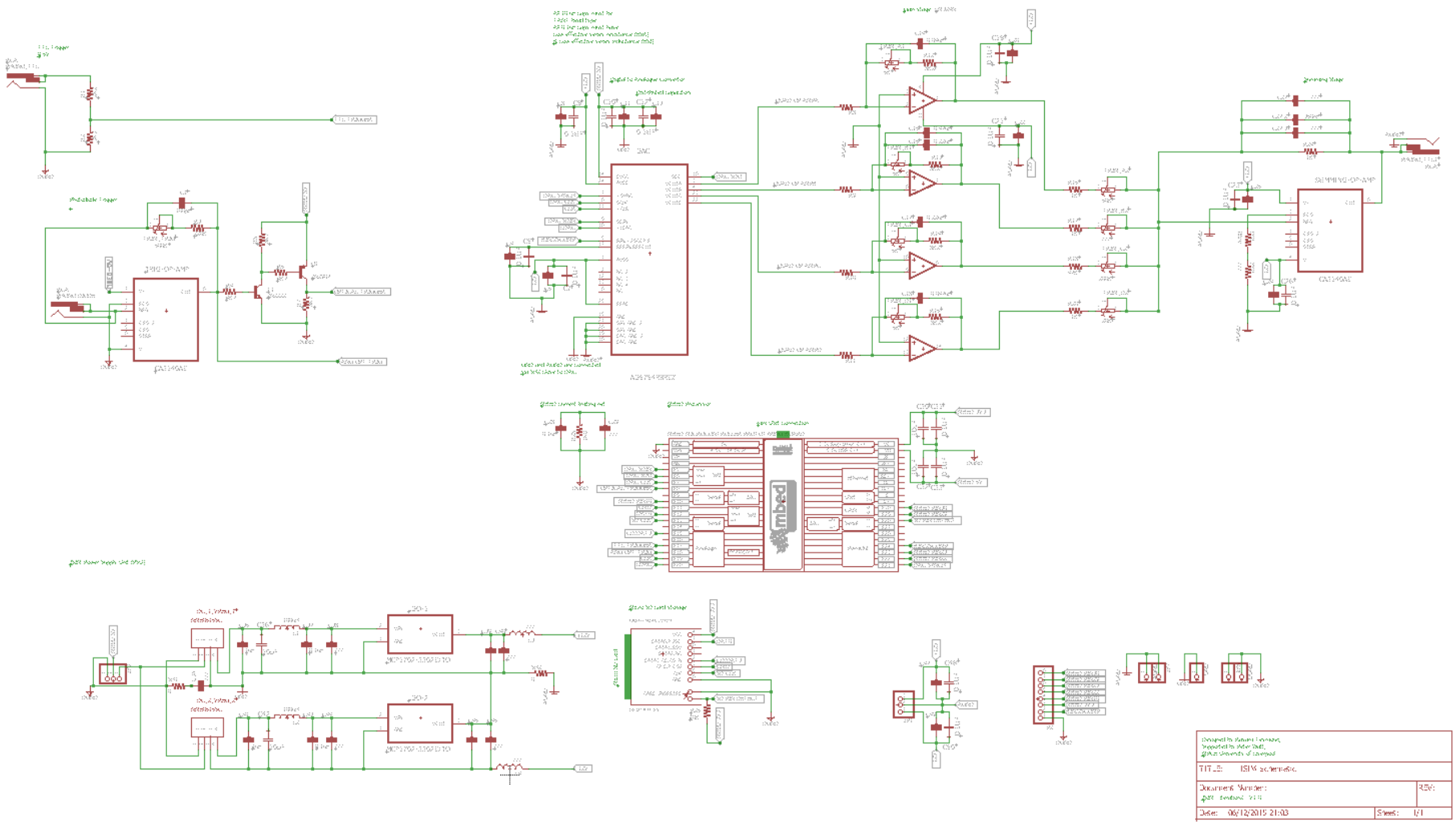

Figure 3.41. Schematic design circuit for iSim version 3. The schematic was next evaluated in EAGLE to generate a 2-layer PCB board. This PCB board was then constructed through outsourcing and populated in department of Medical Physics and Clinical Engineering. Throughout phase three the high-level and low-level software implementation were also optimized and fine-tuned for best user experience.

3.5.5.4 iSim Dynamic range requirements and implementation

In iSim version 1.0, a single-channel, SPI compatible, 12-bit resolution (MCP4922) DAC was implemented to test the concept feasibility and viability. This did not allow enough resolution to reproduce a small signal at low signal to noise ratios. For the lowest SNR of -40 dB, and the largest signal of size 600 µV, the noise amplitude produced is 60,000 µV. The smallest step of the 12-bit DAC at a dynamic range of 60,000 µV is 14.65 µV. This is enough to detect the large 600 µV signal with 40 DAC steps, that is more than the required 15. However, for a fixed dynamic range of 60,000 µV, a small signal of 2 µV will be indistinguishable, this is demonstrated in figure 3.42.

To produce a 2 µV signal with a minimum resolution of 15 DAC steps spanning the signal peak to peak, the step size required is 0.1333 µV. From a fixed dynamic range (DR) of 60,000 µV, the DAC will need to produce 450,000 steps. This is a minimum of 19 bit of required resolution.

DR (µV)	Min Signal (µV)
60,000	220
22,000	80.6
8,060	29.5
2,950	10.8
1,080	4.0
400	1.46

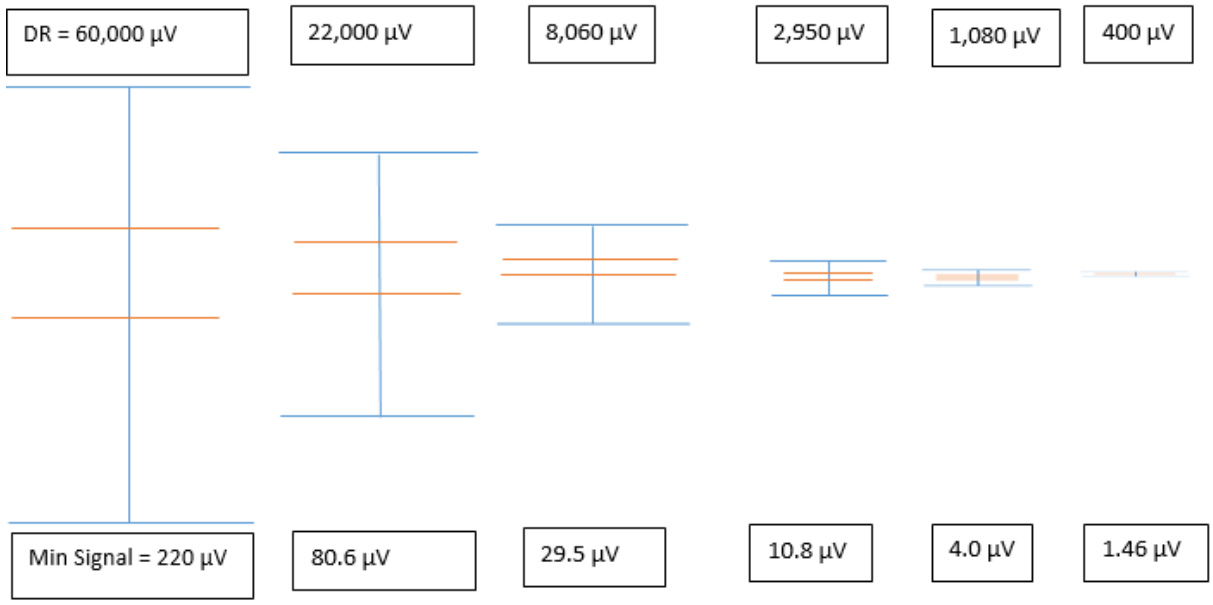

Figure 3.42. Dynamic range requirements based on the selected signal amplitude.

The software package used to generate the user-requested waveforms (implemented through Microsoft Excel®) does not have any knowledge of the hardware capability of iSim. Therefore, not all generated waveforms could be faithfully handled by iSim. The two significant limitations identified during stage one implementation would impact the dynamic range allowed and potentially the morphology of the signal. An Excel® spreadsheet is therefore provided, that enables the user to match the hardware

capability (DAC dynamic range, resolution, required scaling factor and the number of attenuation factors) of iSim (at any particular developmental cycle) to the allowable software-generated waveform.

All unspecified units should be in µV	0.000001				based on minimum S amplitude		based on maximum S amplitude (NOT taken D into account)	
maximum amplitude of S (PP)	600		SNR (dB)		Noise Level	% of S in S+N	Noise Level	S+N
minimum amplitude of S (PP)	29.5			-80	241290	0.010	6000000	6000600
dynamic range (D Volts)	5			-70	76303	0.032	1897367	1897967
number of bits (n)	12			-60	24129	0.100	600000	600600
minimum signal step size (X)	1.97			-40	2413	0.990	60000	60600
				-30	763	3.065	18974	19574
			-20		241	9.091	6000	6600
Max SNR (absolute value)	20		-10		76	24.025	1897	2497
Number of DAC steps	4096		-6		48	33.386	1197	1797
DAC step size (Volts) - LSB	1.22E-03		-3		34	41.450	848	1448
Min error (%)	0.33		1		22	52.875	535	1135
Max error (%)	7		2		19	55.731	477	1077
Required scaling factor (m)	758		3		17	58.550	425	1025
minimum signal (S) amplitude PP (steps)	14.97462		6		12	66.614	301	901
Minimum S (amplitude PP) can be resolved (Volts)	1.83E-02							
Minimum S (amplitude PP) can be resolved (µV)	24							
minimum number of bits required	11.7							

Figure 3.43. Illustrating that for a signal amplitude of peak to peak value in the range of 29.5-600 µV, DAC dynamic range of 5 Volts and a minimum SNR of -20 dB. The DAC with 12-bit resolution can faithfully represent the final waveform.

All unspecified units should be in µV	0.000001				based on minimum S amplitude		based on maximum S amplitude (NOT taken D into account)	
maximum amplitude of S (PP)	400		SNR (dB)		Noise Level	% of S in S+N	Noise Level	S+N
minimum amplitude of S (PP)	2			-80	1972656	0.010	4000000	4000400
dynamic range (D Volts)	5			-70	623809	0.032	1264911	1265311
number of bits (n)	12			-60	197266	0.100	400000	400400
minimum signal step size (X)	0.1		-40		19727	0.990	40000	40400
			-30		6238	3.065	12649	13049
			-20		1973	9.091	4000	4400
Max SNR (absolute value)	40		-10		624	24.025	1265	1665
Number of DAC steps	4096		-6		394	33.386	798	1198
DAC step size (Volts) - LSB	1.22E-03		-3		279	41.450	565	965
Min error (%)	0.03		1		176	52.875	357	757
Max error (%)	5		2		157	55.731	318	718
Required scaling factor (m)	124		3		140	58.550	283	683
minimum signal (S) amplitude PP (steps)	20		6		99	66.614	200	600
Minimum S (amplitude PP) can be resolved (Volts)	2.44E-02							
Minimum S (amplitude PP) can be resolved (µV)	197							
minimum number of bits required	18.6							

Figure 3.44. Illustrating that for a signal amplitude of peak to peak value in the range of 2-400 µV, DAC dynamic range of 5 Volts and a minimum SNR of -40 dB. The DAC with 19-bit resolution can faithfully represent the final waveform.

At this stage (stage one), a single-channel, SPI compatible with the resolution of a 20-bit DAC was next implemented (DAC 1220E). This provided a maximum resolution of 0.0311 µV allowing for a minimum signal amplitude span of 2 µV (with 20 DAC steps to cover small signals) and minimum allowable SNR of -30 dB. This allows for a scaling factor of 153 so that this signal spans the full dynamic range of the DAC.

The following two limitations further restrict the flexibility and accuracy of iSim version 1.0:

- The inclusion of low-frequency and large amplitude, spontaneous noise components such as eye movements, blinks and EMG as well as harmonic components such as mains interference, would saturate the DAC while conveying very little information for low-frequency components. The precious dynamic range will be severely compromised, leaving small room to faithfully replicate the signal and simulated biological noise.
- Tight memory available on MBED, allowing for signal representation of a maximum length of 30 seconds without impacting the signal morphology.

Dynamic range is linked to:

- The DAC specification (e.g. its resolution, number of programmable and independent channels, its dynamic range, and power requirements),
- The iSim power requirements,
- The summing amplification stage and calibration mechanism (fixed or variable),

This demanded a significant hardware modification during phase two. The DAC is therefore considered a critical component within the system and its operations deemed Critical To Function (CTF). Also, during stage two, a method to elevate iSim capability to output waveforms of length greater than 30 seconds was considered to be necessary without any negative impact on signal morphology. This also demanded a major design change to the implemented embedded software including:

- Implementing a software buffer and
- the required multi-threaded application to avoid the bottleneck effect when iSim tries to access the hardware for data samples.

The increase in waveform length has its impacts on hardware too. i.e. design upgrade to the iSim's hardware (that is the addition of an onboard storage unit).

Stage two was split into two sequential stages due to the significant technical risks and limited know-how regarding possible mitigations:

- Feasibility phase within stage two (iSim, as developed under phase one, was versioned at 1.0 and the project was considered complete knowing the existing limitations).
- Develop a working prototype with a significant reduction in technical risks before stage two gate exit.

DAC AD5724R is a 16-bit, SPI capable, digital-to-analogue converter with four simultaneous independently and fully programmable differential channels. The dynamic range of this DAC is also software selectable for individual channels with a nominal full-scale output range of +5 V, +10 V, +10.8 V, +/- 5, 0-10 or 0-10.8 V. The DAC chip has an integrated output amplifier, reference buffers, and proprietary power-up/power-down control circuitry. The only external components needed for this 16-bit DAC are the decoupling capacitors on the supply pins and the reference pin leading to saving in costs and board space. This will also ultimately result in lower noise in the system as well as providing a design that is not very susceptible to external interference (due to lower PCBA component density and the overall reduction in board's total pin count). The DAC has been thoroughly investigated using its commercially available evaluation board together with MBED microcontroller and an external power

supply unit as demonstrated in figure 3.45. It is also determined that the convertor is a monotonic converter as it keeps its last output value for the duration specified by the update rate. A test program was implemented to set the output rate to 1 kHz using a timer object to update the DAC output every 1 ms. The recorded output verifies the output rate of 1 kHz as demonstrated in figure 3.45.

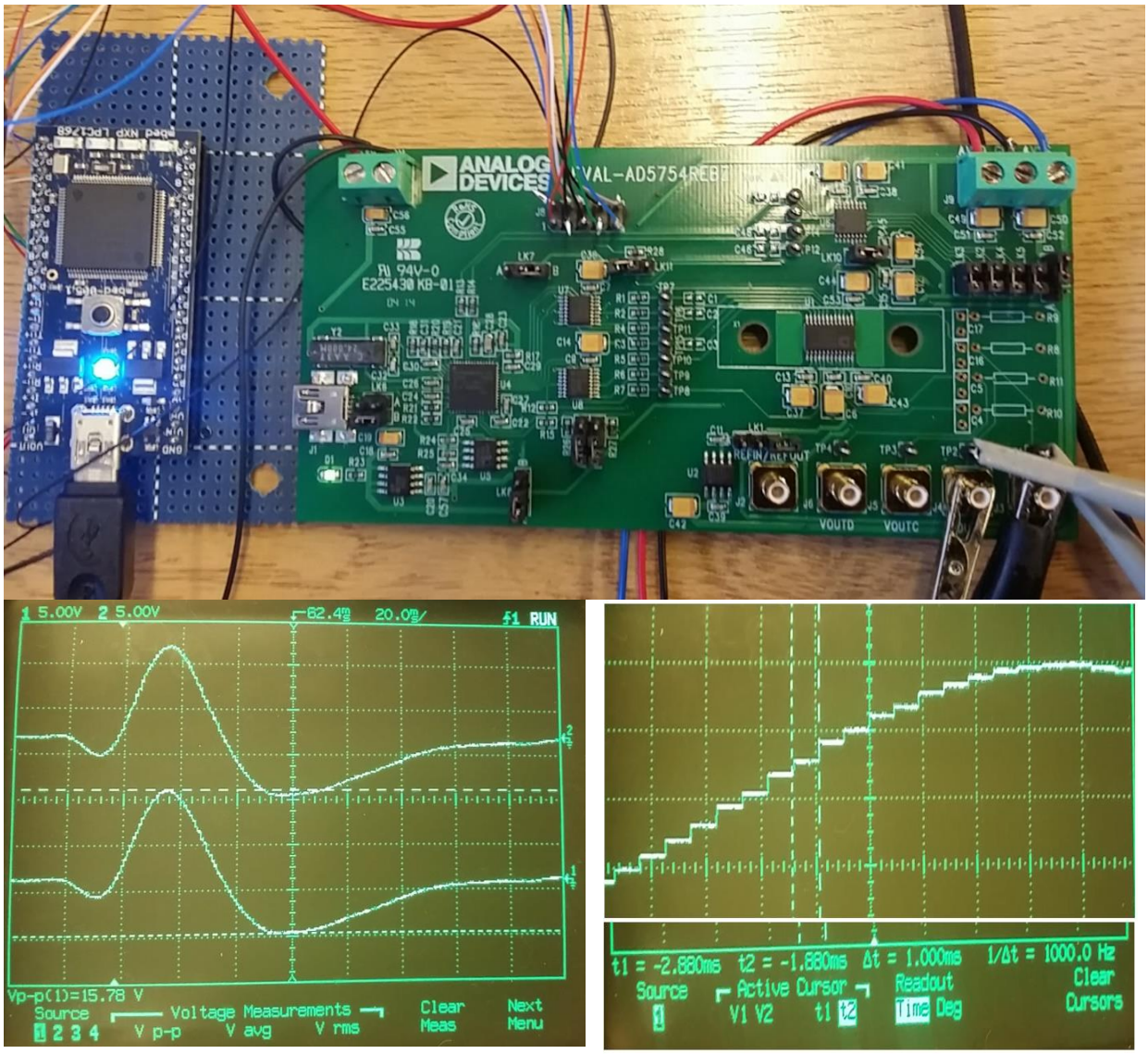

Figure 3.45. (a) Illustration of DAC evaluation board with MBED microcontroller during iSim stage two development. (b) demo DAC output when a standard PERG signal at arbitrary amplitude is programmed. (c) zooming to a section of the output waveform illustrates stepped functionality of the DAC, this clearly demonstrates requirements for a reconstruction filter at the output stage of iSim to smooth the signal and avoid contamination due to these unwanted high-frequency components (stepped edges of the square function).

The analysis of the DAC was performed against its specification sheet and its parameters, such as slew rate. The slew rate determines how fast the DAC can respond to changes at its input. For iSim, it took 4.34 µs to update the DAC output from -9.8 V to + 9.8 V. I.e. spanning the full dynamic range in 4.34 µs or slew rate of 4.5 V/µs which is close in comparison to the stated value of 3.5 V/µs in AD57754R

datasheet). Other important parameters, such as glitch energy, channel cross-talk, dynamic range, resolution, monotonicity, ENOB (effective number of bits) and noise level were investigated as well as DAC Interchannel variability in output rate or timing, which demonstrated that there exists no significant variability between individual DAC channels. The spectral analysis method is used to further characterise the DAC converter through FFT techniques, allowing range of frequency domain specifications to be measured including, SNR, THD (Total Harmonic Distortion) as well as any filtering impact.

The operational rating of the DAC against its clock frequency was investigated, allowing calculation of the maximum sample output rate of the system where the maximum SPI clock frequency is 30 MHz as per DAC specification datasheet (see figure 3.46).

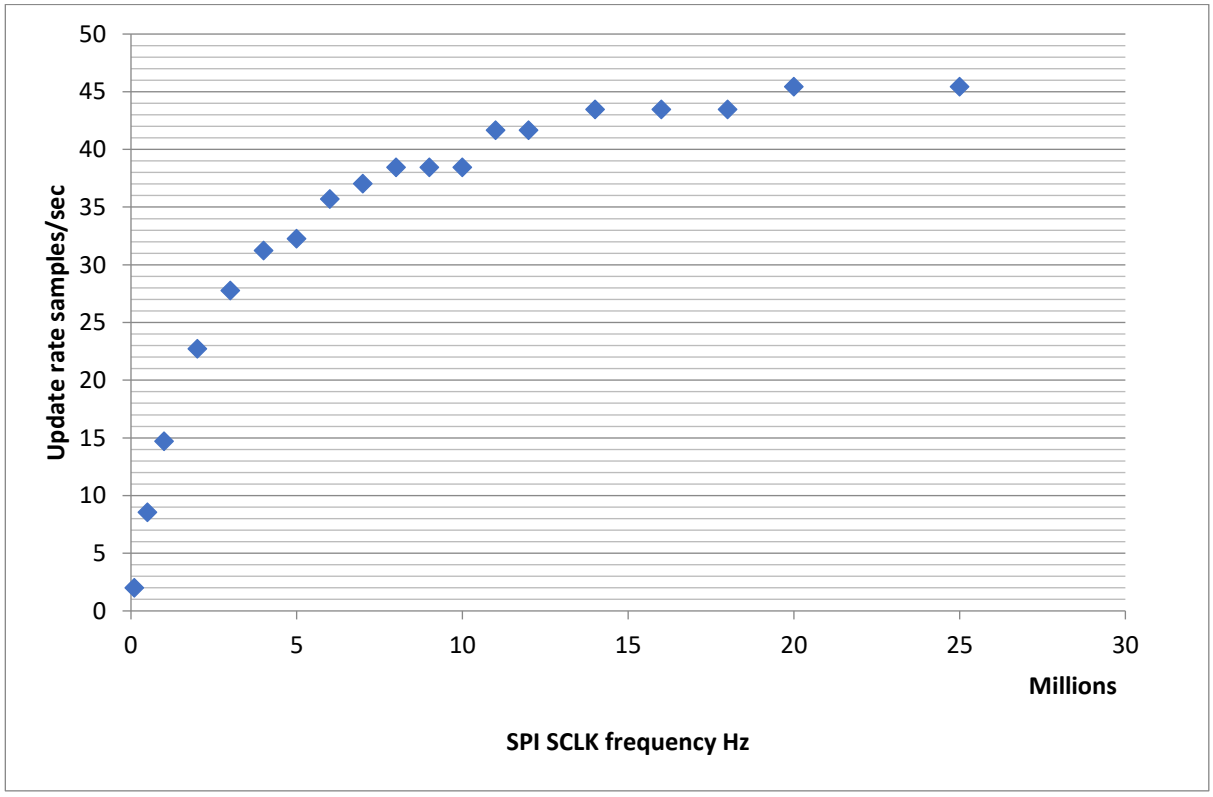

Figure 3.46. DAC update rate vs configured serial peripheral clock frequency.

3.5.5.5 iSim DAC firmware integration

A complete object-oriented class implementation of the DAC (AD5754R) was designed and programmed, allowing access to the DAC internal registers that also inherits the SPI class (its properties and methods), enabling serial communication with the DAC.

During run-time, an instance of this class is created i.e. an object of type AD5754RDAC. This object is then passed to respective function calls as input for further adjustment and querying of its properties (e.g. internal register status). Also, during run-time, the main thread of the iSim firmware has constant access to the DAC's properties, just as it does to any other global value, allowing for better synchronisation and interrupt handling when properties are changed or adjusted.

3.5.5.6 iSim DAC sample rate and output rate

If one is to periodically output samples of data, iSim could be driven at a maximum rate of 14.286 kHz. To avoid changing the waveform timing and hence its morphology, there needs to be a close link between the number of samples in each signal cycle and the designated or requested iSim's output rate. That is for the maximum output rate of 14 kHz, 14 times the number of samples is required compared to the default output rate of 1 kHz. This consequently means a much smoother waveform at the DAC output due to smaller step sizes, hence the output lowpass reconstruction filter would have a wider passband if required.

In MATLAB®, the resample and stairs built-in functions are used to simulate the positive impact of oversampling and increased DAC output rate, as shown in figure 3.47.

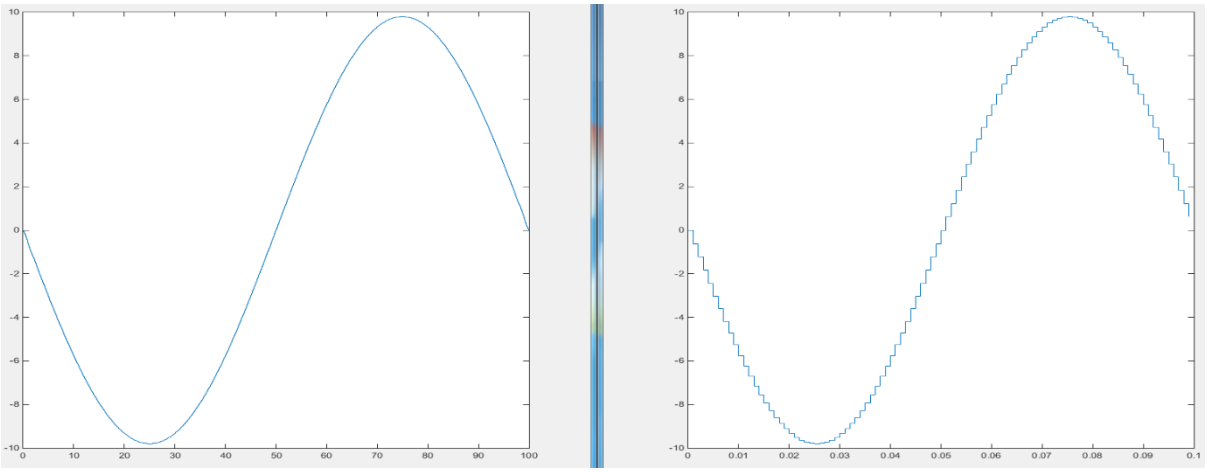

Figure 3.47. Demonstration of Bit rate manipulation using MATLAB® simulation of a simple sinewave. Even zooming to small areas on the left plot in this figure won't make seeing the individual steps any easier. The left plot demonstrates the signal resampled by a factor of 14200. The number of samples in the right plot is 100. The high sample rate mode is used in iSim calibration mode, when one channel is enough to output a clean signal to calibrate the device. That is the software is at its bare minimum operational mode and will not need to spend much time to service other routines.

The maximum iSim output rate against the number of DAC channels updated is calculated as (see figure 3.48):

- Maximum frequency for a single channel = 14.286 kHz (SPI SCLK frequency 1 MHz).
- Maximum frequency when updating two channels = 10.00 kHz (SPI SCLK frequency 1 MHz).
- Maximum frequency when updating three channels = 7.634 kHz (SPI SCLK frequency MHz).
- Maximum frequency when updating all four channels = 6.098 kHz (SPI SCLK frequency 1 MHz).

The upper limit is due to the time that it takes for a DAC output to be updated plus reading a sample from memory. In theory, it is possible to resample a signal of length 500 samples to one of length 14200 x 500 = 7,100,000 samples and increase the output rate accordingly and consequently achieve an improvement in signal integrity. This is not possible in practice since the onboard controller has limited RAM. Thus, the signal file must be stored on another device, hence adding to the overhead.

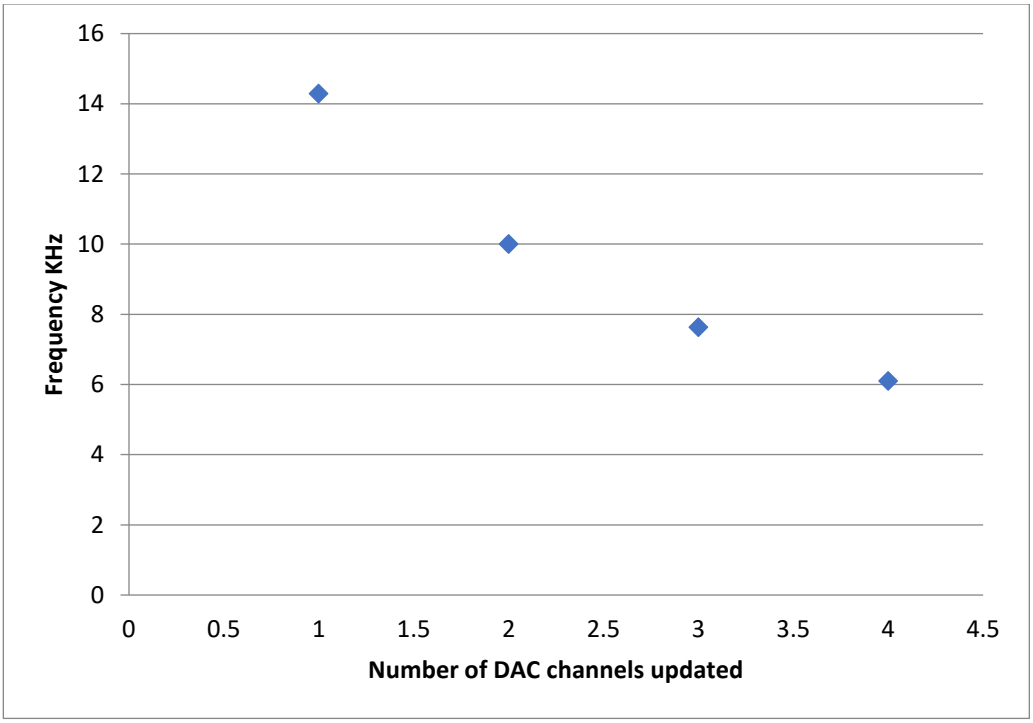

Figure 3.48. Measured iSim output update rate against the number of active channels.

3.5.5.7 iSim maximum signal length

The MBED uses an interrupt ticker that implements a 32-bit integer microsecond counter register, which means it can count to 30 min at most before the counter is reset and timing information is lost. This is entirely within the boundaries of iSim specification. The only rate-limiting factor in stage one development was the overhead of reading samples from storage, which causes a significant bottleneck, forcing the design to store the required output waveform on the MBED onboard the RAM. This limited the maximum waveform duration to 30 seconds when iSim is set at a default output rate of 1kHz. In phase two development, a software buffer implementation meant that such overhead is managed using a multi-threaded application. As this limitation was removed, a storage card could be implemented with enough size to store multiple long-duration files that can be accessed by the microcontroller through an SPI interface. The inclusion of such storage would potentially mean a requirement for a filing system so that access is managed and organised. A microSD card was chosen as the storage unit due to the simplicity of integration of this module with iSim, as well as its low profile and ease of access.

3.5.5.8 iSim trigger methodology

Both hardware and software trigger capabilities are designed into iSim. For the hardware trigger, the source could either be a TTL voltage or optical. The software implementation of the trigger is discussed in a later section.

The optical trigger proved to be more complicated than its TTL counterpart as there are various sources with various luminances that could be used to trigger the device.

- The ISCEV standard states that for PERG the luminance of the white simulation areas should be a minimum of 80 cd.m^{-2}, and there should be a minimum of 80% contrast between the black and white areas.
- For multifocal operation, it specifies that the luminance and contrast should be 100 cd.m^{-2} and 90%, respectively.
- Different electrophysiological centres may use different luminances and have different background intensity settings.
- The illumination may not be uniform.
- Various stimulators may be in use that may cause leakage, such as the Glasgow LED multifocal stimulator. These leakages can be quantified and studied.
- The rate of triggering and hence the response-rate of the phototransistor circuit is also of importance.

It is essential to be able to set the trigger fire on the rising or falling edge of the stimulation onset (white-to-black or black-to-white). The point here is that, for optical triggering, there cannot be a specific light luminance sensitivity setting as the threshold. There must be a method to allow the user to set such a threshold. To accomplish this, a photocurrent-voltage conversion circuit using an operational amplifier was put together that allows for optical-trigger sensitivity adjustment using a 500 kΩ potentiometer in series with a fixed 220 kΩ resistor in the feedback loop of the operational amplifier. To further smooth the op-amp output, and hence reduce the chance of a false trigger, a capacitor is put in parallel with the resistive branch in the feedback loop, providing low pass filtering. The value of the capacitor is chosen to allow for enough rise time for the detection of a pulse and to ensure a high response time. The circuit does not provide any bias, as the non-inverting pin of the operation amplifier is tied to the ground plane (see figure 3.41). The output voltage of the photodiode is then fed to the inverting pin of the amplifier.

To improve the performance, a photodiode with a small active area is selected, and the area is further restricted using surrounding opaque material and by placing the photodiode 5 mm inside the enclosure (see figure 4.40). This reduces the effect of false triggers due to any luminance leakage. As a result, the signal-to-noise ratio of the optical trigger is improved, and hence a more robust performance is achieved.

The sensitivity of the system is adjustable using a potentiometer to the range of 77 cd.m^{-2} - 160 cd.m^{-2}. The analogue signal output of the op-amp is fed to a transistor block to convert the signal to TTL (0-3V3) that is supplied to pin8 of the MBED. This pin is set up as a digital input pin, and the rising edge of the trigger generates an interrupt that is then handled within the call-back routine to output a single cycle of a selected signal at a specified rate. The rate of sample output and the number of samples per cycle of the signal determine the maximum rate that the system can be triggered, and faster trigger rates will not affect this.

3.5.5.9 iSim device Board Zoning

Board zoning is a process of defining general locations of components on the blank PCB before the inclusion of any traces. It goes a little further in that it includes the operation of placing like functions on a board in the same general area, as opposed to mixing them. High-speed components like microcontrollers and DAC are generally placed closer to the power supply with slower parts located

further away and analogue components even further still. With this arrangement, the high-speed logic has less chance of polluting other signal traces. Oscillator chips must be located furthest away from analogue circuitry, low-speed signals, and connectors. This is the strategy that was followed when designing the iSim board. See figure 3.49.

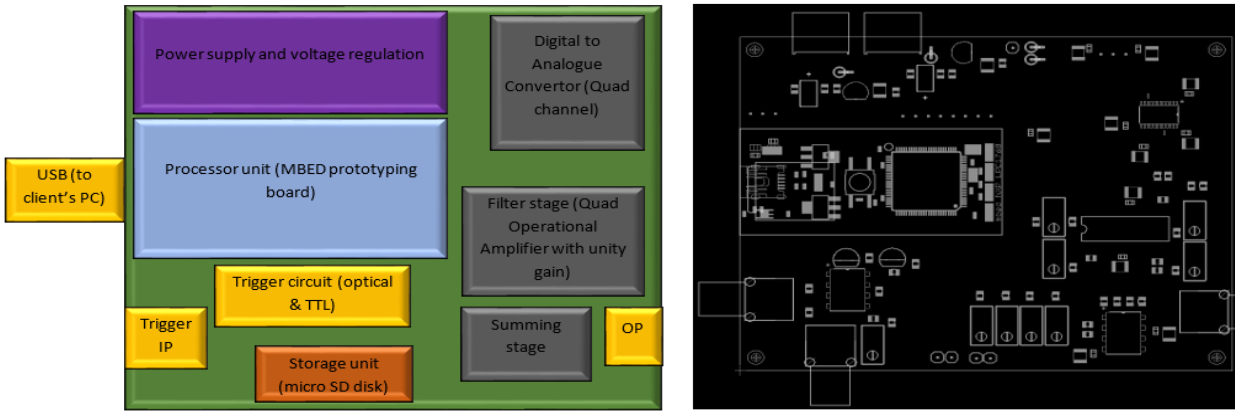

Figure 3.49. Illustration of iSim device board zoning where the placements of the top-level components are defined and mapped.

The iSim board is a two-layer, FRT Tg 130 (isolating material) board. The isolation layer's thickness is 1 mm and 1 oz of copper (greater than 0.035mm). Both sides have a green solder mask with HASL (lead-free) finish. The required Gerber files were created and sent for manufacturing.

In this design, the following criteria were considered and implemented:

- Three Separate ground planes, namely, digital ground plan (DGND), power supply ground plane (GND) and analogue ground plane (AGND). These planes are connected at two points (star connections, SH1 connects DGND to GND and SH2 connects GND to AGND) shown in figure 3.50.
  SH2 is placed right underneath the DAC per the DAC specification sheet to ensure high-quality DAC operation (AD5754R specification sheet for further detail).
- All layout guidelines for the DAC are based on the DAC's specification sheet to ensure the rated performance was achieved. As part of this evaluation, key parameters to check when one receives samples of the DAC, are identified, and it is required to perform inspection of these parameters against the specification as part of first or initial article inspection. All verification test methods are produced, verified and documented.

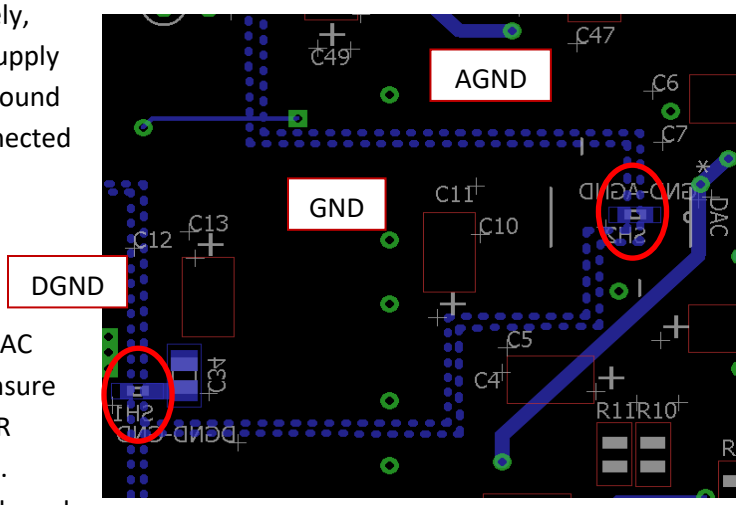

Figure 3.50. illustration of ground star connections.

- MBED and micro SD card are placed in close proximity. This allows better shielding of fast digital components and hence less EMI interfering with analogue circuitry. For example, the fast serial clock line of SD card is isolated from the rest of the circuitry, ensuring better performance of the analogue section on the board. This also provides a single site access for both controller and micro SD card.
- Copper and board thickness.
- Reduction in overall component pin count.
- All components are carefully zoned and grouped, having in mind the effective separation distance. For example, all analogue components are placed close together, and furthest from the rest of components. The MBED and SD card are put together and shielded from the rest of circuitry, and the analogue summing amplification components are grouped furthest away from the digital plane.
- All power lines ($\pm$12V), are 0.8 mm thick and all signal lines are 0.254 mm thick.
- None of the traces has sharp (90^{o}) routes to avoid reflection and hence signal contamination.
- High-speed traces are minimised in length and buried in the ground plane to reduce the coupling of high-frequency noise with other signal traces.
- Potential EMI sources and victims (i.e. circuits that are a potential source of EMI or are potentially susceptible to EMI) were identified as part of the PCB design. For example:
    - Digital clock circuits: these circuits regularly switch and introduce narrowband harmonics.
    - Digital signal circuits: these are traces that carry digital information. These signals have a more random nature than the digital clock and hence are more broadband. If one looks at the least significant bit on the data bus or any other digital trace, these bits usually jump up and down randomly. This effect was visible in the Glasgow operational amplifier design in which it incorporated a 32-bit resolution front-end ADC instrumentation amplifier. These toggling effects are also affected by the encoding system, e.g. binary or two's complement.
    - Power switching circuits: the switching mode power supply and DC-DC converters generate different voltages by switching the current into a transformer and switching on and off rapidly to boost the voltage up (this rate is 100 kHz for the implemented voltage supply booster circuitry). This noise is periodic (i.e. time-locked and challenging to get rid of). However, since the overall LPF (Low Pass Filter) corner frequency is set at 500 Hz, this or any other high-frequency noise is mostly filtered out.
    - All our analogue circuits are highly susceptible to EMI.

- Any noise appearing on the signal traces are internal or external to the iSim electronics. In this design, the potential current loops and critical current path were analysed in conjunction with the path of least impedance for any return currents. This is why the author has tried to have a continuous (with no break) bottom ground plane where possible. At low frequencies, the impedance is dominated by its real part, i.e. resistance. So current will take the path of least resistance (this is true for frequencies of kHz or lower). At higher frequencies (MHz or higher), the impedance is dominated by inductance (the dimensions and abundance of vias on the PCB board become important).
- No digital lines are crossing the analogue plane to digital plane or vice versa. If this was the case, such a path would bridge the isolation gap between the planes and would couple high-frequency noise from DGND to AGND.
- Both layers of the board are poured with copper; this could introduce parasitic capacitances with signal and digital traces, acting as a low pass filter. Due to the frequencies of interest (i.e. low), this won't degrade any of our signal frequency components.
- No high-speed signal traces are running directly under any possible antennas in the circuit (all "through-hole" components, heat sinks, or connectors like phono connectors are possible antennas). This is known as voltage-driven coupling.
- All decoupling capacitors are very close to the designated pins around the DAC and amplifier components.
- The DAC is placed close to the voltage supply pin.
- The length of traces attached to the IO connectors is minimised.
- No high-frequency line is routed under any components.
- All connectors should be located on one edge or corner of the board. Connectors represent the most efficient antenna in any designs. Locating them on the same edge of the board makes it much easier to control the common-mode voltage that may drive one connector relative to another.
- All off-board communication from ISIM is routed through the same USB connector.

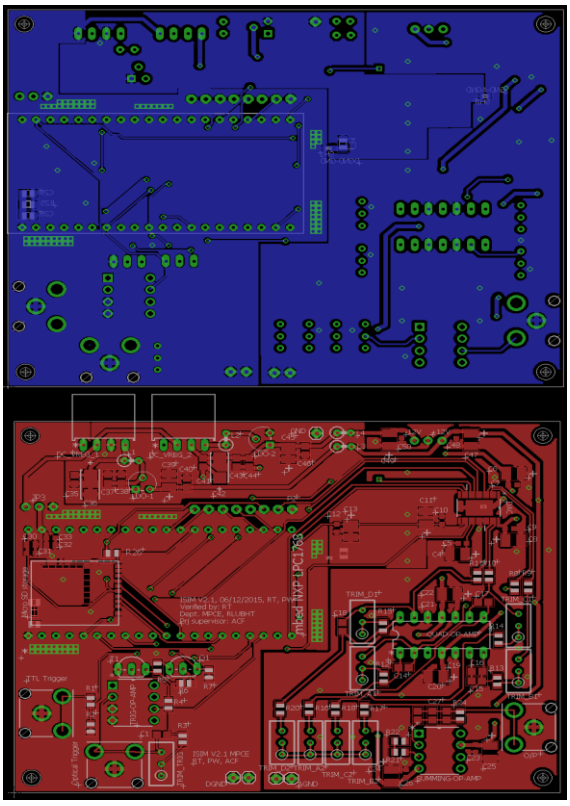

Figure 3.51. Illustration of top and bottom plane and signal routing. Particularly it is evident that the ground plane is kept free of routing where possible ensuring no breaks or discontinuity.

- No high-speed trace is routed close to the edge of the board; this is to contain the generated electric and magnetic field by these lines so that they do not couple noise to and from the board.
- None of the critical signal paths run anywhere near a digital line or in parallel with such lines to avoid capacitive and inductive coupling.
- All digital traces from/to DAC to/from MBED are grouped and buried in the top and bottom ground plane.

3.5.5.9.1 Populating PCB boards – PCBA (PCB Assembly)

The Board was populated in the Department of Medical Physics and Clinical Engineering at the University of Liverpool, RLUBH. All components were purchased from approved vendors, and in cases where an approved vendor could not source the component, rigorous testing at the component level was performed against its specification as part of the First Article Inspection (FAI) and acceptance criteria. The acceptance criteria were determined based on the criticality of the component within the system. Cost of Goods (COGs) is also investigated, bearing in mind that the production of the system is not yet ready to be scaled-up.

Figure 3.52. Illustration of iSim PCB assembly iteration and enclosure testing.

3.5.5.10 iSim device Embedded Software Architecture

The architecture of the iSim embedded software system is described in this section by modularising the software system into software items. iSim embedded Software Detailed Design Specification (DDS) section of this thesis will further decompose the system into its software units. In this document, the term software system, software item, and software unit are used consistently as defined in IEC 62304 standard. figure 3.53 demonstrates an example of a software hierarchy structure.

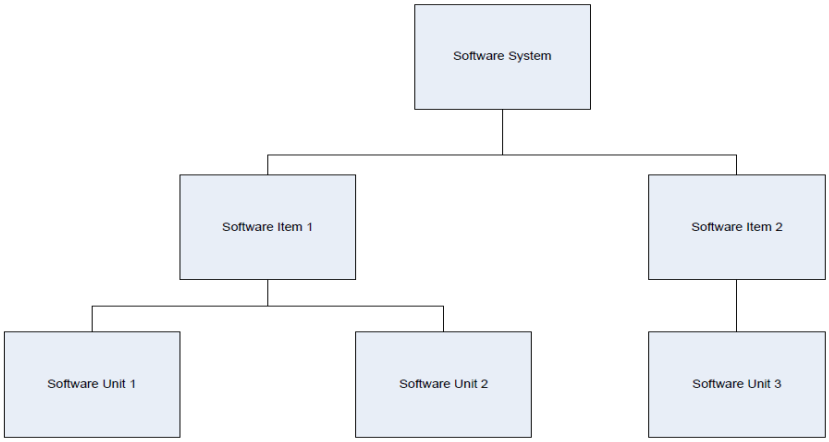

Figure 3.53. Example of software system, items and units.

3.5.5.11 iSim software system decomposition

The iSim embedded software system is limited to the functionality directly related to providing realistic visual electrodiagnostic signals and noise from a device. Consequently, within the software system, there will only be one software item, the iSim embedded Firmware Software Item.

3.5.5.12 iSim embedded firmware

The iSim embedded firmware will manage all software functionality related to providing realistic visual electrodiagnostic signal and noise. Figure 3.54 shows an overview of this firmware. The application program is developed and compiled with relevant libraries and integrated dynamically linked library (DLL) file system using the MBED online platform.

The firmware (application layer in figure 3.54) is responsible for managing the following high-level tasks:

- Control iSim hardware to output and maintain user-specified or requested waveform.
- Handle user inputs.
- Detect the presence or absence of the SD card/storage unit and manages the read and write operations to and from the storage module.
- Manage memory and time to output samples at a user-selected rate, where the default is 1 kHz.
- Detect the presence or absence of the trigger signal, either TTL or flash.
- Manage different modes of operations.
- Enable and control calibration mechanism.

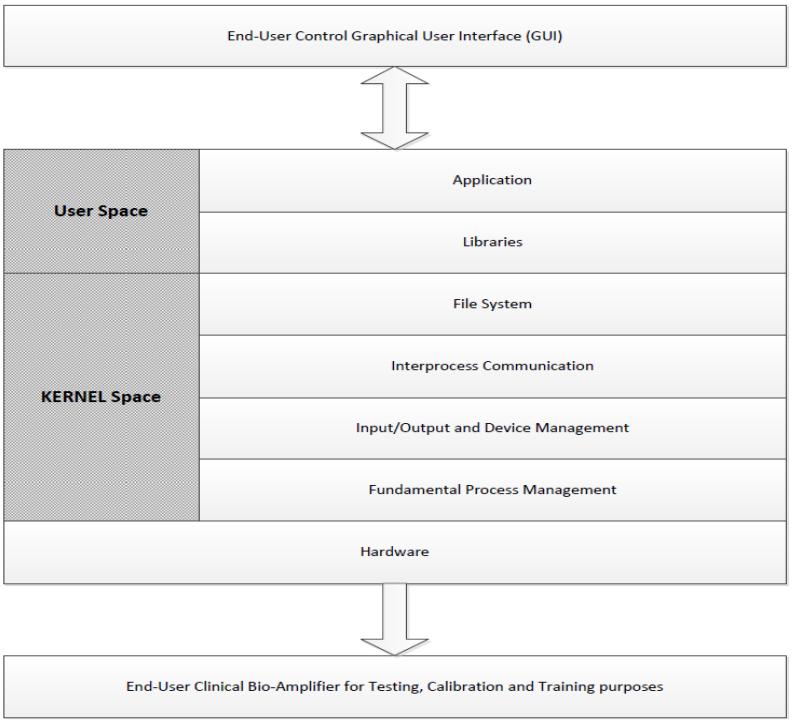

Figure 3.54. Captures the high-level functional inputs and outputs of the firmware software Item.

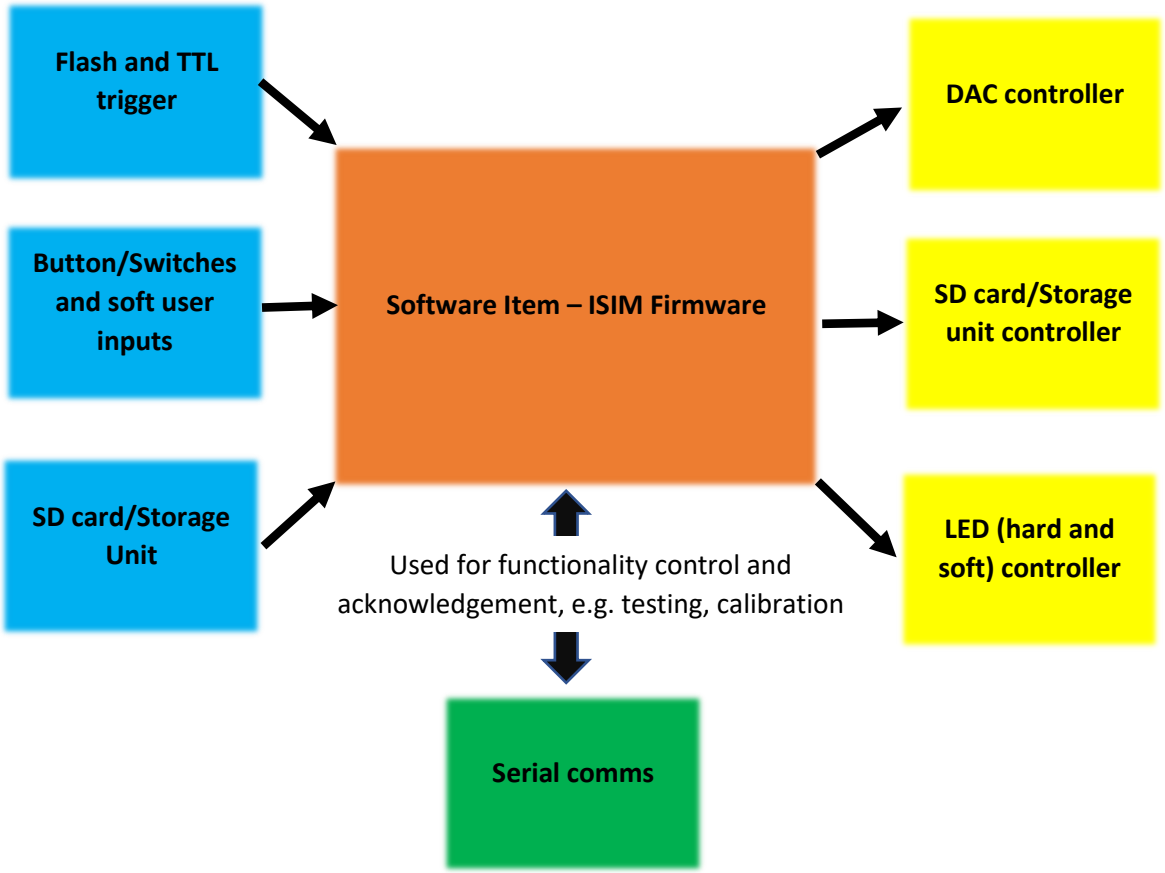

Figure 3.55. High-level functional inputs and outputs of iSim firmware software Item.

3.5.5.13 iSim Software of Unknown Provenance (SOUP)

Off-the-shelf software which has not been developed to known standards but is used in conjunction with or included within a software system is classified as SOUP (figure 3.56). SOUPs are tested using a black-box approach and become a legacy software component as the firmware is upgraded. Use of SOUPs has significantly improved the development time and reduced the development costs and reliability of iSim. The author is aware of the extent of SOUPs used and has investigated the effort it would take to develop all software components from scratch. In many cases, SOUPs were altered slightly to fit their purpose in iSim design, and these changes are documented within the design process.

3.5.5.14 iSim software Detailed Design Specification (DDS)

The purpose of this section is to capture the design rationale driving the implementation of the iSim firmware system.

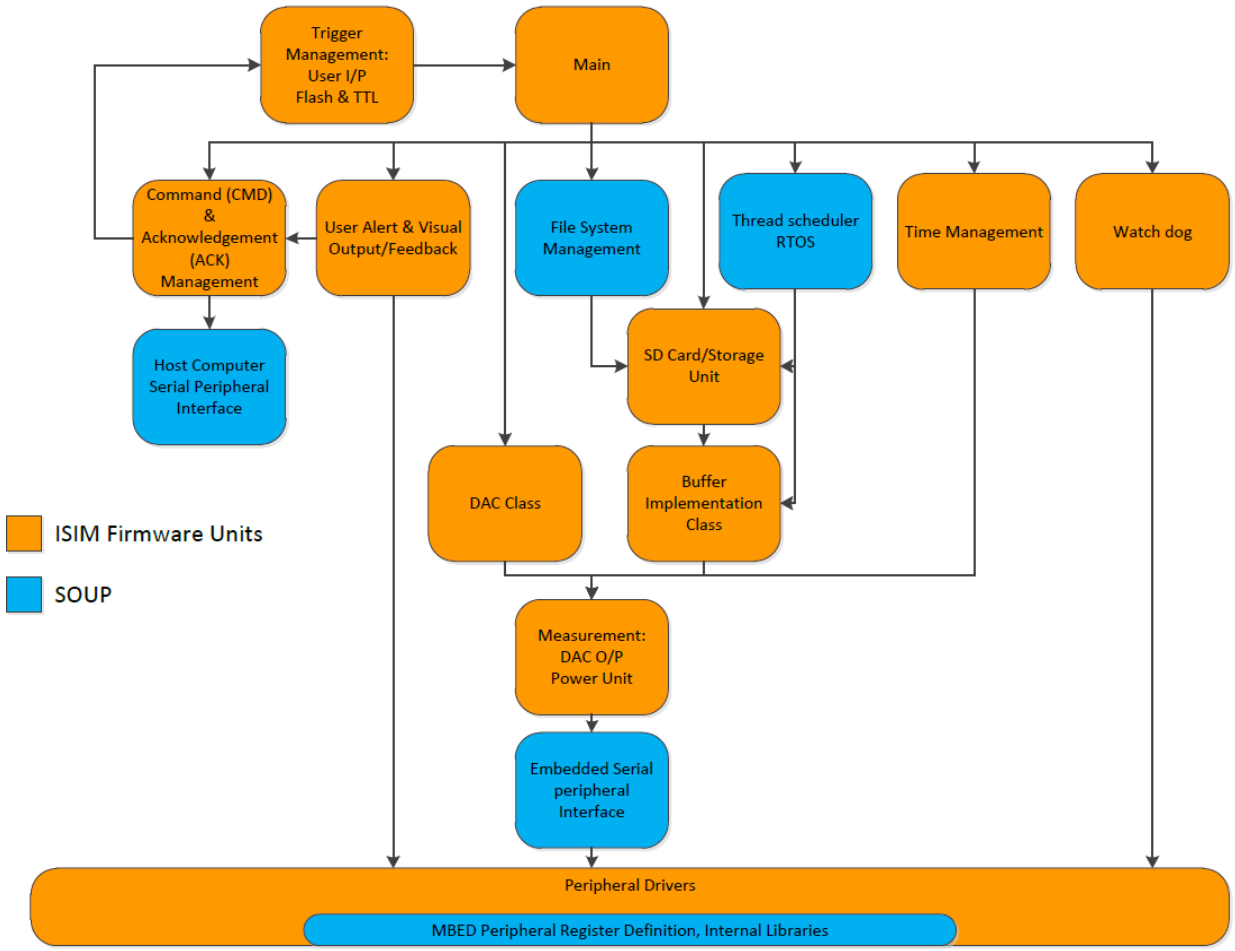

Figure 3.56. iSim embedded firmware architecture. All SOUPs are borrowed pieces of software in the implemented modular design architecture that are fully tested and where needed modified to fit the required design criteria.

3.5.5.15 iSim Real-Time Operating System (RTOS)

Employing an operating system for the iSim micro-controller is necessary as the following top-level functionality needs to be implemented:

- Running multiple processes or functions in parallel.
- Memory management.
- Managing interrupts and event in an efficient and standard way.
- File system management.
- Scheduling among parallel tasks in an automated or customised way.

For example, the following interrupts and hardware peripherals are deployed in the iSim design:

- Interrupts to handle multiple switches and external triggers.
- Host serial communications.
- SD serial communications.

- File system (FATFS) mounting.
- DAC (AD5754R) serial communications.
- USB interface to host PC.
- Execution of multiple tasks in parallel and pre-emptive scheduling.
- Stack switching with minimal overhead.

Using a real-time OS on ARM architecture has many benefits. The architecture supports stack switching without any complications, and almost every chip provides timer and other functions needed for pre-emptive multitasking.

3.5.5.16 iSim embedded software test strategy

It was recognised that, without a test strategy and plan in a complex multi-disciplinary design and development project such as ISIM, the author would struggle to deliver the project on time, to budget and within an acceptable (and agreed) risk profile. The author also recognised that testing would take considerable time. Each module in the design is tested in isolation down to individual critical to function components, which are tested against the supplied specifications. As different modules are integrated, further testing is performed, ensuring no adverse effects. The following testing methodology was implemented:

- Visual verification – for example, checking the workload within each interrupt handler and where criticality exists (CTF code segments), a test plan was developed, and all identified risks were mitigated.
- Black-Box or functional testing – comparison of output data file versus input data file to assess how well the software meets the requirements.
- Coverage or white-box testing – this is to ensure critical segments of code that could have an impact to top-level user requirements are thoroughly tested and verified, for example, DAC Firmware Unit testing was performed as an isolated module and when integrated within the ISIM multi-threaded embedded firmware application.
- Regression testing – throughout the firmware development, it became clear that it is not enough to pass a test once. Every time the program is modified, it was retested to ensure that the changes didn't unintentionally break some unrelated operation.

3.5.5.17 iSim detailed testing structure & implementation

The testing structure and details are design specific, and the following summarises the main criteria tested during the development of ISIM:

- Test duration – Perform testing over long durations to increase the probability of capturing bugs.
- Stress testing – these are tests that intentionally overload input & output channels, memory buffers as well as data flow channels to and from the onboard microSD storage. For example, increasing the microprocessor clock frequency and loading all four channels of the DAC while reading large files from SD storage.

- Boundary value testing – performed mainly to check iSim DAC component to verify the dynamic range and presence of any nonlinearities that may be introduced. Such nonlinearity could significantly affect signal morphology.
- Resource-dependent environmental testing – a desktop computer has more resources than the MBED microcontroller prototyping board. Critical segments of the embedded firmware are written within a resource-rich Integrated Development Environment (IDE) to ensure top-level requirements are met and a test mechanism is identified without worrying too much about details.
- Monitor timing of the read and write operations across the following interfaces:
    - SD/Noise buffer.
    - Noise buffer/Ring buffer.
    - Ring buffer/DAC register.
    - DAC update rate (Sampling rate of iSim).
    - Embedded ring buffer/GUI Ring buffer.
- Atomicity (ensuring thread switching or context switching is managed properly to avoid data corruption – blocking critical sections) of operations and identify areas of risk as well as mitigation and the control mechanisms needed to implement such mitigations.
- Thread lock and protection testing.
- Race detection – this is when the two read and write threads try to access the same variable at once. This was evident in the implementation of the Ring Buffer as we are clearly accessing the same block of memory using two non-synchronized threads in which one is performing the write operations and the other the read operations.
- State Space exploration:
- Through creating Deadlocks (such as the use of `Printf` or `Fread` statements in critical sections of the code and monitoring the behaviour).
    - Violating the user-defined assertions and planning to check the user-defined inputs and capture exceptions accordingly. Identifying the exception types and planning to report this as information or an error. If the risk is probable and can impact critical user defined product requirements, then implement mitigation mechanisms.
    - Generating exceptions (hard code) and performing impact-analysis.
- DAC Serial clock verification against DAC specification.
- Encapsulate the low-level and the high-level programs within code blocks to capture all potential errors without crashing the system, perform a controlled crash, i.e. a system reset.
- The following steps are used to prepare input files to verify that the iSim implementation is consistent and reliable:
    - Generate files to perform testing:
        - Create all required files using the ARMA Excel® interface (front-end user interface communicating via Soap calls to the back-end MATLAB® mathematical engine using MatSOAP© Server). All files are in .txt or .csv format.
    - Prepare files for storage:

        - Create required binary files using a .exe file written in C – See Appendix B for the code implementation.
    - Create a configuration file for the MBED module. MBED will read this file at initialisation stage to configure as required.
    - Using a multi-threaded C code in MBED to perform read and write operations to and from a single buffer.
    - Read from a micro SD card and write to the buffer. Read from the buffer and write to the digital output pin of MBED.
    - Generate an MBED test script that allows for various degrees of testing depending on the changes introduced — for example, MBED to run over a few hours under overloaded operating condition.
- PCBA board noise level testing.
- Power unit voltage stabilisation duration and maximum current intake.
- Calibration potentiometer testing.
- Reconstruction filter testing.
- Output summing amplifier testing.

3.5.5.18 iSim software (main thread) unit description

The main unit is the primary entry point into the iSim firmware. At startup, it initialises all other units and checks for any initialisation errors that would prevent the application from running. Once all modules are initialised, it performs other internal memory initialisation tasks (table 3.3) and enters a finite while loop (table 3.4) which will exit at user request or when the requested simulations have reached its end, see figure 3.57.

Table 3.3: iSim SW unit description.

Software Initialisation Tasks	Encapsulating Unit	Description
System Initialisation	Main Thread	Initialises iSim and initiates communication with iSim GUI.
Operational mode setup	Main Thread	Initialise and enter Normal (default) or Calibration mode (Engineering, Terminal or Terminal + mode) per user request. A hard reset is performed if the mode of operation needs to change.
Initialise Storage unit	Main Thread	Initialise the SD SPI interface.
Storage card file read and onboard verification	Write Thread/Main Thread	Perform a read operation on the content of microSD card and perform initial checking such as file names, extension, length, and size. Send the information (the content of noise and signal folders) to the iSim high-level GUI.
Initialise Ring/Circular Buffer Unit	Write Thread/Main Thread	Sets up the memory buffer and initialises it to zero.
Initialise Thread Unit	Write Thread	Initialises the write operations from SD card to the internal noise buffer memory and continues until it is full.
Initialise DAC	Main Thread	Power up and initialises all four DAC channels to zero.
Initialise timer Unit	Main Thread	Instantiate internal timer objects.

Executed task within the while loop is shown in table 3.4.

Table 3.4: iSim main loop functionality description.

Software While Loop Tasks	Encapsulating Unit	Description
Watchdog Pet	Main Thread	The implemented watchdog timer (software-based) will require a kick every 15-30 seconds otherwise firmware is assumed stuck. This would cause a firmware full reset.
Evaluate Alerts	Main Thread	Monitor all internal flags such as read and write violations, overflow, DAC power up and down error, trigger-in and out error, output rate violation, saturation flag, waveform clipping error, signal polarity error, dynamic range error, sample read violation, missing packet alert, timeout flag, file access & type error, buffer (noise & signal) access error, DAC register setup & read error, microSD attachment error, microSD detachment flag, unknown command error, out of synchronisation error.
Drive DAC	Main Thread	Monitors DAC health status throughout operations, write/reads to/from DAC internal register for data output.
Run Operational State Machine	Main Thread	Monitors and service the state of iSim in all operational mode and adjust the internal registers and variables accordingly.
Check for interrupts (e.g. User Inputs received via Serial Comms Interface)	Main Thread	Check for all internal and external interrupts. External interrupts are composed of user-generated through iSim GUI or external triggers (TTL or optical). Internal interrupts are due to various firmware units functionality during operation.

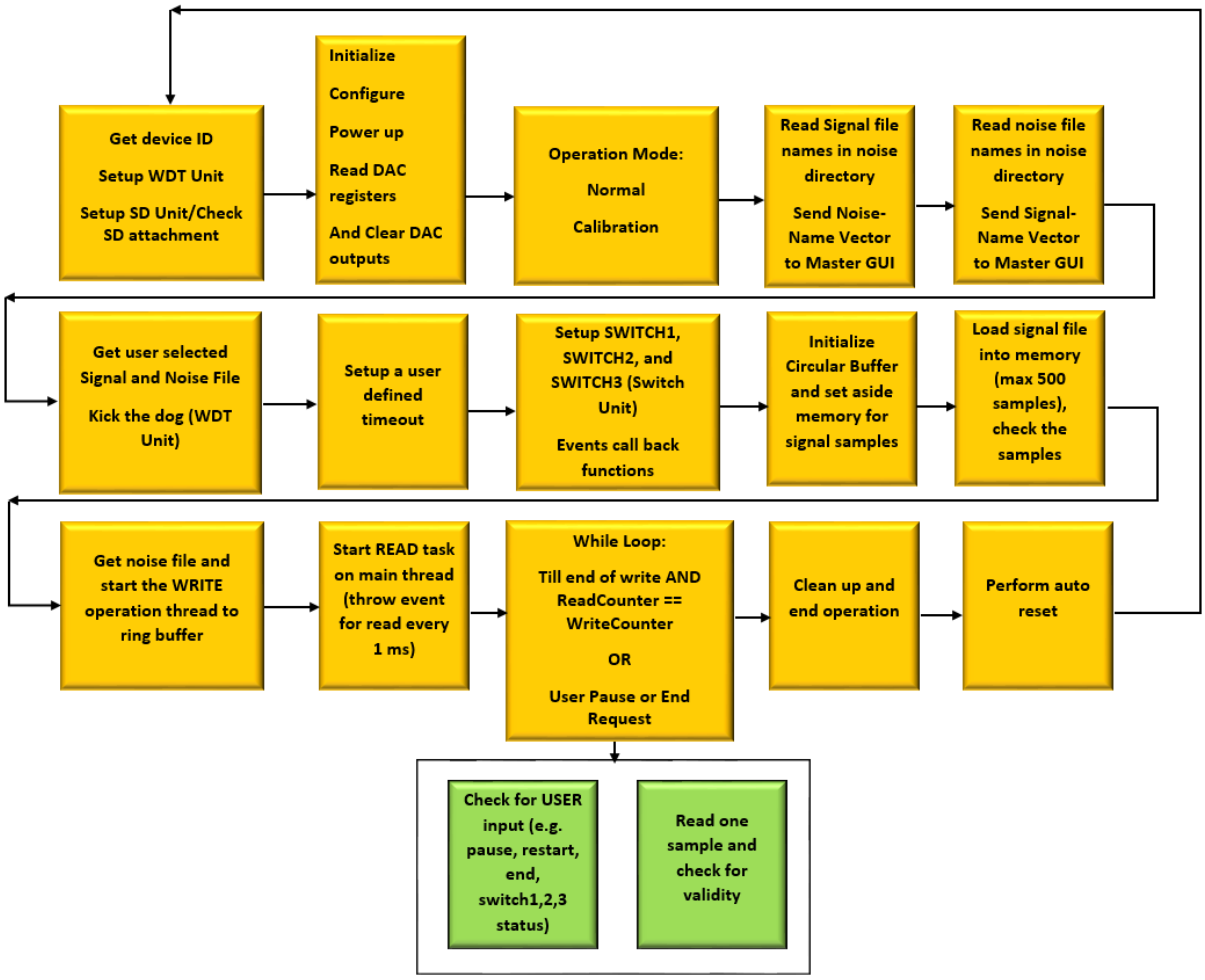

Figure 3.57. Illustration of iSim main thread program flow.

3.5.5.19 iSim file description

In phase two of the iSim developmental cycle, the selected DAC provides a significant improvement in the infrastructure and available flexibility by providing four independent programmable channels. This allows a single signal channel to have sole ownership of the full dynamic range available. That is, the expected signal range is projected over the entire DAC channel (DAC_1) dynamic range. The noise channel has its own assigned DAC channel (DAC_2). The spontaneous noise components (EMG, blinks, and eye movement) are assigned to DAC_3 and harmonic interference to DAC_4. An operational amplifier is configured as a summation amplifier at the output stage of the iSim. A File Application Table File System (FATFS) module is integrated with the embedded firmware (a SOUP unit). The FATFS module sits between the application interface (the iSim firmware) and the storage unit. This module allows the application interface to treat the data bytes on the microSD as files. This has significantly reduced the effort required for reading the files and their associated properties. It also provided a generic layer for the firmware that is independent of the storage unit, i.e. the same firmware could be used with a different storage unit and is not bound to the microSD. The compromise made was the slower access time.

Two files will be required during the initialisation stage:

- Signal file: this is a file of length 500 samples, loaded into the microcontroller memory during the initialisation stage. Any samples beyond this length are ignored. Samples are float types and are represented in the unit of µV.
- Noise file: this is a column vector of float values in units of µV. It can be of a maximum length corresponding to 30 minutes at a sampling frequency of 1 kHz. This file is constructed as shown in figure 3.58 where N = length of noise file/3.

Individual samples or an entire file can be set to zero. This is the case if we want no blinks, eye movements, mains or ERG noise. These settings are also controlled via the GUI. This gives the user the option of suppressing the noise components during the operation. So, for instance, we could have ERG noise samples other than zero in the file but instruct iSim to output zero instead through the master GUI.

Both signal and noise files must be provided as binary files to speed up the read operation. The noise file is constructed, as shown in figure 3.58, to speed up the write operation to the circular buffer since only one file open and close operation is performed to access all noise components.

A software segment is written in C (and incorporated with a C#.NET class within the Top-Level iSim GUI), to convert the text files received from the MatSOAP© Excel® Interface to Binary files for storage in the SD card, see Appendix B for the code implementation.

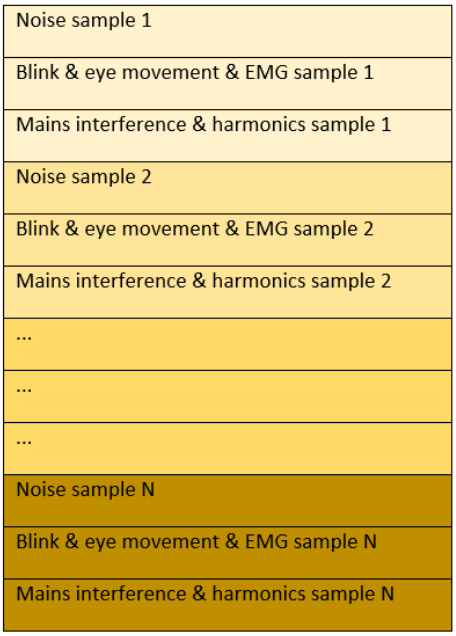

Figure 3.58. Expected iSim noise file structure.

3.5.5.20 iSim embedded ring buffer implementation

A circular buffer is a data structure that wraps from end-to-end. New data overwrites the old data so that it can be written to infinitely. It is ideal for applications in data streaming (a first-in-first-out or FIFO data structure), i.e. for streaming data from the microSD storage unit to the user host computer screen through various allocated memory locations or interfaces, as shown in figure 3.59.

In this architecture, a fixed-sized array is hard-coded, rather than using a dynamic size implementation for the array to avoid the need for a resource-intensive memory reallocation process. The fixed-size array is a contiguous block of memory, and hence it is much faster to access the elements of the array due to the reduced CPU overhead in calculating the next memory location for a read or write operation.

The design application also requires the reading of data from the microSD card and streaming it to a buffer (noise buffer) followed by a read operation from the buffer and a write operation to a generic DIO pin on the MBED prototyping board. This satisfies the requirement of a data streaming operation. Required fixed memory allocation is performed at start-up or during the initialisation phase.

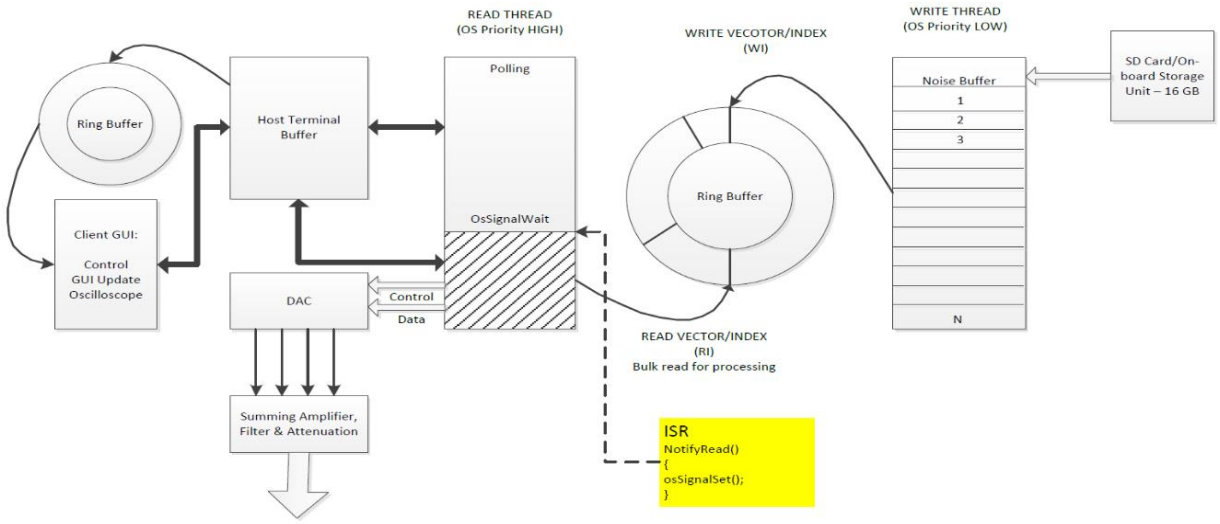

Figure 3.59. Illustration of implemented low and high-level circular buffer in low and high-level software iSim software design. Figure also shows the data flow from the SD storage unit to the client's GUI.

The embedded ring buffer has been implemented and tested as a separate module to ensure timely functionality. This implementation code is provided in Appendix B. The data flow, design infrastructure, and implementation algorithm are illustrated in figure 3.59. This algorithm is used for both embedded and high-level buffer implementation. See Appendix B for the implementation of the high-level ring buffer. This implementation was tested externally to iSim using notepad++ and a generic C/C++ compiler to ensure the code module operates as expected, as well as examining the boundary conditions so that synchronisation between the read and write operations are maintained. The boundary examination was explicitly focused on the read and write speed when they are marginally and significantly different for variable buffer size and data types (the high-level implementation was developed and tested in Visual Studio IDE using C#.NET programming language).

The timing of the read and write tasks was investigated, ensuring synchronisation between the two operations when integrated with iSim. It takes 20 ms to import 500 samples from the microSD to microcontroller onboard memory. This means that it takes over 40 μs (<25 kHz) to read a single sample from the microSD into memory. By default, iSim is set to output samples (more precisely a packet of information) at a rate of 1 kHz. That is, reading three samples (one packet of information) from the ring buffer every 1 ms. It, therefore, takes 334 μs (<3 kHz) to read a single sample from the ring buffer.

Hence: (Read Speed) / (Write Speed) = 25/3 = 8.

That is, the write operation to the ring buffer is almost eight times faster than the read operation. This is shown in figure 3.60. These two operations are run as separate threads in a multithreaded firmware application, where the read thread is responsible for reading from the buffer and driving the respective DAC channel while the write thread is accountable for reading blocks of data (multiple packets) from a designated location in the microSD and writing this to the internal buffer of the iSim. The firmware uses various flags and acknowledgements (ACKs), allowing the state of the machine to be communicated to the user through the iSim GUI, as well as internal firmware communication across the interface of the various software objects and modules.

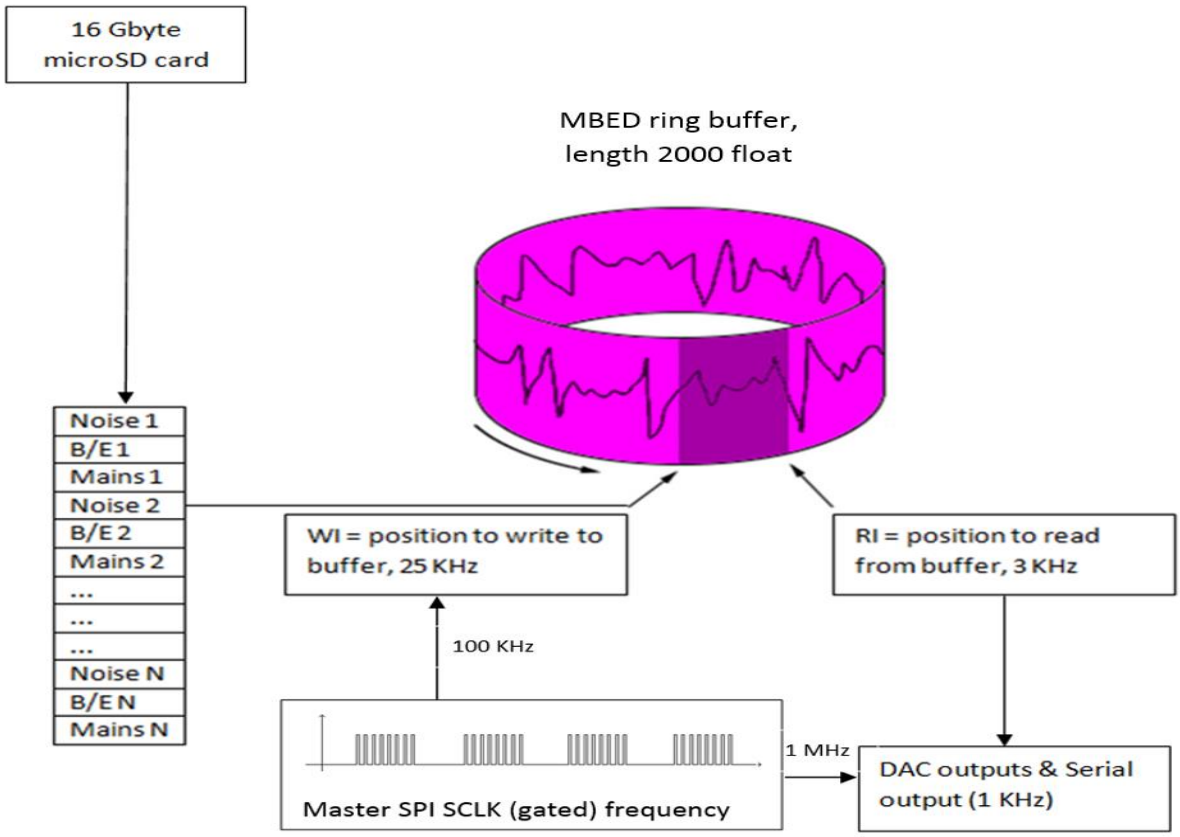

Figure 3.60. Illustrating the timing of the read and write operations and assigned SPI clock frequency to ensure no read and write violation and sustained iSim output sample rate. RI is the Read Index variable holding the position of the next read from the buffer while WI is the Write Index variable that holds the position of the next write to the circular buffer. From the figure and performed calibration, the write and read operations does not occur at the same speed.

iSim communicates, two acknowledgements, or ACKs (`DEV_endini`, `DEV_waiting4start`) over a serial peripheral interface to the host computer. These ACKs mark the end of the initialisation stage and readiness to start the read operation stage from the ring buffer (that is, the Initialise button on the iSim GUI is disabled, and the Start button is enabled).

After `DEV_endini` and before `DEV_waiting4start`, the ring buffer is allowed to fill by setting the main thread to a waiting state (not spinning). Hence the write tasks start for the very first time and begin filling the ring buffer. Next, `DEV_waiting4start` is issued. After this, the main thread is set to spin indefinitely until one of the two following conditions are satisfied:

- WDT timeout (set to 60 seconds) elapses. This causes the program to restart, indicating user inactivity.
- Start command is received on the serial terminal.

While the main task is spinning, the write task is suspended, as its priority level is lower than the main thread and the MBED RTOS is a pre-emptive Operating System (OS).

The spinning is also known as, busy wait, a repeated process to check if a condition is true or false. Here, spinning is mixed with sleeping the thread, to avoid wasting processor resources (clock cycles) spinning and doing nothing while waiting for the user to press start. Instead, on every spin, the main thread is sent to sleep (i.e. no longer scheduled by the scheduler) for 1 ms, at which time the write thread is running and filling up the circular buffer (context switching). By the time the user has pressed start the buffer is full (the read and write indices are equal or RI=WI).

An alternative way to exit the above loop is when the user has defined a quick-start command after initialisation, in which case the while loop will never spin. Thus, the buffer may not be full (due to the initial head start that is given to the write task).

It is not essential to have the buffer full or empty when starting the acquisition. This is just implemented as good practice and useful use of resources.

After the loop exits, the WDT is kicked, and its timer is reset. Next, the device issues a `DEV_readTHR` ACK, indicating that the ticker is attached to enable the read task and its counter is started. This is the interrupt which indicates when the DAC is to output a sample on each of its channels. This timer interrupt is set to the highest priority, and its ISR only sets a boolean flag to true (i.e. an extremely simple execution block). This is to ensure that it is accurate and 100% guaranteed DAC output rate as requested by the user. Its timing has been verified on an oscilloscope when hooked into the TimePin1 DIO pin of MBED (pin 30).

Optical and TTL trigger interrupts are also attached to the microcontroller pins and are called on the rising and falling edge of the interrupt signal, respectively.

Before the execution enters the thread-read polling loop, all flags are reset, and the serial buffer is flushed, and WDT timeout is reset (this sets the device in a known state, identified by its flags).

Note that write task index must always be greater than or equal to the read task index. Any `printf` or other lengthy or blocking operations in either the write or read task can disturb such equilibrium, resulting in sample missing events or alerts being raised. If the read task is much faster than the write task, then unexpected errors can occur which will be captured, causing the device to go through a controlled system crash, i.e. full system reset.

Running the device at a faster rate will increase the read task speed while the write task is fixed due to the system's hardware access overhead. The latter is what limits iSim's output rate to 2.381 kHz. This maximum output rate is calculated based on the experimental testing of all routines, including the following:

- The time that it takes for iSim to read from the temporary noise buffer to the internal ring buffer – this was found to be negligible and ignored.
- The time that it takes to update all four channels of DAC (driving the DAC registers).
- The time that it takes for the operating system to perform other housekeeping routines when iSim is operating in its normal mode.

- SPI serial clock frequency of 1 MHz and 100 kHz for write and Read (write operation to DAC registers, which is performed in the read thread from noise ring buffer), respectively.

Based on the above, a minimum of 420 µs is required and must be allowed before the read thread can repeat itself, giving a maximum output rate of 2.381 kHz. If this is reduced, then iSim firmware will start throwing overflow timing errors which signifies missing packets. This won't result in an iSim reset but is monitored by the master GUI and user is notified as shown by the red box in figure 3.61. However, as this threshold is reduced further, the operation will be terminated by the run time error as the write thread becomes heavily loaded.

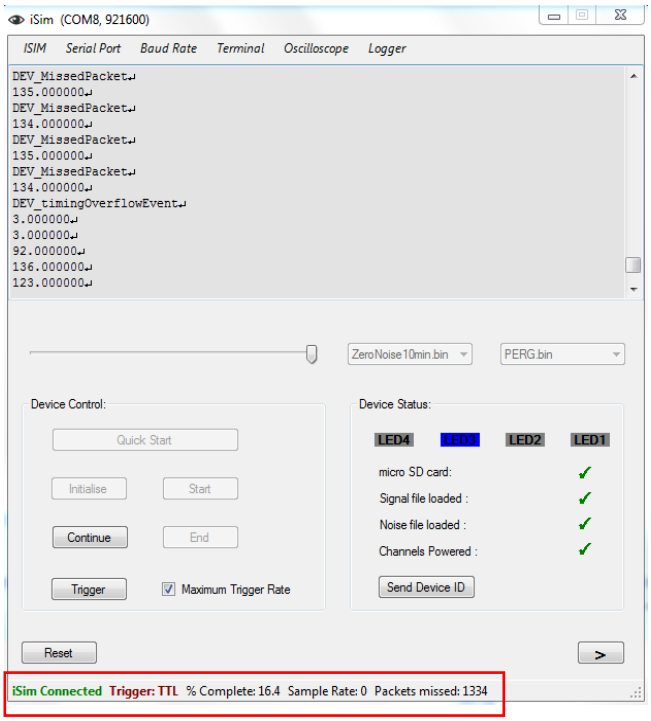

Figure 3.61. illustration of iSim GUI notifying user of missing packets (red box at the footer).

The write thread is the background thread and the main or the read thread is the foreground thread. Therefore, whenever the main thread terminates execution, the write thread will also end.

The write thread will naturally end execution when there are no more values to read from the specified noise file in the microSD, at which point it sets the `FinishWrite` flag to `TRUE` and finish execution. The main thread will finish execution when the `FinishWrite` flag is `TRUE` and when `RI == WI`. At this point, the main thread carries on with cleaning operations and will return.

Other factors introduced to make the processing faster:

- Pre-allocating memory locations.
- Not using dynamic arrays.
- Avoiding memory fragmentation (there is no garbage collection in most embedded systems).
- Using register variables.
- Using faster operations like the shift operator in place of the power (pow) operator.
- Working with binary values.
- Avoiding type conversion as much as possible.
- Using single file storage to read multiple samples, thereby, avoiding overheads in reading from multiple file locations within the SD card.

3.5.5.21 iSim event-driven and polling architecture

In the iSim design, both polling and event-driven architecture were deployed in the low-level software design. This is primarily due to the need to output a sample every 1 ms, i.e. a default output rate of 1

kHz. At the high-level, event-driven programming was employed, where the client's GUI reacts to information received through its Serial Peripheral Interface (SPI) and updates the user accordingly.

3.5.5.22 iSim multi-threaded firmware architecture

There are two threads of execution. One is the main thread (the read thread), and the other is the write thread. The polling section of the main function (while loop) is considered as the read thread. The write-thread executes the function `WriteValue()`.

There are three main global flags in the algorithm design:

- `FinishWrite` boolean flag: indicating when the write thread has finished reading all samples from a specified noise file in SD card.
- `ReadCounter` int flag (RI=Read Index): indicate where to read the next sample from in the embedded ring buffer.
- `WriteCounter` int flag (WI=Write Index): indicates where in the embedded ring buffer to write the next sample to the noise buffer.

The read thread has a window of X ms before it is repeated. X is variable and tested for all possible iSim operational mode. The read thread has the following responsibilities within the X ms window:

- Check the serial buffer for any incoming byte characters (CMD, command characters from the client host GUI) and respond to these accordingly (see firmware API command set in Appendix B).
- Read and process the values from the ring buffer.
- Output the processed values to DAC and signal the DAC (via its control line, LDAC) to update its output.
- Print samples to the serial buffer interface.

The write thread has the following responsibilities:

- Read from the SD storage (Block of data of length N) and write to ring buffer (one sample at a time)
- Set the `FinishWrite` flag when reading from the SD card returns a block of 0 samples. This is where the while Loop in the main function exits naturally (I.e. it is allowed to run until the end of noise file)

The use of the high-level `fread` function makes reading from the microSD card an easy task but requires a long time-block. A closer look at the `fread` function reveals why this is the case. A simulation of the time that it takes to use `fread` to read one sample at a time and one that reads a block of samples was performed as part of the characterisation of the iSim embedded software algorithm. It showed that there is a significant difference between the two operations. Hence, the author has implemented `fread` to read multiple samples each time the write-thread invokes the function callback. This also clearly demonstrates the need to avoid using a traditional polling technique for reading samples from microSD and updating the DAC output, respectively. Figure 3.62 shows the time that it takes for the execution of

the call back function to read from the microSD card, where it is evident that, on average, it takes about 20 ms to read 500 samples from the microSD to the temporary noise buffer.

I.e. this is the time that it takes to load data from the iSim hard drive storage to onboard RAM.

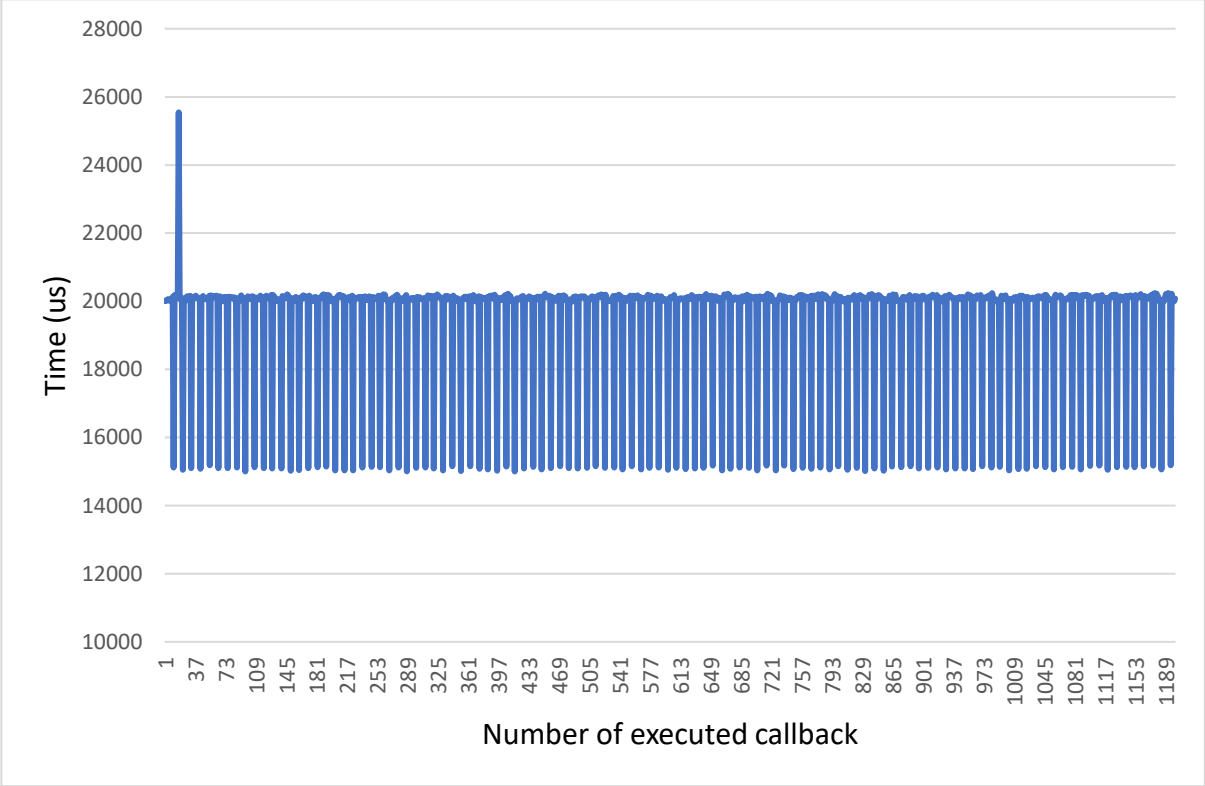

Figure 3.62. Execution time during the implementation of the fread function. Impact of this is shown in figure 3.63.

To validate the link between the observed negative impact on waveform morphology, as seen in figure 3.63, and the overhead caused by reading from the microSD card using `fread` function, an experiment was designed where the write-thread does not perform the read from microSD card but accesses data samples from memory. This simple experiment verified the hypothesis and clarified the design deficiency during stage one development.

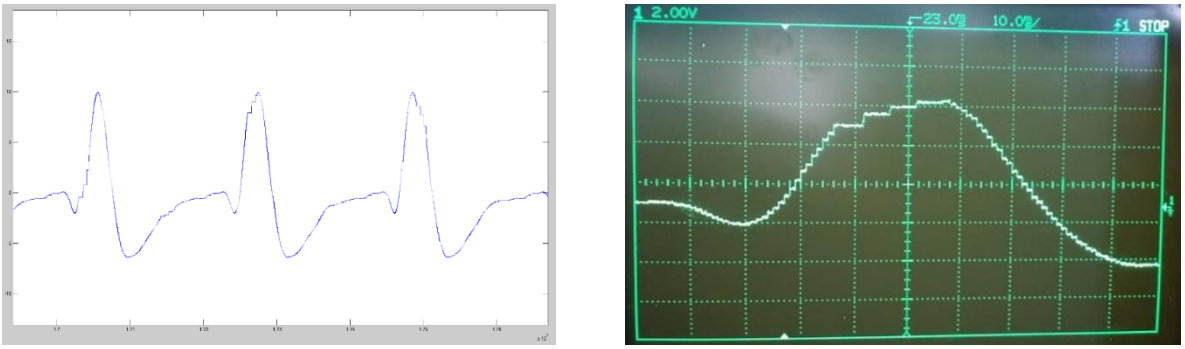

Figure 3.63. Irregular effect and negative impact on signal morphology due to iSim timing error.

The read thread starts by checking the serial buffer for an incoming CMD, and then it waits at `osSignalWait`, as demonstrated in figure 3.60. This causes the thread to go out of scheduler queue and hence no more CPU resources are consumed by it. Under the following two conditions:

- Suppressing all `printf` functions.
- Updating two DAC channels on every iteration.

The read thread waiting time is measured to be 804.8 µs on average, with standard deviation of 2.9 µs. The maximum recorded time is 806 µs and minimum recording time is 792 µs. Enabling the third DAC would result in the statistics to change as follow:

- Average time = 721.7 µs
- Maximum wait time = 724 µs
- Minimum wait time = 676 µs
- STD = 4.0 µs

Adding `printfs` to the code to print the values for generated signals on the serial bus will drastically reduce the recorded wait. The amount of reduction depends on the number of bytes printed.

3.5.5.23 iSim challenge in approximating analogue signals

In producing analogue signals, the sample rate to the DAC must be considered because the stepped-output of a DAC results in high-frequency images. The steps seen in the time-domain signal will translate into high-frequency components at integer multiples of the DAC sample rate plus or minus the fundamental sampling frequency. The effect of increasing the resolution of samples (i.e. sending more samples to the DAC at regular intervals) is to shift these high-frequency images to higher frequency bands. This would, therefore, require the use of a reconstruction filter with a higher 3-dB corner frequency and hence, flatter passband. It would also improve the signal quality as the effect of filter sidebands would be reduced at higher frequency bands.
The expected frequency range from iSim is the ability to simulate very low (near DC) for signal, and noise frequency components (less than 50 Hz), except for the ARMA generated ERG noise channel, bearing in mind the following limiting factors:

- The required minimum number of the `printf` statements (see Appendix B for more details and the experimental results on using the `fprintf` function) to provide adequate visualisation. The GUI is designed having two available modes of operation. One is the calibration mode, including engineering, terminal and terminal+ modes, where `printf` is enabled by default. The other is the User mode where `printf` is disabled. In the engineering mode, the user has the option to disable all `printf` statements to speed up the operation. In User mode, the user cannot enable `printfs`.
- A minimum waiting time that is required by the write thread to read noise blocks from microSD. If all `printfs` are suppressed, the minimum DAC sample rate is 450 µs.
- The hardware limitation on the maximum DAC clock rate. In this design, the DAC clock speed is carefully selected to enable optimal performance, bearing in mind the read speed limit from microSD.

The effect of bit manipulation and read and write speeds as described above is reproduced in MATLAB®. The greater the interpolation (e.g. four times, eight times etc), the smoother the stepped function becomes, and the higher the shift of high-frequency image components (this is shown in figure 3.47).

The maximum DAC sampling rate for the iSim with the current DAC design (DAC software library version 6.0) is just above 2 kHz if all extra `printfs` are disabled. The selected sample rate is linked closely to the number of samples in each signal cycle to avoid unwanted morphology errors.

An alternative to interpolation is the use of an analogue filter. This is implemented in hardware. The analogue filter of a signal generator further smooths the output of the device. Thus, the instrument can accurately represent an analogue signal. Besides, analogue filters provide the added effect of reducing spectral images of the signal.
In line with best design practice, iSim includes both digital and analogue filter implementation. That is, signal interpolation takes place both before building the signal files and during run time.
The timing errors in figure 3.63 are not seen in the provided .NET oscilloscope software on the user's host computer. This is due to the following two reasons:

- The current design outputs the value to the SPI stream as it reads them from the provided file. In other words, no conversion accuracy is included.
- The oscilloscope functions regardless of the relay speed. It provides a continuous real-time plot of data received on the SPI buffer, i.e. it has no time information and hence on the client GUI oscilloscope the samples received are plotted on a fixed set of time coordinates. The drawing coordinates updates every 1000/X Hz. However, there is no plot update along the time axis between the different time windows defined by X ms. So, if no sample received for X+Y ms, the plot will not get updated for the corresponding duration. This has its advantages, for example reducing the workload on the client process and avoiding display flickering effect.

The oscilloscope provides a way of letting the user know the signal that is currently being used as a calibration or test signal. It is not easy (in the context of current design and hardware infrastructure) to display the actual iSim output signal on the client's computer screen. Since further signal processing is performed on the output of the DAC, such as low pass filtering, attenuation and signal summation. Therefore, the scope provides a visual indication and feedback to the user of the current state of the device (running, paused, stopped). The user has access to the scope only in Engineering and Terminal modes. The scope is disabled in user mode, and iSim won't feedback any of the samples to the client's machine in this mode.

If one wants to implement the effect of DAC monotonicity in real-time, it would be necessary to provide a time axis to allow for information on data relay speed, that is, time-stamping the individual samples. Such time stamping can be implemented at two places:

- Client machine.
- MBED processor.

Time stamping on the client machine depends on the resolution of the timers available to us in Windows. The goal here is to timestamp the individual samples received on the SPI buffer stream. The higher the resolution, the more active the processor becomes and hence the higher the power

consumption will be. This becomes especially evident when we use mobile and battery-powered systems like laptops.

The fundamental problem with a software timer in the region of 1ms is that Windows OS is a non-real-time Operating System (NRTOS) and is not suitable for generating regular events around the 1ms mark.

The system timer resolution determines how frequently Windows performs two main actions:

- Update the timer tick count if a full tick has elapsed.
- Check whether a scheduled timer object has expired.

The default timer resolution on Windows 7 is approximately 60 Hz. Some applications can increase this to about 1000 Hz, which reduces the battery run time on mobile systems by as much as 25%.

A greater problem here is the way terminal communication takes place, between a transmitter and receiver. Such communication is purely based on interrupt generation and interrupt handling (ISR, Interrupt service routines). For a non-real time, OS like Windows, this is the main source of difficulty in obtaining accurate timestamps for samples received on the serial peripheral interface.

With an interrupt, the hardware is designed so that the external variables (external to the CPU) can stop the CPU in its tracks and demand attention (with a RTOS, the response of the system to interrupts is more reliable and robust than with a generic OS like windows, RTOSs also allows more control in setting the priority levels for various interrupts). This is the method in which all peripherals communicate with the microprocessor and is the basic block of hardware object-oriented design.

Since both computers and terminals work with whole characters (e.g. eight bits or a byte) but must communicate over a serial line a bit at a time, chips have been developed to do the character-to-serial and serial-to-character conversion. These chips (hardware ICs) are called UARTs (Universal Asynchronous Receiver Transmitters). UARTs are attached to computers via a TX/RX BUS line to Serial interface (in our application, the serial interface communicates via RS232 standards). When the terminal device driver writes a character to the interface card (to be buffered and transmitted one bit at a time along the serial line, with a clock signal to let the other device know when to sample the serial line), it then blocks and waits for an interrupt to be generated by the interface card, letting the OS know that it can send another character. There is no guarantee when the OS will handle this interrupt via the designated ISR in a non-real-time OS.

When it receives an interrupt, the CPU will finish the execution of its current instruction (all CPU instructions are atomic and hence cannot be interrupted), and then it can be interrupted, which means it must change the context. That is, it must save information about what it was doing before context switching. This is just like multi-tasking, where context switching also happens.

It is therefore understandable why fast context switching consumes a lot of power and may even slow the system down, especially in the case of an OS that is not well-suited OS to the task.

The communication between iSim and a host computer is serial. This communication is set to be at its maximum rate, that is a Baud rate of 921600 (921600 symbols per second).

Providing time stamps on the iSim controller is, the next and last option. In the MBED controller, one has access to timers with accuracies in the nanosecond range.

Although `printf()` causes a large overhead, it is still possible to use it with a smaller number of bytes to print to the serial stream. Rather than sending the actual signal values, we could send one character when the flag to generate the signal is set (external or software triggered). This character would mark the start of signal transmission. Since the signal is repetitive and must be constant through different sweeps, we can read the whole signal file (the maximum size of which is an array of 500 floating-point values when the sampling rate is 1 kHz and 2000 floating-point values when iSim is operating at its maximum output rate) at the start of the program, using the terminal or from the MBED folder, and then start outputting the samples to the oscilloscope every time we receive timing information. The timing information is collected but not passed to the client machine in this design and is only used to perform run-time health checks on the read and write threads and to ensure that the onboard OS is keeping its promise of being a RTOS. Any exceptions generated that goes against this will be handled as a warning and, if it continues, will be dealt as fatal error causing iSim to reset.

The cause of such timing errors was investigated further, and it was identified to be a priority issue at the operating system (OS) level. When the read thread priority is set to high and the write priority to low, the problem was resolved, due to a pre-emptive OS implementation.

Setting the priority of the read thread to high gives this thread more of the CPU resources. Also, it is noted that from the timing diagram the read thread spends a lot of time waiting before the notify read ISR (interrupt service routine) is executed. This time is not spent spinning (and hence consuming CPU resources), but the read thread is set in a waiting state and will allow the write thread to execute. Now if the write thread is also in the wait state, there would be no thread in a ready state, and hence the controller is in sleep mode, conserving power. If the write thread is executing and the read thread becomes ready, then the scheduler will interrupt the write thread and give the CPU time slice to the read thread. Thus, we no longer see the timing issue observed in the earlier versions.

The operation was verified by outputting approximately 200,000 data samples at 1kHz, that is 200 seconds of noise data read from the onboard microSD card the samples were sent to DAC's internal registers while the controller monitored the time between the individual data samples. It is evident from figure 3.64 that iSim now behaves like a real-time system and outputs samples at an average frequency of 1/(904.8785 µs) kHz = 1.1 kHz.

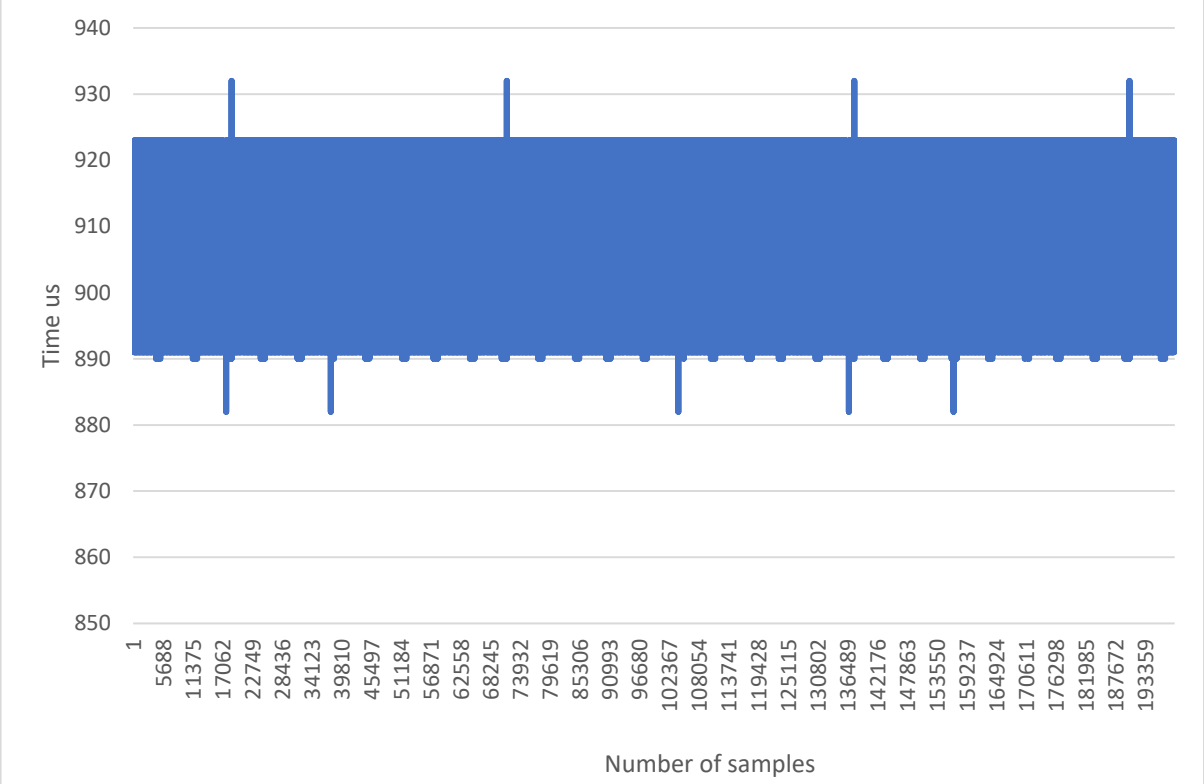

Figure 3.64. The ISR, is kept very simple to avoid timing issues and set its priority to high to avoid it being interrupted by other ISRs.

3.5.5.24 iSim GUI and embedded firmware communication

The communication between the iSim GUI and the embedded firmware is accomplished via a messaging system and a combination of event-driven and polling programming techniques at both ends of the communication channel. The GUI is the master, while the iSim device is the slave in this communication. The GUI takes user inputs and sends these through the communication interface to iSim. These are termed commands (CMDs). iSim will then acknowledge the receipt of these CMDs back to the master (this handshaking mechanism across the interface ensures that messages and commands are received) and subsequently services the received requests. The command execution will result in one or a series of generated acknowledgements (ACKs) that may or may not be placed on the SPI buffer using `printf` statements (the frequency of `printf` statements is kept to a minimum due to their execution overhead). Some of the acknowledgements may only be used internally by the embedded firmware to update flags, which may, in turn, generate further ACK/s. A list of CMDs and ACKs are provided in Appendix B.

Device Acknowledgements or ACKs take the form `DEV_XXXXX`. This signifies a message of type Information, Warning, Error or Confirmation, as described below. (ACKs are generated in response to certain commands or are provided to inform the user of the current machine state. For example, post-DAC configuration, the device provides the DAC's status to the user using, `DEV_DAC_Status_%X` ACK) The ACK types are:

- Confirmation: Those that require actions to be performed based on the ACKs received.
- Errors & Warning: Those that determine if an error or warning has occurred, these will usually cause the whole system to reset. For example, if no files could be found or if files could not be read, then a fatal error has occurred that would warn the user with a brief description about the root cause and would reset the device to the initial known state if it could not be resolved automatically.
- Information Events: These are to let the user know of an event that has occurred which does not require further action, except maybe updating the GUI or other files for later analysis. Depending on the details of the event raised during program execution, this can make it possible to identify various sources of problem such as timing issues, file read issues, missing packets, missing samples, sample count, monitoring the read and write index to the circular buffer, monitoring thread timing and required thread waits etc.

3.5.5.25 iSim high-level software solution package

iSim GUI (see figure 3.66 and 3.67) is a clear, concise, familiar and responsive interface designed and developed to communicate to iSim device and a remote MatSOAP© server through an implemented Serial Peripheral Interface (SPI) and HTTP protocol respectively. This interface has been rigorously tested, and its robustness and friendliness were confirmed through performing human factor-based investigation (simple question and answer sessions) with some target users (clinicians within visual electrodiagnostic centres), through which not only gaps in the design were identified but also usability of the GUI was investigated. feedbacks captured helped to shape the design and improved its reliability, usability and robustness. The Calibration mode of operation was found complex to use and as such the user-mode were introduced. Therefore, the interface consists of two primary modes of operations, that is the user mode and the calibration mode. The calibration mode is further divided into an engineering, terminal and terminal+ mode. Switching between these modes of operations results in a complete reset of the device and the interface except switching between the terminal and terminal+ mode. The interface solution package is developed in C# .NET and is provided as a standalone, installable solution package which is operable on all windows OS. Instruction For Use (IFU) is provided with the installation package that guides the user through installation and detailed functionality of the interface and device. Post successful installation, the interface will subscribe to windows USB controller through probing the .NET Windows Instrumentation Management (WMI) framework wrapper class and will monitor all events that are published through the controller such as USB connected or disconnected events. An event handler would then process the event and enumerate through all USB drivers attached to the host computer and looks for MBED device through its unique USB identifier. If this is found and MBED driver is successfully installed, then GUI can hook up to the driver and automatically configure the SPI communication interface. If the MBED driver is not found, the GUI will automatically try to crawl the MBED web page looking for this driver for download and installation. This makes the interface friendly

and smart capable of establishing communication within 20 seconds from the point the device is first connected (The life cycle development of automatic enumeration and COM port setup has been extensive and started from MATLAB® IDE as demonstrated in figure 3.65. This approach was not friendly, required considerable user inputs and more importantly, the implementation required MATLAB® software installation, or the executable file would be operating system specific and incapable of receiving most of OS events such as USB connection events).

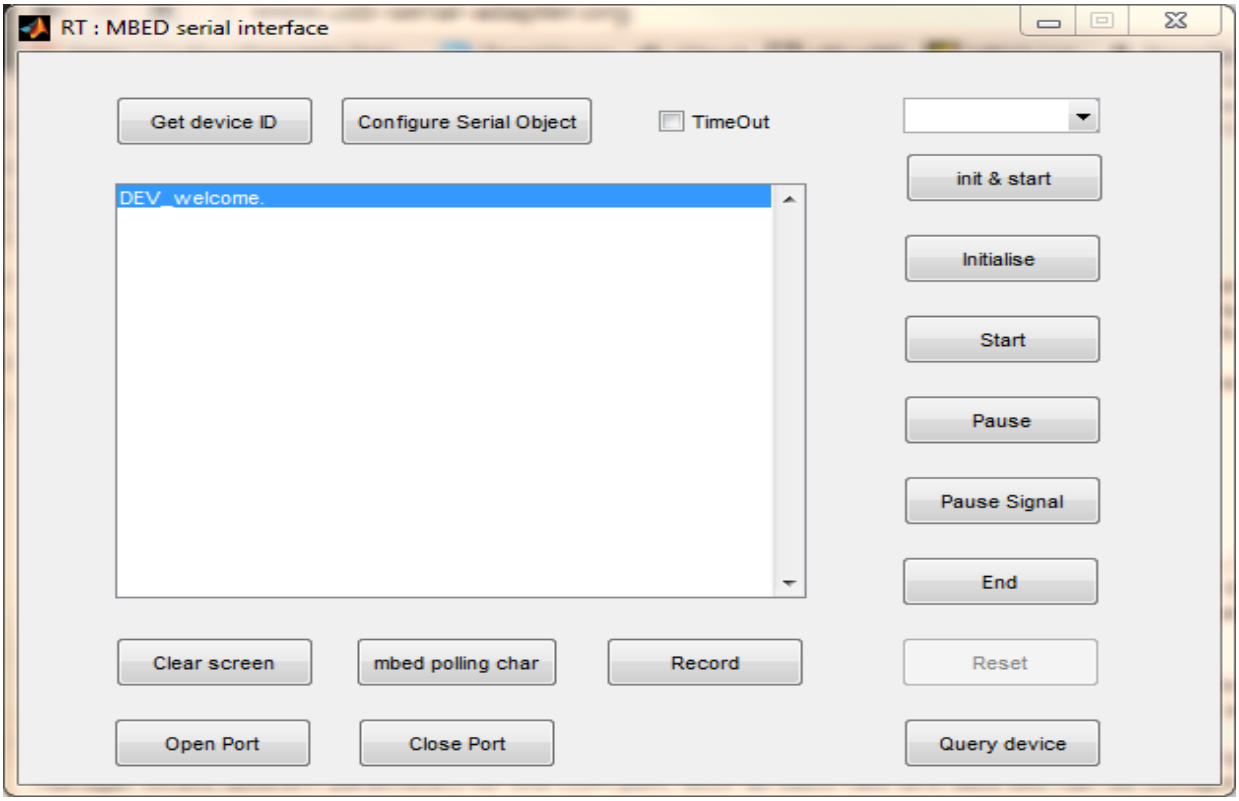

Figure 3.65. Initial MATLAB® GUI to communicate with iSim.

The GUI will always start in default user mode and will initialise the device automatically as soon as the communication is established. This initialisation includes scanning the iSim storage unit (microSD card) to perform the following (as well as other initialisation tasks):

- Scan the signal folder and identify all signal binary files.
- Scan the Noise folder and identify all noise binary files.
- Read (and communicate with the GUI) the name of the files, their file size and signal vector length.
- GUI will then update the file selection dropdown lists and waits for user selection (60 seconds before a WDT is triggered, causing system reset).

The GUI communicates with iSim devices through a command and acknowledgement mechanism, where the interface is the master converting user requests (which are gathered through user interaction with the GUI) into a set of commands (CMDs) and the device is the slave that acknowledges receipts of these commands and execute user requests. Lists of CMDs and ACKs are provided with the installation

package and together with IFU would allow the user to have access to all exposed functionality of the device through any third-party terminal application. The CMD/ACK mechanism ensures that the GUI and the iSim device are always in perfect synchronisation. The GUI captures all data bytes through the SPI buffer on a background thread, and as soon as any data packet is received, it will check and update the GUI accordingly without exhibiting any nonresponsive behaviour. In calibration or engineering mode, the user has access to three pages and switching between these pages while the device is running won't impact on the device operations. It is not possible to keep the top-level modes (user and engineering) of operation simple and have all the device capability available through the implementation of buttons, text fields and other interfaces. The Terminal mode is where the user has access to all the device capabilities and is specifically used when testing the device and its integration with the GUI. The terminal+ mode is the same as the terminal mode but with added buttons to provide some help for quick testing. The terminal mode was the first mode created during stage 1 of the iSim developmental cycle and user mode was the last. User mode was developed with the mindset of 1-click operation from the point that device is first connected to the host computer, with PERG as default signal and ARMA generated noise with SNR of -3 dB as the default noise file with no added spontaneous noise components.

Irrespective of operation mode and selected files, the GUI provides the user with the flexibility of:

- Full DAC configuration.
- Manual and automatic (max rate or interval-based depending on the calculated length of the signal by the device) software trigger as well as iSim hardware trigger capability (optical and TTL).
- User-configurable noise, EMG, blink and eye movement and mains components including, amplitude and SNR.
- Auto-reset and repeat.
- Acting as a pure signal generator (in terminal or terminal+ mode) capable of outputting sine, square, triangular and sinc waveforms with configurable, frequency, amplitude, DC shift, and sampling output rate.
- Upload and download files to iSim microSD card without a need to remove the microSD and uploading the files manually.
- Changing the text properties on the terminal including colour, font etc.
- Providing logging mode, that is the actual samples sent to DAC for conversion to analogue signal.
- Providing an integrated software oscilloscope as a visual indicator of samples sent to the DAC for conversion to analogue signal.

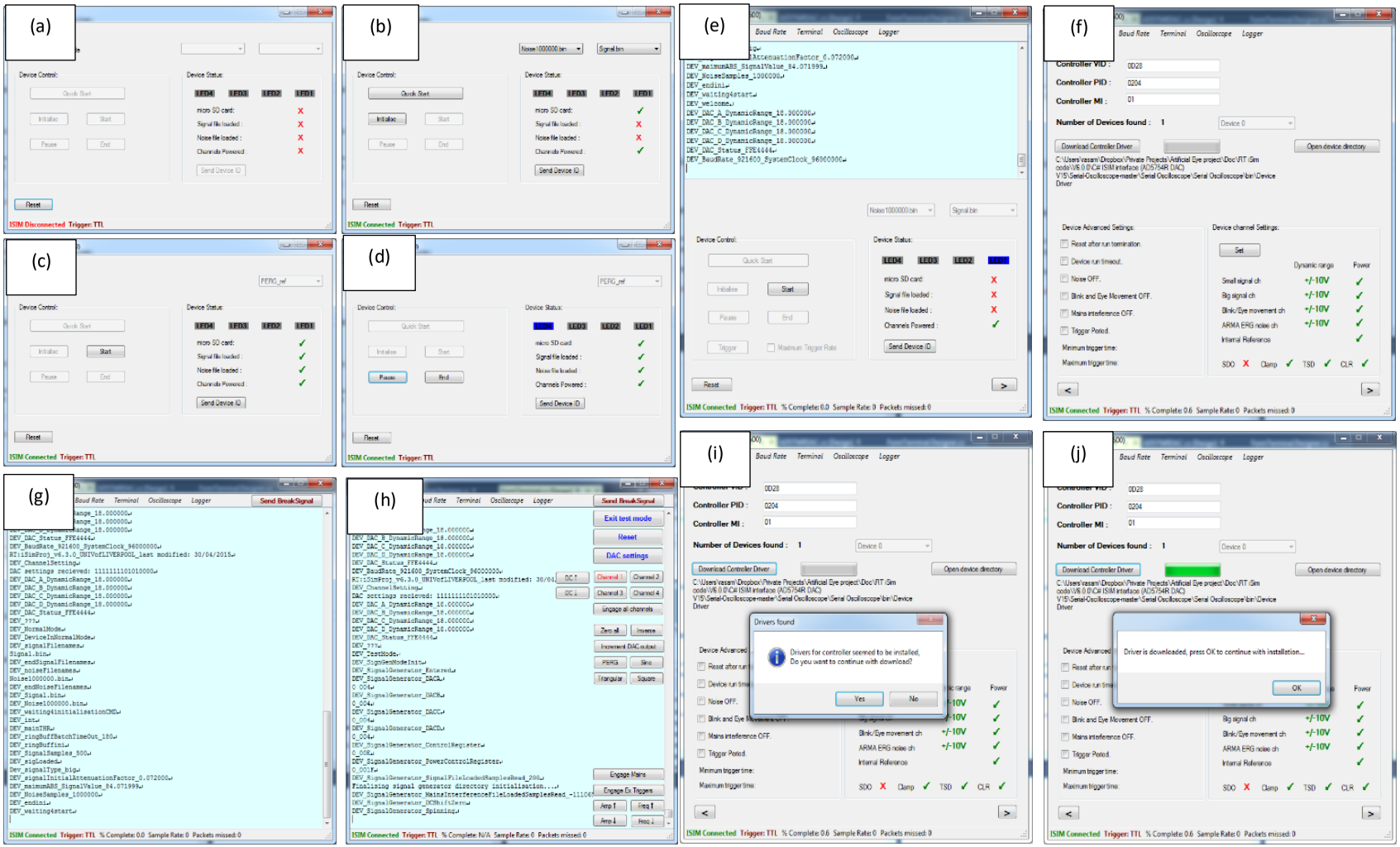

Figure 3.66. iSim GUI. (a) User mode loaded but iSim device is not connected. (b) Same as (a) but iSim device is now connected, micro SD card is connected and iSim channels are powered, communication is established, and device is ready for operation. (c) Same as (b), both signal and noise files are successfully loaded. (d) Device is running. (e) iSim is switched to engineering mode. (f) Engineering mode showing DAC settings applied. (g) iSim is switched to terminal mode of operation. (h) iSim is switched to terminal+ mode of operations with generic waveforms such as sine, square and triangular waveforms available to calibrate iSim itself. (i) and (j) Illustrating, how iSim downloads and installed (accordingly prompting user) the required driver software for a successful operation.

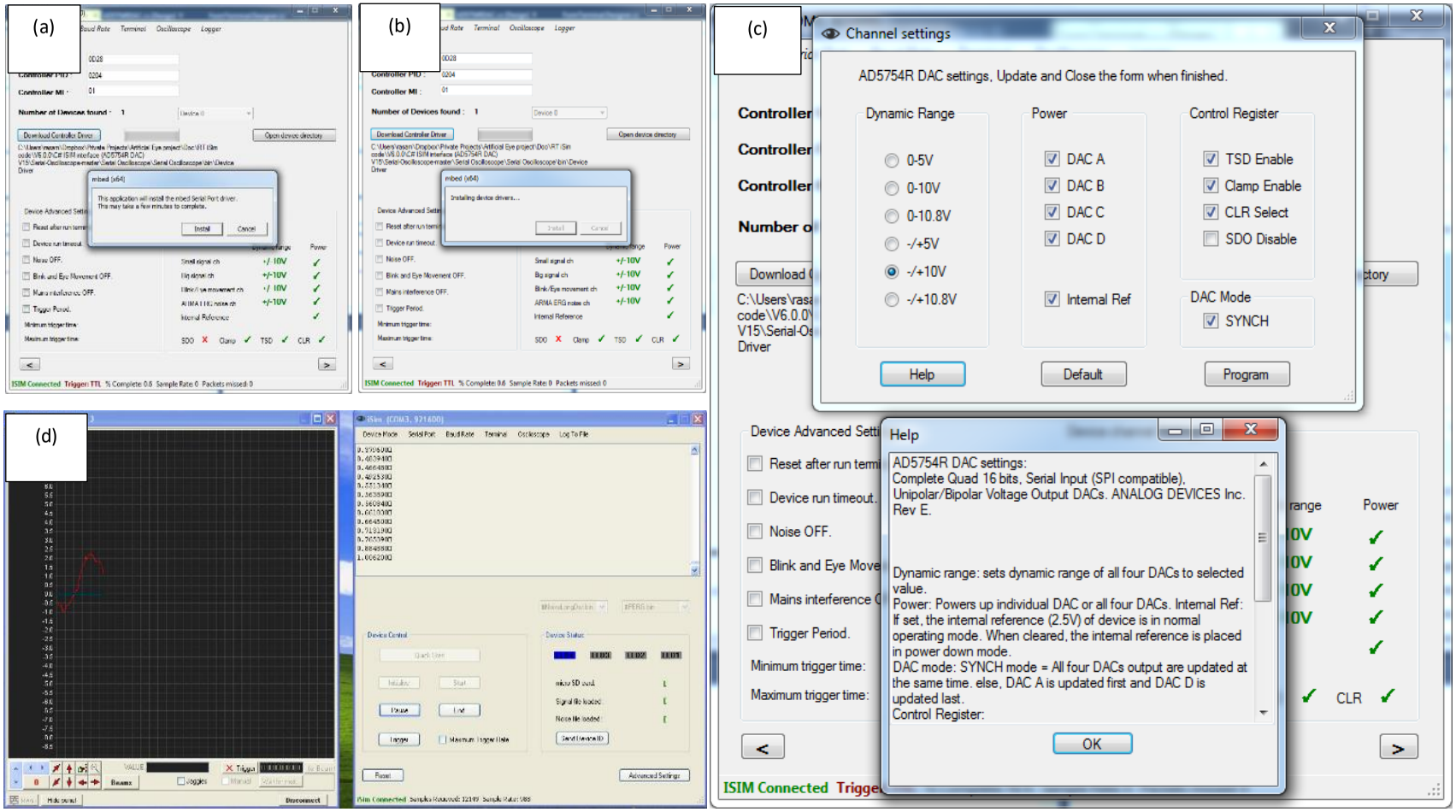

Figure 3.67. iSim GUI. (a) and (b) Illustrating iSim downloading the required driver software and instantiating the installation of these software for a successful operation. (c) iSim integrated DAC GUI. This interface is used to setup iSim channels including, power setting and dynamic range of the individual channels. (d) Illustrating the integrated, on-board oscilloscope that provides the end-user with visualization of data samples that iSim is outputting when in running mode.

3.6 Experimental protocol – Data collection

An initial study was designed to collect ERG response data from twelve normal subjects (see Table 3.5 for inclusion/exclusion criteria) with no eye condition at MPCE RLUBH for the purpose of uploading to the ISIM cloud library enabling remote access and re-use of the data.

The following ERG dependent parameters are considered during study design:

1) The adaptive state of the retina, i.e. scotopic and photopic.
2) Stimulus intensity.
3) Stimulus duration i.e. flash vs long-duration (Note: the retina responds not only to onset of light but also to the cessation of light, and these responses are called ON-response and OFF-response, respectively).
4) Stimulus type, i.e. low-frequency flash stimulus or flicker.
5) Stimulus colour, i.e. white for this study design.

Flash intensities are categorised into LOW, MEDIUM, HIGH and very HIGH as illustrated in the table 4.6 together with the recommended test duration allowing to collect high quality (SNR greater than 120 dB post averaging) data for ISIM library (STANDARD flash corresponds to 3 $cd.s.m^{-2}$ intensity and Xenon 1 setting corresponds to +10 dB above standard flash intensity).

Table 3.5: inclusion and exclusion criteria for data collection.

Inclusion Criteria	Exclusion Criteria
Normal vision with refractive correction (>0.3 logMAR or 6/12 Snellen)	History of ophthalmic disease or ocular trauma
Aged between 20 and 30	History of migraines
Refractive error no greater than +/- 4D	Refractive error >+/- 4 dioptres
Not pregnant	Pregnancy
No history of ophthalmic disease, trauma, or migraines	Subject outside of age range
No history of epilepsy	History of epilepsy
No experience of problems with mydriatic drops (used for pupil dilation)	Experienced problems with dilation before (such as allergic reaction or acute closed angle glaucoma)
Able to attend all necessary sessions	Unable to attend all necessary sessions
Able to consent	Unable to consent
No history of glaucoma	Subject with glaucoma or any family history of the condition

Table 3.6: Flash category and intensities.

Device Flash Intensity Level	Flash category	Duration
NO flashes	NO Blinks/Eye Movement	1 min
NO flashes	Blinks ONLY	1 min
NO flashes	Eye Movement ONLY	1 min
NO flashes	EMG	2 min
LED -40 dB	LOW	2 min (0.5 Hz)
LED -35 dB	LOW	2 min (0.5 Hz)
LED -30 dB	LOW	2 min (0.5 Hz)
LED -25 dB	LOW	2 min (0.5 Hz)
LED -20 dB	LOW	2 min (0.5 Hz)
LED -15 dB	MEDIUM	1 min (0.5 Hz)
LED -10 dB	MEDIUM	1 min (0.5 Hz)
LED -5 dB	~MEDIUM	<1 min (0.5 Hz)
LED -0 dB (STANDARD)	HIGH	20 Sec (0.5 Hz)
LED 5 dB	HIGH/>HIGH	<20 Sec (0.5 Hz)
Xenon 1	>HIGH	2-3 seconds
Xenon 2	>HIGH	2-3 seconds
Xenon 3	>HIGH	2-3 seconds
Xenon 4,5	>HIGH	2-3 seconds

Photopic ERG response, as well as ON-OFF ERG and Flicker responses, were collected (approximately 30 Hz, 2 Hz and 1 Hz flash rates were applied for flicker, photopic and ON-OFF ERG response measurements, respectively. As such time interval between flashes is not long enough in this protocol to maintain scotopic condition even when Ganzfeld background light is turned off. However, as flashes are dimmed and test runs are increased in length to improve averaged response SNR, more pronounced scotopic ERG response characteristics are expected). Periods of no flashes are also used to collect noise signal, blinks, eye-movements and EMG data. To validate the assumption of significant variations in measurements of ERG waveform characteristics such as a- and b-wave, the in-between subject variability was calculated as follow:

- For each intensity level, the variability in a- and b-wave amplitude and implicit times were calculated using equation 3.3.

$$\%\ variability_i = \frac{|maximum - minimum|}{Group\ average} . 100 \quad (3.3)$$

Where $i = intensity\ index$,

$Xenon1\ represents\ index\ 1, and -40\ dB\ flash\ intensity\ represents\ index\ 11.$

$Maximum = maximum\ measured\ parameter\ e.g.\ amplitude\ of\ -wave.$

$Minimum = minimum\ measured\ parameter\ e.g.\ amplitude\ of\ b-wave.$

$Group\ average =$
$average\ of\ the\ measured\ parametres\ across\ all\ subjects\ e.g.\ amplitude\ of\ b-wave.$

Flash duration (ON duration) is set to 500 ms to collect ON-OFF ERG responses at a flash rate of 1 Hz (duty cycle of 50%), and set to 1 ms at a flash rate of 2 Hz for photopic, scotopic ERG response data collection and finally to 1 ms at a rate of 29.4118 Hz to collect Flicker ERG response. All flashes were full-field global flashes presented using Roland Q450 Ganzfeld.

Liverpool bio-amplifier (120 dB CMRR, noise level of less than 3.5 µV P-P and gain of 5000) were used at various sampling frequencies (for ON-OFF ERG and Flicker response data collection, a sampling frequency of 8 kHz were used and for photopic and scotopic as well as noise, blinks, eye-movements and EMG data collection, sampling rate was set at 40 kHz) with filter setting adjusted to 500 Hz and artefact auto-rejection algorithm switched off ensuring raw data is collected without introducing any discontinuities into the records. All measurements were performed with the developed bio-amplifier GUI programmed in MATLAB®, running on a battery-supplied laptop PC. The amplifier itself was powered, programmed and controlled through the USB connection to the PC. Ganzfeld was also programmed and operated through the same GUI and was powered through an isolation transformer block connected to the mains supply. During measurements, the electrode leads were twisted to reduce any common-mode voltage coupling (magnetic interference) and were fixed in place using Microporous tape close to the subject's body, having a short distance (<30 cm) to travel to the amplifier's input (hence reducing the subtended magnetic field pick up area). This setup (together with high common-mode input impedance of $3X10^{10}\Omega$, and shielding the front-end analogue-to-analogue instrumentation amplifier) would mean that there exists a high isolation barrier between amplifier's common and earth ground and any power line interference is expected to be minimal through this route and therefore

majority of such interference would be expected through power-line and subject coupling. The subject under study is set up on a chair in front of the Ganzfeld and distanced from the isolation transformer by a minimum of one meter.

Liverpool DTL electrodes (thread electrodes which are more comfortable to wear over long-running sessions) were placed on the right eye of all subjects for data collection with the un-tested eye, patched. Before the application of the skin surface electrode, the site is cleaned to remove any superficial fatty film which would otherwise increase the electrical impedance and hence degrade the reliability of the measurement [341][342] and conductive EEG paste is used to act as the electrolyte and to ensure good electrical connection in the reference and ground electrodes (see figure 3.68). It is therefore required to reduce the skin impedance to below 5 KΩ. In this study, the author measured and recorded the electrode impedance at the beginning and end of each test (a minimum of 0.5 kΩ and a maximum of 3 kΩ were measured prior to testing and a minimum of 1 kΩ and a maximum of 5 kΩ were measured at the end of the session. The electrode impedance was monitored in between runs, especially if an increased level of noise and interference was visible). Ag/Agcl surface electrodes are used for both ground and reference electrodes due to their highly stable half-cell potentials.

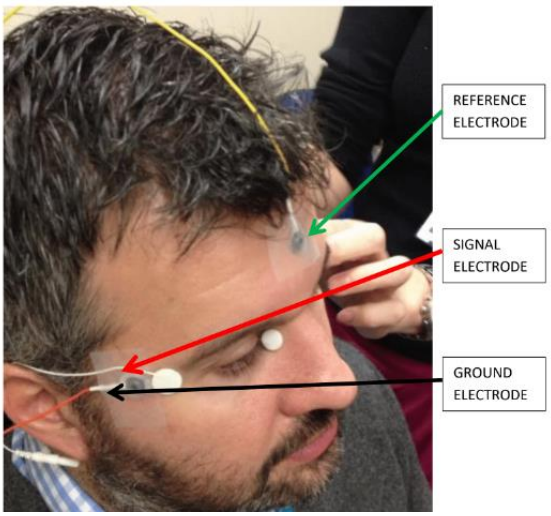

Figure 3.68. Placement of electrodes and subject preparation prior to data collection.

The electrode placement is in such way that (for all subjects) it is draped into the lower fornix to increase the comfort of wearing it over the entire session with a reduced probability of changing it and run-to-run variability. This is at the expense of potential lower ERG recorded signal amplitude. The small adhesive sponge pads at each end of the DTL electrode is placed in the nasal and temporal canthi as illustrated in figure 3.68.

Un-dilated pupils with an average diameter of 4 mm (this was measured manually using a calibrated ruler in the same testing room under the same room illumination for all subjects) were presented with various global flashes per the study protocol.

Data collection test runs, per subject, was performed over the same session with enough rest period in between the test runs and where required the electrode was removed and subject could rest prior to continuing with the respective run and/or session. Subjects were guided throughout the session to ensure, continued focus, and maintained fixation as well as low levels of contamination such as blinks, eye-movement, eye-twitches and EMG during ERG response data collection. Participants were asked about their general feeling after each run to ensure maintained comfort throughout the entire session.

Data collection testing protocol was as a follow:

1) The subject is prepared, and electrodes are attached (Subject is in light-adapted state – ordinary room illumination for at least 10 minutes pre-adaptation phase).

2) Tests are carried out from high to low flash intensities.
3) Flash intensities categorised as LOW are performed over 2 min duration (Flash rate = 0.5 Hz).
4) Flash intensities categorised as MEDIUM are performed over 1 min (Flash rate = 0.5 Hz).
5) Flash intensities categorised as ~MEDIUM are performed over <1 min (Flash rate = 0.5 Hz).
6) Flash intensities categorised as HIGH are performed over 20 seconds (Flash rate = 0.5 Hz).
7) Flash intensities categorised as >HIGH are performed over 5 or 6 flashes/cycles (at a flash rate of 2 Hz this corresponds to 2-3 seconds of acquisition) (Flash rate = 0.5 Hz). These are only carried out if subject agrees to them due to very uncomfortable flash intensity levels.
8) For Low and Medium intensity categories (flash intensity below -10 dB), flashes are applied with no background light and room light turned OFF, this should correspond to less than 10 min. For other categories of flashes, the background light is set at (25 cd – device setting for Ganzfeld Q450) but room light is turned off.
9) 10 minutes in the complete light state is allowed so that subjects can be fully light-adapted. Tests for flash category of higher than MEDIUM (- 10 dB) are performed in the light-adapted state, but room lights are turned off to avoid ambient light.
10) The recording condition, sampling frequency, flash rate, amplifier CMRR, electrode type and model as well as subjects age group, gender, eye colour and tested eye, electrode impedance, etc are recorded carefully and any deviations in the protocol were noted. This information will be provided to end-users of ISIM to ensure traceability and repeatability is maintained (no subject identifier will be exposed).

The following assumptions were made about the retinal responses collected as part of the experimental study design (these assumptions were tested and empirically verified per published results in chapter 5):

- The retinal responses (photopic, scotopic and ON-OFF ERG responses as well as flicker response) collected are stationary.
- Most of the retinal response energy is at low-frequency band, i.e. below 500 Hz.
- Background noise is additive.
- Background noise is weakly stationary.

Chapter 4: Result

4.1 Introduction

This chapter presents the results of the studies introduced in the methodology chapter (chapter 3). ISIM provides a novel platform for generating a selected ERG waveform with user-defined parameters. The verification and validation of ISIM are described, using data from limited experimental testing. The author is mindful of the limited experimental data available. All components of ISIM platform has been tested to ensure fitness for the purpose per the aim and objectives (section 1.6) of this thesis. Section 4.2.1 to 4.2.4 illustrates the verification and validation of the data acquisition system used to perform functional assessment of the retina and the tools and techniques developed to analyse the collected experimental data. The collected data is conditioned and forms part of the ISIM back-end library where access to this library is provided through MatSOAP server. This is in line with Objectives 2, 3 and 4 in section 1.6. Objective 5 is achieved through folder organisation and structuring of files including all programming modules as well as providing a simple, cross operating-system messaging template between the client and server applications. Objective 6 is achieved as illustrated in section 4.2.5 where Magnitude Squared Coherence (MSC) algorithm is implemented in recovering the signal of interest from a simulated, user-specified, noise-contaminated record. These records are produced using the ISIM platform where the platform allows access to a novel signal processing application to recover the original signal of interest. In doing so the user can objectively assess (the feasibility) and verify the effectiveness (specificity) of the selected signal processing packages without any need to perform clinical trials on living test subjects (animals or humans). Section 4.2.6 illustrates the effectiveness of ISIM platform in assessing the clinical system (Roland Consult) in order to capture, assess, scrutinise and verify the governing maximal length sequence, that is implemented by the specific manufacturer. It is illustrated how ISIM can support the user to recover such sequence when the system's artefact rejection algorithm is activated. Such recovery allowed the author to study the Roland system and understand how it categorises the artefacts, register these, reject them and creates the final artefact-free, "bio-signal". The remainder of this chapter describes how the author implemented various types of continuous (e.g. mains interference and the associated harmonics, as well as ERG noise using the MATLAB implementation of ARMAsel algorithm or other types of less realistic noise records such as white noise) and spontaneous noise such as EMG, blinks, eye twitches and eye movement. Other types of low-frequency noise records such as drift have been implemented using Brownian motion implementation in MATLAB. Implementation of fixation error and effect of discontinuities in recorded data (data acquisition system error) and is also investigated and the impact to first and higher-order kernel responses have been demonstrated. The ISIM library is accessed remotely through remote procedural calls to a designated server that ultimately provides a way of expanding the library and ensures better cross-centre collaboration for research and clinical data sharing and future large- or small-scale experiments. The results illustrated in this chapter show that ISIM will generate and output the exact replica of the requested waveform consistently over the entire experimental duration.

4.2 Verification and Validation (V&V): Waveform generation toolset

4.2.1 Bio-amplifier verification & medical safety testing

The designed and developed bio-amplifier was tested and verified before use on human subjects for data collection according to the protocols of the Medical Physics and Clinical Engineering Department at Liverpool University (MPCE). The testing involved the following criteria:

- **Medical Safety and efficacy:** The bio-amplifier was tested using RIGEL L233 (serial number, BIO063) to ensure it is safe for use on human subjects. The test report (See figure 4.1) is maintained under the department's Quality Management System (QMS) and is a controlled document, meaning any change to the design, specification or intended use of the device would require the notification of the management and the re-testing of the amplifier. Testing and recalibration must also be carried out on a yearly basis.
- **The Gain Bandwidth (GBW):** The gain bandwidth (GBW) of the amplifier was verified using a signal generator and performing a sine-sweep (with varying frequency) while sampling the input at 50 kHz, see figure 4.2.a. It was verified that the system does not alter the frequency components below 500 Hz, and the 3-dB point is measured to be at 800 Hz.
- **Amplifier peak-to-peak noise level:** The amplifier peak-to-peak noise level was measured to be less than 3.5 μV. This was determined by shorting the inputs and performing sampling at 40 kHz (the same sampling frequency as used for preliminary data collection) within the intended use environment; results are illustrated in figure 4.3.
- **Amplifiers CMRR:** The amplifiers CMRR was also measured against applied frequency; a known frequency and amplitude sine wave was applied to both differential inputs of the amplifier. Results are illustrated in figure 4.2.b. This shows that the amplifier will successfully reduce the common-mode signal amplitude by at least 118 dB when the maximum frequency component of the input signal is at or below 100 Hz. This range covers the main source of common-mode interference, which is mains supply.
- **Maximum signal amplitude (peak-to-peak):** The maximum signal amplitude (peak-to-peak) that could be applied to the input of the amplifier is 700 μV when the gain of the amplifier was set at 5000. This provides a maximum peak-to-peak potential of 3.5 V to the input of the internal MCC ADC for digitisation post-amplification. The input range of the DAC is set to ∓ 5V, which will ensure higher resolution (16-bits ADC) in a linear operational region throughout the preliminary data collection.

Safety Test Report

Equipment under test:	Bioamp				
Manufacturer:	Clinical Engineering	Model:		Ser. No.:	
Single device/system (D/S):	D				
Owner:	Clinical Engineering	Location:		Test Equip. Model:	RIGEL233
Date of test:	29/9/15	Next Due Date:	28/9/16	Ser. No.:	BIO063

Tests		Mode	Allowed	Measured	Pass/Fail
Insulation Resistance (Mohms)			20	∞	Pass
Earth Continuity (Ohms)			0.2	0.1	Pass
Earth Leakage Current (uA)					
NC		Forward	500	10	Pass
NC		Reverse	500	10	Pass
SFC		Forward	1000	0	Pass
SFC		Reverse	1000	10	Pass
Encl. Leakage Current (u A)					
NC		Forward	100	0	Pass
NC		Reverse	100	0	Pass
SFC (E o/c)		Forward	500	10	Pass
SFC (E o/c)		Reverse	500	10	Pass
SFC (S o/c)		Forward	500	0	Pass
SFC (S o/c)		Reverse	500	0	Pass
Patient Leakage Current (u A)					
NC		Forward	100	0	Pass
NC		Reverse	100	0	Pass
SFC (E o/c)		Forward	500	0	Pass
SFC (E o/c)		Reverse	500	0	Pass
SFC (S o/c)		Forward	500	0	Pass
SFC (S o/c)		Reverse	500	0	Pass
Patient Auxilliary Current (u A)					
NC		Forward	100	0	Pass
NC		Reverse	100	0	Pass
SFC (E o/c)		Forward	500	0	Pass
SFC (E o/c)		Reverse	500	0	Pass
SFC (S o/c)		Forward	500	0	Pass
SFC (S o/c)		Reverse	500	0	Pass
Mains on Applied Part (uA)					
NC		Forward	100	0	Pass
NC		Reverse	100	0	Pass
Phase Reversal		Forward	500	0	Pass
Phase Reversal		Reverse	500	0	Pass
Mains Lead	OK?	Yes			
Plug	OK?	Yes			
Mains Fuse	OK?	3A Yes			

Figure 4.1. Results of Medical Safety testing of the bio-amplifier before using test subjects for data collection for inclusion within the ISIM library. The test was carried out following the medical safety testing procedure under Medical Physics and Clinical Engineering (MPCE) department of the University of Liverpool.

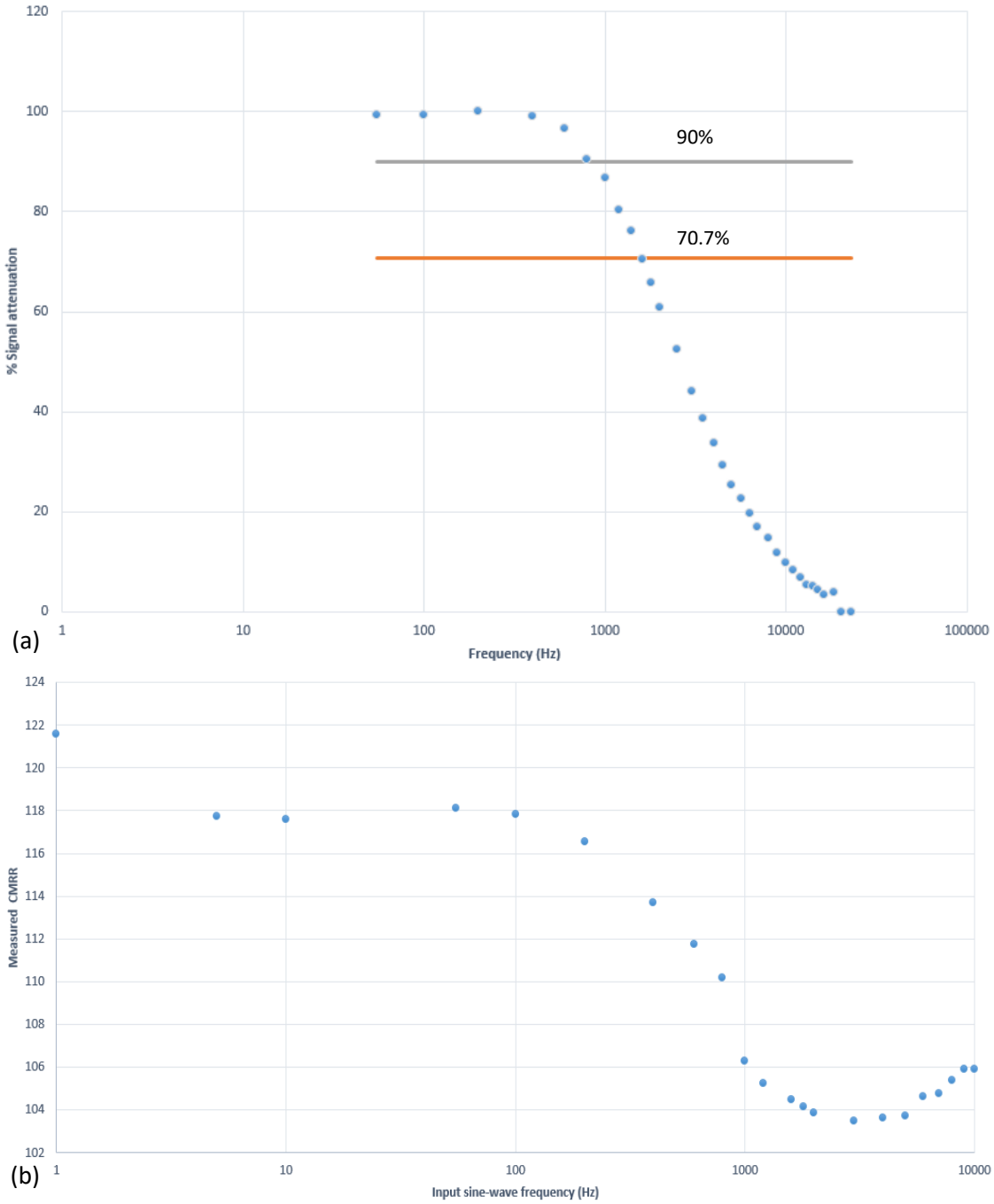

Figure 4.2. (a) bio-amplifier measured Gain Band Width (GBW). Where the grey horizontal line demonstrates the 10% attenuation point, and the orange line represents the 29.3% attenuation point. (b) bio-amplifier measured Common Mode Rejection Ratio (CMRR).

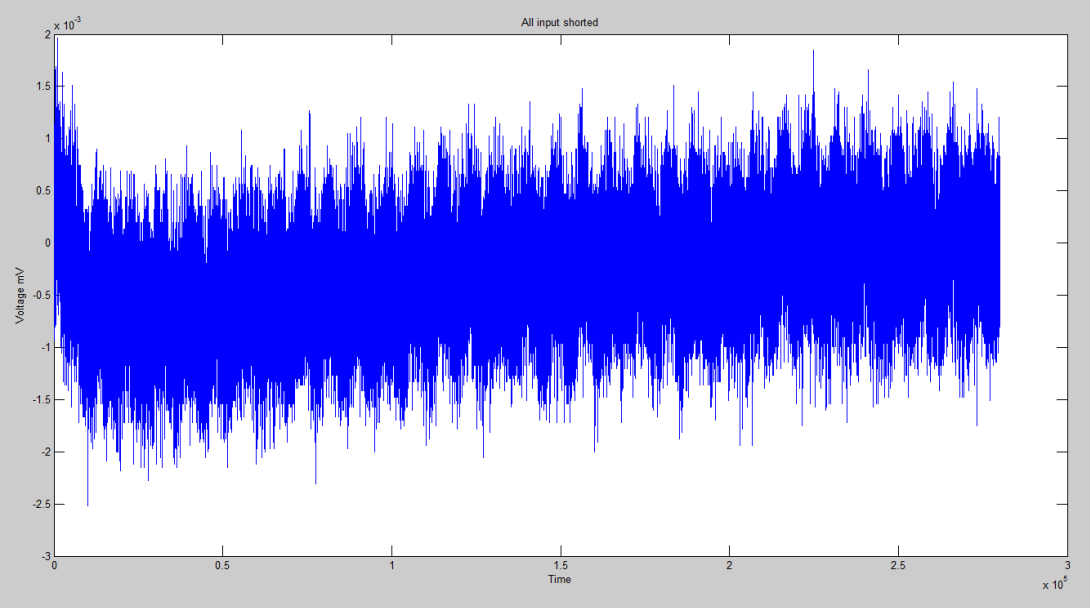

Figure 4.3. Amplifier recorded noise level when inputs are shorted together, and output is measured. Amplifier bandwidth is 0-1000Hz. The sampling frequency is adjusted to 40 kHz. The test is performed in a clinical room at Royal Liverpool and Broadgreen University Hospital. Y-axis is in units of mV with scaling factor of 10^{-3}, I.e. y-values are in µV. The peak-to-peak measured noise level is smaller than 3.5 µV. Roland RETIscan amplifier is reported noise level less than 4 µV (RMS) which is equivalent to approximately 5 µV peak-to-peak.

4.2.2 Data collection & analysis

The ERG signal is an experimentally recorded signal under photopic and scotopic conditions as per the test protocol outlined in section3.6. Post data collection, the record was visually inspected with the help of an experienced clinician to ensure all artefacts are identified and respective cycles are removed. The first five flashes were ignored, ensuring that the stimulator has stabilised. The resulting waveforms are finally added to the ISIM library as raw data. The raw data were then further processed, by averaging and filtering, to generate a single cycle of ERG response.

Before performing any data analysis, such as averaging, a quick record of ERG response (when triggered using standard flash intensity) was collected using a normal subject (the author) and using an open-source software tool (Wavepad Audio editing software). Some of the assumptions on the collected retinal response (section 3.6) were empirically verified (see figure 4.4). Spectral subtraction was used to extract the signal from background additive noise. The noise spectrum was estimated using periods where the ERG signal was absent. Spectral subtraction assumes that the noise is stationary or slowly varies and that the noise spectrum does not vary significantly with time.

If one plays these files using an audio speaker, the removal of background noise could become evident as a more profound heartbeat-like sound post spectral subtraction becomes a dominant tone. Visual inspection of the result based on the selected noise removal process (spectral subtraction) further strengthens that the initial assumptions on the additivity of noise and it being weakly stationary and not changing significantly over time (time or subject independency), holds. The author, however, states this in line with further demonstrating and building tangible evidence that the earlier assumptions on the weakly-stationarity property of visual electrodiagnostic noise signal hold for ISIM engineering application methodology as well as additivity characteristics of the signal.

From the spectrogram analysis of the recorded data in MATLAB® (figure 4.4), one can see that most of the energy of the signal is under 500 Hz. The horizontal axis in figure 4.4 is the time axis and vertical axis the frequency axis. The colour map (figure 4.4.f) represents the energy of various frequency components present in the signal with red the highest and blue the lowest. Through visual inspection, it is also evident that there exists no dependent trend of frequency on time. This can be used to empirically demonstrate that the signal is stationary, or at least there is no dependency on the frequency in time.

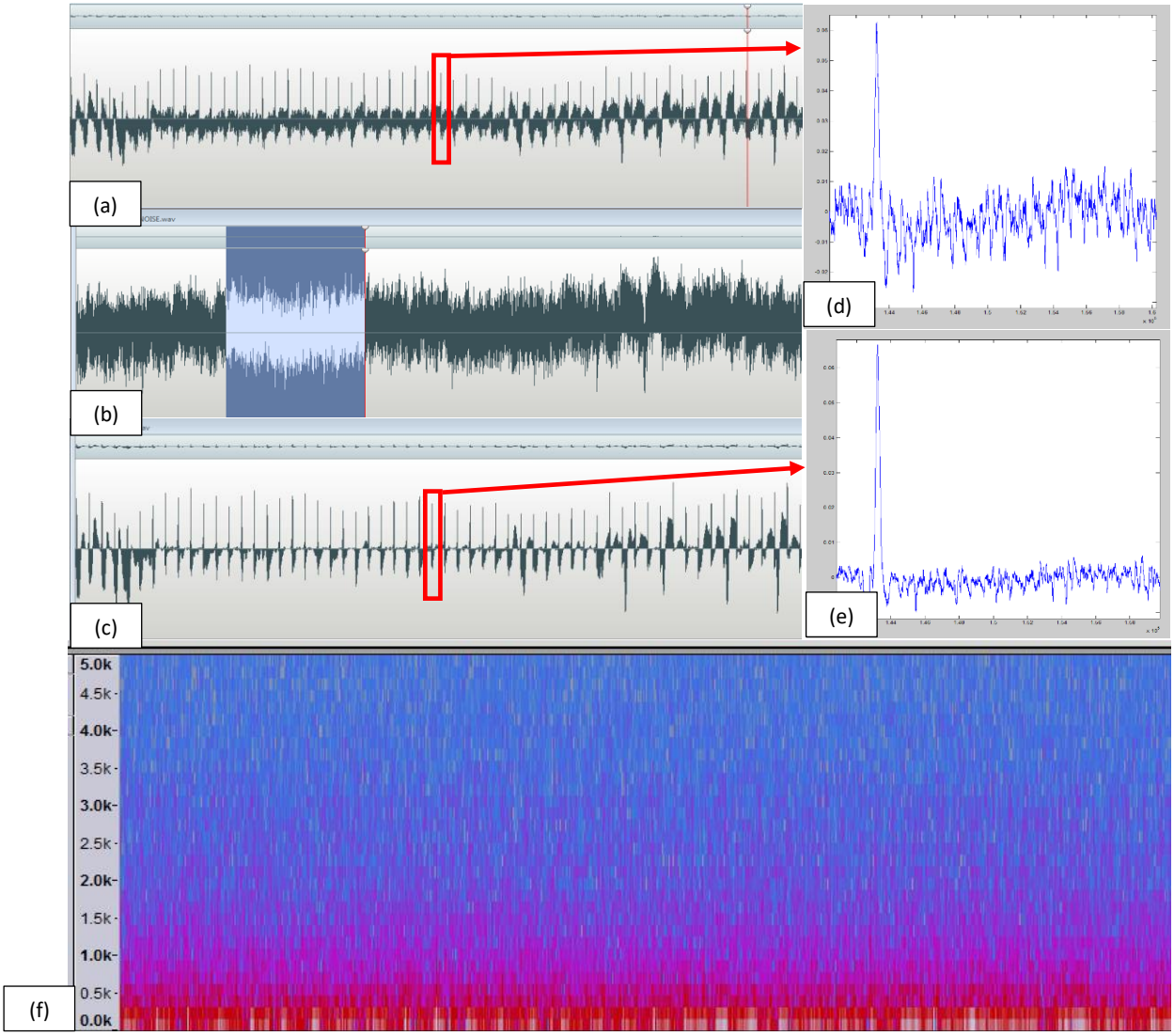

Figure 4.4. Verification of some of the assumptions made about noise and ERG response prior to performing data collection on normal (healthy) subject with no known eye-condition. (a) Record of global or full-field ERG response from a normal subject using Liverpool bio-amplifier and DTL electrodes, under photopic condition using ISCEV standard flash intensity. (b) Record of noise data from the same subject when no stimulus is present. The highlighted section in this record is used for spectral subtraction. (c) Record of ERG response data post spectral subtraction using data record in (a) and (b). (d) A single cycle of the waveform in (a). (e) A single cycle of the data post spectral subtraction procedure. (f) Frequency-time analysis of the record in (c) illustrating stationarity of the data. All voltage records (in a, b, c, d and e) are in mV and time records are in samples (sampling frequency is 8000 Hz, and the bandwidth of the amplifier is set to 500 Hz).

To help with visualisation, removal of artefacts, filtering, decimation (downsampling) and averaging, as well as identifying the parameters of the signal such as a- and b-waves and respective implicit times, a graphical user interface (GUI) was developed in MATLAB® to import the recorded data and perform the required file preparation before addition to the ISIM library. This GUI is illustrated in figure 4.5 where a file of 240 data cycles (2.0083 minutes of recording) is imported. The interface takes two inputs, one MATLAB® native file with a .mat extension (contains both recorded channels and the synchronisation signal) and a text file that contains all necessary information to perform the file preparation. This information is automatically generated by the bio-amplifier GUI during data collection and if not provided the interface will prompt the user to enter the required information before processing. The interface uses the text file and the provided synchronisation signal (red bars in figure 4.5.a) to chop the signal into a set of arrays for each epoch. The epochs are also illustrated in a 3-D plot (figure 4.5.b). A drag and drop operation is implemented that allows the removal of the unwanted epochs. The interface provides for access to the data through exporting to CSV and Excel® files. The Excel® files are prepared automatically through a MATLAB®-Excel® automation service library (developed here). This includes the graphing of user-defined plot/s in Excel® and the saving of the results for later use. This is demonstrated in figure 4.6 and 4.7.

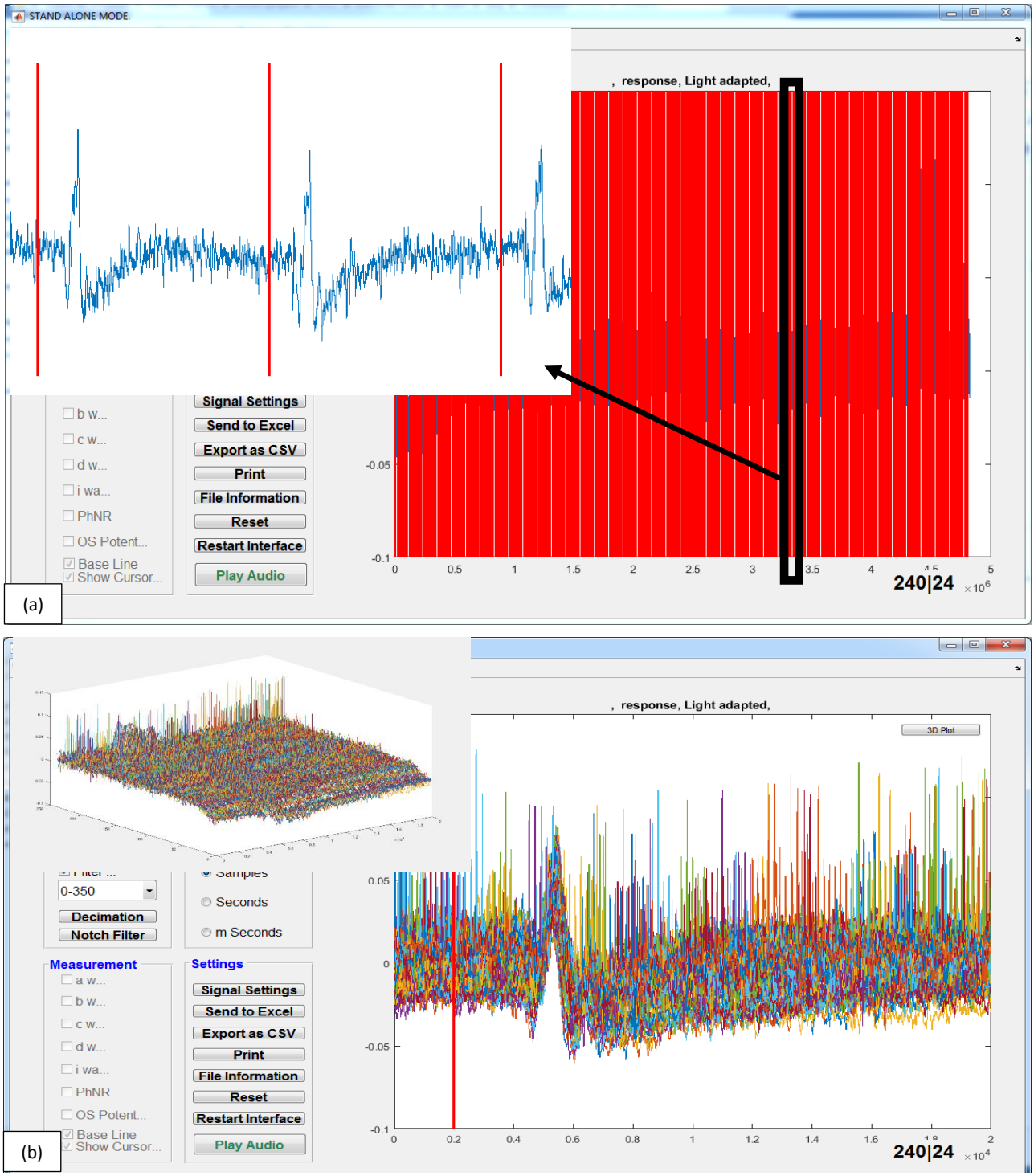

Figure 4.5. (a) Record of full-field photopic ERG from a normal subject at standard flash intensity at a stimulus rate of 2 Hz. A total 240 cycles is recorded. The vertical red lines demonstrate the onset of a flash stimulus minus 100 ms of added pre-flash period (synchronisation point). (b) The record is chopped up into individual cycles, and the resulting array is plotted accordingly. A three-dimension plot in MATLAB® would further help to differentiate the noisy epochs before the averaging process.

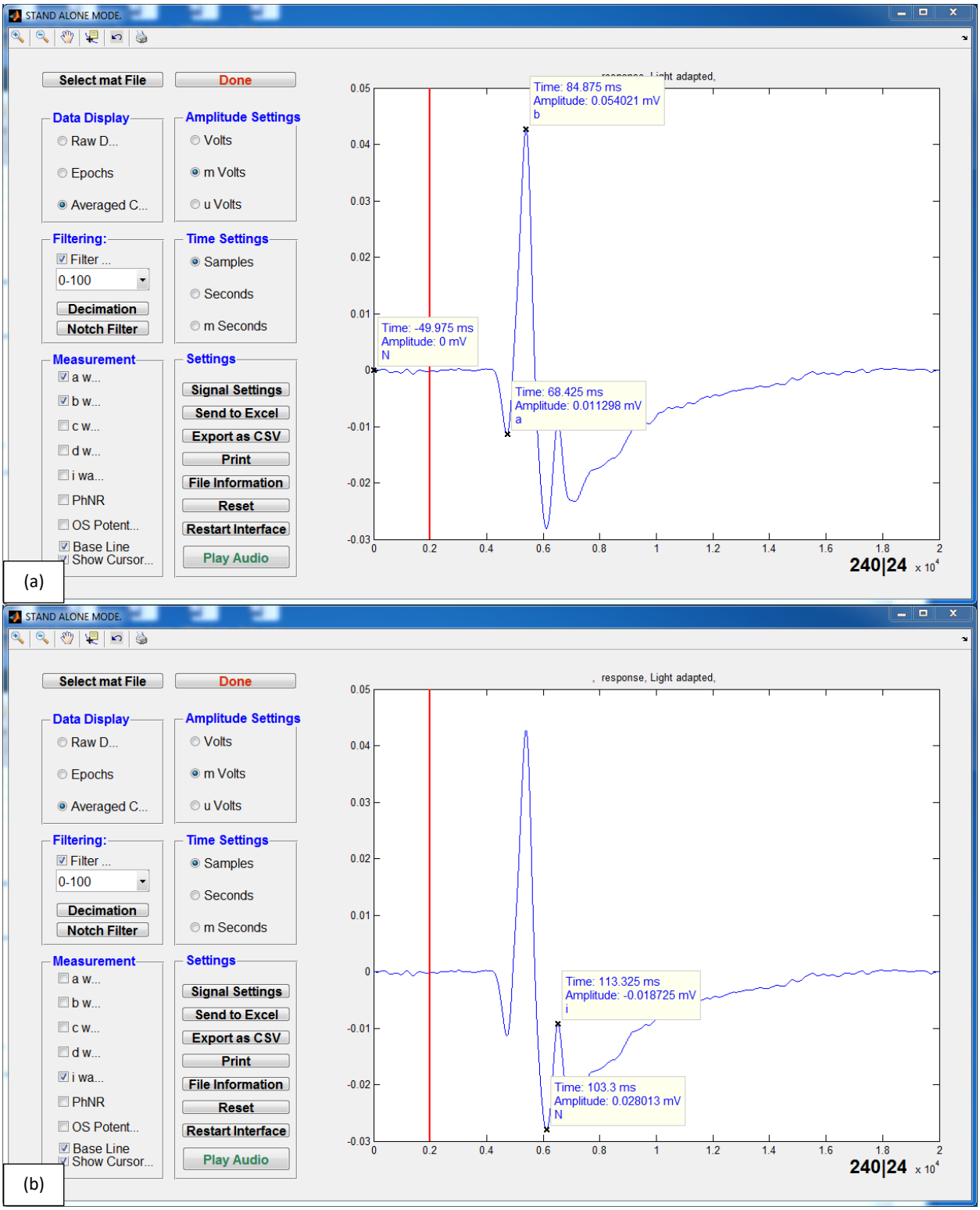

Figure 4.6. The record of figure 4.5 is averaged (post removal of epochs with sharp spikes – potential EMG presence) and filtered (0-100 Hz) and the result is plotted. A pre-flash period of 50 ms is included for accurate windowing of the signal record in later processing. (a) Cursor adjustment to measure the a-wave and b-wave amplitude and implicit time. (b) Cursor adjustment to measure the i-wave amplitude and implicit time.

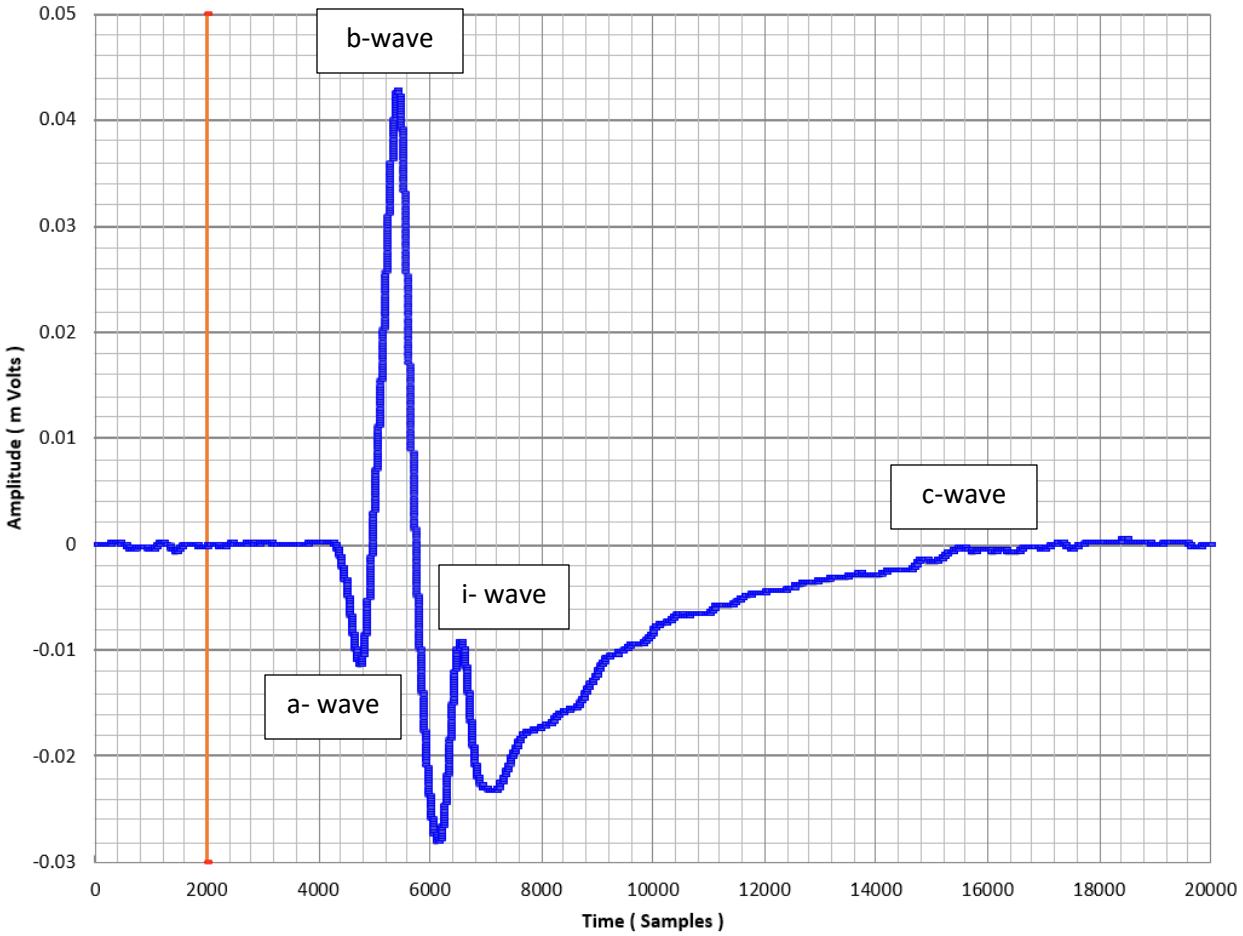

Figure 4.7. The average results in figure 4.6 are transferred to Excel® automatically using the "send to Excel®" button on the analysis GUI. Note that a 50 ms pre-flash period is added to ensure accurate windowing of the record in later processing.

The effects of small artefacts that do not trigger the auto-rejection algorithm are demonstrated in figure 4.8. The data in this figure were collected from a normal subject (subject 5) using ISCEV standard global flashes (LED stimulation). The GUI allows these artefacts to be dragged onto the *bin* (or *temporary storage* area at the bottom right-hand corner of figure 4.8). If the waveforms in the bin area are dropped outside of the figure boundary, MATLAB® will generate a new specialised plotting area to collect these unwanted data cycles, see figure 4.8. Here, seven of the available 86 cycles were removed, meaning 79 cycles were averaged as demonstrated in figure 4.9. Averages with and without the artefacts are illustrated side by side for comparison, which shows that the C-wave is mainly impacted in this example as the artefacts pull down its ascending slope in the averaging process.

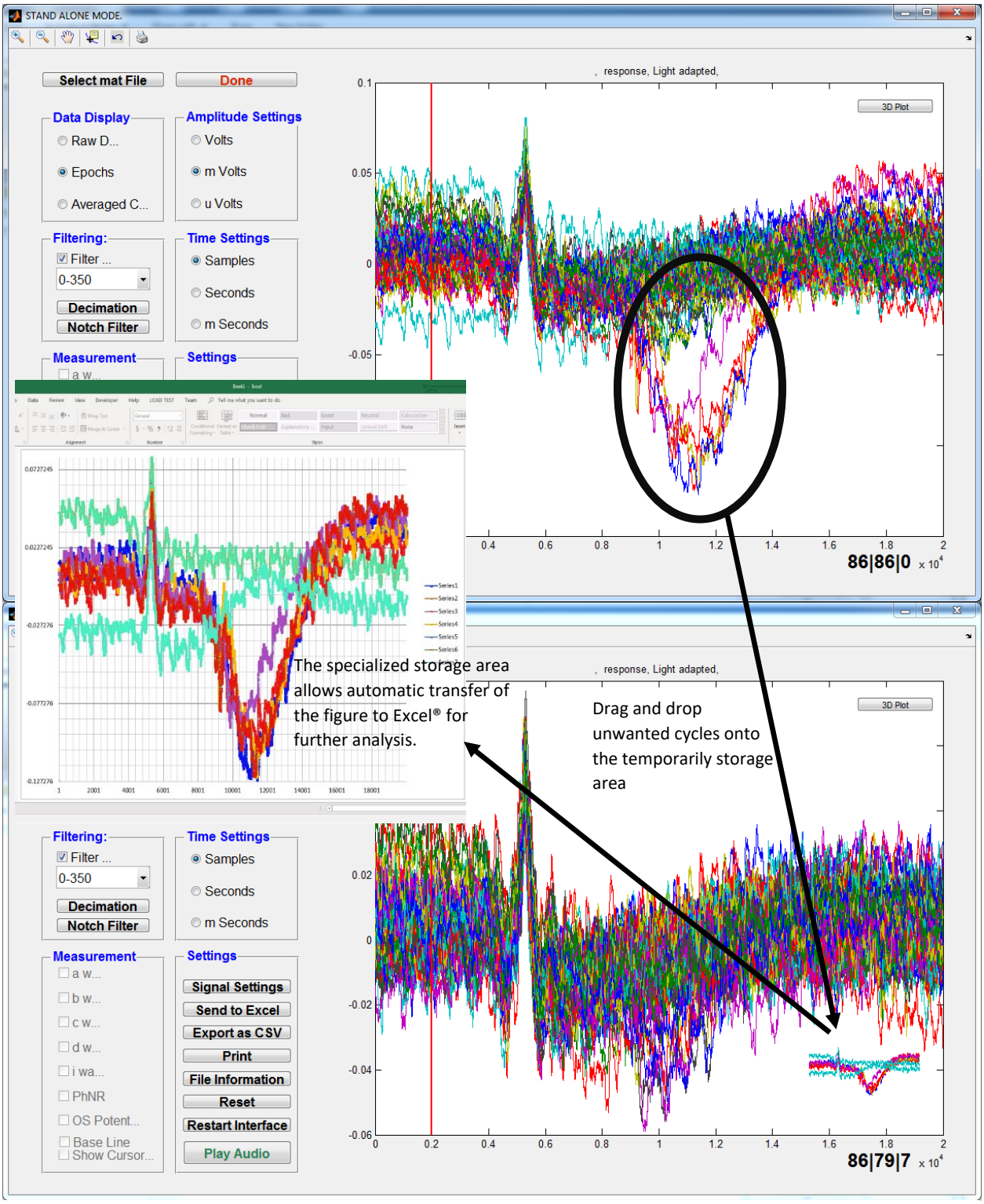

Figure 4.8. Illustration of manual artefact rejection from the raw data record (removal of potential eye-twitches) and automatic transfer of the rejected epochs to Excel® for record storage and further analysis.

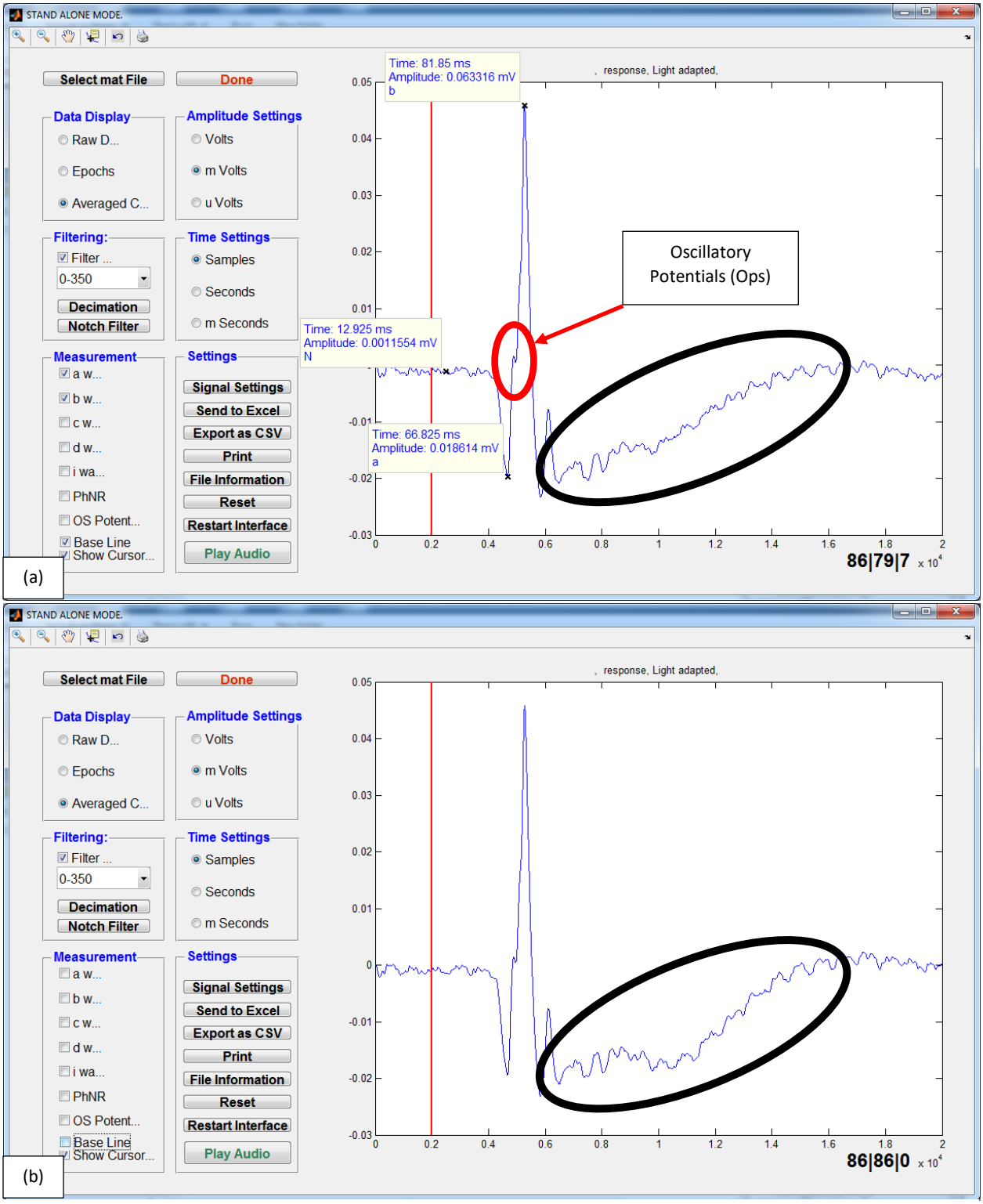

Figure 4.9. (a) Results of averaging the selected epochs, post manual artefact rejection of the waveform in Figure 4.8. Seven epochs were removed prior to averaging and filtering. (b) Averaged result of the epochs without any artefact rejection of the waveform in Figure 4.8. The impact is noticeable (black circled area) with and without any artefact rejection, on the c-wave.

An example of an artefact that triggers the auto rejection algorithm of the amplifier is illustrated in figure 4.10.a, where a normal subject (subject 10) was presented with standard LED flashes. This record shows the data collected and then analysed using the interface to remove contaminated cycles and average the remaining cycles, producing the final grand average (figure 4.10.b).

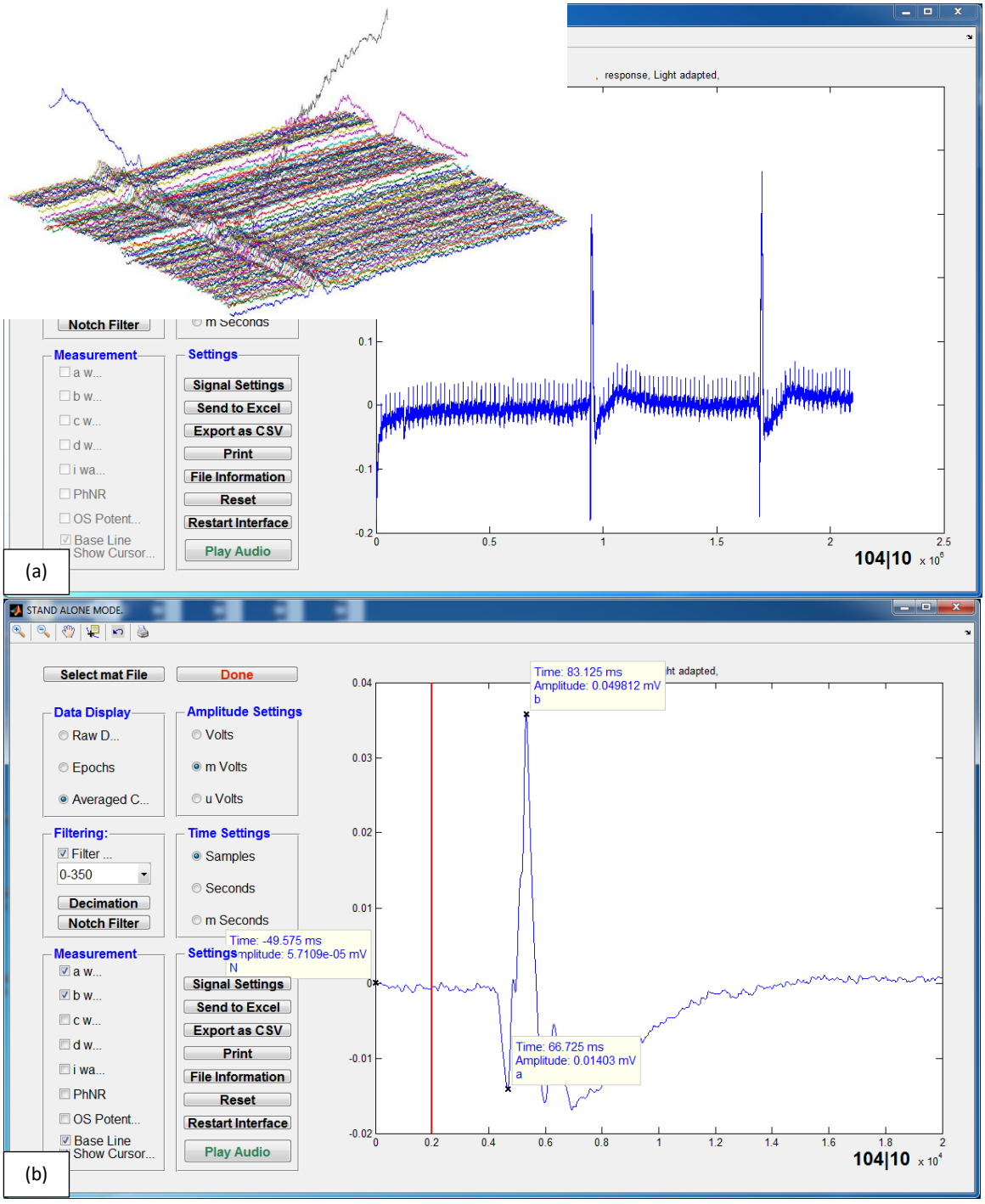

Figure 4.10. (a) An example of an artefact that triggers the auto rejection algorithm of the amplifier – blinks. (b) Averaged result post manual rejection of the raw data record.

A record from a normal subject (subject 12) when standard LED-based full-field flashes were presented is illustrated in figure 4.11.a. Here, the effects of substantial and prolonged EMG, eye twitch and movement, small and large eye blinks are present.

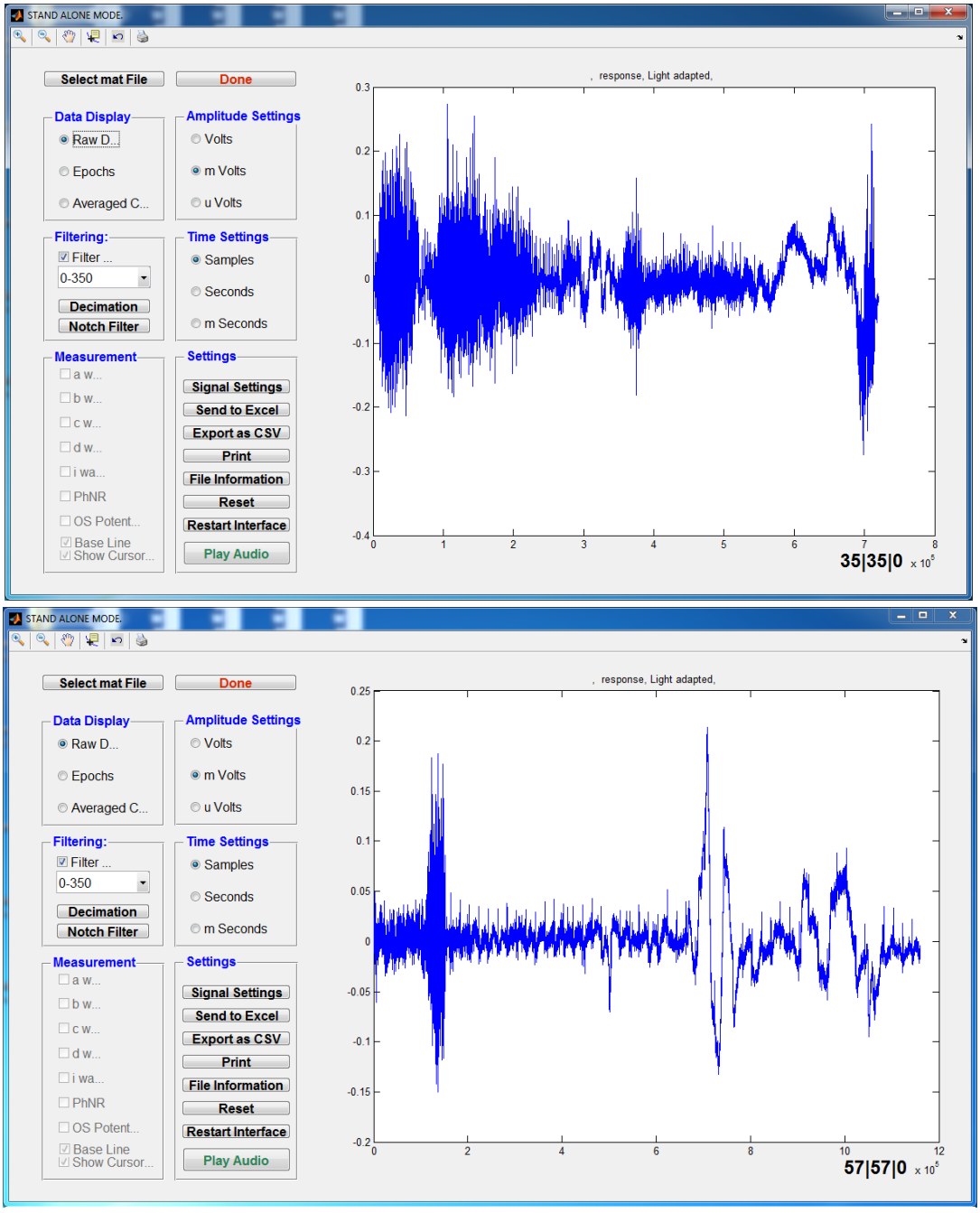

Figure 4.11. Illustrating the effect of EMG, drift, eye-movement and blinks on masking the data (ERG responses) during experimental data collection. (a) The raw data record is discarded due to extensive noise contamination. (b) The data record is retained for further processing; however, the contaminated level of noise is considered too much, and the experiment had to be repeated to ensure a cleaner run.

The author found this record, difficult to analyse and as such it was discarded when building a preliminary ERG library for ISIM platform. Test repetition was performed, where electrodes were taken out, and a rest period was allowed before applying new set of electrodes and adjusting the subject's head to ensure greater comfort. The result of the test repetition is demonstrated in figure 4.11.b.

Post removal of contaminated sections, 50 cycles were averaged, and amplitude and implicit times of the a and b-wave were recorded as shown in figure 4.12.

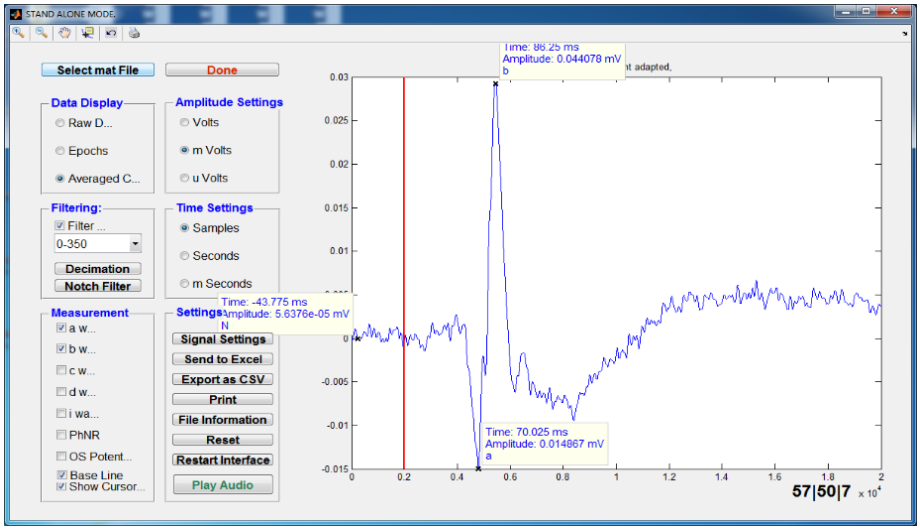

Figure 4.12. Averaged data post manual artefact rejection, averaging and filtering, for the record of figure 5.11.b.

The effect of filtering (0-350 Hz BW against 0-100 Hz BW) is particularly evident between the average responses shown in figures 4.6 and 4.12, where oscillatory potentials (OPs) are seen on the rising edge phase of the b-Wave. These OPs are much faster than the complex a- or b-waves and are of small amplitude. A further example of recorded OPs is demonstrated in figure 4.13 (different normal test subject – subject 4).

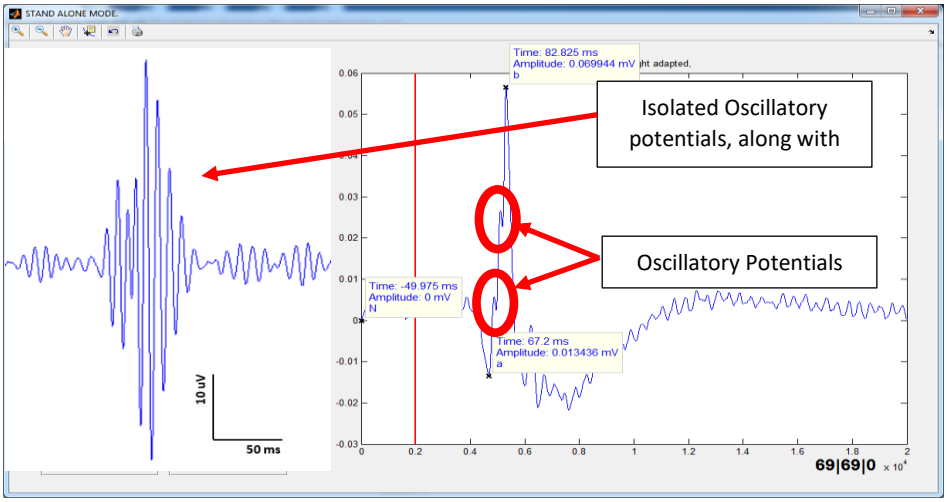

Figure 4.13. Averaged photopic ERG response (photopic with standard flash) from a normal subject with no known eye condition. The data in this figure is filtered from 0-350 Hz, leaving Oscillatory Potentials (OPs) visible on the rising edge of complex b-wave. The average response is band-passed filtered, [100-150] Hz to isolate oscillatory potential through the elimination of the slow, large-amplitude a- and b-waves as illustrated at the left side of the figure.

Figure 4.13 reveals existence of more of these fast oscillatory potentials at the rising edge of the b-wave (OP1 and/or OP2, also known as early wavelets, are seen at MEDIUM and HIGH flash intensities for all subjects as expected as these components are more cone-mediated while higher-index Ops or late wavelets, e.g. OP4, OP5, etc, are more rod-oriented).

Standard full-field flash responses for a total of 10 test subjects were collected and averaged to provide the grand average represented by the solid, white line in figures 4.14 and 4.15. The sampling frequency (fs) and flash frequency were kept constant for all subject at 40kHz and 2 Hz respectively (a decimation factor of 40 was then implemented to reduce the high-frequency jitters through performing running average. This makes the effective sampling frequency to be 1 kHz).

A period of 100 ms of pre-flash stimulus was added before the reconstruction of the final waveform. This is represented by the solid, vertical red line in the figures. This period is added to allow the application of various windowing techniques in later stages of the signal processing phase. Therefore calculation of ERG subcomponents implicit times would require subtracting 100 ms from the measured implicit time.

As the flash intensity reduced, more cycles were required to ensure an adequate SNR. A flash intensity of – 15 dB was found to be the most comfortable by all subjects, as a smaller number of cycles had to be rejected prior to averaging due to contaminating blinks, eye-movement and EMG. The number of rejected cycles increased at both higher flash intensities (above the standard flash intensity or 0 dB level) and below – 20 dB. This could be explained as more blinks, eye twitches and movements were observed when high-intensity flashes were presented. Indeed, flash intensities above Xenon 2 setting were uncomfortable for subjects.

At lower flash intensities (below – 25 dB), a greater number of cycles had to be rejected due to presence of EMG, to the point where up to 75 cycles had to be rejected for subject 5 at a flash intensity of – 40 dB. At the Xenon 1 flash intensity setting of the Roland Consult Ganzefeld, five to a maximum of seven cycles were obtained to obtain the data illustrated in figure 4.14.a. At – 40 dB, up to 250 cycles had to be averaged to obtain the same SNR.

The grand average waveform was windowed (Tukey window), and its length was adjusted to 500 ms for all averaged ERG responses (see figure 4.16). This waveform was added to the ISIM library as the standard full-field ERG response.

The following ERG waveform characteristics were measured for all subjects. The results are illustrated in table 4.1 and figure 4.17.

- The a-wave amplitude – with respect to the baseline (no a-wave could be detected at flash intensities of lower than – 20 dB).
- The b-wave amplitude – with respect to the a-wave.
- The a-wave implicit time (no a-wave could be detected at flash intensities of lower than – 20 dB).
- The b-wave implicit time.

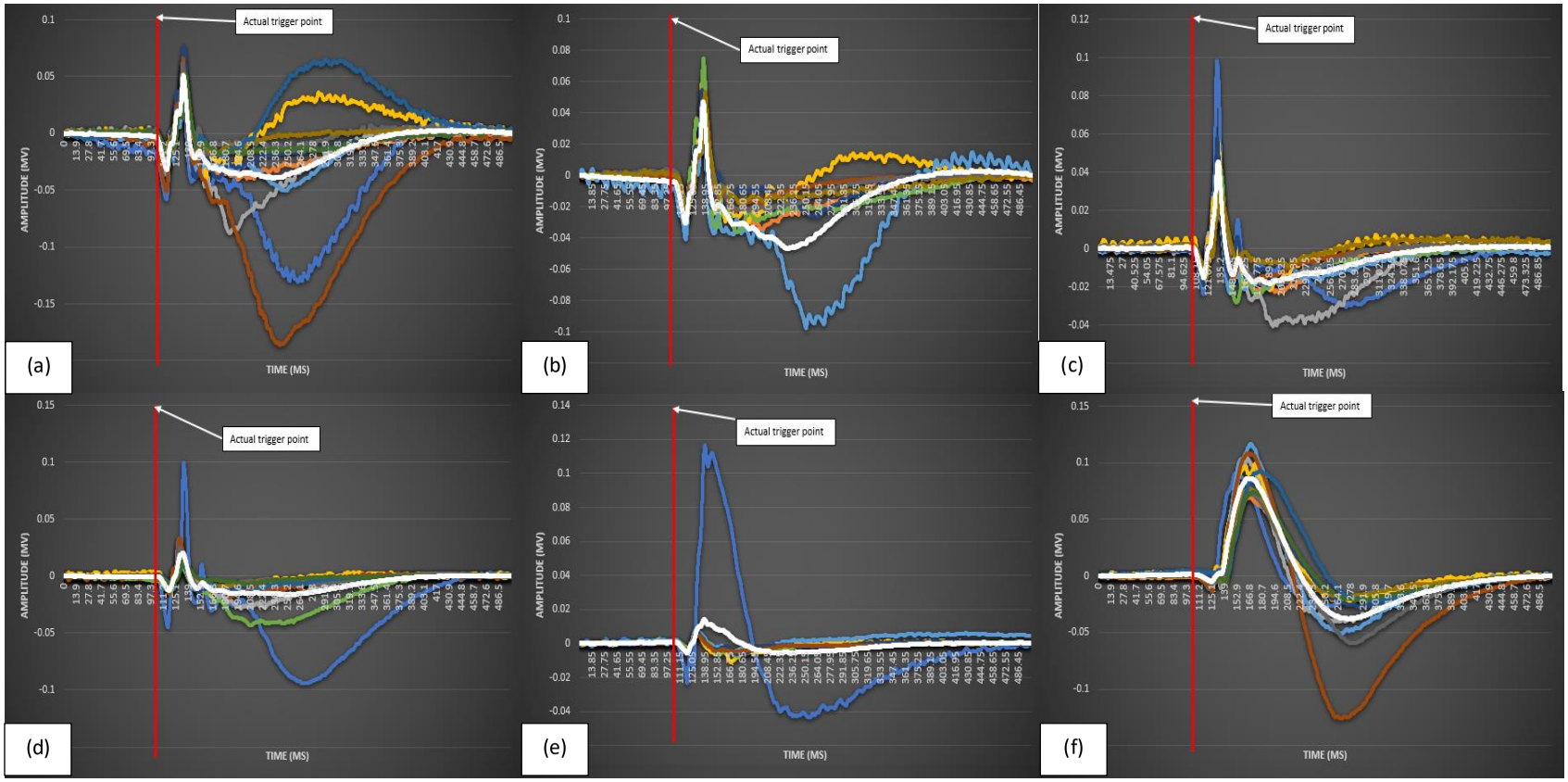

Figure 4.14. ERG response collected from right eye of normal subjects with no eye condition per experimental design in chapter 4 using Roland full field flashes at flash rate of 2 Hz. Liverpool bio-amplifier was used with sampling frequency set at 40 kHz and artefact rejection ratio turned off. Individual responses are collected post manual artefact rejection, decimation by factor of 40 (to simulate sampling frequency of 1 kHz), averaging of the respective epochs and filtering, [0 – 350] Hz. (a) Xenon flash intensity. (b) +5 dB flash intensity. (c) 0 dB (STANDARD) flash intensity. (d) -5 dB flash intensity. (e) -10 dB flash intensity. (f) -15 dB flash intensity.

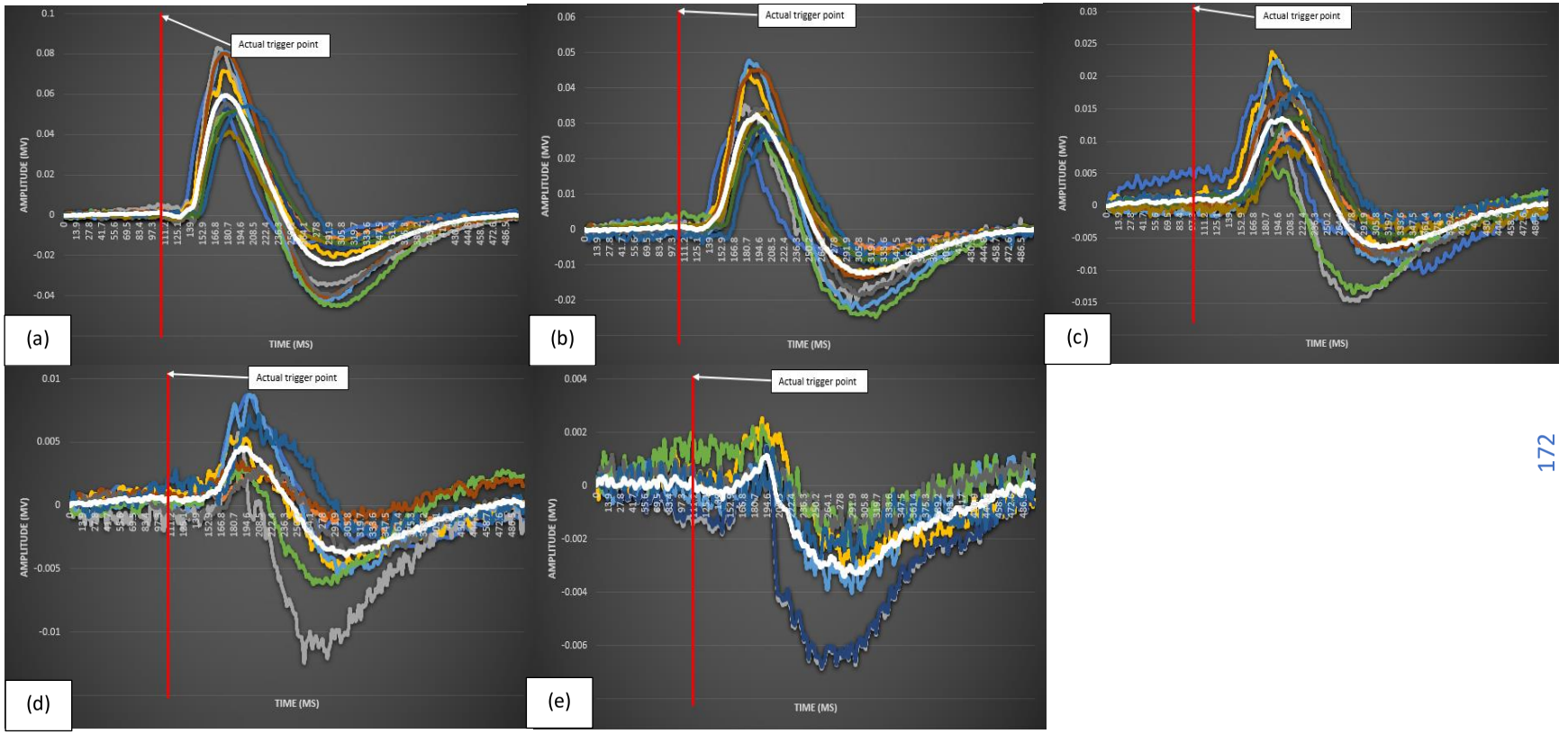

Figure 4.15. ERG response collected from the right eye of normal subjects with no eye condition per experimental design in chapter 4 using Roland full-field flashes at flash rate of 2 Hz. Liverpool bio-amplifier was used with sampling frequency set at 40 kHz and artefact rejection ratio turned off. Individual responses are collected post manual artefact rejection, decimation by factor of 40 (to simulate sampling frequency of 1 kHz), averaging of the respective epochs and filtering, [0 – 350] Hz. (a) -20 dB flash intensity. (b) -25 dB flash intensity. (c) -30 dB flash intensity. (d) -35 dB flash intensity and (e) -40 dB flash intensity.

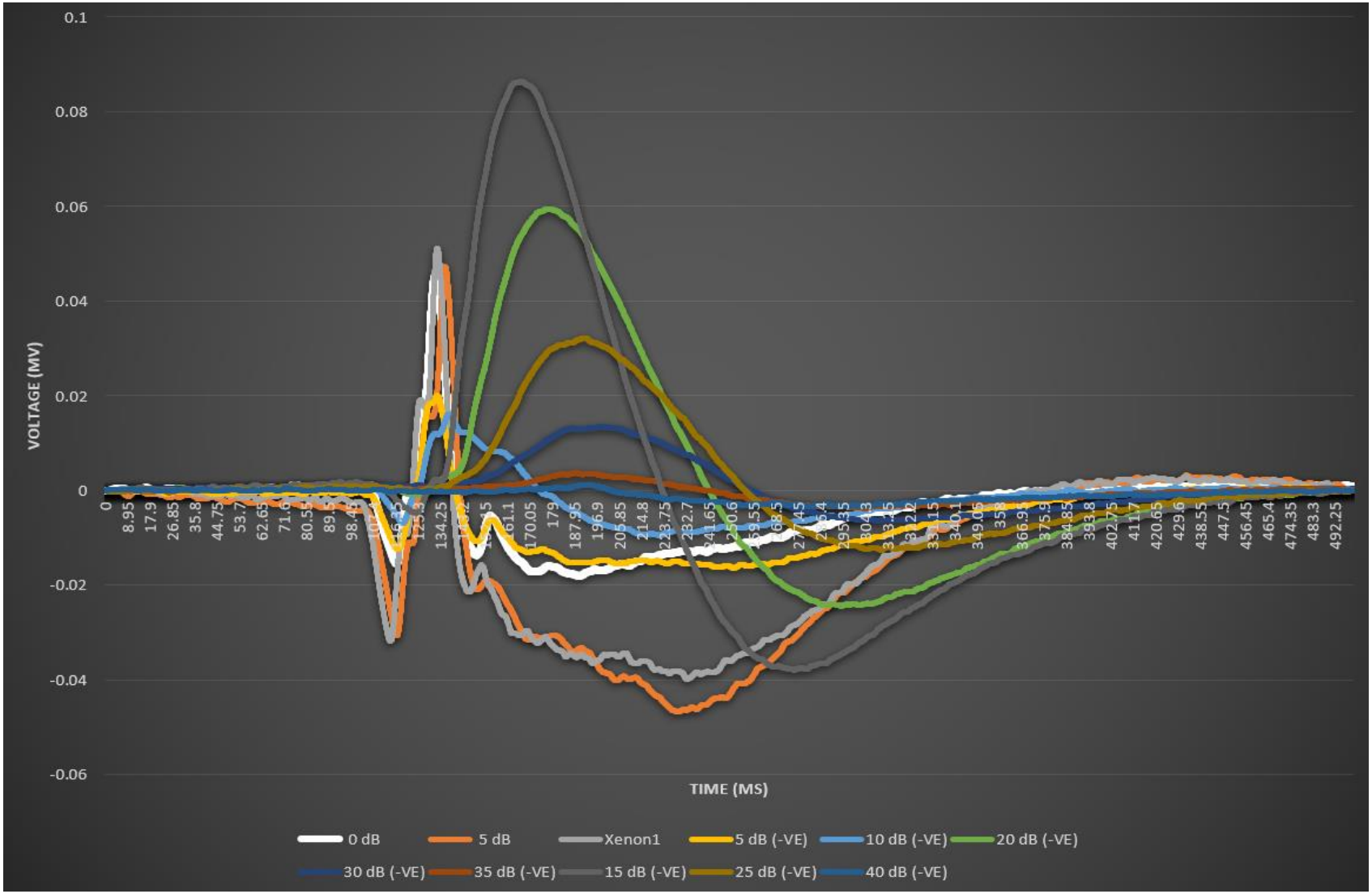

Figure 4.16. Grand average ERG response for all intensity levels (for example, the 0 dB waveform is average of all waveforms in figure 5.14.(c)). All plots are resampled to 1 kHz and filtered to remove DC and high-frequency components, i.e. [0.02 Hz – 350 Hz]. Using Tukey window, ensured no frequency leakage due to presence of any discontinuity. The length of signals are bounded to 500 ms with a 100 ms pre-flash phase. The 0 dB flash intensity (white trace) is equivalent to 3 cd.s.m^{-2}, -10 dB (light blue trace) is equivalent to 0.3 cd.s.m^{-2} etc.

Amplitude (mV)	X1		(+VE)5dB		0dB		(-VE)5dB		(-VE)10dB		(-VE)15dB		(-VE)20dB		(-VE)25dB		(-VE)30dB		(-VE)35dB		(-VE)40dB	
	a	b	a	b	a	b	a	b	a	b	a	b	a	b	a	b	a	b	a	b	a	b
Subject 1	-0.04237	0.07178			-0.02333	0.09799	-0.04413	0.09943	-0.02294	0.1111	-0.01153	0.09116	-0.004523	0.061262		0.02746		0.013775		0.008707		
Subject 2	-0.0302	0.04619	-0.03065	0.0463	-0.01825	0.03288	-0.01081	0.01216			-0.007581	0.06891	-0.004446	0.050214		0.02736		0.009379		0.00256		
Subject 3	-0.02626	0.06357	-0.0251	0.06484	-0.01645	0.05649	-0.00884	0.02544	-0.00517	0.006553	-0.008835	0.1041	-0.005398	0.075277		0.03394		0.01503		0.005726		0.001292
Subject 4	-0.03259	0.06076	-0.03006	0.06175	-0.013	0.0562	-0.01385	0.02772	-0.00486	0.007391	-0.002649	0.09961	-7.34E-05	0.07143		0.04465		0.021753		0.003012		0.00218
Subject 5	-0.03166	0.057767	-0.03237	0.054749	-0.01961	0.04555	-0.01278	0.015	-0.00529	0.005644	-0.005413	0.1164		0.08085		0.04688		0.02253		0.008464		0.001223
Subject 6			-0.02851	0.0576	-0.01977	0.03401	-0.01214	0.01386						0.05342		0.02801		0.006636		0.002858		
Subject 7	-0.02572	0.07725	-0.02106	0.07418	-0.01128	0.04273	-0.00673	0.02316	-0.00346	0.003953	-0.004207	0.08372		0.05322		0.02815		0.009687				0.001425
Subject 8	-0.05113	0.06584	-0.04048	0.073885	-0.02436	0.064144	-0.0154	0.03336	-0.00761	0.0083542	-0.01327	0.1077	-0.003072	0.08035		0.04493		0.01719		0.00253		
Subject 9	-0.03077	0.06164	-0.02974	0.05454	-0.01849	0.05844	-0.01304	0.02583	-0.00697	0.007354	-0.008658	0.07242	-0.003687	0.05552		0.03385		0.01711		0.002631		
Subject 10	-0.01951	0.05281	-0.01916	0.0425	-0.01343	0.03644	-0.00947	0.01833	-0.00438	0.004801	-0.003658	0.07763		0.04148		0.03288		0.008598				0.001034
Subject 11	-0.02066	0.04759	-0.0224	0.041131	-0.01049	0.0303	-0.00914	0.009222			-0.000576	0.09271	-0.000322	0.05392		0.02712		0.01806		0.006477		0.001235
Subject 12	-0.02734	0.05098	-0.0258	0.05355	-0.01464	0.0294	-0.00992	0.01286			-0.007215	0.07382	-0.001003	0.05194		0.02957		0.01356				
Group Average	-0.03151	0.05109	-0.02708	0.0508	-0.01814	0.04411	-0.01227	0.02017	-0.00679	0.01607	-0.004688	0.0863	-0.000925	0.05938		0.03223		0.0133		0.004437		0.001086
Implicit time (ms)	X1		(+VE)5dB		0dB		(-VE)5dB		(-VE)10dB		(-VE)15dB		(-VE)20dB		(-VE)25dB		(-VE)30dB		(-VE)35dB		(-VE)40dB	
	a	b	a	b	a	b	a	b	a	b	a	b	a	b	a	b	a	b	a	b	a	b
Subject 1	13.8	31.9			15.8	31.60	16.6	33.8	19.4	45.6	22.5	52.3	24.8	62.7		68.9		82.9		94.9		
Subject 2	14.9	35.2	17.4	37.7	17.1	33.70	19.6	31.5		31.4	24.8	65.4	25.9	82		95.7		111.5		110.9		
Subject 3	13.4	33.8	17	36.1	17.2	32.20	19.2	30.1	20.8	28.3	26.3	63.9	40.7	72.1		82.7		80.7		86		94.6
Subject 4	14.2	32.9	16.1	35.7	17.7	33.10	17.8	29.8	19.7	28.4	23.5	73.3	28.2	76.6		82		90.8		85.7		90.4
Subject 5	14.2	32.8	16.5	35.5	17.2	32.00	18.8	29.9	19.8		25.6	67.9		76.8		86.9		92.7		95.2		92.3
Subject 6			17.7	37.4	17.9	33.80	19.4	31.9		31.1				83.7		91.3		85.9		87.2		
Subject 7	15.8	33.8	17	37.1	18.5	34.80	20.2	31.5	20	28.1	36.6	65.9		81.7		97.9		109.3		83.2		94.8
Subject 8	13.5	32.9	15.7	35.3	15.9	31.90	18.1	29.3	19.5	29.6	25.2	66.5	27.6	77.2		91.1		103.7		87.7		
Subject 9	14.4	32	16.7	35.1	16	31.70	18.7	29.9	20.6	31.2	36	68.2	41.9	78.9		96.1		106		110.7		
Subject 10	14.6	33	17.5	36.7	16.7	33.00	18.3	31	19.8		33.6	65		82.8		100.1		108.1				92.8
Subject 11	16.2	34.8	17.4	37.1	19.5	34.50	20.8	32.6			41.9	78.6	49.6	98		107.8		116.4		106.6		101.7
Subject 12	17.3	36.4	19.1	38.8	20.3	35.90	21.9	33.6			40.6	72.8	46.2	89.1		102.5		115.6				
Group Average	14.9	33.2	17.4	36.3	16.9	32.6	17.2	33.1	19.9	37.7	24.8	66.9	27.9	78.3		91.7		95.6		92.5		93.5

Table 4.1. Measured amplitude and implicit times of a- and b-wave of recorded ERG data for all 12 normal subjects at 11 intensity levels when global flashes at 2 Hz were presented to the subjects under experimental conditions and protocol as specified in chapter 4. Grey areas are those that the data does not exist, could not be recovered from noise or missing (for example due to increased fatigue level the data collection had to be stopped or flashes were too uncomfortable for the subject to handle). Group averages represents the averaged waveform of all subjects for an intensity level. Each subject was tested the same day and were allowed enough rest time when and where needed. Both a- and b-wave amplitudes where measured with respect to the base-line and a-wave, respectively, while implicit times were measured from the point of actual flash onset.

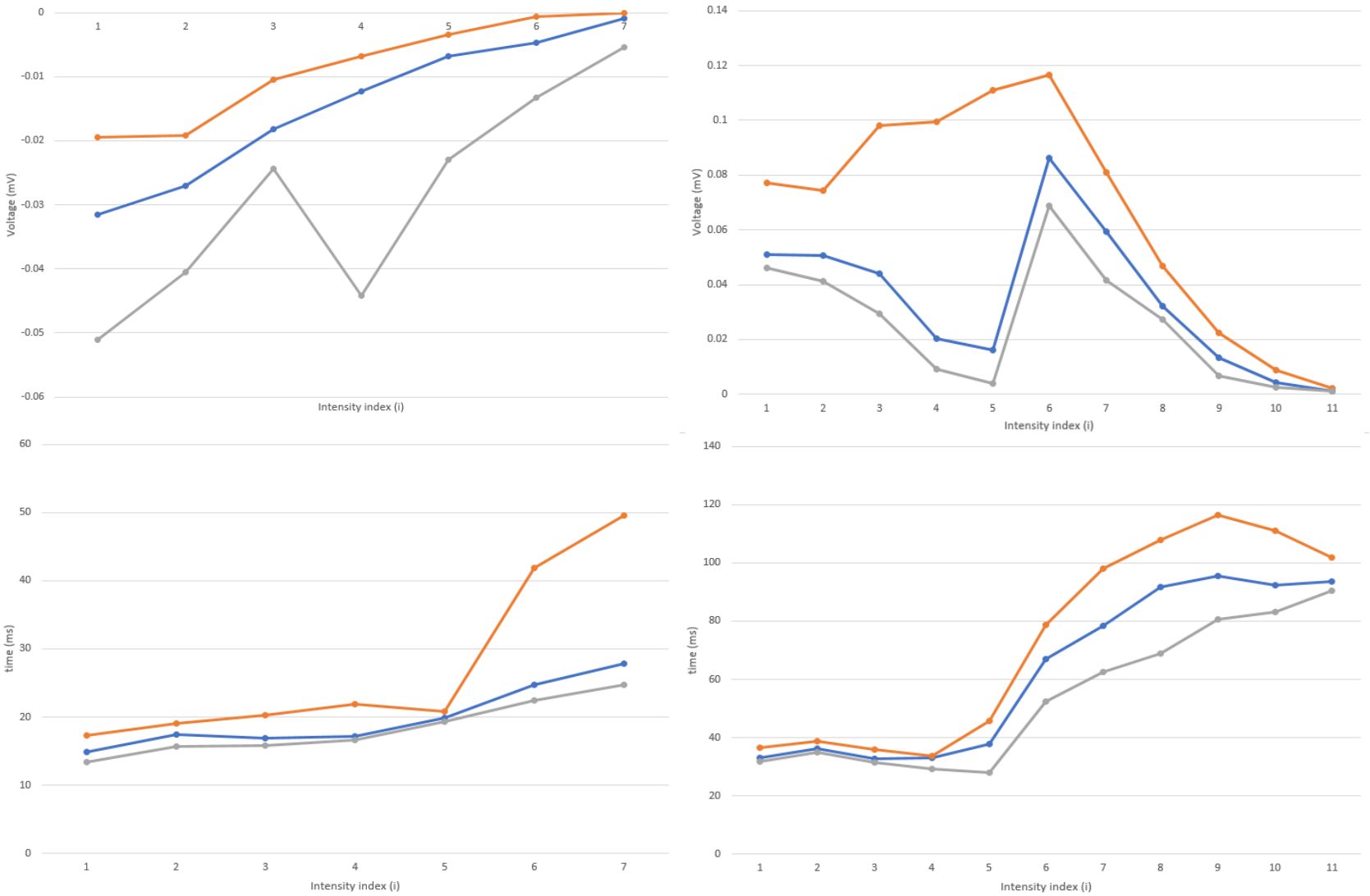

Figure 4.17. (a) a-wave amplitude. (b) b-wave amplitude. (c) a-wave implicit time. (d) b-wave implicit time. In all plots, blue trace represents the measured group average values, orange trace represents the maximum measured value at each intensity level and grey trace represents the minimum measured value at each intensity level.

Table 4.2 illustrates the group average, standard deviation and recorded variability for a- and b-wave amplitudes and implicit times for a group of normal subjects collected to form the RLUBH normal database. The clinical system was Roland Consult, and Gold Foil (GF) electrodes were used on the right eye of all subjects for data collection with and without any pupil dilation. The average measured pupil diameter is 4.2 mm for the un-dilated eye and 7.4 mm for the dilated eye. The recorded electrode impedance is less than 5 kΩ across all subjects. Both Table 4.1 and 4.2 reflect the same demographics including age group, eye colour and ethnicity profiles. The data were collected between June 2013 and January 2014 at St Paul's eye unit RLUBH.

From table 4.2 the following a- and b-wave amplitude ratios and implicit times were calculated (the

Table 4.2. RLUBH un-dialted and dilated full-field ERG normal database alongside the measurment values for all 11 normal subects as part of the work in the scope of this thesis.

	RLUBH normal (Gold Foil electrode, Standard flash, un-dilated eye, photopic)				RLUBH normal (Gold Foil electrode, Standard flash, dilated eye, photopic)				Thesis study normal (Thread electrode, Standard flash, un-dilated eye, photopic)			
	a-wave (ms)	b-wave (ms)	a-wave (μV)	b-wave (μV)	a-wave (ms)	b-wave (ms)	a-wave (μV)	b-wave (μV)	a-wave (ms)	b-wave (ms)	a-wave (μV)	b-wave (μV)
Group Average	17.7	30.9	33.4	126.5	15.7	29.4	42.5	206.5	16.9	32.6	18	44
Standard Deviation (STD)	1	1.1	7.7	44.2	0.5	1.1	12.4	63.7	1.3	1.3	4.3	18.8
Greater than 2 X STD	19.7	33.1	48.9	214.8	16.7	31.6	67.2	333.9	19.6	35.3	26.7	81.8
Smaller than 2 X STD	15.8	28.8	18	38.2	14.6	27.2	17.8	79.1	14.2	29.9	9.5	6.5
%Variability	19.8	11.4	71.5	124.6	11.0	13.3	86.6	107.5	26.6	13.2	76.4	155.5

implicit times are similar, and ratios are considered to be unity) and incorporated into the ISIM back-end mathematical engine to take into account the use of thread or GF electrodes and the effects of pupil dilation when synthesising final waveforms.

- $\frac{b_{RLUBH,Dilated,GF}}{b_{Study,un-dlated,thread}} \approx 4.7$
- $\frac{b_{RLUBH,Dilated,GF}}{b_{RLUBH,un-dilated,GF}} \approx 1.6$
- $\frac{b_{RLUBH,un-dilated,GF}}{b_{Study,un-dilated,thread}} \approx 2.9$
- $\frac{a_{RLUBH,Dilated,GF}}{a_{Study,un-dlated,thread}} \approx 2.4$
- $\frac{a_{RLUBH,Dilated,GF}}{a_{RLUBH,un-dilated,GF}} \approx 1.3$
- $\frac{a_{RLUBH,un-dilated,GF}}{a_{Study,un-dilated,thread}} \approx 1.9$

The experimental setup (section 3.6) used for this study is different from the configuration used to collect the RLUBH normal database. The reported ratios here do seem to be high compared to other studies when comparing different electrode types on ERG responses from healthy subjects. For example, a study by Bradshaw and Hansen et al[64] demonstrated that Gold Foil (GF) electrode responses were on average 4 to 5 times larger than skin-electrode responses recorded in the same laboratory. They also showed that scaling the skin-electrode responses by 4.5 times; would result in the distribution of response amplitudes to be similar to that of the eye contact electrodes in both healthy children and adults. They also found that the waveform morphology is the same, irrespective of the electrode types and the scaling factor used is the same for the entire waveform rather than being different for individual components such as a- or b-wave.

4.2.3 ON & OFF, Scotopic and Flicker ERG response

Flicker responses from five normal subjects with no eye condition were obtained using global standard intensity flashes at 29.4118 Hz with a flash ON duration of 1 ms and a sampling rate of 8000 Hz. Results for one normal subject (the author) are presented in figure 4.18. Five normal subjects were presented with the same global standard intensity flashes at 1 Hz, with a flash duty cycle of 50% (i.e. a flash ON and OFF period of 0.5 seconds) to obtain ON-OFF ERG responses, see figure 4.19 for collected and processed data. The reported data from ISCEV standard in [105] was used to collect, digitise, calibrate and process the scotopic response expected from a normal subject with no eye conditions, see figures 4.20 and 4.21.

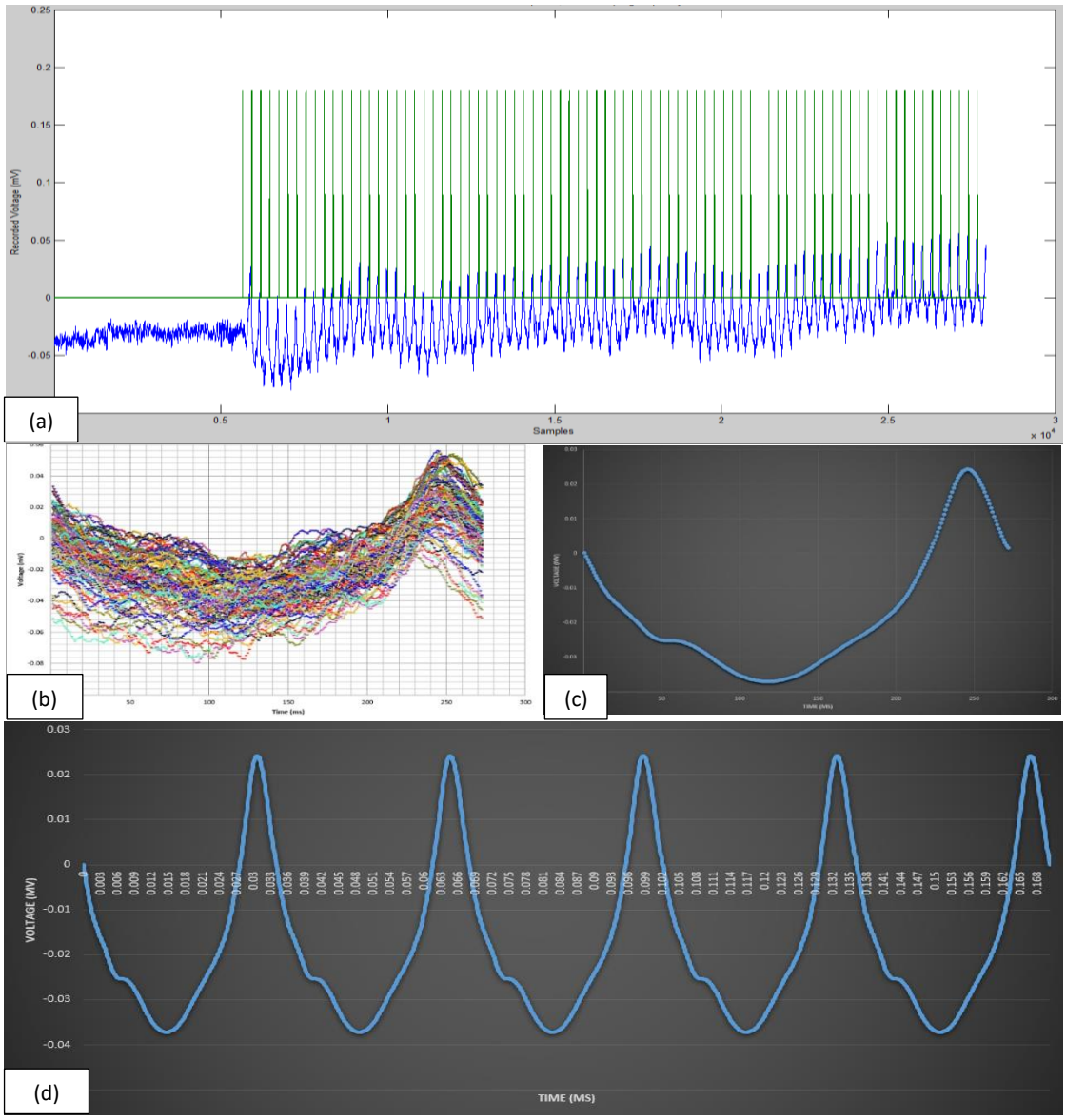

Figure 4.18. (a) Demonstration of normal subject flicker response, using ISCEV standard LED flashes flickering at a rate of 29.4118 Hz. Flash duration is measured to be 1 ms (green trace in (a)) and 100 cycles are averaged (individual epochs or cycles are illustrated in (b)) resulting in the waveform in (c) that is incorporated into ISIM library. (d) concatenating, five copies of (c) resulting in the synthesis of flicker response waveform.

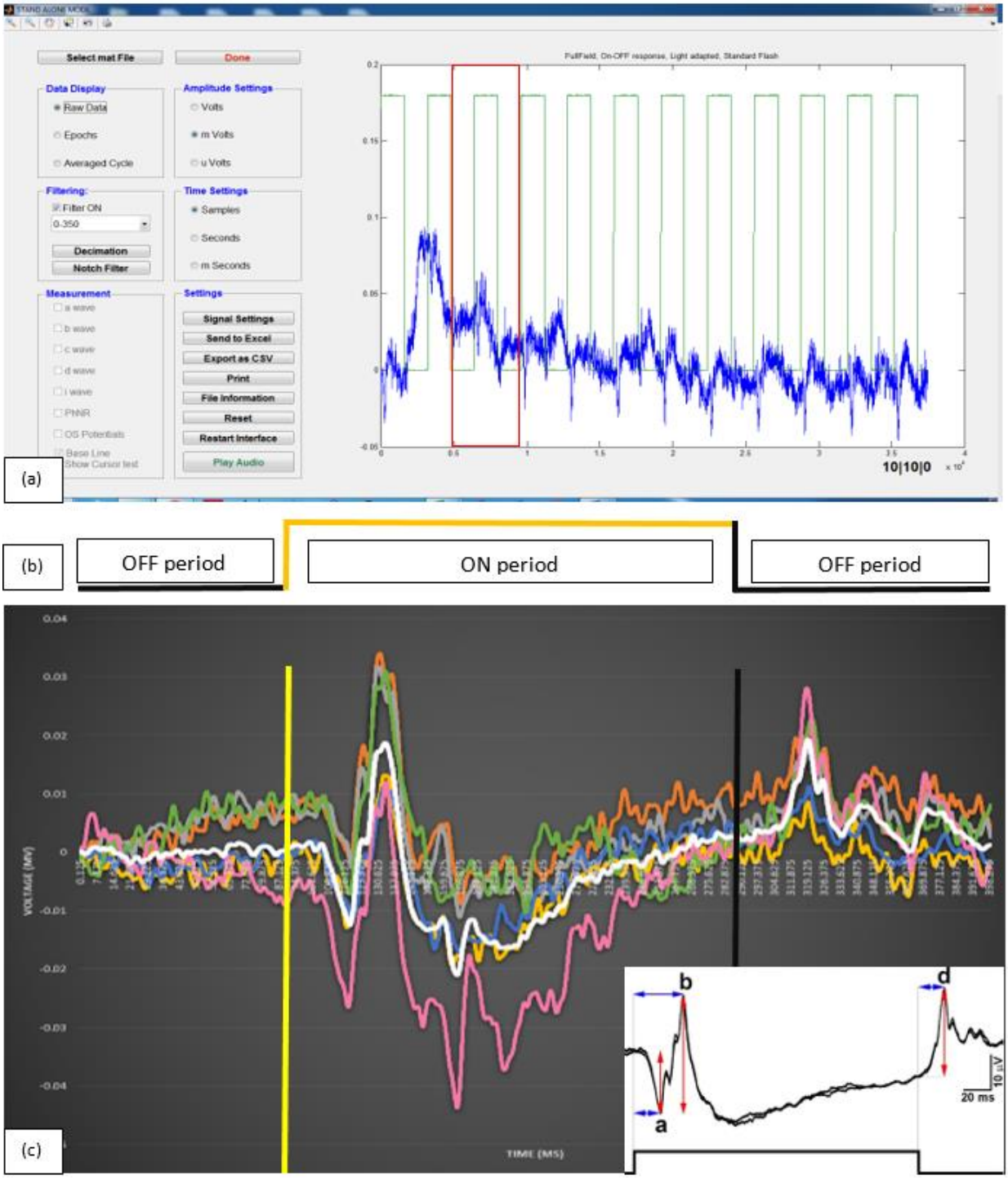

Figure 4.19. Experimentally collected ON-OFF full-field ERG response using standard flash intensity (ISCEV) with a duty cycle of 50%. Five normal subjects with no known eye conditions were tested using Liverpool DTL electrodes and bio-amplifier recording at a sampling rate of 8 kHz. The average cycle (of all subjects) is shown in white and is incorporated into ISIM library for re-use. (a) Subject one, collected raw data (blue trace), and synchronisation signal (green trace). ((b) Illustration of the ON & OFF period of flashes with a duty cycle of 50%. (c) Subjects averaged cycle data together with the grand average in the white trace, marked with the flash onset (yellow vertical line) and flash offset (black vertical line), clearly demonstrating two distinguished ERG ON and OFF responses. This result is a close match with that of ISCEV published results[343] showing re-producibility and repeatability of the experiment to the published standards (lower-right side of (c)).

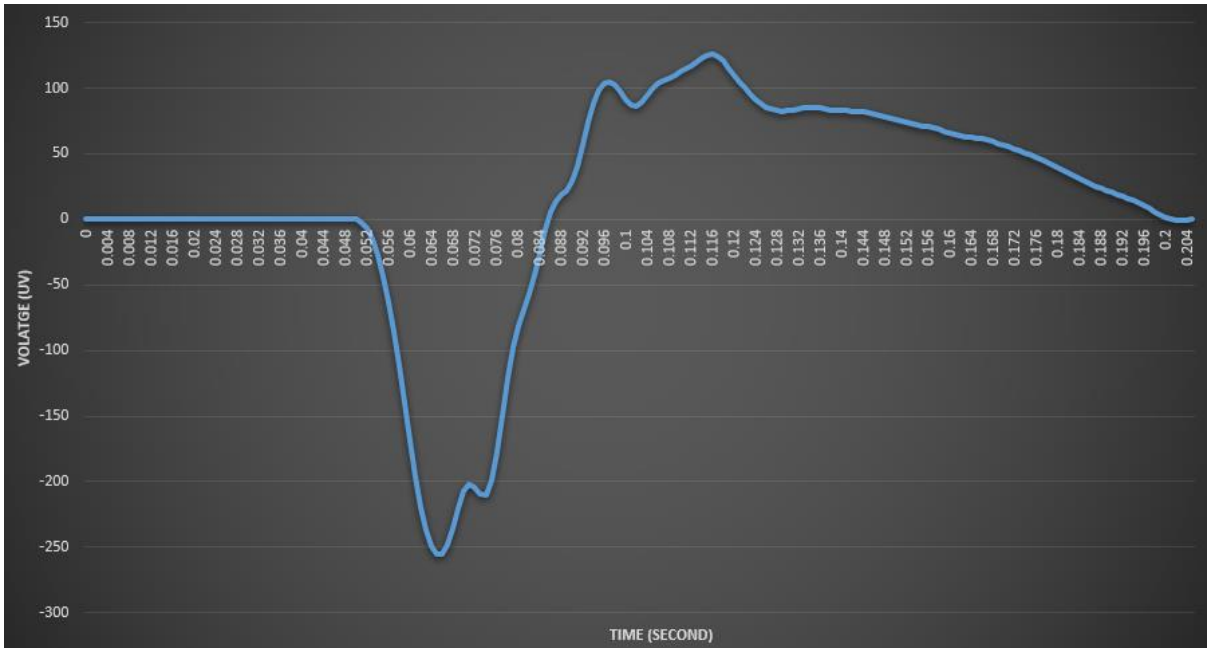

Figure 5.20. Dark-adapted 10.0 ERG response digitised and simulated at a sampling rate of 1 kHz with an added pre-flash period of 50 ms. The response is low-pass filtered at 150 Hz and has a length of 205 ms. [105]

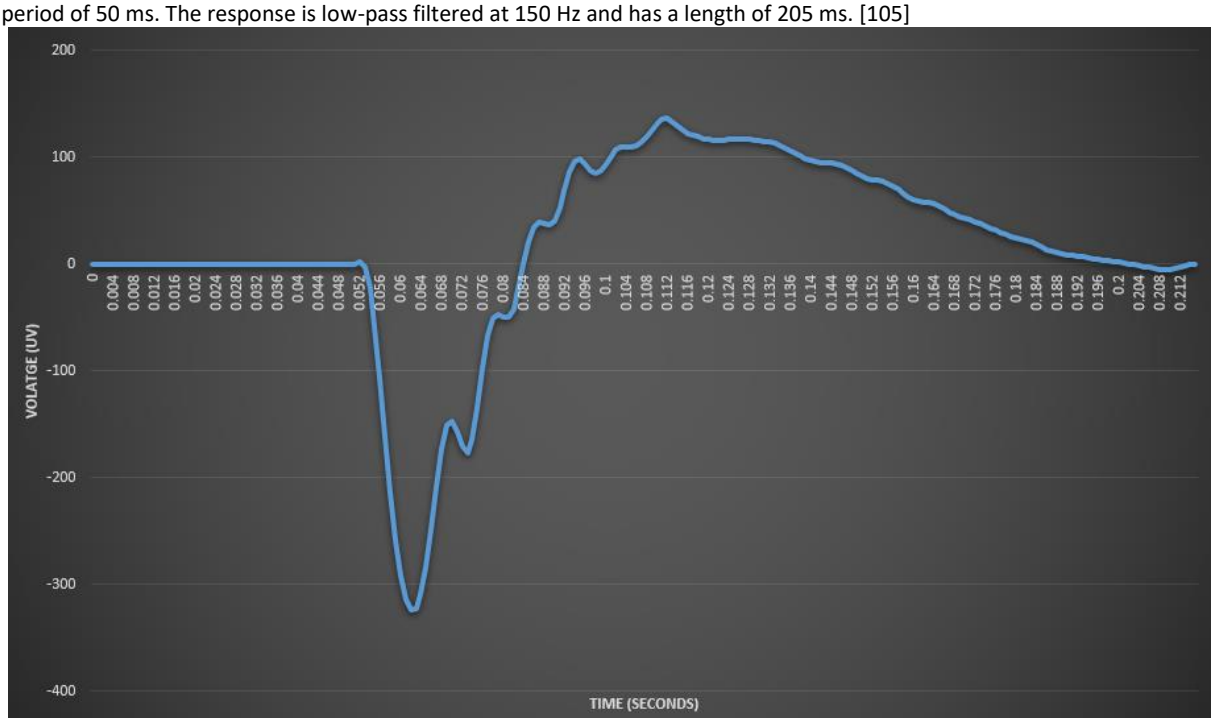

Figure 4.21. Dark-adapted 30.0 ERG response digitised and simulated at a sampling rate of 1 kHz with an added pre-flash period of 50 ms. The response is low pass filtered at 150 Hz and has a length of 212 ms. [105]

4.2.4 Validation of mfERG response simulation & extraction

The simulation of the response for a single hexagonal location using an m-sequence of length 4095 is illustrated in figure 4.22, where the kernels are plugged in using the data illustrated in figure 3.14. The final simulated waveform is illustrated in figure 4.22.b, where one cannot recognise the original kernels without further processing. This installation can be used standalone or can be operated in real-time, where it reads the incoming flash triggers and produces the required waveform, having provided the necessary kernel table. The generated waveform, illustrated in figure 4.22.b, could be fed into the GUI of figure 4.23 to extract the original kernels, as described in chapter 3. This software plugin could also be used to perform real-time cross-correlation as trigger flashes are fired and registered by the iSim device.

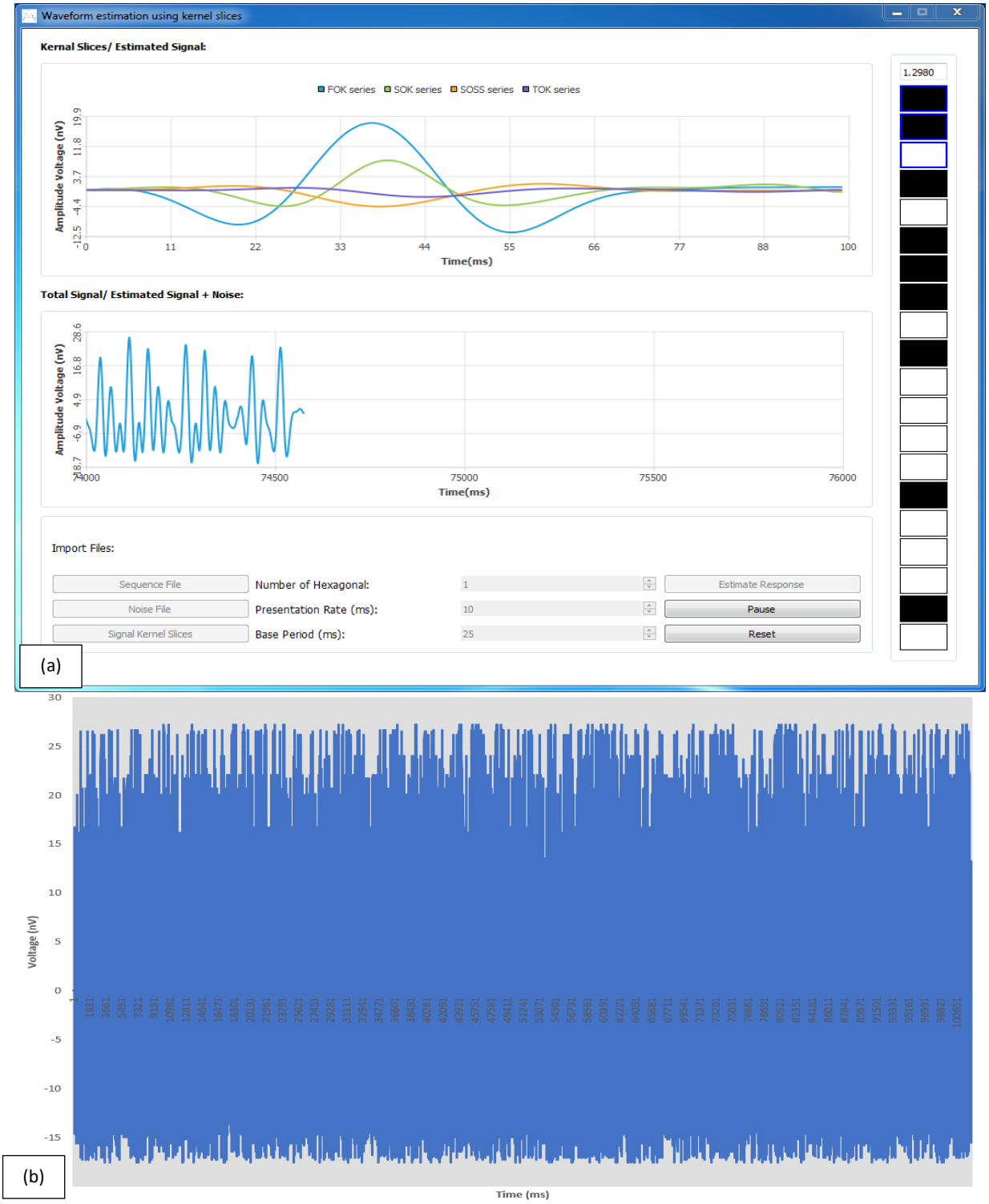

Figure 4.22. (a) GUI used to simulate a mfERG waveforms based on several hexagonal locations to simulate: base-period (overlap), imported m-sequence array, noise file and kernel table. (b) the simulated waveform for one hexagonal location with a base-period of 25 ms, and an m-sequence of length 4095. Noise is zero and kernel table consists of FOK, SOK, SOSS and TOK slices obtained from Sutter paper[44].

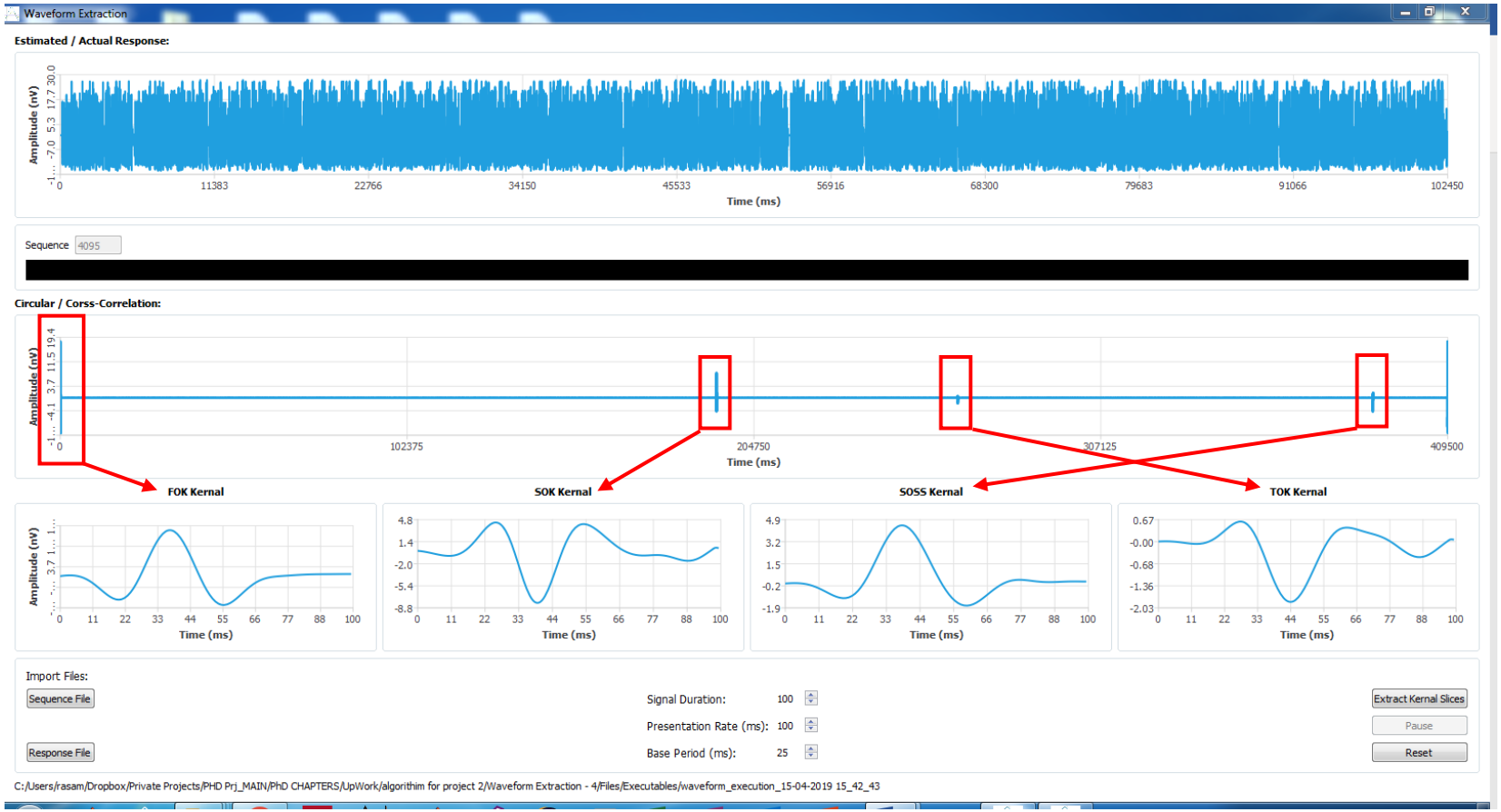

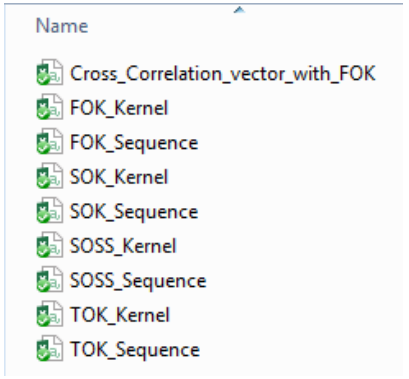

Figure 4.23. The GUI used to extract the nonlinear simulated or actual retinal kernel responses. In this validation, the top waveform is the estimated waveform illustrated in figure 5.22.b. The central plot demonstrates the calculated cross-correlation in real-time against the received m-sequence. The m-sequence could be collected from the actual mrERG monitor screen using iSim or could be provided and imported as a text or CSV file, in this example the sequence has been imported and is the same as the coding sequence of figure 5.22. The cross-correlation is then calculated based on the provided base-period (25 ms) and a memory length of two previous base-periods. The decoded results are next plotted based on the requested signal duration (100 ms in this example, however if longer duration is requested, user will obtain 0 everywhere after the 100th sample point if the coding/decoding sequence contains the correction term; otherwise a DC offset will be evident). The interface will only require the mother m-sequence or the sequence responsible for the FOK response, as it will calculate the SOK, SOSS and TOK sequences and will have these saved as CSV files as illustrated at the bottom, right-hand side of this figure.

4.2.5 Magnitude Squared Coherence algorithm verification

This section demonstrates the applicability of a statistical approach that is novel in the visual electro-diagnostic field - Magnitude Squared Coherence (MSC). The section also demonstrates the effectiveness of the ISIM platform in implemented new signal processing techniques. The aim could be to test, verify and validate or simply demonstrates the feasibility of a novel technique (which is the case here). The developer could also use ISIM platform to verify applicability of an already existing analysis methods using robust and consistent signal generation. For the latter, ISIM platform would provide, the nosie-free and contaminated waveform at various degrees of complexity so that the developer can truly challenge the signal enhancing package.

One of the objectives of ISIM is to demonstrate that the shortcomings of some procedures (e.g. when an ensemble average is taken as an estimate of the underlying response which is assumed stationary and the sampling frequency is not available, or the confidence limits of the cardinal points are unknown), can be mitigated by mathematical methods which can be readily applied to data across the majority of clinical visual electro-diagnostic instruments. The test signal preparation is illustrated in figure 4.24, and the MSC analysis result is shown in figure 4.25.

- Reference templates were made from epochs windowed using a Tukey function.
- No spontaneous artefacts were included in template synthesis.
- The MSC index of response present/not present was established using a Magnitude Squared Coherence statistic (referred to the reference template above): SNR estimate and detection probability reported explicitly ($p<0.05$, MSC_i (MSC index)=true).
- One cycle of the signal is then reconstructed using the significant MSC indexed frequency components with a p-value at or below 0.05, using the synthesis of noisy data to estimate the amplitude of these significant frequency components.

The clinical ERG can be objectively reported using a robust and statistically well-informed model by means of mathematical resources optimised for ease-of-use and accessibility. The use of Tukey windowing accommodates variable discontinuities in the data record and enables implementation across a range of clinical settings in the field of visual electro-diagnostics.

It should be noted that the test statistic of the MSC algorithm assumes that the signal can be modelled as a weakly stationary Gaussian process. However, it is conceivable that some signals do not satisfy this assumption, and therefore there is no guarantee that the algorithm will reject the null hypothesis at the nominal level (e.g. 0.05). A possible safeguard against this problem, which also helps in reducing the impact of false discoveries intrinsic in the use of p-values, is to greatly reduce the significance level required to declare a discovery, for example using $p = 0.001$ or even smaller. ISIM accommodates this type of user intervention, so the tool remains fully useable even in cases where deviations from the assumptions are suspected.

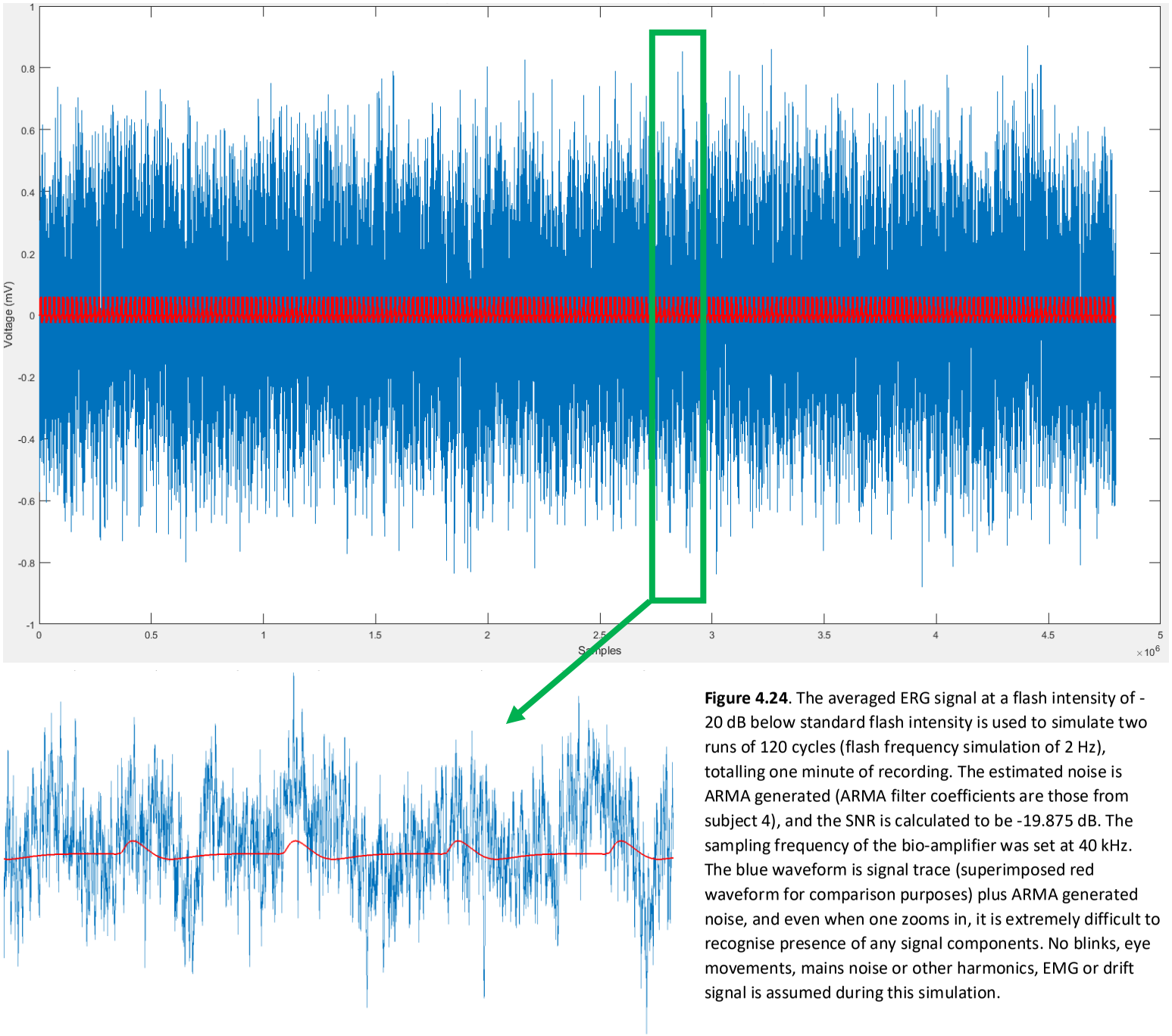

Figure 4.24. The averaged ERG signal at a flash intensity of -20 dB below standard flash intensity is used to simulate two runs of 120 cycles (flash frequency simulation of 2 Hz), totalling one minute of recording. The estimated noise is ARMA generated (ARMA filter coefficients are those from subject 4), and the SNR is calculated to be -19.875 dB. The sampling frequency of the bio-amplifier was set at 40 kHz. The blue waveform is signal trace (superimposed red waveform for comparison purposes) plus ARMA generated noise, and even when one zooms in, it is extremely difficult to recognise presence of any signal components. No blinks, eye movements, mains noise or other harmonics, EMG or drift signal is assumed during this simulation.

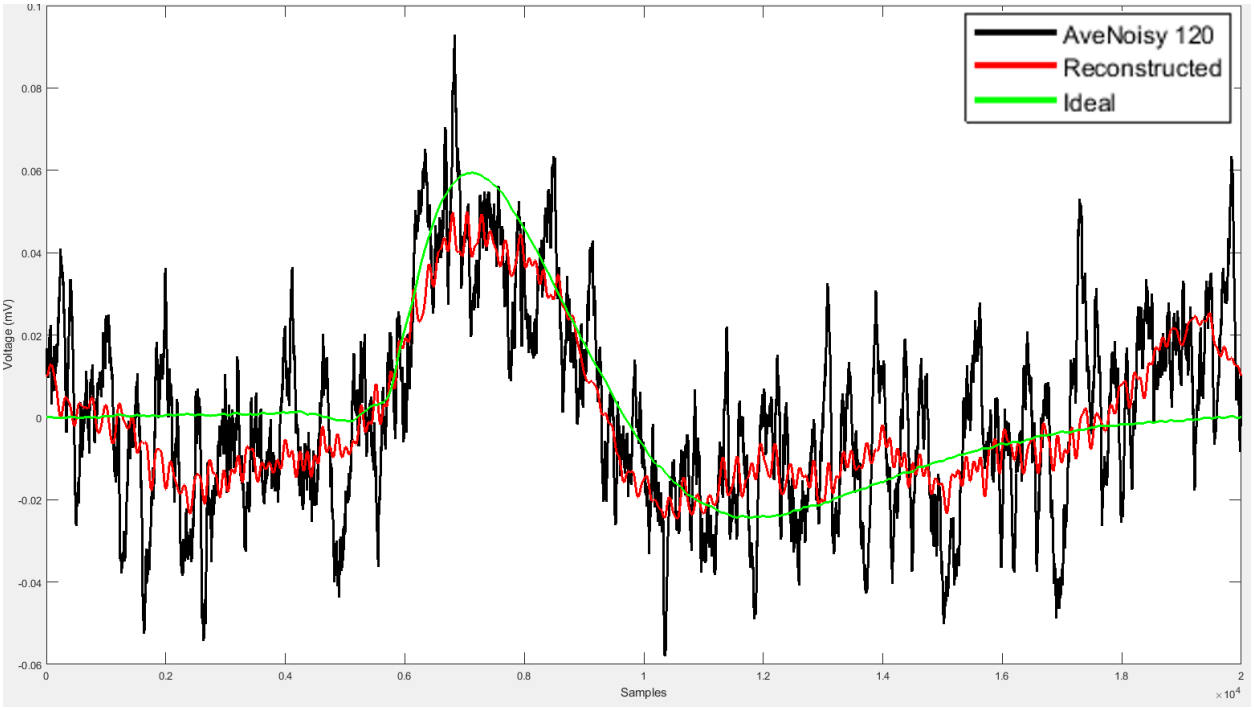

Figure 4.25. Time-domain representation of averaged noisy cycle (black trace), clean signal (green trace, for reference only) and the MSC re-constructed signal cycle (red trace) where only the significant (p-values at or below 0.05), frequency components below 350 Hz are considered to re-construct the signal.

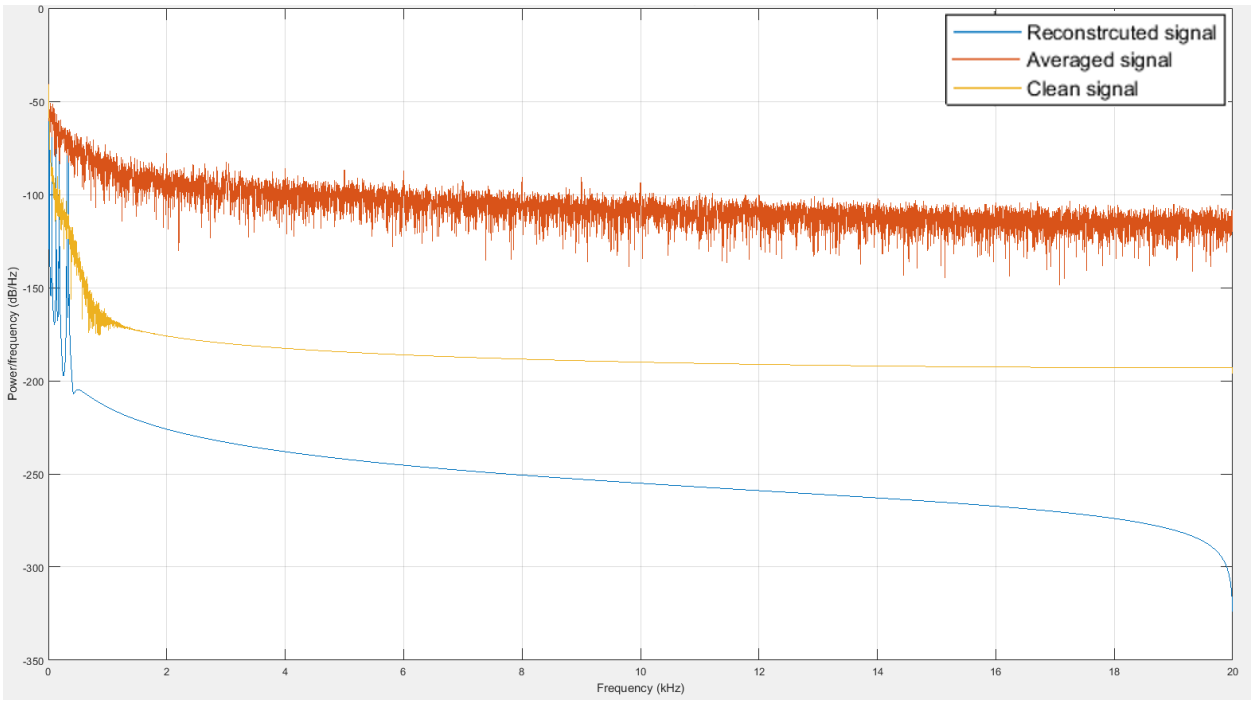

Figure 4.26. Frequency spectrum analysis of the averaged noisy data (brown trace), clean signal (yellow trace) and MSC re-constructed signal (blue trace), where only the significant (p-values at or below 0.05), frequency components below 350 Hz are used to reconstruct the signal.

The blue trace in the frequency spectrum (figures 4.26 and 4.27) demonstrates the reconstructed signal using the most significant frequency components at or below the low-pass corner frequency of 350 Hz (peaks at [2, 4, 6, 8, 10, 16, 22, 60, 132, 178, 186, 312, 316, 344] Hz) identified by the MSC algorithm when 240 cycles of noisy data are fed as the input to the algorithm. (The default filter corner frequency, significance assignment and frequency component selections are 350Hz, 0.05 and automatic, respectively.) The user of the MATLAB® GUI can manually set these parameters as required. The algorithm's output is all frequency components with an associated p-value. The peaks are those frequency components with p values of 0.05 or lower. To accurately plot the frequency spectrum using the MATLAB® built-in Pwelch function, a Kaiser window is applied, and frequency resolution is set to the length of one cycle of the signal (maximum resolution). A spectrogram of the reconstructed signal is illustrated in figures 4.28, where it is evident that most of the signal energy is in the lower frequency band (below 350 Hz), as expected. The spectrogram of the original clean cycle and the averaged cycle is also demonstrated for comparison purposes. (Note the range of the frequency spectrum when comparing these three figures).

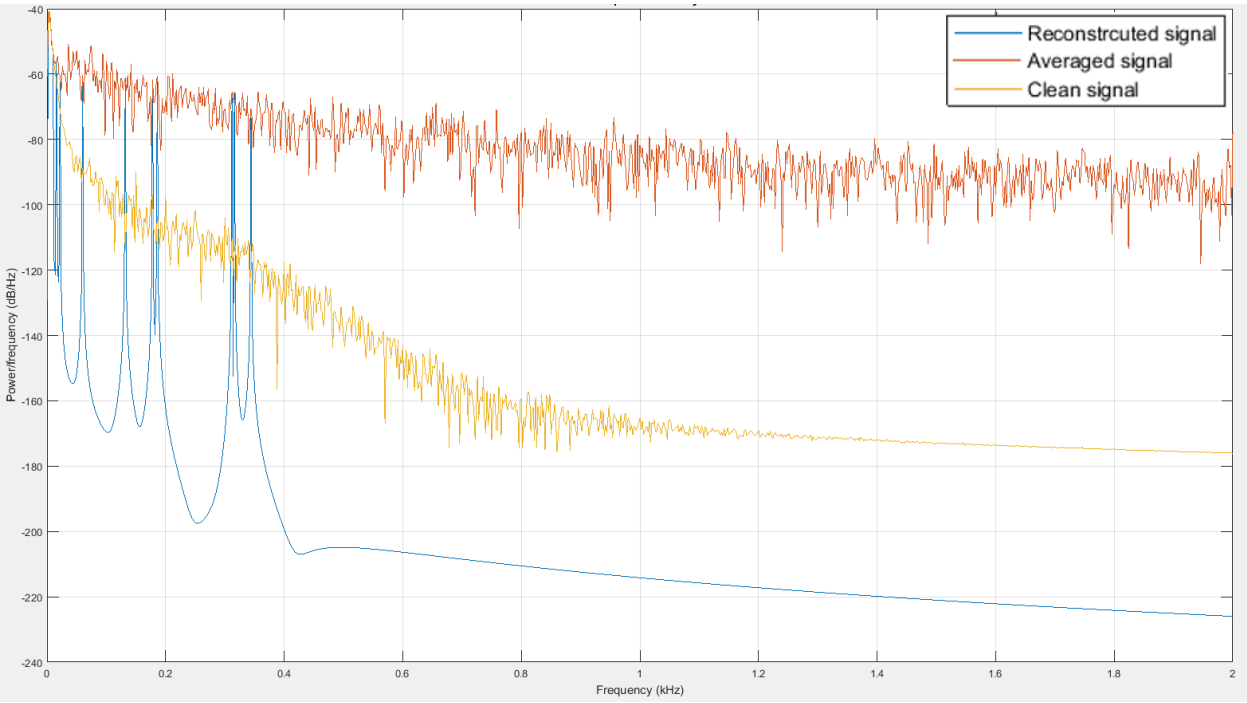

Figure 4.27. Frequency spectrum analysis (same as figure 5.26 with frequency limits set to 0-2kHz) of the averaged noisy data (brown trace), clean signal (yellow trace) and MSC re-constructed signal (blue trace), where only the significant (p-values at or below 0.05), frequency components below 350 Hz are considered to re-construct the signal based on the observed noisy waveform.

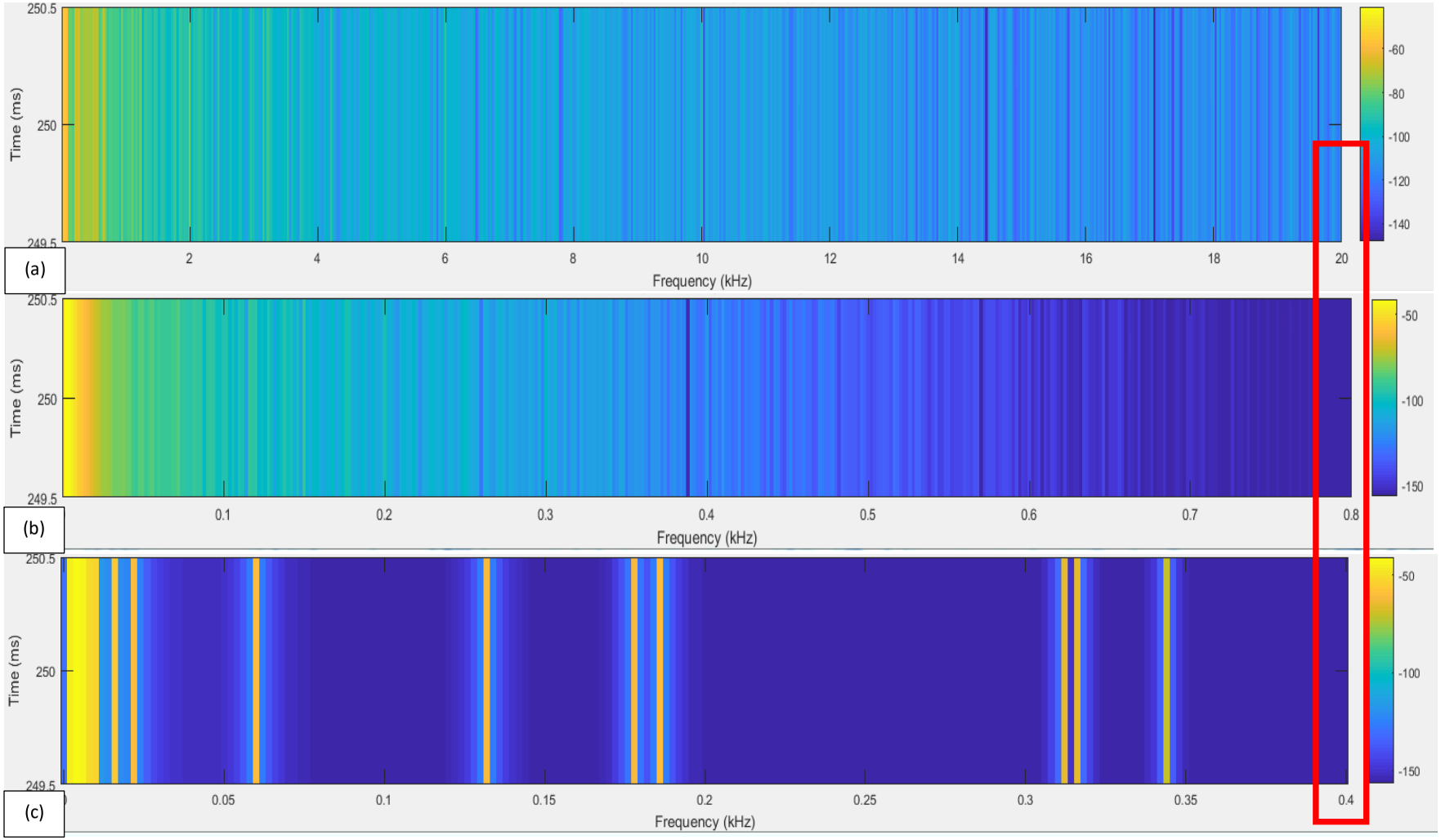

Figure 4.28. Frequency-time analysis. (a) Spectrogram of the averaged noisy signal. Presence of high-frequency noise components are clear compared to the clean signal and reconstructed signal spectrogram of (b) and (c) respectively. (b) Spectrogram of the original clean signal. It is evident that most of the energy of the signal is contained at low () below 45 Hz) frequency band. (c) Spectrogram of the reconstructed signal through identification of significant frequency components present in the noisy waveform using MSC algorithm and low-pass filtering. The bandwidth of the signal is smaller than 350 Hz, and as it can be seen there are distinct high-energy lines in the estimated, re-constructed signal.

4.2.6 Verification of clinical system (Roland RETIscan) artefact rejection algorithm

Post data collection, the author (with help from a trained clinical scientist) used the developed MATLAB® analysis GUI tool to visualise the collected signal epochs and remove contaminated cycles with biosignal artefacts such as blinks, eye movement and EMG. As explained previously, the bio-amplifier and associated software platform will reject artefacts with a large amplitude, as defined by a pre-set threshold, during data collection. This process is an online process although the user will have access to the full raw data recorded during the examination, which allows the manual removal of the artefacts including those that the automatic artefact rejection algorithm could not register as an artefact and therefore would have gone undetected. This manual process is superior compared to the automatic artefact rejection process as it also allows for rejection of contaminated cycles where the biosignal baseline is impacted due to artefacts occurring in previous periods. Therefore, the manual artefact rejection process avoids, as much as possible, problems in the frequency domain where the artefactual periods last longer than the discarded period where the artefact happened, but not causing the automatic rejection system to register it as an artefact.

Post manual artefact removal process; a windowing technique is implemented (such as a Tukey or Rectangular window in MATLAB) to smooth the epochs at both ends and ensure the epochs originate and return to the baseline before averaging and filtering. In the design of Liverpool bio amplifier system, both on-line and off-line artefact rejection processing is implemented having in mind that the off-line signal processing is performed on the recorded raw biosignal data (it is noted that the process of artefact removal and rejection is never perfect whether performed manually or automatically).

Working with the Kelvin Vision prototype amplifier (which was reliant on high-speed data streaming from amplifier to the host computer), provided an opportunity to understand other types of artefacts present beside the biosignal artefacts such as blinks. Timing artefacts may occur if the Operating System (OS) does not respond promptly to processing requests generated by the amplifier or is too busy servicing other tasks. At which point data losses (or as the developers of the Kelvin Vision amplifier Application Interface termed this, "*Missing Packets*") occurs, that can trigger the system's timing artefact rejection algorithm.

Both biosignal and timing artefacts can result in triggering the rejection algorithms and would require some sort of processing to recover from them. ISIM can simulate timing errors as described in section 4.2.10 so that the developers of signal processing algorithms and manufacturers of visual electrodiagnostic instruments can verify their solution accordingly. This section of the thesis will deal with biosignal artefacts.

iSim can be used to understand the biosignal artefact rejection algorithm for verification (test the system once against the manufacturer's specification) and validation (to ensure that the system will re-produce the same result if the same or similar input applied at different times) purposes. The test signals are generated by ISIM back-end mathematical engine where blinks, eye-movement and EMG artefacts are actual biological signal segments collected (and processed) from human subjects as part of the data collection phase (see figure 4.29).

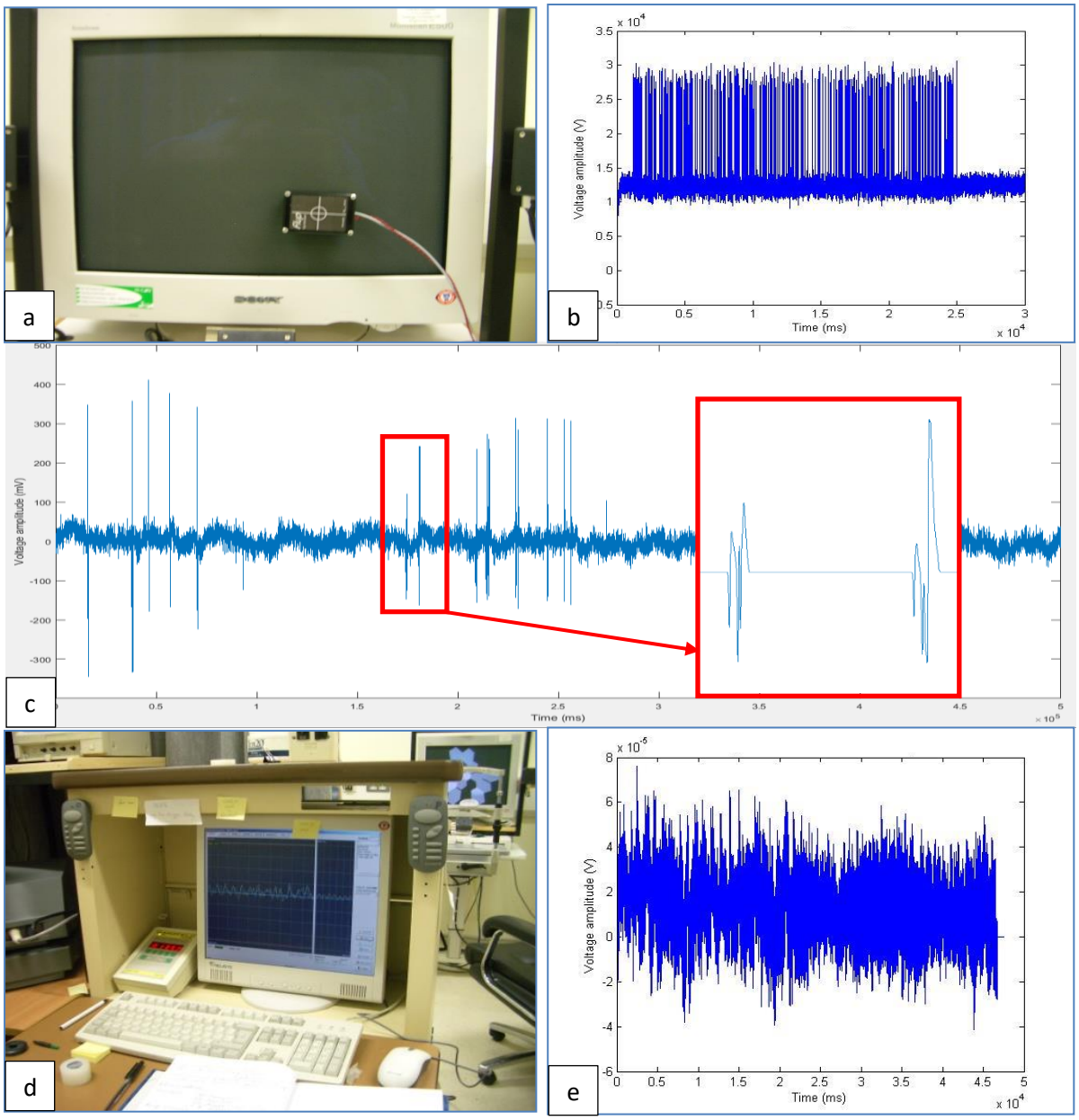

Figure 4.29. Roland RETISCAN artefact rejection ratio verification & m-sequence capture using iSim.

(a) Placement of photodiode (as part of initial development) on the Roland RETIscan CRT screen.
(b) Collected raw photodiode data as recorded on the Roland RETIscan system.
(c) Generated test signal (at – 20 dB SNR) at the sampling frequency of 1000 Hz with known locations of the injected artefacts) using ISIM with blinks and eye-movement to verify the Roland RETIscan artefact rejection algorithm.
(d) Roland RETIscan setup at RLUBH.
(e) Roland RETIscan "biofile". The raw data collected from Roland RETIscan system over the entire 511 steps of the governing m-sequence, with the blinks and eye-movements (artefacts), removed.

The Roland RETIscan CRT screen used, had a frame refresh rate of 60 Hz. The clinical setting of 5 frames per base-period gave 83 ms as the system base-period. From the specification, the ON frame is only white for approximately 1-2 ms, and the underpinning m-sequence length that drives the stimulus was 511 steps long. The Roland samples the signal at 1021 Hz. This signal was low pass filtered using a

second-order low pass Butterworth filter with the cut-off frequency of 25 Hz to get rid off as much high-frequency noise as possible. The test signal included some ARMA noise (-20 dB SNR) so that some features of the signal trace could be used to help visualise the duration of the biosignal that was ignored when recovering from the artefact. The recorded biosignal (post artefact rejection) was then re-sampled at 500 Hz. This re-sampling process would further reduce some high-frequency jitters. The best-fit line (in the least-squares sense) is subtracted from the data or remove any DC offsets. The recorded signal was normalised with respect to its standard deviation to compensate for differences in gain of the head-box preamplifier. The same signal processing was performed on the generated signal from ISIM so that comparison between the Roland processed signal and the input signal could be made (see figure 4.30 for an example of the input trace created using ISIM and processed through Roland RETIscan system).

Comparing the input waveform with the processed output (through Roland RETIscan system) does not require any synchronisation signal to align the two traces. This is the case as one has access to both the control and artefactual sequences. Also, the location where these sequences are captured from won't change the analysis and verification results as biosignal artefacts are picked up by the electrode that carries the summed, localised responses to the Roland preamplifier head-box.

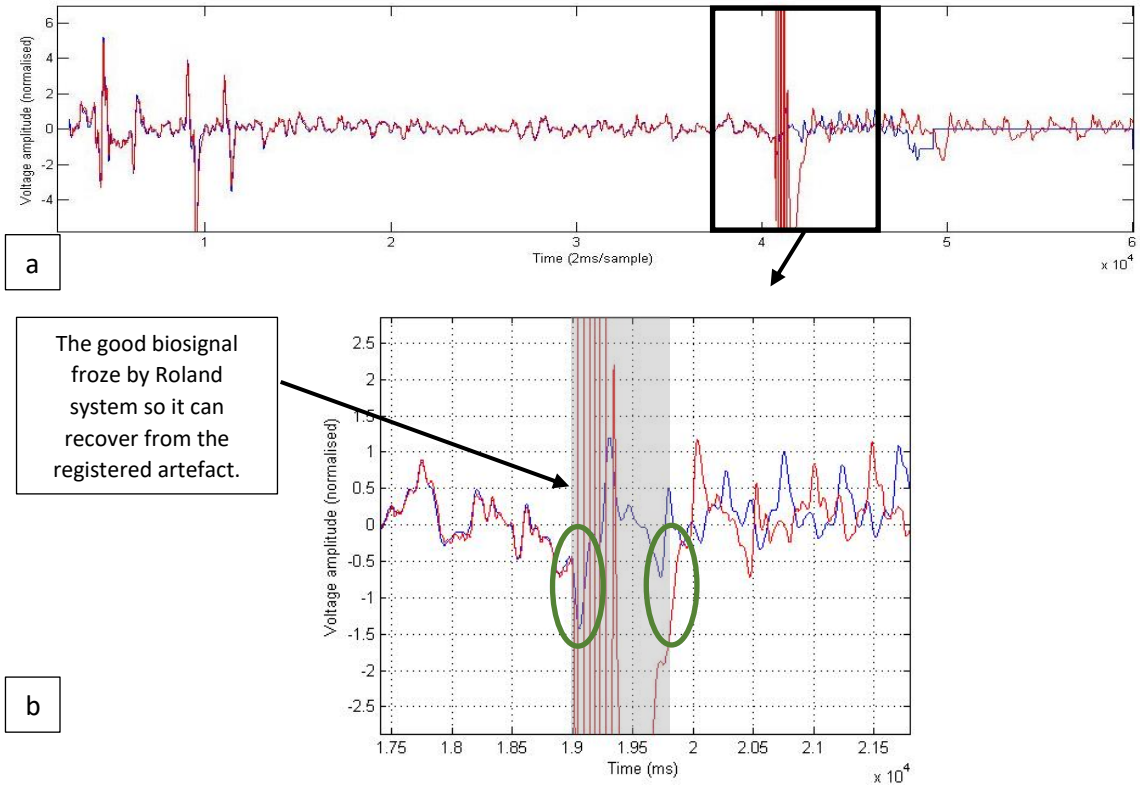

Figure 4.30. (a) a segment of data produced using ISIM contaminated with small and large amplitude artefacts. The Red trace is the input waveform into the Roland RETIscan preamplifier head-box. The blue trace is the processed biofile obtained from Roland. The first few small-amplitude artefacts are not recognised as artefacts by the automatic rejection algorithm of the Roland RETIscan system. The ample amplitude artefact at the end of the trace is registered as an artefact by the system. (b) The blue trace provides clues as to how the system has recovered from the artefact. That is the system has been off-line for approximately 0.5 seconds (greyed-out box), and the system has stitched the traces together to form a continuous signal with no artefacts. The way the two traces are stitched together can introduce artificial jump in the baseline of the signal and hence introduce unwanted artificial noise (this is illustrated using the green ovals where the traces are stitched together).

To examine the Roland RETIscan artefact rejection algorithm, the captured sequence data when artefacts present, and when there are no artefacts (control sequence) are compared. iSim is used to create the artefactual signals used to drive the inputs of the RETIscan amplifier and to capture the flash sequence using its optical input.

Section 3.2.3 described how iSim is used to verify if the captured sequence is a true m-sequence when no artefacts are present at the input of the clinical system. The same methodology is used to capture the sequence when artefacts are present, but without trying to verify if the captured sequence is, in fact, an m-sequence. The artifactual sequence will not be a true m-sequence if it passed through the algorithm in figure 3.8. It is easy to visualise the differences between the control and artefactual sequences through plotting the differential number of steps between flashes (as illustrated in figure 3.9.d for the control sequence). The plots will match precisely to the point that the system registers the first artefact. One can also see that the steps between the flashes in the artefactual sequence may not always correspond to an integer multiple of the base-period.

The duration of the sequence skipped back when it encountered an artefact can be verified, as illustrated in figure 4.31 and 4.32. For RETIscan system, this duration is not constant and depends on multiple factors.

Registered artefact-length is the period where the system is held off-line, the biosignal is frozen, and all stimulus patterns are turned off. As soon as the signal returns below the artefact threshold level, the number of steps to skip back is calculated. The system attempts to start the stimulation from the calculated point. Most artefacts are bi-phasic, so just before the system resumes normal operation, it may be interrupted again. The time difference between these interrupts could also impact how the system registers the artefacts, i.e. as a single or multiple artefact. It is observed that, if this time difference is less than 0.5 seconds, then the system sees this as a single artefact. Other factors that determine the number of steps that the Roland RETIscan skips back to recover from the registered artefact/s are:

1. Length of the previous step in the sequence when artefact occurred.
2. The number of sequentially encountered or more precisely registered artefacts.
3. The number of sequence steps between consecutive artefacts.

The recovery from the registered artefact/s, will, therefore, result in processed biosignal trace to lag the input trace by several steps (base-periods). The total steps lagged is the number of steps skipped back (approximately 0.5 seconds) plus those where the artefact is occurring.

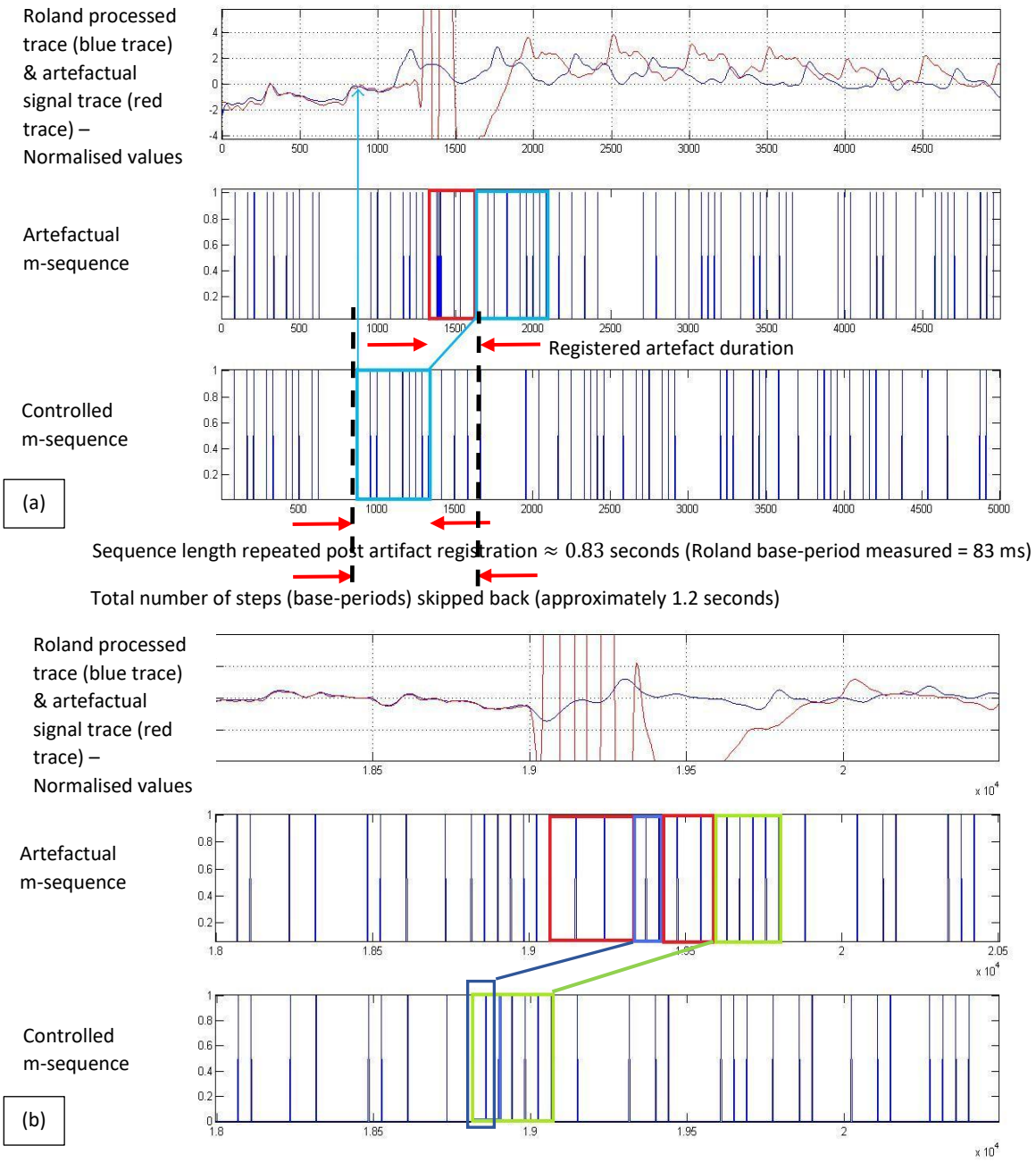

Figure 4.31. The highlighted red steps show periods where an artefact is occurring, blue steps (b) show where the stimulus was repeated but another artefact was encountered so the attempt was discarded. The green steps in the sequence show a second and successful attempt to recover from the artefact and continue through the remainder of the sequence steps. From this quick verification using iSim, it is evident that (without going into any further investigation) the number of steps to be skipped back is dependent upon several factors. These are the step that the sequence is currently running; the length of the preceding steps in the sequence; and the length of the artefact. Using iSim, the procedure (the clinical system under investigation) carries out to perform artefact rejection could be outlined (not further studied here). iSim can help to accurately and objectively determine this procedure with no impact (or change) to the clinical setup and minimal impact on the clinic hours.

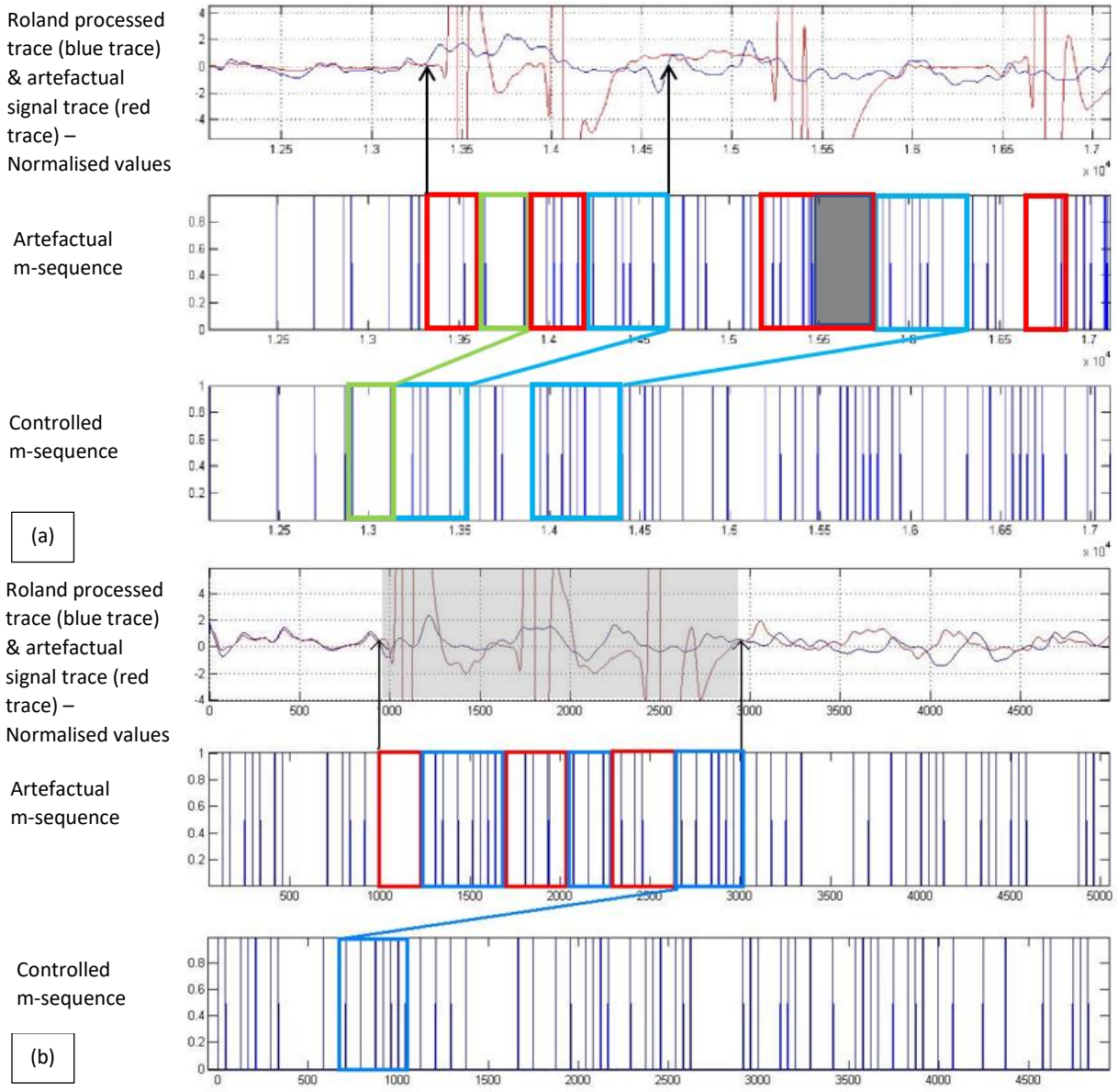

Figure 4.32. The highlighted red steps show periods where an artefact is occurring. The green highlight show where Roland RETIscan attempted a sequence skip back followed immediately by another artefact. The blue regions show a successful attempt to recover from artefact/s. (a) Illustrates the Roland artefact rejection algorithm in dealing with artefacts separated by greater than 0.5 seconds. The backout region in the plot of artefactual m-sequence shows where Roland RETIscan is stationary while the artefact returns toward the baseline. (b) Illustrates the behaviour of Roland RETIscan artefact rejection algorithm when dealing with artefacts separated by less than 0.5 seconds. The greyed-out region shows the recording segment of the signal ignored when Roland tries to recover from the three-consecutive artefacts. Careful examination of this figure shows how Roland stitches the signal segments to create the artefact-free trace (blue trace).

Since artefacts might occur in between the steps, the system will freeze the "good" biosignal and then tries to recover from it. For a number of data sets (single artefacts of length smaller than 300 ms) recorded using Roland RETIscan system, the length of the sequence that skipped back is calculated. This is performed after measuring the artefact length and the total length of the trace that was removed. This verified that the Roland RETIscan system would effectively remain stationary for as near to 0.5

seconds as it is possible. This is only an approximate as the number of sequence steps skipped back also depends on the preceding sequence step (see figure 4.31.a).

There is a delicate balance between the number of times that the sequence is allowed to skip back and the strategy in place on how to categorise a series of consecutive artefacts as a single artefact. This is a compromise between the overall examination duration and the amount of artificial noise added to the final processed biosignal trace. Every time the system, successfully skips back, it stitches two signal trace together, introducing jumps in the DC offset as illustrated in figure 4.30 and 4.33.

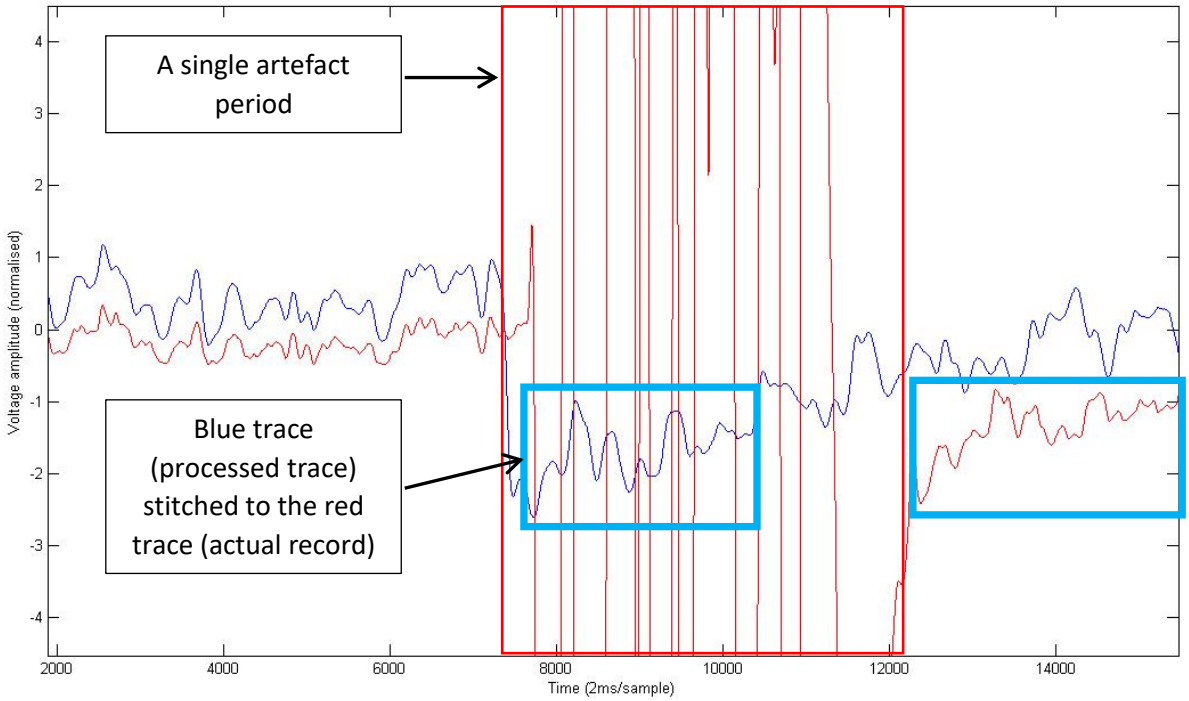

Figure 4.33. Illustrating stitching mechanics of the Roland RETIscan system to recover from the artefact. This has introduced a pronounced DC offset into the artefact-free trace (blue trace).

It was not an aim of this thesis, to define and investigate, how the system will stitch the signals and if it does perform any interpolation to avoid sharp edges in the time domain. Any potential stitching method must be carefully tested and verified as the data obtained in a base-period is specific to the particular ON/OFF pattern preceding it. Unlike the Roland system, the VERIS contains a proprietor artefact elimination scheme that finds and subtracts blinks and eye-movement artefacts. This is advantageous as the signal superimposed on the artefact is preserved only if the artefact does not exceed the amplifier and the analogue-to-digital converter dynamic range. VERIS[344] also implemented replacing the noisy signal segments with "*reliable alternate data*". It is not the aim of this thesis to discuss various methods and strategies for removing artefacts. The VERIS system is not investigated in this study; however, ISIM remains useable to check its artefact rejection algorithm through subtraction or use of alternative, reliable data segments.

4.2.7 Mains interference simulation & verification

Data from the UK national grid (measured frequency values) over a two-day period with one-minute resolution were analysed to obtain the statistics below (all measured using MATLAB®), see figure 4.34. See Appendix B for the original raw data representing the statistics below.

- Minimum value = 49.8220 Hz
- Maximum value = 50.2070 Hz
- Mean value = 49.9992 Hz
- Standard deviation = 0.0476 Hz
- Median = 49.9950 Hz
- Mode = 49.9700 Hz
- % of data below mean = 53.2
- % of data above mean = 46.8
- % of data outside [49.9, 50.1] = 3.0093
- % of data outside [49.95, 50.05] = 28.3
- Skewness = 0.2657
- Kurtosis = 3.1627

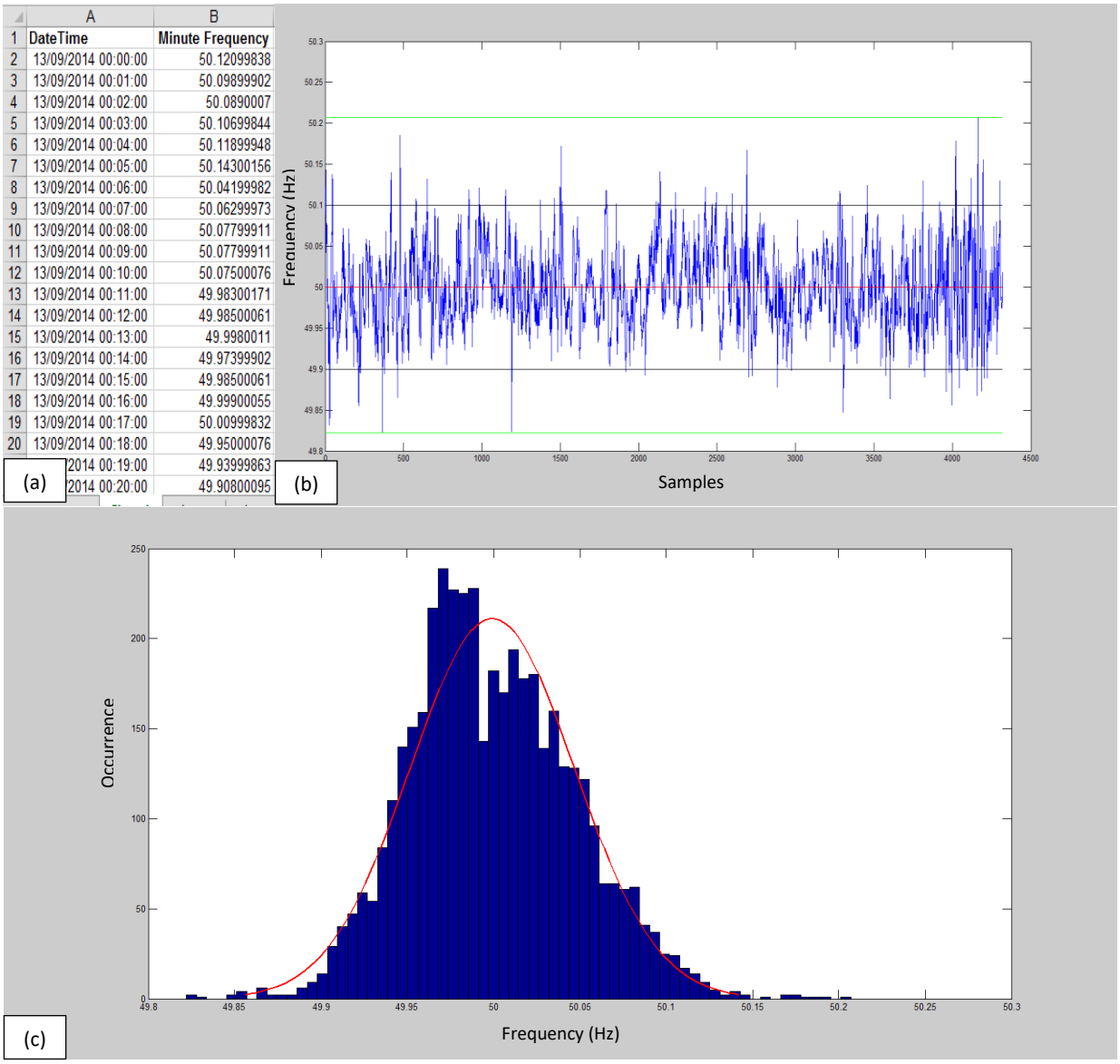

Figure 4.34. (a) Obtained UK National Grid generated mains supply frequency data over two consecutive days with a resolution of 1 minute. (b) The plot of a sample of the data from the population (a), in MATLAB®. The red horizontal line marks the 50 Hz, black horizontal lines mark the boundaries of [49.95, 50.05] Hz and the green horizontal lines mark the boundaries of [49.9, 50.1] Hz. (c) The histogram plot of the population data. The red fit is one for a normal distribution, where comparing this with that of the histogram of the data, one can see that the distribution is not normal.

The mains signal was recorded (see figure 3.23, for equipment setup) through a wall socket in the RLUBH eye clinic and sampled at 2000 Hz using a 12-bits MCC USB ADC (Measurement Computing Device USB-1208FS). The data was then migrated to MATLAB® and resampled to a frequency of 1 kHz for further analysis. The zero-crossing of the recorded waveform was calculated in MATLAB® to measure the recorded mains supply frequency against time. A histogram of the frequency variations (mains fundamental frequency component only) from cycle-to-cycle is shown in figure 4.35. The mean and median statistics of differential positive- and negative-slope zero-crossings were measured to be 40 ms, i.e. it is observed that approximately every 40 ms (or two cycles, assuming a fixed 50 Hz fundamental

frequency) the frequency of the recorded mains data is changing according to the measured distribution of figure 4.35.

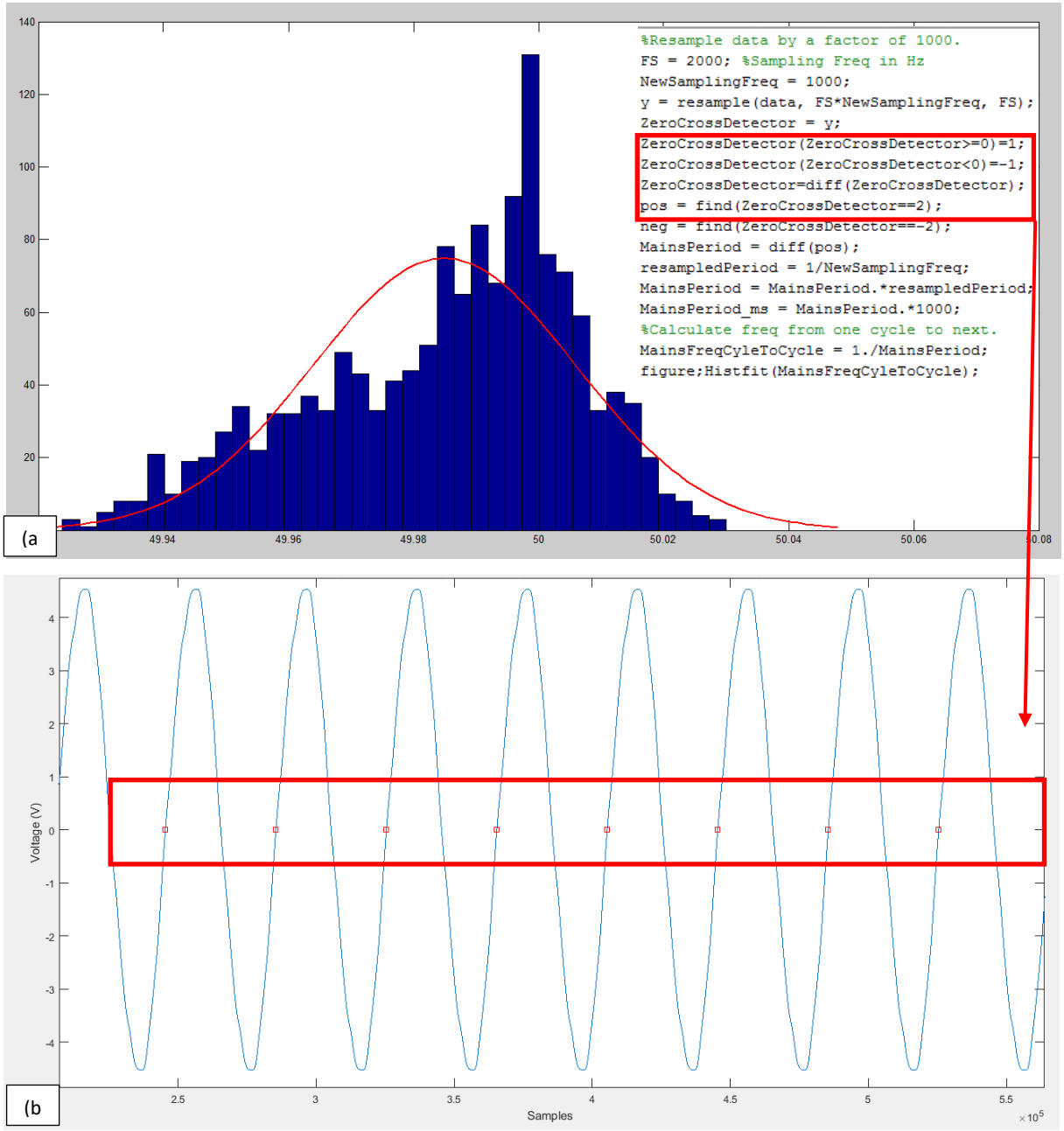

Figure 4.35. The recorded data is resampled first (1000 Hz) where the change in signal power (recorded mains data) due to resampling process was calculated to be three orders of magnitude lower than the total mains data power and hence insignificant. Next zero-crossings were measured per the MATLAB® script illustrated in this figure. The positive differential zero-crossing points are marked using the red square in (b). The frequency variation from cycle-to-cycle was then measured, and histogram of the result is plotted in (a).

To gain knowledge of harmonic distortion of the fundamental frequency component, the power spectral density function (PSD) was calculated in MATLAB® and plotted in figure 4.36.a, using a single 30 seconds data segment. The spectrogram of this data segment is also plotted in figure 4.36.b. It shows strong peaks at odd harmonics. This suggests that the harmonics may not be part of the mains signal recorded but due to some other nonlinear effects that are present. Such nonlinear effects can be due to attachment of a nonlinear load to the mains network at a nearby place. The analysis also demonstrates that most of the power is at low frequency (<100 Hz) with no DC component. Also, live feed showed that the mains record seems to be stationary at frequencies below 320 Hz. This makes it possible to simulate the mains frequency using our ARMA statistical package so that one can take into account any voltage-time-dependency.

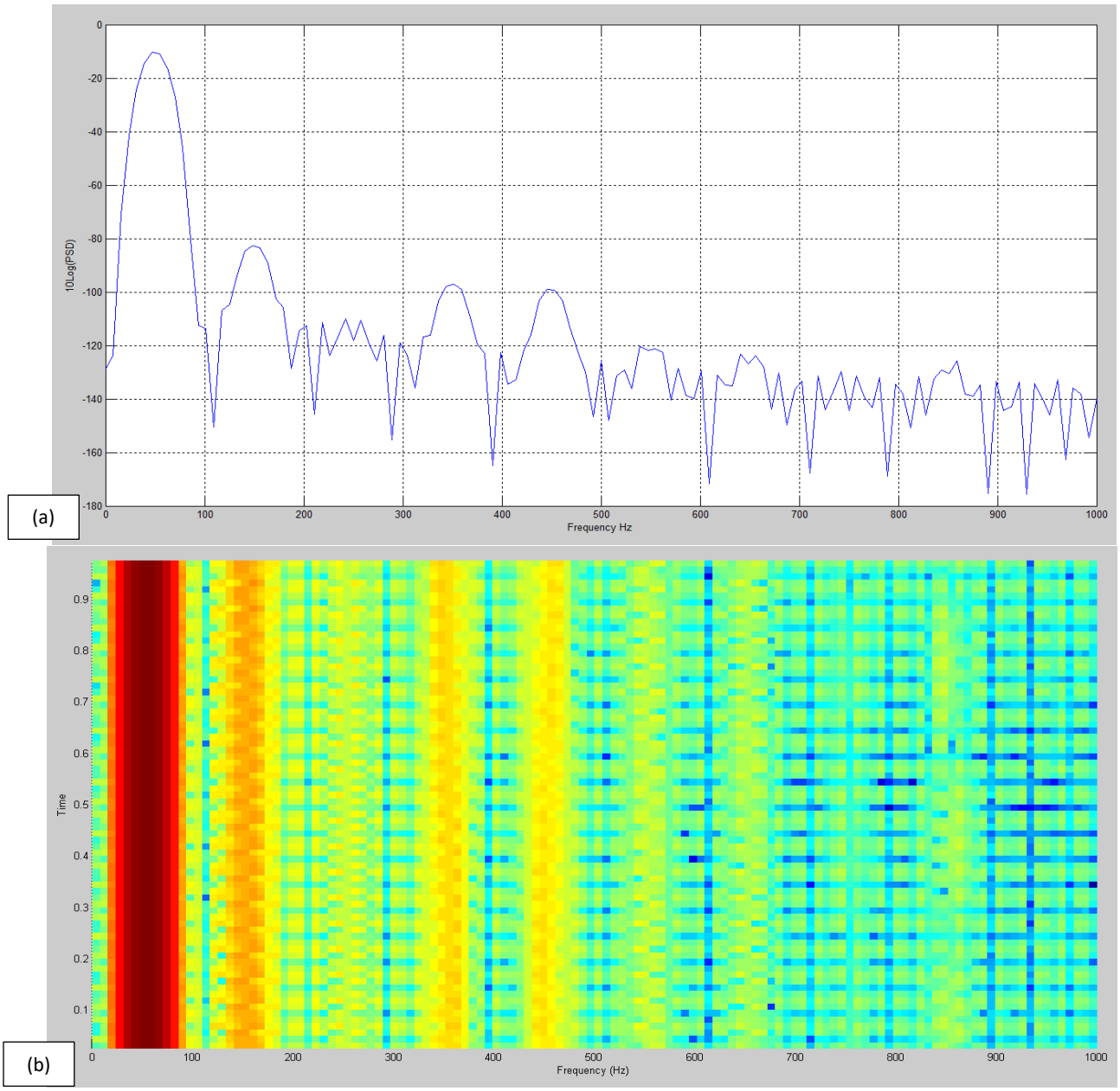

Figure 4.36. (a) Power spectral density (PSD) for collected mains supply data. (b) Respective spectrogram plot.

The power spectral density was modified by increasing the frequency resolution and using a Tukey window with lower side-lobe to capture all significant frequency components in the recorded mains supply data (see figure 4.37).

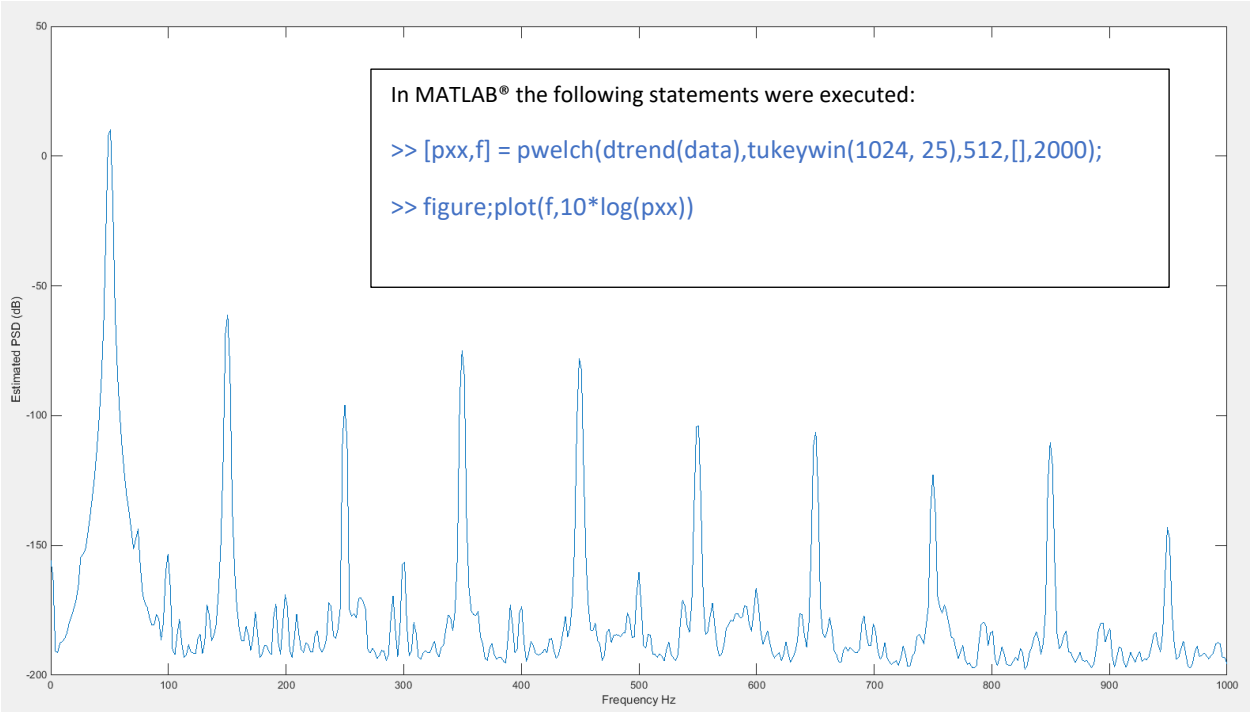

Figure 4.37. Power Spectral Density (PSD) for collected the main supply data, and the associated MATLAB® script for plotting it.

The modified periodogram shows a well-defined fundamental frequency component and its associated harmonics. The total harmonic distortion (THD) of the input signal which returns the ratio of the power of all harmonic content to the fundamental signal was measured to be -29.97 dB, which contributes to a strong vector of harmonics contaminating the mains fundamental frequency component. (The most significant harmonic is the third and is about 30 dB down from the fundamental. This is where most of the distortion is occurring). SNR and SIND (signal-to-noise and distortion ratios) are measured to be of magnitude 46 and 30 dB, respectively, and the calculated SIND and THD are similar. Most of the distortion is due to harmonic distortion in the recorded mains data with the 3rd harmonic being the most significant component (see figure 4.38 and figure 4.39).

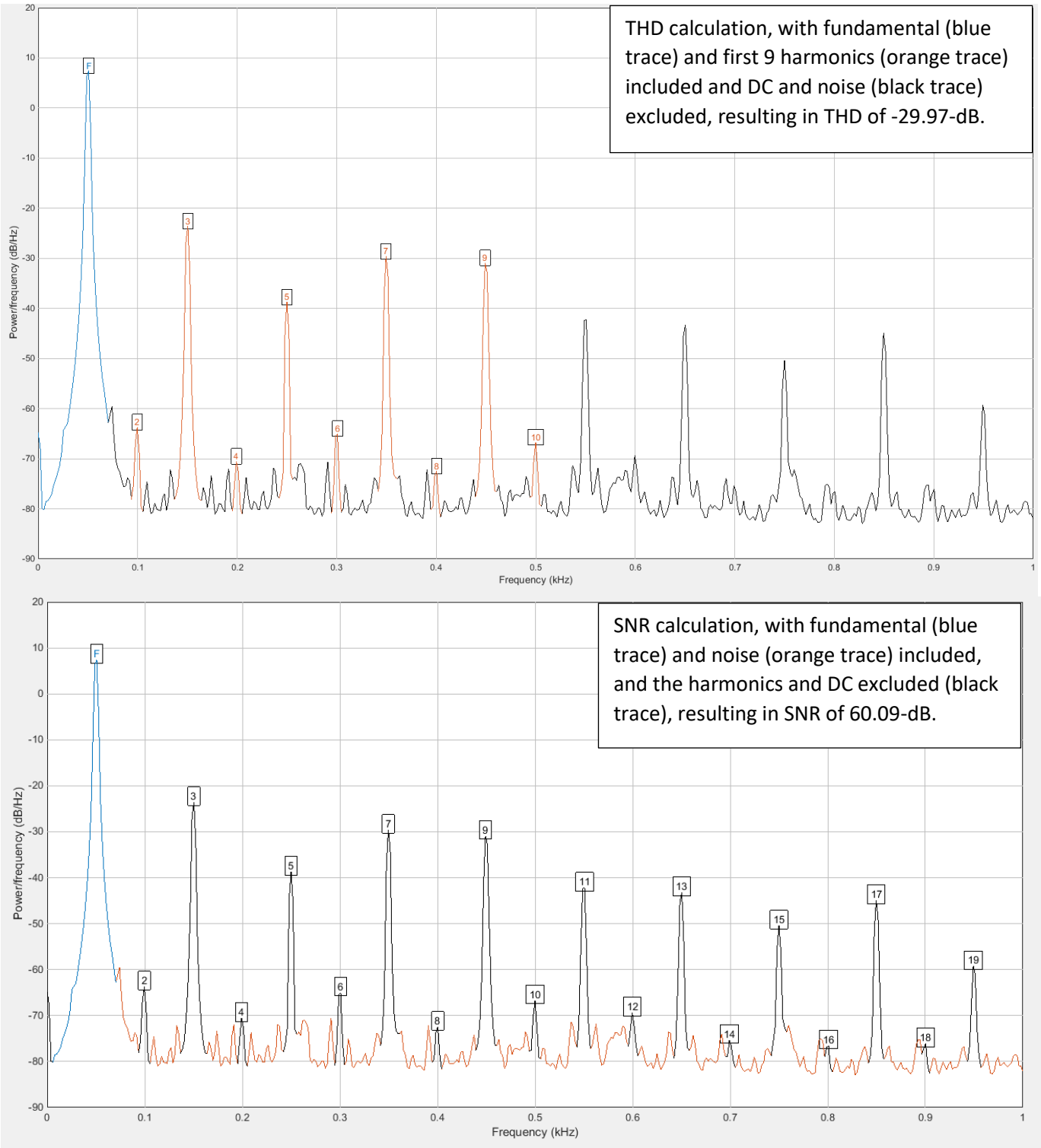

Figure 4.38. THD (top plot) and SNR calculation for collected mains supply data from the clinic wall socket, using MATLAB® PSD calculation.

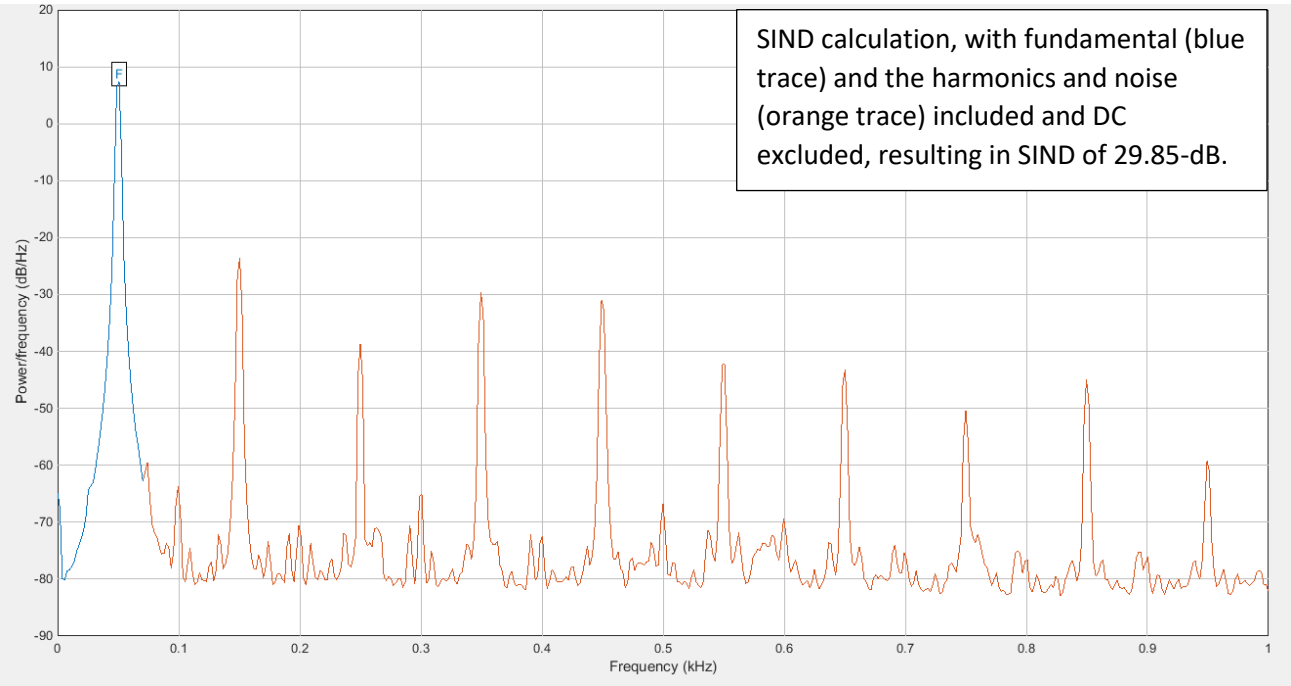

Figure 4.39. SIND calculation for collected mains supply data from the clinic wall socket, using MATLAB® PSD determination.

The most straightforward estimation of the mains interference is obtained by using a sine wave with a fixed fundamental frequency to generate the mains data with the user-specified duration and amplitude (see figure 4.40 for a representation of such a simulation using a 50 Hz fundamental component and the associated 1st and 2nd harmonics, having the same power as the fundamental frequency).

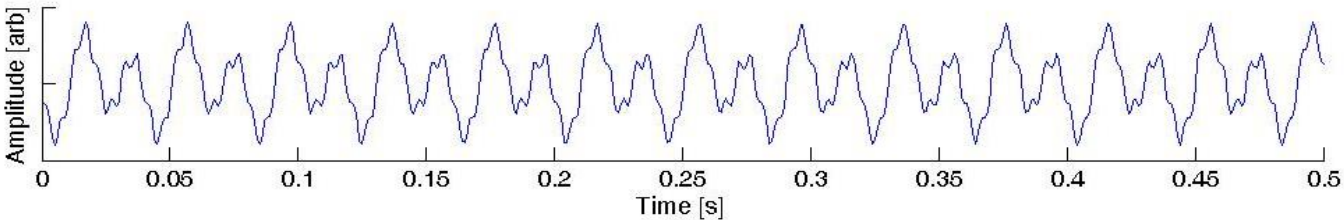

Figure 4.40. Mains supply interference estimation/modelling using a single 50 Hz and 1st and 2nd harmonics.

If one varies the frequency component of the sine wave, then a more realistic approximation to the mains interference signal could be made. A MATLAB® function was developed to generate a mains interference waveform, while allowing the fundamental frequency component of the signal to vary, based on values drawn at random from a specified distribution (vector of fundamental frequency components). The user can specify the required number of harmonics and the amplitude of the fundamental component. The amplitude of the associated harmonics can be specified as a percentage of the fundamental or, if not specified, adjusted automatically based on power ratio conversion to amplitude ratio as observed by the PSD illustrated in figure 4.36 (i.e. 30 dB converts to amplitude reduction by a factor of 31.62 for the first observed odd harmonics, and 70 dB converts to a reduction by a factor of 3162 for the first even harmonic). The mean, standard deviation, kurtosis and skewness are those measured from UK national grid data. In MATLAB®, the Pearsrnd function is used to generate a vector (m rows and one column) of numbers drawn from the normal distribution in the Pearson system with mean, `mu`, standard deviation, `sigma`, skewness, `skew`, and kurtosis, `kurt` (figure 4.38

shows the histogram of the generated frequency-time series where mu = 49.9992 Hz, sigma = 0.0476, skew = 0.2657, kurt = 3.1627 and the requested length of the frequency vector = 200). The function uses a normalised unit amplitude (in units of mV unless otherwise stated) for the fundamental component. The amplitude of the final waveform is user-defined through the available GUI. The function also takes another optional input that defines the duration of each fundamental frequency component before switching to the next component and so on. This optional input if left blank will be set to 40 ms (at a default sampling frequency of 1 kHz). To ensure no discontinuity when stitching together the various segments of the mains waveform, the function will calculate the phase of the segment at its end and will start the next segment from this point in time plus an overhead of $\frac{1}{sampling\ frequency\ (Hz)}\ ms$.

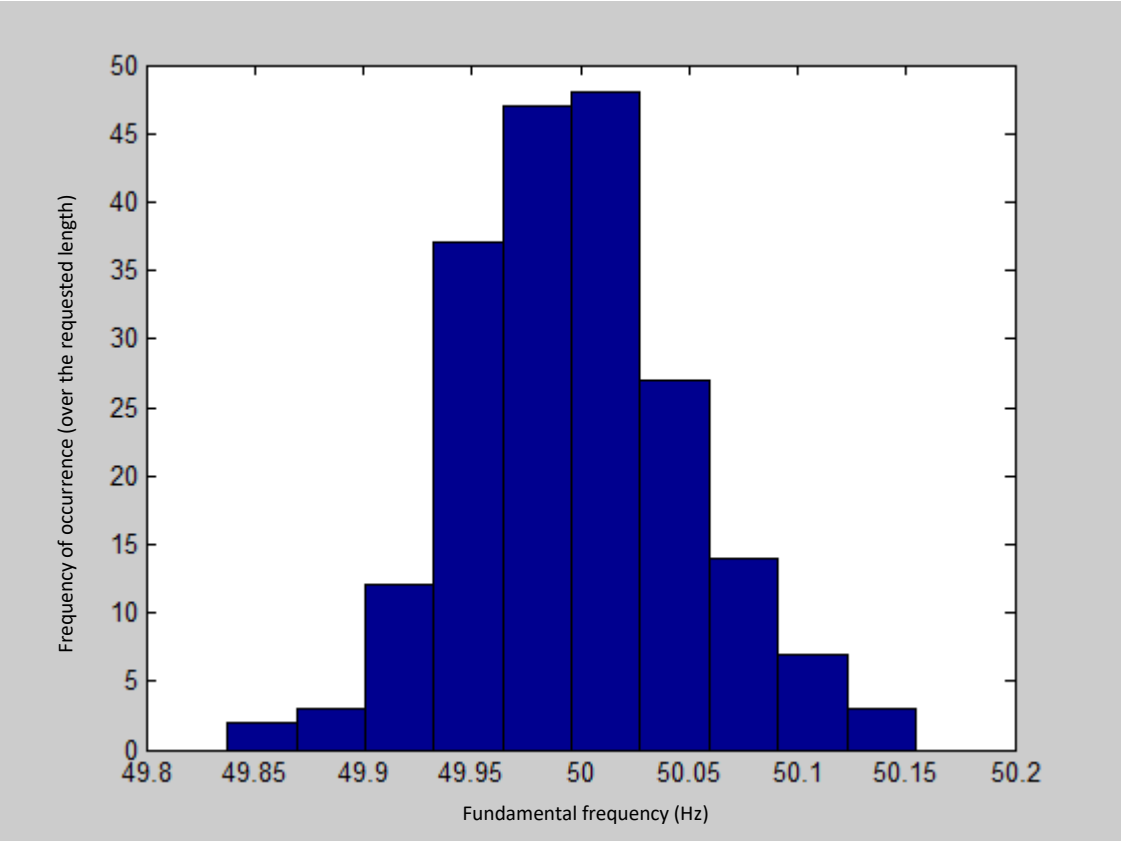

Figure 4.41. Histogram of the frequency data selected at random to be used for simulation of mains interference while varying the fundamental (and associated harmonics) frequency.

The result of one second of simulated mains interference in both the time and frequency domains is illustrated in figure 4.42, where a sampling frequency of 1 kHz is assumed. This simulation shows strong similarities with the interference data recorded from the mains wall socket at RLUBH eye clinic. The simulation (red trace) is generated using 25 fundamental frequency components selected at random from a distribution represented by the histogram data of fFigure 4.41. The frequency is allowed to switch between the individual components every 40 ms. The associated harmonics are integer multiples of the fundamental component and the highest order harmonic included in the simulation is the 8th harmonic. Individual cycles are next added together without any resampling or interpolation to avoid adding any unwanted low-frequency noise. Signal continuity was ensured to prevent any unwanted high-frequency noisy data to the simulation.

(a)

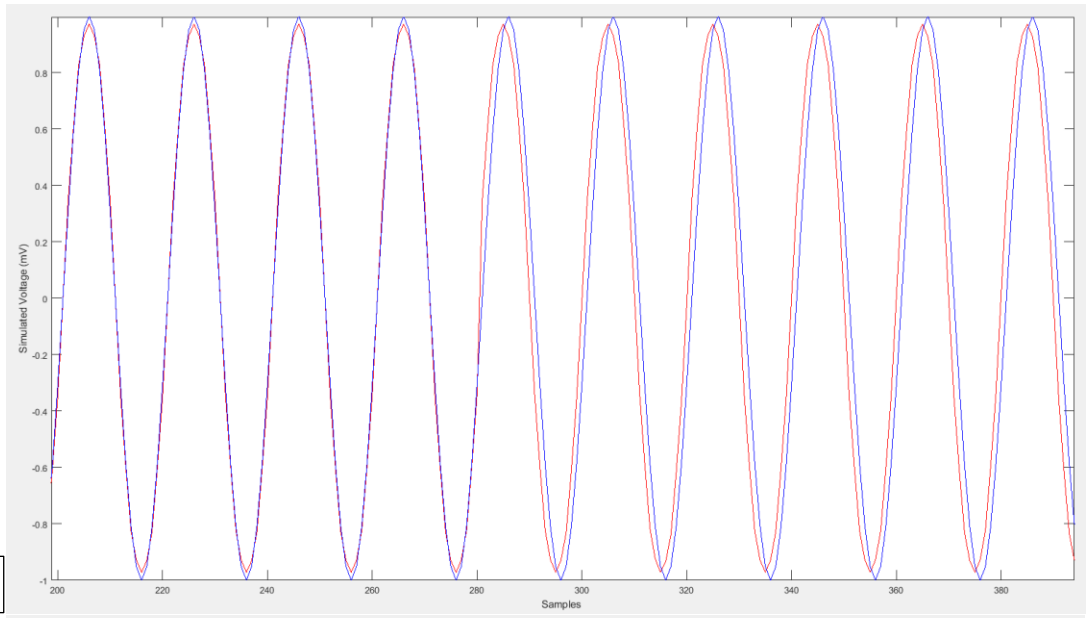

(b)

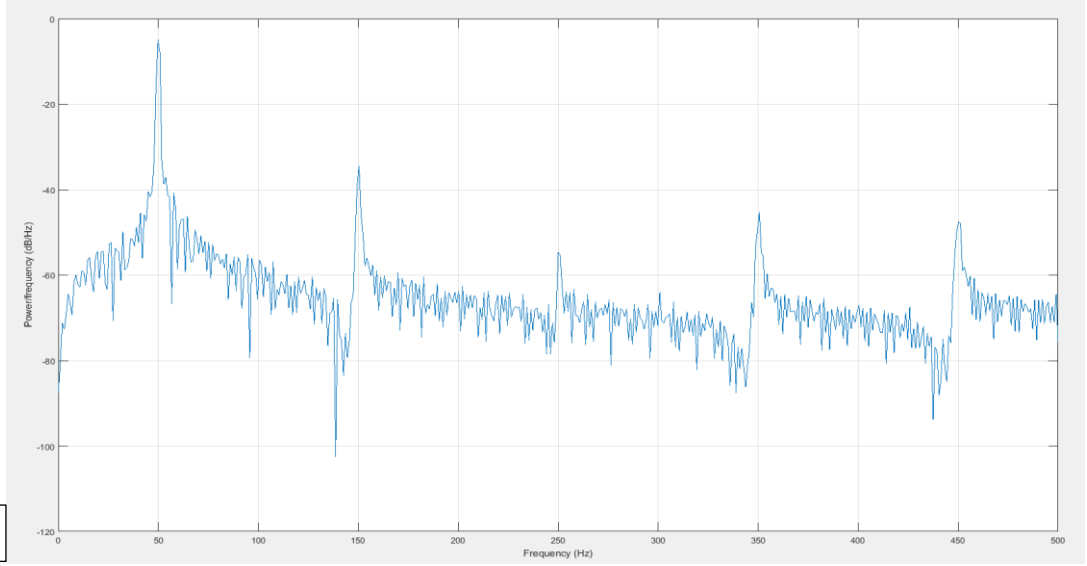

Figure 4.42. (a) time-domain plot of simulated mains interference (red) against a single 50 Hz component simulation (blue). The length of generated data is 1 second. Red trace contains the following fundamental frequency components and its associated harmonics:

[49.9236,50.0315,50.0181,49.9939,49.9772,50.0286,49.9134,50.0007,50.0885,49.9977,50.0421,50.0499,49.9822,50.0172, 50.0033,49.9551,49.9986,50.0300,49.9840,50.0261,49.9752,49.9751,50.016,50.0338,49.9780]

(b) illustrates the frequency domain representation of the simulated data.

The analysis to this point has not considered any time-dependencies between frequency data and has assumed that the frequency "vector" follows a normal distribution. A fixed interval between cycles with different fundamental frequency was assumed with a default value of 40 ms. It is shown that both the recorded data from RLUBH clinic and the data originating from the national grid show nonlinear behaviour and distortion. They also do not demonstrate a normal distribution, as illustrated in the normal probability plot of figure 4.43.

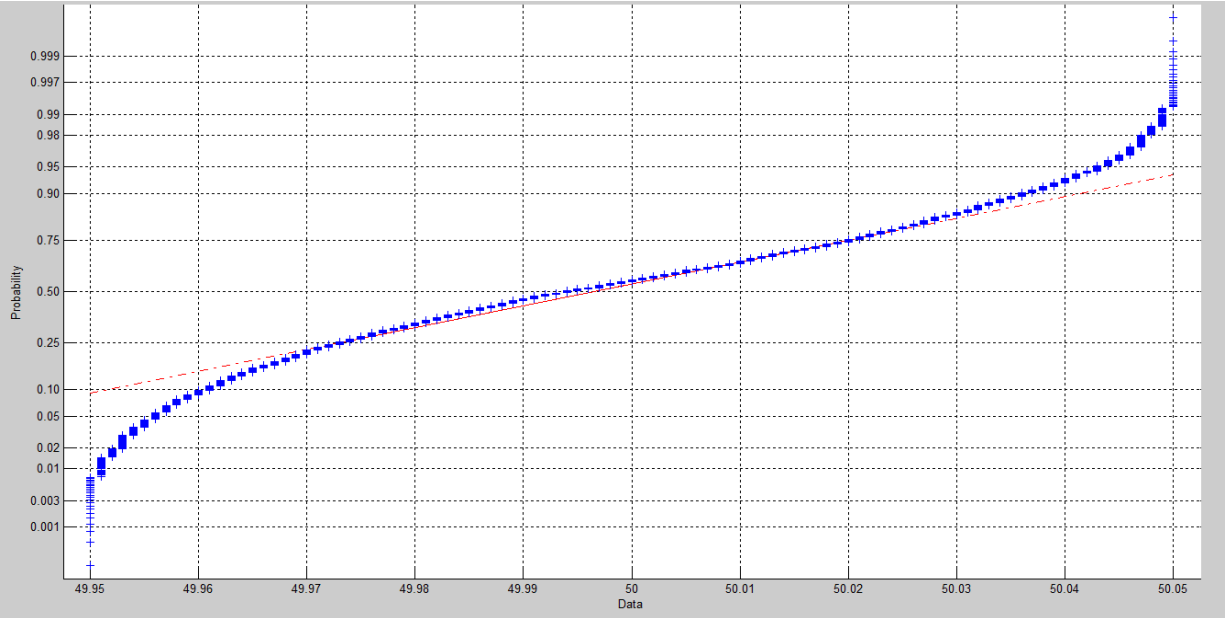

Figure 4.43. Normal probability plot of the frequency data supplied by the UK national grid (blue trace) against the normal probability plot of a theoretical normally distributed data (red trace).

An Auto-Regressive model (AR) was created to simulate the mains interference using the ARMA algorithm (Appendix A.5) based on the recorded data from the mains supply. Next, the frequency spectrum of the simulated data was plotted using MATLAB® for comparison with that of the measured frequency of the actual record. Results are shown in figure 4.44.

Based on the results of figure 4.41, the dynamic modelling of the mains interference is selected as the best approximation to simulate this noise component. The ISIM user is also provided with the mains data collected from the eye clinic at RLUBH with which to generate contamination of any requested ERG waveform. Such data can also easily be obtained at different centres and integrated into ISIM.

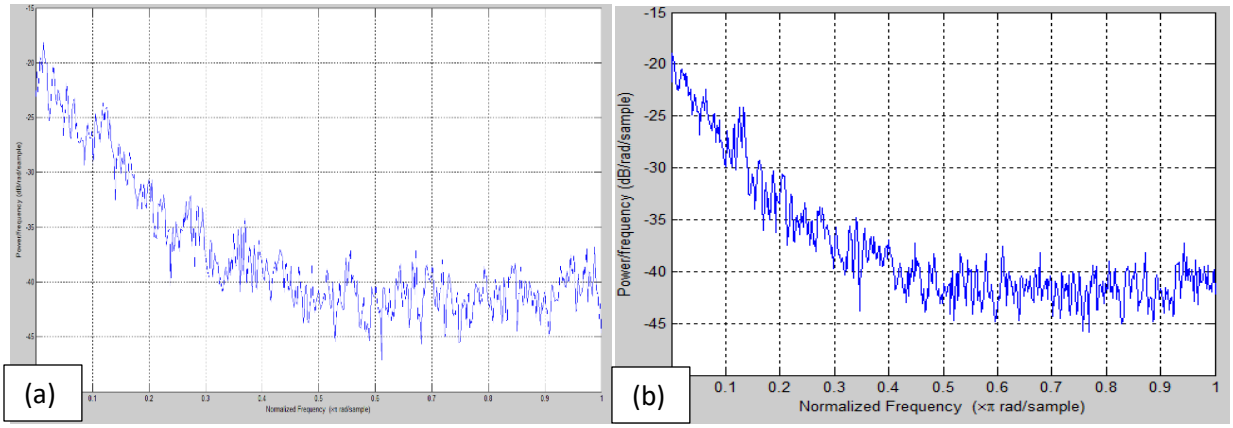

Figure 4.44. The frequency spectrum of the variations in mains frequency of the recorded data (a) against the ARMA simulated mains data frequency variations (b).

4.2.8 Simulating drift

Drift in measurements is simulated using a few lines of MATLAB® code to generate a random walk. The result is normalised within a range of ±1 V and finally multiplied by a factor of 5, avoiding saturation of the iSim internal amplifiers as well as the DAC, see figure 4.45.

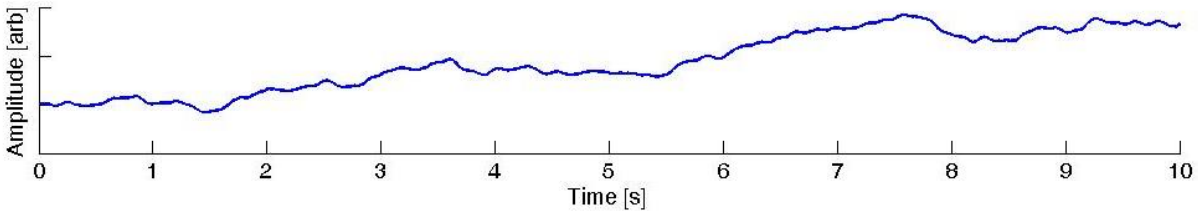

Figure 4.45. Illustrating of drift simulation.

4.2.9 ARMA noise simulation

ISIM can create white noise as well as other types of coloured noise, such as pink, Brownian and blue noise to contaminate the generated signal waveform, see figure 4.46. Different types of coloured noise can be generated at the user's request, such as violet noise, which is also known as differentiated white noise, and finally, grey noise. Visual inspection of coloured noise signals in the time, or frequency domains demonstrate the differences in the nature of the noise. It is also possible to listen to noise and distinguish between different combinations and types of noise encountered when measuring, collecting or estimating the ERG noise signal.

More accurate simulation of noise was performed using the auto-regressive moving average (ARMA) algorithm. Each subject was prepared for noise collection as per the outlined experimental design in chapter 3. With the help of an experienced visual electro-diagnostic clinical scientist, sections of each record with no EMG, eye-movement or blinks were selected and used as input to estimate the subject-specific ARMA filter coefficients. These coefficients were then incorporated into the ISIM library as MATLAB® structures (saved as *.mat* files at the backend server) to generate noise data based on the requested SNR and the required data-length. The frequency spectrum of the estimated noise was then

compared with that of the actual data. Figure 4.47 shows results obtained from one normal subject with no known eye condition. The frequency spectrum shows higher power per frequency at low frequency (below 40 Hz) bands and spikes at 50 Hz, and the associated odd harmonics up to the 9^{th} harmonic (sampling frequency is 1 kHz). The spike locations are matched with the obtained mains data collected from the wall socket at the clinic room, clearly demonstrating that mains interference has induced components in the data. The simulated data also illustrates that both the low-frequency components of the noisy data and the induced mains interference are reproducible using the ARMA model.

Using this data, it is possible to measure the stray capacitance that exists between the subject's body and earth (C_{body} in figure 3.26.b). Assuming that the decoupling capacitance between the subject's body and the power lines (C_{pow} in figure 3.26.b) is a typical value of 3 pF provides a displacement current (i_1 in figure 3.26.b) of approximately 0.2 μA that flows through the body and C_{body} to earth. This causes a potential drop across this impedance that would appear on the electrode leads as a common-mode voltage signal. Note that, due to the patient and amplifier setup and its design, the i_2 current in figure 3.26.b is assumed to be 0 – see section 3.6. Figure 3.26 does not reflect the electrode setup for ERG recording and is one for ECG recording; however, the principles are similar for a generic bio-potential amplifier. The measured power of the 50 Hz component is approximately 20 dB above the noise level with RMS (Root Mean Square) value of approximately 6.5 mV. From the measured CMRR of 120 dB for the amplifier, this means 64.2 V_{rms} will appear on the subject's body as common-mode voltage. This is the voltage drop across Cbody with a displacement current of 0.2 μA. The capacitance of C_{body} is now calculated to be approximately 10 pF at the fundamental frequency of 50 Hz for subject 1. This stray capacitance was estimated to be the same for all other subjects under the experimental conditions specified in section 3.6. This is expected as the body size of all subjects was roughly the same, and the amount of clothing/insulation was also similar.

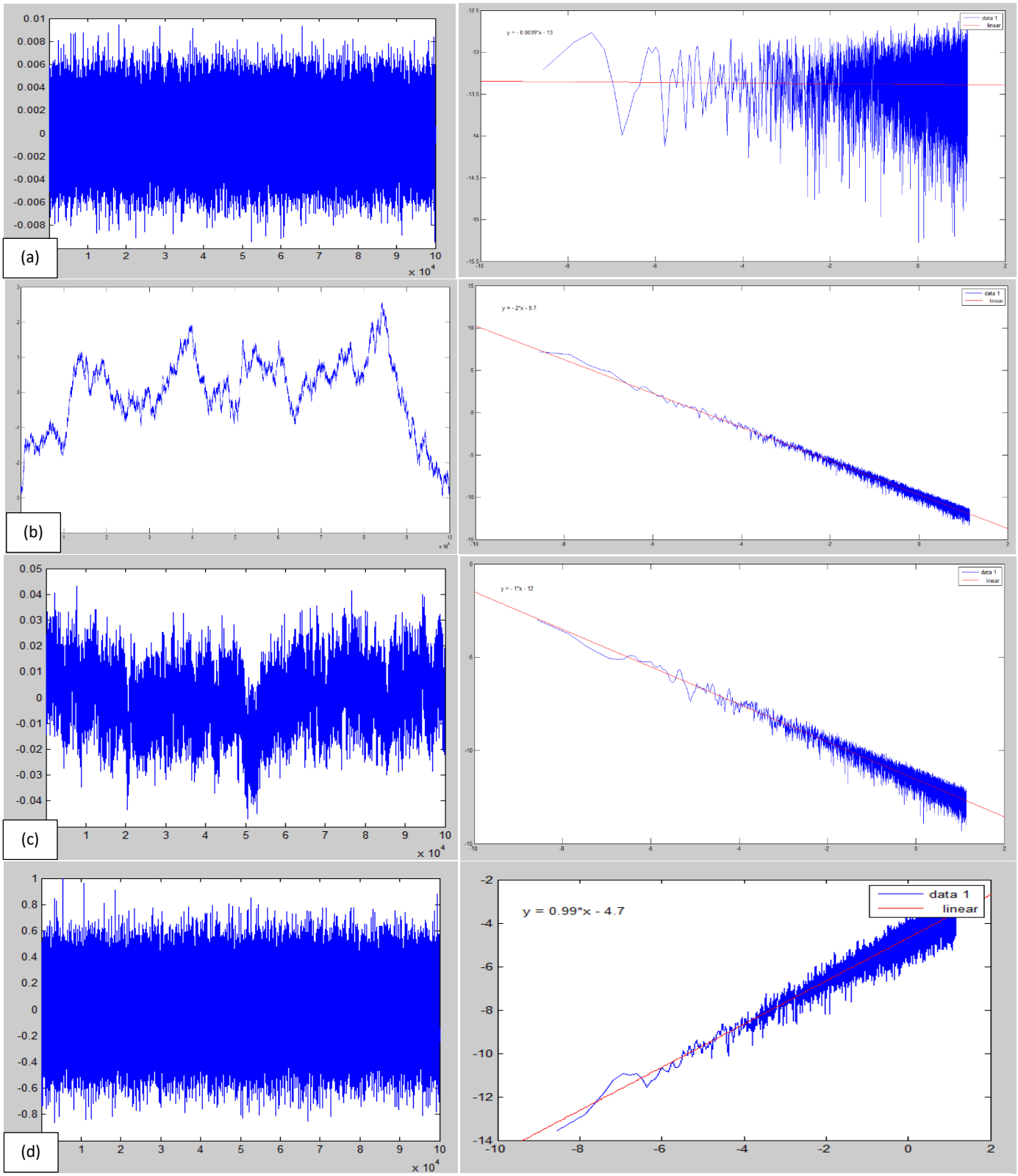

Figure 4.46. Illustrating plots of some of the generated coloured noise in both time-domain (plots in the left-hand column) and frequency-domain (plots in the right-hand column). Time-domain plots are arbitrary amplitudes against the requested number of samples. The frequency-domain plots are those obtained through application of the Pwelch function in MATLAB® (Log-Log plots). (a) white noise. (b) Brownian noise. (c) pink noise. (d) blue noise.

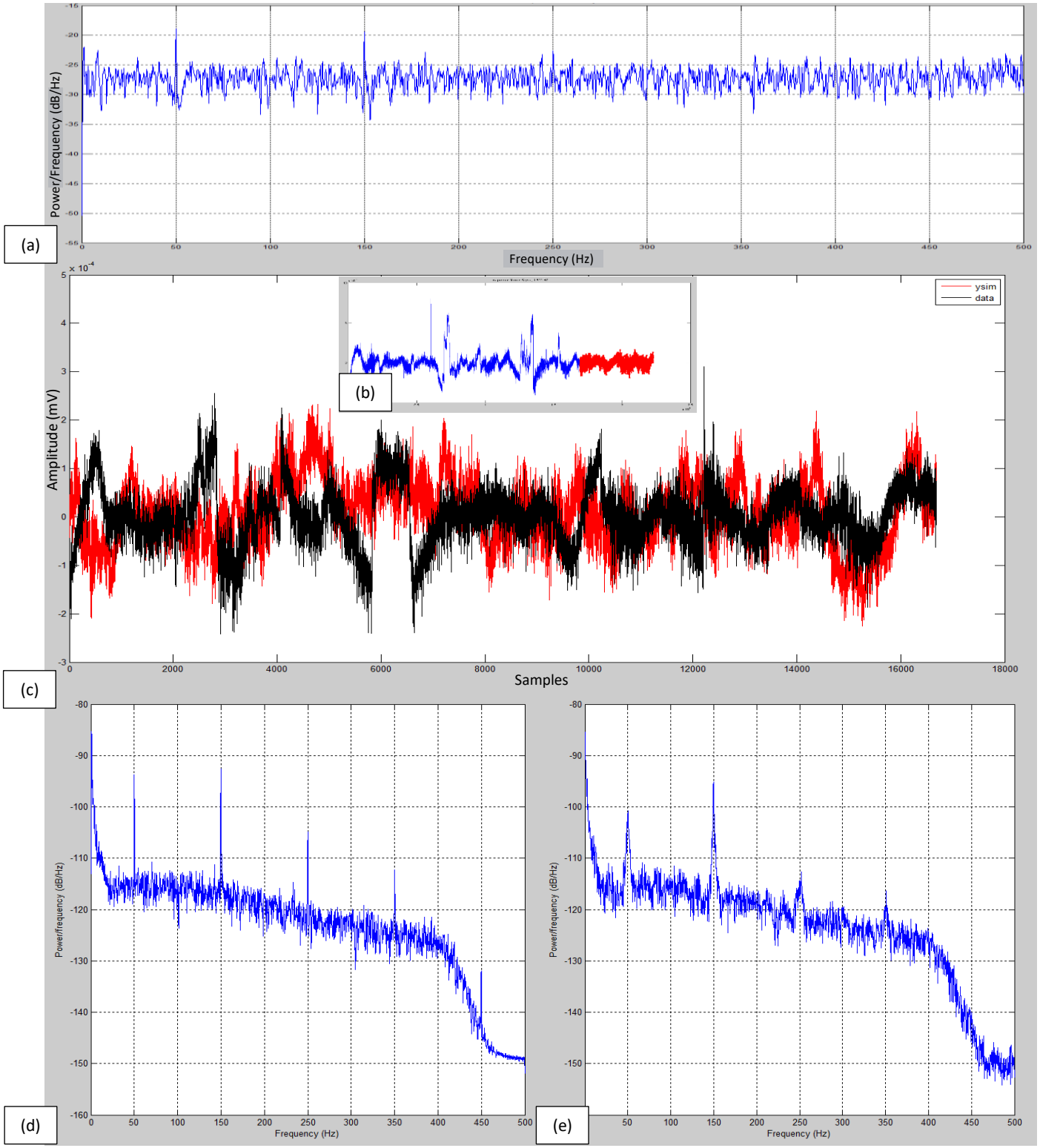

Figure 4.47. (a) Frequency spectrum of the noise data triggering the filter to generate the recorded data segment. This resembles the spectrum for white noise. (b) Original noise record collected at a Nyquist frequency of 500 Hz, using Liverpool bio-amplifier & thread electrode on subject's right eye with no flash stimulus present and no background light. A section of this record (red brushed area) is selected with no blinks, EMG or eye-movements, to be used for ARMA filter coefficient estimation (filter order is 200 for this subject). (c) Black trace: Selected region of the voltage record in (a), Red trace: simulated data using the subject's ARMA filter. (d) Frequency-power spectrum of the selected region. (e) Frequency-power spectrum of the simulated data (red waveform in ((c)).

4.2.10 Other types of artificial noise/errors simulation

ISIM allows for the generation of other kinds of noise, such as that due to non-uniform sampling frequency and the presence of discontinuities. These types of error data is typically used to test and develop novel statistical signal processing packages, which areused for dealing with such errors in the measuring system. Figure 4.48 demonstrates a sample of a pattern electroretinogram (PERG) waveform (simulated at a sampling frequency of 1 kHz) sampled non-uniformly (blue trace) against the same length of the waveform that is uniformly sampled.

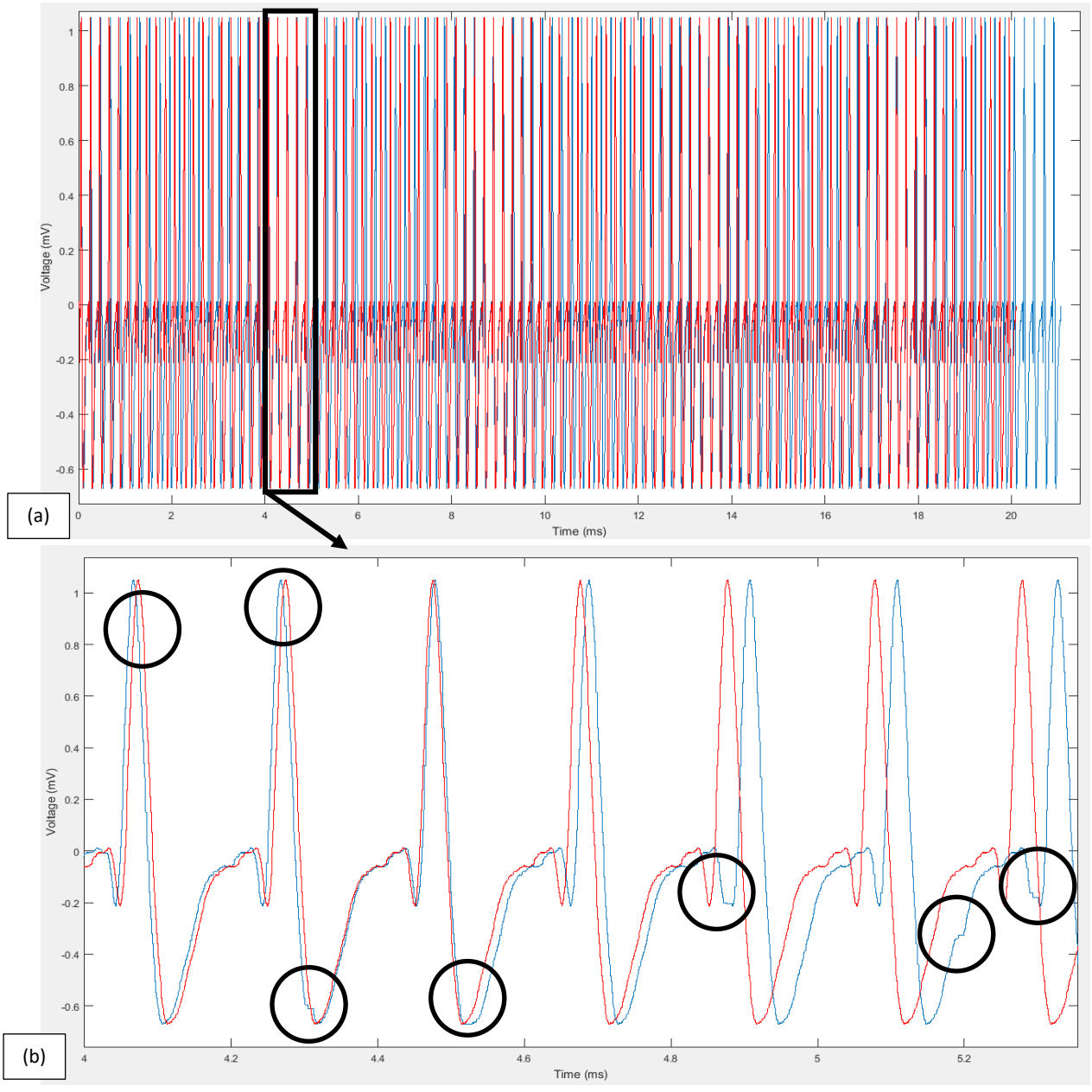

Figure 4.48. Illustration of nonuniform sampling period using ISIM waveform generation toolset. (a) Red trace is the clean waveform for reference and blue trace is the same waveform as in (a) with introduced nonuniform sampling intervals. (b) The black circles show points in in the waveform where the error is introduced.

Simulating frequency leakage through introducing discontinuities at either end of one cycle of the signal waveform (via switching off the window operation when preparing the signal file) and missing signal samples (see figure 4.49) are two methods that are used to simulate discontinuity errors in the prepared file. In MATLAB®, a random section of data of a user-specified length is replaced by NaNs (Not a Number) to simulate missing packets or data.

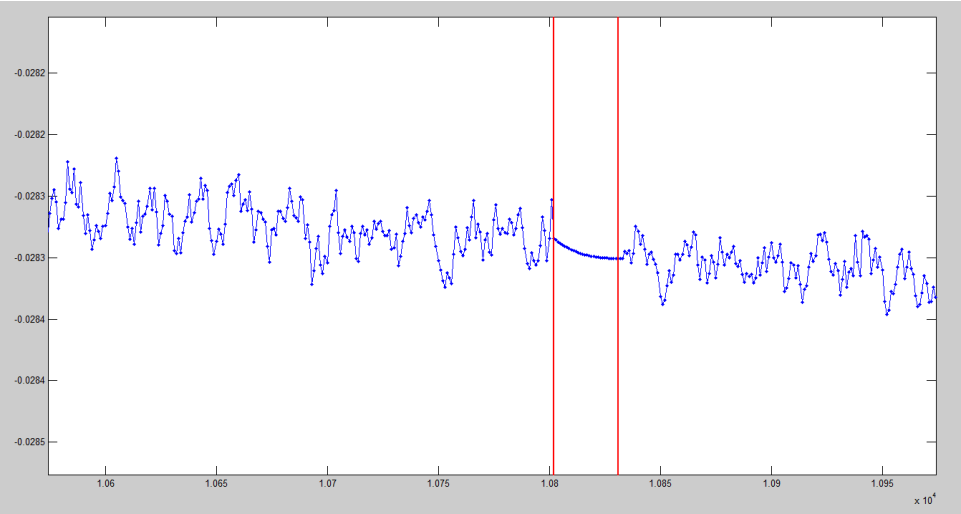

Figure 4.49. A record of simulated ERG response (photopic) contaminated with noise and simulated missing samples or packets of information as illustrated by the region enclosed by vertical red lines.

4.3 ERG Excel® GUI (Liverpool ERG Simulator)

The Excel® interface is available to download from the Liverpool MPCE server and can be used as a stand-alone application or can be instantiated from within the ISIM GUI. The interface is the same as far as a user is concerned. It is available for download for use with a 32- or 64-bit Windows Operating System. Once the file is downloaded and opened, it prompts the client to configure its setting to communicate with a remote or locally installed MatSOAP© server, requests the type of communication (Synchronous or Asynchronous operation) and an email address to serve as a unique identifier (client ID), see Appendix B.

The client ID (Identification Number) is used to organise all generated files at the server-end into the client's folder and as such avoids any cross-client-communication as demonstrated in Appendix B. A user's data is initially stored in one centralised folder location called temp_folder to avoid server cluttering. Once the MATLAB® engine is finished with waveform synthesis, the output files are stored in the user-specific folders. These files include JPEG, MAT, CSV and TEXT files which are made available for download having assigned a session-specific file ID name. Other files are created and deleted accordingly during run-time and are for the use of the engine only.

The Liverpool ERG simulator (the client Excel® GUI) is illustrated in Appendix B, where most of the MATLAB® engine functionality is exposed to the clients when using ISIM to generate a waveform. The interface was tested and verified to ensure there were no faults with individual operations on both synchronous and asynchronous communications. Examples of the generated waveforms based on specific user requirements are shown in figures 4.50 and 4.51 and 4.52.

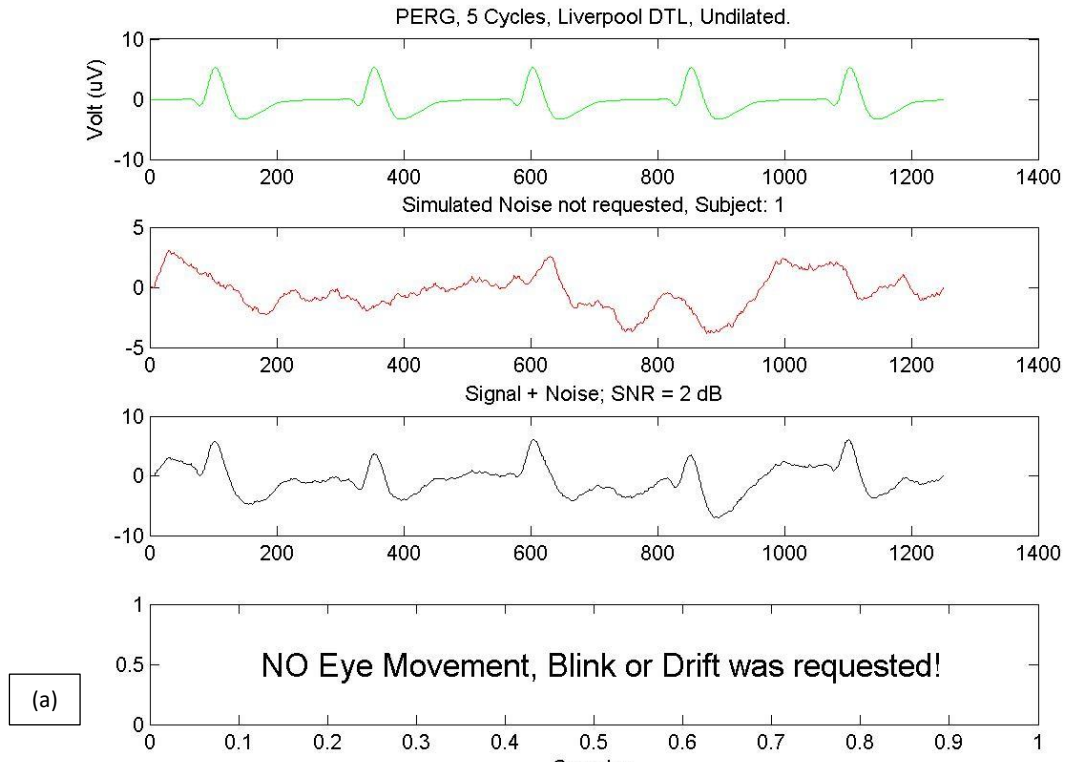

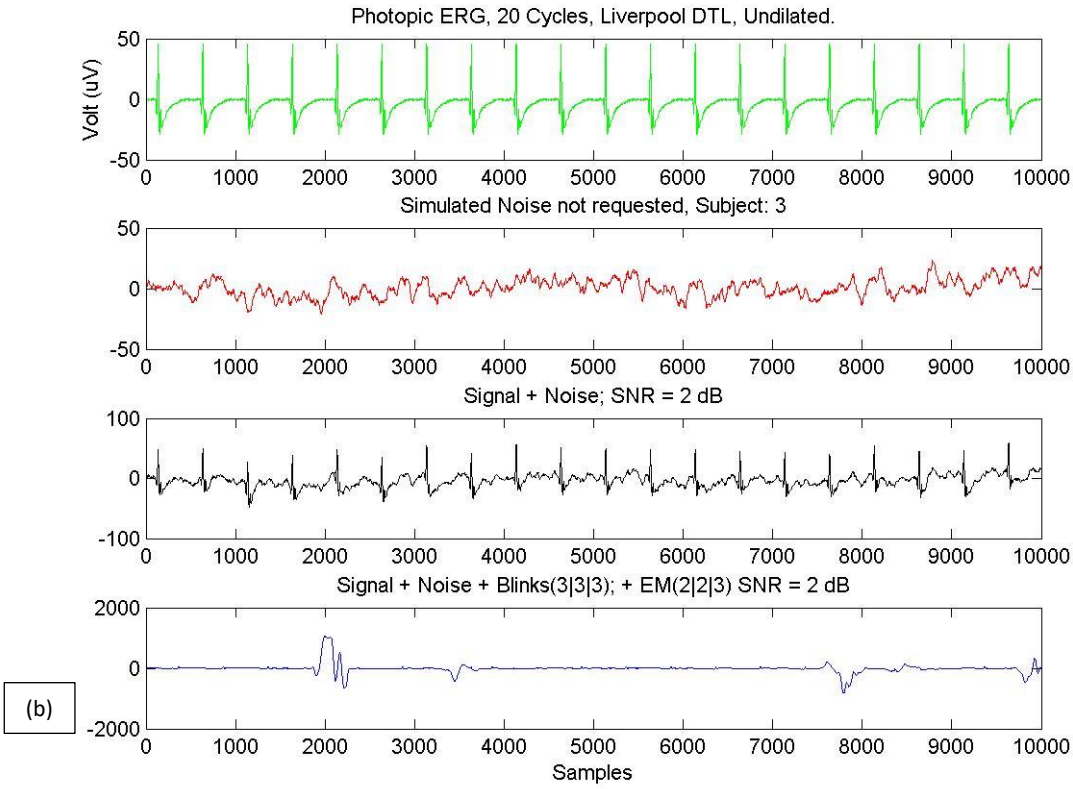

Figure 4.50. Examples of generated waveforms using Liverpool ERG simulator GUI. (a) 5 cycles of PERG signal with ARMA generated noise at +2 dB without eye-movement, blinks, EMG, mains interference or drift. (b) 20 cycles of photopic ERG (standard flash) with a +2 dB ARMA generated noise, 3 Blinks and 2 eye-movements.

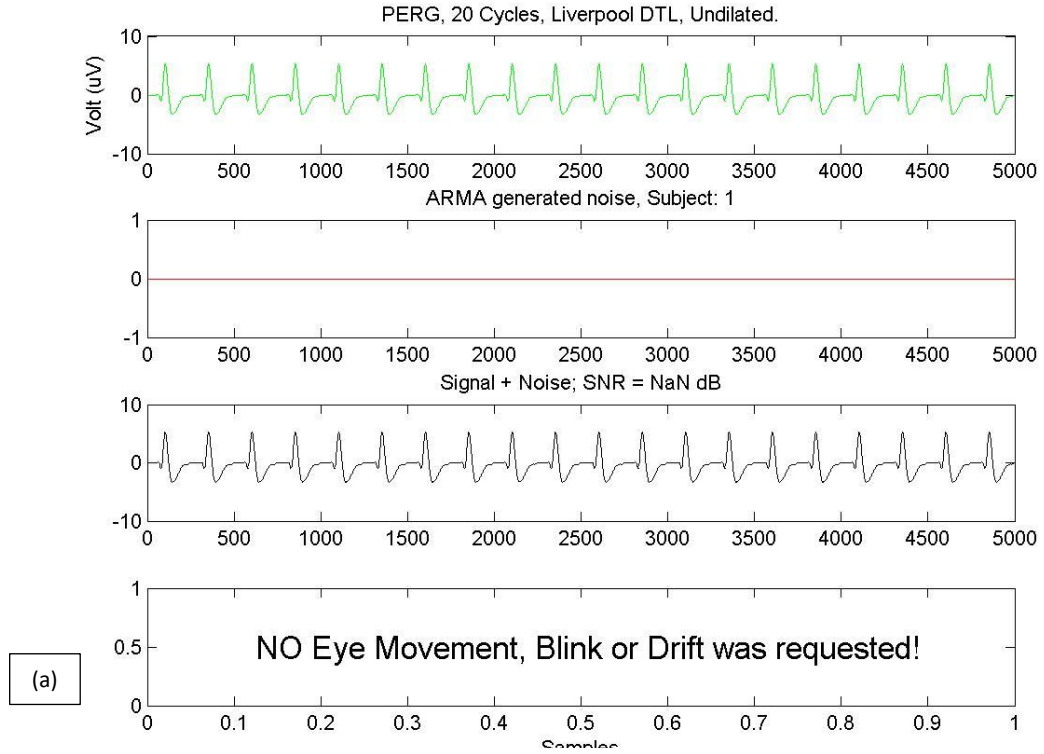

(a)

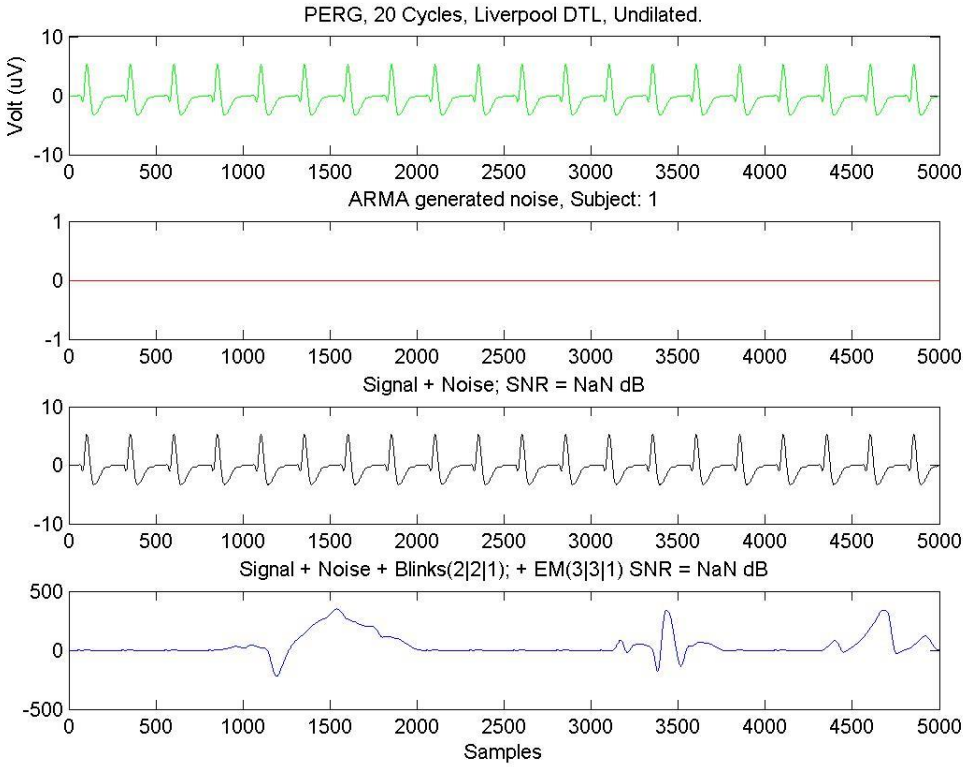

(b)

Figure 4.51. Examples of generated waveforms using Liverpool ERG simulator GUI. (a) 20 cycles of PERG signal without noise, eye-movement, blinks, EMG, mains interference or drift. (b) 20 cycles of PERG signal without noise, 2 blinks and 1 eye-movement.

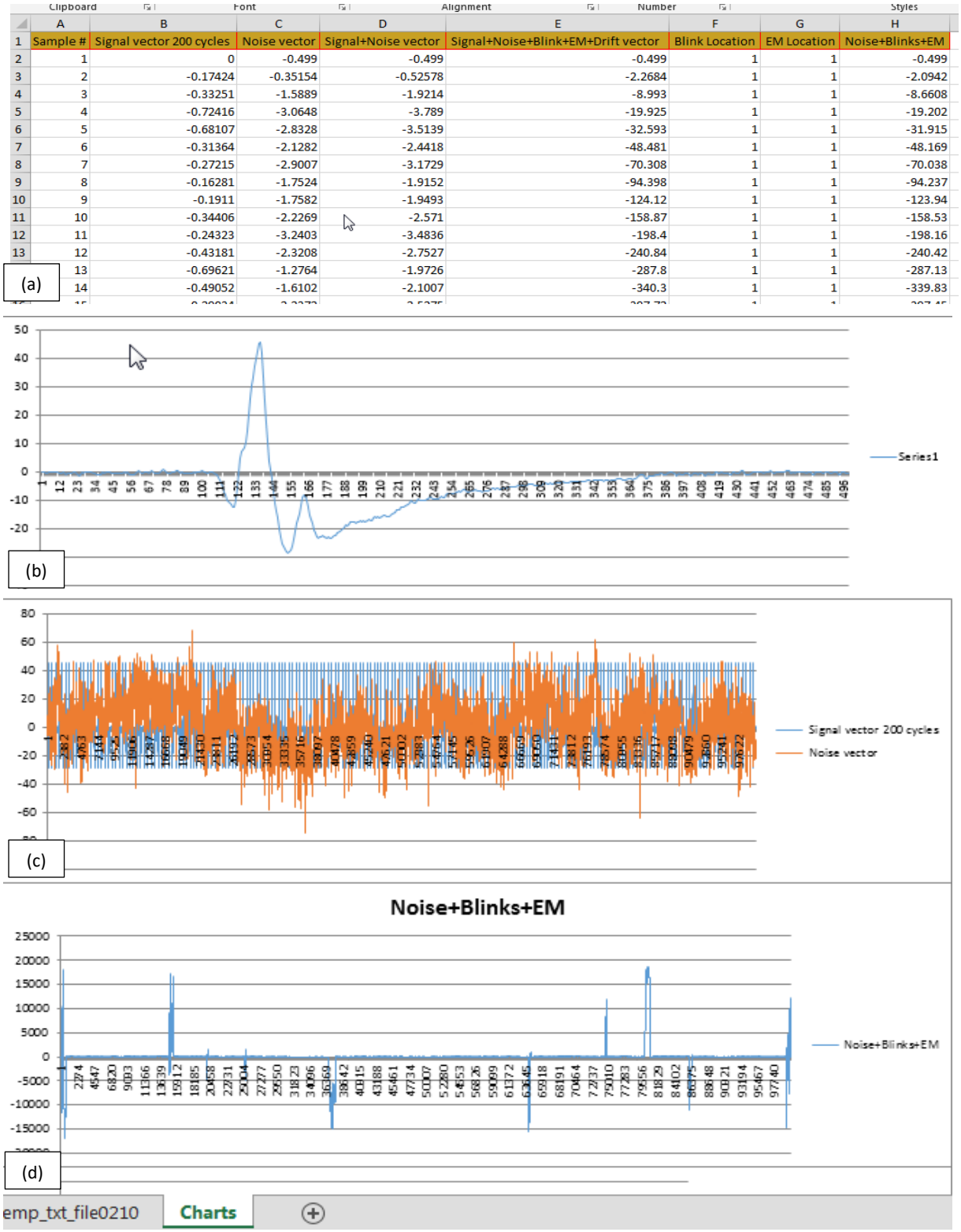

Sample #	Signal vector 200 cycles	Noise vector	Signal+Noise vector	Signal+Noise+Blink+EM+Drift vector	Blink Location	EM Location	Noise+Blinks+EM
1	0	-0.499	-0.499	-0.499	1	1	-0.499
2	-0.17424	-0.35154	-0.52578	-2.2684	1	1	-2.0942
3	-0.33251	-1.5889	-1.9214	-8.993	1	1	-8.6608
4	-0.72416	-3.0648	-3.789	-19.925	1	1	-19.202
5	-0.68107	-2.8328	-3.5139	-32.593	1	1	-31.915
6	-0.31364	-2.1282	-2.4418	-48.481	1	1	-48.169
7	-0.27215	-2.9007	-3.1729	-70.308	1	1	-70.038
8	-0.16281	-1.7524	-1.9152	-94.398	1	1	-94.237
9	-0.1911	-1.7582	-1.9493	-124.12	1	1	-123.94
10	-0.34406	-2.2269	-2.571	-158.87	1	1	-158.53
11	-0.24323	-3.2403	-3.4836	-198.4	1	1	-198.16
12	-0.43181	-2.3208	-2.7527	-240.84	1	1	-240.42
13	-0.69621	-1.2764	-1.9726	-287.8	1	1	-287.13
14	-0.49052	-1.6102	-2.1007	-340.3	1	1	-339.83

Figure 4.52. The back-end ISIM engine, will create text, CSV, mat and image (JPEG) files once it is finished with waveform synthesis. All these files are then available to download through the Liverpool ERG simulator GUI. Once the CSV/Text file is received, the interface will parse the data accordingly and will present the data in two separate worksheets as demonstrated by (a) through to (d). These worksheets are generated automatically by the background macro written in VBA.

4.4 Verification and Validation of the iSim device

4.4.1 iSim SNR verification

The ISIM hardware (iSim) consists of an ARM microprocessor, a multi-channel 16-bit D-to-A convertor, and a very low-noise voltage amplifier with a passband of [0.0 … 500] Hz and balanced output impedance of 4.7 kOhm. Modern biopotential amplifiers used in visual electrophysiological clinics are a combination of analogue and digital processing units as well as advanced digital signal processing post-acquisition of the collected biosignal waveform. Calibration of these amplifiers must take into account the noise environment so to allow accurate characterisation of such systems. A PERG signal (with a peak-to-peak amplitude of 30 mV) is used as the test signal to establish the iSim SNR as shown in figure 4.50. The SNR of iSim channels A to D were measured using a PICOSCOPE technology oscilloscope to be 92, 90, 90 and 94 dB, respectively when the DAC dynamic range is set to $\pm\ 10\ V$ and the output sampling rate to 1 kHz with all four channels active. The measured SNR is obtained with probes placed at the output of the quad-channel operational amplifier stage with low pass filter feedback set at 500 Hz for all channels. Measured SNR at the output of the summing stage is 90 dB.

Post SNR calculation the default hardware low-pass filter corner frequencies for iSim channels are set to:

- Channel A: 400 Hz
- Channel B: 45 Hz
- Channel C: 150 Hz
- Channel D: 300 Hz

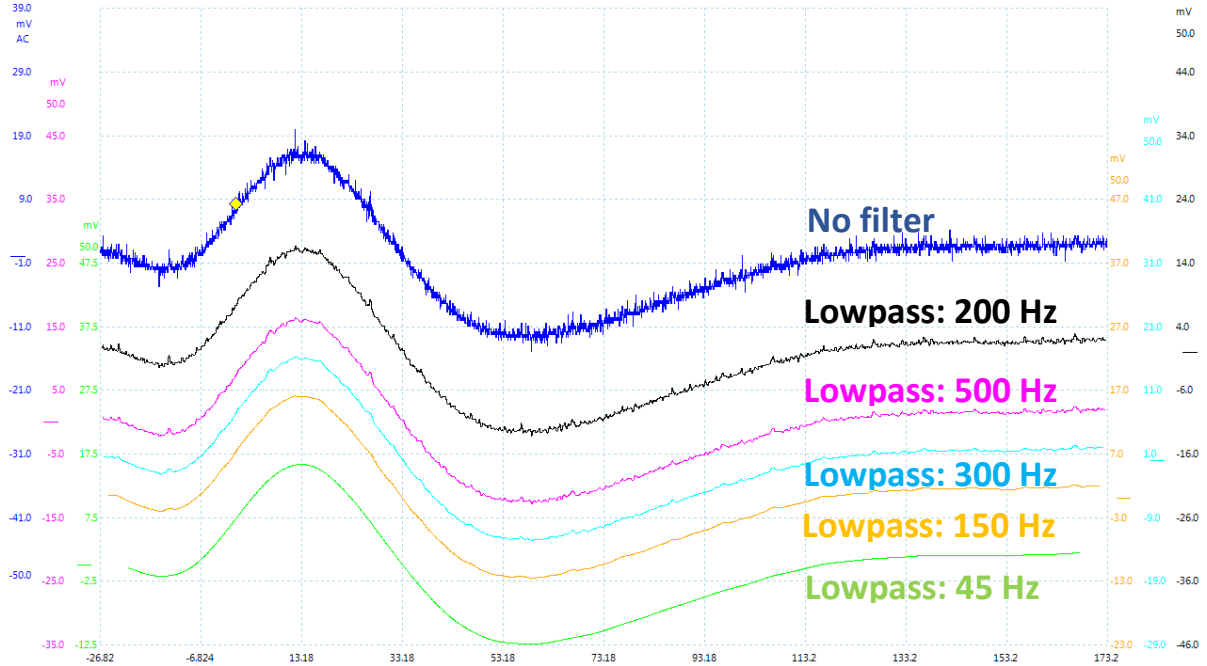

Figure 4.53. iSim device simulating PERG signal (driving the inputs of an oscilloscope) and filtering the output accordingly with a lowpass corner frequency of 45, 150, 200, 300 and 500 Hz to measure the channels specific SNR and the SNR at the output of the summing amplifier.

The high-frequency spikes (noise) on the blue trace in figure 4.53, are captured as shown in figure 4.54, where the glitch repetition duration is measured to be 13.5 microseconds with a duration of 2.3 microseconds and an amplitude of approximately 20 mV. A comparison with the DAC specification sheet suggests that these spikes are inherent to the DAC system and originate from digital-to-analogue conversion. These glitches are injected into the analogue output when the input code in the DAC register changes (that is the DAC is updating). The same phenomenon occurs on the output of DAC channels when another channel is updating, this is known as DAC channel crosstalk. These glitches are of high frequency and will be filtered out on all available channels.

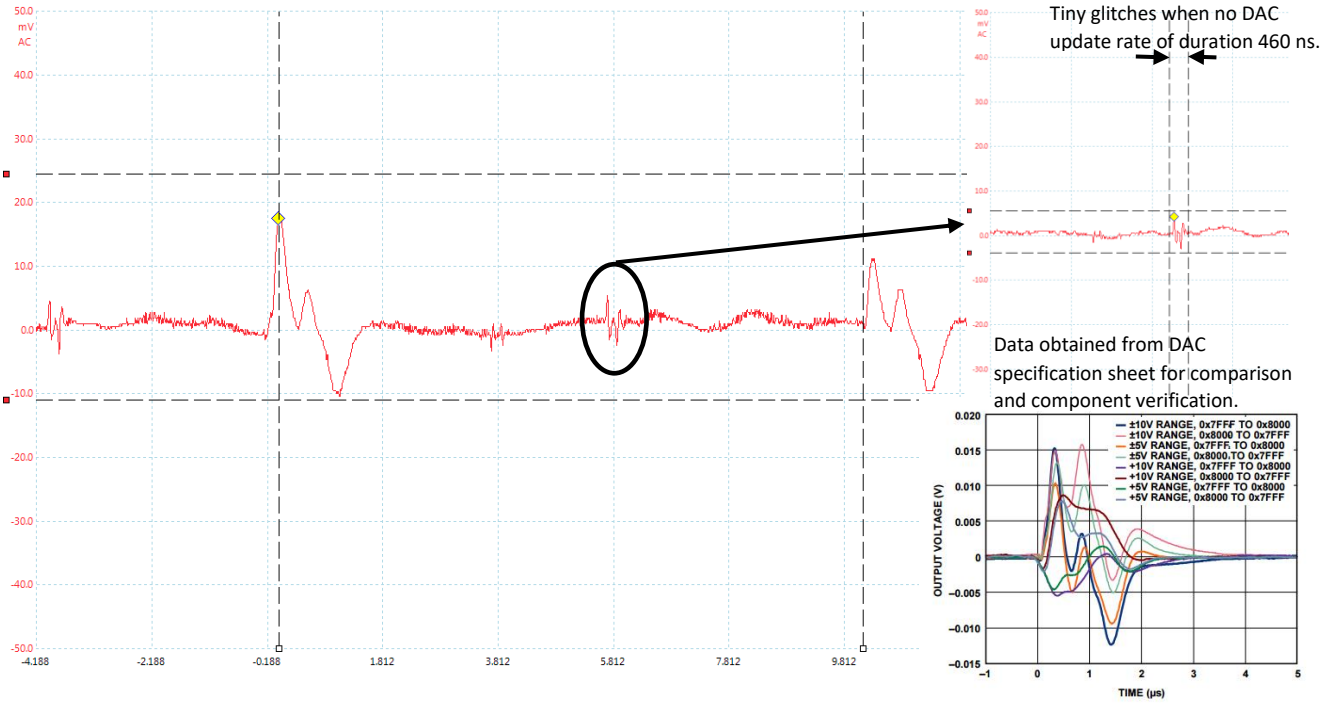

Figure 4.54. Illustration of glitch response due to DAC register update and comparison with DAC data sheet as part of Critical To Function (CTF) component inspection and verification.

Two versions of the Roland RETPORT/SCAN system have been tested using the ISIM. Figure 4.55 illustrates the response collected by these systems where the significant parameters of the ERG wave (a and b-wave amplitudes) are automatically calculated and cursors are further adjusted by the clinician.

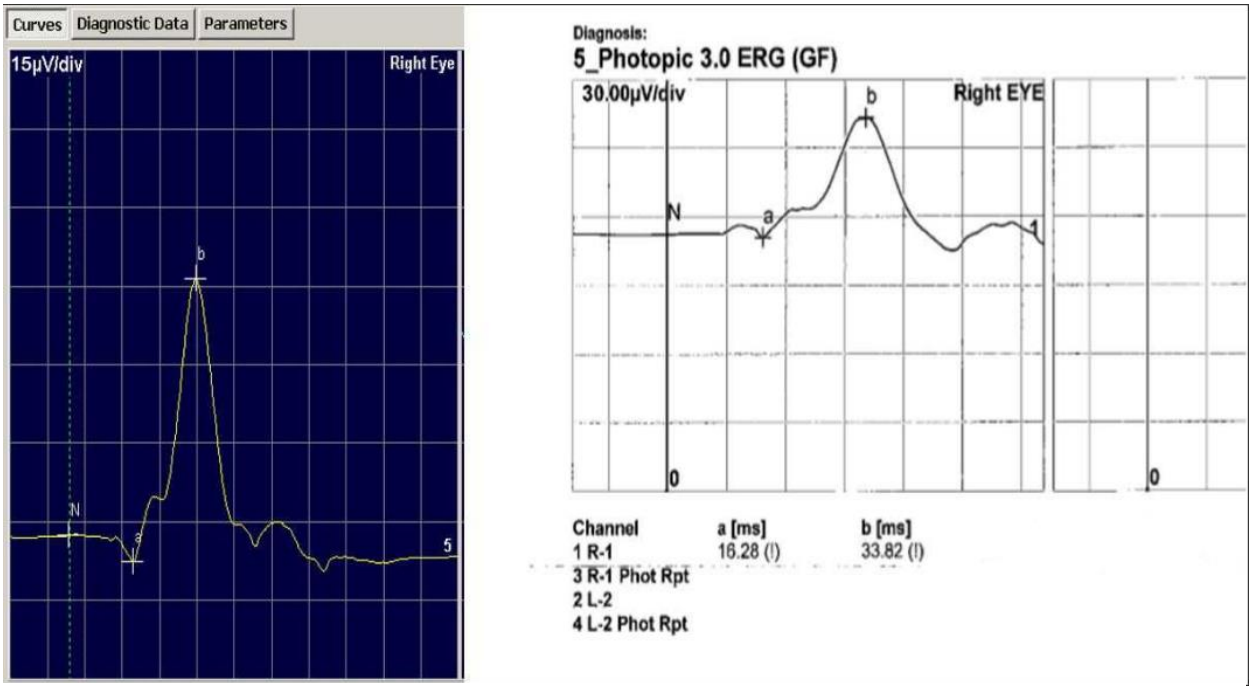

Figure 4.55. iSIm device is tested and verified at RLUBH eye clinic centre using Roland visual electro-diagnostic system with a record of photopic ERG signal (at standard flash). The record in this picture was obtained after three cycles having no noise or other types of artefacts added to the input trace.

4.5 Chapter conclusion

In this chapter, the designed Liverpool bio amplifier is verified against its initial design specification requirements. The verification showed similar characteristics compared to both Roland and Kelvin Vision biosignal amplifiers including CMRR, noise level, adjustable sampling frequency, adjustable artefact rejection threshold voltage, and adjustable bandwidth. The Liverpool bio amplifier also provided a simple and easy to use Graphical User Interface (GUI). The GUI provides two main plotting areas to display the real-time biosignal, and the averaged and filtered trace. The amplifier can operate in both continuous and trigger mode and its hardware and software capability to buffer data allow for maintained integrity of the biosignal when operating at a high sampling frequency of up to 100 kHz. The required safety testing was performed before data collection as illustrated in figure 4.1. The amplifier is also capable of interfacing and driving the Kelvin Vision Multifocal Stimulator (MFS) and Roland Ganzfeld stimulator using a provided Pulse Width Modulated (PWM) synchronisation signal. The amplifier was designed and developed to collect continuous records of various types of interferences and visually evoked biosignals so that the assumptions made at the end of chapter 3 are empirically verified. The collected signals are also embedded within the ISIM back-end library for later use. Using the collected traces some novel applications of iSim are put into test. These include:

- Verify the underpinning sequence for various stimulation locations of the Roland RETIscan system

- Decode and better understand the underpinning mechanisms for Roland RETIscan auto rejection algorithm
- Verify and visually demonstrate that MSC algorithm could be a useful technique in extracting significant signal frequency components in traces with very low SNR
- Mathematical simulation of ERG noise using ARMA filter as the linear estimator (or use actually recorded ERG noise) to contaminate the clean signal trace at a user-specified SNR
- Simulate other types of artefacts, including EMG, mains interference and its associated harmonics, drift and DC shift
- Investigation of the effect of fixation error during mfERG stimulation and demonstrating the impact of fixation error on first and higher-order kernels
- Simulate the effect of discontinuities in recorded data as well as a non-uniform sampling of the recorded data

Toward the end of the chapter, demonstration of the Excel® GUI to download the data from a designated server is provided, where users could synthesis the type of record they require for particular testing. This was used to create the required traces to investigate the Roland RETIscan artefact rejection algorithm as well as verification of the MSC algorithm as a viable signal processing tool in low SNR visually evoked biopotentials such as PERG. The iSim device noise level is also measured and the SNR and filter setting for individual DAC channels are calculated.

Chapter 5: Discussion, Conclusion, Limitations and Future work

5.1 Discussion

Experimental studies to develop new tools and techniques for accurate calibration of the visual electrodiagnostic instrumentation are limited. ISCEV (International Society for Clinical Electrophysiology of Vision) latest publication on guidelines to standardise calibration techniques is published almost 17 years ago[281]. The requirement for regular, traceable and precise calibration techniques has been discussed in, [281][282][345][225] and is regulated by strict standards, including FDA's 21 CFR Part 820, Quality System Regulation (QSR) and ISO 13485.

Most electrodiagnostic systems can now provide automated calibration of their clinical data acquisition subsystem. Laboratories need to rely on the manufacturer's recommendations and guidelines on the calibration of their instrumentation[281], but the accountability on determining if the recording standards are actually met is with the clinical electrophysiologist[65]. There are no technical studies reported to understand if these recommendations are different and how any such differences could be quantified.

The inconsistencies between the limited number of studies, technical reviews and the importance of accurate, reliable and up to date calibration, suggest that there are still gaps in the practice. There is also no appropriate standardised calibrator, accepted by the international community in visual electrophysiology for use in calibration of visual electrophysiological instrumentation. A unified and standardised calibration method would make the work in visual electrophysiology more reproduciable[346].

Torok (2014) [347] presented a poster on a new calibration method for ERG, PERG, mfERG, EOG and VEP measurement. His battery-powered calibrator is a sine or square wave generator that is capable of operating at both continuous and transient modes. In transient mode, a known amplitude sine or square wave with a fixed time delay is produced every time the device is triggered by a light source such as a Ganzfeld. This allowed voltage calibration of the equipment, including its phase delay and phase linearity (see figure 5.1).

Ding et al (2017)[283] used a mathematical technique to create a more realistic simulation of the clinical human electrophysiological signals. These waveforms were used as the calibrating waveform using a developed physical device to drive the input of the clinical system (see figure 2.22). They used literature to identify the significant peaks and valleys of the most frequently encountered visual electrophysiological signals such as PERG and ERG. A sawtooth waveform is then obtained by connecting these points, and finally, a low pass filter is used to smooth the signal and limit its frequency bandwidth. The amplitude of the constructed waveform is then adjusted to span the full dynamic range of a 20 bit Digital to Analogue Converter (DAC) before attenuation of the waveform based on the selected signal category (e.g. PERG, Pattern VEP or ERG). The delay time is another critical parameter that is preloaded into the memory of the device, ensuring traceability to literature. Their system performance is based on its ability to test for amplitude and latency time when calibrating the clinical system under both visual and pattern stimulation (the amplitude and latency are the two parameters that are commonly used for diagnosis in clinical electrophysiology[281]). They concluded that their system could be a convenient tool as a more frequent (daily) calibrator. They also claimed that their device could be implemented as a

useful research tool that improves long term data stability and could be a facilitator as an inter-laboratory data share for both diagnostic and research purposes. They further concluded that the device could be implemented as an EEG, ECG and EMG calibrating system through loading the necessary electrophysiological data into the onboard memory of the signal generator.

From the published paper by Ding et al[283], it is not clear on how the device is used to perform data share amongst workers in the visual electrophysiological centres. It is also not clear on how the dynamic range of the device is adjusted to compensate for various electrophysiological signals ranging from one µV to a few hundreds of mV in the case of an ECG or EMG signal. The device only outputs a single cycle of a mathematically constructed waveform when triggered by an optical source and as such does not provide means to challenge the clinical data acquisition system using contaminated noise (continuous or spontaneous).

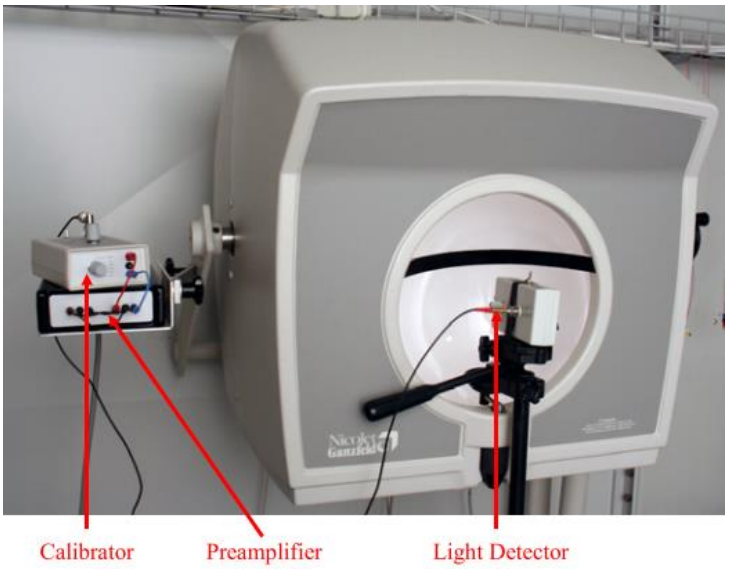

Transient Modes (triggerable):

ERG: a-Wave (25 ms) and b-Wave (50 ms)
PERG: N35 (35 ms) and P50 (50 ms)
mfERG: N1 (15 ms) and P1 (30 ms)
VEP: N75 (75 ms) and P100 (100 ms)

Continouos (free-running) Modes:

Mxn: Maximal Nominal Voltage (DC)
Min: Minimal Nominal Voltage (DC)
Baseline: 0 V
Sinussoidal Wave: 1 Hz, 2 Hz, 5 Hz, 10 Hz
Square Wave: 0.5 Hz, 1 Hz, 2 Hz, 5 Hz and 10 Hz

Figure 5.1. The proposed calibrator able to provide objective measures on the phase delay and phase linearity of the amplifier and signal processing system, implemented by the clinical setup. Torok[347] states that most visual electrodiagnostic laboratories are potentially unable to do the basic, ISCEV recommended calibration procedure of their setup as they may lack suitable test equipment. Torok claims that the presented device solves this problem and allows accurate calibration of the recording equipment without experience in electronics.

This study aims to design and develop the required infrastructure, tools and techniques necessary to address the gaps in current practice with regards to the calibration of visual electrophysiology data acquisition system, closer collaboration and data sharing amongst scientists and researchers, quality assurance and finally training staff in the field of visual electrophysiology. The platform is termed ISIM

(Eye Simulate), and it is compromised of both software and hardware components (the hardware component is termed iSim), allowing generation and delivery of realistic waveforms to facilitate one to address the above gaps.

ISIM provides a realistic simulation of visual electrophysiology waveforms as well as the supplementary information required to accurately interpret the data before re-using it (i.e. providing a well-described dataset so that any original interpretation or conclusion can be reproduced without loss of traceability on the data itself or on the methods used to collect the data). The data provided could be synthesised mathematically or could be actual data collected under some experimental condition (e.g. in accordance with an experimental protocol that outlines the use of specific electrodes, stimuli configuration, instrumentation, retinal adaptation status, etc). The data is a combination of simulated or actual biological neuro-responses and background noise. The noise trace is used to contaminate the simulated electrophysiological signal and is a combination of continuous and spontaneous components. An example of a continuous record is the ARMA generated background noise combined with mains interference and its associated higher-order harmonics. EMG, blinks and eye movements are examples of physiological spontaneous noise components.

ISIM is the only available platform that allows the researcher to calibrate the clinical instrumentation system using actual or realistic visual electrophysiological data. It enables the worker to accurately and more frequently calibrate the acquisition system. This provides a considerable advantage over traditional methods (e.g. signal generators) as it allows calibration of the clinical instrumentations over the entire frequency range of most commonly recorded visual electrophysiological signals (e.g. scotopic and photopic ERG, pattern ERG or PERG, VEP, and pattern VEP, flicker and ON-OFF ERG response simulation).

Advances in technology and methodology have dramatically increased the volume and complexity of the data recorded in visual electrophysiological experiments[348][349]. KCL sponsored RETeval All Comers Trial (REACT) study, completed in 2018, is one example in accumulating a vast amount of data from approximately 1000 participants in a relatively short period (around one year). ISCEV recognises that progress in visual electrophysiological science, increasingly depends on collaborative efforts, exchange of data and re-analysis and re-visiting previously recorded data. This view is also shared widely across all branches of science in the 21st century, where scientific research is more data-intensive and collaborative than in the past[349]. It has become a challenge in the field of neuroscience to ensure, data stays accessible, data processing is reproducible, and data can be shared and reused by various centres[350]. Sobolev and Stoewer et al [350] points out that efficient data management is particularly challenging for the area of electrophysiology. The field faces significant inherent variability (see figure 1.6), a large variety in experimental methodology, a considerable variation in the number of data acquisition systems[351] and their individual calibration requirements[65], different file formats which are often vendor-specific and undocumented, variety of electrode type and configurations, stimuli and overall experiment paradigm. This creates complex metadata (data and the required additional data about the experiment and test subjects) to be structured, organised and managed efficiently before it can be shared (see figure 1 in [350]). By sharing and analysing well-described electrophysiological data, scientists can develop new algorithm and tools, teach and train beginners, validate the different hypothesis, and potentially make some novel scientific discoveries[348].

To date, no initiatives have been made that supports data sharing in visual electrophysiology. There are many platforms available in other areas[348], and the pros[352] and cons[349] of data sharing[353][354] is discussed in cardiology, radiology[355], neuroscience[350][356], MRI[357], cancer research[358], EMG and EEG[356][359][360]. The regulations have also improved in the last decade to ensure the information stemming from clinical trials is available to patients and clinicians helping to mitigate the problem with selective publications and outcome reporting[353][361]. The control of raw data remains with those who generate it and sharing it, is not a legal requirement, but may be seen as good practice. The imperative to ensure "*open science & innovation*"[348] is to find and support successful pathways to share data that best serve the interest of patient care[353][361].

ISIM provides the first novel, flexible, cloud-based, data integration/access platform that structures, organises, processes and makes the de-identified visual electrophysiological data accessible over the internet through MatSOAP server. The server manages client-service communication using SOAP as the query protocol and MATLAB as the logical layer to process user requests. The service allows for data download and upload (text files as the standardised file format), data visualisation (where the service provides images of the waveforms and graphical plots of the data in MS Excel application, see figures 4.50, 4.51 and 4.52) and online analysis (for example, software tools that analyse the captured binary sequences governing the system's mfERG ON and OFF patterns). These functionalities promote collaboration and make an unprecedented amount of data available to clinicians and researchers to ultimately improve the quality of research-based health care and reduce the short term costs of expensive data collection[353]. It allows for improved quality assurance as it enables reproducibility of large-scale data analysis.

ISIM is the only available platform that allows for a single point of coordination and access for the visual electrophysiological data. This is of great advantage, primarily when research project span multiple geographically sparsely distributed institutes and requires seamless sharing and interpretation of data that originates from various resources. ISCEV also recommends that individual laboratories establish their normal databases and use this as the reference point for diagnosis rather than relying on published norms[281]. There are many studies and published literature that aimed at establishing large normal databases that could be used by other centres as their reference point[92][157][362][363]. There are also many published studies that aimed at publishing normal databases for specific region, country or a specific ethnic group[81][87]. There exist inconsistencies between published ISCEV guidelines on the use of centre specific normal database as the true reference point for each centre and attempts by many scientific groups in visual electrophysiology that encourages the use of published norms as the centre's reference point. This inconsistency suggests that there are gaps in practice on what constitutes an acceptable normal database that could be used by other centres as their reference point for diagnosis. ISIM provides methods to not only publish the centre's raw data and normal parameters but also to publish the contextual data, i.e. data that completely describes what is meant by normal from the centre's perspective and how the data was collected including tools and techniques used to collect such data. ISIM provides the required mechanism to share this metadata amongst workers in different centres and hence improves the patient data transferability among these centres.

There are significant challenges before an electrophysiological data platform can be operational. These include difficulties in data transfer, data storage, standardisation of data format, data visualisation and cloud computing as well as tools and algorithm to perform online data analysis and integration (see

figure 1 in [348]). Building a sound infrastructure for data sharing and preservation is not the only challenge per the survey by Tenipir et al[349]. They found that insufficient time and lack of funding are the leading reasons why scientists won't make their data available electronically (other reasons such as no place to put the data are barriers to sharing data). They also found that systems that make it quick and easy to share data can help to improve the sharing culture amongst scientists. ISIM is the infrastructure that makes it easy to structure, store and share data in a standardised format.

ISIM modular and scalable design architecture allows for efficient management of an increased number of transactions to the server by adding new devices to the network, upgrade their versions (hardware or software) and extend its capability by adding new algorithms, physical storage and new processes. A typical programming module is treated as a black box as far as ISIM is concerned, i.e. the input to the module and its output are the only parameters that need to be managed so that the functionality of the module is exposed to the end-users for re-use. This modular design allows for ISIM backend capability to be easily extended to include a new algorithm and enabling scientists to run their code on the cloud.

In addition to providing a practical calibration tool and the infrastructure for an organised and standardised data-sharing platform, ISIM enables one to create a fully customisable waveform. The SNR of the generated waveform can be customised by the clinician or the researcher allowing them to objectively challenge the acquisition system and investigate the performance of signal processing toolboxes in extracting signals buried in realistic noise (i.e. poor SNRs). The impact of electrode types is also included as a simple scaling factor when synthesising visual electrophysiological responses. The electrode-type scaling factor could easily be traced back to a published study using a specific instrumentation and study protocol. Since ISIM allows publication of study result together with the supplementary information, it will support the operator to make sense of any potential variations between different scaling factors in various electrode comparison studies. The impact of intensity and the retinal light adaptation is not a simple scaling of a standard template. Changes in the retinal adaptation and stimulus intensity results in changes in physiological response morphology. A library of various signal epochs, which are traceable to a specific publication, is organised and stored at the backend server. Access to this library is made possible using a simple dropbox menu in the ISIM front-end graphical user interface (GUI).

iSim also provides a novel mechanism to include other interferences such as mains interference. It allows the worker to verify the clinical system's performance in steps of increased complexity when dealing with periodic interferences. This is particularly important as the filter settings of the amplifier section of ERG recording systems have a large impact on the waveforms of the recorded responses[364]. For example, a single frequency sinusoid could be created and combined with the waveform to objectively verify the performance of the clinical system's notch filter at removing 50 or 60 Hz mains component and at the same time evaluate the impact of the notch filter on the signal of interest. Bock and Gerth et al[364] investigated the effect of a notch filter in removing lines interference and its impact on the first- and second-order kernel slices of the mfERG. They used 11 normal subjects (two runs per test subject with the line rejection filter setting active and inactive respectively) and a function generator to create sinewaves with a constant frequency and peak to peak amplitude to investigate the magnitude and phase response of the amplifier. Any accurate conclusion on the FOK and SOK responses due to the impact of notch filter would require a template response for both the first- and second-order kernel of the mfERG as both inter- and intra-session variability can induce changes in the waveform in

each measurement. This standard template would act as the reference point to accurately investigate the effect of a notch filter in both removing the lines interference as well as the frequency spectrum of the FOK and SOK responses. Bock concluded that that the notch filter must not be used when one is to investigate the second-order kernels, but due to higher SNR, it can be used to eliminate the effect of substantial mains interference when one is studying the FOK responses. Bock also stated that if the results of different labs are to be compared then the filter settings of these laboratories must be known and kept the same. ISIM can reproduce the same recording data using the same FOK, SOK and higher-order response templates and SNR with the same contaminating line interference to accurately and objectively compare the effect of filter setting in removing substantial line interference and its impact on the frequency spectrum of the results. Using this technique, different laboratories could adjust their filter setting to ensure higher data comparability.

Representing lines interference as a single 50 or 60 Hz sinusoid is not an accurate simulation. ISIM can support synthesising more complicated representations of the line interference by adding additional harmonics, varying the frequency of the fundamental component or contaminating the clean signal with a record of actual mains interference and then drive the inputs of the instrumentation amplifier using this generated waveform[333]. ISIM provides software modules to extract the first- and higher-order kernel responses post-filtering (other filtering approaches such as mains and harmonics estimation and subtraction[333] could be tested at this stage on the same data available using ISIM). The user can build a quick notch filter module in MATLAB per the specification published by the investigator (as an example for such filter description, see Bock et al, MATLAB notch filter specification implemented as part of their study in [364]) and test the impact of the notch filter post kernel slice extraction and compare this to the standard reference template.

non-physiological artefacts such as line interference are modelled using ISIM as described in section 4.2.7. Other non-physiological artefacts such as electrode artefacts, electrode lead movement artefacts, if isolated, can be included as part of the ISIM continuous noise component library. These artefacts can then be included as part of the extended ISIM library to synthesise realistic visual electrophysiological waveforms. In addition to these artefacts and the methods of removing them, the need for robust methods for automated and on-line removal of physiological artefacts[327] is particularly acute as healthcare technology development undergoes the transition to delivering more point of care (POC) delivery in monitoring environment other than hospitals[365]. An automated algorithm will also standardise preprocessing of the records by eliminating or at least reducing bias from human influence[331]. Such bias could be due to varying level of artefact rejection skills by different human observer[366]. It is challenging to determine the performance of various artefact removal techniques on real or mathematically generated artefactual data. In the first case (using real data), one does not have access to the actual desired data (same recorded data that is not corrupted by the artefact), so performance is measured with respect to uncorrected data[367]. In the second case, the model fidelity is the determining factor. In these models, a mathematically generated artefact does not fully capture the underlying physiological mechanisms, becoming an approximation to the physiological dynamics that produce it. These underlying physiological mechanisms are essential in providing the required level of knowledge on the Spatio-temporal profile of the neural and artefactual activities that are needed to train a pattern classifier in a model before it accredited as a fully automated artefact removal algorithm[366][331].

It is demonstrated that iSim is capable of simulating waveforms with actual blinks, eye-movement and EMG epochs (actual data allows preservation of the artefactual dynamics when one is reproducing experimental data using ISIM). This realistic simulation will enable one to objectively assess to what extent the true visual electrophysiology signal (e.g. ERG, or PERG) is recovered or deteriorated by different correction algorithms that are implemented by the clinical system. Such a system's verification includes testing the system to see if it does register the artefact, how it deals with multiple artefacts, avoids unnecessary data loss due to removal of artefactual signal segments and how it performs when it tries to recover from the registered artefacts. Chapter 4.2.6 showed how ISIM is used to investigate the artefact removal algorithm in Roland RETIscan. This was addressed by creating an artefactual trace, challenging the data acquisition and processing of the Roland RETIscan system by driving its input using this trace. Capturing the artefactual sequence and comparing this with the non-artefactual or control m-sequence allowed the author to verify the logic that Roland uses to recover from a registered artefact/s. The author found that this recovery depends on how the system categorises multiple artefacts and wherein the sequence the artefact is registered.

ISIM allows the investigator to obtain the true accuracy, specificity and sensitivity[323] of any automated signal processing method or toolboxes. This is possible as ISIM provides both the desired reference exemplar and the realistically simulated test data so that one can genuinely investigate the performance of new signal processing techniques and methodologies. Using ISIM one can ensure a continued supply of realistic data to challenge a novel signal processing package before any statistical significance could be made and a new discovery could be announced. This type of verification can work to bolster the findings of the investigator as one can determine whether conclusions are robust to various assumptions[354]. This, together with any re-analysis performed on the same data set or signal processing package, could expose errors or inconsistencies in the data that cast doubt on the validity of the initial findings or else can support it and allow it to be generalised.

In addition to quality assurance, fixation error is often challenging to capture as the operator has little information and feedback on when it occurs, how much the test subject or patient fixate away from the target and its frequency of occurrence. A considerable challenge in synchronising fixation drifts with the recorded signal exists. This makes it a challenge to quantify fixation quality during a recording session[250]. The author demonstrated a simple example in illustrating the impact of fixation on first-, second- and higher-order kernels of the mfERG using tools and software available in the ISIM package. Through this example, the author showed the effect of fixation error is most visible on higher-order kernels for an m-sequence of length 4096. More sophisticated experiments could be devised, using ISIM, to simulate the fixation error and objectively determine the impact of this type of error on the extracted kernel responses. Doing so one is enabled to quantify the quality of fixation and adjust the mfERG setting accordingly to minimise the impact of poor fixation quality during recording sessions.

ISIM's initial referenced signal and artefact templates are gathered from data published in the literature as well as data collected inhouse. In house data collection required the author to devise robust tools and techniques to acquire traceable data to the latest ISCEV standards at the time of writing this thesis. This included designing and building a biopotential amplifier and the high-level control software. The acquisition system is a 16-bit ADC with sampling throughput of up to 100 kHz and a 32-bit central processing unit (CPU). The front-end amplifier contains a block of analogue-to-analogue amplification allowing an overall CMRR of 120 dB. The control software is designed so that the amplifier is

synchronised with the Roland Ganzfeld stimulator enabling operation in both transient and continuous modes. Adapting to ISCEV standards and alignment with the state-of-the-art requirement of a commercial data acquisition system[225] facilitated the interoperability and comparability of experiments, models and simulations. The author also needed to gather extensive knowledge of biological and non-biological sources of variability to control and where possible to isolate these sources when collecting the reference templates. The author obtained a single data set from twelve healthy volunteers. This data set included background noise, EMG, blink and eye movement artefacts, mains interference and associated harmonics. Photopic ERG signal at various intensities, Photopic ON-OFF ERG responses and flicker ERGs are also collected using Liverpool thread electrode dropped under the eyelid for improved signal stability (see chapter 3.6). A custom-built biopotential amplifier was designed and developed to obtain the continuous record of raw data ensuring no missing data samples. No automatic rejection algorithm is implemented, and all artefacts are identified and manually removed using expert help. The author created the required MATLAB software tools to analyse and annotate the data. Reference templates for photopic ERG, flicker, ON and OFF ERG responses were created and stored at the back-end library after decimation, averaging, low pass filtering and windowing the epochs. Similarly, standards templates for blinks and eye movements as well as EMG epochs were created and stored at the back-end library. Algorithms were also designed to simulate voltage drift, nonuniform sampling error and missing data segments. Algorithm allowing the user to simulate the background noise using white or coloured noise generation as well as a more realistic ARMA simulation were also created. To build on this progression, new experimental data is needed. This should include further isolation of noise and signal sources. Previously collected data could also be included through sharing and closer collaboration with the originators of these data sources. Through closer collaboration and a more comprehensive review of already existing publications, the effect of pupil dilation, eye colour, age, gender, etc, can be quantified as potentially a single scaling parameter within ISIM backend mathematical engine. These scaling factors can be applied to a reference template allowing a mathematical synthesis for any of these attributes, which may help to normalise data further.

5.2 Conclusion

The objective 1 in section 1.6 is achieved as demonstrated in introduction (chapter 1) and literature search (chapter 2). These chapters provided the needed comprehensive review in the field of visual electrophysiology providing a history on the instrumentation and techniques as well as the applicable standards and their development. The foundations of visual electrodiagnostic include the disciplines of psychophysics, neurophysiology, electronics, mathematics, computer science, statistic and medicine. The discussion in chapters 1 and 2 provided a review of the developments and progress made to date, in each of these domains. Therefore, these chapters form the necessary foundation of the work presented in the later part of this thesis.

Section 3.3 of chapter 3 describes the development of a custom-built biopotential amplifier and its integration with Kelvin Vision Multi Focal Stimulator (MFS) and Roland Ganzfeld. The required embedded and top-level Graphical User Interface (GUI) and the associated signal processing analysis toolboxes was developed and documented accordingly. Section 4.2 demonstrates the performed Medical safety test result for the amplifier as well as other performed technical testing, demonstrating the comparability of the amplifier with most commercially available systems (Roland and Kelvin Vision).

The design, implementation and verification & validation of this measurement system provides the required evidence in meeting objective 2 in section 1.6. The development (and the accompanying calibration of the system) enabled the author to faithfully collect visual electrophysiological data, that is traceable back to the ISCEV standards (photopic, scotopic, ON-OFF, and flicker full-field and multifocal ERG responses at various flash rates and intensities as well as biological and non-biological noise records, including eye-movement, blinks, EMG, mains-supply-induced noise and the associated harmonics and finally the background continuous ERG noise). The data collection was performed on 13 normal subjects in the same demographic of those included in the St Paul's electrodiagnostic unit's normal database. The procedure for data collection is described in section 3.6 and the results and analysis are documented in chapter 4. The collected data were processed (the development of necessary algorithms to process the data is described in chapter 3 and the results are documented in section 4.2.2 to 4.2.10) and included into ISIM platform preliminary reference library, ultimately satisfying objective 4 in section 1.6.

During this project, I have developed a comprehensive platform to help visualise the impact of different filter settings, demonstrate the effectiveness of various recording strategies in removing realistic noise and offer an opportunity to compare different acquisition systems and perform realistic calibration of visual electrodiagnostic instrumentation. This platform (ISIM) provides the required evidence for meeting objective 3 in section 1.6, where its development is documented in chapter 3.

Further, the same platform has the capability of accessing whether a system is using a genuine m-sequence or not as well as allowing the operator to evaluate system's specific algorithms such as automatic artefact rejection algorithm (evidence for objective 6 in section 1.6). Roland system was used to verify ISIM's capabilities in collecting and analysing the governing m-sequence when its artefact rejection algorithm is triggered and when it is not triggered. This supported the aim of this thesis to better understand the implemented algorithm as documented in section 4.2.6.

Objective 7 in section 1.6 is achieved as demonstrated in section 4.2.5. The author has provided Magnitude Squared Coherence (MSC) algorithm as a novel technique in recovering the visual electrophysiological signal of interest from a contaminated record with low Signal to Noise Ratio (SNR). This signal processing package is included in the ISIM platform and results of using the platform to validate the package is documented in section 4.2.5.

This device may help operators, often with clinical backgrounds, by giving them the opportunity to assess their data collection strategies or indeed assess new equipment. There is potential with future collaboration to upload numerous datasets, from different platforms, normalising these platforms by playing the same waveforms through each and identifying how they change, of course, this could only be achieved with a great deal of collaboration, which requires facilitated data sharing across different centre's. As the platform provides the required infrastructure for data re-use through cloud-based tools, it provides the required means to expand the software library, ensure scalability, maintainability, reproducibility, repeatability and encourage closer cross-centre collaboration. The capability of the system to communicate through cloud gateways is documented in section 4.3, where a light front-end MS excel spreadsheet is used as the client's command centre to communicate with the back-end server

processing engine through MatSOAP server (a custom-built and optiomised server application providing remote access as described in section 3.4). This will satisfy objective 5 in section 1.6.

5.3 Limitation

The following are identified as limitations of this thesis. These are due to constraints on the available funding, time, human resources and willing collaborators.

Research on visual electrophysiology and processing of big neuro data devices and biomarkers could progress significantly if accurate and real-time collaborative efforts could be organised. Further technological improvements (see section 5.3) could play a significant role in facilitating, promoting and influencing, different workers in the field of visual electrodiagnostic and research to adapt ISIM into their normal busy schedule. Such adaption would provide a continuum of quality surveillance data on iSim/ISIM allowing to further validate the platform and improve its functionality. It also increases the size of the back-end library, acting as a single point of reference to pull data from by various centres for calibration, training, validation novel signal processing packages, etc.

1. Greater validation of the ISIMs ability to compare and contrast several centres data, developing transfer factors for differing electrode types, with respect to work already published. The author proposed one such study, compiled all relevant documentation for ethics approval and ensured the study protocol was in place and approved by the head of the visual electrodiagnostic unit and head of the department. The proposed multi-variate, multiple regression statistical modelling of the data and its analysis was approved, and the declaration form was signed by Dr Antonio Eleuteri on 21st December 2015. The study timeline to completion was also agreed, as illustrated in Appendix C. The study did not take place as the author could not secure the required contract term with the University of Liverpool. See Appendix C for the study proposal.
2. Systematic and large-scale (centre specific or cross-centre) reproducibility study using ISIM/iSim.
3. Systematic and comprehensive evaluation and validation of ISIM/iSim capabilities under various clinical instrumentation operating conditions, such as the impact of changing clinical instrumentation filter setting on the collected waveform.
4. Systematic and comprehensive comparison study using iSim in conjunction with various commercially available data acquisition systems (including implemented signal processing packages).

5.4 Future work

From a clinical research perspective, iSim/ISIM is seen as a starting point with significant potential in transforming the current clinical practice and research cultures into a more organised and collaborative approach. Part of which would be to help harmonise responses across platforms, facilitating the ability to see how responses recorded on different systems might change or look. Combined with other more established changes of waveform with electrode type, gender, pupil dilatation etc might help to create a greater scientific foundation for clinical decisions to be made.

Such approaches have proven effective in research and clinical advances in other neuroscience areas such as EEG, EMG and ECG community. The author suggests the following technological advances to be incorporated into the future development of iSim that would allow for a more user-friendly, robust and accurate implementation of iSim/ISIM. This ultimately would make iSim/ISIM an ever more appealing

technological toolset at the hands of clinician across the globally distributed visual electrodiagnostic centres.

1. Incorporation of wireless technology over the short, medium or long-range into iSim:
   This would connect iSim to the cloud services, directly from the box and could potentially allow operation of the device through elegant mobile applications or an integrated touch screen technology.
2. Battery operated device:
   This was originally specified by the author and is currently work in progress at the time of writing this thesis (see figure 5.2). Mr Peter Watt leads the implementation of the battery operation circuitry at the department of Medical Physics and Clinical Engineering (MPCE) of the University of Liverpool (UoL). The battery operation would result in significant Printed Circuit Board (PCB) noise level reduction, ultimately improving the available dynamic range of the system and speeding up the calibration procedures.
3. Other technological advances that would result in the reduction of the system noise level. These include:
   - Using multi-layered PCB board, allowing for separation of the digital, analogue signal and ground lines.
   - Striping out un-used electronic components of the MBED prototyping board and reduce the overall pin count and board component density.
4. Improve onboard memory of the system:
   Improving onboard memory (RAM) of the system can result in faster access time to retrieve data from the memory. This enables greater time window in the internal logic of iSim for other operations as well as checking the retrieved data and updating the DAC output register. This ultimately means faster data sample throughput and hence improved overall signal morphology without loss of data due to reduced risk of overwriting conditions.
5. Increase the number of optical inputs to concurrently monitor visual stimuli from multiple spatial locations on the screen (proposed to be 103 locations):
   This feature would be a significant step that increases the performance of the device when simulating retinal responses under mfERG setting. It also provides the mechanism for simultaneous, independent verification of the underpinning m-sequences for all spatial locations in a mfERG setting.
6. Extending the ISIM front end application from Excel interface to a webpage interface, mobile phone application interface, etc. and improve the back-end data management and maintenance.

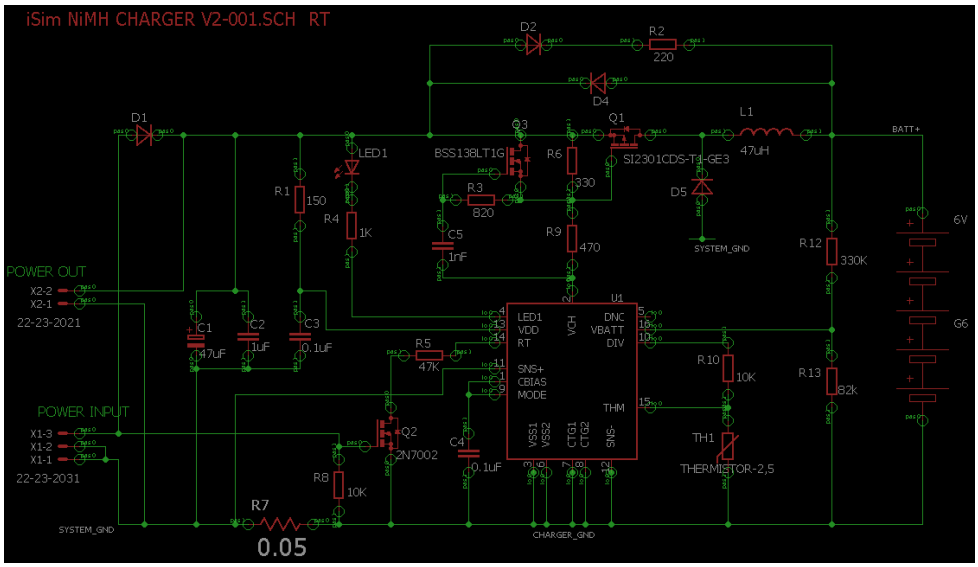

Figure 5.2. Proposed standalone iSim (currently work in progress) device without requirements to connect to a nearby host computer for operations. (a) Left: Push-Button based application of iSim with few selected waveforms. Right: Illustrating input and output connections. (b) Illustrating the implemented battery operation device – This is currently under verification testing by Mr Peter Watt ant MPCE. (c) A modified DS2715 (Maxim Dallas Semiconductor) charger controller switch mode application circuitry for five NiMH battery cells in series.

Appendix A: Mathematical background

A.1 Hypothetical linear and nonlinear system response

A hypothetical system response for a double-input experiment is illustrated in figure A.1.a, reproduced from figure 1 in Larkin et al 1979[320]. Time-between-pulses demonstrated as $|\tau_1 - \tau_2|$ where Larkin measured that there would not be any significant activity in the second-order kernel when time-between-pulses is greater than 120 ms. Assuming the system in this example is first-order time-invariant, then first-order responses are identical. If one considers that the system is also linear under specific experimental setting, then the total response to the double-input experiment becomes linear sum of two responses (dashed curve in figure A.1.b), that is superposition holds. However, where the system behaviour cannot be modelled as linear, the response to double-input experiment may behave as shown by the red trace in figure A.1.c. Since this is different compared to the expected linear response, one can conclude, nonlinear interactions between consecutive responses to the first and second pulses.

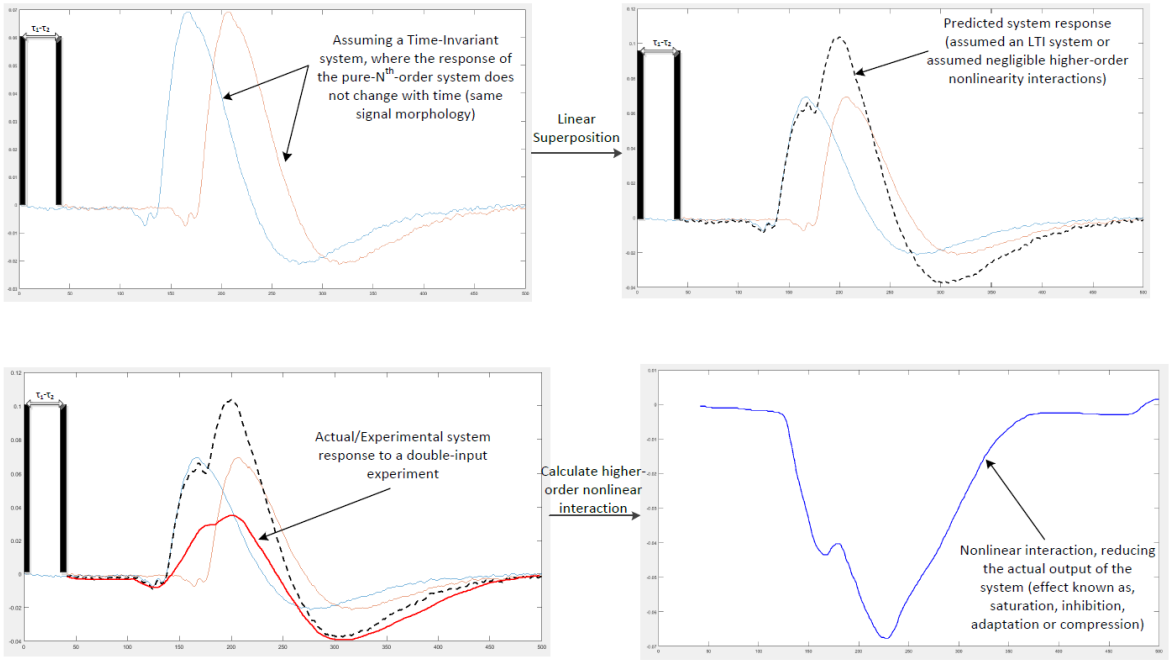

Figure A.1. (a-d) Illustrating an elegant method of calculation of the system's higher-order nonlinear interactions in a double-pulse experiment[320]. It also demonstrates the difference between a linear and nonlinear system characteristic. X-axes demonstrate time after first and second pulses and y-axes demonstrate, amplitudes in units of measurement. Figure (d) is magnified by a factor of 2 along the amplitude axis (y-axis).

In this generic, hypothetical example, one may use a simple method to calculate the nonlinear effect using expression (A.1). The impact of nonlinearity is negative in amplitude (figure A.1.d) and hence is termed adaptation or suppression.

$$A(t) = Nonlinear\ Interaction\ (t) = Predicted\ Linear\ response\ (t) - Actual\ system\ response\ (t) \quad \text{(A.1)}$$

A.2 Double-flash experiment (based on Sutter's work)

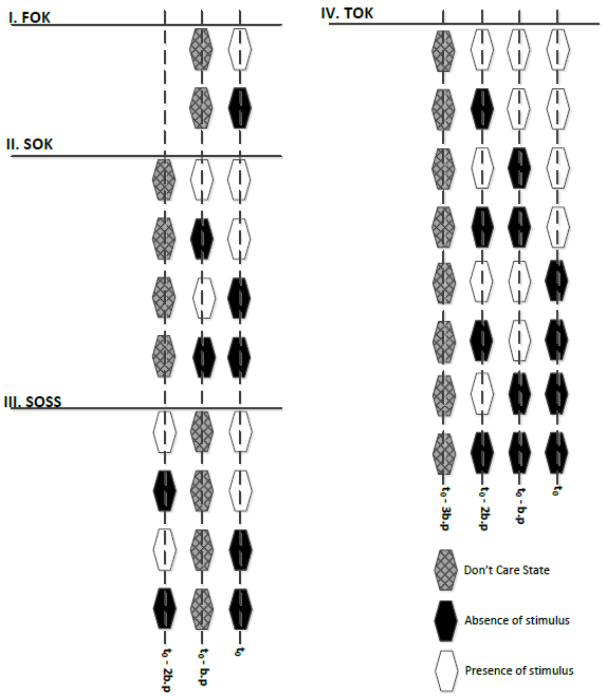

Figure A.2. Illustration of binary stimulus allowing to derive non-zero kernel responses. This illustration provides an assessment of the impact of the previous two flashes on current flash (at $t_0 = 0$). Therefore, two delay operations are considered resulting in adaptation of a second-order nonlinear model. Each section of this figure is termed in line with the same language adapted by Sutter[44][241] (that is FOK, SOK, SOSS and TOK). To derive the kernel responses for a second-order system, a window of three base-period is selected. However, the system remains a second-order nonlinear system as only changes at input, extending to 2 pervious b.p. (i.e. a memory-length of 2b.p.) are considered to deviate the response of the system at $t = t_0$ from that of an LTI system (higher-order delays considered to have negligible impact and hence are ignored). The adaptive model uses a window of length three b.p. to estimate the future response of the system and hence it is a third-order system with respect to this response-estimation and a second order with respect to assessment of LTI-response-deviation.

During focal ERG stimulation, if the pseudorandom flashes (pulses) are presented at an integer multiple of constant intervals (base-periods abbreviated by b.p.) controlling a single retinal stimulation patch (and the sampling frequency is selected so that there exists no aliasing effect), then different slices of a second-order kernel could be described as:

- $|\tau_1 - \tau_2| = 1.b.p.(flash\ train: 11) \Rightarrow SOK\ (First\ slice\ of\ second-order\ kernel)$
- $|\tau_1 - \tau_2| = 2.b.p.(flash\ train: 101) \Rightarrow SOSS\ (Second\ slice\ of\ second-order\ kernel)$
- $|\tau_1 - \tau_2| = 3.b.p.(flash\ train: 1001) \Rightarrow SOTS\ (Thrid\ slice\ of\ second-order\ kernel$
- $|\tau_1 - \tau_2| > N.b.p. \Rightarrow (flash\ train: 100 \ldots 1) \Rightarrow Higher\ order\ slices\ of\ second-order\ kernel$

The above definition of various slices of the second-order kernel is valid for a purely second-order system where the effect of the previous flash on the current response is investigated assuming system's memory of Nxb.p ms. So if previous flash is distanced by 1xb.p then the kernel slice is termed SOK. If it is separated by 3xb.p then it is termed SOTS and so on.

A.3 Walsh transform

Sutter (1991)[42] introduced Binary m-transform by replacing all 0's by 1's and the 1's by -1's in an array of binary m-sequences obtained from all cyclical-shifts of the mother m-sequence (sequence generated through modulo-2 feedback shift register with an appropriately selected set of tabs). The zeroth-element was then added as a cycle of its own (when all entries of the shift register are zero) to the matrix ensuring maintained symmetrical property. Sutter showed that the rows and columns of the matrix are orthogonal with respect to other rows and columns respectively. Therefore the generated m-transform matrix is an orthogonal matrix. Sutter then showed that all Walsh transform, and m-transform matrices of dimension 2^n (length is 2^n, as the zeroth element is now added) are in the same equivalence class (i.e. equivalent) of Hadamard matrices. A method of developing m-transform matrices was then demonstrated through the implementation of a shift register.

It was demonstrated that cross-correlation[321] is an effective and efficient method to characterise retinal function, knowing its input and output. Sutter further improved the efficiency of the calculation of cross-correlation operation to a single Fast Walsh transform that is performed in place of cross-correlation. This method effectively replaces the convolution by multiplication which is then preceded and followed by simple addition and subtraction through the use of the Walsh-Hadamard matrix.

Sutter's FWT matrix used to extract the individual kernel responses from the recorded mfERG response is illustrated in table A.1.

Table A.1: Walsh Transform matrix representation.

Flash train	Kernel Slice		(000)	(001)	(010)	(011)	(100)	(101)	(110)	(111)		Walsh Functions	Number of sign change (zero-crossing)
		j	0	1	2	3	4	5	6	7			
		x											
***	(000)	0	+1	+1	+1	+1	+1	+1	+1	+1	=	$\boldsymbol{\varphi_0}$	0
**f	(001)	1	+1	-1	+1	-1	+1	-1	+1	-1	=	$\boldsymbol{\varphi_1}$	7
f	(010)	2	+1	+1	-1	-1	+1	+1	-1	-1	=	$\boldsymbol{\varphi_2}$	3
*ff	(011)	3	+1	-1	-1	+1	+1	-1	-1	+1	=	$\boldsymbol{\varphi_3}$	4
f**	(100)	4	+1	+1	+1	+1	-1	-1	-1	-1	=	$\boldsymbol{\varphi_4}$	1
f*f	(101)	5	+1	-1	+1	-1	-1	+1	-1	+1	=	$\boldsymbol{\varphi_5}$	6
ff*	(110)	6	+1	+1	-1	-1	-1	-1	+1	+1	=	$\boldsymbol{\varphi_6}$	2
fff	(111)	7	+1	-1	-1	+1	-1	+1	+1	-1	=	$\boldsymbol{\varphi_7}$	5

First two digits (from left to right) = Pre-stimulus history and the third digit represent status of current stimulus.

The m-transform hides vast amounts of mathematical and engineering knowledge into a class of operation defined through simple addition and subtraction to extract kernel slices from the recorded retinal response and vice versa when using specific m-sequence array to govern stimulation patches (see figure A.3). The transform is independent of the stimulation sequence that is used as well as the spatial location which the sequence controls. The reversibility of this transform makes it even more useful,

allowing construction of algorithms to simulate retinal waveform under specific experimental setting through providing kernel slice table as input to the algorithm. It also makes it possible to extract the original kernels and associated slices using a simple cross-correlation technique.

It is also worth mentioning that the precise algorithm that is implemented amongst different commercially available systems (such as VERIS Scientific system, the AccuMap ObjectiVision, the RETIscan Roland system, MetroVision and SHIL Multi-focal Imager) may vary but the main principle here is that the sequences must be generated so they remain independent in both the time and space domain. Cross-correlation (see Appendix A.4) would then allow extraction of the spatiotemporal signals and even the cross-kernel responses (effect of the stimulus of one region on another) and/or induced components.

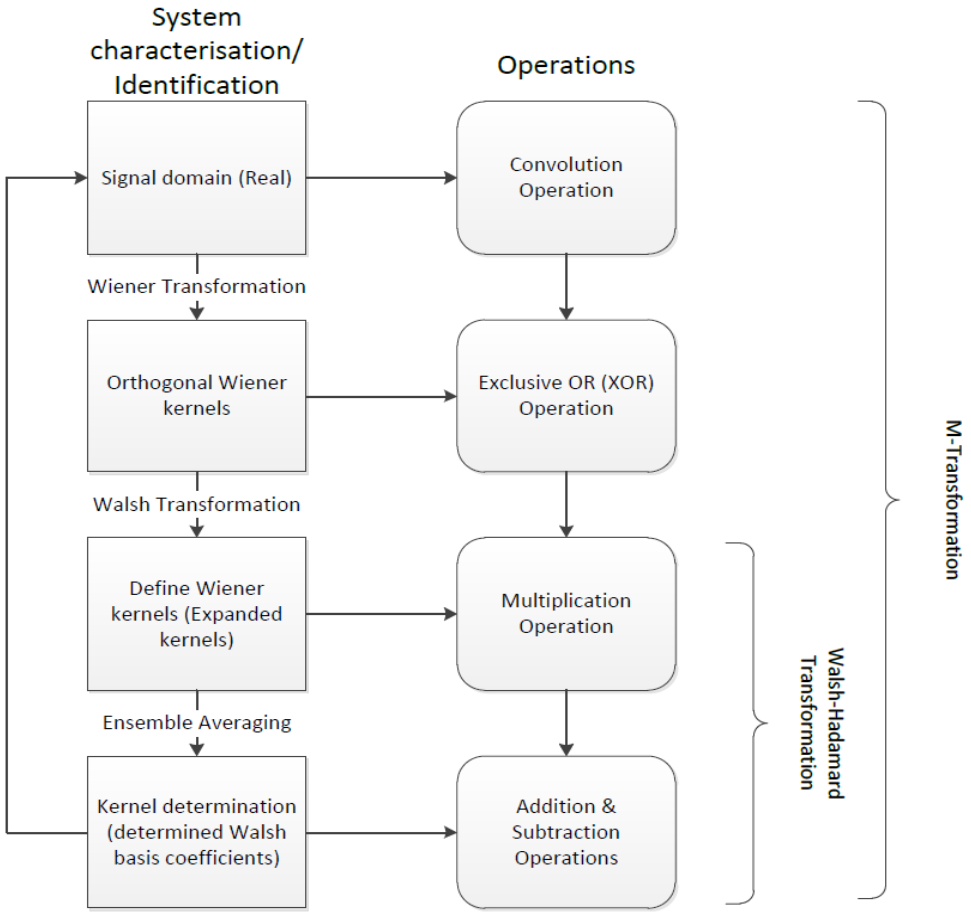

Figure A.3. System characterisation, operations and transformation through the use of powerful m-transform, which is in the same equivalent class of Walsh transform.

A.4 Cross-correlation method in nonlinear system characterisation

Volterra series is used to explain the relationship between input and output of a dynamic nonlinear time series[368]. The main issue with Volterra representation is that, even if the invoking signal is GWN, the H-functionals lack orthogonality[48]. This complicates the use of Volterra representation for complex nonlinear systems[369] such as the retina. To overcome this issue, one can either use Gram-Schmidt orthogonality procedure applied to the representative polynomial or use the Wiener approach developed by Wiener (1958)[312] to form a set of orthogonal basis functionals, termed G-functionals.

Two approaches are discussed in figure A.4:

1- One where Wiener G-functionals are developed/defined through ensuring orthogonalisation of G-functionals with lower-order Volterra H-functionals and next verifying orthogonality of n^{th} order G functionals with lower-order (m^{th}-order) G-functionals.
2- And the second approach is to mathematically determine/obtain G-functionals through cross-correlation procedure first developed by Lee and Schetzen (1965)[321]. The cross-correlation procedure would allow for investigation of the properties of the retina via knowledge of its input and output only, i.e. back-box (nonparametric) approach to retinal characterisation.

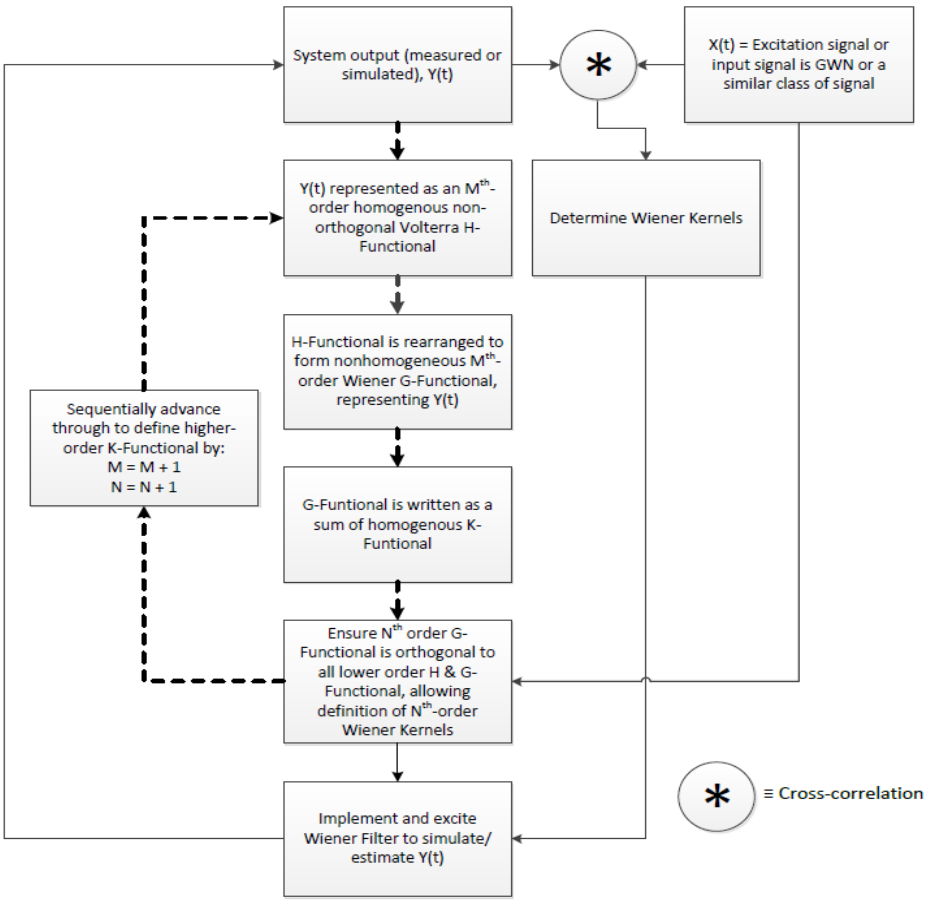

Figure A.4. Methods of defining G-Functional.

A.5 the ARMAsel model selection algorithm

A.5.1 Introduction

Three types of time series models can be distinguished, autoregressive (AR), moving average (MA) and the combined type (ARMA).

In general, an ARMA(p,q) process can be written as[370]:

$$x_n + a_1 x_{n-1} + \mathrm{L} \; + a_p x_{n-p} = \varepsilon_n + b_1 \varepsilon_{n-1} + \mathrm{L} \; + b_q \varepsilon_{n-q} \qquad (1)$$

where ε_n is a sequence of independent identically distributed random variables with zero mean and variance σ_ε^2.

We recover the AR and MA processes with *q*=0 and *p*=0, respectively.

By using the *z*-transform notation, we can write eq.1 compactly as:

$$A(z)x_n = B(z)\varepsilon_n$$

where the *A*(*z*) operator, say, is defined as:

$$A(z) = 1 + a_1 z^{-1} + \mathrm{L} \; + a_p z^{-p}.$$

The ARMAsel algorithm[371] allows selection of a suitable model for an observed time series, by choosing a model in the three classes AR, MA and ARMA. First an AR(*p*) model is fitted; then a MA(*q*) model is fitted; finally, an ARMA(*r*,*r*-1) model is fitted. In all cases, the parameters are automatically selected. The performances of the three models, estimated by the prediction error, are compared, and the one with the lowest error estimate is chosen. For further details, see [370] and [371].

A.5.2 AR estimation

It is well known that order selection algorithms based on asymptotic criteria [371] can give biased estimates which usually result in overfitting of the time series of length *N*, if the model order is higher than 0.1*N*.

For a given model order *p*, Burg's algorithm[370] provides an estimate of the model parameters. Based on these estimates, we may define the residual variance, which is a measure of the fitness of the model to the time series that has been used for estimation of the parameters themselves:

$$S^2(p) = \frac{1}{N-p} \sum_{i=p+1}^{N} \left[x(i) - \sum_{j=1}^{p} \hat{a}_j x(i-j) \right]^2.$$

It can be shown that the minimum of the following Combined Information Criterion provides an estimate of optimal model order[371]:

$$CIC(p) = \ln S^2(p) + \max\left[\prod_{i=0}^{p}\frac{1+\frac{1}{N+1-i}}{1-\frac{1}{N+1-i}} - 1, 3\sum_{i=0}^{p}\frac{1}{N+1-i}\right].$$

A.5.3 MA estimation

Theoretically, a MA(*q*) model is equivalent with an AR(∞) model[370], by using the relationship B(*z*)=1/A(*z*).

Durbin's method[370] uses the estimated parameters of a *long* AR model to approximate the MA model. In this case, we first estimate an AR model using CIC(*p*), and we use 2*p*+*q* as order of the intermediate AR model[372]. The MA order is selected by minimising the Generalised Information Criterion:

$$GIC(q) = \ln S^2(q) + 3q / N.$$

A.5.4 ARMA estimation

Durbin's method[370] can be used to estimate the ARMA(r,r-1) model. We first estimate an AR model using CIC(*p*). We then estimate an intermediate AR model of order 3*p*+2*r-1*. The procedure then involves using the estimated intermediate AR from MA estimation and updating cyclically the autoregressive part[372]. Selection of the optimal order can be obtained by minimising:

$$GIC(2r-1) = \ln S^2(2r-1) + (6r-3) / N.$$

Appendix B: Software algorithms and code & Hardware design

This thesis is accompanied by a cloud location (DropBox location: https://www.dropbox.com/sh/oz3kxophnhe7nl5/AAABGsSZg1IsxXFEmoQsW1Uza?dl=0), allowing the reader to download the accompanying files and data records referenced within the main text of this thesis.

The shared top-level directory is further split into multiple folders. The terminology used within the text of this thesis, the folder name and the file names provide an adequate clue as to the purpose of the file and its relation with regards to this thesis. All programming software codes are annotated extensively describing the functionality, input requirements and expected outputs. The annotations make these software modules self-explanatory and easy to read, re-use and understand.

With over thousands of files shared and hundreds of thousands of software programming lines in this cloud directory, it seems a little pointless to index them here.

The files in this directory are of the following types/formats:

- Software files (C, C++, C#, MATLAB, JAVA).
- CAD files (used for circuit design such as EAGLE).
- MS Word and Excel files.
- Collected biological raw data, mains record and their accompanying processed and conditioned files (these are mainly in MATLAB's native file format, .MAT). The collected biological data include EMG, blink, eye movement and noise files as well as the recorded electroretinogram biosignal.

The directory contains files to document the following:

- Liverpool bio amplifier circuit design, testing and description.
- Liverpool bio amplifier control software (MATLAB package) – see figure B.1.
- Liverpool bio amplifier MBED embedded C/C++ code – see figure B.2.
- iSim circuit design.
- iSim embedded C/C++ software code including the module that allows for the simulation of mfERG waveform based on received optical input – see figure B.3 for a visualisation of the implemented C++ array.
- iSim high-level C# software code and the accompanying Graphical User Interface (GUI) installation file and user guide.
- iSim command (CMD) and acknowledgement (ACK) specification datasheet allowing to interface with the iSim hardware from a terminal application or other user-selected environment (IDEs) capable of establishing an RS232 communication protocol
- ISIM MATLAB back-end engine software package and structure.
- ISIM MatSOAP server modified for 60 seconds timeout and the accompanying installation file. Figure B.4 illustrates the algorithm implemented for communication between thin MS Excel client application GUI and the back-end MATLAB engine using

MatSOAP as the designated SOAP server enabling both synchronised and asynchronised communication protocols.

- ISIM back-end library including the eye movement, blink, EMG, noise and mains interference data folders (processed data).
- ISIM maximally length sequence (m-sequence) simulator and extractor C++ code and GUI along with the installation files.
- ISIM m-sequence generator MATLAB toolbox.
- ISIM m-sequence verifier MATLAB toolbox.
- ISIM MSC algorithm implemented in MATLAB.
- Collected raw data, analysed and conditioned data files per the data collection protocol of section 3.6 of this thesis.
- Royal Liverpool and Broadgreen University Hospital (RLUBH) normal ERG and mfERG dataset incorporated within ISIM package.
- Mains interference data collected from RLUBH visual electrodiagnostic clinic room and the accompanying MATLAB toolbox to simulate mains interference.
- MATLAB implementation of figure digitisation toolbox.
- MATLAB implementation for random-walk implementation.
- MATLAB implementation toolbox of white, coloured and ARMA noise.
- MS Excel Visual Basic for Application (VBA) client code and GUI implementation used to communicate with ISIM back-end engine.
- Glasgow Multi-Focal Stimulator (MFS) MATLAB toolbox and integration file (allowing synchronisation with Liverpool bio amplifier GUI).
- Glasgow MFS MS Excel semi-automatic calibration file (also integrated with the Liverpool bio amplifier GUI control software package).

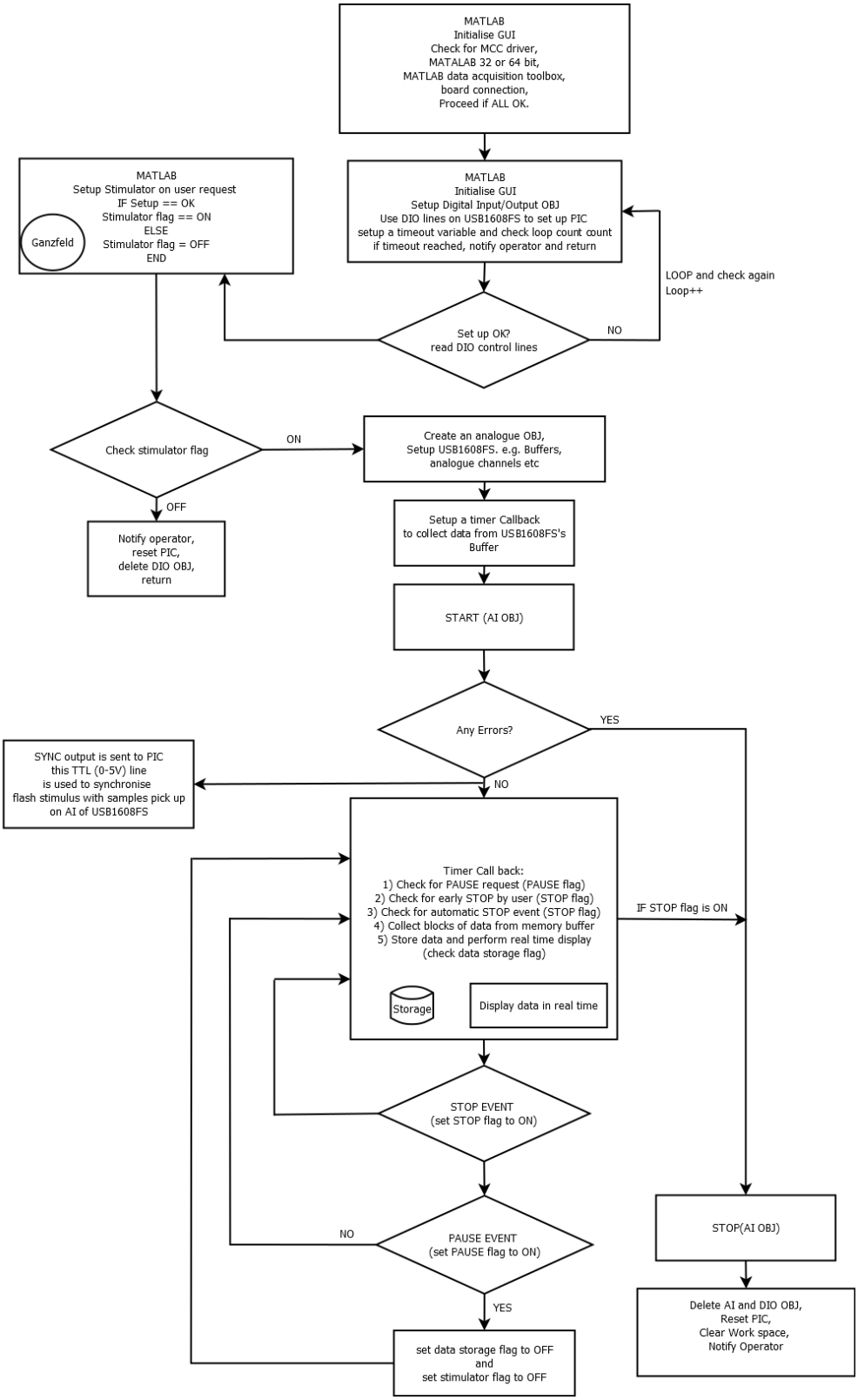

Figure B.1. Liverpool bio amplifier control software flowchart. The control software is fully synchronised with Roland Ganzfeld stimulator and Glasgow MFS LED-based stimulator.

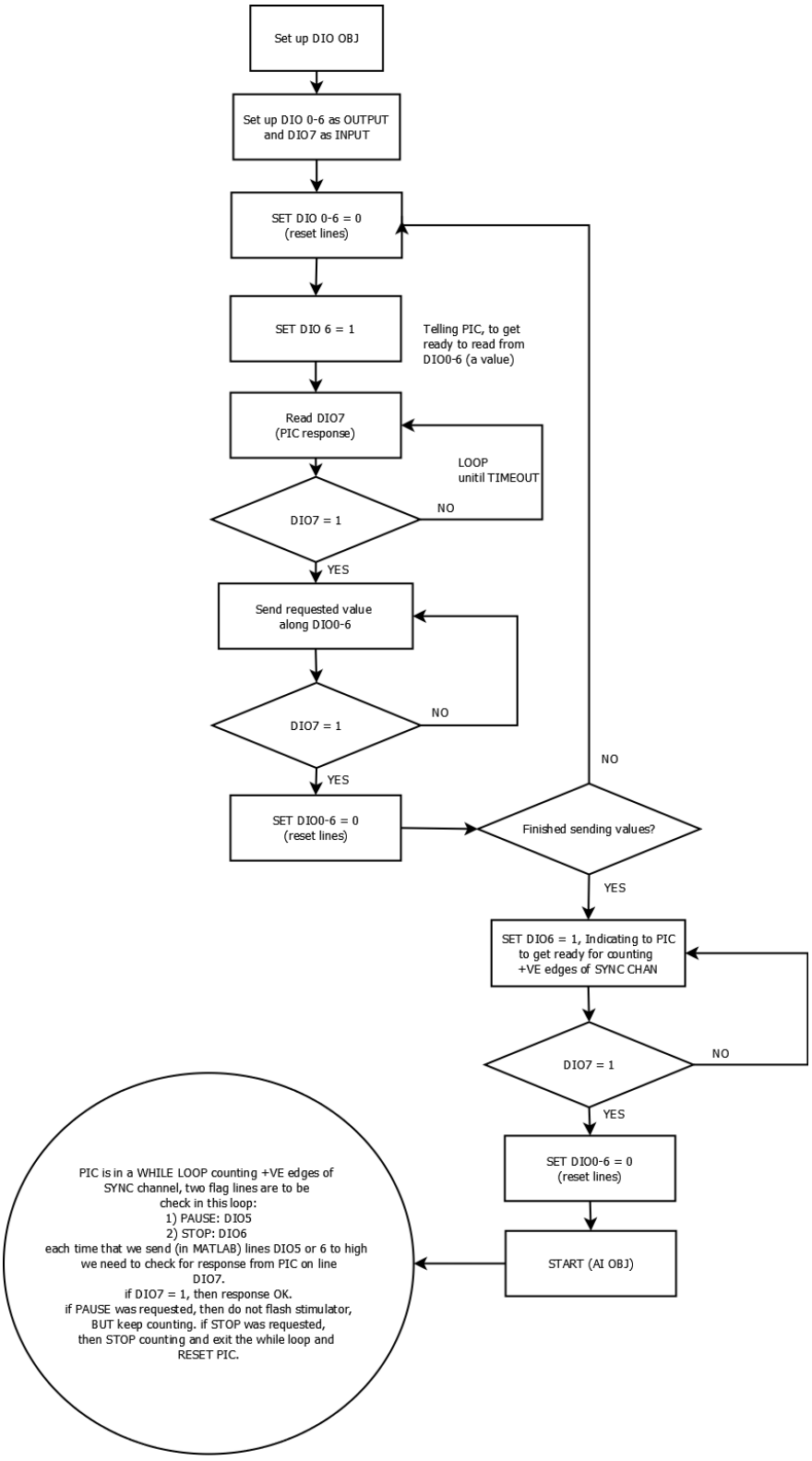

Figure B.2. Liverpool bio amplifier MBED embedded software code implementation flowchart. This software provides the required synchronisation with the high-level MATLAB control software and the stimulators (Roland Ganzfeld and Glasgow MFS).

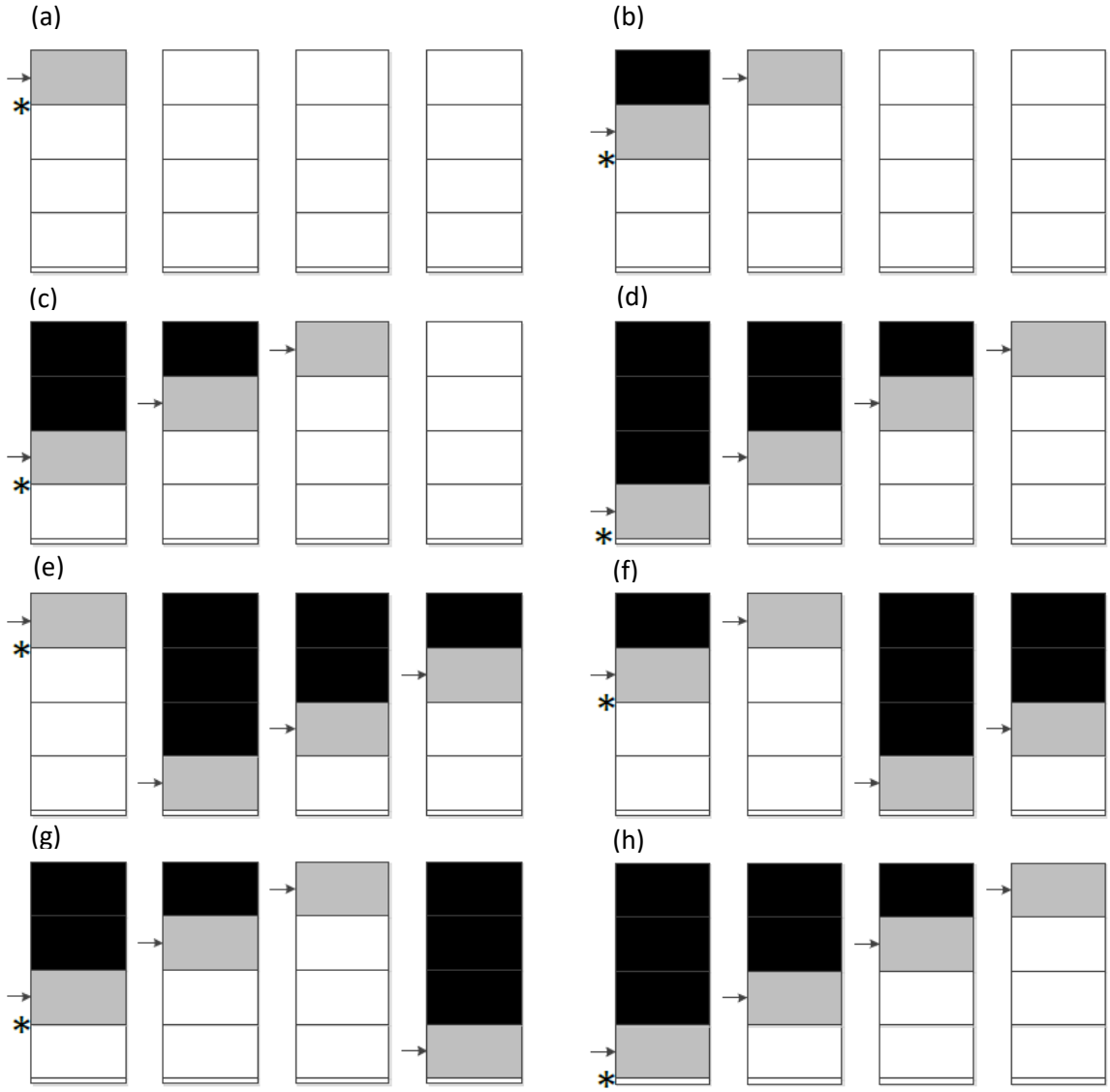

Figure B.3. Memory array represented in each (a) – (h) illustrates how signal memory buffer is managed at each call to timer object callback function. Each array represents the buffer state in between frames separated by b.p + 1 ms. This example assumes a b.p of 25 ms is selected. The asterisk denotes the time at which the timer object is triggered, and its call back is due execution. Arrows represent the index ($Index_{(i,j)}$) to the memory block (M_i) where the next signal sample is taken from and sent to the output. Each block is of length 100 ms and assuming a fixed sampling output rate of 1 kHz, it would contain 100 floating-point number. Since timer object is called four times before iSim scans through one memory block, four such blocks are required to be initialised so that 100 ms second of signal could be generated and sent to the Digital to Analogue Conversion (DAC) unit. The amplitude values (A) stored in each memory block is determined during timer object callback function based on values of memory register and signal array binary string representation. The output of Sample-Vector-Calculation module is then represented by:

$output\ sample = \sum_{i=1}^{4} A(index_{(i,j)}), where\ j = 1, 2, 3, \ldots, 100$

If measured or selected b.p = 10 ms, then one would require initialising ten such arrays to accurately calculate signal output samples. If b.p = 100 ms, then the system is assumed to be linear and only FOK will be used to represent the output signal. White regions demonstrate unread samples, black regions demonstrate scanned areas and grey regions demonstrates areas that are in the process of being scanned at a rate of 1 kHz in-between frames.

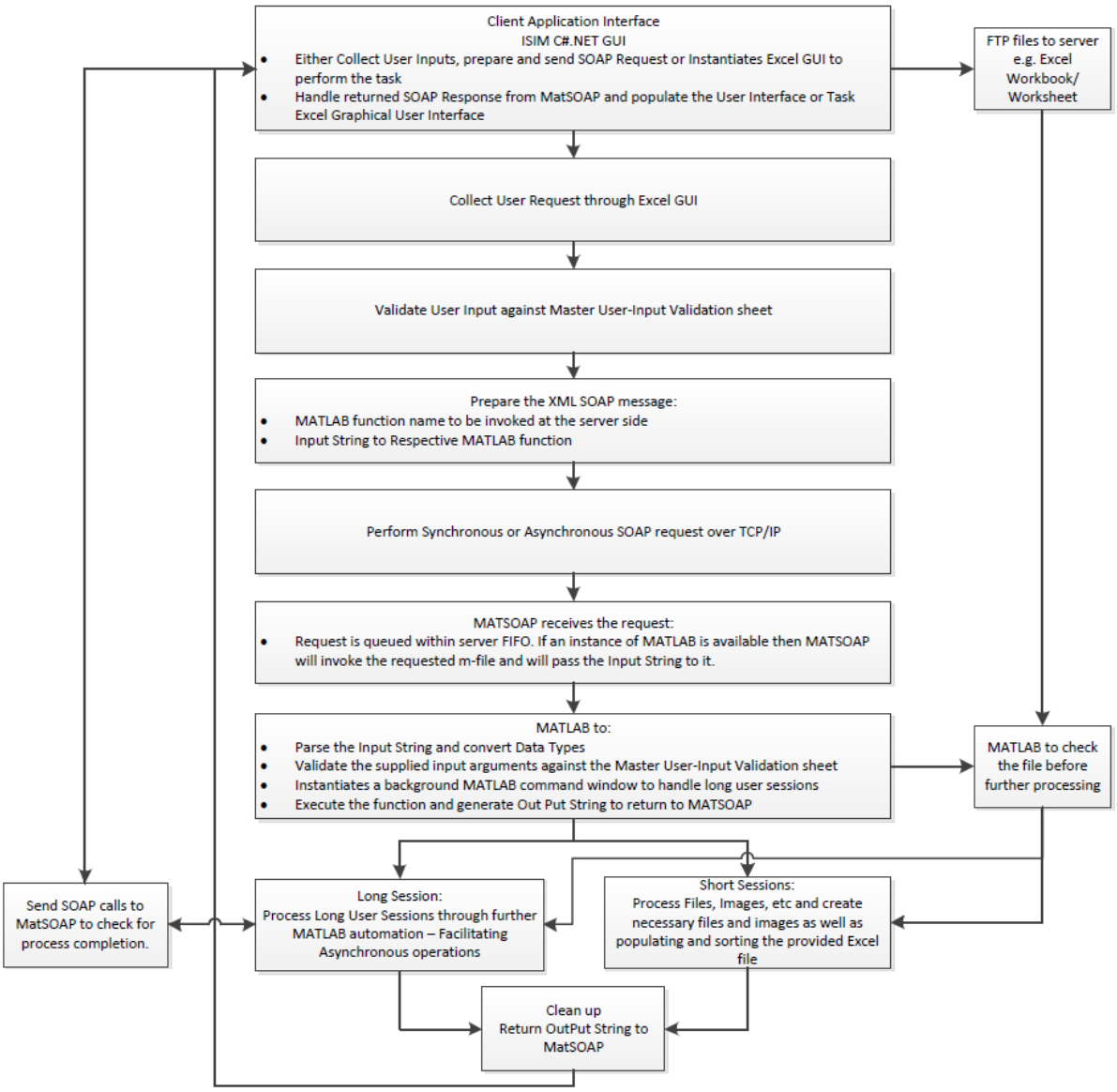

Figure B.4. The client application (MS Excel) – MatSOAP – MATLAB communication algorithm.

Appendix C: The proposed ethics research protocol & verified statistical analysis

Refer to, https://www.dropbox.com/sh/oz3kxophnhe7nl5/AAABGsSZg1IsxXFEmoQsW1Uza?dl=0, for the complete ethics protocol and the accompanying approved statistical analysis. The timing for completion of the proposed study and the sign off on the recommended statistical analysis is illustrated in figure C.1.

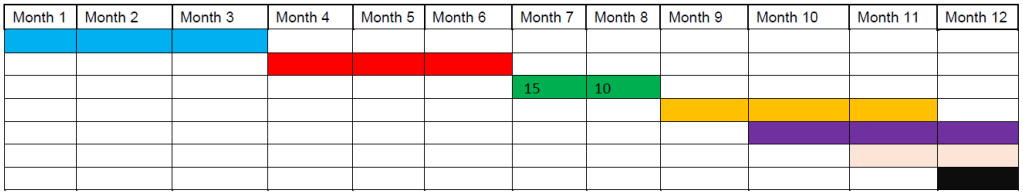

Notes:

1. Ethics Approval process is estimated as three-month process provided all required documents are in place.
2. The study site will be within UK so no time is planned for any translation (e.g. as part of submission to other competent authority beside MHRA)
3. The numbers inside the boxes refer to the minimum number of volunteers we aim to recruit in that month to reach our recruitment target.
4. Recruitment will begin before the study is initiated to ensure that clinic dates are well organised ensuring an expedited delivery of outcomes.

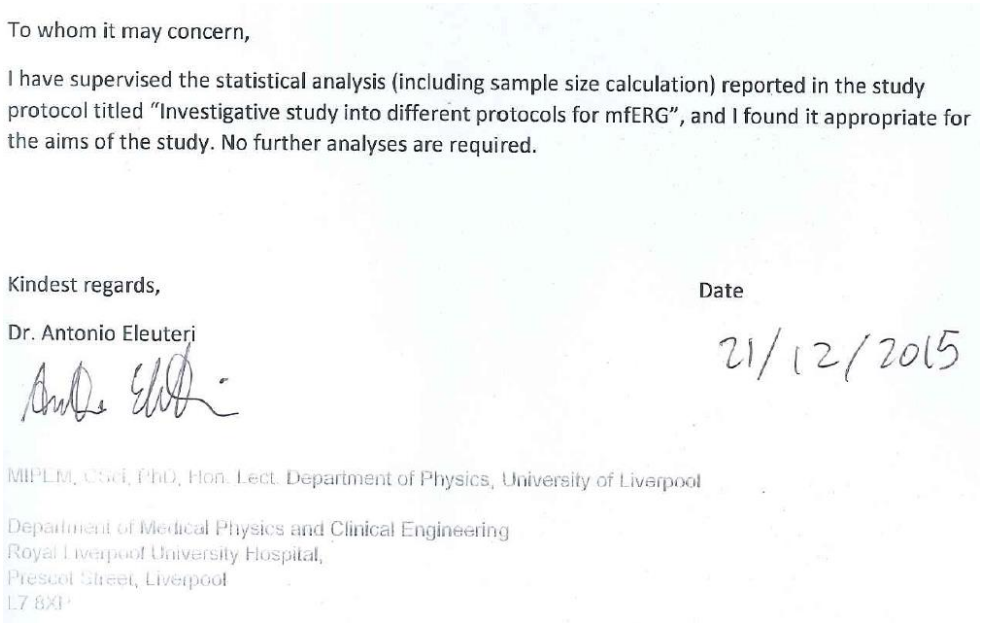

To whom it may concern,

I have supervised the statistical analysis (including sample size calculation) reported in the study protocol titled "Investigative study into different protocols for mfERG", and I found it appropriate for the aims of the study. No further analyses are required.

Kindest regards,

Date

Dr. Antonio Eleuteri

21/12/2015

MIPEM, CSci, PhD, Hon. Lect. Department of Physics, University of Liverpool

Department of Medical Physics and Clinical Engineering
Royal Liverpool University Hospital,
Prescot Street, Liverpool
L7 8XP

Figure C.1 (a) The proposed timing for a study to investigate and assess the reproducibility, reliability, variability (inter- and intra-subject and session) and SNR of different protocols for mfERG (per the proposed study design), using a multi-variate, multiple regression statistical model and analysis approved by Dr Antonio Eleuteri (b).
It is clear from the timeline that, a study (single-centre) of this size (see Appendix D) would take roughly 12 months to perform the analysis and write up. The timing for peer review and publications are not included.

References

[1] R. H. Masland, “The Neuronal Organization of the Retina,” *Neuron*, vol. 76, no. 2, pp. 266–280, 2012.

[2] J. B. Demb and J. H. Singer, “Functional Circuitry of the Retina,” *Annu. Rev. Vis. Sci.*, vol. 1, no. 1, pp. 263–289, 2015.

[3] M. Helmstaedter, K. Briggman, S. Turaga, V. Jain, S. Senug, and W. Denk, “Connectomic Reconstruction of the Inner Plexiform Layer in the Mouse Retina,” *Nature*, vol. 500, no. 7461, pp. 168–174, 2013.

[4] S. Seung, “Towards functional connectomics,” *Nature*, vol. 471, no. 3, pp. 171–172, 2011.

[5] R. Marc, B. Jones, C. Watt, J. Anderson, C. Signulinsky, and S. Lauritzen, “Retinal Connectomics: Towards Complete, Accurate Networks,” *Bone*, vol. 37, no. 1, pp. 141–162, 2013.

[6] M. F. Cordeiro, R. Nickells, W. Drexler, T. Borrás, and R. Ritch, “High-resolution ocular imaging: Combining advanced optics and microtechnology,” *Ophthalmic Surg. Lasers Imaging*, vol. 40, no. 5, pp. 480–488, 2009.

[7] E. Garcia-Martin *et al.*, “Electrophysiology and optical coherence tomography to evaluate parkinson disease severity,” *Investig. Ophthalmol. Vis. Sci.*, vol. 55, no. 2, pp. 696–705, 2014.

[8] A. R. Whatham, V. Nguyen, Y. Zhu, M. Hennessy, and M. Kalloniatis, “The value of clinical electrophysiology in the assessment of the eye and visual system in the era of advanced imaging,” *Clin. Exp. Optom.*, vol. 97, no. 2, pp. 99–115, 2014.

[9] J. Ng, “The Time is Now for Visual Electrophysiology,” *Int. J. Ophthalmic Pathol.*, vol. 01, no. 01, pp. 1–2, 2012.

[10] Jaakko Malmivuo and Robert Plonsey, *Bioelectromagnetism: Principles and Applications of Bioelectric and Biomagnetic Fields*. 1995.

[11] R. W. Rodieck, *The first steps in seeing*. 1998.

[12] G. E. Holder, G. G. Celesia, Y. Miyake, S. Tobimatsu, and R. G. Weleber, “International federation of clinical neurophysiology: Recommendations for visual system testing,” *Clin. Neurophysiol.*, vol. 121, no. 9, pp. 1393–1409, 2010.

[13] H. Kolb, E. Fernandez, and R. Nelson, *Webvision: The Organization of the Retina and Visual System*. Webvision, 2005.

[14] T. Euler and R. H. Masland, “Light-Evoked Responses of Bipolar Cells in a Mammalian Retina,” *J. Neurophysiol.*, vol. 83, no. 4, pp. 1817–1829, 2017.

[15] E. M. Callaway and J. J. Nassi, “Parallel processing strategies of the primate visual system,” *Nat. Rev. Neurosci.*, vol. 10, no. 5, pp. 360–372, 2009.

[16] W. B. Thoreson and S. C. Mangel, “Lateral interactions in the outer retina,” *Prog. Retin. Eye Res.*, vol. 31, no. 5, pp. 407–441, 2012.

[17] M. F. Marmor, “Vision, eye disease, and art: 2015 Keeler Lecture,” *Eye*, vol. 30, no. 2, pp. 287–303, 2016.

[18] H. Asi and I. Perlman, “Relationships between the electroretinogram a-wave, b-wave and oscillatory potentials and their application to clinical diagnosis,” *Doc. Ophthalmol.*, vol. 79, no. 2, pp. 125–139, 1992.

[19] K. T. Brown, “The Electroretinogram: Its components and Their Origins,” *Vision Res.*, vol. 8, pp. 633–677, 1968.

[20] K. T. Brown and T. N. Wieselt, “Intraretinal Recording with Micropipette Electrodes in the Intact Cat Eye,” *J. Physiol*, vol. 149, pp. 537–562, 1959.

[21] T. Tomita and Y. Torihama, “Further Study on the Intraretinal Action Potentials andd on the Site of ERG Generation,” *Dep. Physiol. , Tokyo Women’s Med. Coll. Ushigome , Tokyo*, 1956.

[22] R. Hanitzsch, “Intraretinal isolation of PIII subcomponents in the isolated rabbit retina after treatment with sodium aspartate,” *Vision Res.*, vol. 13, no. 11, pp. 2093–2102, 1973.

[23] E. A. Newman, “Current source-density analysis of the b-wave of frog retina.,” *J. Neurophysiol.*, vol. 43, no. 5, pp. 1355–1366, 2017.

[24] K. T. Brown and T. N. Wiesel, “Localization of Origins of Electroretinogram Components by Intraretinal Recording in the Intact Cat Eye,” *J. Phy8iol*, vol. 158, no. 2, pp. 257–280, 1961.

[25] X. Xu and C. J. Karwoski, “Current source density analysis of retinal field potentials. II. Pharmacological analysis of the b-wave and M-wave,” *J. Neurophysiol.*, vol. 72, no. 1, pp. 96–105, 2017.

[26] S. Sharma, S. L. Ball, and N. S. Peachey, “Pharmacological studies of the mouse cone electroretinogram,” *Vis. Neurosci.*, vol. 22, no. 5, pp. 631–636, 2005.

[27] N. Tian and M. M. Slaughter, “Correlation of dynamic responses in the ON bipolar neuron and theb-wave of the electroretinogram,” *Vision Res.*, vol. 35, no. 10, pp. 1359–1364, 1995.

[28] R. A. Shiells and G. Falk, “Contribution of rod, on-bipolar, and horizontal cell light responses to the ERG of dogfish retina,” *Vis. Neurosci.*, vol. 16, no. 3, pp. 503–511, 1999.

[29] M. Fujii, G. A. Sunagawa, M. Kondo, M. Takahashi, and M. Mandai, “Evaluation of micro Electroretinograms Recorded with Multiple Electrode Array to Assess Focal Retinal Function,” *Sci. Rep.*, vol. 6, no. July, pp. 1–12, 2016.

[30] R. Granit, “The Components of the Retinal Action Potential in Mammals and their Relation to the Discharge in the Optic Nerve,” *Physiol. Lab. Oxford*, 1911.

[31] O. Textorius, “The Influence of Stimulus Duration on the Human D.C Registered c-Wave,” *Acta Ophthalmol.*, vol. 55, no. 4, pp. 561–572, 2009.

[32] *Slow Potentials and Microprocessor Applications: Documenta Ophthalmologica Proceedings Series*, vol. 37. 1983.

[33] P. A. Hock and M. F. Marmor, “Variability of the Human C-Wave,” vol. 37, pp. 151–157, 2011.

[34] S. E. G. Nilsson and B. E. Andersson, “Corneal D.C. recordings of slow ocular potential changes

such as the ERG c-wave and the light peak in clinical work - Equipment and examples of results," *Doc. Ophthalmol.*, vol. 68, no. 3–4, pp. 313–325, 1988.

[35] D. C. Hood, "Assessing retinal function with the multifocal technique.," *Prog. Retin. Eye Res.*, vol. 19, no. 5, pp. 607–46, Sep. 2000.

[36] M. F. Marmor, A. Serrato, and R. Tzekov, "Comparison of conventional ERG parameters and high-intensity A-wave analysis in a clinical setting," *Doc. Ophthalmol.*, vol. 106, no. 3, pp. 281–287, 2003.

[37] L. Wachtmeister, "Basic research and clinical aspects of the oscillatory potentials of the electroretinogram," *Doc. Ophthalmol.*, vol. 66, no. 3, pp. 187–194, 1987.

[38] C. Gerth, "The role of the ERG in the diagnosis and treatment of Age-Related Macular Degeneration.," *Doc. Ophthalmol.*, vol. 118, no. 1, pp. 63–8, Feb. 2009.

[39] E. J. Berrow, H. E. Bartlett, F. Eperjesi, and J. M. Gibson, "The electroretinogram: a useful tool for evaluating age-related macular disease?," *Doc. Ophthalmol.*, vol. 121, no. 1, pp. 51–62, Aug. 2010.

[40] J. C. Armington, "The Electroretinogram, The Visual Evoked Potential, and the Area-Luminance Relation," *Vis. Res*, vol. 8, pp. 263–276, 1967.

[41] K. Shinoda, C. S. Matsumoto, and H. Ohde, "Objective Assessment of Local Retinal Function by Focal Macular and Multifocal Electroretinograms," 2003.

[42] E. E. Sutter, "The Fast *m* -Transform: A Fast Computation of Cross-Correlations with Binary *m* -Sequences," *SIAM J. Comput.*, vol. 20, no. 4, pp. 686–694, 1991.

[43] E. E. Sutter, T. Smith, K. Eye, and S. Francisco, "Noninvasive Testing Methods : Multifocal Electrophysiology," pp. 142–160, 2010.

[44] E. Sutter, "The interpretation of multifocal binary kernels.," *Doc. Ophthalmol.*, vol. 100, no. 2–3, pp. 49–75, Jan. 2000.

[45] F. J. MacWilliams and N. J. a Sloane, "Pseudo-Random Sequences and Arrays.," *Proc. IEEE*, vol. 64, no. 12, pp. 1715–1729, 1976.

[46] P. H. W. Chu, H. H. L. Chan, and S. J. Leat, "Effects of unsteady fixation on multifocal electroretinogram (mfERG).," *Graefes Arch. Clin. Exp. Ophthalmol.*, vol. 244, no. 10, pp. 1273–82, Oct. 2006.

[47] L. Thaler, a. C. Schütz, M. a. Goodale, and K. R. Gegenfurtner, "What is the best fixation target? The effect of target shape on stability of fixational eye movements," *Vision Res.*, vol. 76, pp. 31–42, Jan. 2013.

[48] H. W. Chen *et al.*, "Nonlinear analysis of biological systems using short M-sequences and sparse-stimulation techniques.," *Ann. Biomed. Eng.*, vol. 24, no. 4, pp. 513–36, 1996.

[49] R. P. Hagan, A. C. Fisher, and M. C. Brown, "Examination of short binary sequences for mfERG recording.," *Doc. Ophthalmol.*, vol. 113, no. 1, pp. 21–7, Jul. 2006.

[50] R. P. Hagan, A. C. Fisher, and M. C. Brown, "Investigation of the temporal properties of the retina

using the m-sequence.," *Doc. Ophthalmol.*, vol. 123, no. 3, pp. 179–85, Dec. 2011.

[51] C. Pieh, M. B. Hoffmann, and M. Bach, "The influence of defocus on multifocal visual evoked potentials.," *Graefes Arch. Clin. Exp. Ophthalmol.*, vol. 243, no. 1, pp. 38–42, Jan. 2005.

[52] a M. Palmowski, T. Berninger, R. Allgayer, H. Andrielis, B. Heinemann-Vernaleken, and G. Rudolph, "Effects of refractive blur on the multifocal electroretinogram.," *Doc. Ophthalmol.*, vol. 99, no. 1, pp. 41–54, Jan. 1999.

[53] C. M. Poloschek and M. Bach, "The mfERG response topography with scaled stimuli: Effect of the stretch factor," *Doc. Ophthalmol.*, vol. 119, no. 1, pp. 51–58, 2009.

[54] E. E. Sutter and D. Tran, "The field topography of ERG components in man--I. The photopic luminance response.," *Vision Res.*, vol. 32, no. 3, pp. 433–46, Mar. 1992.

[55] C. M. Poloschek and E. E. Sutter, "The fine structure of multifocal ERG topographies," *J. Vis.*, vol. 2, no. 8, p. 5, Dec. 2002.

[56] D. C. Hood *et al.*, "ISCEV standard for clinical multifocal electroretinography (mfERG) (2011 edition).," *Doc. Ophthalmol.*, vol. 124, no. 1, pp. 1–13, Feb. 2012.

[57] D. Keating, S. Parks, and a Evans, "Technical aspects of multifocal ERG recording.," *Doc. Ophthalmol.*, vol. 100, no. 2–3, pp. 77–98, Jan. 2000.

[58] D. Browning and C. Lee, "Test-retest variability of multifocal electroretinography in normal volunteers and short-term variability in hydroxychloroquine users," *Clin. Ophthalmol.*, vol. 8, p. 1467, Aug. 2014.

[59] F. C. Gundogan, G. Sobaci, and M. Z. Bayraktar, "Intra-sessional and inter-sessional variability of multifocal electroretinogram," *Doc. Ophthalmol.*, vol. 117, no. 3, pp. 175–183, 2008.

[60] Á. García-García, F. J. Muñoz-Negrete, and G. Rebolleda, "Variability of the multifocal electroretinogram based on the type and position of the electrode," *Doc. Ophthalmol.*, vol. 133, no. 2, pp. 99–108, 2016.

[61] D. W. Cockcroft, F. Faaaai, P. Nair, F. Frcpc, P. Nair, and F. Frcpc, "Reproduced with permission of the copyright owner . Further reproduction prohibited without," *J. Allergy Clin. Immunol.*, vol. 130, no. 2, p. 556, 2012.

[62] a C. Cheng, C. P. Pang, a T. Leung, J. K. Chua, D. S. Fan, and D. S. Lam, "The association between cigarette smoking and ocular diseases.," *Hong Kong Med. J.*, vol. 6, no. 2, pp. 195–202, Jun. 2000.

[63] M. Bock, M. Andrassi, L. Belitsky, and B. Lorenz, "A comparison of two multifocal ERG systems.," *Doc. Ophthalmol.*, vol. 97, no. 2, pp. 157–78, 1999.

[64] K. Bradshaw, R. Hansen, and A. Fulton, "Comparison of ERGs recorded with skin and corneal-contact electrodes in normal children and adults.," *Doc. Ophthalmol.*, vol. 109, no. 1, pp. 43–55, Jul. 2004.

[65] R. Karanjia, M. W. ten Hove, and S. G. Coupland, "Electroretinograms and Normative Data."

[66] N. Meziane, J. G. Webster, M. Attari, and a J. Nimunkar, "Dry electrodes for electrocardiography," *Physiol. Meas.*, vol. 34, no. 9, pp. R47–R69, Sep. 2013.

[67] M. He and P. Lachapelle, “Reproducibility of ERG responses obtained with the DTL electrode,” vol. 39, pp. 1069–1070, 1999.

[68] C. A. Grimbergen, A. C. Mettingvanrijn, and A. Peper, “A method for the measurement of the properties of individual electrode-skin interfaces and the implications of the electrode properties for preamplifier design .’,” no. 991667, pp. 2382–2383.

[69] G. B. Arden, C. R. Hogg, and G. E. Holder, “Gold foil electrodes: a two-center study of electrode reliability.,” *Doc. Ophthalmol.*, vol. 86, no. 3, pp. 275–84, Jan. 1994.

[70] L. Esakowitz, A. Kriss, and F. Shawkat, “A Comparison of Flash Electroretinograms Recorded from Burian Allen, Jet, C-Glide, Gold Foil, DTL and Skin Electrodes,” pp. 169–171, 1993.

[71] R. R. Hidajat, J. L. McLay, M. J. Elder, D. H. Goode, J. P. Morton, and C. D. Burley, “A comparison of two patient-friendly ERG electrodes.,” *Australas. Phys. Eng. Sci. Med.*, vol. 26, no. 1, pp. 30–4, Mar. 2003.

[72] M. Kuze and Y. Uji, “Comparison Between Dawson , Trick , and Litzkow Electrode and Contact Lens Electrodes Used in Clinical Electroretinography,” vol. 5155, no. 00.

[73] A. Kriss, “Skin ERGS : their effectiveness in paediatric visual assessment , confounding factors , and comparison with ERGS recorded using various types of cornea1 electrode,” *Int. J. Psychophysiol.*, vol. 16, no. 1, pp. 137–146, 1994.

[74] N. Mohidin, M. K. H. Yap, and R. J. Jacobs, “Electrodes for Multifocal Electroretinography (mfERG): A Comparison of Four Electrodes Types,” *Sains Malaysiana*, vol. 43, no. 7, pp. 1089–1094, 2014.

[75] M. Yoshii *et al.*, “A basic investigation of multifocal electroretinogram: reproducibility and effect of luminance.,” *Jpn. J. Ophthalmol.*, vol. 44, no. 2, pp. 122–7, 2000.

[76] W. a Verdon and G. Haegerstrom-Portnoy, “Topography of the multifocal electroretinogram.,” *Doc. Ophthalmol.*, vol. 95, no. 1, pp. 73–90, Jan. 1998.

[77] A. V Chappelow and M. F. Marmor, “Effects of pre-adaptation conditions and ambient room lighting on the multifocal ERG.,” *Doc. Ophthalmol.*, vol. 105, no. 1, pp. 23–31, Jul. 2002.

[78] C. Gerth, S. M. Garcia, L. Ma, J. L. Keltner, and J. S. Werner, “Multifocal electroretinogram: Age-related changes for different luminance levels,” *Graefe’s Arch. Clin. Exp. Ophthalmol.*, vol. 240, no. 3, pp. 202–208, 2002.

[79] H. Langrová, E. Zrenner, A. Kurtenbach, and M. W. Seeliger, “Age-related changes in retinal functional topography,” *Investig. Ophthalmol. Vis. Sci.*, vol. 49, no. 11, pp. 5024–5032, 2008.

[80] W. K. Tam, H. Chan, B. Brown, K. W. Leung, V. Woo, and M. Yap, “Aging and mfERG topography,” *Eye*, vol. 20, no. 1, pp. 18–24, 2006.

[81] M. M. Parvaresh, L. Ghiasian, K. Ghasemi Falavarjani, M. Soltan Sanjari, and N. Sadighi, “Normal values of standard full field electroretinography in an Iranian population,” *J. Ophthalmic Vis. Res.*, vol. 4, no. 2, pp. 97–101, 2009.

[82] C. Gerth, E. E. Sutter, and J. S. Werner, “mfERG response dynamics of the aging retina.,” *Invest. Ophthalmol. Vis. Sci.*, vol. 44, no. 10, pp. 4443–50, Oct. 2003.

[83] G. G. Celesla, D. Kaufman, and S. Cone, “Effects of age and sex on pattern electroretinograms and visual evoked potentials,” *Electroencepnalography chmcal N Eur. ,* vol. 68, no. 3, pp. 161–171, 1986.

[84] S. Tobimatsu, S. Kurita-Tashima, M. Nakayama-Hiromatsu, K. Akazawa, and M. Kato, “Age-related changes in pattern visual evoked potentials: differential effects of luminance, contrast and check size,” *Electroencephalogr. Clin. Neurophysiol. Evoked Potentials*, vol. 88, no. 1, pp. 12–19, 1993.

[85] R. Sharma, S. Joshi, K. D. Singh, and A. Kumar, “Visual evoked potentials: Normative values and gender differences,” *J. Clin. Diagnostic Res.*, vol. 9, no. 7, pp. 12–15, 2015.

[86] P. de F. Dotto, A. Berezovsky, P. Y. Sacai, D. M. Rocha, and S. R. Salomão, “Gender-based normative values for pattern-reversal and flash visually evoked potentials under binocular and monocular stimulation in healthy adults,” *Doc. Ophthalmol.*, vol. 135, no. 1, pp. 53–67, 2017.

[87] M. Mahjoob, J. Heravian Shandiz, A. Mirzajani, A. Ehsaei, and E. Jafarzadehpur, “Normative values of visual evoked potentials in Northeastern of Iran,” *J. Optom.*, pp. 1–6, 2019.

[88] A. Al Abdlseaed, Y. McTaggart, T. Ramage, R. Hamilton, and D. L. McCulloch, “Light- and dark-adapted electroretinograms (ERGs) and ocular pigmentation: comparison of brown- and blue-eyed cohorts.,” *Doc. Ophthalmol.*, vol. 121, no. 2, pp. 135–46, Oct. 2010.

[89] P. Gonzalez, S. Parks, F. Dolan, and D. Keating, “The effects of pupil size on the multifocal electroretinogram.,” *Doc. Ophthalmol.*, vol. 109, no. 1, pp. 67–72, Jul. 2004.

[90] C. M. Poloschek and M. Bach, “Can we do without mydriasis in multifocal ERG recordings?,” *Doc. Ophthalmol.*, vol. 118, no. 2, pp. 121–7, Apr. 2009.

[91] L. R. Barbosa Júnior, “Normative Study of the Full Field Electroretinogram in Cats: a Fast Dark-Adaptation Curve,” *Adv. Ophthalmol. Vis. Syst.*, vol. 4, no. 3, 2016.

[92] S. R. Simão S, Costa M, Â, Sun J, K, Cunha-Vaz J, “Development of a Normative Database for Multifocal Electroretinography in the Context of a Multicenter Clinical Trial,” *Ophthalmic Res*, vol. 57, pp. 107–117, 2017.

[93] W. W. Harrison, M. A. Bearse, J. S. Ng, S. Barez, M. E. Schneck, and A. J. Adams, “Reproducibility of the mfERG between instruments,” *Doc Ophthalmol*, vol. 119, no. 1, pp. 67–78, 2009.

[94] E. Huigen, “Noise characteristics of surface electrodes,” 2001.

[95] M. Brigell, M. Bach, C. Barber, K. Kawasaki, and a Kooijman, “Guidelines for calibration of stimulus and recording parameters used in clinical electrophysiology of vision. Calibration Standard Committee of the International Society for Clinical Electrophysiology of Vision (ISCEV).,” *Doc. Ophthalmol.*, vol. 95, no. 1, pp. 1–14, Jan. 1998.

[96] W. Lin and X. Fan, “Software development practice for FDA-compliant medical devices,” *Proc. 2009 Int. Jt. Conf. Comput. Sci. Optim. CSO 2009*, vol. 2, pp. 388–390, 2009.

[97] IMDRF SaMD Working Group, “Software as a Medical Device: Application of Quality Management System,” *Int. Med. Device Regul. Forum*, 2015.

[98] International Medical Device Regulatory Forum, “IMDRF Software as a Medical Device (SaMD),” 2013.

[99] Food and Drug Administration, “N41 Software as a Medical Device (SAMD): Clinical Evaluation Guidance for Industry and Food and Drug Administration Staff,” pp. 1–32, 2017.

[100] N. Riaz, S. L. Wolden, D. Y. Gelblum, and J. Eric, “Collaborating and sharing data in Epilepsy Research,” vol. 118, no. 24, pp. 6072–6078, 2016.

[101] M. Ihle *et al.*, “EPILEPSIAE - A European epilepsy database,” *Comput. Methods Programs Biomed.*, vol. 106, no. 3, pp. 127–138, 2012.

[102] J. C. Dean Hart and D. Papakostopoulos, “Electrodiagnostic evaluation of the visual system: the role of the clinician,” *Int. J. Psychophysiol.*, vol. 16, no. 2–3, pp. 121–129, 1994.

[103] B. Young, E. Eggenberger, and D. Kaufman, “Current electrophysiology in ophthalmology: A review,” *Curr. Opin. Ophthalmol.*, vol. 23, no. 6, pp. 497–505, 2012.

[104] J. Somlai, *Neuro-Ophthalmology*. 2016.

[105] D. L. McCulloch *et al.*, “ISCEV Standard for full-field clinical electroretinography (2015 update),” *Doc. Ophthalmol.*, vol. 130, no. 1, pp. 1–12, 2015.

[106] L. L. Emanuel, “Ethics and the Structures of Healthcare,” *Cambridge Univ. Press*, vol. 9, no. 2, pp. 151–168, 2000.

[107] A. R. Whatham, V. Nguyen, Y. Zhu, M. Hennessy, and M. Kalloniatis, “The value of clinical electrophysiology in the assessment of the eye and visual system in the era of advanced imaging.,” *Clin. Exp. Optom.*, vol. 97, no. 2, pp. 99–115, Mar. 2014.

[108] M. Piccolino, “Visual images in Luigi Galvani’s path to animal electricity,” *J. Hist. Neurosci.*, vol. 17, no. 3, pp. 335–348, 2008.

[109] C. Cajavilca, J. Varon, and G. L. Sternbach, “Luigi Galvani and the foundations of electrophysiology,” *Resuscitation*, vol. 80, no. 2, pp. 159–162, 2009.

[110] M. Piccolino, “Luigi Galvani and animal electricity: Two centuries after the foundation of electrophysiology,” *Trends Neurosci.*, vol. 20, no. 10, pp. 443–448, 1997.

[111] G. Finkelstein, “Mechanical neuroscience: Emil du Bois-Reymond’s innovations in theory and practice,” *Front. Syst. Neurosci.*, vol. 9, no. September, pp. 1–4, 2015.

[112] J. M. and R. Plonsey, “Bioelectromagnetism: Principles and Applications of Bioelectric and Biomagnetic Fields,” *Elem. Sonata Theory Norms, Types, Deform. Late-Eighteenth-Century Sonata*, no. June 2019, pp. 603–610, 1995.

[113] Thomas F. Collura, “History and Evolution of Electroencephalogtaphic Instruments and Techniques.” 1993.

[114] M. Drazek, M. Lew, S. Lew, and A. Pomianowski, “Electroretinography in dogs: A review,” *Vet. Med. (Praha).*, vol. 59, no. 11, pp. 515–526, 2014.

[115] A. Balicka, A. Trbolová, and T. Vrbovská, “Electroretinography (A Review),” *Folia Vet.*, vol. 60, no. 1, pp. 53–58, 2016.

[116] M. A. ALI, *Vision in fishes: new approaches in research*. 1975.

[117] and M. B. John R. Heckenlively, Geoffrey B. Arden, *Principles and Practice of Clinical Electrophysiology of Vision*. 2006.

[118] T. H. E. Time, R. Of, C. I. N. The, and F. Gotch, "Physiology, University of Oxford. (With," 1900.

[119] C. Zywietz, "A Brief History of Electrocardiography-Progress through Technology," *Biosignal Inst. Biosignal Process. …*, pp. 1–10, 2003.

[120] T. Shipley and M. T. Anton, "The human electroretinogram in the first day of life," *J. Pediatr.*, vol. 65, no. 5, pp. 733–739, 1964.

[121] C. Fisch, "Centennial of the string galvanometer and the electrocardiogram," *J. Am. Coll. Cardiol.*, vol. 36, no. 6, pp. 1737–1745, 2000.

[122] W. Einthoven and W. A. Jolly, "the Form and Magnitude of the Electrical Response of the Eye To Stimulation By Light At Various Intensities," *Q. J. Exp. Physiol.*, vol. 1, no. 4, pp. 373–416, 1908.

[123] L. A. Riggs, "Electrophysiological techniques for studying visual function in man: A historical overview," *J. Opt. Soc. Am.*, vol. 67, no. 11, p. 1451, 1977.

[124] J. E. H. S. Gasser, "A Stidy of the Action Currents of Nerve with the Cathode Ray Oscilligraph," *Lab. Pharmacalogy Physiol. Washingt. Univ. Sch. Med.*, 1922.

[125] B. Matthews, "A New Electrical Recording System for Physiological Work," *J. Physiol.*, vol. 65, no. 3, pp. 225–242, 1928.

[126] L. A. Riggs, "Continuous and reproducible records of the electrical activity of the human retina," *Proc. Soc. Exp. Biol. Med.*, vol. 48, no. 1, 1941.

[127] A. McAllan, J. Sinn, and G. W. Aylward, "The Effect of Gold Foil Electrode Position on the Electroretinogram in Human Subjects," *Vis. Res*, vol. 29, no. 9, pp. 1085–1087, 1988.

[128] G. B. Arden, R. M. Carter, C. Hogg, I. M. Siegel, and S. Margolis, "A gold foil electrode: Extending the horizons for clinical electroretinography," *Investig. Ophthalmol. Vis. Sci.*, vol. 18, no. 4, pp. 421–426, 1979.

[129] R. William, W. Dawson, G. L. Trick, and C. A. Litzkow, "Improved electrode for electroretinography," *Invest. Ophthalmol. Vis. Sci.*, vol. 18, no. 9, pp. 988–991, 1979.

[130] G. Karpe, "a Routine Method of Clinical Electroretinography," *Acta Ophthalmol.*, vol. 40, no. 70 S, pp. 15–31, 1962.

[131] A. Bjork and G. Karpe, "the Clinical Electroretinogram V. The Electroretinogram in retinitis Pigmentosa," *Acta Ophthalmol.*, vol. 37, no. 3, pp. 294–301, 1945.

[132] G. Karpe, "Apparatus and method for clinical recorded of the electroretinogram," *Doc. Ophthalmol.*, vol. 2, no. 1, pp. 268–276, 1947.

[133] G. Karpe, T. Kornerup, and B. Wulfing, "The clinical Electroretinogram VIII. The Electroretinogram in Diabetic Retinopathy," *Acta Ophthalmol.*, vol. 239, no. 7, pp. 2292–2297, 1964.

[134] G. Karpe, K. Rickenbach, and S. Thomasson, "The Clinical Electroretinogram The Normal Electroretinogram above Fifty Years of Age," *Acta Ophthalmol.*, vol. 37, no. 3, pp. 294–301, 2009.

[135] G. Karpe and K. Tansley, “The Relationship Between the Change in the Electroretinogram and the Subjective Dark-Adaptation Curve,” *J. Physiol*, pp. 272–279, 1947.

[136] G. Karpe, “Early Diagnosis of Siderosis Retinae by the Use of Electroretinography,” *Doc. Ophthalmol.*, vol. 2, no. 1, pp. 277–296, 1947.

[137] G. Karpe and I. Rendahl, “The Clinical Electroretinogram VI. The Electroretinogram in Detachment of the Retina,” vol. 30, 1951.

[138] G. Karpe and B. Vainio-Mattila, “The Clinical Electroretinogram III. The Electroretinogram in Cataract,” *Eye Clin. Karolinska Sjukhuset, Stock.*, vol. 29, 1948.

[139] H. Kaneko, T. Sigumachi, and O. Nakagawa, “ASimplified Set Up for Clinical Electroretinography. The ERG Recorded at High Stimulus and Adaptation Levels,” pp. 462–472, 1945.

[140] R. Dhanda, “Clinical application of electro-retinography,” *Mahatma Gandhi Meml. Med. Coll. Indore, India*, vol. 9, no. 1, pp. 33–38, 1956.

[141] E. G. Niemeyer and C. Huber, “Techniques in Clinical Electrophysiology of Vision,” *Doc. Ophthalmol.*, vol. 31, p. 523, 1982.

[142] J. Rover and M. Huttel, “The Amplitude of the C Wave in the Human ERG as a Function of the Luminance Energy of the Stimulus,” *Springer-Verlag*, vol. 217, pp. 299–307, 1981.

[143] M. Fioretto, C. Orione, C. Ciurlo, E. Volpi, C. Burtolo, and G. P. Fava, “Electrical activity of retinal pigment epithelium evaluated by EOG and c-wave,” pp. 59–62, 2011.

[144] G. B. Arden, A. Barradat, and J. H. Kelsey, “New clinical Test of Retinal Function Based upon the Standing Potential of the Eye,” *Brit. J. Ophthal*, pp. 449–467, 1962.

[145] R. H. Steinberg, “Interactions between the retinal pigment epithelium and the neural retina,” *Doc. Ophthalmol.*, vol. 346, 1985.

[146] M. F. Marmor, “Clinical electrophysiology of the retinal pigment epithelium,” *Doc. Ophthalmol.*, vol. 76, no. 4, pp. 301–313, 1991.

[147] G. B. Arden and J. H. Kelsey, “Changes produced by light in the standing potential of the human eye,” *J. Physiol.*, vol. 161, no. 2, pp. 189–204, 1962.

[148] J. S. Barlow, “The early history of EEG data-processing at the Massachusetts Institute of Technology and the Massachusetts General Hospital,” *Int. J. Psychophysiol.*, vol. 26, no. 1–3, pp. 443–454, 1997.

[149] E. L. Rabin, Arnold R. Berson, “A Full-Field System for Clinical Electroretinography,” no. 7, 1974.

[150] S. Kimura, “Photically Central Visual Electrically System of Elicited the Responses Squirrel in the Monkey,” vol. 51, pp. 19–51, 1964.

[151] B. Matthews, “A New Electrical Recording System for Physiological Work,” *Physiol. Lab. Cambridge*, 1928.

[152] E. D. Adrian and H. C. Matthews, “The Interppretation of Potential Waves in the Cortex,” *Physiol. Lab. Cambridge*, pp. 440–471, 1934.

[153] E. D. Adrian and H. C. Matthews, “The Berger Rhythm: Potential Changes from the Occipital Lobes in Man,” *Physiol. Lab. Cambridge*, vol. 57, 1934.

[154] R. Kline, “Harold Black and the Negative-Feedback Amplifier,” *IEEE Control Syst.*, vol. 13, no. 4, pp. 82–85, 1993.

[155] W. M. Siebert, “Processing Neuroelectric Data,” 1959.

[156] W. A. Clark, R. M. Brown, M. H. Goldstein, C. E. Molnars, D. F. O’Brien, and H. E. Zieman, “The Average Response Computer (ARC): a Digital Device for Computing Averages and Amplitude and Time Histograms of Electrophysiological Response,” *Ire Trans. Biomed. Electron.*, vol. 8, no. 1, pp. 46–51, 1961.

[157] K. A. Kooi and B. K. Bagchi, “Visual Evoked responses in Man: Normative Data,” *J Clin Diagn Res*, vol. 9, no. 7, 1956.

[158] W. Buxton *et al.*, “Interaction at Lincoln laboratory in the 1960’s: looking forward - looking back,” *CHI ’05 Ext. Abstr. Hum. factors Comput. Syst.*, pp. 1162–1167, 2005.

[159] M. Bouguer, *Essai d’optique sur la gradation de la lumière*. 1729.

[160] D. L. Mcculloch and R. Hamilton, “Essentials of photometry for clinical electrophysiology of vision,” pp. 77–84, 2010.

[161] W. E. K. Middleton, “Bouguer , Lambert , and the Theory of Horizontal Visibility,” *Hist. Sci. Soc.*, vol. 51, no. 2, pp. 145–149, 1960.

[162] D. Whitaker and D. B. Elliott, “Simulating age-related optical changes in the human eye,” *Doc. Ophthalmol.*, vol. 82, pp. 307–316, 1992.

[163] O. Paper, “Age-Related Changes in Spectral Transmittance of the Human Crystalline Lens in situ,” vol. 0021, pp. 174–180, 2012.

[164] J. M. Artigas, A. Felipe, A. Navea, and A. Fandi, “Spectral Transmission of the Human Crystalline Lens in Adult and Elderly Persons : Color and Total Transmission of Visible Light,” vol. 53, no. 7, pp. 4076–4084, 2012.

[165] P. K. Kaiser, “Sensation Luminance: A New Name to Distinguish CIE Luminance from Luminance Dependent on an Individual Spectral Sensetivity,” *Vis. Res*, vol. 28, no. 3, pp. 455–456, 1988.

[166] T. . Goodman, “The Use of Terms and Units in Photometry – Implementation of the CIE System for Mesopic Photometry,” 2016.

[167] Y. Ohno *et al.*, “Principles governing Photometry,” 2019.

[168] L. T. Troland, “On the Measurement of Visual Stimulation Intensities,” *Exp. Psychol.*, vol. 2, no. 1, 1917.

[169] H. Kragh, “Photon : New light on an old name,” pp. 1–16, 2014.

[170] S. Hecht, S. Shlaer, and M. Pirenne, “Energy, Quanta and Vision: Threshold Energies for Vision,” vol. 1941, pp. 819–840, 1942.

[171] D. V Norren and J. J. Vos, “Spectral Transmission of the Human Ocular Media,” *Vis. Res*, vol. 14,

no. 1973, pp. 1237–1244, 1974.

[172] V. Polo *et al.*, “Assessment of the ocular media absorption index,” vol. 8, pp. 7–9, 1997.

[173] K. H. Ruddock, “The Effect of Age upon Colour Vision - II. Changes with Age in Light Transmission of the Ocular Media,” *Vis. Res*, vol. 5, pp. 47–58, 1965.

[174] H. Mactier, S. Maroo, M. Bradnam, and R. Hamilton, “Ocular Biometry in Preterm Infants : Implications for Estimation of Retinal Illuminance,” pp. 453–457.

[175] E. A. Boettner and J. R. Wolter, “Transmission of the ocular media,” pp. 776–783, 1962.

[176] A. Roset, “The Relative Sensitivities of Television Pickup Tubes , Photographic Film , and the Human Eye *,” pp. 293–300, 1942.

[177] Y. Shimada and M. Horiguchi, “Stray Light – Induced Multifocal Electroretinograms,” pp. 1245–1251, 2003.

[178] H. B. Barlow, “Measurments of the Quantum Efficiency of Discrimination in Human Scotopic Vision,” *J. Phy8iol*, vol. 160, no. 1, pp. 169–188, 1962.

[179] H. B. Barlow, “A Method of Determining the Overal Quantum Efficiency of Visual Discriminations,” *J. Phy8iol*, vol. 160, pp. 155–168, 1962.

[180] A. Van Meeteren, “On the Detective Quantum Efficiency of the Human Eye,” *Vis. Res*, vol. 18, no. 1959, pp. 257–267, 1977.

[181] J. A. Martínez-Roda, M. Vilaseca, J. C. Ondategui, M. Aguirre, and J. Pujol, “Effects of aging on optical quality and visual function,” pp. 518–525, 2016.

[182] K. Kamiya, K. Umeda, H. Kobashi, K. Shimizu, T. Kawamorita, and H. Uozato, “Effect of Aging on Optical Quality and Intraocular Scattering Using the Double-Pass Instrument,” vol. 37, no. April, pp. 884–888, 2012.

[183] M. Shahidi and Y. Yang, “Measurements of Ocular Aberrations and Light,” vol. 81, no. 11, pp. 853–857, 2004.

[184] M. L. Hennelly, J. L. Barbur, D. F. Edgar, and E. G. Woodward, “The effect of age on the light scattering characteristics of the eye,” vol. 18, no. 2, pp. 197–203, 1998.

[185] A. Guirao, G. Manuel, E. Geraghty, S. Norrby, and P. Artal, “Function of Age in a Normal Population,” vol. 40, no. I, 1998.

[186] D. B. Elliott, “Contrast Sensetivity Decline with Ageing: A Neural or Optical Phenomenon?,” *Ophlhal. Physiol*, vol. 7, no. 4, pp. 415–419, 1987.

[187] F. Diaz-Douton, A. Benito, J. Pujol, M. Arjona, L. Gu, and P. Artal, “Comparison of the Retinal Image Quality with a Hartmann-Shack Wavefront Sensor and a Double-Pass Instrument,” *Invest. Ophthalmol. Vis. Sci.*, vol. 47, no. 4, pp. 1710–1716, 2006.

[188] W. S. Stiles and B. H. Crawford, “The Luminous Efficiency of Rays Entering the Eye Pupil at Different Points,” pp. 428–450, 1932.

[189] W. S. Stiles and B. H. Crawford, “The liminal Brughtness Increment as a Function of Wave-Length

for Different Conditions of the Foveal and Parafoveal Retina," pp. 496–530, 1933.

[190] G. Westheimer, "Directional sensitivity of the retina : 75 years of Stiles – Crawford effect," *Proc. Biol. Sci.*, vol. 275, no. 1653, pp. 2777–2786, 2008.

[191] R. A. Applegate, "Parametric representation of Stiles-Crawford functions : normal variation of peak location and directionality," vol. 10, no. 7, pp. 1611–1623, 1993.

[192] C. E. Sternheim and L. A. Riggs, "Utilization of the Stiles-Crawford Effect in the Investigation of the Origin of Electrical Responses of the Human Eye," *Vis. Res*, vol. 8, pp. 25–33, 1968.

[193] A. W. Snyder and C. Pask, "The Stiles-Crawford Effect - Explanation and Consequences," *Vis. Res*, vol. 13, pp. 1115–1137, 1973.

[194] M. E. Clinic, M. E. Clinic, and S. Hospital, "Stiles – Crawford effect in focal macular ERGs from macaque monkey," vol. 12, pp. 1–7, 2012.

[195] P. Gonzalez, S. Parks, F. Dolan, and D. Keating, "The effects of pupil size on the multifocal electroretinogram," *Doc. Ophthalmol.*, vol. 109, no. 1, pp. 67–72, 2004.

[196] A.-M. Gagne, J. Lavoie, M.-P. Lavoie, A. Sasseville, M.-C. Charron, and M. Hebert, "Assessing the impact of non-dilating the eye on full-field electroretinogram and standard flash response," *Doc Ophthalmol*, vol. 121, no. 3, pp. 167–175, 2010.

[197] C. Q. Davis, O. Kraszewska, and C. Manning, "Constant luminance versus constant retinal illuminance stimulation in flicker ERGs," *Doc. Ophthalmol.*, vol. 134, no. 2, pp. 75–87, 2017.

[198] C. M. Poloschek and M. Bach, "Can we do without mydriasis in multifocal ERG recordings ?," *Doc. Ophthalmol.*, vol. 118, no. 2, pp. 121–127, 2009.

[199] R. Hagenah, "Simultaneous Recording of Pupillary Hippus and EEG," vol. 218, no. 1978, pp. 213–218, 2000.

[200] B. Laeng and U. Sulutvedt, "The Eye Pupil Adjusts to Imaginary Light," *Psychol. Sci.*, vol. 25, no. 1, pp. 188–197, 2014.

[201] K. Daniel and J. Beatty, "Pupil Diameter and Load on Memory," *Science (80-.).*, vol. 154, no. 3756, pp. 1583–1586, 1966.

[202] P. R. K. Turnbull, N. Irani, N. Lim, and J. R. Phillips, "Origins of Pupillary Hippus in the Autonomic Nervous System," *Invest. Ophthalmol. Vis. Sci.*, vol. 58, no. 1, pp. 197–203, 2017.

[203] B. H. Crawford, "The Dependence of Pupil Size upon External Light Stimulus under Static and Variable Conditions," *Proc. R. Soc.*, vol. 121, no. 823, pp. 376–395, 1936.

[204] H. Bouma and L. C. J. Baghuis, "Hippus of the Pupil: Periods of Slow Oscillation of Unknown Origin," *Yision Res*, vol. II, pp. 1345–1351, 1971.

[205] B. C. Goldwater, "Phychological Significance of Pupillary Movements," *Psychol. Bull.*, vol. 77, no. 1943, pp. 340–355, 1972.

[206] J. L. Fernández-torre, A. Paramio-paz, and I. L. L. Ríos, "Pupillary hippus as clinical manifestation of refractory autonomic nonconvulsive status epilepticus: Pathophysiological implications," *Eur. J. Epilepsy*, vol. 63, no. 9, pp. 102–104, 2018.

[207] E. J. German, M. A. Hursf, and D. Wood, “Evaluation of the pinhole pupillometer,” vol. I, no. 6, pp. 484–495, 1998.

[208] H. H. Telek, “The Effects of Age on Pupil Diameter at Different Light Amplitudes,” vol. 3, no. 2, pp. 80–85, 2018.

[209] P. Gouras, “Electroretinography : Some basic principles,” *Invest. Ophthalmol. Vis. Sci.*, vol. 9, no. 8, pp. 557–569, 1970.

[210] E. P. Johnson, “The Electrical Responses of the Human Retina During Dark-Adaptation,” *Exp. Psychol.*, vol. 39, no. 5, pp. 597–609, 1947.

[211] R. M. Boynton and L. A. Riggs, “The Effect of Stimulus Area and Intensity upon the Human Retinal Response,” *Exp. Psychol.*, vol. 42, no. 4, 1951.

[212] R. G. Devoe, H. Ripps, and H. G. Vaughan, “Cortical Responses to Stimulation of the Human Fovea,” *Vfsion Res*, vol. 8, pp. 135–147, 1968.

[213] D. Finkelstein, P. Gouras, and M. Hoff, “Human electroretinogram near the absolute threshold of vision,” *Invest. Ophthalmol. Vis. Sci.*, vol. 7, no. 2, pp. 214–218, 1968.

[214] R. D. Gunkel, D. R. Bergsma, and P. Gouras, “A Ganzfeld Stimulator for Electroretinography,” *Arch. Ophthalmol.*, vol. 94, no. 4, pp. 669–670, 1976.

[215] G. K. Diprose and M. J. Smith, “Computer-controllable variable-intensity ganzfeld stimulator for electroretinography,” *Med. Biol. Eng. Comput.*, vol. 23, no. 5, pp. 496–497, 1985.

[216] C. Gargini, G. C. Demontis, L. Cervetto, and S. Bisti, “Analysis of pharmacologically isolated components of the ERG.,” *Vision Res.*, vol. 39, no. 10, pp. 1759–66, May 1999.

[217] A. E. Weymouth and A. J. Vingrys, “Rodent electroretinography: Methods for extraction and interpretation of rod and cone responses,” *Prog. Retin. Eye Res.*, vol. 27, no. 1, pp. 1–44, 2008.

[218] J. Heck and I. Rendahl, “Components of the Human Electroretinogmm. An Analysis in Normal Eyes and in Colour Blindness. Preliminnry Report.,” no. 1942, 1957.

[219] D. Yonemura, Y. Masuda, and M. Hatta, “The Oscillatory Potential in the Electroretinogram,” *Jpn. J. Physiol.*, vol. 13, no. 2, pp. 129–137, 2011.

[220] D. Yonemura, K. Tsuzuki, and T. Aoki, “Clinical Importance of the Oscillatory Potential in the Human ERG,” *Acta Ophthalmol.*, vol. 51, no. 2, pp. 50–95, 2001.

[221] W. H. Seiple, I. M. Siegel, R. E. Carr, and C. Mayron, “Evaluating Macular Function Using the Focal ERG,” *Invest Ophthalmol Vis Sci*, vol. 27, no. 7, pp. 1123–1130, 1986.

[222] P. Errico, B. Falsini, V. Porciatti, and F. M. Cefala, “The human focal electroretinogram as a function of stimulus area,” pp. 41–48, 1990.

[223] C. A. Curcio, K. R. Sloan, R. E. Kalina, and A. E. Hendrickson, “Human Photoreceptor Topography,” vol. 523, pp. 497–523, 1990.

[224] J. B. Jonas, U. Schneider, and G. O. H. Naumann, “Count and density of human retinal photoreceptors,” *Graefe’s Arch Clin Exp Ophthalmol*, vol. 230, no. 6, pp. 505–510, 1992.

[225] John R.Heckenlively and Geoffrey B.Arden, *Principles and Practice of Clinical Electrophysiology of Vision*, Second. 2001.

[226] D. Ophthalmologica, K. A. Publishers, S. Florida, and J. A. H. V. Hospital, "The clinical utility of the foveal electroretinogram : A review," pp. 313–325, 1990.

[227] M. A. B. Brazier and J. V Casby, "Summation of Retinal Potentials," vol. 217, no. August, 1961.

[228] B. G. S. Brindley and G. Westheimer, "The Spatial Properties of the Human Electroretinogram," *J. Physiol*, vol. 179, pp. 518–537, 1965.

[229] T. S. Aiba, M. Alpern, and F. Maaseidvaag, "The Electroretinogram Evoked by the Excitation of Human Foveal Cones," *J. Physiol*, vol. 43, no. 1, pp. 43–62, 1967.

[230] G. B. Arden and J. L. K. Bankes, "Foveal Electroretinogram as a Clinical Test," *Brit. J. Ophihal*, vol. 50, 1966.

[231] I. M. Siegel and R. E. Carr, "Electrodiagnostic and psychophysical testing in retinal disease." .

[232] S. A. Burns, A. E. Elsner, and M. R. Kreitz, "Analysis of nonlinearities in the flicker ERG," *Optometry and Vision Science*, vol. 69, no. 2. pp. 95–105, 1992.

[233] G. Gong, T. Helleseth, and P. V. Kumar, "Solomon W . Golomb — Mathematician , Engineer , and Pioneer," *IEEE Trans. Inf. Theory*, vol. 64, no. 2, pp. 2844–2857, 2018.

[234] K. W. Cattermole, "Shift Register Sequences," *Electron. Power*, vol. 14, no. 4, pp. 166–167, 1968.

[235] S. J. Fricker and J. J. Sanders, "A new method of cone electroretinography: the rapid random flash response," *Invest Ophthalmol Vis Sci*, vol. 14, no. 2, pp. 131–137, 1974.

[236] P. E. B. Bovernick, "United States Patent, 4846567, Eric Sutter," no. 19, 1989.

[237] D. C. Hood, J. G. Odel, C. S. Chen, B. J. Winn, and M. Electroretinogram, "The Multifocal Electroretinogram," vol. 23, no. 3, pp. 225–235, 2003.

[238] R. C. Reid, J. D. Victor, and R. M. Shapley, "The use of m-sequences in the analysis of visual neurons: linear receptive field properties.," *Vis. Neurosci.*, vol. 14, no. 6, pp. 1015–27, 1997.

[239] M. J. Korenberg and I. W. Hunter, "The Identification of Nonlinear Biological Systems - Wiener," *Ann. Biomed. Eng.*, vol. 18, pp. 629–654, 1990.

[240] V. Z. Marmarelis, "Wiener analysis of nonlinear feedback in sensory systems.," *Ann. Biomed. Eng.*, vol. 19, no. 4, pp. 345–82, Jan. 1991.

[241] E. E. Sutter, "Imaging visual function with the multifocal m-sequence technique.," *Vision Res.*, vol. 41, no. 10–11, pp. 1241–55, Jan. 2001.

[242] W. Kosnik, J. Fikre, and R. Sekuler, "Visual fixation stability in older adults.," *Invest. Ophthalmol. Vis. Sci.*, vol. 27, no. 12, pp. 1720–5, Dec. 1986.

[243] C. Tosha, M. B. Gorin, and S. Nusinowitz, "Test-Retest Reliability and Inter-Ocular Symmetry of Multi-Focal Electroretinography in Stargardt Disease," vol. 35, no. 1, pp. 63–72, 2010.

[244] K. B. Pedersen, A. K. Sjølie, A. H. Vestergaard, S. Andréasson, and F. Møller, "Fixation stability and

implication for multifocal electroretinography in patients with neovascular age-related macular degeneration after anti-VEGF treatment," *Clin. Exp. Ophthalmol.*, vol. 254, no. 10, pp. 1897–1908, 2016.

[245] S. Samet, E. G. Gonz, M. S. Mandelcorn, M. H. Brent, and L. Tarita-nistor, "Changes in Fixation Stability with Time during Binocular and Monocular Viewing in Maculopathy," pp. 1–9, 2018.

[246] J. M. Henderson, "Human gaze control during real-world scene perception," vol. 7, no. 11, pp. 498–504, 2003.

[247] M. J. Steinbach, L. Tarita-nistor, I. Gill, and E. G. Gonza, "Fixation Stability Recording : How Long for Eyes," vol. 94, no. 3, pp. 311–316, 2017.

[248] F. Di Russo, S. Pitzalis, and D. Spinelli, "Fixation stability and saccadic latency in e lite shooters," vol. 43, pp. 1837–1845, 2003.

[249] C. N. C. Engineering, "The stability of human eye orientation during visual fixation," vol. 142, pp. 2–5, 1992.

[250] J. a Chisholm, D. Keating, S. Parks, and a L. Evans, "The impact of fixation on the multifocal electroretinogram.," *Doc. Ophthalmol.*, vol. 102, no. 2, pp. 131–9, Mar. 2001.

[251] M. Kondo, Y. Miyake, and M. Horiguchi, "Clinical Evaluation of Multifocal Electroretinogram," vol. 36, no. 10, pp. 2146–2150, 1995.

[252] D. C. Hood, W. Seiple, K. Holopigian, and V. Greenstein, "A comparison of the components of the multifocal and full-field ERGs," *Vis. Neurosci.*, vol. 14, no. 3, pp. 533–544, 1997.

[253] S. Wu and E. Sutter, "A topographic study of oscillatory potentials in man," *Vis. Neurosci.*, vol. 12, no. 6, pp. 1013–1025, 1995.

[254] M. A. Bearse, Y. Shimada, and E. E. Sutter, "Distribution of oscillatory components in the central retina," *Acta Ophthalmol.*, vol. 100, no. 2–3, pp. 185–205, Mar. 2000.

[255] M. Kondo and M. Yozo, "Assessment of local cone on- and off-pathway function using multifocal ERG technique," *Doc. Ophthalmol.*, vol. 100, no. 2–3, pp. 139–154, 2000.

[256] L. Tan, M. Kondo, M. Sato, N. Kondo, and Y. Miyake, "Multifocal pupillary light response fields in normal subjects and patients with visual field defects," vol. 41, pp. 1073–1084, 2001.

[257] D. Keating, S. Parks, D. Smith, and A. Evans, "The multifocal ERG: unmasked by selective cross-correlation," *Vision Res.*, vol. 42, no. 27, pp. 2959–2968, 2002.

[258] C. S. Matsumoto *et al.*, "What monitor can replace the cathode-ray tube for visual stimulation to elicit multifocal electroretinograms?," *J. Vis.*, vol. 14, no. 9, pp. 2–2, 2014.

[259] T. Meigen and A. Friedrich, "Zur Reproduzierbarkeit von multifokalen ERG-Ableitungen," *Ophthalmologe*, vol. 24, no. 288, pp. 713–718, 2002.

[260] P. C. Jacobi, K. Miliczek, and E. Zrenner, "Experiences with the international standard for clinical electroretinography : normative values for clinical practice , interindividual and intraindividual variations and possible extensions," pp. 95–114, 1993.

[261] M. Gauvin, J. Lina, and P. Lachapelle, "Advance in ERG Analysis : From Peak Time and Amplitude

to Frequency , Power , and Energy," vol. 2014, 2014.

[262] M. Gur and I. Gath, "Time and Frequency Analysis of Simultaneously Recorded Corneal and Non-Corneal Electroretinogram," vol. 1, pp. 172–174, 1979.

[263] Y. Han, "Towards optimal filtering of 'standard' multifocal electroretinogram (mfERG) recordings: findings in normal and diabetic subjects," *Br. J. Ophthalmol.*, vol. 88, no. 4, pp. 543–550, Apr. 2004.

[264] A. Maiti, M. Uparkar, S. Natarajan, N. Borse, and J. Walinjkar, "Principal components ' analysis of multifocal electroretinogram in retinitis pigmentosa," no. 9, 2007.

[265] R. Barraco, D. P. Adorno, and M. Brai, "An approach based on wavelet analysis for feature extraction in the a -wave of the electroretinogram," *Comput. Methods Programs Biomed.*, vol. 104, no. 3, pp. 316–324, 2011.

[266] S. S. Nair and K. P. Joseph, "Biomedical Signal Processing and Control Wavelet based electroretinographic signal analysis for diagnosis," *Biomed. Signal Process. Control*, vol. 9, pp. 37–44, 2014.

[267] R. Barraco, D. P. Adorno, M. Brai, and L. Tranchina, "A comparison among different techniques for human ERG signals processing and classificatio," *Phys. Medica*, vol. 30, no. 1, pp. 86–95, 2014.

[268] T. Wright, J. Nilsson, and C. Gerth, "A comparison of signal detection techniques in the multifocal electroretinogram," *Doc Ophthalmol*, vol. 117, no. 2, pp. 163–170, 2008.

[269] S. Parks, D. Keating, T. H. Williamson, A. L. Evans, A. T. Elliott, and J. L. Jay, "Functional imaging of the retina using the multifocal electroretinograph : a control study," *Br. J. Ophthalmol.*, vol. 80, no. 9, pp. 831–834, 1996.

[270] K. S. M. Fung, F. K. Lam, F. H. Y. Chan, P. W. F. Poon, and J. G. Lin, "Adaptive neural network filter for visual evoked potential estimation," *Proc. ICNN'95 - Int. Conf. Neural Networks*, pp. 2293–2296, 1995.

[271] R. S. Ledley and L. B. Lusted, "Reasoning foundations of medical diagnosis," vol. 130, no. 3366, 1959.

[272] P. J. G. Lisboa, E. C. Ifeachor, W. D. Penny, W. G. Baxt, M. F. Jefferson, and N. Pendleton, "Artificial Neural Networks in Biomedicine," vol. 25, pp. 211–214, 2002.

[273] E. Systems and E. Engineering, "Diagnosis of the macular diseases from pattern electroretinography signals using artificial neural networks," vol. 30, pp. 361–366, 2006.

[274] M. F. Marmor, "An international standard for electroretinography," vol. 1961, pp. 299–302, 1989.

[275] L. H. Van Der Tweel, "Some Proposals for Standardization of ERG Equipment," *Acta Ophthalmol.*, vol. 70, 1962.

[276] L. H. van Der Tweel, R. Carr, K. A. Hellner, T. Lawwill, G. H. Van Lith, and Y. Tazawa, "Report of the Committee on Instrumentation and Procedures in Visual Electrophysiology at the request of the Concilium Ophthalmologicum Universale," *Doc. Ophthalmol.*, vol. 51, no. 4, pp. 383–395, 1981.

[277] J. . Barlow, A. Kamp, H. . Morton, A. Ripoche, H. Shipton, and D. . Tchavdarov, "EEG

Instrumentation Standards (Revised 1977): Report of the Committee on EEG Instrumentation Standards of the International Federation of Societies for Electroencephalography and Clinical Neurophysiology," pp. 144–150, 1977.

[278] M. F. Marmor and E. Zrenner, "Standard for clinical electroretinography (1994 update)," pp. 199–210, 1995.

[279] M. F. Marmor and E. Zrenner, "Standard for clinical electroretinography (1999 update)," pp. 143–156, 1999.

[280] F. Michael, E. Graham, and W. Mathias, "Standard for clinical electroretinography (2004 update)," 2004.

[281] M. Brigell, M. Bach, C. Barber, K. Kawasaki, and A. Kooijman, "Guidelines for calibration of stimulus and recording parameters used in clinical electrophysiology of vision. Calibration Standard Committee of the International Society for Clinical Electrophysiology of Vision (ISCEV).," *Doc. Ophthalmol.*, vol. 95, no. 1, pp. 1–14, Jan. 2003.

[282] R. P. Hagan, K. J. Quinn, L. Milner, R. L. Robinson, and A. F. TakTak, "Reproducibility Of Visual Electrophysiology Recordings Between Laboratories: The Importance Of Regular Calibration," *IVOS Investig. Ophthalmol. Vis. Sci.*, vol. 53, no. 14, 2012.

[283] X. Ding, W. Liu, J. Zhang, and L. Zhao, "A method and system to simulate human electrophysiological activity," vol. 25, no. 18, 2017.

[284] R. Aliazizi, M. Elt, R. Hagan, R. Laflin, and A. Eleuteri, "iSim: A Smart ERG Signal Generator for Calibration of Instruments and Alignment of Recording Regimes Across Clinical Laboratories," *12th BriSCEV Course Conf.*, p. 20, 2014.

[285] G. Nicoletti, G. De Crecchio, B. Falsini, G. Ambrosio, M. Ahmadi, and S. Kastner, "ISCEV Symposium Program Listing (in chronological order)," *Doc. Ophthalmol.*, vol. 129, no. S1, pp. 3–11, 2014.

[286] Ó. S. B. Heidelberg *et al.*, "ISCEV symposium program listing (in chronological order)," *Doc. Ophthalmol.*, vol. 130, no. S1, pp. 3–9, 2015.

[287] G. E. Holder, C. Gerth-kahlert, K. Landau, and J. V. M. Hanson, "53rd Symposium of International Society for Clinical Electrophysiology of Vision (ISCEV), 23–27 June 2015, Ljubljana, Slovenia," *Doc. Ophthalmol.*, vol. 130, no. S1, pp. 11–58, 2015.

[288] J. R. Grigg *et al.*, *56th Annual Symposium of the International Society for Clinical Electrophysiology of Vision (ISCEV 2018) : Reims, France, 18-23 June 2018*, vol. 136. 2018.

[289] K. Fujinami *et al.*, "54th ISCEV Symposium, Singapore, August 13, 2016–August 18, 2016," *Doc. Ophthalmol.*, vol. 133, no. S1, pp. 9–41, 2016.

[290] K. Reinhard *et al.*, "Step-By-Step Instructions for Retina Recordings with Perforated Multi Electrode Arrays," vol. 9, no. 8, 2014.

[291] M. Fujii, G. A. Sunagawa, M. Kondo, and M. Takahashi, "Evaluation of micro Electroretinograms Recorded with Multiple Electrode Array to Assess Focal Retinal Function," *Nat. Publ. Gr.*, no. November 2015, pp. 1–13, 2016.

[292] Y. Krakova, H. Tajalli, S. Thongpang, and Z. Derafshi, “Spatial differences in corneal electroretinogram potentials measured in rat with a contact lens electrode array,” *Doc Ophthalmol*, vol. 129, no. 3, pp. 151–166, 2014.

[293] E. Sundrnark, “Recording of the Human Electroretinogram with the Contact Glass,” *Acta Ophthalmol.*, vol. 37, 1959.

[294] R. Yin *et al.*, “Soft transparent graphene contact lens electrodes for conformal full-cornea recording of electroretinogram,” *Nat. Commun.*, 2018.

[295] A. S. John and C. P. Price, “Existing and Emerging Technologies for Point-of-Care Testing,” vol. 35, no. 3, pp. 155–167, 2014.

[296] N. M. Farandos, A. K. Yetisen, M. J. Monteiro, and C. R. Lowe, “Contact Lens Sensors in Ocular Diagnostics,” pp. 792–810, 2015.

[297] C. Biosensors, R. C. Tseng, C. Chen, S. Hsu, and H. Chuang, “Contact-Lens Biosensors,” 2018.

[298] K. Asakawa *et al.*, “New Mydriasis-Free Electroretinogram Recorded with Skin Electrodes in Healthy Subjects,” vol. 2017, 2017.

[299] A. E. Hobby *et al.*, “Effect of varying skin surface electrode position on electroretinogram responses recorded using a handheld stimulating and recording system,” *Doc. Ophthalmol.*, vol. 137, no. 2, pp. 79–86, 2018.

[300] K. Kato, M. Kondo, M. Sugimoto, K. Ikesugi, and H. Matsubara, “Effect of Pupil Size on Flicker ERGs Recorded With RET eval System : New Mydriasis-Free Full-Field ERG System,” no. 2595, 2015.

[301] F. J. Ascaso, “Noninvasive Continuous Monitoring of Tear,” vol. 93, no. 4, pp. 426–434, 2016.

[302] P. Teikari *et al.*, “An inexpensive Arduino-based LED stimulator system for vision research,” *J. Neurosci. Methods*, vol. 211, no. 2, pp. 227–236, 2012.

[303] S. Maehara, N. Itoh, Y. Itoh, S. Wakaiki, K. Tsuzuki, and T. Seno, “Electroretinography Using Contact Lens Electrode with Built-In Light Source in Dogs,” 2005.

[304] S. Mizunoya, K. Kuniyoshi, and M. Arai, “Electroretinogram contact lens electrode with tri-color light-emitting diode,” pp. 497–500, 2001.

[305] Y. W. Y. Yip, T. C. Man, C. P. Pang, and M. E. Brelén, “Improving the quality of electroretinogram recordings using active electrodes,” *Exp. Eye Res.*, vol. 176, no. June, pp. 46–52, 2018.

[306] A. Pourahmad and A. Mahnam, “Evaluation of a Low‐cost and Low‐noise Active Dry Electrode for Long‐term Biopotential Recording,” *J Med Signals Sens*, vol. 6, no. 4, pp. 197–202, 2016.

[307] J. Xu, S. Mitra, and C. Van Hoof, “Active Electrodes for Wearable EEG Acquisition : Review and Electronics Design Methodology,” *IEEE Rev. Biomed. Eng.*, vol. 10, no. 1, 2017.

[308] M. Thoma and M. Morari, *Block Oriented Nonlinear System Identification*. Springer, 2010.

[309] H. M. Sakai, K. Naka, and M. J. Korenberg, “White-noise analysis in visual neuroscience,” no. 1988, pp. 287–296, 1988.

[310] A. J. Zele *et al.*, “A Temporal White Noise Analysis for Extracting the Impulse Response Function of the Human Electroretinogram,” vol. 6, no. 6, 2017.

[311] R. D. Nowak, “Nonlinear system identification,” *Circuits, Syst. Signal Process.*, vol. 21, no. 1, pp. 109–122, 2002.

[312] N. Wiener, *Nonlinear problems in random theory*. The Massachusetts Institute of Technology, 1958.

[313] V. Volterra, *Theory of Functionals and of Integral and Integro-Differential Eqution*s. Dover, New York, 1930.

[314] A. A. C. A. Jayathilake, A. A. I. Perera, and M. A. P. Chamikara, “Discrete Walsh-Hadamard Transform in Signal Processing Discrete Walsh-Hadamard Transform in Signal Processing,” *IJRIT Int. J. Res. Inf. Technol.*, vol. 1, no. 1, pp. 80–89, 2013.

[315] S. Mandelbrojt, “The Mathematical Work of Jacques Hadamard,” *Am. Math. Mon.*, vol. 85, no. 1, pp. 2–26, 2019.

[316] J. Hadamard, *Calcul Des Variations*. 1910.

[317] A. A. Khan and N. S. Vyas, “Non-Linear Parameter Estimation Using Volterra and Wiener Theories,” *J. Sound Vib.*, vol. 221, pp. 805–821, 1999.

[318] G. Palm and T. Poggio, “The Volterra Representation and the Wiener Expansion: Validity and Pitfalls,” *SIAM J. Appl. Math.*, vol. 33, no. 2, pp. 195–216, 1977.

[319] A. Usakova, J. Kotuliakov, and M. Zajac, “Using of Discrete Orthogonal Transforms for Convolution,” *J. Electr. Eng.*, vol. 53, no. 9, pp. 285–288, 2002.

[320] R. M. Larkin, S. Klein, T. E. Ogden, and D. H. Fender, “Nonlinear Kernels of the Human ERG,” *Nature*, vol. 237, no. 5349, pp. 55–56, 1979.

[321] Y. W. Lee and M. Schetzen, “Measurement of the wiener kernels of a non-linear system by cross-correlation,” *Int. J. Control*, vol. 2, no. 3, pp. 237–254, 1965.

[322] M. Schetzen, “Nonlinear System Modeling Based on the Wiener Theory,” *Measurement*, vol. 6, no. 1997, pp. 1557–1573, 1981.

[323] A. C. Fisher *et al.*, “Comparison of human expert and computer-automated systems using magnitude-squared coherence (MSC) and bootstrap distribution statistics for the interpretation of pattern electroretinograms (PERGs) in infants with optic nerve hypoplasia (ONH),” *Doc. Ophthalmol.*, vol. 131, no. 1, pp. 25–34, 2015.

[324] A. F. G. Taktak, A. Eleuteri, S. P. Lake, and A. C. Fisher, “Decision support systems in cancer,” pp. 227–227, 2008.

[325] A. F. G. Taktak, A. Eleuteri, S. P. Lake, and A. C. Fisher, “A web-based tool for the assessment of discrimination and calibration properties of prognostic models,” *Comput. Biol. Med.*, vol. 38, no. 7, pp. 785–791, 2008.

[326] F. Matsuo, J. F. Peters, and E. L. Reilly, “Electrical Phenomena Associated with Movements of the Eyelid,” *Electroencephalogr. Clin. Neurophysiol.*, vol. 38, no. 1965, pp. 507–511, 1975.

[327] A. Tandle, S. Bhakti Vedanta Marg Vile Parle, M. -, and N. Jog, “Classification of Artefacts in EEG Signal Recordings and Overview of Removing Techniques,” *Int. J. Comput. Appl.*, no. Icct, p. 46, 2015.

[328] S. Kanoga and Y. Mitsukura, “Review of Artifact Rejection Methods for Electroencephalographic Systems,” in *Electroencephalography*, 2017, p. Chapter 6: 69-89.

[329] J. S. Barlow and A. Remond, “Eye Movement Artifact Nulling in EEGs by Multichannel On-Line EOG Subtraction,” *Electroencephalogr. Clin. Neurophysiol.*, vol. 2, no. 1977, pp. 418–423, 1981.

[330] M. Iwasaki *et al.*, “Effects of eyelid closure, blinks, and eye movements on the electroencephalogram.,” *Clin. Neurophysiol.*, vol. 116, no. 4, pp. 878–85, Apr. 2005.

[331] C. A. Joyce, I. F. Gorodnitsky, and M. Kutas, “Automatic removal of eye movement and blink artifacts from EEG data using blind component separation,” vol. 41, 2004.

[332] M. M. Stecker, “The effects of automatic artifact rejection on evoked potential recordings,” vol. 32, pp. 247–259, 2002.

[333] M. R. Keshtkaran and Z. Yang, “A Fast, robust algorithm for power line interference cancellation in neural recording,” *Neural Eng*, vol. 11, no. 2, pp. 1–18, Feb. 2014.

[334] R. V Baratta, M. Solomonow, B. H. Zhou, and M. Zhu, “Methods to reduce the variability of EMG power spectrum estimates,” *J. Electromyogr. Kinesiol.*, vol. 8, no. 5, pp. 279–85, Oct. 1998.

[335] D. P. Dobrev, T. D. Neycheva, and N. Tsvetanov, “High-Q Comb Filter for Mains Interference Suppression,” pp. 47–49, 2009.

[336] I. Sadiq, A. M. Zuberi, I. Zaman, A. Hassan, and T. Zaidi, “Adaptive removal of power-line interference from high resolution ECG,” vol. 2012, no. August, pp. 324–326, 2012.

[337] D. Berry, F. Duignan, and R. Hayes, “An Investigation of the use of a High Resolution ADC as a Digital Biopotential Amplifier,” *IFMBE Proc.*, no. January 2009, 2009.

[338] G. C. Carter, C. H. Knapp, and A. H. Nuttall, “Estimation of the Magnitude-Squared Coherence Function Via Overlapped Fast Fourier Transform Processing,” *IEEE Trans. Audio Electroacoust.*, vol. 21, no. 4, pp. 337–344, 1973.

[339] S. Malekpour, J. A. Gubner, and W. A. Sethares, “Measures of generalized magnitude-squared coherence: Differences and similarities,” *J. Franklin Inst.*, vol. 355, no. 5, pp. 2932–2950, 2018.

[340] A. Fisher, R. Aliazizi, and R. Hagan, “Recovery of the ERG from very low SNR recordings using a robust frequency domain approach: an Internet open source implementation,” *Acta Ophthalmol.*, vol. 90, no. 9, pp. 0–0, 2012.

[341] A. Peper and C. A. Grimbergen, “Investigation into the origin of the noise of surface electrodes,” *Med. Biol. Eng. Comput.*, vol. 40, no. 3, pp. 332–338, 2002.

[342] E. S. Kappenman and S. J. Luck, “The Effects of Electrode Impedance on Data Quality and Statistical Significance in ERP Recordings,” vol. 47, no. 5, pp. 888–904, 2011.

[343] M. Sustar *et al.*, “ISCEV extended protocol for the photopic On–Off ERG,” *Doc. Ophthalmol.*, vol. 136, no. 3, pp. 199–206, 2018.

[344] EDI, “VERIS Clinic 5.1, Visual Evoked Response Imaging System, Reference Guide.” p. Chapter 2, Page 12, 2006.

[345] G. Regan, F. McCaffery, K. Mc Daid, and D. Flood, “Medical device standards’ requirements for traceability during the software development lifecycle and implementation of a traceability assessment model,” *Comput. Stand. Interfaces*, vol. 36, no. 1, pp. 3–9, 2013.

[346] K. Dickersin and E. Mayo-Wilson, “Standards for design and measurement would make clinical research reproducible and usable,” *Proc. Natl. Acad. Sci.*, vol. 115, no. 11, pp. 2590–2594, 2018.

[347] B. Török and S. Gallen, “Calibration device for ERG , PERG , mfERG , EOG and VEP recording equipment,” no. June 2006, p. 9007, 2014.

[348] Y. Chen, Z. Y. Wang, G. Yuan, and L. Huang, “An overview of online based platforms for sharing and analyzing electrophysiology data from big data perspective,” *Data Min. Knowl. Discov.*, vol. 7, no. 4, pp. 1–25, 2017.

[349] C. Tenopir *et al.*, “Data sharing by scientists: Practices and perceptions,” *PLoS One*, vol. 6, no. 6, pp. 1–22, 2011.

[350] A. Sobolev *et al.*, “Integrated platform and API for electrophysiological data,” *Front. Neuroinform.*, vol. 8, no. APR, pp. 1–9, 2014.

[351] W. W. Harrison, M. A. Bearse, J. S. Ng, S. Barez, M. E. Schneck, and A. J. Adams, “Reproducibility of the mfERG between instruments,” *Doc Ophthalmol*, vol. 119, no. 1, pp. 67–78, 2009.

[352] D. J. Conrado, M. O. Karlsson, K. Romero, C. Sarr, and J. J. Wilkins, “Open innovation: Towards sharing of data, models and workflows,” *Eur. J. Pharm. Sci.*, vol. 109, no. June, pp. S65–S71, 2017.

[353] J. S. Ross and H. M. Krumholz, “Ushering in a new era of open science through data sharing: The wall must come down,” *JAMA - J. Am. Med. Assoc.*, vol. 309, no. 13, pp. 1355–1356, 2013.

[354] M. J. Pencina *et al.*, “Supporting open access to clinical trial data for researchers: The Duke Clinical Research Institute-Bristol-Myers Squibb Supporting Open Access to Researchers Initiative,” *Am. Heart J.*, vol. 172, pp. 64–69, 2016.

[355] F. Sardanelli, L. M. Sconfienza, G. Di Leo, M. Alì, M. G. Hunink, and N. Houssami, “To share or not to share? Expected pros and cons of data sharing in radiological research,” *Eur. Radiol.*, vol. 28, no. 6, pp. 2328–2335, 2018.

[356] R. Moucek *et al.*, “Software and hardware infrastructure for research in electrophysiology,” *Front. Neuroinform.*, vol. 8, no. March, pp. 1–15, 2014.

[357] R. A. Poldrack and K. J. Gorgolewski, “Making big data open: Data sharing in neuroimaging,” *Nat. Neurosci.*, vol. 17, no. 11, pp. 1510–1517, 2014.

[358] H. A. Piwowar, R. S. Day, and D. B. Fridsma, “Sharing detailed research data is associated with increased citation rate,” *PLoS One*, vol. 2, no. 3, 2007.

[359] T. G. M. Van Erp *et al.*, “Infrastructure for sharing standardized clinical brain scans across hospitals,” *2011 IEEE Int. Conf. Bioinforma. Biomed. Work. BIBMW 2011*, pp. 1026–1028, 2011.

[360] J. B. Wagenaar, B. H. Brinkmann, Z. Ives, G. A. Worrell, and B. Litt, “A multimodal platform for

cloud-based collaborative research," *Int. IEEE/EMBS Conf. Neural Eng. NER*, pp. 1386–1389, 2013.

[361] A. Thorogood and B. M. Knoppers, "Can research ethics committees enable clinical trial data sharing?," *Ethics, Med. Public Heal.*, vol. 3, no. 1, pp. 56–63, 2017.

[362] S. . Coupland and D. Wu, "International Multicenter Normative ERG Database Using the ISCEV Standard," *IOVS Investig. opthalmology Vis. Sci.*, vol. 47, no. 13, 2006.

[363] B. Fortune, X. Zhang, D. C. Hood, S. Demirel, and C. A. Johnson, "Normative ranges and specificity of the multifocal VEP," *Doc. Ophthalmol.*, vol. 109, no. 1, pp. 87–100, 2004.

[364] M. Bock, C. Gerth, and B. Lorenz, "Impact of notch filter use on waveforms of First- and Second-Order-Kernel responses from multifocal ERGs," pp. 1–16, 1999.

[365] K. T. Sweeney, H. Ayaz, T. E. Ward, M. Izzetoglu, S. F. McLoone, and B. Onaral, "A methodology for validating artifact removal techniques for physiological signals," *IEEE Trans. Inf. Technol. Biomed.*, vol. 16, no. 5, pp. 918–926, 2012.

[366] W. Wu *et al.*, "ARTIST: A fully automated artifact rejection algorithm for single-pulse TMS-EEG data," *Hum. Brain Mapp.*, vol. 39, no. 4, pp. 1607–1625, 2018.

[367] F. Grouiller, L. Vercueil, A. Krainik, and C. Segebarth, "A comparative study of different artefact removal algorithms for EEG signals acquired during functional MRI," *Neuroimage*, vol. 38, no. 1, pp. 124–137, 2007.

[368] Y. H. Ku and A. A. Wolf, "Volterra- Wiener Functionals for the Analysis of Nonlinear System," *J. Franklin Inst.*, vol. 281, no. 1, pp. 9–26, 1965.

[369] C. M. Cheng, Z. K. Peng, W. M. Zhang, and G. Meng, "Volterra-series-based nonlinear system modeling and its engineering applications: A state-of-the-art review," *Mech. Syst. Signal Process.*, vol. 87, no. Part A, pp. 340–364, 2017.

[370] A. Papoulis, *Probability, Random Variables, and Stochastic Processes*, 3rd ed. McGraw-Hill, 1991.

[371] P. M. T. Broersen, "Finite Sample Criteria for Autoregressive Order Selection," *IEEE Trans. SIGNAL Process.*, vol. 48, no. 12, pp. 3550–3558, 2000.

[372] P. M. T. Broersen, "Autoregressive Model Orders for Durbin's MA and ARMA Estimators," *2454 IEEE Trans. SIGNAL Process.*, vol. 48, no. 8, pp. 2454–2457, 2000.